

ISBN 978-4-901668-37-8

PROCEEDINGS

International Symposium on GeoInformatics for Spatial-Infrastructure Development in Earth and Allied Sciences

Phitsanulok, Thailand, 2-4 September 2021

Editors: Chaiwiwat VANSAROCHANA, Tanyaluck CHANSOMBAT and Venkatesh RAGHAVAN



The Japan-Vietnam Geoinformatics Consortium (JVGC)

JVGC Technical Document No.10

PROCEEDINGS

International Conference on GeoInformatics for Spatial-Infrastructure Development in Earth and Allied Sciences

GIS-IDEAS 2021

Conference Founders: Nghiem Vu KHAI & Takashi FUJITA

Conference Chairs: Venkatesh RAGHAVAN & Chaiwiwat VANSAROCHANA

Editors: Chaiwiwat VANSAROCHANA, Tanyaluck CHANSOMBAT and
Venkatesh RAGHAVAN

Organized by



**Naresuan University, Osaka City University &
Japan-Vietnam Geoinformatics Consortium**

Supported by

Hanoi University of Mining and Geology (VN)

Hanoi University of Natural Resources & Environment (VN) Japan

Geotechnical Consultant Association (JP)

Japan Society of Geoinformatics (JP)

i-bitz Company Ltd. (TH) and Geoinformatics International (TH)

2-4 September 2021, Phitsanulok, Thailand

From the Editors

The International Conference on GeoInformatics for Spatial-Infrastructure Development in Earth & Allied Sciences (GIS-IDEAS) 2021 was a special event in many ways. Previous GIS-IDEAS International Conferences between 2002 to 2018 were organized in collaboration with premier academic institutions in S.R. Vietnam. GIS-IDEAS 2021 marked the 10th in the conference series and first event to be organized in hybrid (online/onsite). The conference was to be organized in 2020 but was delayed due to the pandemic situation. GIS-IDEAS 2021 was hosted onsite at Naresuan University (NU), Thailand and in online mode between 2-4 September 2021.

The conduct of GIS-IDEAS Conferences is based on the spirit of mutual cooperation and openness. The GIS-IDEAS provides a platform for sharing of knowledge and valuable experiences and help promote collaborations and scientific exchanges between not only between students, researchers and practitioners Thailand, Vietnam, and Japan but also our other colleagues involved in developing and promoting Geoinformatics technologies.

We are indeed gratified with the overwhelming support for GIS-IDEAS 2021 from the international scientific community. We hope that the conference will continue to fulfill the expectations of participants and prove worthy of the trust and patronage of our peers.

We would like to express our gratitude to Naresuan University, Osaka City University, and the Japan-Vietnam Geoinformatics Consortium (JVGC) for all the support for successful organization of GIS-IDEAS 2021. We would like to particularly thank Honorary Prof. Dr. Kanchana Ngourungsi, President of Naresuan University, Dr. Nghiem Vu Khai, Founder of JVGC & Former Vice-Minister of Science and Technology, S.R. Vietnam, Prof. Muneki Mitamura, Osaka City University and Asst. Prof. Peerasak Chaiprasart, Naresuan University for their constant encouragements and invaluable support.

We thank all the contributors for sharing the outcome of their research that made the publication of the conference proceedings possible. We would also like to record our sincere gratitude to the committee members GIS-IDEAS 2021 and the Faculty, staff, and students of Naresuan University for helping in various ways. We express our deepest thanks to all the supporters and participants of GIS-IDEAS 2021, without their cooperation, organizing the event would not be possible.

We sincerely hope that the deliberations of GIS-IDEAS 2021 would kindle many innovative ideas and further academic exchanges in Geoinformatics research. We seek your continued patronage and cooperation.

Chaiwiwat Vansarochana, Tanyaluck Chansombat and Venkatesh Raghavan

20 January 2022

GIS-IDEAS 2021

2-4 September, 2021, Phitsanulok, Thailand

Contents

Session I

Health GIS

- S-1-2** Application of GIS technique and BENMAP Model for studying impacts air pollution on public health : A case of Ho Chi Minh City, Vietnam 1
S-1-3 Public space capacity estimations during COVID-19 pandemic using geospatial analysis: A case study of Naresuan University, Thailand 7

Session II

Hazards and Disaster

- S-2-1** Drainage density and valley erosion index at deep-seated landslides in the central Kii Mountains, Southwest Japan 12
S-2-2 Assessing the Landslide susceptibility in Samdrupjongkhar Dzongkhag using Machine Learning Models 18
S-2-3 Flood Risk Area Mapping with Logistic Regression: A Case Study of Phuntsholing City in Bhutan 26

Session III

Health GIS

- S-3-1** Relationship between daily number of COVID-19 cases and climate factors using multiple linear regression analysis method in Thailand 32
S-3-2 Cluster Pattern Identification of the COVID-19 Pandemic in Thailand 38
S-3-3 The Study of Vaccination Priority in Thailand: An GWR Analysis 44
S-3-4 Development of GEO-IOT in emergency medical care and services planning using U-BLOX GPS based on web GIS 50
S-3-5 GIS based analysis for emergency relief and rescue and disaster mitigation 58
S-3-6 The spread of COVID-19 in the context of regional geography 64

Session IV

Hazards and Disaster

- S-4-1** Landslide susceptibility Mapping using Logistic Regression Model : A case studies in the Van Yen, Yen Bai Province 69

- S-4-2** Hydrological Impact of Dual-Polarization Doppler Radar Data in mountainous areas: A case study of Typhoon Vipha (2020) in Upper NAN 76
S-4-3 An analysis and identification of flooded areas with data from SENTINEL-1 SATELLITES Yoshikatsu NAGATA 83
S-4-4 Generation of indicators to assess the flood vulnerability index in Hoi An City, Vietnam 89

Session V

Remote Sensing

- S-5-1** Machine Learning for Urban Types Detection Using Sentinel-1 And Sentinel-2 96
S-5-2 Estimating CHLOROPHYLL-A variations with temporal MODIS data time series 102
S-5-3 Above ground biomass estimation using multispectral SENTINEL-2 MSI DATA : A preliminary experiment in Wangchan forest learning center, Thailand 109
S-5-4 Air pollution NO₂ assessment using RS and GIS in Ho Chi Minh City and Neighborhood Period 2015-2019 115

Session VI

Hazards and Disaster

- S-6-1** Flood risk field survey using mobile GIS in Pua subdistrict, Pua district, Nan province, Thailand 121
S-6-2 Landslide susceptibility using Analytic Hierarchical Process in northern Thailand 129
S-6-3 Flood extent detection with differencing water indices using LANDSAT 8 data 136

Session VII

Remote Sensing

- S-7-1** Correlation of Drought Index Effected by El Nino Phenomenon Using Remote Sensing 142
S-7-2 Comparison of geographic images with SSIM and MSE algorithms 148
S-7-3 Linking between meteorological drought and land use/land cover in the Ba river basin 156

Session VIII

Web-GIS and Area Informatics

- S-8-1** Economic crops predictive system using artificial intelligence and GIS 162

S-8-2	GIS application for updating the information of waste transportation in Lien Chieu district, Danang city, Vietnam	170
S-8-3	Geo-Informatics evaluation of characteristics and amounts of microplastics contaminated in water surface level: Case of Songkhla Lake, THAILAND	178
S-8-4	Historical changes and variants of community level place names in the northeast of Thailand: A spatiotemporal-oriented study based on maps of early 20th century	185

Session IX

Spatial Analysis

S-9-1	A web-based seasonal geomorphological and coastal dynamics monitoring system : Case studies in Myanmar	191
S-9-2	Possibility in identifying suitable areas for urban green space development using GIS-BASE MULTI-CRITERIAL analysis and AHP WEIGHT METHOD in Dong Ha city, Vietnam	199
S-9-3	Building a GIS-BASED decision support model on land use planning for rubber plantation under the effect of typhoons in Quang Binh province, Vietnam	205
S-9-4	The survey of vertical temperature distribution within sea water column using geoinformatics technology, case study : The upper gulf of Thailand	213
S-9-5	Application of kriging interpolation method on building the digital elevation models for Ninh Kieu and Cai Rang districts of Can Tho city	219

Session X

Web Mapping, IoT

S-10-2	Implementation of web technology for smart farming monitoring and controlling using IoT, BLYNK APP and NODEMCU ESP8622	227
S-10-3	Online and real-time environment monitoring system using ESP8266 and wireless sensor networks	234
S-10-6	Development of smart location tracking system based on GPS GY-NEW-8M MODULE, REID, and online GIS technology	240

Session I

Poster – With full paper

P-1-1	Isarithm Mapping of Pandemic Covid-19 Significant Area with Kriging Surface and Semi-Variance Analysis	248
--------------	--	-----

P-1-2	A Machine learning approach to building a digital map of COVID-19	254
P-1-3	The formal alleviation of people suffering and cost reduction during the COVID-19 epidemic in Thailand	260
P-1-4	Interests and Knowledge of the People on Non-Pharmaceutical Measures - DMHTT of Thailand During the Third Wave of the COVID-19 Pandemic	267
P-1-5	Development of web map application for maximizing emergency vehicle service area for elderly people	272
P-1-6	Accuracy and effectiveness of 3D model reconstruction from UAV photogrammetry for physical road safety investigation	279
P-1-7	Study of the Accuracy of UAV survey technology for topology mapping on discrepancy terrain conditions	285
P-1-8	Shoreline change analysis using Sentinel-2A imagery data in Ben Tre, Vietnam	294
P-1-9	The use of NDVI and NDBI techniques for monitoring the growth of maize; A case study of Mae Phrik District, Lampang Province	300
P-1-10	Application of UAV multi-spectral camera for estimating bananas disease infestations in complex farming in Phitsanulok province	306

Session II

Poster – With full paper

P-2-1	Efficiency of MRC Flash Flood Guidance System (MRCFFGS) for Northeastern Thailand: Case Study of Tropical Strom Impact in 2019-2020	313
P-2-2	Web Map of Vietnam protected areas	319
P-2-3	Web-based database and spatial database management system : Application of disabled person in Phetchabon province	325
P-2-4	Using GIS to analyze factors affecting the apartment price. Case study : Neighborhood of Ho Chi Minh metro (Line 1)	333
P-2-6	Integration of geographic information systems and universal soil loss equation for soil erosion assessment in Dong Phu district, BINH PHUOC province, Vietnam	339
P-2-7	Capacity building on water and natural resources in SOUTH-EAST ASIA- benefits from the WANASEA PROJECT	347
P-2-9	Application of geographic information system with field experiment to assess suitable zonation mapping for rice cultivars under projected GLOBAL WARMING in Lower Northern Thailand	357
P-2-10	Application of GIS on building the geographic database for Ninh Kieu and Cai Rang districts of Can Tho city	364

P-2-11 Mapping surface water quality zone by GIS and spatial interpolation IDW – Case study in Can Tho city, Vietnam 370

Abstracts – Without full paper

A-1-1 Monitoring The Multi-Temporal Pattern of A COVID-19 Situation in Thailand Through Geospatial Data
Chudech Losiri amd Asamaporn Sithi

A-2-5 Assess the relationship between the Surface Urban Heat Island (SUHI) and Urbanization in Ho Chi Minh City
Vo Thi My Tien and Ho Dinh Duan

A-2-8 Study on extending the supply water pipe network at Binh Thuy district, Can Tho city
Ngan Nguyen Vo Chau, Giang Nam Nguyen Dinh and Minh Khoa Tran

APPLICATION OF GIS TECHNIQUE AND BENMAP MODEL FOR STUDYING IMPACTS AIR POLLUTION ON PUBLIC HEALTH: A CASE OF HO CHI MINH CITY, VIETNAM

Hoang Ngoc Khue Vu^{1,2}, Thoai Tam Nguyen^{1,2}, Thi Thuy Hang Nguyen^{1,2}, Ricardo Simon Carbajo³, Quan Le³, Rajnish Rakholia³, Bang Quoc Ho^{1,2,*}

¹Institute for Environment and Resources (IER), Ho Chi Minh City 700000, Vietnam; vhnk1304@gmail.com (H.N.K.V.); thoaitam1986@gmail.com (T.T.N.); hangnguyen6769@gmail.com (T.T.H.N.)

²Department of Science and Technology, Vietnam National University-Ho Chi Minh City (VNU-HCM), Ho Chi Minh City 700000, Vietnam

³ Ireland's National Centre for Applied Artificial Intelligence (CeADAR) / University College Dublin, Ireland; ricardo.simoncarbajo@ucd.ie; quan.le@ucd.ie, rajnish.rakholia@ucd.ie

142 To Hien Thanh St., Dist.10., HCMC

*Correspondence: bangquoc@yahoo.com

ABSTRACT

Vietnam's urban areas have faced serious environmental pollution issues, including: water pollution, municipal waste and air pollution. Air in Ho Chi Minh city is polluted by PM_{2.5} (particle matter with a diameter is less than 2.5 μm, so-called PM_{2.5}), O₃, CO, NO₂ and TSP which greatly affects public health. Ho Chi Minh City (HCMC) had 8,640,000 inhabitants with a total of 7,339,552 motorcycles and 637,323 automobiles. There are about 2,807 factories releasing air emissions, 2,061,957 households and 5,096 restaurants in the city. A comprehensive study is required to evaluate the impacts of air pollution levels on public health in this city. The aim of this study is to: (i) Application GIS technique to distribute air pollution concentration, population and public health diseases in the city and (ii) Then apply BENMAP theory model to calculate the mortality rate from three causes, namely Ischemic Heart Disease (IHD), cardiopulmonary, and lung cancer due to air pollution. The results showed that the annual average concentrations of NO₂ were higher than the standard of Vietnam National Technical Regulation on Ambient Air Quality (QCVN 05: 2013 40 μg/m³) and World Health Organization (WHO) (40 μg/m³). The annual average concentrations of PM_{2.5} were 23 μg/m³ and were also much higher than the WHO (10 μg/m³) standard by about 2.3 times. PM_{2.5} was found to be responsible for about 1136 deaths, while the number of mortalities from exposure to NO₂ and SO₂ was 172 and 89 deaths, respectively.

Keywords: GIS Technique; health impacts; Air pollution; BENMAP model; Ho Chi Minh City

1. INTRODUCTION

According to the National Environmental Status Report, Vietnam is facing an increase in air pollution, especially in megacities such as Hanoi or Ho Chi Minh City (HCMC). HCMC is the largest city in Vietnam with its position as the political, economic, scientific and cultural center of the country. Rapid urbanization rate leads to increased traffic pressure to meet the transportation demand of 8.6 million people in the city. HCMC has the highest number of vehicles in the country, accounting for about 9 million private vehicles in April 2017, up 5.4% compared to 2016 while public transport systems and the infrastructure has not met the rapid demand. In addition, HCMC has 2800 factories having chimneys to release air pollutants (including 19 manufacturing and industrial zones, 30 industrial clusters on an area of 1,900 ha,

and numerous factories and enterprises located separately around the city). All activities including transportation, industry, construction, domestic cooking, etc could cause serious air environment problems. Monitoring data collected between 2012 and 2016 indicated that levels of particulate matter (PM) and noise in urban areas including HCMC remained high in the last 5 years. Nearly 80% of total suspended particulate (TSP) samples exceeded the National technical regulation in ambient air quality (Vietnamese Standard QCVN 05:2013) in this period, especially at the high traffic density, industrial and crowded resident areas. NO_x and CO concentrations at the traffic area also exceeded the QCVN 05:2013 in this period. HCMC has 27% days exceed the standard of PM_{2.5} in 2016-2017. These high pollutant concentrations were associated with an increase in the risk of human health in HCMC (Bang, 2017, Ly et., 2019). Air pollution event on 22 Sep. 2019 showed that the number of patients admitted for respiratory diseases at the Saigon General Hospital in District 1 has increased by 5-10 percent compared to normal days, it was even overloaded and all doctors and nurses had to work around the clock.

It is an urgent need to study the impacts of air pollution on public health in Ho Chi Minh City. Therefore, the research on “Application of GIS technique and BENMAP model for studying impacts air pollution on public health: a case of Ho Chi Minh City, Vietnam” was carried out. The aim of this study is: (i) Application GIS technique to distribute air pollution concentration, population, and public health diseases in the city and (ii) Then apply BENMAP theory model to calculate the mortality rate from three causes, namely Ischemic Heart Disease (IHD), cardiopulmonary, and lung cancer due to air pollution.

2. MATERIALS AND METHODS

The effects of air pollution on health have been studied and proven on a global scale. Generally, the health effect from air quality can be estimated by using an impact function relating to the levels of air pollution change, the exposure population, the baseline incidence rate and the relative risk coefficient from an epidemiological study. This impact function can be described as the following formula (equation 1) and Figure 1:

$$\Delta Y = Y_0 (1 - e^{-\beta \Delta PM}) Pop \quad (1)$$

Where Y_0 is the death rate baseline in the study area (%); β - the effect estimate calculated by relative Risk – RR relating to the specific change in pollutant concentration and can be found in the cohort studies; ΔPM - the air quality change (increase or decrease) in pollutant concentration ($\mu g/m^3$ or ppb); and Pop - the exposed population in the study area (people). This study presents these parameters as a map layer, including: the pollutant concentration data which is the output of the CTM model for yearly-average of PM_{2.5}, NO₂ and SO₂ at cell resolution; the number of exposed people collected from the Statistic Office of HCMC for the year of 2017; the relative risk coefficients for each parameter are obtained from the report of Health Effects Institute by Daniel Krewski and colleagues (Table 1) (Krewski et al., 2009); and the death rate baseline is from Vietnamese A6 mortality reporting system (A6 system).

The study of Krewski has been carried out for 18 years, involving approximately 360,000 participants residing around the USA in 1980 and increasing up to around 500,000 people in 2000. These people were fully tracked for the levels of PM_{2.5} exposure and their status is also recorded on their diseases and mortality. The RR value in Table 2 shows that PM_{2.5} was strongly associated with the death due to lung cancer and IDH with the RR is higher than those of the other pollutants. Meanwhile, there is the weaker association between the disease and the mass of the larger size of particles, as well as with the concentration of SO₂.

Table 1. The relative risk of pollutants and selected cause of deaths

Pollutants	Cause of deaths	<i>Incremental Change</i>	Risk Factor
<i>PM_{2.5}</i>	Cardio-pulmonary	10 µg/m ³	1.09 (1.06–1.12)
	Lung cancer		1.11 (1.11–1.20)
	IHD		1.15 (1.04–1.18)
<i>NO₂</i>	Cardio-pulmonary	10 ppb	1.01 (1.00–1.02)
	Lung cancer		1.01 (0.97–1.01)
	IHD		1.02 (1.00–1.03)
<i>SO₂</i>	Cardio-pulmonary	5 ppb	1.02 (1.01–1.03)
	Lung cancer		1.00 (0.98–1.02)
	IHD		1.04 (1.02–1.05)

Source: Krewski et al., 2009

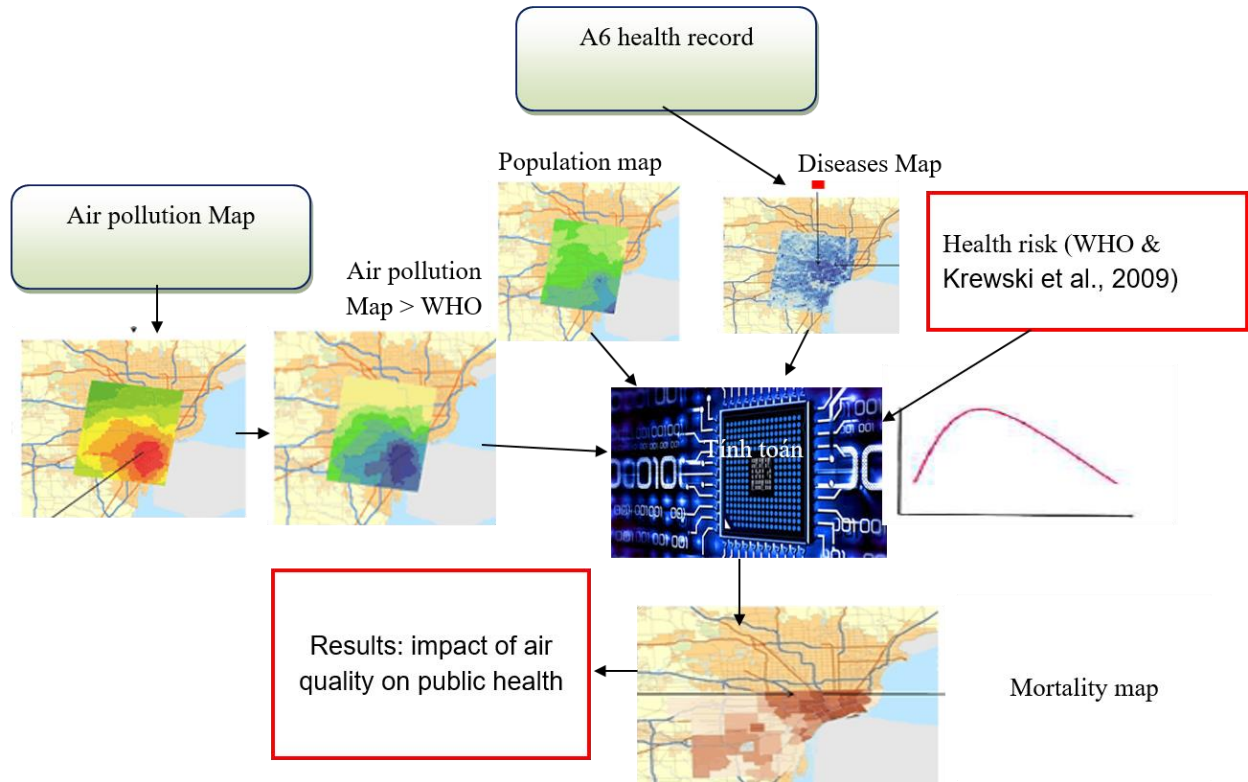


Figure 1. Methodology to studying impacts air pollution on public health

For mortality baseline incident rate in HCMC, the total number of deaths were gathered from the Ministry of Public Health in the form of the Vietnamese A6 mortality reporting system. This is a data set built from 1992 to record the death from the commune level, aggregated then and posted to the central level. Health storage system A6 in Vietnam recorded relatively full (94%) the number of deaths and correctly classified the top 3 causes of death (accounting for 66% of total deaths) which is related to the circulatory system, cancer and trauma. The mortality data for three main causes of death such as IHD, cardio-pulmonary and lung cancer.

As recorded from the A6 health system of Ho Chi Minh City, there were about 6,630 deaths per year related to cardiopulmonary disease (accounting for 30.05% of total deaths), 3,314 deaths due to IHD (accounting for 15.02% of total deaths) and 437 deaths from lung cancer (accounting for 2.00% of total deaths).

Air emission inventory

A comprehensive emission inventory in HCMC in 2019 was conducted by following the top-down and bottom-up approaches. The estimation of the emission of different types of sources including the line, point, area, and biogenic source was conducted. Traffic sources accounted for the largest emissions for almost all pollutants. Motorcycles were the dominant emission source of all pollutants for on-road sources, accounting for 35.3%, 91.4%, 65.4%, 70.4%, 99.4% and 79.9% of the total line sources emissions for NO_x, CO, SO_x, NMVOC, CH₄ and PM_{2.5}, respectively.

3. RESULTS AND DISCUSSIONS

The air quality model used in this study is the Chemical Transport Model (CTM). The model was developed by CSIRO and detailed description model by the document of The Centre for Australian Weather and Climate Research (Cope, 2009). For simulations that require complex chemical transformation, CSIRO developed an enhanced version of TAPM referred to as TAPM-CTM (Cope, 2009). The advances of TAPM-CTM compared to TAPM were analyzed thoroughly in the study of Bang, 2018 (Bang, 2019) in which the prognostic model provides the meteorological fields that drive dispersion of emissions and pollutant concentrations CTM.

The results in Figure 2 also show that the annual average concentration of NO₂ was 67.1 µg/m³, higher than QCVN 05: 2013 (40 µg/m³). In contrast, the annual levels of PM_{2.5} was 23 µg/m³, levels of SO₂ was 19.2 µg/m³ which is lower than QCVN 05: 2013 (25 µg/m³ and 50 µg/m³). The average annual concentration of PM_{2.5} in HCMC is lower than QCVN 05: 2013 (25 µg/m³). However, the PM_{2.5} levels in most areas in the city were about two times higher than WHO recommendations (10 µg/m³), with the exception of some areas in the south of the city (Can Gio District). The highest concentration was in District 4 and District where there are many ports and activities. These results were relatively similar to the PM_{2.5} pattern observed by using continuous monitoring in the period of 2011-2015.

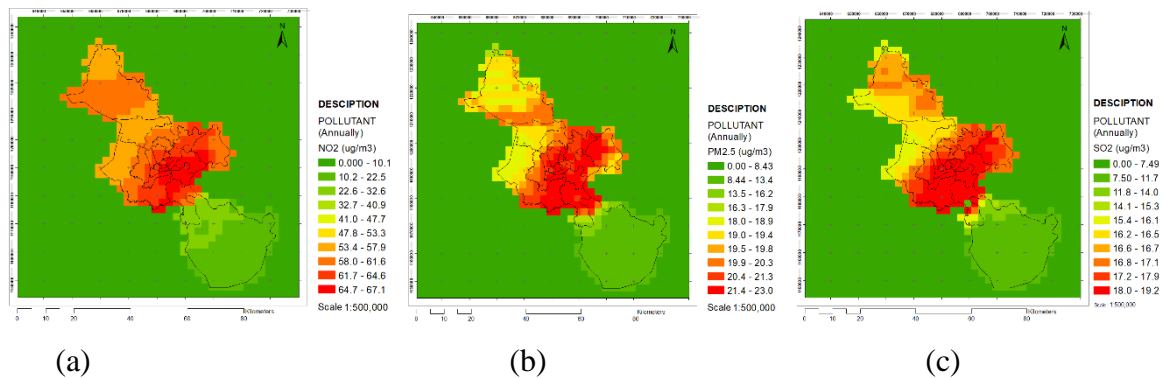


Figure 2. Air pollution dispersion map for (a) NO₂, (b) PM_{2.5}, (c) SO₂ annually in HCMC

The total mortality cases are found to be 1396 for three diseases (lung cancer, cardio-pulmonary and IHD) due to PM_{2.5}, SO₂, and NO₂ pollutant levels. PM_{2.5} has the highest impact in terms of mortality with a total of 1.136 deaths, followed by NO₂ with 172 cases and 89 cases by SO₂. The number of deaths from PM_{2.5} accounts for 81% of total mortality among 3 pollutants (PM_{2.5}, SO₂, and NO₂). The second-largest impact is NO₂ accounting for about 12.2 % and the third pollutant is SO₂ about 6.3%. This result of highest death due to PM_{2.5} is consistent with the air quality monitoring data done by the HCMC environmental monitoring center (the PM_{2.5} is usually higher than QCVN 05:2013) and consistent with the results of PM_{2.5} air quality modeling in this study (the annual average concentrations of PM_{2.5} is much higher than WHO (10 µg/m³) about 2.3 time). PM_{2.5} is responsible for the largest number of mortality from cardio-pulmonary disease with 715 cases, followed by NO₂ with 83 cases, and finally SO₂ with 43 cases.

4. CONCLUSION

This research paper has presented the preliminary study about the application of GIS technique to distribute air pollution concentration, population and public health diseases in the city application BENMAP theory model to calculate the mortality rate from three causes, namely Ischemic Heart Disease (IHD), cardiopulmonary, and lung cancer due to air pollution. Air pollution has high impacts on public health in HCMC. The total mortality cases are found to be 1396 for three diseases (lung cancer, cardio-pulmonary and IHD) due to population exposure to the combination of PM_{2.5}, SO₂, and NO₂ pollutant levels. Among these air pollutants, PM_{2.5} has the highest impact in terms of mortality with a total of 1.136 mortality, followed by NO₂ with 172 cases and 89 cases by SO₂. HCMC's government should develop measures to reduce air pollution as soon as possible to protect human health.

5. REFERENCES:

Bang, Q. HO, Vu Hoang Ngoc Khue, Nguyen Thoai Tam, Kristofer Lasko, 2017. *Air pollution emission inventory and air quality modeling for Can Tho City, Mekong Delta, Vietnam*. Air Quality, Atmosphere & Health, pp 1–13.

Ly Thi Mai Luong, Tran Ngoc Dang, Nguyen Thi Thanh Huong, Dung Phung, Long K Tran, Do Van Dung, Phong K Thai, 2019. *Particulate air pollution in Ho Chi Minh city and risk of hospital admission for acute lower respiratory infection (ALRI) among young children*. Environ Pollution Journal. doi: 10.1016/j.envpol.2019.113424. Epub 2019 Oct 18.

Krewski, D., Jerrett, M., Burnett, R. T., Ma, R., Hughes, E., Shi, Y., ... & Thun, M. J., 2009. *Extended follow-up and spatial analysis of the American Cancer Society study linking particulate air pollution and mortality (No. 140)*. Boston, MA: Health Effects Institute.

Cope, M., Lee, S., 2009. *Chemical transport model – user manual CAWCR Technical Report No. 016*.

Bang, H.Q., Hiep, N.D., Khue, V., Hien, T.T., 2018. *Photochemical smog modelling using the air pollution chemical transport model (TAPM-CTM) in Ho Chi Minh city, Vietnam*. Environmental Modeling & Assessment Springer International Publishing: 1-16.

ACKNOWLEDGEMENTS

The authors gratefully acknowledge Irish Research Council COALESCE Research Fund 2019 – IRC-COALESCE-2020-31 under the HealthyAIR project to support this research.

Public space capacity estimations during COVID-19 pandemic using geospatial analysis: A case study of Naresuan University, Thailand

Tanyaluck Chansombat¹, Pathana Rachavong¹, Maythawee Janthra² and Jiranya Duangfu²

¹**Thailand Geographical Association, Email:** pathanar@gmail.com, tanyalaks@nu.ac.th

²**Geographic Information Sciences, Naresuan University
Email:** jiranya@nu.ac.th, maythaweej63@nu.ac.th

ABSTRACT

As many provinces in Thailand have eased lockdown restrictions to combat the COVID-19 pandemic, people are returning to their daily lives. Unfortunately, because of the growing use of public spaces, this often leads to an increase in illnesses. This raises problems regarding how to avoid premature lockdowns and how to regulate spatial distance in different regions throughout the epidemic. Although the need for a COVID-19 vaccine is critical for disease control, limiting measures in areas such social distancing in public venues with limited capacity are equally vital. This study aims to use GIS analysis to implement appropriate social distancing protocols and capacity estimations of public space areas, both indoor and outdoor, in Naresuan University, which incorporate approximately 2-meters between individuals in determining how many people should be let in to access a given space allowing some space for people to move around. The study finds that GIS can greatly contribute to planning safer ways to open recreational and public space areas and to adhere for social distancing guidelines during the pandemic.

1. INTRODUCTION

The COVID-19 pandemic is riddled with unknowns, many of which have a spatial dimension that leads to a geographic and potentially mappable knowledge of the outbreak. Thus, in health science, research needs include the ability to analyze the COVID-19 phenomena using several types of variables, spatial analysis and spatiotemporal aspects, geographic influence on decision-making and everyday life, and predictive modeling of the disease's evolution. With the classification of COVID-19 as a global pandemic, the use of geospatial and statistical technologies has become even more important.

This COVID-19 theme necessitates interdisciplinary analysis, and geography is one of the few disciplines that claims to provide a synthetic approach to the interplay between biophysical and human variables (Turner, 2002), by approaching the environment from a holistic perspective and focusing on the forms and processes that coexist in a geographical space (Sauer, 1925). These are placed in a geographical, territorial, locational, and landscape context by geography. The environment-society dialectic must be understood in the perspective of geography's integrative approach (Pattison, 1964).

This study aims to use analysis to implement appropriate social distancing protocols and capacity estimations of public space areas, both indoor and outdoor, in Naresuan University, which incorporate approximately 2-meters between individuals in determining how many people should be let into access a given space allowing some space for people to move around. The study finds that GIS can greatly contribute to planning safer ways to open recreational and public space areas and to adhere for social distancing guidelines during the pandemic.

2. METHODS AND STATISTICAL ANALYSIS

2.1 Study area

Naresuan University (NU) is one of a well-recognized government universities located in Phitsanulok Province, northern Thailand. It was established on 29 July 1990, which was named after the King Naresuan the Great. The university has about 20,000 full-time students. The university has an area of 2.08 square kilometers.

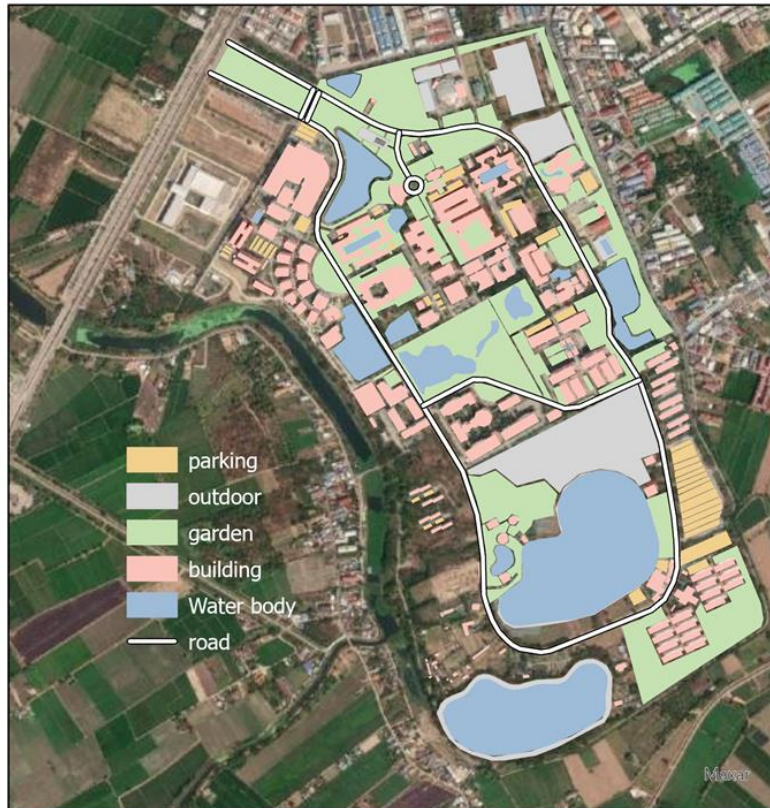


Figure 1. Naresuan university map

2.2 Data collection

Seven outdoor spaces across the university were identified based on satellite imagery and shapefile polygons were created and calculated the areas ArcGIS Pro as a tool (Figure.1).

2.3 Data analysis

Social distancing, or physical distancing, means limiting close contact with people we don't live with, both indoors and outdoors. It's one of the best tools we must prevent the spread of COVID-19, even if ones have been vaccinated.

One-meter social distancing is recommended by China, Denmark, and France; 1.5 meters by Australia, Germany, and Italy; and six feet, or 1.8 meters, by the United States. Meanwhile, the United Kingdom has announced that it will relax its policy, which has been criticized by leading scientists. When it comes to coronavirus, the truth is that we don't yet know how far is too far. The virus was identified in the air as far as four meters away from sick patients in a COVID-19 unit, according to a recent study. However, according to a research cited by the WHO, the

chance of transmission decreases dramatically with one meter or more from an infected individual and decreases even more with additional distance. In this study we adapted the 1.8 meters rule as our analysis according to US CDC. For this work, bubbles that allowed for efficient 2-meter social distance in public space were intended to be created (Figure 2.)

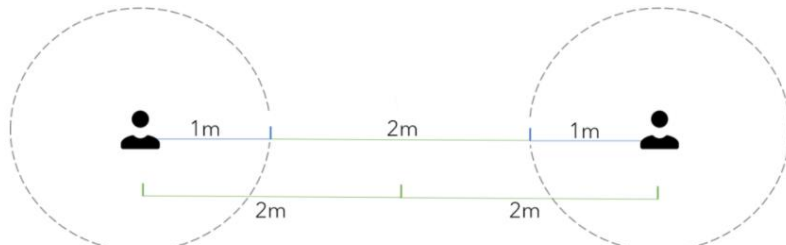


Figure 2. Diagram of efficient 2-meter social distance in public space bubbles.



Figure 3. Efficient 2-meter social distance in public space circle. (Courtesy: Shutterstock/elenabsl)

Firstly, the public spaces were selected (Figure 4a) then the Generate Tessellation tool was used to create a series of hex grids across the public space areas (Figure 4b). The area of the Generate Tessellation tool area is defined as 13.856m^2 to create a 2m distance between each bubble.

Then the Feature to Point tool was applied to identify a point feature in the center of each hexagon (Figure 4c). 1m buffer using the Buffer tool was created using point feature function (Figure 4d). This results in a series of evenly spaced circles representing a social distance, with a 2m gap between each circle (Figure 4e). Finally, buffer polygons were clipped to the selected areas and removed the hex grid (Figure 4f).

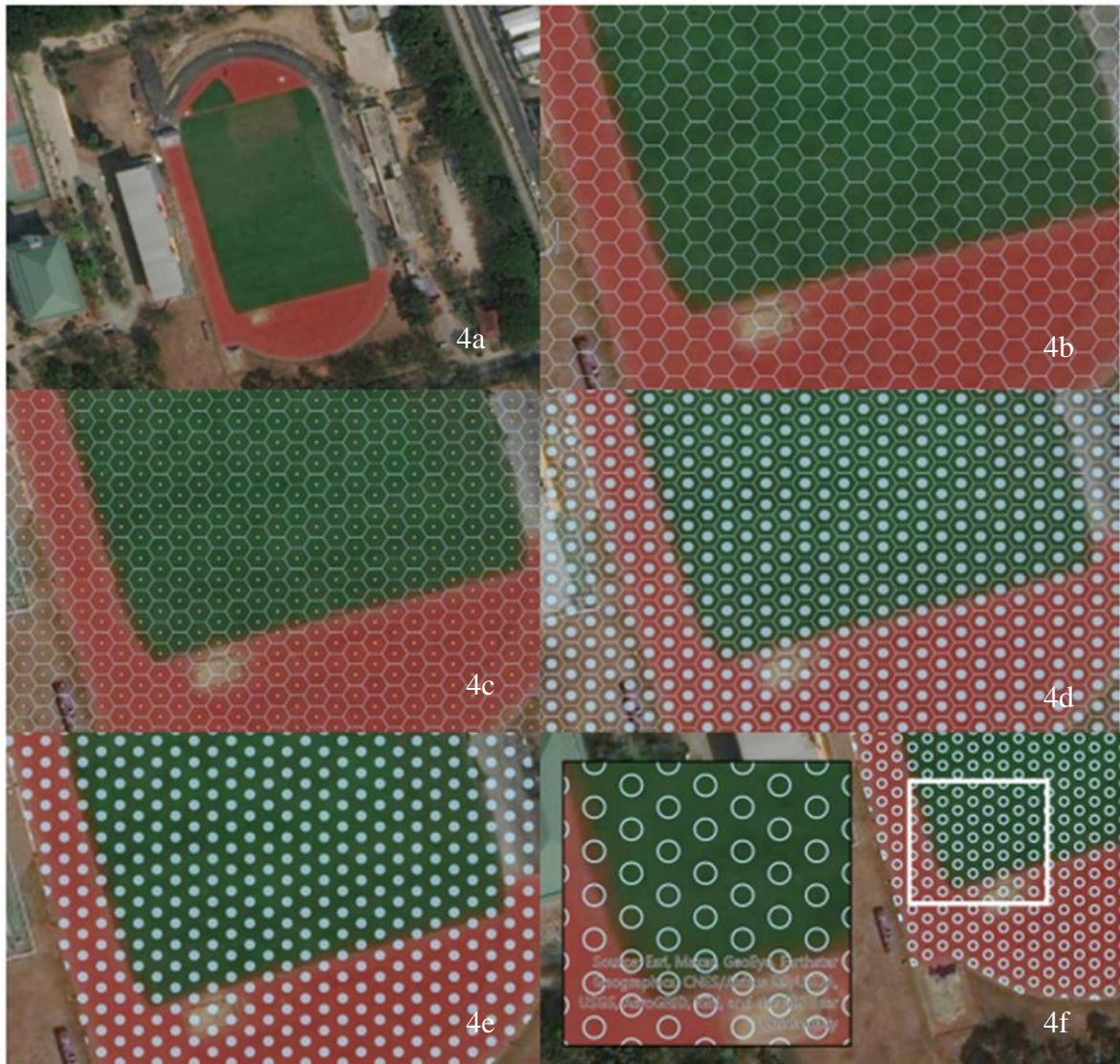


Figure 4. Steps of efficient 2-meter social distance in public space bubbles creation using GIS.

3. RESULT AND DISCUSSION

The analysis found that the BEC Football Field space has the biggest area of 16,450 m² which allows 1,170 people to use the space under the 2m distancing rule at a specific time. NU Main Stadium has the area of 14,980 m² with 1,070 people followed by NU Plaza Track, Reservoir Running Track, NU Track, King Naresuan Statue, and Outdoor Performance Space, respectively. This analysis limits the use of public space at around 22 percent of the total area during the COVID-19 pandemic.

Table.1 Place names and public space limit of each open areas in Naresuan University

ID	Place Name	Area (m2)	Public Space Limit (person)	Public Space Limit Area (m2)	Public Space Limit (%)
1.	BEC Football Field	16,450	1,170	3,580	21.8
2.	NU Main Stadium	14,980	1,070	3,260	21.8
3.	NU Plaza Track	8,970	830	1,945	21.7
4.	Reservior Running Track	7,865	730	1,720	21.9
5.	NU Track	5,080	460	1,120	22.0
6.	King Naresuan Statue	2,260	170	490	21.7
7.	Outdoor Performance Space	1,930	140	420	21.8

4. CONCLUSION

The study finds that the simple analysis of GIS can greatly contribute to planning safer ways to open recreational and public space areas and to adhere for social distancing guidelines during the pandemic. In other words, when assessing how many people should be allowed into a given space, authorities could benefit from utilizing estimates for social distance that include roughly 2-meters, or about six feet, between persons. Given the spatial dimensions and total area for public space at the institution, authorities should apply social distancing to assess the number of people they can accommodate. This would help to prevent or at the very least minimize huge gatherings from becoming possible super spreader events, which might quickly increase infection rates.

5. REFERENCES

- Bark, S.2020. Investigation into beaches in the UK and how many people could be reasonably accommodated, <https://www.geospatialpr.com/2020/07/02/esri-uk-analysis-reveals-beach-capacity-ahead-of-holiday-season/>
- Pattison, W.D. . 1964. The four traditions of geography. *J. Geogr.*, 63, pp. 211-216
- Turner, B.L.2002. Contested identities: human-environment geography and disciplinary implications in a restructuring academy, *Ann. Assoc. Am. Geogr.*, 92 (1) (2002), pp. 52-74
- Sauer, C.O.1925.The Morphology of Landscape, *University of California, Oakland, CA, USA*, pp. 19-53

DRAINAGE DENSITY AND VALLEY EROSION INDEX AT DEEP-SEATED LANDSLIDES IN THE CENTRAL KII MOUNTAINS, SOUTHWEST JAPAN

Muneki Mitamura¹ and Kazuma Kasahara¹

¹Geosciences, Osaka City University
3-3-138 Sugimoto, Sumiyoshi, Osaka 558-8585, Japan
Email: mitamura@osaka-cu.ac.jp

ABSTRACT

The central part of the Kii Peninsula is a mountainous area composed of Cretaceous accretionary prisms with undulations of about 1000 m. Many mountain slopes have gravitational rock creep. The heavy rains of the Typhoon Talas (2011) caused many deep-seated landslides. Most of the landslide slopes are dip slopes facing northwest. This typhoon moved slowly, causing continuous rainfall of 20-40 mm/hour, with total rainfall of over 800 mm for five days in this area. It is clear that rainwater infiltration has led to destabilization of mountain slopes, and it is important to evaluate the hydraulic properties of mountain slopes. Therefore, using 5 m DEM data measured before 2011, we evaluated the drainage density and valley undulations, which are indicators related to rainwater infiltration on rock creep slopes.

The drainage density was calculated by dividing the valley length by the dimensions of the tributary catchment extracted on QGIS using 5 m DEM. Two-dimensional wavelet analysis using a Mexican Hat filter was performed to evaluate the degree of valley erosion. Since the convolution integration is performed for a 5 m DEM with a filter size of 9×9 , the undulations of the representative wavelength of 20 m of the terrain are evaluated.

As a result of examining the target area of 10 km square, the drainage density is relatively low on the northwestern slope, which is a dip slope, and among them, the landslide traced areas tends to be low. Valleys with a negative wavelet coefficient close to zero using the Mexican Hat filter have a small degree of erosion, and are evaluated as shallow. Comparing the wavelet coefficient distributions of the entire area and the landslide area, it was found that the proportion of shallow valleys with a coefficient of less than 0 to -5 or more is predominant in the landslide area. The small drainage density and the predominance of shallow valleys in the landslide area suggest that no significant surface water is produced in those drainage areas. Opposite slopes tend to have high valley densities, and many surface collapses are observed, but few lead to deep-seated landslides. Therefore, it was clarified by DEM analysis that bedrocks in the dip slope is loosened by rock creep and is prone to rainwater infiltration. It can be seen that such slopes tend to lead to deep-seated landslides.

1. INTRODUCTION

Typhoon Talas (2011) passed through the west Japan from 30th August to 4th September 2011 (Japan Meteorological Agency, 2013). This typhoon led to the heavy rain record that the total precipitation for 5 days in the southeastern part of the Kii Peninsula more than 1000 mm. The maximum record was 1652 mm for 72 hours and total precipitation of 1814 mm at Kami-kitayama Village, Nara. This total precipitation for 5 days is roughly equivalent to the annual rainfall average of Japan and 60% of the annual rainfall in this area.

Deep-seated landslides more than 10,000 m² in area have been confirmed 54 locations by Nara Prefecture (Figure 1). 13 sites of these large scale landslides induced natural damming of river channels with debris deposits (Kinki Regional Development Bureau, Ministry of Land, Infrastructure and Transport, 2013). These landslides mostly occurred in dip slopes consisting of the Cretaceous accretionary complex of the Shimanto Group (Kishu

Shimanto Research Group, 2012).

It is clear that rainwater infiltration has led to destabilization of mountain slopes, and it is important to evaluate the hydraulic properties of mountain slopes. Therefore, using 5 m DEM data measured before 2011, we evaluated the drainage density and valley undulations, which are indicators related to rainwater infiltration on rock creep slopes.

2. GEOLOGICAL SETTING

The 10 km square research area is located in the central part of the Kii Mountains, where the main stream and tributaries of the Totsukawa River flow, forming a canyon with undulations over 500m.

Deep-seated landslides mainly occurred in the Cretaceous accretionary complex of Shimanto Group (Kishu Shimanto Research Group, 2012). Oceanic and terrigenous facies are alternated in each tectonostratigraphic unit consisting of several thrust sheets. The oceanic facies intercalated in the lower part of thrust sheet is well sheared, and formed the tectonic mélange. The shear deformation is stronger in the older complex units located in northern part of the Shimanto Group terrain. The basal shear plane of large scale landslide is mainly formed in the lower part of the thrust sheet consisting of muddy tectonic mélange zone. Because thrust sheets generally incline toward north or northwest in this area, north or north western slopes are in the dip slope situation. Almost deep-seated landslides are occurred in dip slope areas (Figure 2).

3. DEM DATA AND ANALYTICAL METHODS

The DEM dataset which was provided by the Kinki Regional Development Bureau, is 5 meter intervals ground elevation data which records the pre-disaster terrain by airborne LiDAR in 2010. The former topography of the deep-seated landslide in 2011 can be evaluated with this data set. We selected and analyzed a data set of about 10 km square in a mountainous area where major collapses occurred frequently (Figures 1, 2). National Research Institute for Earth Science and Disaster Prevention, Japan (NIED, 2005) published the digital archive for landslide distribution maps. NIED detected topographical traces formed by landslide movement with 1970s aerial photographs on an approximate 1:40,000 scale.

The analysis work was done using QGIS. The valley lines were extracted by the method using the Median Filter of Iwashashi (1994). The tributary catchment area was extracted using “r.watershed” tool, which is one of the GRASS raster tools under 500 meshes of minimum size of exterior watershed basin. The drainage density was calculated by dividing the valley length by the dimensions of each tributary catchment area. Valley reliefs were carried out using a 2D wavelet analysis with a 9×9 Mexican Hat digital filter (Booth *et al.*, 2009; Fujisawa and Kasai, 2009). Since a 5 m DEM set is used, evaluation will be

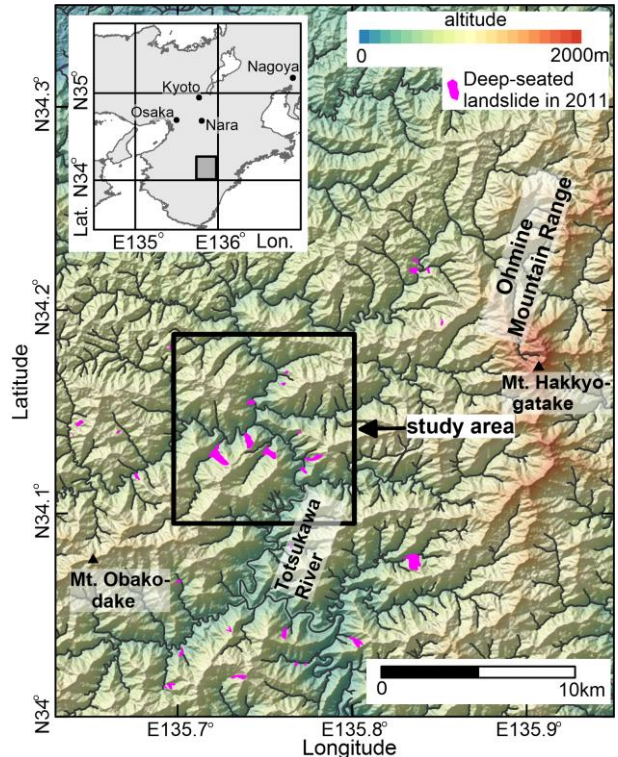


Figure 1. Location map of study area

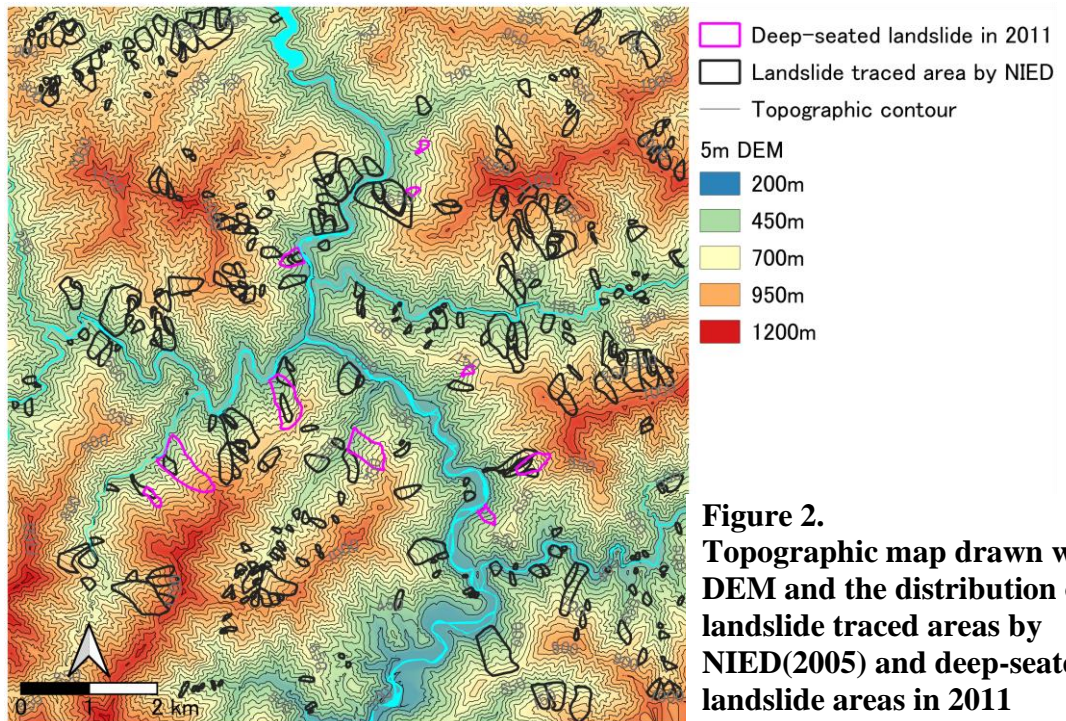


Figure 2.
Topographic map drawn with 5m DEM and the distribution of landslide traced areas by NIED(2005) and deep-seated landslide areas in 2011

performed for reliefs of representative wavelength 20 m. The results of the 2D wavelet analysis were statistically evaluated in tributary catchment areas and landslide areas.

4. RESULTS

4.1 Drainage density

Detected tributary catchment areas are 3570 plots, and the range of those dimensions are from 2 to 8 ha. The drainage density shows a distribution with an average of 26.2 km^{-1} and a standard deviation of 7.6 km^{-1} . Figure 3 shows the distribution of valley densities in different colors. Most of the major ridge lines which are shown by hatched lines in Figure 3, extend NE-SW direction. It can be seen that the drainage density of the tributary catchment area on the northwestern slope of the main ridge line is smaller than that on the southeastern slope. There are many landslide traces on the NIED landslide map on the northwestern slope, and deep-seated landslides have also occurred. Valley densities are rated low in most of these areas.

4.2 Valley Relief

Figure 4 shows the distribution of wavelet coefficients evaluated by the Mexican Hat digital filter. The distribution of wavelet coefficients indicates that the ridges with large positive values and valleys with significant negative values are repeated on the southeast side slopes of the main ridge line, and those slopes are rich in undulations. On the other hand, the northern or western slopes of the major ridge lines have low undulations and valleys in those areas are poorly developed.

5. DISCUSSION

5.1 Valley Erosion Index

The distribution of wavelet coefficients indicates poor valley development on the

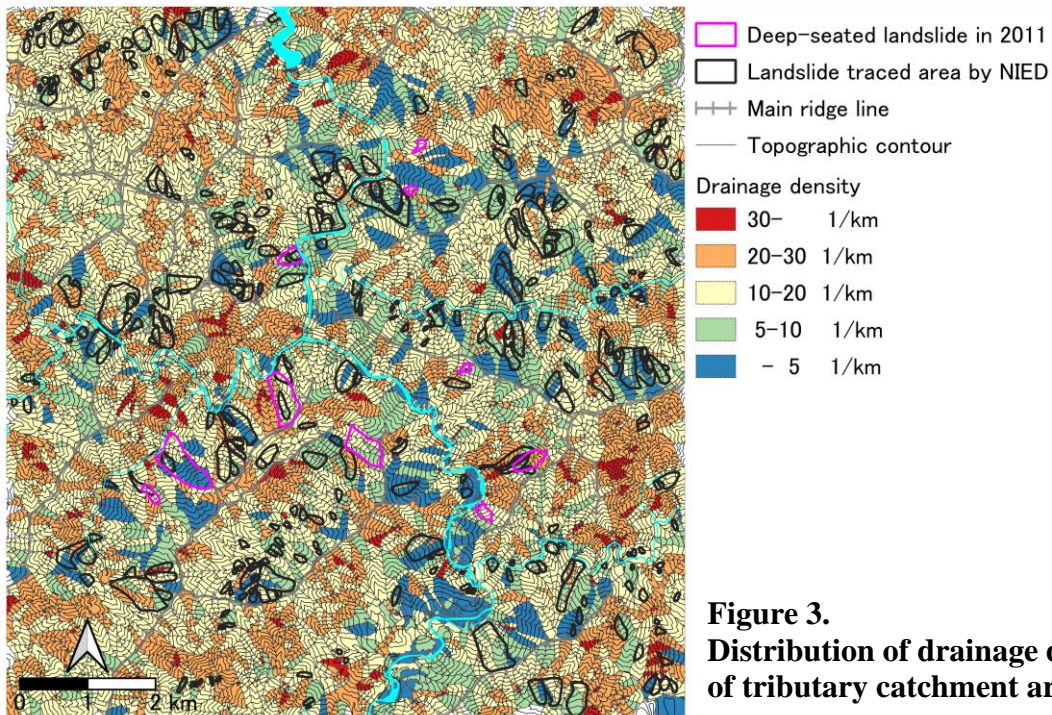


Figure 3.
Distribution of drainage density of tributary catchment area

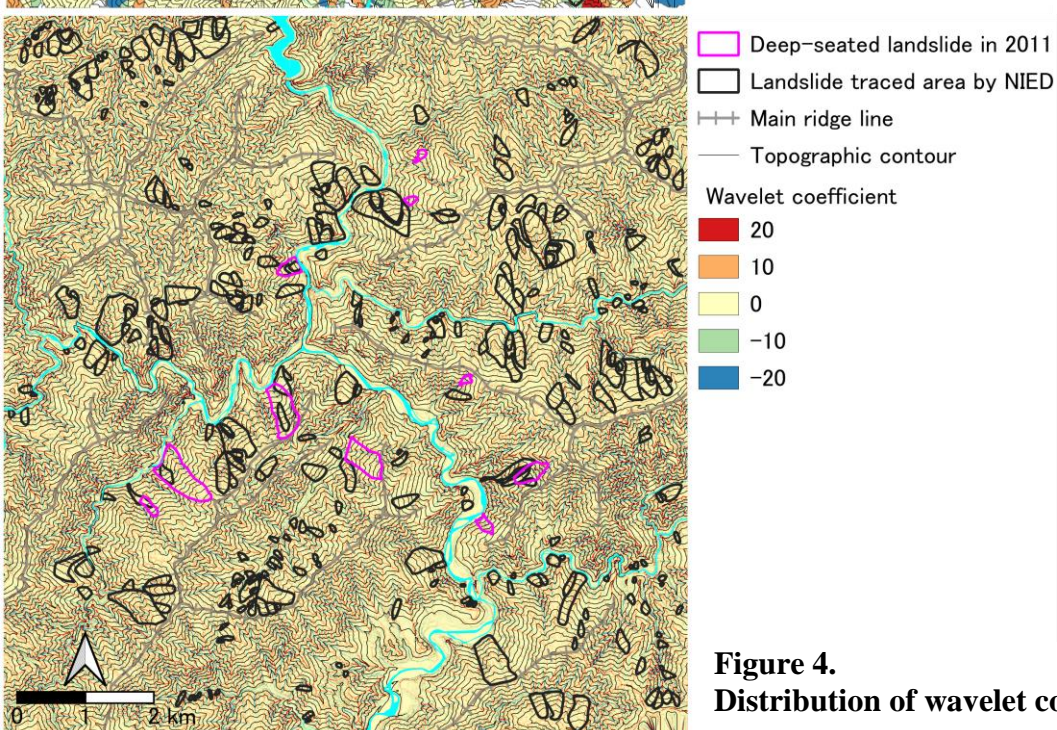


Figure 4.
Distribution of wavelet coefficient

northwest side of the main ridge line. We compared the distribution statistics of wavelet coefficients along the valley line in the entire survey area and the landslide area. Figure 5 shows the distribution of wavelet coefficients in each area. There is a difference in the distribution between the wavelet coefficients value range of -5 to less than 0 and the range of -20 to -10. In landslide areas, the proportions in the wavelet coefficients value range of -5 to less than 0 are predominant. While, in the range of -20 to -10, the distribution ratio of landslide traced area is relatively low. The former topography of deep-seated landslide areas has a similar tendency.

Therefore, the ratio of the range of -20 to -10 to the range of -5 to less than 0 was evaluated as the valley erosion index in each landslide traced area. A small value of the

valley erosion index indicates that the valley development is poor. Almost valley erosion indexes in landslide traced areas and the former topography of deep-seated landslide areas are less than 1 (Figure 6).

5.2 Rock Sliding and Valley Development

The northeast-southwest direction of the main ridge lines corresponds to the strike direction of the main geological structure in this area. Since the main inclination direction of the Shimanto accretionary prism in this area is north or northwest, the northwestern region to the main ridge line is in a dip slope. As shown in Figure 2, it is clear that the drainage density of the tributary catchment area in this region tends to be small. The low drainage density region suggests the situation of significant infiltration of rain water (Horton, 1945). Dip slopes are prone to rock sliding from deeper positions, destabilizing the slopes. Instability of the slope leads to the formation of cracks in the bedrock and promotes rainwater infiltration. As a result, those situations are reflected in the topographical characteristics of small drainage density. The small valley erosion index also shows poor valley development, suggesting a situation where surface water erosion of the valley is small. Almost these indexes at landslide traced areas and former topography of deep-seated landslide areas are small. Therefore, the small drainage density and the small valley erosion index in this area can be one of effective indicators of the destabilizing area.

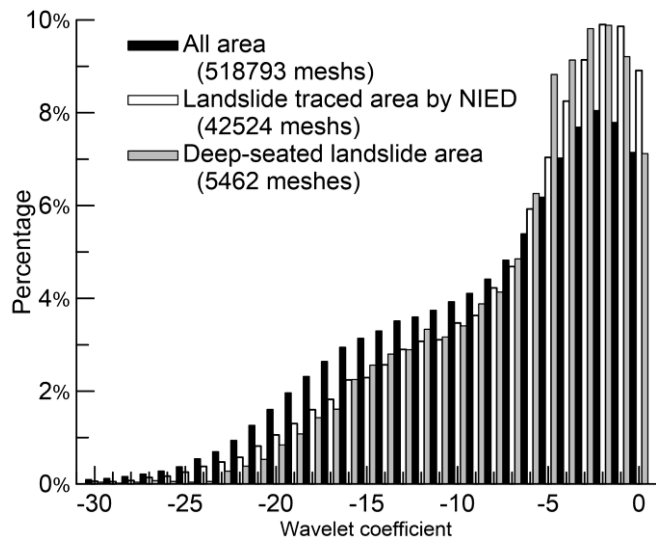


Figure 5.
Comparison of wavelet coefficient histograms among all areas and landslide areas

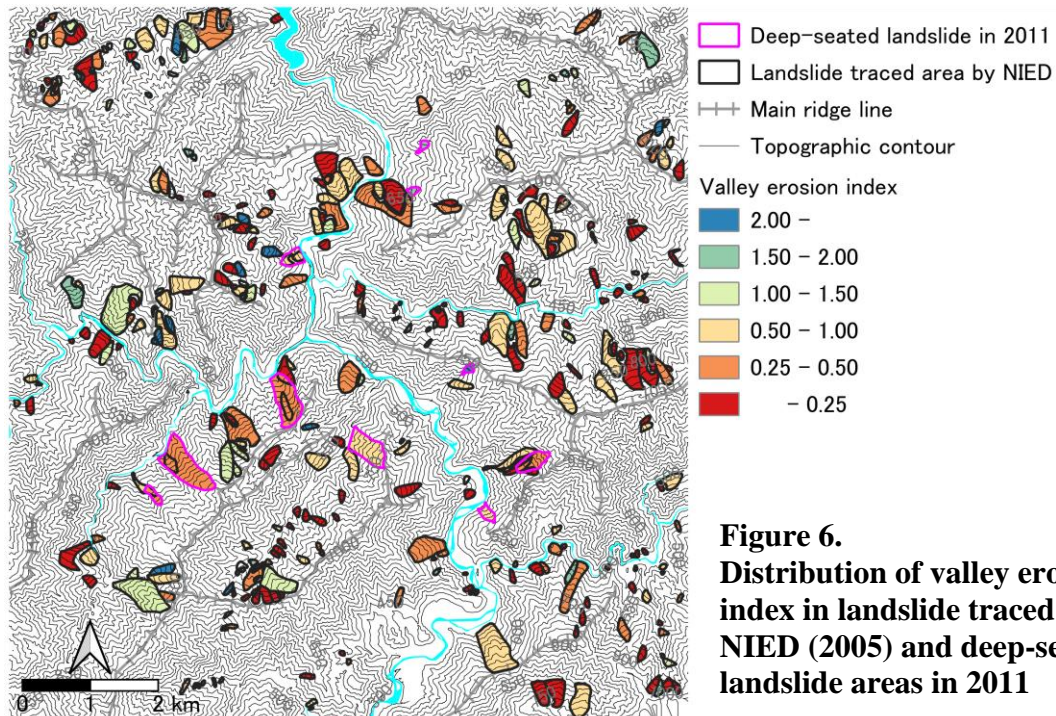


Figure 6.
Distribution of valley erosion index in landslide traced areas by NIED (2005) and deep-seated landslide areas in 2011

5. CONCLUSION

Using 5m DEM data before the occurrence of a large-scale heavy rain disaster, we evaluated the drainage density related to rainwater infiltration in the landslide traced area and the occurrence area of deep seated landslide area mountain slopes composed of Cretaceous accretionary prisms. The drainage density in the dip slope area was relatively low, and the evaluation was also low in the landslide area. The newly devised valley erosion index, which is the distribution ratio on wavelet coefficients of -20 to -10 to the range of -5 to less than 0, also shows a tendency similar to drainage density.

DEM analysis clarified that bedrocks in the dip slope is loosened by rock creep and is prone to rainwater infiltration. It can be seen that such slopes tend to lead to deep-seated landslides. Therefore, the small drainage density and the small valley erosion index in this area can be one of effective indicators of the destabilizing area.

6. ACKNOWLEDGMENT

We thank the Ministry of Land, Infrastructure, Transport and Tourism Kinki Regional Development Bureau for the providing 5m DEM data of the survey area. And we also thank Dr. Tamotsu Matsui and other related members at the Calamity Science Institute for their valuable discussions.

7. REFERENCES

- Booth, A.M., Roering, J.J., Perron, J.T., 2009. Automated landslide mapping using spectral analysis and high-resolution topographic data: Puget Sound lowlands, Washington, and Portland Hills, Oregon. *Geomorphology*, 109, 132-147.
- Fujisawa, K. and Kasai, Y., 2009. Data Analysis Manual of on Aeronautical Laser Surveying in Landslide Area. *Technical Note of PWRI*, Public Works Research Institute, Tsukuba, JAPAN, No. 4150, 43p.
- Horton, R.E., 1945. Erosional development of streams and their drainage basins: hydrophysical approach to quantitative morphology. *Geological Society of America Bulletin*, 56, 275-370.
- Iwashashi, J., 1994. Development of landform classification using digital elevation model. *Annals of Disaster Prevention Research Institute of Kyoto University*, 37, B-1,141-156.
- Japan Meteorological Agency, 2013. Typhoon Talas relevant information -Portal-.
https://www.jma.go.jp/jma/en/typhoon_Talas.html.
- Kinki Regional Development Bureau, Ministry of Land, Infrastructure and Transport, 2013. *Memoir of Disaster Correspondence on 2011 Typhoon Disaster in Kii Peninsula*. Ministry of Land, Infrastructure and Transport, 200p.
- Kishu Shimanto Research Group, 2012. *New Perspective on the study of the Cretaceous to Neogene Shimanto Accretionary Prism in the Kii Peninsula, Southwest Japan*. The Association for the Geological Collaboration in Japan, Monograph 59, 295p.
- NIED, 2005, *Landslide Maps* (1:50000 scale), Vol. 23, Wakayama and Tanabe, 27maps, - Portal-. https://dil-opac.bosai.go.jp/publication/nied_tech_note/landslidemap/pdf-23.html.

Assessing the Landslide susceptibility in Samdrupjongkhar Dzongkhag using Machine Learning Models

Vasker Sharma*, Thongley, Phurba Tamang, Dechen Wangmo, Lobzang Dorji, Jigme Tenzin.

Department of Civil Engineering and Surveying, Jigme Namgyel Engineering College, Dewathang,
Samdrupjongkhar, Royal University of Bhutan.

vaskersharma.jnec@rub.edu.bt *, thongley.jnec@rub.edu.bt, phurbatamang.jnec@rub.edu.bt,
dechenwangmo.jnec@rub.edu.bt, lobzangdori.jnec@rub.edu.bt, jigmetenzin.jnec@rub.edu.bt

ABSTRACT

Natural hazards that are associated with landslides are predominant in a hilly and mountainous area owing to several causative factors that trigger the landslides in a region. In this study, Machine Learning Models such as Artificial Neural Network (ANN) and Logistic Regression (LR) and conventional methods like Weight of Evidence (WoE) were used to develop the Landslide susceptibility maps (LSM) for Samdrupjongkhar Dzongkhag in Bhutan, which could be used for land management in strategic areas. The causative factor was kept the same for all the methods. The landslide inventory was developed based on field observation in conjunction with Remote sensing data. The landslide data were divided into training and testing data with 70% for training the model and 30% for testing. The AUC success rate for the LSM was 64%, 93%, and 89% for WoE, ANN, and LR respectively. Similarly, the AUC prediction rate was 58%, 88%, 89%, for WoE, ANN, and LR respectively. From the validation, it was found that the LR method followed by ANN is better than WoE in predicting the landslide occurrence zones. From the study, it emerged out that, slopes facing South-East to South-West were more prone to landslide failures. This is mainly attributed to the monsoon which brings rain from the south and mostly precipitates on the south-facing slopes making it more vulnerable to landslides. Also slope value per se tends to influence the landslides predominantly. This perhaps offers preliminary ways to identify the landslide zones in spatially large areas where geotechnical studies become strenuous and costly.

Keywords: Landslides, Susceptibility mapping, ANN, Logistic regression, WoE.

1. INTRODUCTION

The regions in the Himalayan area are ever more faced with natural hazards due to flooding and landslides which are mostly associated with an increased amount of rainfall. While flooding has been mostly associated with extreme rainfall events, landslides are attributed to a multitude of other causative factors besides rainfall events. Landslide-related risks have been rampant especially along the highways in the hill and mountains impacting the environment, infrastructures such as roads and bridges, and livelihood owing to intense and erratic rainfall patterns which are most likely induced by climate change and other anthropogenic activities. Further, as per climate projection (IPCC, 2014), South Asia is expected to receive a higher amount of rainfall leaving the region in a vulnerable state. However, rainfall alone is not the leading cause of landslides in these regions. The immediate factor after rainfall is the disturbances caused by construction per se along the highways which causes the slope instability. These constructions include new road construction, road widening works, and routine maintenance which makes the slope more susceptible to increased infiltration due to the removal of vegetation along the road corridor. The slope of the area per se can be a good indicator of the landslide susceptibility in the hilly region however the slopes with a firm rock material are less likely to fail than the loose soil with the same slope. Further, distance to stream and erosive power of the stream aggravate the problem. The geological structure of the Himalayas is such that there are several roughly east-west trending major thrust and faults with several weak and crushed zones. Such areas are susceptible to numerous landslides along with these linear structures. Further, the orientation of folds and bedding, foliation, and joints in the rocks also play a vital role in landslide events (Upreti & Dhital, 1996). Therefore, it necessitates identifying the causative factors and their contribution in

triggering the landslides in the region. The southern foothill of Bhutan receives the highest rainfall than any part of the country and these regions report the highest number of landslides and roadblocks. The expenditure incurred by the Royal Government of Bhutan (RGoB) is enormous for the maintenance of roads due to landslides (Wangchuk, 2019; Nima, 2020; Wangdi, 2015).

Although several researchers (El Jazouli et al., 2020; Prakasam et al., 2020; Pasierb et al., 2019; Mondal, 2016), assessed the landslides from a geological, geotechnical, and geophysical standpoint, it can be very costly owing to the use of sophisticated equipment in analyzing the geology of the affected areas. The cost is further escalated when such assessment is carried out on large spatial areas. Therefore, simplistic morphological, and environmental factors can be considered to assess the landslides on a large spatial scale using GIS employing different mapping methods. Numerous studies (Thongley & Vansarochana, 2021; Arzu et al., 2010; Erenler et al., 2012; Kavzoglu et al., 2014; Feizizadeh & Blaschke, 2013; Yilmaz, 2010) have studied the landslide considering myriads of factors in producing Landslide Susceptible Maps (LSM) where such maps were produced using different mapping methods such as Index of Entropy (IoE), Weight of Evidence (WoE), Frequency Ratio (FR), Analytical Hierarchical Process (AHP), Logistic Regression (LR), Support Vector Machine (SVM), Artificial Neural Networks (ANN).

Therefore, there is a need for landslide hazard zonation for the identification of potential landslide areas via remote sensing and GIS techniques. Thus, effective management and mitigation measures could be reciprocated and referred to these potential landslide areas. In this study, we aim to prepare the landslide inventory using field surveying, GIS, and remote sensing techniques and identify the most prominent causative factors triggering the landslide in the region. The study will also prepare a prediction map using the weight of evidence, artificial neural network, and logistic regression. The study can also put forward site-specific mitigation measures to prevent landslides and road subsidence.

1.1 STUDY AREA

The Kingdom of Bhutan is situated on the southern slopes of the Eastern Himalayas and being a part of the young fold-thrust Himalayan Mountain belt, more than 90 percent of the country's area is topographically rugged and geologically very fragile. Monsoonal winds are most intense between June to September, making Bhutan the wettest country within the Himalayan range (Sharma & Adhikari, 2020). Rainfall-induced slope failure is the most common geo-environment hazard in the country. Samdrupjongkhar Dzongkhag, known for its industrial and commercial trade routes in the country, connects the rest of the eastern part of the country to the neighboring country, India.

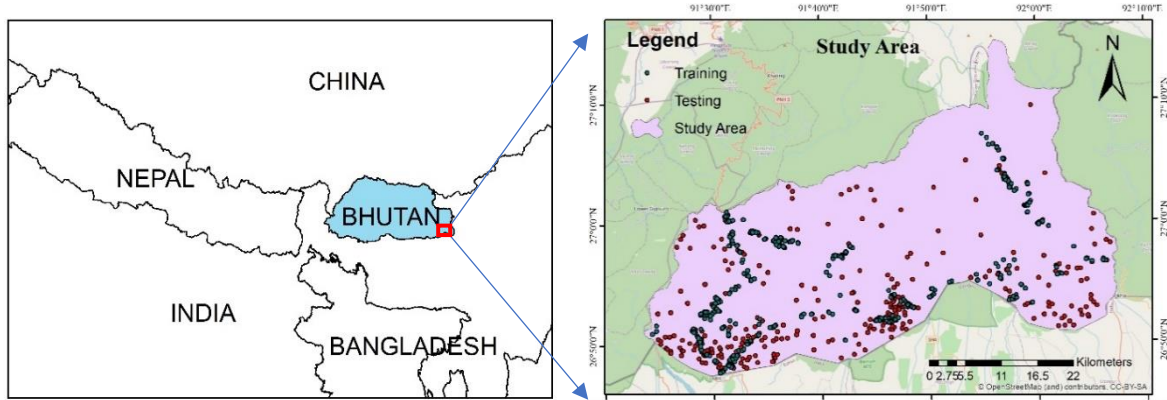


Figure 1 Study Area

2. DATA AND METHODS

The remotely sensed data such as Digital Elevation Model (DEM) and Landsat data (2020) has been obtained from www.usgs.gov.bt. Further locally available data like land use data and geological maps were also obtained for the analysis. Using DEM, various causative factors such as elevation, aspect, and slope were generated in the form of a raster layer. Further different raster like geological map, distance to road, distance to stream, FAO soil, and rainfall were also generated. Finally, Normalized Differential Vegetation Index (NDVI) was generated from Landsat data. A total of nine factors were considered in this study. However, the aspect data were further segregated into eight parts considering different aspect angles. Therefore, for the ANN and logistic regression model, a total of sixteen factors were considered. The factors are well represented in Fig. 2.

2.1 Data Preparation

The landslides inventory for training and testing were digitized using GIS from Google Earth which were further confirmed by field surveying. A total of 1675 points were digitized of which 1172 (70%) points were used for training the model while 503 (30%) points were used for testing the model. Within the training data, there are 812 landslide points while there are 274 landslides points in testing data.

The data from the raster layers mentioned above were extracted based on the location of training and testing data. The extracted data were then normalized using min-max normalization given by equation 1. The training and testing data was used in ANN and logistic regression model.

$$y = \frac{x - \min(x)}{\max(x) - \min(x)} \quad (1)$$

Where y is the normalized data, x is the original extracted data.

2.2 Weight of Evidence (WoE) Method

The Weight of Evidence (WoE) is a data-driven quantitative statistical method (Bonham-Carter et al., 1988). Initially, the weight of evidence is developed for the mineral potential study. However, several authors have applied for the prediction of landslides, floods, and groundwater potential (Dahal et al., 2008). For landslide susceptibility assessment, the landslide probability is determined using the weight of the factors (evidence). In this method, a series of mathematical calculations are required and the detail of mathematical procedures are explained by (Van Westen, 2002). Two types of data required for the WoE were landslide inventory and landslide factors (Roy et al., 2019). The weight describes the probability of landslide occurrence in the case of the presence as well as the absence of the evidence (Kayastha et al., 2012). In this method, the positive and negative weights (W^+ and W^-) are assigned to each pixel of the factor classes and calculated using Equation 2 and Equation 3. W^+ expresses the chances of occurrence of a landslide in the case of the evidence being present and its magnitude indicates the positive association between landslide event and the factor class (Neuhäuser et al., 2012). On the other hand, W^- describes the chances of landslide in case of absence of the evidence and its magnitude indicates a negative association between the landslide event and the factor class (Neuhäuser et al., 2012).

$$W^+ = \log_e \frac{P\{B | S\}}{P\{B | \bar{S}\}} \quad (2)$$

$$W^- = \log_e \frac{P\{\bar{B} | S\}}{P\{\bar{B} | \bar{S}\}} \quad (3)$$

Where P is the probability, B is the presence of potential landslide factor, while \bar{B} is the absence of a potential landslide factor. S is the presence of landslide and \bar{S} is the absence of landslide.

The difference between W^+ and W^- is known as weight contrast C , which indicates the spatial association between classes of the factor and landslides events. The $C > 0$, if the spatial association is positive while $C < 0$, if the spatial association is negative and $C = 0$ if the spatial association is lacking (Carranza, 2004).

$$C = W^+ - W^- \quad (4)$$

Where C is the weight contrast of W^+ and W^- .

To develop LSM, all the classes of the factors are reclassified using the contrast value (C). Then, add all the reclassified factors. Equation 5 is used for the development of the LSM.

$$LSM_{WOE} = \sum_{i=1}^n C_{ij} \quad (5)$$

Where LSM is a landslide susceptibility map, and C_{ij} is the contrast for class i of conditioning factor j , n is the number of factors.

2.3. Artificial Neural Network (ANN)

ANN model was developed using the R-programme, where a backpropagation algorithm was employed to adjust the weight and bias. The stopping criteria for the model was set by the error threshold of 0.01 and logistic function was used as an activation function in the model. The learning rate for the model was set at 0.0001.

Mathematically, the neural network is expressed as:

$$y = f \sum_{i=1}^N w_i \times x_i + b \quad (6)$$

Where y is the output vector and x_i is the input vector in the neural network, N is the number of neurons, w_i is the connection weight between input and output, f is the activation function, and b is the bias term.

Weights and bias are adjusted using the ANN's back-propagation algorithm, where the objective function (also known as loss function) is the error between the network's output and the observed output. The error is minimized using the optimization algorithm known as "Gradient descent" which minimizes the error value by taking steps from an initial guess until it reaches the best value. This makes Gradient descent useful when it is not possible to solve where the derivative of the objective function is equal to zero. The step size is usually calculated by providing the learning rate and is expressed as follows:

$$\text{step size} = \text{slope of objective function} \times \text{learningrate} \quad (7)$$

2.4 Logistic Regression (LR)

Logistic regression is employed when the response variable is a categorical variable involving 0/1. It models non-normal distribution and used the logit link function given by (4)

$$\log\left(\frac{y}{1-y}\right) = \beta_0 + \beta_1 \cdot x_1 + \dots + \beta_n \cdot x_n + \varepsilon \quad (8)$$

Where y is the probability of occurrence of landslide event while $(y/1-y)$ is the odds ratio and $\log(y/1-y)$ is the log odds ratio. β_0 is the intercept and $\beta_1, \beta_2, \dots, \beta_n$ are coefficients that measure the contribution of each independent variable (x_1, x_2, \dots, x_n) which are landslide

influencing factors and ε is the error.

3. RESULTS AND DISCUSSION

The landslide susceptibility maps have been produced using the methods described above and are shown in Fig 2.

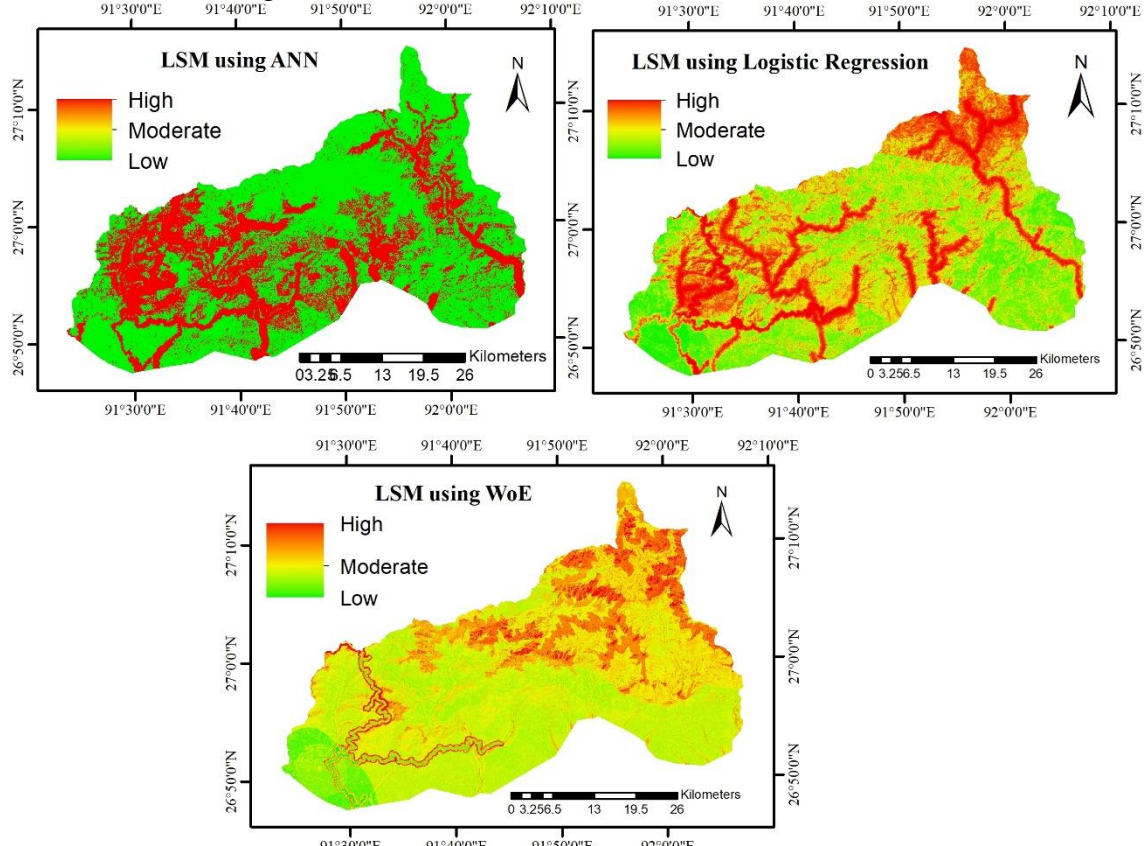


Figure 2 Landslide Susceptibility Maps

Although the model like ANN and LR yields better predictivity (Fig 3) of the landslide zones, a few clarifications are indispensable considering the overall interpretation of the weights generated by the model. From the model weights it is found that slope and aspect with south, southeast, and southwest have been the most influencing factor causing landslides in the region. It is because the majority of the monsoon rainfall falls on the slopes facing south which always remain in the grip of landslides. However, the factor like rain perse has relatively low weight for all the models indicating their low influence on the landslides. But it is an obvious fact that the intensity of rainfall invariably causes landslides and such ambiguity in the model weights is mainly due to the non-availability of adequate rainfall stations in the region. In this study only two rainfall stations were available and the rainfall intensity from these two stations has been interpolated over the whole region where actual rainfall in the region is either over or under-represented. This explains the non-influence of the rain on landslides in this study. It is also observed that the majority of the factors in the study do not tend to influence the landslides in the region.

From the Receiver Operating Characteristics (ROC) curve (Fig 4), it is observed that the success rate for ANN and LR is 93% and 89.48% respectively while for WOE is 64.15%. Similarly, the prediction rate for ANN and LR is 87.92% and 89.88% respectively while for WOE is only 58.10%. ANN and Logistic regression prove to be the better predictability models for assessing the landslide susceptibility zones. However, models like ANN takes an enormous

amount of computation time to train and test the model and therefore LR can be a preferred method to preliminary assess the landslide zones given the instant computation time. Although predictability from the WOE method is strikingly low in this study, generally they have a better edge in explaining the influence of subfactors on the landslides which ANN and Logistic regression cannot.

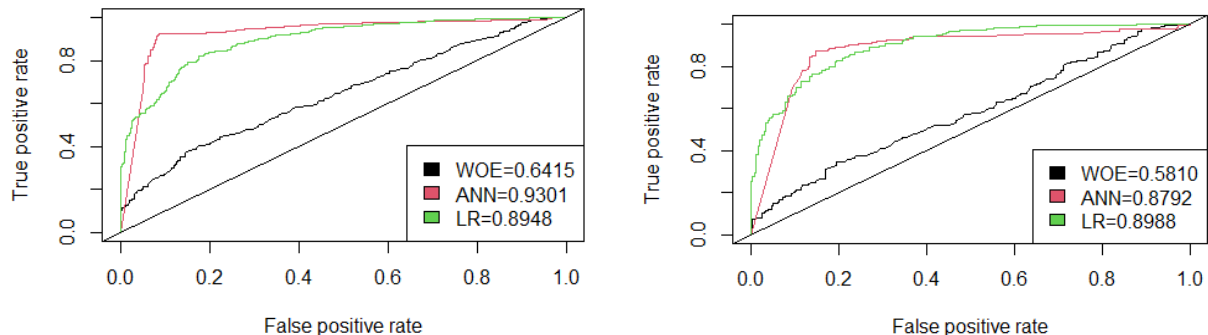


Figure 3 ROC-AUC curve (a) Success rate (b) prediction rate

4. CONCLUSION AND RECOMMENDATIONS

Natural hazards in the form of landslides are a common sight in the hilly and mountainous areas especially during the event of extreme rainfall and occasional earthquakes. Such hazards necessitate identifying the most prominent causative factor responsible for landslides in the region. Although various geotechnical and geophysical investigations can identify the causative factors, such investigation is enormous and costly especially if the investigation is carried out at a large spatial scale. Therefore, simple spatial analysis using Machine learning and other conventional techniques is a viable option in identifying the causative factors at a large spatial scale. Here in this study, ANN, LR, and WoE have been used to identify the causative factors causing the landslides in the region. From the models, it was observed that ANN and logistic regression yielded better predictability, while the WOE has low predictability. The prediction rate for ANN and Logistic regression is 87.9% and 89.88%, while for WOE the prediction rate is only 58%. Although ANN has a better predictability rate, it takes an enormous amount of computation time and therefore LR can be a preferred method for assessing the landslide susceptibility zones. From the model weights, it also emerged that slope and Aspect (South, Southwest, and South East) are the most influencing factors for the landslides in the region. Although rain is widely known as the cause of the landslide, the model weights did not justify the cause which was mainly attributed to the unavailability of an adequate rainfall station in the region. Nevertheless, from the visual observation in the region rainfall has been the major factor influencing the landslides in the region.

Further, the hills and mountains formed in the region are geologically young and weak, therefore the soils and slopes in these regions are fractured and weathered making them prone to slope failures(DGM, 2016). From the field, it was also observed that the soil along the highway and in the localized region was sandy-granular. This perhaps has a great influence on the stability of the slopes in the region as the rainwater infiltrating into such soil renders them unstable as they are not able to withstand the pore pressure. Furthermore, the landslide is more prominent in anthropologically active areas where road construction and widening are predominant. To reduce the landslide impact, detailed geo-technical investigations are deemed necessary on strategic location whereby site-specific mitigation measures could be employed. The mitigation measures range from constructing bio-engineering slopes and facilitating drainage especially along the highways where there is a higher chance of landslide failures. It

is also believed that the non-frame method is an innovative slope stabilization technique and a disaster prevention technology widely adopted in Japan (Pokhrel, 2015) which could be reciprocated in Bhutan as well.

5. REFERENCES

- Bonham-Carter, G., Agterberg, F., & Wright, D., 1988. Integration of geological datasets for gold exploration in Nova Scotia. *Photogrammetric Engineering and Remote Sensing*, 54(11), 1585-1592.
- Caranza, E. J. M., 2004. Weights of evidence modeling of mineral potential: a case study using small number of prospects, Abra, Philippines. *Natural Resources Research*, 13(3), 173-187.
- Dahal, R. K., Hasegawa, S., Nonomura, A., Yamanaka, M., Dhakal, S., & Paudyal, P., 2008. Predictive modelling of rainfall-induced landslide hazard in the Lesser Himalaya of Nepal based on weights-of-evidence. *Geomorphology*, 102(3-4), 496-510.
- DGM (Department of Geology and Mines)., 2016. *Integrated Geo-Hazard Risk Assessment of Critical Landslide at Arong / Lamsorong , Samdrupjongkhar-Trashigang Highway , under Samdrupjongkhar Dzongkhag*. Thimphu, Bhutan: Ministry of Economic Affairs.
- El Jazouli, A., Barakat, A., & Khellouk, R., 2020. Geotechnical studies for Landslide susceptibility in the high basin of the Oum Er Rbia river (Morocco. *Geology, Ecology, and Landscapes*, 1–8. <https://doi.org/10.1080/24749508.2020.1743527>
- Erener, A, & Duzgun, H. S. B., 2012. Landslide susceptibility assessment : what are the effects of mapping unit and mapping method ? *Environ Earth Sci*, 66, 859–877. <https://doi.org/10.1007/s12665-011-1297-0>
- Erener, Arzu, & Duzgun, H. S. B., 2010. Improvement of statistical landslide susceptibility mapping by using spatial and global regression methods in the case of More and Romsdal (Norway . *Landslides*, 7, 55–68. <https://doi.org/10.1007/s10346-009-0188-x>
- Feizizadeh, B., & Blaschke, T., 2013. GIS-multicriteria decision analysis for landslide susceptibility mapping : comparing three methods. *Nat Hazards*, 65, 2105–2128. <https://doi.org/10.1007/s11069-012-0463-3>
- IPCC (Intergovernmental Panel on Climate Change., 2014. *Climate Change 2014 Synthesis Report. Contribution of Working Groups I, II and III to the Fifth Assessment Report of the Intergovernmental Panel on Climate Change [Core Writing Team, R.K. Pachauri and L.A. Meyer (eds.)]*. IPCC, Geneva, Switzerland.
- Kavzoglu, T., Sahin, E. K., & Colkesen, I., 2014. Landslide susceptibility mapping using GIS-based multi-criteria decision analysis , support vector machines , and logistic regression. *Landslides*, 11, 425–439. <https://doi.org/10.1007/s10346-013-0391-7>
- Mondal, S., 2016. Geomorphic Threshold and Landsliding in Paglajhora Sinking Zone, Darjiling Himalaya. *International Journal of Research in Geography*, 2(1), 1–13.
- Nima., 2020, July 15. The cost of keeping the Gelephu-Trongsa highway open. *Kuensel*. Retrieved from <https://kuenselonline.com/the-cost-of-keeping-the-gelephu-trongsa->

highway-open/

Pasierb, B., Grodecki, M., & Gwóźdż, R., 2019. Geophysical and geotechnical approach to a landslide stability assessment: a case study. *Acta Geophysica*, 67, 1823–1834.
<https://doi.org/10.1007/s11600-019-00338-7>

Pokhrel, N., 2015, October 28. Non-frame method to stabilize slopes. *Kuensel*. Retrieved from <https://kuenselonline.com/non-frame-method-to-stabilize-slopes/>

Prakasam, C., Aravindh, R., Nagarajan, B., & Kanwar, V. S., 2020. Site-specific geological and geotechnical investigation of a debris landslide along unstable road cut slopes in the Himalayan region, India. *Geomatics, Natural Hazards and Risk*, 11(1), 1827–1848.
<https://doi.org/10.1080/19475705.2020.1813812>

Sharma, V., & Adhikari, K., 2020. Rainfall and Rainy days trend and ENSO Phenomena in Himalayan Kingdom of Bhutan. *International Journal of Spatial Temporal and Multimedia Information Systems*. <https://doi.org/10.1504/IJSTMIS.2020.10035484>

Thongley, & Vansarochana, C., 2021. Spatial Zonation of Landslide Prone Area Using Information Value in the Geologically Fragile Region of Samdrup Jongkhar-Tashigang National Highway in Bhutan. *Environment and Natural Resources Journal*, 19.
<https://doi.org/10.32526/ennrj/19/2020171>

Uperti, B. N., & Dhital, M. R., 1996. *Landslide Studies and Management in Nepal*. International Center for Integrated Mountain Development (ICIMOD. Kathmandu, Nepal: ICIMOD.

Wangchuk, K., 2019. More than Nu 4 M worth of roads damaged in Samdrup Jongkhar by the onset of monsoon. Retrieved April 22, 2021, from <http://www.bbs.bt/news/?p=117939>

Wangdi, T., 2015, September 15. Mitigating slides at Reutala and Box Cutting roads. *Kuensel*. Retrieved from <https://kuenselonline.com/mitigating-slides-at-reutala-and-box-cutting-roads/>

Yilmaz, I., 2010. Comparison of landslide susceptibility mapping methodologies for Koyulhisar , Turkey : conditional probability , logistic regression , artificial neural networks , and support vector machine. *Environ Earth Sci*, 61, 821–836.
<https://doi.org/10.1007/s12665-009-0394-9>

Flood Risk Area Mapping with Logistic Regression: A Case Study of Phuntsholing City in Bhutan

Thongley Thongley^{1*}, Chaiiwat Vansarochana² and Vasker Sharma¹

¹Department of Civil Engineering and Surveying, Jigme Namgyel Engineering College, Royal University of Bhutan

Email: thongley21@gmail.com, vaskarsharma@jnec.edu.bt

²Faculty of Agriculture, Natural Resources and Environment, Naresuan University, Phitsanulok, Thailand, 65000

Email: chaiiwatV@gmail.com

ABSTRACT

Flood is one of the most frequent natural disasters in the different parts of the world. Phuntsholing city which is located in southern Bhutan also experiences several floods every year. Phuntsholing city is a commercial hub of Bhutan which is bordered with the Indian state of West Bengal. The Phuntsholing city cooperation has a plan to expand its area due to the rapid increase in population. However, some of the areas are prone to flood during the monsoon season. Therefore, this study aimed at developing a flood risk map at Phuntsholing using the logistic regression model. The factors used for this study area are elevation, terrain slope, soil type, lithology, distance from streams, flow accumulation, topographic wetness, index normalized difference vegetation index. The collinearity among these factors was checked using tolerance (TOL) and variance inflation factors (VIF) which should be more than 0.1 for TOL and less than 5 for VIF. All the factors have more than 0.1 for TOL and less than 5 for VIF. During the initial field survey, a total of 26 flood points were identified which is divided into training datasets (70%) and validation datasets (30%). The training dataset is used to train the selected factors while the validation datasets are used to validate the generated map. The generated flood map is divided into five classes namely: very low(22.71%), low(24.25), moderate(18.91%), high(23.95%), and very high(10.18%). The success rate of the flood map is 0.895 (89.5%) and the prediction rate is 0.9622 (96.22%) which is accurate enough for engineers and urban planners for future references.

Keywords: flood, logistic regression, variance inflation factor, tolerance, success rate, prediction rate

1. INTRODUCTION

Flood is one of the most frequent natural disasters in the world. As per the International disaster database Centre for Research on the Epidemiology of Disasters (CRED), the flood claimed the life of 2,383,739 people, injured 124,4492, and 77,004,216 became homeless from the span of 1900-2021 in Asia alone (EM-DAT, 2021). The flood affected nearly 99 million people every year between 2000 and 2008 around the world (McClean, 2010). Urban development needs appropriate studies to minimize the damages caused by the flood.

Flood risk identification, event planning, and preparedness are crucial for flood risk reduction. One of the most common methods for risk reduction is preparing a flood risk map in the most vulnerable area. There are numerous methods to prepare a flood risk map which starts from simple statistical calculation to advance machine learning techniques. This study uses logistic regression is used to preparation of the flood risk map. The logistic regression requires a dichotomous dependent variable and several independent variables. The dichotomous variable is prepared during flood inventory while the independent variables are

prepared from several datasets.

The report published by the Intergovernmental Panel on Climate Change (IPCC) in 2014 forecasted that Bhutan will experience a 5% decrease in rainfall during the dry season, and an 11% increase during the monsoon (Acharya, 2017). This may be true because the southern parts of Bhutan receive torrential rainfall during the monsoon season causing numerous floods. Bhutan is also vulnerable to glacial lake outburst floods (GLOFs) due to the huge amount of perpetual snow and ice creating many glacial lakes. There are around 2,674 glacial lakes are covering an area of about 107 sq.km in northern Bhutan threatening the low-lying places from the GLOF(Mool et al., 2001). Phuntsholing has vulnerable to flood due to its location in the low-lying terrain and contains numerous rivers such as Torsa river, Singyechu, and many other numerous petty rivers. The flood left 400 families homeless and 43 people went missing in August 2000 at the Pasakha area of Phuntsholing city(Tshering & Sithey, 2008). Asian Development Bank (ADB) has drafted a document about the expansion of Phuntsholing city by 66hectare which cost around \$53m (ADB, 2018). However, it is very important to look into the possibility of flood events in the future at the time of town planning.

Therefore, this study aimed at developing a flood risk map of Phuntsholing city in Bhutan using the logistic regression model. This study is expected to guide urban planners for the future planning of the town, and flood risk management

2 Study Area

Phuntsholing (**Figure 1**) is located strategically on the Indo-Bhutan border at 89°23'E longitude and 26°52'N latitude. Phuntsholing is the second largest city of Bhutan and it is the main commercial hub of Bhutan with the majority of goods imports and export transit through Phuntsholing. Phuntsholing city is located at an elevation of about 293m above mean sea level characterized by a tropical monsoon climate. Its average annual precipitation is about 2953mm with a long rainy season and short dry winter season. The highest temperature recorded at Phuntsholing is about 40degree celsius.

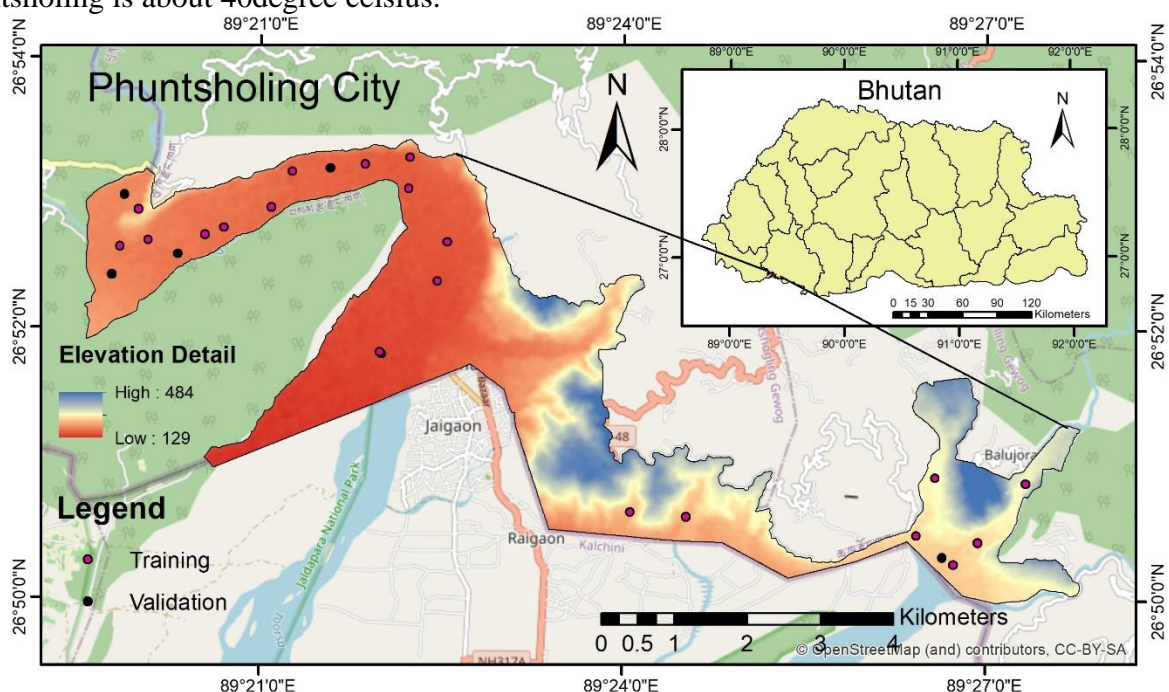


Figure 1. Phuntsholing City in Bhutan

3. Materials and methods

3.1 Flood Inventory

The flood inventory was done through google earth and field visits. A total of 26 flood points and an equal number of non-flood points were identified which is divided into a training dataset (70%) and validation dataset (30%) as shown in **Figure 1**. The training datasets were used to train the factors while the validation datasets were used to validate the generated map.

3.2 Dataset collection and preparation of factors.

The datasets were collected from ALOS PALSAR DEM, FAO soil map, Geological map of Bhutan, and sentinel 2 data. The elevation map, slope gradient, flow accumulation, and topographic wetness index were derived from ALOS PALSAR DEM while soil data was derived from the Food and Agriculture Organization of the United Nations (FAO). Similarly, the lithological map was derived from the geological map of Bhutan, and the normalized difference vegetation index was derived from the sentinel 2 image. All the factors were resampled to 12.5m spatial resolution.

3.3 Multi-collinearity diagnosis

Logistic regression is sensitive to collinearity among the factors and it is important to check the collinearity among the factors. It is important to examine the collinearity among the independent factors. Multicollinearity is caused by the high correlation between the independent factors (Tehrany, Jones, & Shabani, 2019). The tolerance (TOL) and variance inflation factor (VIF) are commonly used to check multi-collinearity. The TOL and VIF are calculated using Equations 1 and 2.

$$TOL = 1 - R^2 \quad (1)$$

$$VIF = \frac{1}{TOL} \quad (2)$$

The non-collinearity should have a tolerance of more than 0.1 and a VIF of less than 5 (Tien Bui et al., 2019).

3.4 Logistic Regression Model

Logistic regression is a multivariate statistical method and it is widely used in flood and landslide risk analysis. The logistic regression requires several independent variables on a single dichotomous outcome variable (Mind'je et al., 2019). The single dichotomous variable contains binary points (1 and 0) whereby 1 indicates flood point and an equal number of 0 indicates non-flood point. The logistic regression evaluates the correlation between the flood event and the influencing factors (Tehrany et al., 2019).

The probability (p) of the flood in logistic regression is calculated using Equation 3.

$$P = \frac{1}{1 + e^{-z}} \quad (3)$$

where p is the probability of flooding which ranges between 0 to 1 on an S-shaped curve. Z represents a linear combination and it is using Equation 4.

$$Z = b_0 + b_1x_1 + b_2x_2 + b_3x_3 + b_nx_n \quad (4)$$

where b_0 is the intercept of the model, b_i ($i = 0, 1, 2, \dots, n$) represents the coefficients of the logistic regression model, and x_i ($i = 0, 1, 2, \dots, n$) denotes the independent variables (Lee & Sambath, 2006).

3.5 Accuracy assessment for the flood risk map

The accuracy assessment is an important step to check the reliability and efficiency of the map (Tehrany et al., 2019). The accuracy assessment of the generated flood map was done using the Area Under the Curve (AUC) of the Receiver Operating Characteristics (ROC) curve. The AUC is calculated using Equation 7. The ROC curve is constructed False Positive Rate (FPR) on the x-axis and True Positive Rate (TPR) on the y-axis (Thongley & Vansarochana, 2021b). The AUC is interpreted as excellent (0.9-1.0), very good (0.8-0.9), good (0.7-0.8), moderate (0.6-0.7), and poor (0.5-0.6) (Thongley & Vansarochana, 2021a). The sensitivity and specificity are calculated using the equation 5 and 6.

$$\text{TPR} = \frac{\text{TP}}{\text{TP} + \text{FN}} \quad (5)$$

$$\text{FPR} = \frac{\text{FP}}{\text{FP} + \text{TN}} \quad (6)$$

$$\text{AUC} = \frac{\sum \text{TP} + \sum \text{TN}}{\text{TP} + \text{TN} + \text{FP} + \text{FN}} \quad (7)$$

Where TP is true positive, TN is true negative, FP is false positive, FN is false negative

4. RESULT AND DISCUSSION

4.1 Multi-collinearity diagnosis and flood risk mapping

The multi-collinearity was checked using TOL and VIF. The factors were considered non-collinear if TOL is more than 0.1 and VIF is less than 5. Table 1 shows the coefficient, TOL and VIF for individual factors. It is noticed that all the independent factors are free of collinearity.

Table 1. Coefficient of factors and the value of tolerance (TOL) and Variance Inflation Factor (VIF)

Factors	Coefficient	Collinearity Statistics	
		TOL > 0.1	VIF < 5
Dist from river	-0.005	0.462	2.164
Elevation	-0.270	0.373	2.683
Flow Accumulation	0.001	0.884	1.132
Lithology	0.139	0.798	1.254
Slope gradient	0.044	0.609	1.642
Soil	0.555	0.875	1.143
TWI	-0.040	0.781	1.281
Constant	4.595		

The coefficients from Table 1 were used to calculate linear combination Z(Equation 3) which will ultimately be used to calculate the flood probability P (Equation 3) and generate a flood risk map.

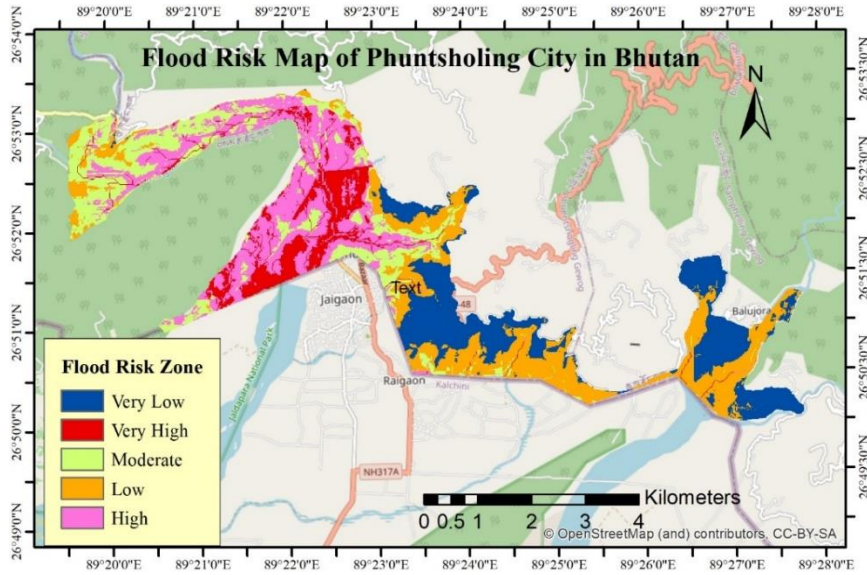


Figure 2. Flood Risk Map of Phuntsholing city in Bhutan.

The generated flood map (**Figure 2**) is divided into five classes based on the jenk classification due to its clear breakpoint between the classes (Toshiro, 2002). The five classes constitute very low (22.71%), low (24.25), moderate (18.91%), high (23.95%), and very high (10.18%).

4.2 Validation result of the flood risk map

The success rate shows the reliability of the model using trained data while the prediction rate shows the future prediction capability of the flood risk map (Thongley & Vansarochana, 2021b). The success rate of the flood risk map is 0.895 which falls under very good category while the prediction rate is 0.9622 which falls under the excellent category for the flood prediction (**Figure 3**).

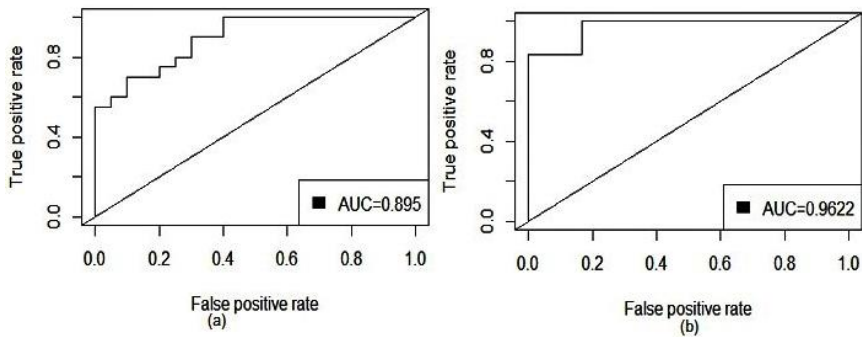


Figure 3. ROC Curve for validation (a) Success rate curve, (b) Prediction rate curve

5. CONCLUSION

The flood risk map is a preliminary step for minimizing major disasters due to the flood. The logistic regression is a simple and effective model for the preparation of the flood risk map in conjunction with the remote sensing data and geographic information techniques.

The generated map is a reliable map for future use due to its good performance with a success rate of 0.895 and excellent prediction rate of 0.9622. The final output shows a perfectly good result while comparing with the past flood area. The natural break classification shows the very high-risk area constitutes 10.18% of the total area. This study recommends not to plan any future developmental activities in the very high flood risk area which is 10.18%.

Since the success rate of the flood map is very good, the planners, engineers, and politicians can use it for future planning purposes while the researchers can also apply the logistic regression model for their future studies. It also recommends future researchers to study the highest volume of river water in the specified time and its return period for the prevention of possible loss of lives.

6. REFERENCES

- Acharya, G. 2017, Flash floods the dangerous new normal in Bhutan. Retrieved from <https://www.thethirdpole.net/en/climate/bhutan-flash-floods/>
- ADB. 2018. *Proposed Loan and Grant Kingdom of Bhutan: Phuentsholing Township Development Project* Asian Development Bank.
- EM-DAT. 2021. *The International disaster database*. .
- Lee, S., & Sambath, T. 2006. Landslide susceptibility mapping in the Damrei Romel area, Cambodia using frequency ratio and logistic regression models. *Environmental Geology*, 50(6), 847-855.
- McClean, D. 2010. World disasters report 2010: focus on urban risk *World Disasters Report 2010: Focus on urban risk*: International Federation of Red Cross and Red Crescent Societies (IFRC).
- Mind'je, R., Li, L., Amanambu, A. C., Nahayo, L., Nsengiyumva, J. B., Gasirabo, A., & Mindje, M. 2019. Flood susceptibility modeling and hazard perception in Rwanda. *International journal of disaster risk reduction*, 38, 101211.
- Mool, P. K., Wangda, D., Bajracharya, S. R., Kunzang, K., Gurung, D. R., & Joshi, S. P. 2001. Inventory of glaciers, glacial lakes and glacial lake outburst floods. Monitoring and early warning systems in the Hindu Kush-Himalayan Region: Bhutan. *Inventory of glaciers, glacial lakes and glacial lake outburst floods. Monitoring and early warning systems in the Hindu Kush-Himalayan Region: Bhutan*.
- Tehrany, M. S., Jones, S., & Shabani, F. 2019. Identifying the essential flood conditioning factors for flood prone area mapping using machine learning techniques. *Catena*, 175, 174-192.
- Thongley, T., & Vansarochana, C. 2021a. Landslide Identification and Zonation Using the Index of Entropy Technique at Ossey Watershed Area in Bhutan. *Applied Environmental Research*, 43(1), 102-115.
- Thongley, T., & Vansarochana, C. 2021b. Spatial zonation of landslide prone area using information value in the geologically fragile region of Samdrup Jongkhar-Tashigang national highway in Bhutan. *Environment and Natural Resources Journal*, 19(2), 122-131.
- Tien Bui, D., Khosravi, K., Shahabi, H., Daggupati, P., Adamowski, J. F., Melesse, A. M., . . . Bahrami, S. 2019. Flood spatial modeling in northern Iran using remote sensing and gis: A comparison between evidential belief functions and its ensemble with a multivariate logistic regression model. *Remote Sensing*, 11(13), 1589.
- Toshiro, O. 2002. Classification Methods for Spatial Data Representation. *Center for Advanced Spatial Analysis. University College London. London*.
- Tshering, D., & Sithey, G. 2008. Climate change and health in Bhutan. *Thimpu: Royal Society for Protection of Nature*.

Relationship between daily number of COVID-19 cases and climate factors using multiple linear regression analysis method in Thailand

¹Napatsawan Tubkrit, ²Tanyaluck Chansombat

**Department of Natural Resources and Environment,
Faculty of Agriculture Natural Resources and Environment, Naresuan University,
99 Moo 9 Tanbon Thapho Amphoe Muang, Phitsanulok, Thailand**

¹Email: napatsawan61@nu.ac.th, ²tanyalaks@nu.ac.th

ABSTRACT

A novel coronavirus, now referred to as 2019 Novel Coronavirus (2019-nCoV), is an emerging disease that the World Health Organization had declared a pandemic on 11 March 2020. In this study, the relationship between climatic factors affecting the spread of the virus in Thailand from 01 June 2021 to 30 July 2021 was studied using multiple linear regression analysis method in R. Factors used in the study comprised minimum temperature (°C), maximum temperature (°C), precipitation level (mm) and wind speed (m/s). The results showed that the daily cases was significantly related to maximum temperature in Bangkok ($r = 0.2315$; $p = 0.000529$), Samutprakan ($r = 0.2448$; $p = 0.0208$), and Chonburi ($r = 0.2057$; $p = 0.00242$). The finding might be useful as a contribution to a policy making in terms of the awareness of covid-19 and other airborne infectious diseases outbreak during rainy season in Thailand.

1. INTRODUCTION

Coronavirus disease (COVID-19) is an infectious disease caused by a novel severe acute respiratory syndrome coronavirus 2 (SARS-CoV-2) (WHO, 2020). In early December 2019, an outbreak of COVID-19 originally occurred in Wuhan City, Hubei Province, China and later on January 30, 2020, the World Health Organization declared the outbreak as a pandemic incident with Public Health Emergency of International Concern. On January 12, 2020, in Bangkok, Thailand, the first COVID-19 patient was discovered. The infection has since spread throughout the country affecting various provinces.

Extreme climatic conditions could play a role in the virus's rapid spread, according to Wang et al., 2010's study. COVID-19's potential spread may also be predicted by latitude and seasonality (Sajadi et al., 2020). Certain climatic circumstances have also been recognized as predisposing factors in previous studies on respiratory disorders (D'Amato et al., 2014). Climate factors such as temperature, rainfall, and wind speed may act as biological catalysts in the relationship between covid-19 and humans in this scenario. Virus transmission is influenced by a variety of parameters such as host behavior, host defensive mechanisms, and virus infectivity (Cory, 2015), as well as population density and environmental conditions (Brown et al., 2008).

This study aims to examine the relationship between climatic factors and COVID -19 infection in top three highest numbers of covid 19 provinces of Thailand consisting of Bangkok, Samutprakan, and Chonburi provinces. This study utilized a secondary data analysis of covid-19 surveillance data from the Department of Disease Control, Thailand, and weather data from the website of Thai Meteorological Department. Minimum temperature (°C), maximum temperature (°C), precipitation level (mm), and wind speed (m/s) are the elements of climatic data.

2. Methods and Statistical Analysis

2.1 Study area

Thailand's climate is influenced by its location in the tropical monsoon zone of mainland Southeast Asia, as well as certain physical factors that affect precipitation distribution. Beginning in May, warm, humid air masses from the Indian Ocean travel northeastward across the region, depositing large amounts of precipitation; rainfall peaks in September. The northeast monsoon brings cool, generally dry air in a southwesterly flow between November and February, resulting in cooler temperatures across much of the country. In March and April, stagnant air creates a distinct hot-and-dry inter-monsoonal phase. Average temperatures are relatively stable through the year ranges between 25 and 29 °C.

2.2 Data collection

A secondary data analysis of covid-19 surveillance data was retrieved from the Department of Disease Control, Thailand, and weather data was downloaded from the website of Thai Meteorological Department. Minimum temperature (°C), maximum temperature (°C), precipitation level (mm), and wind speed (m/s).

2.3 Data analysis

The linear regression analysis was used to analyze the relationships between covid-19 daily new cases and climate elements. An analysis at 95% confidence interval was applied.

3. RESULT AND DISCUSSION

During the third phase of pandemic in Thailand since early of April 2021, Covid-19 new cases dramatically increased in Thailand, especially during May to July. Descriptive summary of the climate data suggests (Table 1.) a minimum temperature of 22.1 °C and the highest maximum temperature of 37.2 °C during the study period. In addition to that, the lowest recorded rainfall was 0 mm whereas the highest was 63.8 mm. The lowest wind speed recorded with value of 18.53 m/s and highest wind speed of 83.4 m/s.

Table 1. Variables descriptive statistics.

Variables	Bangkok			Samutprakan			Chonburi		
	Min	Max	Mean	Min	Max	Mean	Min	Max	Mean
Daily new cases	624	3997	1810	124	1386	543	10	1062	341
Min temp (°C)	22.3	28.5	25.93	24.6	28	26.45	24	29.7	27.03
Max temp(°C)	30.1	36.6	33.32	29.5	38	33.36	30.1	37.2	33.96
Precipitation (mm)	0	41.1	4.37	0	63.8	3.52	0	41	4.67
Wind speed (m/s)	27.8	83.4	39	22.24	79.69	35.21	18.53	59.3	30.94

3.1 Spatial Pattern Analysis

The total number of cases (from 1 April to 28 July 2021) in each province and the rate of the disease were mapped using GIS. The number of cases and infection rate are divided into five categories

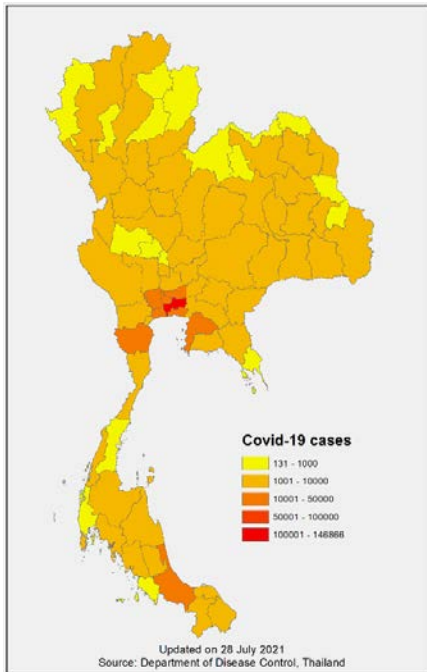


Figure 1. The province-level of COVID-19 cases Thailand on 28 July 2021. The map shows the number of COVID-19 daily cases. The number of cases is divided into five categories and illustrated by colors from light yellow (low number) to deep red (high number), respectively.

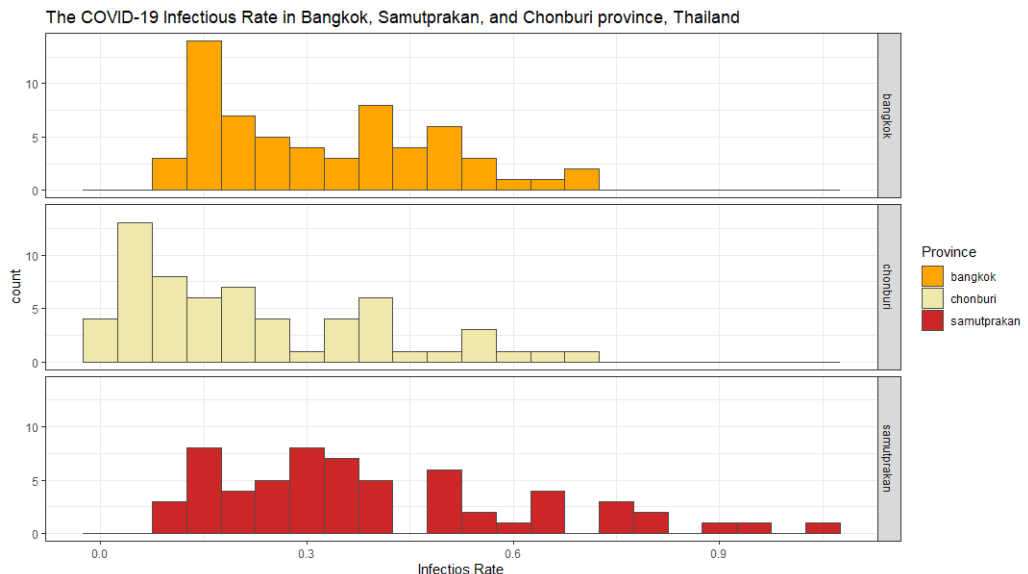


Figure 2. The COVID-19 infectious rate in Bangkok, Samutprakan, and Chonburi province, Thailand on 28 July 2021.

3.2 Multiple Linear Regression Analysis

Table 2. Multiple Linear Regression Analysis

Climatic factors	Bangkok	p-value Samutprakan	Chonburi
Minimum temperature (°C)	0.97536	0.082	0.91656
Maximum temperature (°C)	0.000529 ***	0.0208 *	0.00242 **
Precipitation(mm)	0.748486	0.7784	0.20502
Wind speed (m/s)	0.624421	0.4182	0.48519
Multiple R-squared	0.2315	0.2448	0.2057

*** Significance level of 0.0001

** Significance level of 0.001

* Significance level of 0.01

Among the four weather variables, maximum temperature data in Bangkok ($r = 0.2315$; $p = 0.000529$), Samutprakan ($r = 0.2448$; $p = 0.0208$), and Chonburi ($r = 0.2057$; $p = 0.00242$) was negatively significant with covid-19 cases. On the other hand, minimum temperature, precipitation, and wind speed were not significantly associated with covid-19 daily cases.

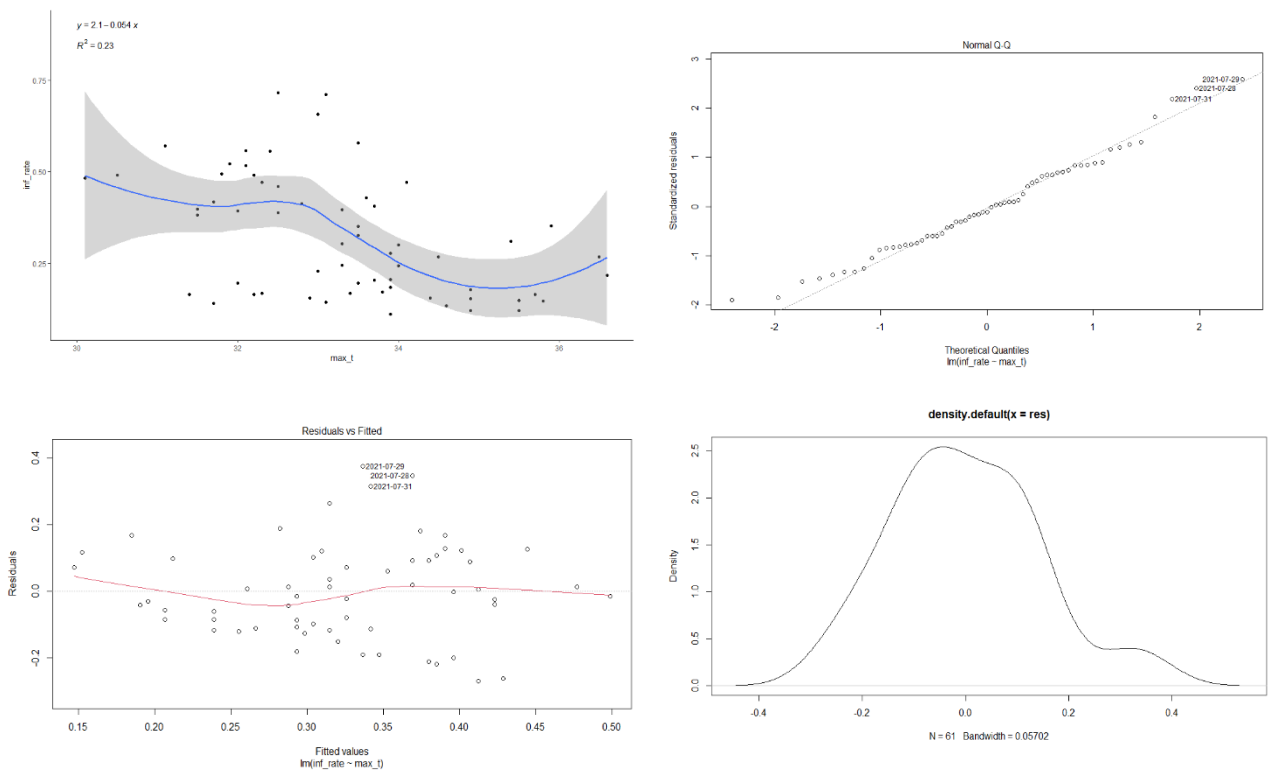


Figure 3. Diagnostic plots of the residuals from the linear regression analysis model (Bangkok province)

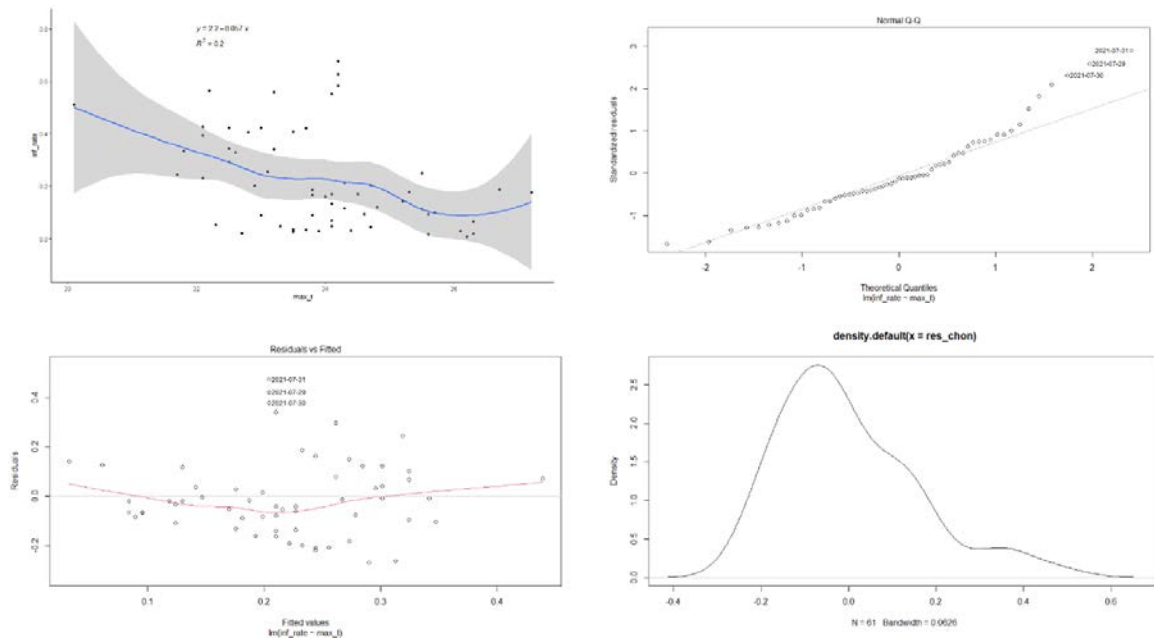


Figure 4. Diagnostic plots of the residuals from the linear regression analysis model (Samutprakan province)

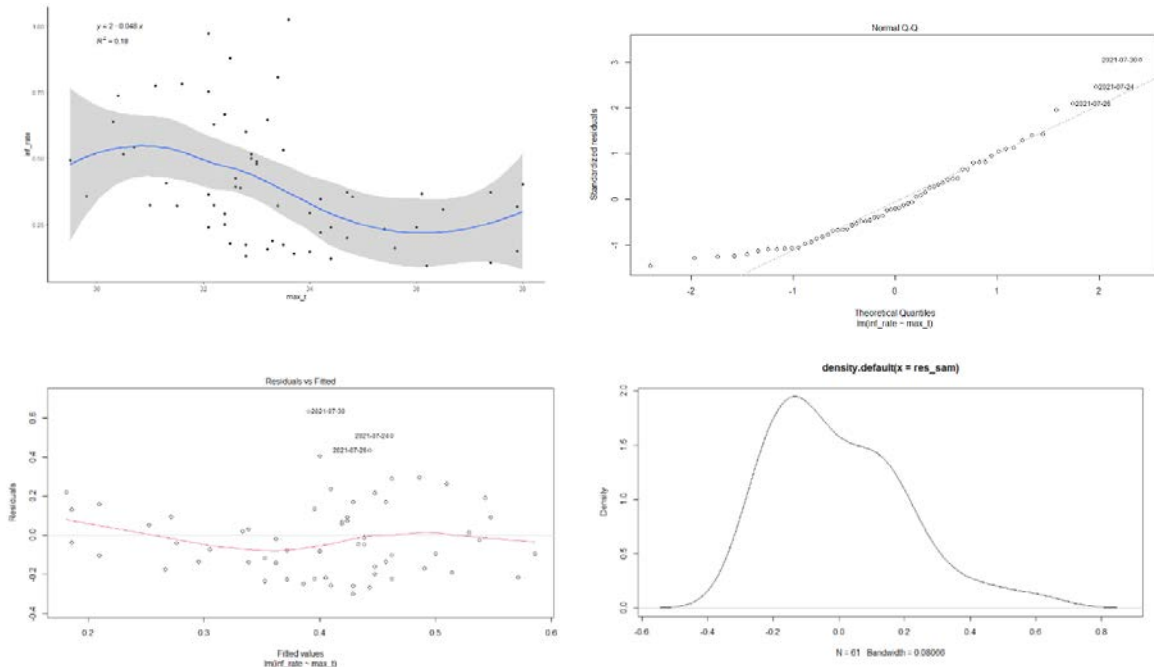


Figure 5. Diagnostic plots of the residuals from the linear regression analysis model (Chonburi province)

The result of this study shows that the pattern of climate elements delivers a scenario of the incidence of covid-19 in Thailand. It is found that maximum temperature negatively associates with occurrence of Covid-19 (Table 2). This finding is consistent with prior research that has found a link between temperature and human West Nile Virus infections (Ruiz et al., 2010). The result of this study also relates with a recent finding by Wang, J., et al. (2020) where their study claimed that high temperature lessens the transmission of Covid-19. However, there are a range of viewpoints on the positive association between temperature and new cases, with some claiming that people are more likely to disobey lock-down rules and thus become infected. However, the finding of this study is in contrast with Mesay M. (2020) which stated that maximum temperature and normal temperature are positively associated with covid-19.

4. CONCLUSION

Maximum temperature associate with the decreasing of incidence rate of daily covid-19 cases in Bangkok, Samutprakan, and Chonburi provinces, Thailand. In contrast to the weather conditions, it is considered that factors such as high social mobility, population density, household condition affect new covid-19 in metropolitan area like Bangkok. Bangkok, Samutprakan, and Chonburi provinces are the main economic destinations for job seekers who come from various regions. High population density of these areas allows covid-19 transmission to be very rapid (Kuchler et al., 2020).

5. REFERENCES

- Brown, H.E., Childs, J.E., Diuk-Wasser, M.A., Fish., D., 2008, **Ecologic factors associated with West Nile virus transmission, northeastern United States**, Emerg. Infect. Dis., 14 (10) (2008), p. 1539
- Cory, J.S., 2015, **Insect virus transmission: different routes to persistence**, Current Opinion in Insect Science, 8 (2015), pp. 130-135
- D'Amato, G., Cecchi, L., D'Amato, M., Annesi-Maesano, I. 2014, **Climate Change and Respiratory Diseases**, Eur Respiratory Soc (2014)
- Kuchler, T., Russel, D., Stroebel., J., 2020, **The Geographic Spread of COVID-19 Correlates with Structure of Social Networks as Measured by Facebook**, pp. 0898-2937
- Mesay Moges Menebo, 2020, Temperature and precipitation associate with Covid-19 new daily cases: A correlation study between weather and Covid-19 pandemic in Oslo, Norway, Science of The Total Environment, Volume 737, 139659, ISSN 0048-9697
- Ruiz, M.O., Chaves, L.F., Hamer, G.L., Sun, T., Brown, W.M., Walker, E.D., Kitron, U.D., 2010, **Local impact of temperature and precipitation on West Nile virus infection in Culex species mosquitoes in northeast Illinois, USA**, Parasites & vectors, 3 (1) (2010), p. 19
- Sajadi, M.M., Habibzadeh, P., Vintzileos, A., Shokouhi, S., Miralles-Wilhelm, Amoroso, F. A., 2020, **Temperature and Latitude Analysis to Predict Potential Spread and Seasonality for COVID-19**, (Available at SSRN 3550308)
- Wang, J., Tang, K., Feng, K., Lv W., 2020, **High Temperature and High Humidity Reduce the Transmission of COVID-19**
- WHO, 2020, **Coronavirus disease 2019 (COVID-19) situation report** – Retrieved from https://www.who.int/docs/default-source/coronaviruse/situation-reports/20200301-sitrep-41-covid-19.pdf?sfvrsn=6768306d_2

Cluster Pattern Identification of the COVID-19 Pandemic in Thailand

¹Maythawee Jantha, ²Pathana Rachavong and ³Tanyaluck Chansombat

Department of Natural Resources and Environment,
Faculty of Agriculture Natural Resources and Environment, Naresuan University,
99 Moo 9 Tanbon Thapho Amphoe Muang, Phitsanulok, Thailand
¹Email: maythweej63@nu.ac.th, ²Email: pathanar@gmail.com, ³Email: tanyalaks@nu.ac.th

ABSTRACT

The novel coronavirus (COVID-19) pandemic poses a serious threat to human health worldwide. Thailand has more than 300,000 infected as of June 2021. To understand disease transmission patterns, it is necessary to know outbreak patterns. In this study, we survey COVID-19 cases in Thailand from March 1, 2020, to July 28, 2021 using Open Government Data of Thailand. Country-level cases and disease rates are mapped using a geographic information system (GIS). Overall disease trends in Thailand and in 77 provinces are analyzed using K-means clustering analysis in R.

Based on the results from K-means analysis, the results show that the optimal k value to form a cluster of 2 is accepted. Cluster 1 contains 1 province which is Bangkok, Cluster 2 consists of 62 provinces, and Cluster 3 contains 9 provinces based on COVID-19 data.

There are specific patterns of disease curves and are assigned to clusters. The results of this study provide insights into creating disease control and mitigation strategies.

1. INTRODUCTION

Coronavirus disease (COVID-19) is an infectious disease caused by a novel severe acute respiratory syndrome coronavirus 2 (SARS-CoV-2) (WHO, 2020). In early December 2019, an outbreak of COVID-19 originally occurred in Wuhan City, Hubei Province, China and later on January 30, 2020 the World Health Organization declared the outbreak as a pandemic incident with Public Health Emergency of International Concern (Harapan et.al., 2020). In Thailand, the first COVID-19 patient was found on 12 January 2020 in Bangkok. Since then, the disease has spread to several provinces in the country. Thailand has faced the third wave of the pandemic outbreak which started from 1 April 2021. As of 30 July 2021, more than 578,375 cases of COVID-19 have been reported in Thailand. (CDC Thailand, 2021)

The K-means algorithm is helpful in segmenting a heterogeneous population into more homogeneous subgroups and it also offers a better view of applicant characteristics and needs, which may lead to more targeted rehabilitation options (Armstrong, et.al., 2012). This technique is a cluster algorithm that provides several competence advantages (Li and Haiyan 2012). Pattern recognition plays a vital role in exploring meaningful information and detecting complex relationships from a large data set, such as identifying risk factors and illustrating the trend of a disease. Cluster analysis is one of the approaches to pattern recognition which groups objects with similar attributes into the same cluster. Therefore, objects have high similarity within cluster while low similarity between clusters. Identifying geospatial patterns of COVID-19 is also essential for disease mitigation because it helps to illustrate the extent and impact of the pandemic, develop public health policies and aid decision making and community action. The objective of this study is to identify the patterns of the COVID-19 cases in Thailand by applying K-means clustering analysis to identify these patterns (Wu, J. and Sha, S., 2021).

2. Methods and Statistical Analysis

2.1 Data Collection and Processing

The COVID-19 data was obtained from Website of Department of Disease, Thailand, which are publicly assessable from the website. The daily-country level data that started from 12 January 2020 to the present are updated daily. Considering there were only very few cases before January 2020, the data were removed before 1 April 2021. Therefore, the data in our analysis start on 1 March 2021 up until 28 July 2021. Spatially, the data from 77 provinces were included.

Two datasets were generated from the dataset for separate analyses. For spatial pattern analysis, the data were grouped by the date to obtain the total number of cases in each province on the latest day of the study period. For K-means clustering and time-series analysis, the data were aggregated by province and risk to obtain the daily new case data during the study period in each state. Data were analyzed using the K-Means Clustering method in R Software version 3.6.3.

2.2 Spatial Pattern Analysis

To demonstrate the spatial distribution of COVID-19 cases, the total number of cases (up to 28 July 2021) in each province with a geographic information system (GIS) was mapped. The rate of the disease using the total number of cases in each province divided by the population in that province is also calculated.

2.3 Temporal Trend Analysis

To achieve a trend of daily cases in Thailand during the third wave of the COVID 19 outbreak, time series data are plotted in descending order based on the total case number and genders from 1 April – 28 July 2021.

2.4 K-Means Clustering

K-means clustering is applied to explore the pattern of disease clusters in different provinces. K-means clustering is a simple and common unsupervised machine learning algorithm for exploratory data analysis to get an intuition about data structure which divides the data into subgroups or clusters. The province with a similar disease cluster curve will be grouped into the same cluster. The K-means algorithm functions as following processes. First, the algorithm specifies the number of clusters (K); second initialize K centroids and calculate the distance between each centroid and each data point; third, the data points that have the shortest distance to a centroid are grouped in the same cluster; fourth, calculate the new centroid based the data points in a cluster; and fifth, repeat the process from until the centroids are stable (Likas et.al., 2003)

3. Result and Discussion

3.1 Spatial Pattern Analysis

The total number of cases (from 1 April to 28 July 2021) in each province and the rate of the disease were mapped using GIS. The number of cases and infection rate are divided into five categories.

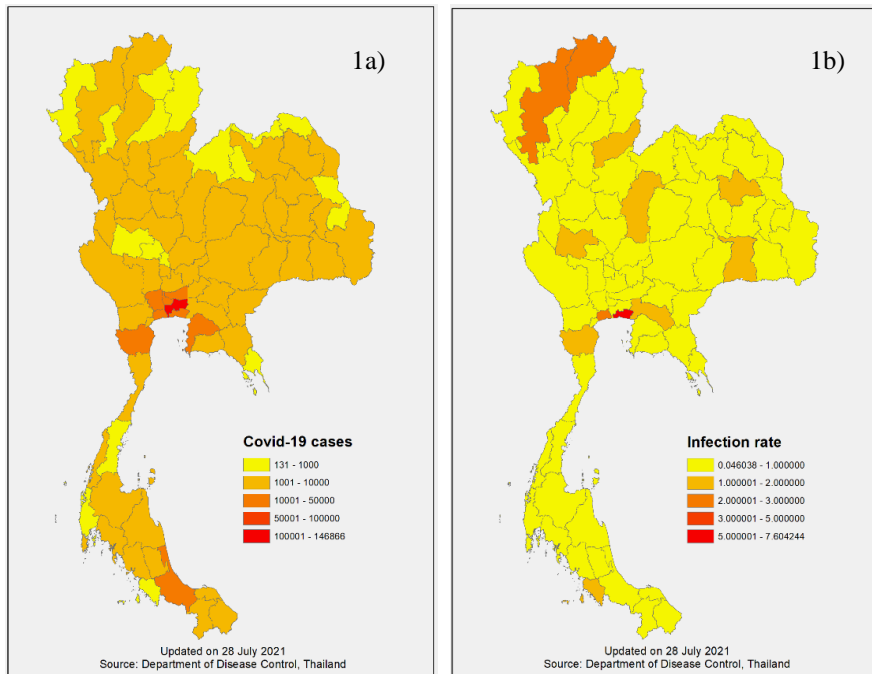


Figure 1. The country-level of COVID-19 cases Thailand on 28 July 2021. The map shows the number of COVID-19 cases (1a) and infection rate in each province (1b). The number of cases and infection rate is divided into five categories and illustrated by colors from light yellow (low number) to deep red (high number), respectively.

3.2 Temporal Trend Analysis

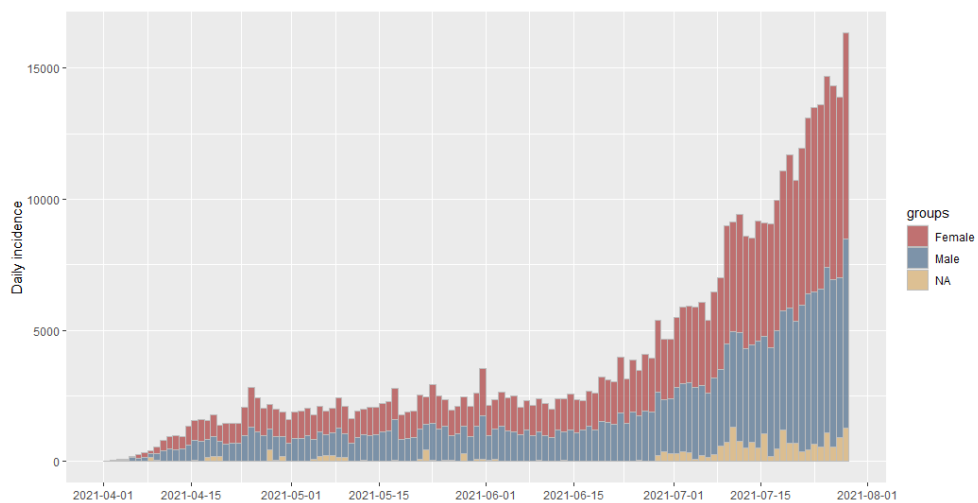


Figure 2. Trend of daily cases in Thailand during the third wave of the COVID 19 outbreak, time series data are plotted in descending order based on the total case number and genders from 1 April – 28 July 2021.

The trends of daily cases in 77 provinces are demonstrated in Fig. 2. In the early of state (1 April –31 April), the disease curve was quite low, However, the case number increased quickly and formed a large peak in mid-May and increasingly risen in June and July.

3.3 K-Means Clustering

The total within-cluster sum of squares (WSS) and Silhouette method were plotted. Based on the spatial pattern analysis of COVID-19 in Thailand, two to five main clusters in study period were observed. From the WSS plots, the K value as two for the whole period analysis was selected. K-means algorithm to initialize the centroids of clusters was applied using R package.

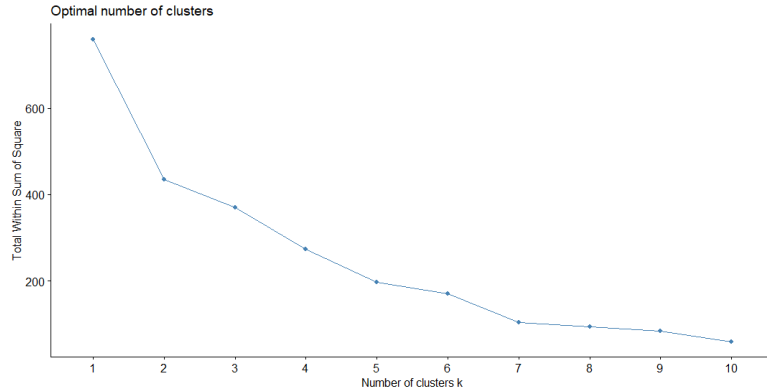


Figure 3. K value cluster analysis using the total within-cluster sum of squares (WSS) method.

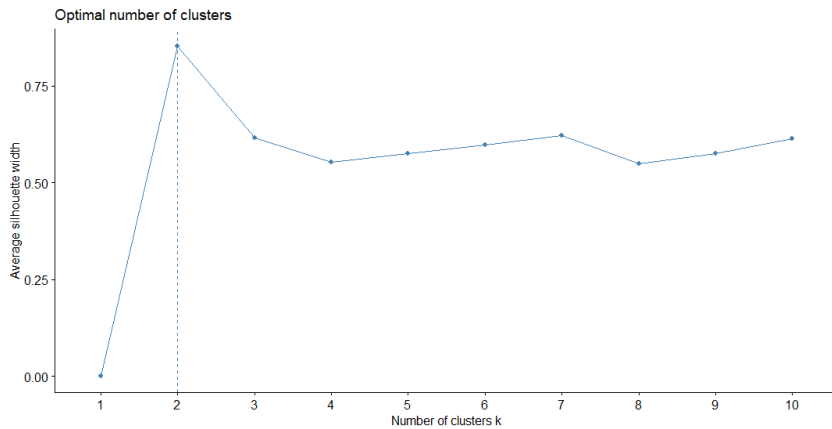


Figure 4. K value cluster analysis using the Silhouette method.

In Fig. 1, Bangkok apparently is the biggest cluster in Thailand, the province became the epicenter of the outbreak. This is due to Bangkok is the capital city and the most densely populated city of Thailand. The optimal number of k groups was determined using commonly used methodologies namely within-cluster sum of squares (WSS) and Silhouette Statistics. The results can be seen in Fig. 3 and 4.

Based on Fig. 3 and 4, the WSS method and the Silhouette method obtained optimal clusters at $k = 2$. Therefore, based on the results from K-means analysis, the optimal k value to form a cluster is 2 is accepted. As shown in Table 1, Cluster 1 contains 1 province which is Bangkok, Cluster 2 consists of 62 provinces, and Cluster 3 contains 9 provinces based on COVID-19 data (Fig. 5).

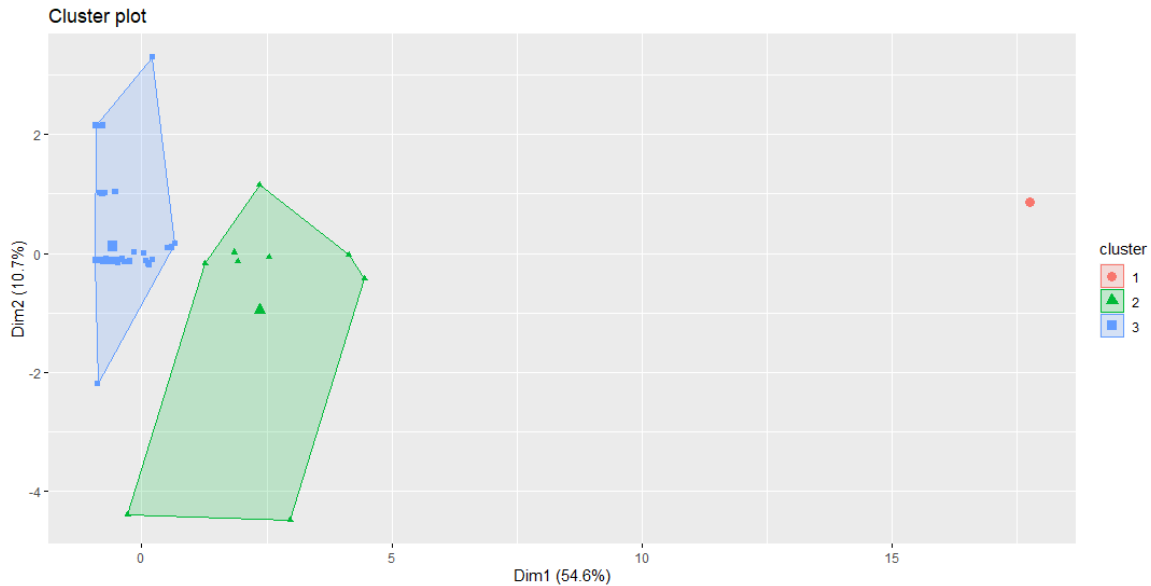


Figure 5. Cluster analysis using K value = 2

Table 1. Cluster analysis using K-means analysis

Cluster 1	Cluster 2			Cluster 3
Bangkok	Amnatchareon Buriram Chaiyaphum Chiangrai Lopburi Mukdahan Nakornpathom Nakornsithammarat Nongbualamphu Petchabun Phraya Prachuabkhirikhan Rayong Roi-ed Saraburi Srakaew Suphanburi Trad Udonthani Yala	Ang-thong Chacherngsoa Chantaburi Chumphon Mahasarakam Nakornnayok Nakornratchasima Nan Nongkhai Phang-nga Phichit Phrae Ranong Roi-ed Satun Srisaket Suratthani Trung Uthaiyathani Yasotorn	Buengkarn Chainat Chiangmai Loei Meahongson Nakornpanom Nakornsawan Narathiwat Pattani Phattalung Phitsanulok Prachinburi Ratchaburi Sakonnakhon Samutsonkram Singburi Sukhothai Surin Ubonratchathani Uttaradit	Ayuddhaya Chonburi Nonthaburi Pathumthani Petchaburi Samutprakan Samutsakorn Songkhla Tak

4. CONCLUSION

The result of this study is expected to provide input to the government in making policies related to restrictions on community activities and to provide insights into creating disease control and mitigation strategies of COVID-19 in Thailand. This study is according with Zarikas, et.al. (2020), Azarafza, et.al. (2021), and Dahlan, A., et.al. (2021) which stated that clustering active cases in a region is useful for drawing conclusions about the disease impact which spreads rapidly in an area and the pattern of transmitting infection between provinces can be estimated using the clustering method. Therefore, it can be determined that K-means clustering method is one of effective methods to illustrate disease spread patterns and also provide alternative solutions related to this distribution pattern of the COVID-19 outbreak in Thailand.

5. DATA AVAILABILITY

The data in this study can be accessed at: Website of Department of Disease, Thailand.
[\(https://ddc.moph.go.th/covid19-dashboard/\)](https://ddc.moph.go.th/covid19-dashboard/)

6. REFERENCES

- Armstrong, J.J., Zhu, M., Hirdes, J.P., Stolee, P., 2012. *K-Means cluster analysis of rehabilitation service users in the home health care system of ontario: examining the heterogeneity of a complex geriatric population.* Arch. Phys. Med. Rehabil. **93**(12), 2198–2205
- Azarafza, M., Azarafza, M., Akgun, H., 2021. *Clustering method for spread pattern analysis of coronavirus (covid-19) infection in iran.* J. Appl. Sci. Eng. Technol. **3**(1), 1–6 (2021)
- Dahlan, A., S. Susilo, Ansari, S.A., R. Rusli and Rahmat, H., 2021 *The application of K-means clustering for province clustering in Indonesia of the risk of the COVID-19 pandemic based on COVID-19 data.* Qual Quant. <https://doi.org/10.1007/s11135-021-01176-w>
- Department of disease control, Ministry of Public Health, Thailand., 2021. *COVID-19 Thailand Data,* <https://ddc.moph.go.th/covid19-dashboard/>
- Likas, A., Vlassis, N., Verbeek, J.J., 2003. *The global k-means clustering algorithm.* Pattern Recognit **36**, 451–461.
- Wu, J. and Sha, S., 2021. *Pattern Recognition of the COVID-19 Pandemic in the United States: Implications for Disease Mitigation.* Int. J. Environ. Res. Public Health **2021**, **18**, 2493. <https://doi.org/10.3390/ijerph18052493>
- Zarikas, V, Poulopoulos, S.G., Gareiou, Z., Zervas, E., 2020. *Clustering analysis of countries using the covid-19 cases dataset.* Data in Brief **31**, 105787

The Study of Vaccination Priority in Thailand: An GWR Analysis

Pathana Rachavong¹ Jiranya Duangfoo² and Tanyaluck Chansombat¹

¹Department of Natural Resources and Environment, Naresuan University, Thailand

Email: pathanar@gmail.com, tanyalaks@nu.ac.th

²Geographic information science section, Department of Natural Resources and Environment, Naresuan University, Thailand

Email: jiranyad64@nu.ac.th

ABSTRACT

The study, titled The study of VACCINATION PRIORITY in Thailand: An GWR Analysis, aimed to study the distribution of COVID-19 vaccine in Thailand by using data from Mahidol University's vaccine transport tracking system to analyze the spatial correlation of distribution of COVID-19 vaccine and covid-19 outbreak coefficient using geospatial programs. The results showed that the allocation of the COVID-19 vaccine in Thailand was reasonably distributed across areas with a high cumulative population, with a correlation coefficient of 79.03%. However, the central region in the provinces surrounding Bangkok and the eastern region are allocated relatively large compared to the remote areas.

1. INTRODUCTION

When the supply of vaccines for COVID-19 in the early stages of vaccine development success is limited. This raises the question of how countries should prioritize distribution of available vaccines. It is also necessary to act transparently and based on evidence of incidences related to knowledge and uncertainty of the epidemic, risk profiles, vaccine efficacy, and immunizations. The nature of the population exists to exemplify the priority allocation of vaccines. Bubar et al. (2020) studied and presented a model for vaccine distribution priorities. They assessed the impact of the established strategies, in order of importance, on cumulative epidemic incidence and mortality. Demographic factors such as age, exposure, and prevalence of contagious immunity were considered. Regarding vaccine factors, including imperfections of vaccine availability and efficacy caused by age differences.

A study by Bubar et al. (2020) found that epidemic vaccines should be given priority to adults aged 20-49 in order to reduce the cumulative incidence of epidemic and adult populations over 60 in order to reduce the death rate from infection of the epidemic. Examples of priorities were drawn from studies in the People's Republic of China, South Korea, Italy and the United States. In the People's Republic of China, vaccines are provided to essential workers, including health, law enforcement, safety, nursing homes, social welfare institutions, community services, energy, food and transportation, and employees/. International students (49.7 million). This information can be prioritized for vaccination to maintain essential services in the early stages of the vaccination program. Later, the elderly, people with underlying health conditions, and pregnant women (563.6 million) may be vaccinated to reduce the number of severe cases of COVID-19. This includes hospitalizations, intensive care, and death. Lately, the vaccination program could be extended to target adults without health conditions and children (784.8 million) to reduce symptomatic infection and/or stop the spread of the virus when given 10 million doses per day. The two-dose vaccination schedule will take 1 week to inoculate the necessary practitioners but will likely take up to 7 months to vaccinate 70% of the population.

In South Korea, effective vaccination strategies have been developed that will reduce the number of deaths and the incidence of infection. One characteristic of COVID-19 is that symptoms, severity, and mortality vary with age. When vaccination is limited, an age-based vaccination prioritization strategy should be used to reduce the incidence of epidemics and public mortality. Choi et al. (2021) developed an age-structured model to describe the dynamics of COVID-19 transmission, including vaccination. Using models and actual epidemiological data in Korea, infection probabilities were assessed for each age group under different levels of social distancing in Korea. and examine effective age-based vaccination strategies to reduce the number of confirmed cases and deaths from COVID-19. The study found that in areas with low levels of social distancing, vaccination was prioritized for the age group with the highest transmission rates to largely reduce the incidence. But in areas where social distancing is high, vaccination is prioritized for older age groups to reduce infection and reduce mortality. Vaccination for the elderly is the best strategy in all situations of social distancing that affects vaccine allocation and its effectiveness on reducing disease incidence and mortality.

In Italy, an automated decision-making system (ADM) has been introduced to determine the priorities of COVID-19 vaccination both by the Italian Federation of General Practitioners and by regional authorities in Lombardy, Valle d'Aosta, and Piedmont. The ADM system analyzed to find the right solution and found that all systems share a common ground. That is to maximize the efficiency of vaccine distribution. While the priority was given to the elderly and those at high risk due to co-morbidities, in which patients had more than one health condition and individualized overall medical history. Italy is not the only country where vaccine prioritization algorithms have been adopted, for example the "QCovid" algorithm deployed in the UK. This has led to inflated risk score claims due to missing data and general doubts about its reliability in the scientific community. Similar issues have been highlighted in Bavaria, Germany and in the United States.

In the United States, a dynamic model of transmission has been created using a parametric segmented model to capture current understanding of the epidemiological nature of COVID-19. This includes the main source of group differences. (sensitivity, severity, and contagion rate). It examines three alternative policy objectives: reducing infection, age at death, or mortality. A dynamic strategy model that evolves with the population's epidemiological status has been modeled, finding that this time resilience is critical to public health goals. Typically older key practitioners are targeted first. However, it depends on the purpose. Younger employees are prioritized for spreading control or older workers for direct mortality control. When the goal is to reduce deaths versus non-target approaches, prioritizing prevents deaths between 20,000 (when non-drug interventions are severe) and 300,000 (when non-drug interventions are weak). Study showed that proper prioritization is susceptible to a number of factors, especially the effectiveness and supply of vaccines, transmission rates, and the size of initial infections.

This research aims to study the distribution of the COVID-19 vaccine in Thailand by analyzing the spatial correlation of the COVID-19 vaccine distribution and the coefficient showing the spread of COVID-19. using geospatial program to display the results as a spatial description on the choropleth map

2. METHODOLOGY

2.1 Data Management

This research was based on information from the website "The researcher" located at <https://covid-19.researcherth.co>. This website collects domestic vaccination data in daily cumulative reports since the first vaccination date. The report began on March 24, 2021, showing cumulative data by province. The data analyzed herein is the cumulative number of people vaccinated as of July 18, 2021 by categorizing the vaccinated recipients into 2 groups: the elderly and the general public, as shown in Figure 1 below.

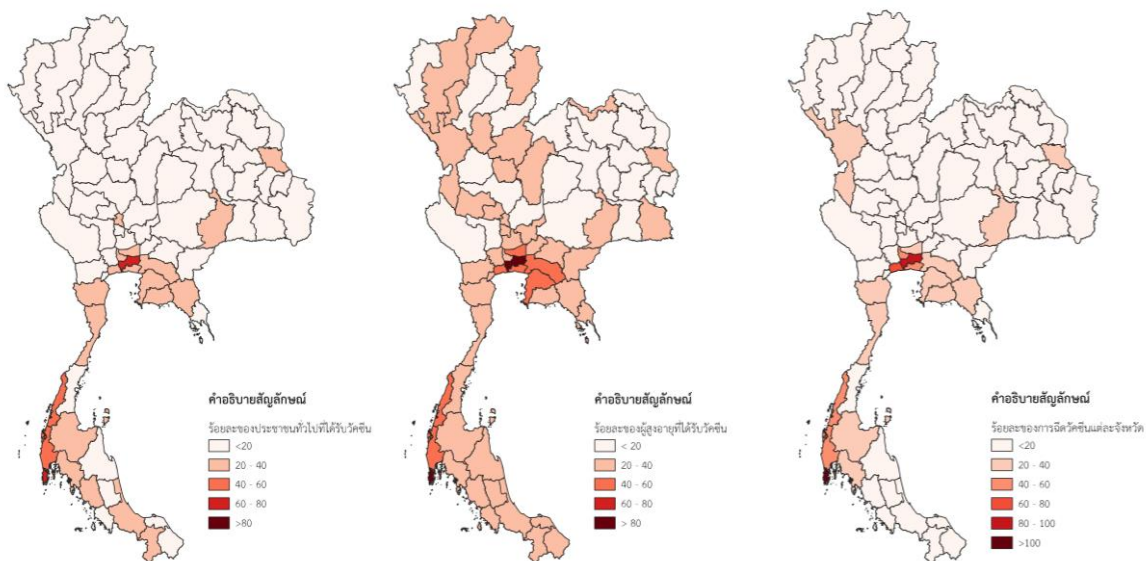


Figure 1. Vaccine distribution in different areas of Thailand

2.2 Method of Data Analysis

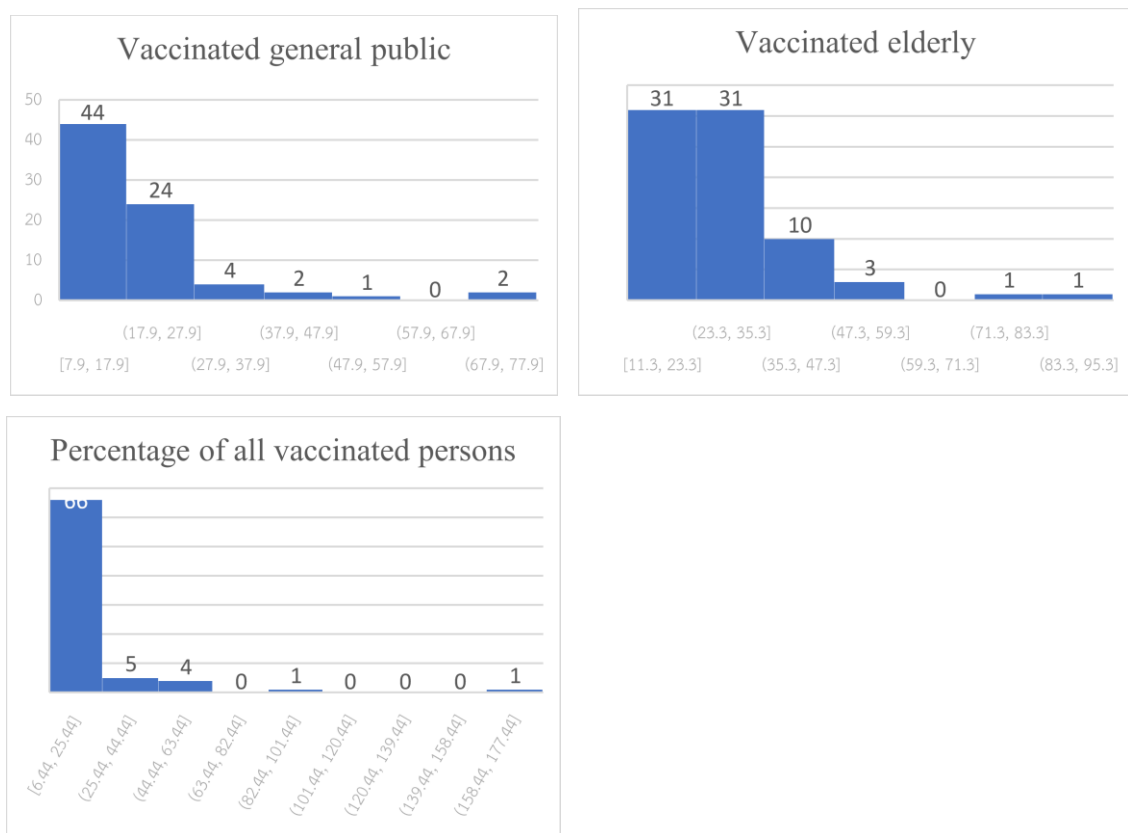
A spatial analysis of data to show the distribution of vaccine allocations to the entire population at risk, comprising the elderly and the general public, across all 77 provinces of the country. Descriptive statistics were used in the analysis to preliminarily show the distribution of the data. Geographically weighted regression analysis was performed on a geospatial program with Explanatory Variables and Dependent Variables by province in 77 provinces.

3. RESULT AND DISCUSSION

On average, people in each province of Thailand are vaccinated on average 18.95% of the total population. The elderly were vaccinated with an average of 27.74 percent of the entire provincial population. And the general public receives vaccination, an average of 19.21 percent of the population of the whole province with a standard deviation of 22.56, 14.17 and 12.29, respectively. The provinces with the highest proportion of vaccinated populations were Phuket and Bangkok, accounting for 174.4 percent and 87.79, while Kalasin Province Only 6.44 percent of people were vaccinated.

Table 1 Vaccine Distribution in Thailand

	General Public	Elderly	Percentage of all vaccinated persons
AVG.	19.21428571	27.74415584	18.95
STD.	12.28845965	14.17100908	22.55581406
MAXIMUM	74.1	91.2	174.40
MINIMUM	7.9	11.3	6.44
MEDIAN	15.3	25.6	12.57
MODE	11.4	33.6	#N/A
SKEWNESS	2.79923333	2.080428963	4.968450401

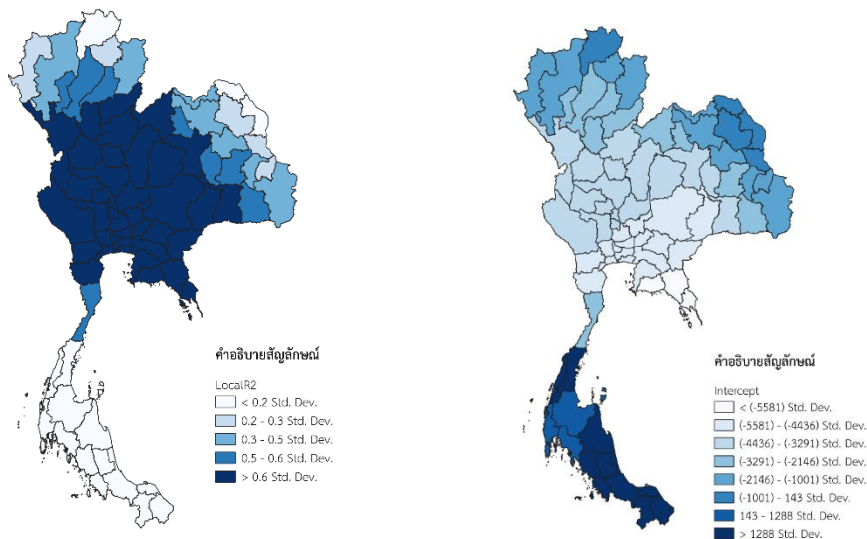
**Figure 2** Vaccine distribution in Thailand

From the descriptive statistics analysis, the results are shown in Table 1 and Figure 2. It was found that skewness = 2.80, 2.08 and 4.97, respectively. In most provinces, more than 60 provinces have been allocated vaccinations to the people in the range of not more than 35%.

From the results of Geographically Weighted Regression showing the relationship of vaccination allocation in each province was found that the R² value of 0.79 indicates that the vaccination allocation in Thailand is consistent with the area with cumulative infection among the people in that province.

Table 3. The spatial relationship model parameters.

Bandwidth	2.37
ResidualSquares	855623342.8
EffectiveNumber	11.26
Sigma	3607.67
AICc	1489.86
R2	0.79
R2Adjusted	0.75

**Figure 3.** A map showing the spatial distribution of Explanatory variables' Influence towards Dependent variable through the two parameters: local coefficients and local intercepts.

The results of this GWR analysis were used to create a map showing the correlation coefficient of each province as shown in Figure 3. It was found that the central region, the eastern region, and some parts of the northeastern region, and the northern region was allocated an amount of vaccine that was clearly consistent with the cumulative number of infections.

4. CONCLUSION

From the descriptive statistic and GWR analysis, the allocation of the COVID-19 vaccine in Thailand spreads across areas with a reasonable cumulative number of cases, with a correlation coefficient of 79.03%. The central region in the provinces surrounding Bangkok and the eastern region received relatively large vaccination allocations compared to the remote areas.

5. REFERENCES

- Buckner, Jack H., Chowell, Gerardo., and Springborn, Michael R. (2020). “Dynamic Prioritization of COVID-19 Vaccines When Social Distancing is Limited for Essential Workers.” *medRxiv*. (December). doi: 10.1101/2020.09.22.20199174
- Chiusi, Fabio. (2021). “COVID-19 vaccine prioritization algorithms in parts of Italy.” *Algorithm Watch*. Available on <https://algorithmwatch.org/en/italy-covid19-vaccine-prioritization-algorithms/>.
- Choi, Yongin., Kim, James Slghee., Kim, Jung Eun., Choi, Heejin., and Lee, Chang Hyeong. (2021). “Vaccination Prioritization Strategies for COVID-19 in Korea: A Mathematical Modeling Approach.” *Int J Environ Res Public Health.* 18(8) (April). doi: 10.3390/ijerph18084240.
- Yang, Juan., Zheng, Wen., Shi, Huilin., Yan, Xuemei., Dong, Kaige., You, Qian., Zhong, Guangjie., Gong, Hui., Chen, Zhiyuan., Jit, Mark., Viboud, Cecile., Ajelli, Marco., and Yu, Hongjie. (2021). “Who should be prioritized for COVID-19 vaccination in China? A descriptive study.” *BMC Medicine.* 19(45) (February). doi.org/10.1186/s12916-021-01923-8

DEVELOPMENT OF GEO-IOT IN EMERGENCY MEDICAL CARE AND SERVICES PLANNING USING U-BLOX GPS BASED ON WEB GIS

**Rhutairat Hataitara¹, Kampart Piyathamrongchai¹, Venkatesh Raghavan²
and Sittichai Choosumrong^{1*}**

¹Department of Natural Resources and Environment, Faculty of Agriculture Nature Resources and Environment, Naresuan University, Phitsanulok Province, Thailand 65000

² Urban Engineering Course , Graduate School of Engineering, Osaka City University, Sugimoto, Sumiyoshi-ku, Osaka, Zip-code: 558 -8585

* Corresponding author: E-mail: sittichaic@nu.ac.th.

ABSTRACT

Emergency Medical Care and Services Planning (EMCSp) System has been developed to help and reduce the amount of injury because of the delay in transporting the patient. Due to the original system used by the National Institute For Emergency Medicine to call the 1669 hotline and 1699 mobile application, residents or patients had to have a phone or smartphone to report an emergency and current location from smartphone.

The proposed system has been developed based on the Internet of Things (IoT) technology, Global Positioning System (GPS) and Web Map Application. Thus, in the development of this system, we have designed and developed an IoT system for notification of an incident instead of using phone call or mobile application. An IoT based application was developed, which can track down the position in real-time. The developed system is designed for user friendly equipment by simple one button service. Patient can simply press the button on the sensor device to report and send GPS location of emergency events. The location and other information will be displayed on the Web Map Application. EMS staff can easily know where patients are and make a plan to go to the patient location for rescuing. The main target of users for this system is aging people and disabled people who might not familiar with technology on mobile applications.

1. INTRODUCTION

The change in population structure has brought many countries into an aging society. Thailand Found the proportion of the elderly population in 2020, aged 60 years and over, more than 12 million people, or about 18% of the total population, and in 2021 will increase to 20% of the total population. Making Thai society into an aging society. Under the aging society, health issues are important to the health system as the elderly are a group of ailments. In which 95% of Thai elderly people have illnesses or health problems, as follows: hypertension 41%, diabetes 18%, disabled 6%, and bedridden 1% (Department of Health, 2013). Illness and chronic disease are also the leading causes of limitation or loss of the elderly's ability to care for themselves. Leading to the occurrence of a condition elderly disability. As a result, the elderly have higher dependency needs. Currently, there are many channels of communication for EMS service incidents, for example, by telephone via number 1669, using the ThaiEMS 1669 application, Mobile Application 1669, and Application TTRS Video (call center for hearing and speech impaired), etc. The recipient of the incident is the Information Gathering and Dispatch center

(IGDc) in each Province. The IGDc operates 24 hours. The staff at IGDc use GPS navigation from IGDc location as start point to go to location of patient based on the caller.

However, using telephones to report the location of an accident by the elderly might be difficult to explain and take a long time to communicate to locate the location. The cause of the whistleblower may not be able to control his or her consciousness. Telling the location of the accident point is not completely correct where the driver chooses a route and that delays reaching the patient's location. Due to this problem, patients might get rescue late and timely medical treatment. May cause death or impairment of organs affecting the inability to function normally. This can also make a mild injury or illness worsen. Therefore, these problems are important to find solutions for the elderly population to have easy and convenient access to EMS services. The use of Geographic Information Systems (GIS), Global Positional System (GPS) and Internet of Things (IoT) technology can be used to find the location of an accident.

IoT is an arrangement of interrelated computing gadgets, mechanical and digital machines, objects, animals or individuals that are given one kind of an identifier and the capacity to exchange information over a system without requiring human-to-human or human-to-PC communication. IoT is a new concept that has evolved from the convergence of wireless technologies. Wireless communication is the transfer of information or signal between two or more points that are not connected by an electrical conductor. IoT devices equipped with Wi-Fi allow machine-to-machine communication. The sensor and actuator can be set up in different places but they are working together over an internet network. Message Queuing Telemetry Transport (MQTT) is a messaging protocol designed for lightweight M2M communications and resource-constrained wireless connectivity. Features in MQTT such as an asynchronous communication model, low memory footprint for low network bandwidth applications, support for network disruptions with QOS features and low power consumption are key enablers for a reliable and low-latency two-way communication using wireless cellular Internet connectivity.

This research aims to develop a Smart Emergency Notification System with IoT (SENS-IoT) based sensors that display real-time location information of the patient's home. The study was created using the U-blox GPS module as a home locator. The location coordinates are processed by NodeMCU and alerts via MQTT and Line Notify are sent to the operator's mobile phone. The information will be displayed as a map with information of the home location via web application and mobile application.

2. METHODOLOGY

2.1 System design

Development of a SENS-IoT with specified location sensors to access emergency medical services with U-Blox GPS and Web GIS application. The working design is, when the patient presses a button, NodeMCU ESP8266 will send the location and information in JSON format via

MQTT. The GPS location of the patient's house will send and take into account to the central database. GeoServer working as Web Map Service (WMS) displayed point data on the web application and mobile application. At the same time, will send an alarm to Line Notify of the officer's mobile phone. When staff got alarm information, he/they can easily find the location on Web Map Application. Patients and plans to go to the patient facility to save lives.

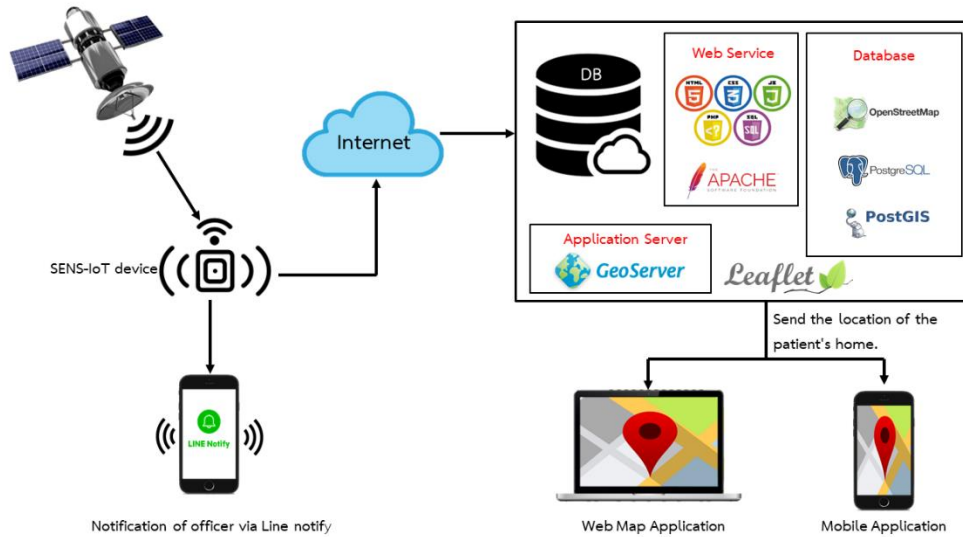


Figure 1. Research Conceptual Framework.

3. SYSTEM DEVELOPMENT

In this research, the developers have used GPS U-blox 6m to determine the location of the area and use it. A NodeMCU ESP8266 microcontroller to connect to the Internet and send location data from U-blox to LINE Notify , MQTT servers and Database Server.

3.1 u-blox 6 GPS Modules

The NEO-6 module series is a family of stand-alone GPS receivers featuring the high performance u-blox 6 positioning engine. These flexible and cost effective receivers offer numerous connectivity options in a miniature 16 x 12.2 x 2.4 mm package. Their compact architecture and power and memory options make NEO-6 modules ideal for battery operated mobile devices with very strict cost and space constraints.

The 50-channel u-blox 6 positioning engine boasts a Time-To-First-Fix (TTFF) of under 1 second. The dedicated acquisition engine, with 2 million correlators, is capable of massive parallel time/frequency space searches,enabling it to find satellites instantly. Innovative design and technology suppresses jamming sources and mitigates multipath effects, giving NEO-6 GPS receivers excellent navigation performance even in the most challenging environments.



Figure 2. u-blox 6 GPS Modules.

3.2 NodeMCU

The NodeMCU is an open-source firmware and development kit that helps you to prototype your IoT product with few Lua script lines. The Development Kit, based on ESP8266, integrates GPIO, PWM, IIC, 1-Wire and ADC all in one board. The ESP8266 is the name of a micro controller designed by Espressif Systems. The ESP8266 itself is a self-contained WiFi networking solution offering as a bridge from existing microcontroller to WiFi and is also capable of running self-contained applications. This module comes with a built in USB connector and a rich assortment of pin-outs. With a micro USB cable, you can connect a NodeMCU device to your laptop and flash it without any trouble, just like Arduino. It is also immediately breadboard friendly. The MQTT library has been ported to the ESP8266 SoC platform and committed to the NodeMCU project. After this, the NodeMCU was able to support the MQTT IoT protocol using Lua to access the MQTT broker.

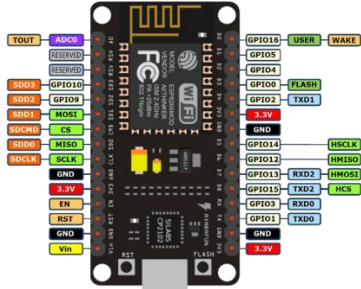


Figure 3. NodeMCU Pinout.

3.3 Emergency button for the elderly with NodeMCU and GPS

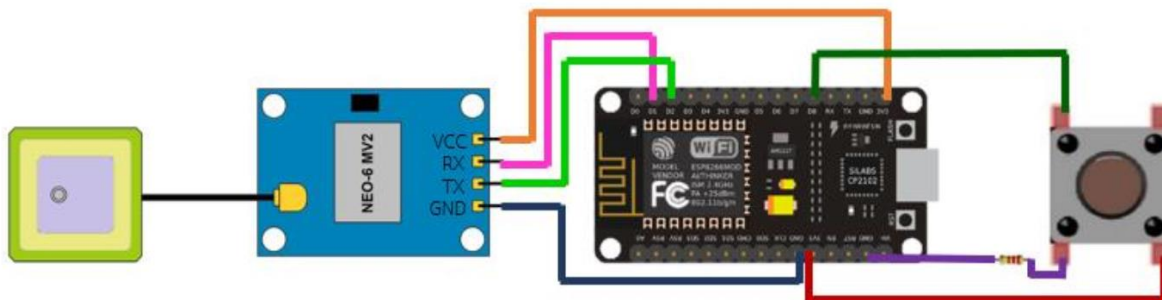


Figure 4. Emergency button for the elderly with NodeMCU and GPS.

Connected the VCC and GND of the GPS module to the 3.3v and GND pins on the NodeMCU board, and connected the Tx of the GPS module to the D2 of the NodeMCU and Rx of the GPS module to D1 of the NodeMCU board. Connected one push switches by Connected the VCC and GND on the NodeMCU board and pin D8 of the NodeMCU board as connected button for press the emergency button.



Figure 5. Prototype System Circuit.

3.4 MQTT

MQTT is a machine-to-machine / “Internet of Things” publisher-subscriber based connectivity protocol. It was designed as an extremely lightweight publish/subscribe messaging transport. It is useful for connections with remote locations where a small code footprint is required and network bandwidth is extremely expensive. Message Queueing Telemetry Transport is an ISO standard publish-subscribe based messaging protocol. It works on top of the TCP/IP protocol. The publish-subscribe based messaging pattern requires a message broker.

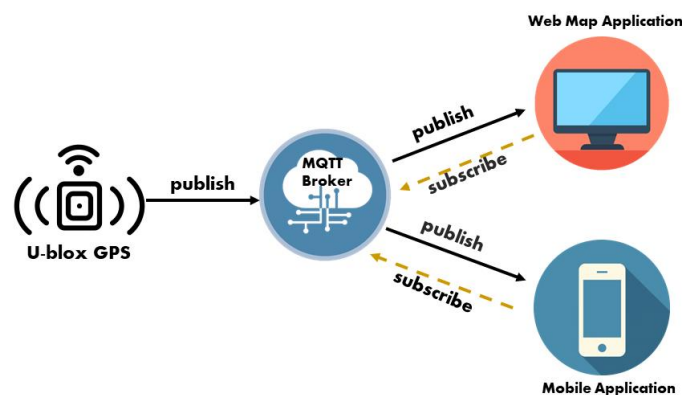


Figure 6. Message queuing telemetry transport protocol model.

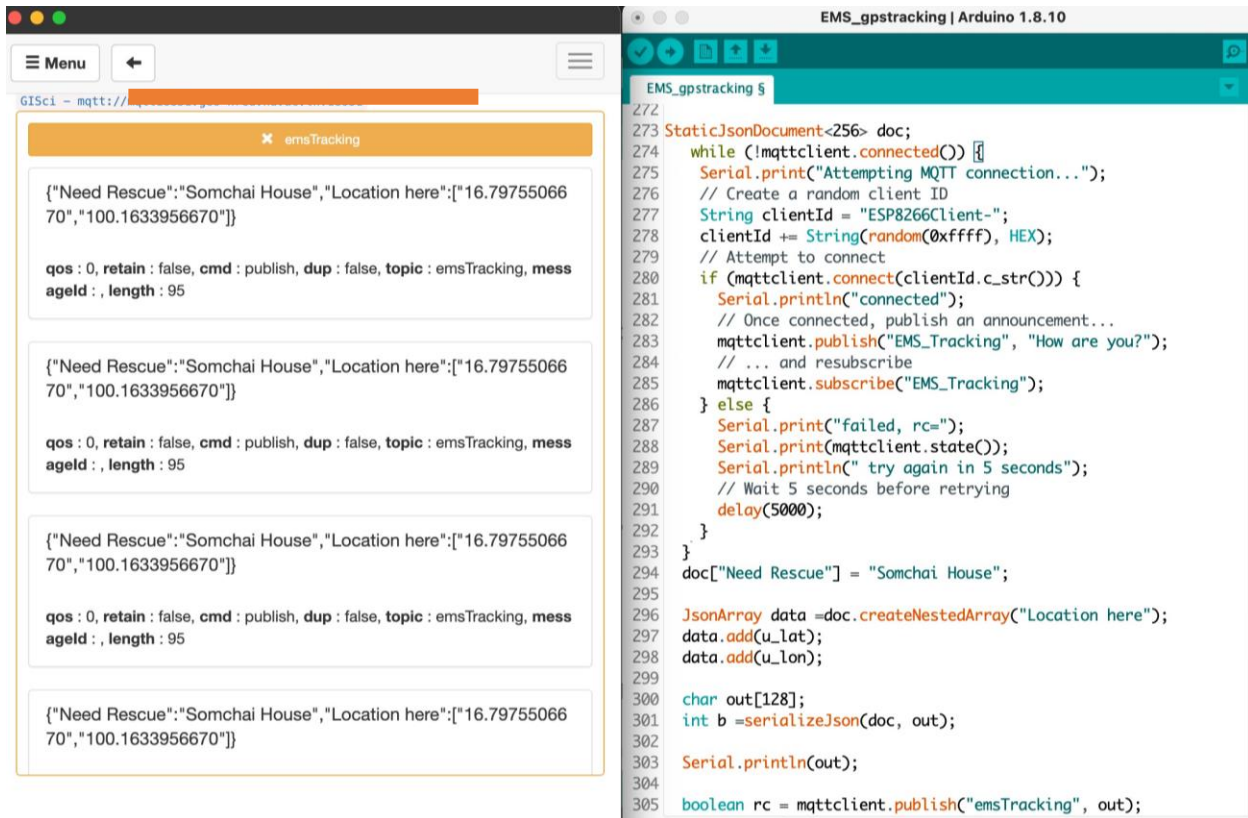


Figure 7. Data Publish and Subscribe.

4. RESULE

When patient press the button on the device, the location will send an alarm message to LINE notify (Figure 8) and send point data to spatial database in the server. Then, the point data from spatial database will show on Web Map Application (Figure 9).

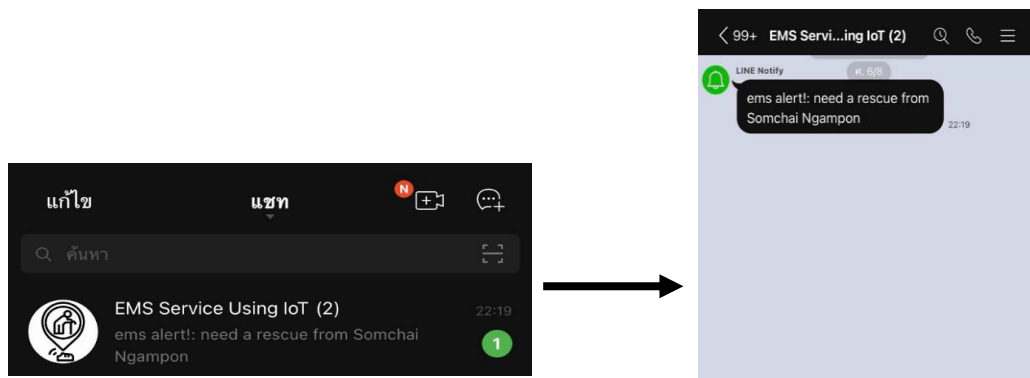


Figure 8. Message alert through LINE notify.

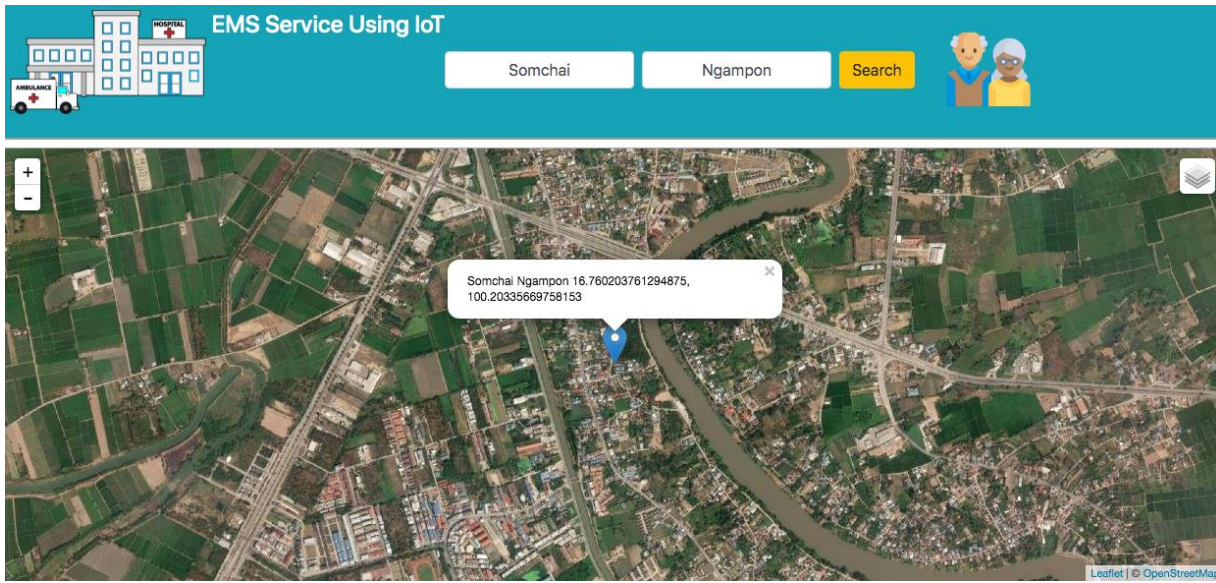


Figure 9 . Web Map Interface to show the patient's location from push the GPS device.

5. DISCUSSION AND CONCLUSION

- Based on the results of the survey, the system using the U-blox neo 6m GPS module and NodeMCU can transmit the location of the patient's home effectively.
- The accuracy of the GPS module was around 10m outdoor and 25m indoor. These figures can be dramatically reduced by using a GPS module with a higher accuracy.
- Connecting the neo6 m GPS module to a satellite requires a considerable time of about 5 minutes, especially if the GPS module is in a confined space.
- IoT is a new internet application which leads to an era of smart technology where there exists thing-thing communication rather than human-human communication. Through IoT, each and every object in this world can be identified, connected and take decisions independently. It has taken its birth from mobile computing and ubiquitous computing. Technologies such as RFID, wireless sensor networks and embedded systems play a vital role in forming an IoT application. It is used in many applications in healthcare, agriculture, smart buildings, transportations etc.
- This work can be developed in conjunction with location search system and navigation systems. To help patients with pgRouting /OpenRouteService.

6. REFERENCE

Bergenheim, W., Sarjakoski, L. and Sarjakoski, T., 2009. A Web Processing Service for GRASS GIS to Provide on-line Generalisation. 12th AGILE International Conference on Geographic Information Science 2009, Leibniz University Hannover, Germany.

- Choosumrong, S., Raghavan, V., Delucchi, L., Yoshida, D. & Vinayaraj, P. (2014). Implementation of Dynamic Routing as a Web Service for Emergency Routing Decision Planning. International Journal of Geoinformatics, 10(2), 13-20.
- Choosumrong, S., Raghavan, V., Jeefoo, P. & Vadaddi, N. (2016). Development of Service Oriented Web-GIS Platform for monitoring and evaluation using FOSS4G. International Journal of Geoinformatics, 12(3), 67-76.
- Choosumrong, S., Raghavan, V., Jeefoo, P. and Vadaddi, N., 2016. Development of Service Oriented Web-GIS Platform for Monitoring and Evaluation using FOSS4G. International Journal of Geoinformatics, Vol. 12, No.3,67-77.
- Devaraju, A., Jirka, S., Kunkel, R. and Sorg, J., 2015. Q-SOS- A Sensor Observation Service for Accessing Quality Descriptions of Environmental Data. ISPRS International Journal of Geo- Information, No.4,1346-1365.

GIS BASED ANALYSIS FOR EMERGENCY RELIEF AND RESCUE AND DISASTER MITIGATION

Chamnan Kumsap¹ Teeranai Srithamarong² and Suriyawate Boonthalarath³

Defence Technology Institute
47/433 Moo 3, Ban Mai, Pak Kret, Nonthaburi 11120, Thailand

¹Email: chamnan.k@dti.or.th

²Email: teeranai.s@ dti.or.th

³Email: suriyawate.b@ dti.or.th

ABSTRACT

This research was aimed to contribute GIS capabilities to military emergency relief and rescue and disaster mitigation that require the detailed analysis of an area and environment prior to performing a mission. At an ultimate goal of maintaining faulty mechanic equipment that consists of backhoes and tailgate trucks for the Mobile Development Unit 31 of the Armed Forces Development Command to prevent and solve public and disasters problems in Pua district of Nan province, the objective was to use GIS for a route selection mission of Mobile Development Unit 31 in the mission of disaster prevention and solution. A sample road network database covering Pua district was prepared and tested for the simulation of an optimal route selection based on an actual landslide incident in the district reported by the news media. The Mobile Development Unit 31 was set as the starting point of the routing while the landslide location was set as the target point. Field survey along the selected route was presented as proof of concept. More factors dictating route selection were recommended for a more accurate route selection.

1. INTRODUCTION

The Armed Forces Development Command is a military agency under the Ministry of Defense. It is an ally member of the Department of Disaster Prevention and Mitigation under the Ministry of Interior. It has an important duty in preventing and solving public problems and disasters. Its direct report units are scattered throughout Thailand to reach the problems of the people in every corner of the country. Therefore, they are the military unit that is faced with a wide variety of public services and disasters according to the area of responsibility. Units in the northern part are located in mountainous region with high mountain terrain, they often encounter landslides. Most of the equipment under responsibility is mechanical such as backhoes or tailgate trucks, etc. Most of them have been in use for more than 10 years and therefore have deteriorated over time. Mobile Development Units have also attempted to maintain their conditions to help the people. Therefore, if principles and technology can be applied to enable the units to continue to operate the faulty equipment, the units will perform the disaster prevention and mitigation mission in the best interest of the people in the area.

This research project is a collaboration between Defence Technology Institute and Mobile Development Unit 31 or MDU31 of Armed Forces Development Command. The goal is to use Geographic Information Systems (GIS) to transform geospatial data into a tool for emergency relief and rescue and disaster mitigation. The database will be used for disaster management which requires the detailed analysis of the area and environment prior to performing the mission. This will contribute to the maintenance of MDU31's faulty mechanic equipment in order for the MDU31 to prevent and solve public and disasters problems in the study area of Pua district in Nan province. The objective is to use GIS to support the MDU31 in the mission of disaster prevention and solution in response to landslides in the study area by optimal route selection for the transport of the faulty mechanical equipment. The technology to maintain the state of mechanic equipment will be introduced to the units and the principles and processes will be tested in the actual problem area.

2. GIS IN DISASTER MANAGEMENT

Coppock (1995) conducted a brief survey of the diversity of such hazards and made an attempt to review what had been written in the past, a task made difficult by the wide range of interests involved. The review showed that, within the GIS field proper, relatively little had been published and that, within the disciplines studying natural hazards, few papers described operational systems that were applied routinely, four examples of which were summarized. van Westen (2000) discussed that the collection and management of spatial data from remote sensing and GIS were regarded proper to handle a large amount of data and had demonstrated their usefulness in disaster prevention, preparedness and relief. The objectivity and reproducibility of assessment were considerably improved by sequential imagery interpretation with quantitative description of the factors and well defined analytical procedures and decision rules, which were applied to come to the hazard assessment. In response to the previous discussion, Johnson (2000) claimed that GIS was the foundation for emergency management. As soon as potential emergency situations were identified, mitigation needs could be determined and prioritized. Utilizing existing databases linked to geographic features in GIS made quick displays of values at risk possible. Thus, the closest and quickest response units could be selected, routed, and dispatched to an emergency once the location was known. The review of Tomaszewski et al. (2015) provided interdisciplinary literature from a variety of spatially-oriented disaster management fields and demonstrated progress in various aspects of GIS for disaster response. They further concluded that a GIS for disaster response research agenda and provided a list of resources for researchers new to GIS and spatial perspectives for disaster management research.

3. GIS BASED DISASTER MITIGATION CONCEPT

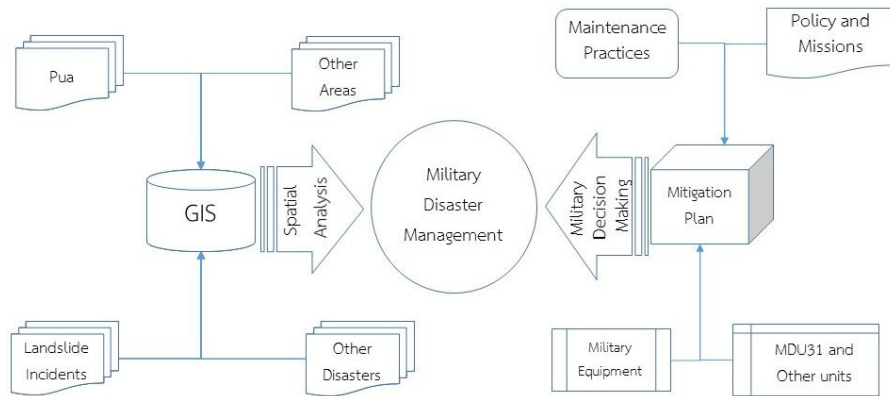


Figure 1. Concept of GIS based analysis for disaster mitigation.

The engagement of GIS and disaster mitigation is proposed for military disaster management as shown on Figure 1. All geo-referenced data is handled in GIS with emphasis on landslide data and previous records of the incidents. This GIS systematic approach can be applied to other areas with frequently incurred disasters. The spatial analysis capability of GIS plays a major role on the GIS side of the management while a military decision making alternatives is the output result of disaster mitigation component. Policy and missions will drive the mitigation plan while regions under responsibility contributes how decision is made and equipment allocated.

4. RESEARCH METHODOLOGY

The research methodology proposed in this project is illustrated in Figure 2. Four stages are followed to implement GIS based disaster mitigation that returns optimal routes to dispatch military equipment from MDU31 to landslide sites.

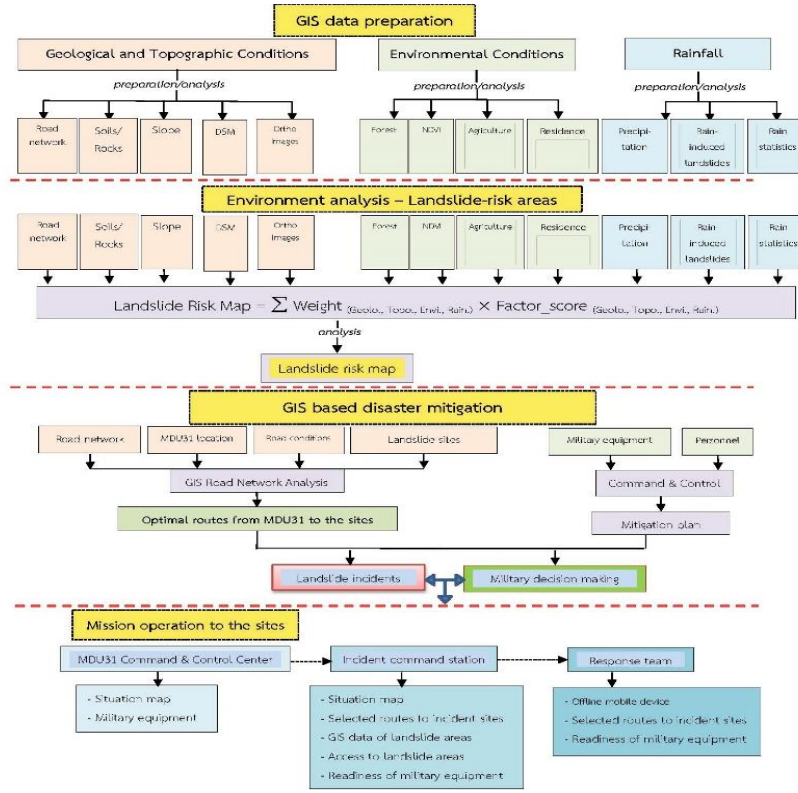


Figure 2. Use of GIS based disaster mitigation to access landslide sites.

4.1 GIS data preparation

GIS data preparation was to ensure essential geo-spatial layers are ready for further analysis processes. Four types of data were central to the spatial analysis for a landslide risk map. Geological and topological conditions were integral in nature while environmental ones needed further GIS data manipulation before the analysis. Rainfalls were largely regarded as dynamic especially precipitation and rain-induced landslides. Rain statistics were influential factors to the magnitude of rainfall to landslide incidents.

4.2 Environment analysis for landslide-risk areas

The analysis of environments for landslide – risk areas to produce a landslide – risk map took the summation of weighted 4 factors. GIS data layers describing geological and topological conditions each carry a 30% combined weight percentage while those containing environmental and rain conditions were each carry a 20% combined weight percentage. The result map revealed those patches prone to landslides. Though a road layer was weighted in the weighting process, it next provided accessibility to the mapped landslide sites.

4.3 Mitigation command and control

Prior to implementing this stage, a road network needed to complete connecting edges and nodes so that the network analysis could be reiterated for starting and end points. Road attributes describing surface, lane number, width intersections etc. were conditions that later

determined whether military vehicles and equipment on which they could be transported from the analyzed starting to end points. Records of vehicle maintenance and regular checks were data for command and control of the vehicles for the mission (Figure 3 left) in which the traffic was completely blocked by the landslide (Figure 3 right).



Figure 3. Maintenance practices (left) before mission in the site (right).

4.4 Onsite mission operation

This three cascaded operation of figure 2 includes command and control from the MDU31 center, holding a big picture situation map and complete military equipment database, incident station commanding the mission upon the selected routes to the sites with an offline copy of dataset from the center, and the team responding to the incident with mobile devices to track the selected routes and handling the military equipment at the landslide sites.

5. CASE STUDY

In order to achieve the objective of this research article, case studies of a landslide incident retrieved from online media was showcased, road network data was analyzed for the route selection mission of MDU31 in disaster prevention and solution. The following describes the case study extracted from the lowest portion of Figure 2 in response to the objective.

5.1 Landslide-prone study area

As part of the MDU31 landslide disaster management project, Pradabmook and Laosuwan (2021) reported the research output that Nan Province had areas prone to soil erosion of about 3,685.206 km² or equal to 57.73% due to the topology characterized by forest and mountain for almost 75 %. Where agricultural activities were found to be planted on the mountain with steepness of more than 5% in a total area of 6,975.325 km² or equal to 60.80%.

5.2 GIS road network

Yi et al (2012) calculated the shortest evacuation routes between affected points and shelters or Origin - Destination ranking model where considerable roads and land features and other environmental factors when the closest facilities and routes were selected, selection criteria and approach methods could be suggested for future events. Likewise, in this research the network of roads was formed by the connectivity of arc segments constituting an individual road. Then, road network database consisted of Edge to connect components such as sections or intersections, Junction to connect arcs, and Turn to define directions. Connectivity analysis came in two types i.e. group connectivity and road connectivity within the same group. The latter connectivity connected roads of the same group in two types namely Endpoint connectivity for simulating object crossover and Vertex connectivity for dividing a line segment into sub-segments. A snapshot of Pua road network dataset is shown on Figure 4.

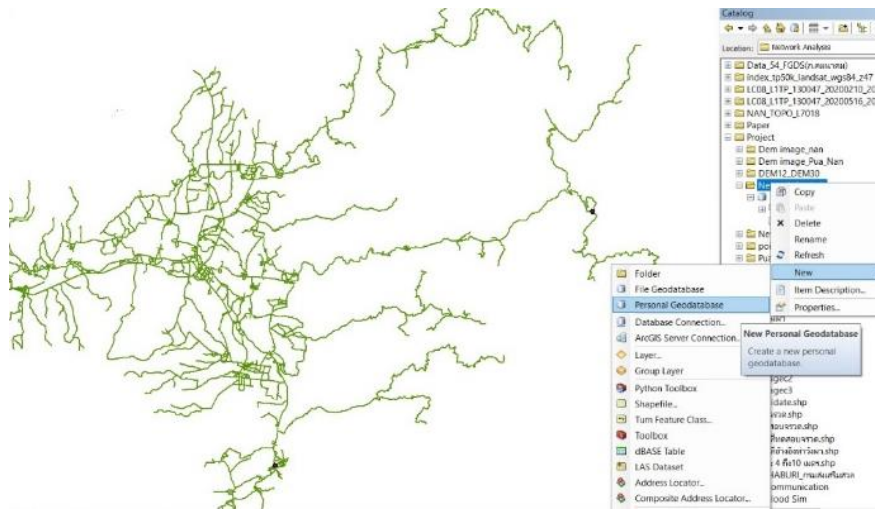


Figure 4. Pua district road network dataset.

5.3 Actual landslide incident

According to Siamrath online (at <https://siamrath.co.th/n/97454#>) on 17 August 2019 at 16:34 Nan province local time, there were heavy rains day and night and 60 villages of Nan province were at risk of flooding and landslide blocking the road linking Pua district to Bo Kluea district. Along the road from Pua to Bo Kluea at the front gate to Doi Phu Kha National Park, the road was blocked by sliding mountain.

6. ROUTE SELECTION AND VALIDATION

6.1 Route selection

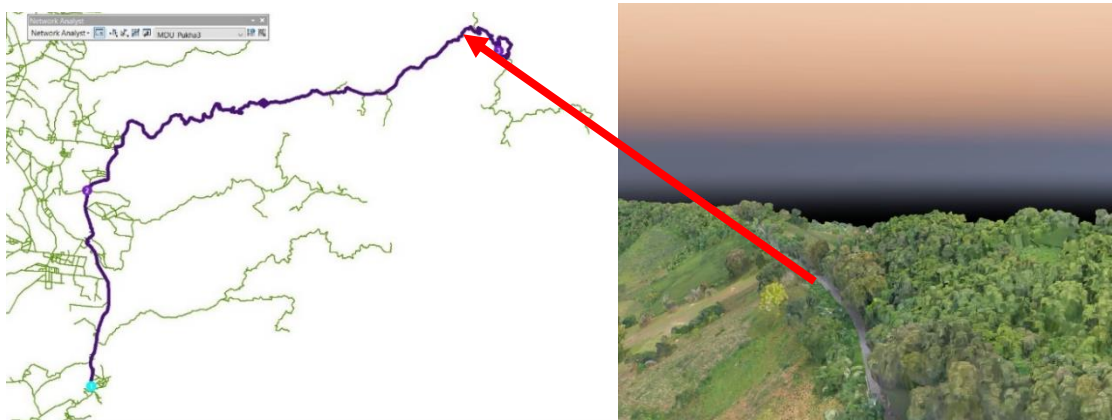


Figure 5. Selected route and simulation for validation.

The road network analysis for route selection returned the route result as shown on Figure 5 left. The starting point of the route began at MDU31 (see the lower left), traversed along National Highway No. 1080, National Highway No. 1258 and Nan Rural road No. 2047 to end at the landslide incident area as reported online by the media. The total distance was measured at 30.3927 km.

6.2 Selected route validation

Figure 5 right was a snapshot extracted from the flythrough simulation of the selected route generated from the 5 cm. resolution mosaic of orthoimagery being draped on the DSM of the same resolution. An arrow is to provide a visual link from the snapshot to the selected route resulted from the road network analysis. Road surface was assumed to be concrete with the sufficient road width to accommodate military vehicle to transport to the site. Road characteristics input to GIS attributes were on the way in the project. Site ground survey could have best validated the selection but the COVID-19 pandemic made it impossible.

7. RESULT AND DISCUSSION

The route of 30.3927 km. distance was selected from the dataset to demonstrate the integrated GIS and military decision making for the MDU31 to access the actual landslide site. The route was simulated to illustrate the road conditions sufficient for the transport of MDU31 vehicles and equipment to the blocked road of the landslide site. However, the complete use of GIS based analysis for emergency relief and rescue and disaster management for optimal access to landslide sites was subject to further studies of DTI ongoing project for MDU31. Road conditions were recommended for the more accurate route selection. More surveys to update the road dataset were under development as well as integral military decision making of MDU31 for the disaster management. Other landslide sites as reported by the press will be input to the analysis for solutions to test and evaluation of the dataset for road network analysis.

8. REFERENCES

- Coppock, J.T., 1995. GIS and Natural Hazards: An overview from a Gis Perspective. In: Carrara A., Guzzetti F. (eds) Geographical Information Systems in Assessing Natural Hazards. Advances in Natural and Technological Hazards Research, vol 5. Springer, Dordrecht. https://doi.org/10.1007/978-94-015-8404-3_2.
- Johnson, R., 2000. GIS Technology for Disasters and Emergency Management. An ESRI White Paper - May 2000. Redlands, USA. 12p.
- Kumsap, C., 2018. Concept of Mobile C4ISR System for Disaster Relief. *National Defense Studies Institute Journal*, January – April 2018, Vol 9 No.1, pp. 7 – 19.
- Kumsap, C., Witheetrirong, Y., and Pratoomma, P., 2016. DTI's modeling and simulation initiative project to strive for the HADR mission of Thailand's ministry of defence. *Proceedings of the 6th International Defence and Homeland Security Simulation Workshop*, September 26-28 2016, Cyprus, 44-51.
- Pradabmook, P. and Laosuwan, T. 2021. The Integration of Geo-informatics Technology with Universal Soil Loss Equation to Analyze Areas Prone to Soil Erosion in Nan Province. *ARPJ Journal of Engineering and Applied Sciences*, Vol. 16 No. 8, 823-830.
- Robert, O. P., Kumsap, C. and Janpengpen, A., 2018. Simulation of counter drugs operations based on geospatial technology for use in a military training simulator. *International Journal of Simulation and Process Modelling*, Nol.13 No.4, pp. 402 - 415.
- Tomaszewski, B., Judex, M., Szarzynski, J., Radestock, C. and Wirkus, L., 2015. Geographic Information Systems for Disaster Response: A Review. *Journal of Homeland Security and Emergency Management*. June 2015. DOI: 10.1515/jhsem-2014-0082.
- van Westen, C.J., 2000. Remote Sensing for Natural Disaster Management. *International Archives of Photogrammetry and Remote Sensing*. Vol. XXXIII, Part B7. pp. 1609 - 1617.
- Yi, C., Park, R. S., Murao, O., and Okamoto, E., 2012. Emergency management: Building an O-D ranking model using GIS network analysis. *Journal of Disaster Research*, Vol.7 No.6, 793-802.

The spread of COVID-19 in the context of regional geography

Jiranya Duangfoo¹ and Pathana Rachavong²

¹ Geographic Information Sciences, Naresuan University

²Thailand Geographical Association, Email: pathanar@gmail.com

Email: jiranyad63@nu.ac.th

ABSTRACT

The spread of COVID-19 in the context of regional geography aims to study the spatial patterns of the global COVID-19 outbreak situation. We collect data from the World Health Organization and Worldmeter website, the data obtained is the highest cumulative infection and the date of the highest number of countries with more than 10,000 infected cases with 80 countries in total, the data was divided into 14-day intervals for the COVID-19 outbreak. In addition, the outbreak zones are divided into 6 longitude - zones and 4 latitude - zones. The descriptive statistical methods are used to analysis. We discover that it was spread from the early Eastern Hemisphere countries to the countries in the Western Hemisphere at a later time. It was also found that It has spread from tropical regions to warmer regions.

1. INTRODUCTION

Over the past few decades, there have been ongoing outbreaks of serious emerging infectious diseases, such as Severe Acute Respiratory Syndrome (SARS), which have spread over the course of the year 2002-2003. SARS began to spread from China and spread throughout the world. More than 8,000 people have been infected with a 10% death rate. Middle East Respiratory Syndrome (MERS: Middle East Respiratory syndrome (MERS), which is an epidemic in Middle Eastern countries especially Saudi Arabia, infects more than 2,000 people, with a death rate of 35 percent.

The coronavirus disease 2019 outbreak started in China. It originated in a seafood market in Wuhan, the capital city of Hubei Province and was a hub for transportation to several major cities in the People's Republic of China. The first group of infected people were workers and customers of the Huanan Seafood Wholesale Market. Later, on March 11, 2020, the World Health Organization declared the novel coronavirus disease 2019 a pandemic. The number of deaths increased rapidly. The current mortality rate from the disease is about 5.1%. The majority of patients with severe symptoms are the elderly and people with underlying medical conditions such as heart disease and diabetes.

In the first phase of the outbreak in January There are 9,837 cases worldwide, 214 deaths, and 186 recoveries. The country with the most cumulative infections is China. There are a total of 9,692 infected people. In February, the outbreak spread to neighboring countries and the epidemic in China has accumulated 85,403 cases worldwide and 2,924 deaths. In March to April, the outbreak began to spread to Asia. Middle East and Europe, with a total of 750,890 infections worldwide in March and 36,405 deaths. During May, the outbreak hit Europe and began spreading to the Americas, with 5,934,936 infections and 367,166 deaths. Later in June, Covid-19 began to spread to South America and Russia, with 10,185,374 cases worldwide and 503,862 deaths. In July-August, many countries started having 2nd and 3rd rounds such as Japan, Australia, Singapore, and India.

The objective of this research is to study the spatial pattern of the global COVID-19 outbreak to provide spatial data on the spread of COVID-19 for infection prevention and control.

2. METHODOLOGY

2.1 Data Collection and Management

This study compiled data from the World Health Organization and the worldometers.info website. The information obtained is the cumulative number of infected people and the maximum number of infected people. In the data collection, the period during the COVID-19 outbreak was divided into 14 days of infection. In addition, the epidemic zone is divided into 6 zones according to longitude and 4 zones according to latitude. Descriptive statistics were then used to analyze the distribution and present the data by displaying the number of cases of each country broken down by time and region to reveal outbreak patterns in the context of regional geography. The results of the data analysis were then displayed on the choropleth map to show the distribution patterns of the infected in a given time period and region.

3. RESULT AND DISCUSSION

In the study of the spread of COVID-19 in the context of regional geography, it is divided into two parts: the world time zone region and the global climate region. The research results are as follows.

3.1 Spread of COVID-19 by region, world time zone

The spread of COVID-19 by region is divided into six epidemic zones, 60 degrees each, from the east end to the west.

The results showed that there were a total of 42,857,292 cumulative cases, located in zones 2-6, 14.583 percent, 7.914, 8.602, 11.232 and 0.524, respectively. All of these infections were from the outbreak between February 12 and September 30. The highest number of infected people in each zone were in zones 2 and 5, 156,000 and 147,000, respectively, as shown in Table 1.

The COVID-19 outbreak in Zone 2 has the highest number of cases, totaling 156,000. The highest-infected country is the United States, with the highest number of infections, with 78,763 as of June 24. Argentina had the highest number of cases of 12,701 cases as of September 17, and Peru had the highest number of cases of 10,143 as of August 16.

As for the COVID-19 outbreak in zone 3, the number of confirmed cases is 97,000, with Brazil having the highest number of cases at 70,869 on 29 July and Spain with the highest number of cases at 70,869. The highest number of confirmed cases was 10,854 as of March 20.

For the COVID-19 outbreak in Zone 4, the highest number of confirmed cases totaled 108,000. The country with the highest number of infections was South Africa. The highest number of cases were 13,944 as of July 24, and France had the highest number of cases of 13,498 as of September 19.

While the COVID-19 outbreak in Zone 5 has the highest number of cases totaling 147,000, the country with the highest number of infections is India. The highest number of cases were 97,859 as of September 11, China's highest number of cases was 14,108 as of February 12, and Russia's highest number of cases was 11,656 as of May 11.

And the COVID-19 outbreak in zone 6 has the highest total number of cases of 11,000. The country with the highest infection is the Philippines. The highest number of cases were 6,871 as of August 10, and Japan recorded the highest number of cases at 1,998 as of August 3.

It can be seen that the COVID-19 disease that first emerged at the Huanan Seafood Wholesale Market in Wuhan, Hubei Province, People's Republic of China since the end of 2019. There was a heavy outbreak in the province during February-March and spread to surrounding countries, most notably Japan, South Korea, Hong Kong, Singapore and Thailand, all of which are in zone 5 according to Table 1. Then, into April-May, the outbreak spread westward into zones 4 and 3, the Middle East and Europe, with the worst outbreak countries including Iran, Italy, France, Germany and the United Kingdom. And by the time of June to August, there has been another outbreak spreading to the west. by crossing the Atlantic Ocean into North and South America This is in zone 2 with the highest outbreaks in the United States, Canada, Brazil and Peru. Meanwhile, the countries in zones 5 and 4 also started a second round of outbreaks, namely the People's Republic of China, Iran, Japan and South Korea.

3.2 Spread of COVID-19 divided by global climate zone

In the study of the COVID-19 epidemic by region, the global climate zone was organized into four zones based on latitude, 32 degrees each, counting from the northernmost 84 degrees north to the southernmost 80. degrees south, which each zone has a different climate.

The results showed that a total of 42,857,292 cumulative cases were found in zones 1-4, 26.169 percent, 9.329, 2.367 and 5.103, respectively. All of these infections were from the outbreak between February 12 and September 30, with the highest number of infections in each zone were in Zones 1 and 2, with 301,000 and 134,000 cases respectively, as shown in Table 2.

The COVID-19 outbreak in Zone 1 has the highest number of cases totaling 301,000. The country with the highest number of infections is India. The highest number of cases were 97,859 as of September 11. The United States had the highest number of cases of 78,763 as of June 24. China had the highest number of cases 14,108 as of February 12. France had the highest number of cases of 13,498 as of 19. September and Spain recorded the highest number of cases of 10,854 as of March 20. The COVID-19 outbreak in Zone 2 had the highest total number of cases, totaling 134,000. The highest number of cases were 70,869 as of July 29. Colombia had the highest number of cases at 13,056 on August 19, and Peru had the highest confirmed cases of 10,143 as of August 16.

For the Covid-19 outbreak in Zone 3, the highest number of infected people totaled 36,000. The country with the highest number of infections is South Africa. The highest number of cases were 13,944 as of July 24 and Argentina. The highest number of cases were 12,701 as of September 17, while the COVID-19 outbreak in Zone 4 had the highest total number of cases totaling 50,000. The highest number of cases were 11,656 as of May 11 and the United Kingdom. The highest number of confirmed cases was 7,860 as of April 10.

It can be seen that the Covid-19 epidemic was severe in the People's Republic of China throughout February - May and has spread to surrounding countries. Importantly, India, Iran, Italy and Spain, all of which are in Zone 1, according to Table 2. Then, when entering April-May, the outbreak spread northward to Zone 4 with countries with outbreaks. hard consists of Russia and United Kingdom And when it enters August - September, it has spread to the south into South America and Australia. These are in zones 2 and 3, with outbreaks predominantly

in Brazil, Peru, Chile, South Africa and Australia. Meanwhile, countries in zone 1 have begun to have outbreaks.

Table 1. The spread of COVID-19 in the context of regional geography – by time zone.

	Cumulative number of infected people (million)	Maximum number of infected people	The date of maximum number of infected people	Time of the outbreak (14 Days)											
				1	2	3	4	5	6	7	8	9	10	11	12
Longitude 2	14.583	0.156	24 April - 17 September											(12)	(15)
Longitude 3	7.914	0.097	10 April - 18 September					(5)	(6)						
Longitude 4	8.602	0.108	20 March - 30 September					(5)	(6)						(14) (15)
Longitude 5	11.232	0.148	12 February - 21 September	(2)								(9)			(15)
Longitude 6	0.524	0.011	3 March - 10 August											(13)	

Table 2. The spread of COVID-19 in the context of regional geography – by climate zone.

	Cumulative number of infected people (million)	Maximum number of infected people	The date of maximum number of infected people	Time of the outbreak (14 Days)											
				1	2	3	4	5	6	7	8	9	10	11	12
Latitude 1	26.169	0.301	12 February - 19 September	(2)	→	(5)									(13) (14) (15)
Latitude 2	9.329	0.134	29 July - 16 August												(13) (14)
Latitude 3	2.367	0.036	24 July - 17 September							↓					(14) (15)
Latitude 4	5.103	0.05	10 April - 30 September						(7)	(9)					

4. CONCLUSION

In the study of the spread of COVID-19 in the context of regional geography by time zone The study managed to divide the epidemic area into 6 zones according to the longitude zone 60 degrees from the eastern end to the western end.

The study shows that COVID-19 first emerged in the People's Republic of China since the end of 2019 and spread heavily throughout February-March and has spread to surrounding countries. When entering April - May, there has been an outbreak spreading to the west. Entering June-August, the outbreak spread further westward, crossing the Atlantic Ocean into North and South America. It can be concluded that COVID-19 has spread from countries in the Eastern Hemisphere in the early stages to countries in the Western Hemisphere later.

In the study of the COVID-19 outbreak, in the context of geographic regions divided by climate zones, the epidemic zone was organized into four zones, each 32 degrees latitude, from 84 degrees north to the north. southernmost 80 degrees south. Each zone has different weather conditions. The study shows that the outbreak of COVID-19 began in the People's Republic of China during February-May and has spread to surrounding countries located in Zone 1. Then

in April - May, the outbreak spread north to the zone 4 and into the August - September outbreak spread south into South America and Australia, which are in the zone. 2 and 3 conclude that COVID-19 has spread from tropical regions to temperate regions.

5. REFERENCES

- Khataee, Hamid., Scheuring, Istvan., Czirok, Andras., and Neufeld, Zoltan. (2021). "Effects of social distancing on the spreading of COVID-19 inferred from mobile phone data." *Nature: Scientific Report*. 11(1661) (January) doi.org/10.1038/s41598-021-81308-2
- Liu, Yang., Morgenstern, Christian., Kelly, James., Lowe, Rachel., and Jit, Mark. (2021). "The impact of non-pharmaceutical interventions on SARS-CoV-2 transmission across 130 countries and territories." *BMC Medicine*. Vol 19, Number 40 (February). doi.org/10.1186/s12916-020-01872-8.
- Patiño-Lugo, Daniel F., Vélez, Marcela., Salazar, Pamela Velásquez., Vera-Giraldo, Claudia Yaneth., Vélez, Viviana., Marín, Isabel Cristin., Ramírez, Paola Andrea., Quintero, Sebastián Pemberthy., Martínez, Esteban Castrillón., Higuita, Daniel Andrés Pineda., and Henandez, Gilma. (2020). "Non-pharmaceutical interventions for containment, mitigation and suppression of COVID-19 infection." *Colombia Medica*. vol. 51, no. 2. (April). doi.org/10.25100/cm.v51i2.4266
- Rundle, Chandler W., Presley, Colby L., Militello, Michelle., Barber, Cara., Powell, Douglas L., Jacob, Sharon E., Atwater, Amber Reck., Watsky, Kalman L., Yu, Jiade., and Dunnick, Cory A. (2020). "Hand hygiene during COVID-19: Recommendations from the American Contact Dermatitis Society." *Journal of American Academic Dermatol*. 83(6) (December): pp.1730-1737. doi: 10.1016/j.jaad.2020.07.057.
- Li, Yanni., Liang, Mingming., Gao, Liang., Ahmed, Mubashir Ayaz., Uy, John Patrick., Cheng, Ce., Zhou, Qin., and Sun, Chenyu. (2021). "Face masks to prevent transmission of COVID-19: A systematic review and meta-analysis." *Am J Infect Control*. 49(7) (July): pp.900-906. doi: 10.1016/j.ajic.2020.12.007.

LANDSLIDE SUSCEPTIBILITY MAPPING USING LOGISTIC REGRESSION MODEL: A CASE STUDIES IN THE VAN YEN, YEN BAI PROVINCE

Xuan Quang Truong¹, Xuan Luan Truong³, Thi Thanh Thuy Pham¹,

Thi Thu Ha Le¹, Ngoc Hoan Nguyen¹, Chi Cong Nguyen², Thi Hai Yen Phi¹

¹Faculty of Information Technology, Hanoi University of Natural Resources and Environment

²Faculty of Geology, Hanoi University of Natural Resources and Environment

41A, Phu Dien Road, Bac Tu Liem, Hanoi, Vietnam

Email: txquang@hunre.edu.vn

³Faculty of Information Technology, Hanoi University of Mining and Geology

18 Pho Vien, Duc Thang Ward, Tu Liem District, Hanoi, Vietnam

Email: truongxuanquang@gmail.com

ABSTRACT

Landslide is one of the most complex natural phenomena and is quite common in Vietnam. Recently, Machine learning models are applying in order to improve accuracy of creating landslide susceptibility map and combining into the system as the prediction model for early warning and forecasting. The logistic regression model is widely used for prediction analysis in a variety of applications. Landslide susceptibility mapping, prediction analysis is important to predict the areas which have high potential for landslide occurrence in the future. The study area is in Van-Yen in the northern province of Yen Bai. Landslide inventory maps (300 landslides) were compiled by reference to historical reports and aerial photographs. All landslides were randomly separated into two data sets: 70% were used to establish the models (training data sets) and the 30% for validation (validation data sets). 11 factors were considered as conditioning factors related to landslide including: road, geology, fault, aspect, slope, topographic wetness index, NDVI, stream power index, plan curvature, profile curvature and river. The accuracy of the results was evaluated by using ROC. The area under the curve (AUC) for the logistic regression model was 0.903.

1. INTRODUCTION

Landslides are very common, occurs in a variety of form in the mountain areas of Vietnam. Landslide happens due to many reasons such as poor condition of soil together with long-term rainfall or mud and/or rocks slide downhill due to gravity. In Vietnam, northern areas and central region are the most affected by landslide. From 2001 to 2010, natural disasters such as floods, flash floods, landslides, droughts, salinity and other types of natural disasters cause 9.500 deaths and missing, causing losses of about 1.5% of annual GDP. In 2020 Natural disasters cost Vietnam 1.6 bln including landslide, Vietnam was hit by 14 storms that triggered heavy flooding and 130 people have died and missing cause of landslides based on Vietnam Disaster Management Authority report (VDMA 2021). The rainfall-triggered landslide is especially exacerbated in countries that are located in storm centers of the world, including Vietnam (Truong et al, 2018).

The landslide occurrence is a complex process which is a combination of multiple interacting factors. In order to minimize the damage due to landslides, machine learning

methods are suitable when a direct mathematical relationship cannot be established between cause and effect (Shano et al, 2020). Recently, methods for landslide susceptibility assessment have relied on statistical-based approaches and data-driven approaches. Such as a logistic regression (Pourghasemi et al. 2013) and (Tsangaratos and Ilia 2016); artificial neural networks (Pradhan and Lee 2010) and (Bhardwaj and Venkatachalam 2014); support vector machines (Peng et al. 2014) and (Chen et al. 2018); Naive Bayes (Tsangaratos & Ilia 2016); decision trees models (Pradhan 2013); and random forest (Catani et al. 2013) and (Truong, X.Q et al. 2018) or hybrid machine learning approach (Truong, X.L et al. 2018).

The main purpose of this study is to use logistic regression analysis for landslide susceptibility mapping of Van Yen district, Yen Bai province. Remote sensing data along with data collection from the field in study area have been used to generate the landslide susceptibility areas for the Van Yen district. The collection of landslide inventories was compiled from Geo-Web portal of the Vietnam Institute of Geosciences and Mineral Resources VIGMR (VIGMR, 2020), 302 landslides have been identified. The factors such as slope, aspect, geology, distance from fault, distance from river, distance from road, normalized difference vegetation index (NDVI) and stream power index (SPI), Profile Curvature, Plan Curvature have been used to facilitate the quantification of landslide.

2. STUDY AREA

The study area is the Van Yen district (Figure 1) of the Yen Bai province. Yen Bai province is located on the northern part of the Vietnam. Yen Bai province is between in the latitude 21° 24'N and 22° 16' N and between 103° 56'E and 105° 03'E. The study area is covered with an 1.391,54 km². The lowest area is about 20m above sea level, the high mountain area has an elevation from 300 - 1.700m, mainly concentrated in the north west. 70% of study area is occupied by slope angles, those are higher than 15°. The average temperature ranges between 18 and 20°C and rainfall varies between 1500 mm and 2200 mm/yr, average annual humidity is between 83%-87%. There are two main seasons: a rainy season spanning from April to October, and a dry season starting from November to March. The study area is located in an active tectonic region with the relatively fast movement of the Red River fault zone that results in continuously landslide occurrences over the years (Truong, X.Q et al, 2018). The history of landslides that have caused damages to life, property, and infrastructures, they were investigated by the VIGMR in 2013 and 2017. These landslides mainly occur along national road and at various topographic types after heavy rain or/and human activities.

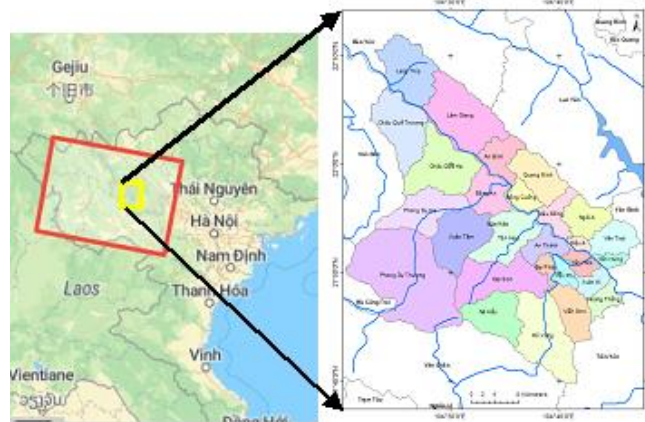


Figure 1: Study area

3. LANDSLIDE CONDITIONING FACTORS

In this paper, 11 factors were studied based on the data available and general geo-environment of the study area as shown in (Table 1). The condition factors are slope, aspect, altitude, landcover, lithology, soil type, distance to fault, distance to river, rainfall. A digital elevation model (DEM) from ALOS PALSAR data with 12.5 m resolution was used to process slope, aspect, elevation, topographic wetness index (TWI), stream power index (SPI), plan curvature and profile curvature maps using QGIS 2.16.3. Normalized Difference Vegetation Index (NDVI) was created from sentinel-2. The geology and fault maps at scale 1:50.000 was provided by the Ministry of Natural Resource. The river and road maps were used from the Vietnam national atlas with scale 1:50.000. The categories of each layers were defined in the (Table 1).

Table 1. Landslide conditioning factors and their classes

Type	Classes	Number of class pixels	Landslide points	SI
distance to faults (m)	0-50	395353	90	1.076
	50-100	318816	54	1.186
	100-200	558240	73	0.927
	200-500	1546065	114	0.354
	>500	6115621	161	-0.675
Plan Curvature	-1	3869564	109	-0.182
	0	992414	52	0.438
	1	4072097	141	0.024
Profile Curvature	-1	4296900	147	0.011
	0	64641	33	0.412
	1	3990763	122	-0.100
NDVI	≤0	12207	25	5.0308
	0 – 0.2	1246475	160	9.8429
	0.2 – 0.4	638461	293	6.8225
	0.4 – 0.6	400772	413	9.0381
	0.6 – 0.8	184817	326	9.7929
	≥0.8	106719	429	5.0308
River	0-25	779239	42	0.466
	25-50	757665	48	0.628
	50-100	1411858	96	0.698
	100-200	2189294	55	-0.296
	200-300	1391479	32	-0.385
	≥300	2404560	29	-1.032
SPI	-13 to -5	3265726	164	0.395
	-5 - 0	281298	15	0.455
	0 - 5	264804	6	-0.400
	5 - 10	361359	13	0.062
	10 - 14	4760888	104	-0.436
Slope	0-5°	624239	54	0.939
	5-10°	885595	71	0.863
	10-15°	1143726	57	0.388
	15-20°	1538329	46	-0.122
	20-25°	1551737	36	-0.376
	25-30°	1384137	16	-1.073
	30-40°	1400540	21	-0.812
	40-50°	340851	1	-2.444
Aspect	≥50 °	64921	0	0.939
	-1	74552	0	0
	35-72 and 320-360	627791	20	-0.091
	72-113	1692255	72	0.197

113-156	1117460	44	0.120
156-198	1035447	43	0.173
198-238	1131021	48	0.194
238-279	1264409	28	-0.455
279-320	1026233	28	-0.246
Geology	29 classes	values: -2.39 to 3.95	
Distance to Road	05 classes	values: -2.73 to 1.40	
TWI	04 classes	values: -0.26 to 0.19	

The statistical index (SI) method is applied for landslide susceptibility analyses in this study and was proposed by (Bui 2011) and Van Westen (1997). In this method, the weight for a parameter class, such as a slope class or NDVI class, is defined as the natural logarithm of the quotient as follows:

$$w_i = \ln \left(\frac{\frac{N_{i,j}}{A_{i,j}}}{\frac{N_T}{A_T}} \right) \quad (1)$$

Thus, supposing that j is a category within the factor i , then the LSI for this category with $N_{i,j}$, the number of landslides in category j of the factor i , $A_{i,j}$ the area of this category, N_T the total number of landslides and A_T the total area under investigation (Figure 2).

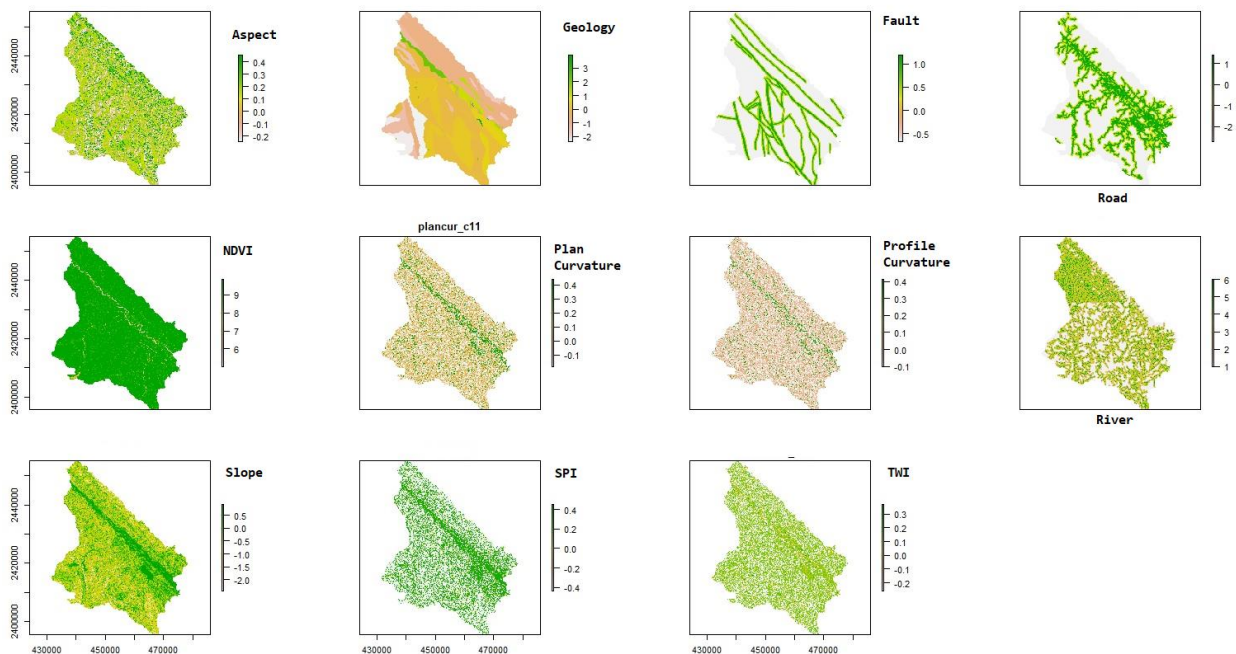


Figure 2: statistical index of factors based on Table 1

4. LANDSLIDE SUSCEPTIBILITY MAPPING USING LOGISTIC REGRESSION

Logistic regression is a mathematical modeling that can be applied for examination the presence or absence of outcome based on the values of a set of predictor variables (Lee 2005). The logistic regression function $f(z)$, which is defined as:

$$f(z) = \frac{1}{1+e^{-z}}; z = \alpha + \beta_1 x_1 + \beta_2 x_2 + \dots + \beta_n x_n \quad (2)$$

where z is a linear sum of a constant α and products of independent variables $x_i (i = 0, 1, 2, \dots, n)$ and their corresponding coefficients $\beta_i (i = 0, 1, 2, \dots, n)$.

For building landslide model, the landslide inventory map was randomly divided into a training dataset of 70% (210 landslides with 2,781 pixels) for building the landslide models and a validation dataset 30% (92 landslides with 716 pixels). Using the logistic regression coefficients, landslide susceptibility index was calculated and then the landslide susceptibility map was obtained (Figure 3). The linear sum of the constant and the product of the independent variables and their corresponding coefficients are calculated as shown below:

$$z = -1.81 - 1.19 * aspect + 0.69 * geology + 0.44 * fault + 0.96 * road + 0.2367 * NDVI + 0.98 * river - 1.28 * curvature_plan + 1.49 * curvature_profile + 0.29 * slope - 0.88 * SPI + 0.88 * TWI$$

5. RESULT AND DISCUSSION

In this paper, we have evaluated the logistic regression for landslide susceptibility assessment for Van Yen district of the Yen Bai province. Data processing for each factor was analyzed based on QGIS 2.16.3. The landslide inventory (302 landslide locations) and 11 landslide conditioning factors (slope angle, slope aspect, plan curvature, profile curvature, topographic wetness index, stream power index, NDVI, distance to roads, distance to rivers, distance to faults and geology) were used for building the logistic regression model.

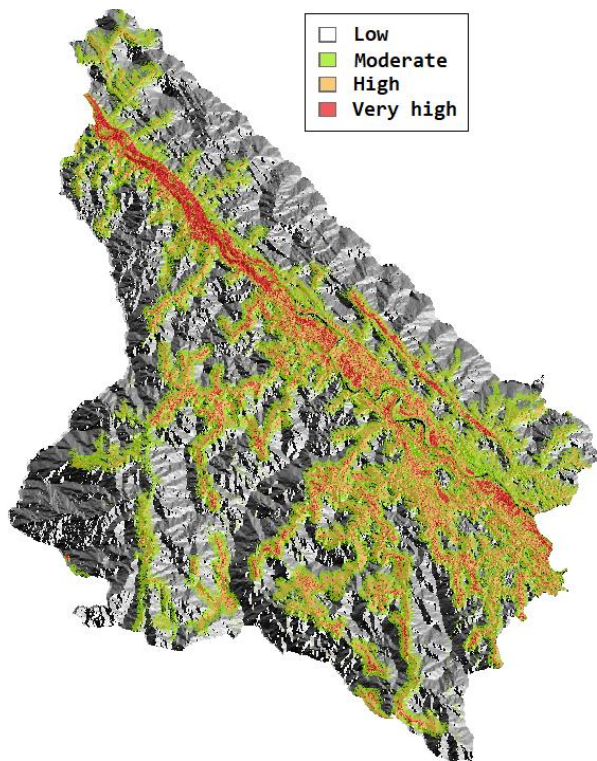


Figure 3: Landslide susceptibility mapping using Logistic Regression

The ROC curve can be used to provide predictions of the performance of the model. The ROC curve is a two-dimension graph showing true-positive rate (vertical axis) and false-positive (horizontal axis). The area under the ROC curve (AUC), which is the summarized information of the plot, it can be used to estimate the validity of the model, accuracy or the overall quality of a model (Hosmer and Lemeshow 2000). Areas under the curves (AUC) were calculated (Figure 4). The result shows that, the logistic regression has AUC=0.903 (Figure 4).

As the result from regression model, the landslides happen in many and densely along the road through Dong An, Chau Que Ha, Dong Cuong communes. The results are given in a medium-scale map, this will clarify the details of high and very high susceptibility area related to landslide risk.

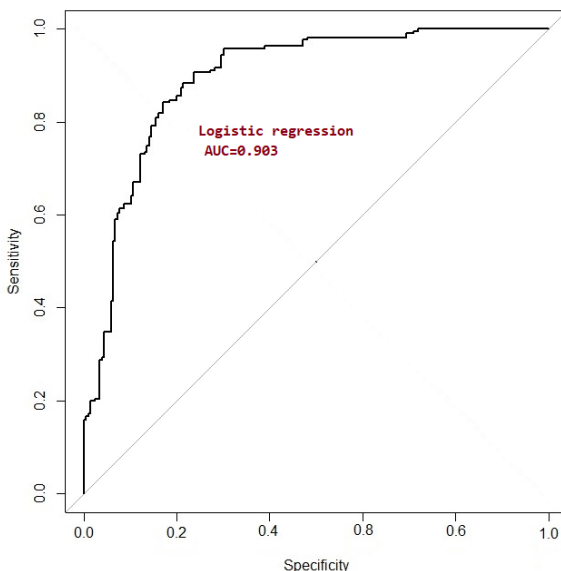


Figure 4: The receiver operating characteristic (ROC) curve

The landslide susceptibility maps of this study may be support to local administrator in order to manipulate in decision makers, slope management and land use planning. The accuracy of the logistic regression model can be improved if the landslide inventory map was updated or other factors such as land use land cover, soil maps are included in the analysis.

6. ACKNOWLEDGMENTS

This work is supported by the Bilateral Scientific Research project between Vietnam and Italy, code: NDT/IT/21/14 funded by Ministry of Science and Technology of Vietnam (MOST) and Funded by a grant from the Italian Ministry of Foreign Affairs and International Cooperation

REFERENCES

- Bhardwaj A, Venkatachalam G. 2014. Landslide hazard evaluation using artificial neural networks and GIS. In *Landslide science for a safer geoenvironment*. Cham: Springer; p. 397–403.
- Bui, D.T., Lofman, O., Revhaug, I. et al. Landslide susceptibility analysis in the Hoa Binh province of Vietnam using statistical index and logistic regression. *Nat Hazards* 59, 1413 (2011). <https://doi.org/10.1007/s11069-011-9844-2>
- Chen, W.; Pourghasemi, H.R.; Naghibi, S.A. A comparative study of landslide susceptibility maps produced using support vector machine with different kernel functions and entropy data mining models in China. *Bull. Eng. Geol. Environ.* 2018, 77, 647–664.
- Catani, F., Lagomarsino, D., Segoni, S., & Tofani, V. (2013). Landslide susceptibility estimation by random forests technique: Sensitivity and scaling issues. *Natural Hazards and Earth System Sciences*, 13(11), 2815–2831
- Lee S (2005) Application of logistic regression model and its validation for landslide susceptibility mapping using GIS and remote sensing data journals. *Int J Remote Sens* 26(7):1477–1491. doi:10.1080/01431160412331331012.
- Hosmer DW, Lemeshow S (2000) Applied logistic regression, 2nd edn. Wiley, New York.

- Pradhan B, Lee S. 2010. Landslide susceptibility assessment and factor effect analysis: backpropagation artificial neural networks and their comparison with frequency ratio and bivariate logistic regression modelling. *Environ Model Softw.* 25:747–759.
- Pradhan B. 2013. A comparative study on the predictive ability of the decision tree, support vector machine and neuro-fuzzy models in landslide susceptibility mapping using GIS. *Comput Geosci.* 51:350–365.
- Pourghasemi, H.; Moradi, H.; Aghda, S.F. Landslide susceptibility mapping by binary logistic regression, analytical hierarchy process, and statistical index models and assessment of their performances. *Nat. Hazards* 2013, 69, 749–779.
- Shano, L., Raghuvanshi, T.K. & Meten, M. Landslide susceptibility evaluation and hazard zonation techniques – a review. *Geoenviron Disasters* 7, 18 (2020). <https://doi.org/10.1186/s40677-020-00152-0>
- Tsangaratos P, Ilia I. (2016). Comparison of a logistic regression and Naive Bayes classifier in landslide susceptibility assessments: the influence of models complexity and training dataset size. *CATENA*. 145:164–179.
- Truong, X.L; Mitamura, M; Kono, Y; Raghava, V; Truong, X.Q; Do, T.H; Bui, T.D; Lee, S. Enhancing prediction performance of landslide susceptibility model using hybrid machine learning approach of bagging ensemble and logistic model tree, *Appl. Sci.* 2018, 8(7), 1046; <https://doi.org/10.3390/app8071046>.
- Truong, X.Q., Truong, X.L., Dang, T.K.L Nguyen., T.D; Nguyen., D.A. Landslide susceptibility mapping using random forest model in Lao Cai Province, Vietnam, *GIS-IDEAS 2018, Geoinformatics for Rural-Urban Synergy* (2018)
- VIGMR, Vietnam institute of geosciences and mineral resources (2020) <http://www.canhbaotruotlo.vn/> (accessed on Dec, 2020)
- Van Westen CJ (1997) Statistical landslide hazard analysis. ILWIS 2.1 for Windows Application guide. ITC Publication, Enschede
- VDMA, Vietnam Disaster Management Authority (2021) <http://phongchongthientai.mard.gov.vn/> (accessed on 12, Aug 2021)

Hydrological Impact of Dual-Polarization Doppler Radar Data in mountainous areas: A case study of Typhoon Vipha (2020) in Upper NAN Basin

Fatah Masthawee^{1,2}, Chaiiwat Vansarochana¹, Pattara Sukthawee², Nattapon Mahavik¹, Nuttapong Panthong² and Rattana Prakhammintara²

¹Faculty of Agriculture Natural Resources and Environment, Naresuan University
Naresuan University, Phitsanulok 65000, Thailand

²Hydrometeorological Division, Thai Meteorological Department
4353 Shukhumvit Rd., Bangna, Bangkok 10260, Thailand
Email: fatah_m@yahoo.com

ABSTRACT

Weather Radar observation is a remote sensing measurement. It uses electromagnetic wave reflection. It is expected to reflect rainfall droplets and interpret rainfall values. Not only rainfall droplet reflection but other objects also reflected by the radar beam. They are including living things such as birds and bats, and non-living things like mountains, airplanes, and buildings. Thus, it is necessary to filter these objects out. This study aims to improve rainfall measurement by filtering with Velocity and Cross correction ratio. The result shows that the radar-based has more accuracy. When utilizing radar-based rainfall as an input for hydrological model, the statistical score are RMSE = 32.38, MAE = 11.18 and PE = 26.1. The result is not different from directed-measurement rainfall. Due to radar-based rainfall missing in some areas, causing the hydrological model error. If the improved radar-based rainfall equation is used, the hydrological model will show an accurate result.

1. INTRODUCTION

A weather radar is an important tool for meteorological services and atmospheric study agencies. Recently, dual-polarization is developed which can detect more accurate raindrops. A High-resolution forecast is required by the public and can be done with a numerical weather forecast for many purposes such as an input dataset of the multi-dimension flood simulation. Spatial rainfall with high resolution is the prominent of this tool not only temporal but also area. To calculate Aerial rainfall from radar, a mathematic equation is applied with data from rain gauge (Villarini and Krajewski, 2010). Radar-based rainfall still has some uncertainty - for example, the weakness of signal by blockage and reflection of the object. Dual polarization can reduce this kind of uncertainty of radar-based rainfall (Dufton and Collier, 2015).

One of many reasons that rainfall from radar has an uncertainty is the reflection of objects that do not raindrop, sometime it reflects surface matters called ground clutter. Living things or biological scatterers also blocks radar beam such a bird and bug, in some cases, non-living thing flying such as an airplane and sea wave clutter. Static technic can erase noise from a none-movement object, but dynamics filter technic from one axis and two axes can filter ground clutter and achievement in a variety of noise clutter (Dufton and Collier, 2015)

The Upper Nan River basin is selected as the study area, located in the north of Thailand, This area is out of reach of a rain gauge, nearest rain names Thun Chang, it is river source area of Nan river basin. Because of flood problems in this area in the wet season, and lack of water

in the dry season, it depends on natural river flow without structure management although Nan river basin has Sirikit dam in lower of basin only solve a problem in the lower basin. Flood in the upper area has an effect to a landslide which affect to many people living in this area. People in a lower area such as the Chao Phraya basin also have an effect of this phenomenon because of the geography of the confluence of the river basin. Alternate land use is also the reason for floods in the study area.

In this study, radar-based rainfall is used as an input of the hydrological model name Tank model to address the efficiency of the rainfall dataset from radar. The outlet of Tung Chang water station is selected as a study point, the first order station in the river basin operated by TMD. Rainfall is the main factor that triggers the river flow in basin difference from other point stations that receive water from the upper area.

2. METHODOLOGY

2.1 Study area

Upper Nan river basin is sub-basin of Nan river basin has $2,221.82 \text{ km}^2$ as 6.36% of the Basin covers seven districts as following Chaleam Prakeat, Chiang Klang, Tha Wang Pha, Thung Chang, Boa Klea, Pua, and Song Keaw in Nan province. The topography of the Basin is a source of water in the watershed and has a mountainous area and high ground 1400 – 1900 meter mean sea level with five rivers. Population Depends on Agriculture for occupation (DWR, 2018)

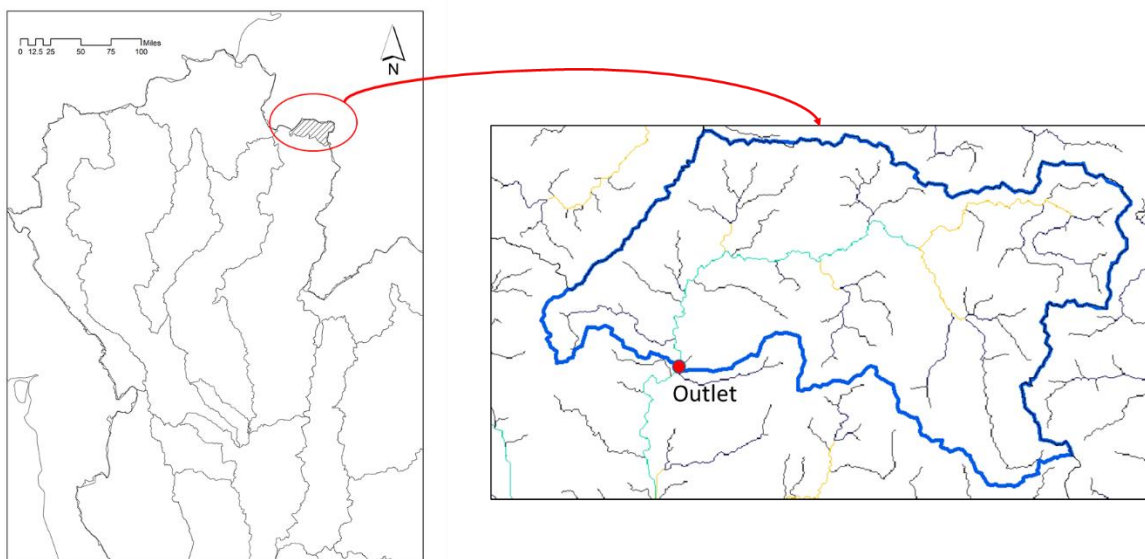


Figure 1. Study area

This study aims to find the performance of radar-based rainfall as input of Tank model for Tung Chang station when heavy rainfall during tropical cyclone event occurring in 2019

2.2 Data collection

1. Radar-based rainfall from Tha Wang Pha radar station in Nan province from 2-5 August 2010 which affect by tropical storm Vipa collecting in UF file format interval 15 minutes in temporal by TMD database.

2 Point rainfall by TMD serviced by Climate information service, CIS from 1 January 2018 to 21 April 2020 for adjusting the Tank model.

3 Water level and volume from RID and TMD from 1 January 2018 to 21 April 2020

2.2 Data collection

The main purpose of using Radar-based rainfall is to extend the rainfall network in a remote area which rain gauges not covering on the far side of the basin. The remote area is a water source with the natural flow and non-controlling system with dangerous river shape, narrow and steep shape, water level changes rapidly causing to harm people in a riparian area. The flow chart of the study shows in the figure below.

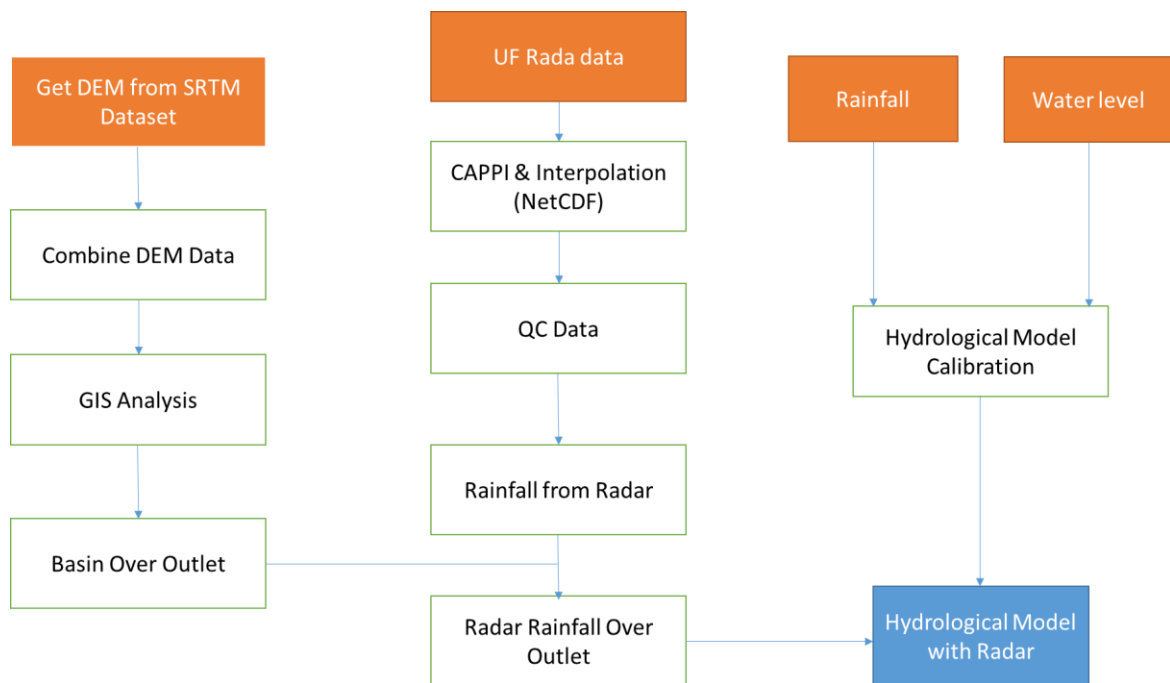


Figure 2 workflow of the study

Script for analysis data is created in NetCDF File and TIFF File that suitable GIS tasks such as ArcGIS and QGIS. The parameter is the magnetic reflection of raindrops, velocity, and Cross-correlation ratio compress as CAPPI at 1km vertical high as shown in the figure 3.

How to devise clutter from raindrop, velocity, and cross-correlation ratio are utilized. If the object stays still, it is no movement and velocity equal to zero. Likewise, cross-correlation ratio is the relation of refection between two axes, when cross-correlation ratio near 1, it's rain.

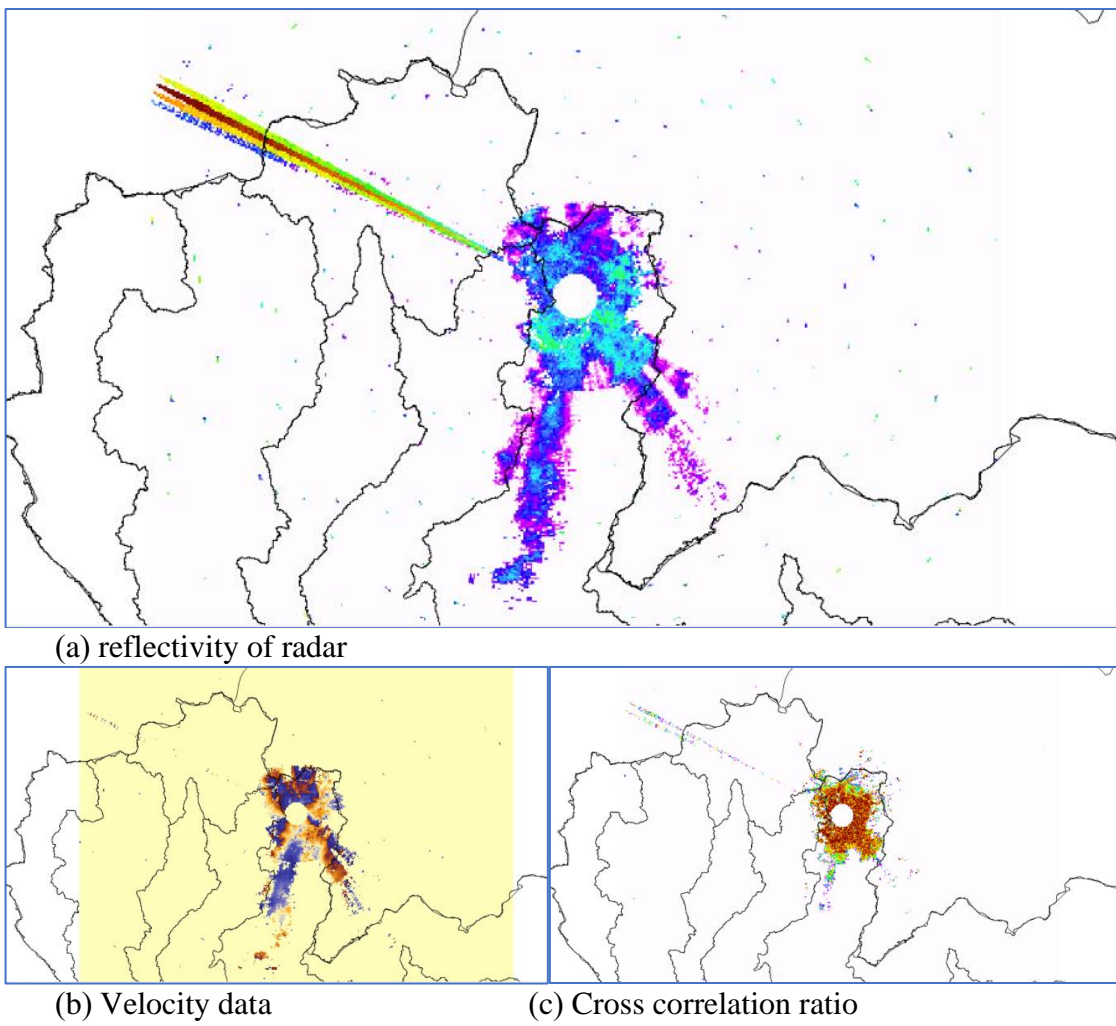


Figure 3. Radar data

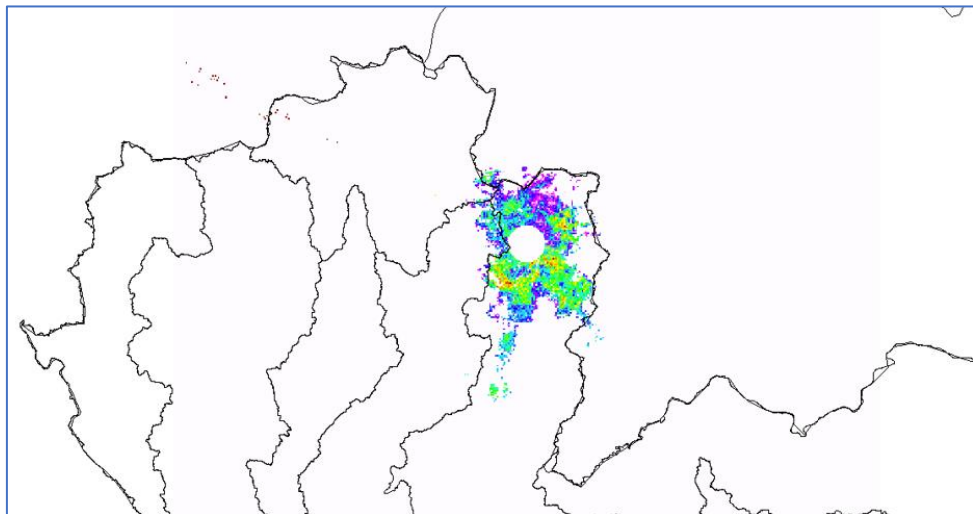


Figure 4. filtered radar data

The transformation from reflectivity to rain rate, Z-R relation equation is adopted with $Z = 250R^{1.2}$. this equation is suitable for tropical weather zone (Einfalt et al.,2004) when R stands for rain rate(mm/h) and Z is radar reflectivity (mm^6/m^3).

To compute drainage area in study basin and fine water volume that fill in the Tung Chang river station, GIS is applied to analyze rainfall in watershed.

Tank model is written in computer program names python and uses rain gauge network data set to calibrate and verify Tank

Tank Model is one of a user-friendly hydrological model in term of setting model and calibrating lumped properties. Tank is arranged vertical and represents surface interflow and base flow depend on the modeler decision. (Sugawara et al., 1995)

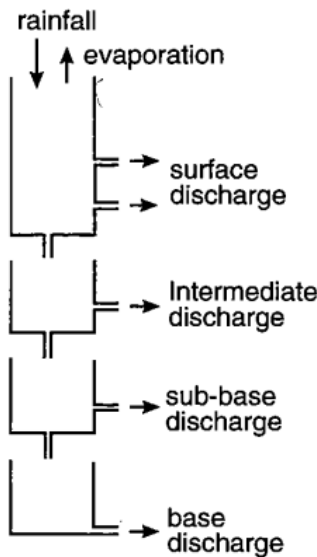


Figure 5 Tank model

3. RESULT AND DISCUSSION

Radar based-rainfall and rain gauge network dataset from 2-5 August 2010 which triggers heavy rainfall widespread in northern Thailand by tropical storm Vipa is used as input of Tank model separated in two cases: 1. Tank model with radar rainfall 2. Tank model with a rain gauge. The result shows that discharge that generating from remotely sensed data is slightly lower than rain gauge input data. This can adjust the radar equation to improve the accuracy of rainfall input. However, Statistical verification points out less error from radar base model than rain gauge base including mean absolute error (MAE), root mean square error (RMSE) and percentage error (PE).

The result from using Velocity and Cross-correlation ratio to filter noise from Radar rainfall product found that filtering is good enough when erasing mountain in water source area at upper of study basin as shown in figure 7(a). The point that showing in the picture means filtering successfully and figure 7(b) shows flirted rainfall map and the missing area can be replaced by composting with a nearby radar station and satellite rainfall too.

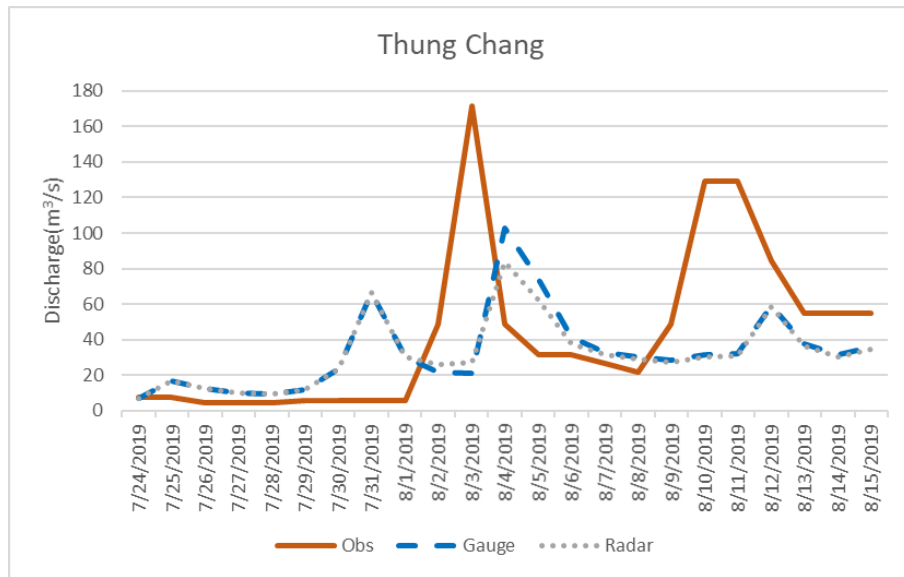


Figure 6 Discharge from observation, rain gauge input, and radar input

Table 1. Error of Tank model comparing radar base model and gauge base model

Input data	RMSE	MAE	PE
Rain gauge	35.25	12.95	30.22
Radar	32.38	11.18	26.11

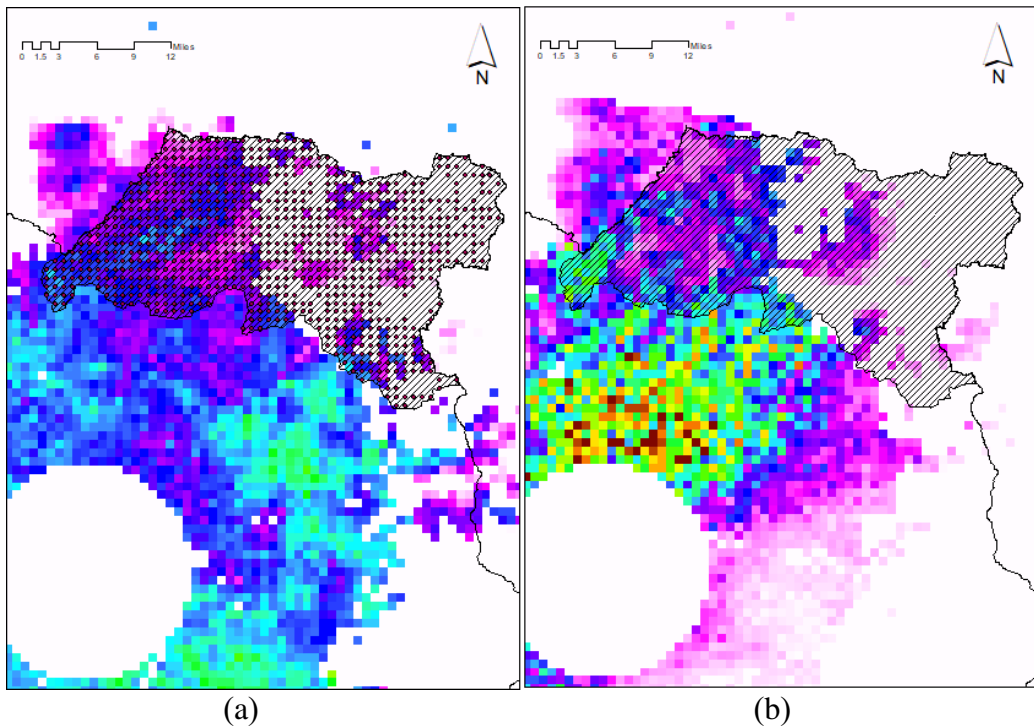


Figure 7. Data filtering

(a) Filtering with Velocity and Cross correlation ratio

(b) Filtered rain fall map

The equation with $Z = 250R^{1.2}$ is suitable for the tropical area where air mass convection and condense to rainfall, but Marshall and Parmer with $Z = 200R^{1.6}$ applied in this study, rainfall volume is diminished and needs calibration for more accuracy. On the other hand, Mean-field bias (MFB), Range dependent adjustment (RDA), Special bias adjustment (SBA), or Static local bias adjustment and range dependent adjustment (SRD) may be tested in the next experiment with ground truth (Mahavik, 2017)

This study is not a separate Tank model in a wet and dry period when calibration model, error take place come from this reason. This is because water levels change rapidly in the transition phase of wet and. If separate wet-dry season, the result will be improved.

The rainfall data set that uses as an input of the model is an aerial rainfall with the whole basin, some periods or some stations are missing and need to interpolate the data set causing a small amount of rain volume in a basin to fulfill with bias correction.

Moreover, filtering radar rainfall makes some error with missing data and need to fill the gap of missing data with another radar station. Lastly, some data set has an error with false rainfall event, no rain with rain data, it is a main source of error in the model, Radar can be used as truth checked of this event.

4. REFERENCES

- Dufton D. R. L., and Collier C. G., 2015. Fuzzy logic filtering of radar reflectivity to remove non-meteorological echoes using dual polarization radar moments. *Atmospheric Measurement Techniques*. 8:3985-4000.
- DWR, 2018. *Nan Basin System*.
- Einfalt, T., Arnbjerg-Nielsen, K., Golz, C., Jensen, N. E., Quirmbach, M., Vaes, G. and Vieux, B., 2004. Towards a roadmap for use of radar rainfall data in urban drainage. *Journal of Hydrology*. 299:186-202.
- Sugawara, M. 1995. Tank model. In: V.P. Singh (Ed.), *Computer models of watershed hydrology*. Water Resources Publications, Highlands Ranch, Colorado.
- Mahavik, N., 2017. Bias Adjustments of Radar Rainfall during Seasonal March of the Summer Monsoon in the Middle of Thailand. *International Journal of Applied Environmental Sciences*. 12(4): 577-594.
- Villarini, G. and Krajewski W.F., 2010. Review of the different sources of uncertainty in single polarization radar-based estimates of rainfall. *Surveys in Geophysics*, 31: 107–129.

AN ANALYSIS AND IDENTIFICATION OF FLOODED AREAS WITH DATA FROM SENTINEL-1 SATELLITES

Bussaba Samdaengchai¹, Somsarit Sinnung², Pattanapol Meena³, and Teerawong Laosuwan^{4*}

^{1,3,4} Department of Physics, Faculty of Science, Mahasarakham University, Maha Sarakham, Thailand

² Defence Technology Institute, Office of the Permanent Secretary of Defence, Nonthaburi, Thailand

*Corresponding author: teerawong@msu.ac.th

ABSTRACT

Flooding in Thailand has caused damage to people including property, houses, commercial buildings, factories and agricultural land. Sukhothai is one of the provinces in Thailand that floods every year. The main purpose of this study was to analyze and identify flood areas with data from sentinel-1 satellites in Sukhothai province, conducting data analysis with SNAP and ArcGIS programs. The data analysis showed that the data from August 25, 2020 with flooding areas was 96.751 km². Compared to the flood area data obtained from Geo-informatics and Space Technology Development Agency (GISTDA), which has a total flood area of approximately 106.632 km², there was a difference of approximately 9.593%. The differences may be due to different actions taken in the management and creation of data, including the processing of data to determine the extent of the flooding. Moreover, it found that the geographical nature of Sukhothai province is that the river flows from north to south, passing about 170 km, which causes repeated flooding, especially in Si Satchanalai, Sawankhalok, Sri Samrong, Sukhothai, and Kong Krailat districts.

1. INTRODUCTION

Water is an important resource in the livelihoods of humans and living things. In the last 10 years, the world has had more natural disasters, especially water disasters. There are many forms of water-related hazards. Floods are a form of water hazard that cause social, economic, and environmental damage (Rotjanakusol et al., 2019). From the recent flooding situation in Thailand, especially in late 2010, there were floods in the northeastern region, early 2011 floods and land sledging in many provinces of the south and the most severe in 50 years were floods that occurred in central and Bangkok during 2011. When it is said that all regions of Thailand have experienced flooding, direct impacts on people's lives, property, buildings, buildings, and infrastructure, agriculture and pets.

It also indirectly affects natural conditions, human-social conditions, such as demographic changes, well-being, health and diseases, human development, and economic and political conditions. These days of impact will intensify. The damage and subsequent losses are beyond predictable (Rotjanakusol et al., 2020). The lowlands of the Yom River are important lowlands for farmers' agriculture in Sukhothai, but the area of agriculture has experienced flooding. A 1998 flood study by the Irrigation Department found that the river capacity of the Yom River from upstream to Mueang Sukhothai district would be between 1,500-3,000 m³/s, and since The District of Sukhothai has reduced its capacity to 300-600 m³/s. Due to the bottleneck, drainage in the water season is not as good as it should be. It caused flooding in two lowlands along the banks of the Yom River (Phrae News, 2007).

Flooding in Thailand has caused damage to property, houses, commercial buildings, factories, and agricultural land (Asian Disaster Reduction Center, 2012), which Sukhothai has flooded every year and is a lowland area with Yom River flowing through the province. When the rainy season comes, there is quite a lot of rainfall in the area, along with rainfall in the

northern regions that flow down to Sukhothai. This resulted in flooding in study areas and affected the lives of property and agricultural lands of the people in the area in order to build knowledge in planning to prevent natural disasters from expanding. If people have knowledge of software data and processing, it can effectively explore, analyze data, and process areas affected by flooding during disasters (Ministry of Agriculture and Cooperatives, 2017; Zhang et al., 2020; Gašparović & Klobučar, 2021). Remote sensing technology is a science and technology used to record the characteristics of objects in reflection and radiation of electromagnetic energy without direct contact (Uttaruk & Laosuwan, 2016; Laosuwan & Uttaruk, 2016; Singh & Singh, 2017; Uttaruk & Laosuwan, 2018; Rotjanakusol, T., & Laosuwan, 2018; Prohmdirek et al., 2020; Jomsrekrayom et al., 2021). Remote sensing technology is constantly evolving and with satellite data, it can be used to create spatial data to solve these flooding problems. Therefore, this research focuses on analyzing and identifying flood areas with data from the Sentinel-1 satellite to determine the extent and trends of flood areas, to provide prevention, surveillance, as well as to assess flood damage, and to reduce the impacts in a wider range of risks that may increase.

2. AREA OF THE STUDY

Sukhothai Province (Figure 1) has 9 main administrative regions: Mueang Sukhothai, KhiriMas District, Ban Dan Lan Hoi District, AmSri Samrong, Sawankhalok District, Thung Saliam District, Si Satchanalai District, Srinakharinwirot District. The total number of sub-districts is approximately 6,592 km².

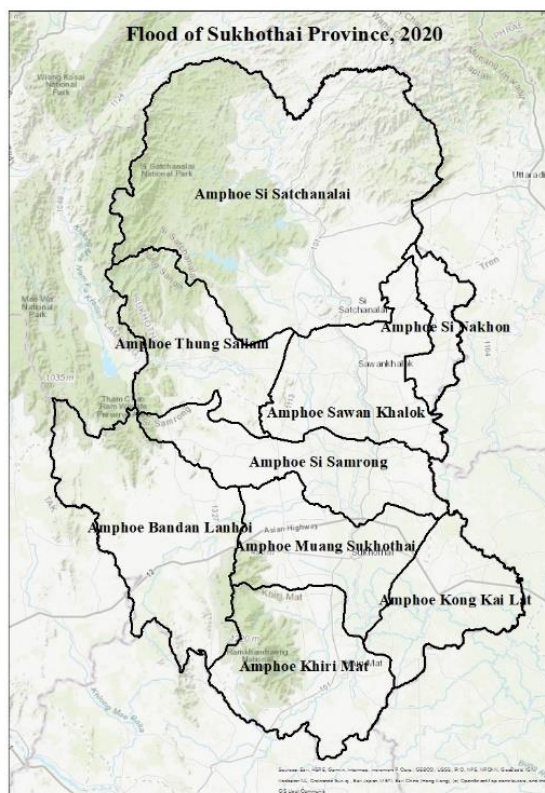


Figure 1. Sukhothai Province.

3. METHODOLOGY

The research was based on data from the Sentinel-1 satellite, recorded on August 25, 2020 in the Sukhothai area from the Copernicus Open Access Project Information Service website provided by the European Space Agency (ESA). The data used as Interferometric Wide Swath (IW) GRD level-1 data has a spatial resolution of 5x20 m, a orientation width of 250 km, which is an intberration. Therefore, the use of research requires increasing the quality of data from satellites in the SNAP program to analyze flood areas effectively.

The procedure is shown as follows:

- 1) Apply Orbit File updates the satellite's orbital data value to be more accurate because the receiver time has not been modified,
- 2) Noise Removal reduces the noise available in satellite image data. The next step is calibrate to calibrate the signal value of the resulting power. The result at this stage is Sigma0_vv,
- 3) Speckle Filtering eliminates interference found in Salt and Paper data by using a Lee Sigma 9x9 filter,
- 4) Terrain correction is an adjustment to the tolerances resulting from the terrain,
- 5) Create Vector creates a Vector data layer for Digital samples in the water area to collect Sigma0 statistics, then analyzes sigma0 statistics of flood areas,
- 6) Binarization by Thresholdization method with Sigma0 Mean in Study Area with Band Math, and
- 7) Export view as image of flood area export for analysis in Arc GIS program

4. RESULT

In this study, the researchers compared the flood area boundary results (Figure 2 - 5) using analytical data showing flood areas to analyze differences with GISTDA's published flood data.

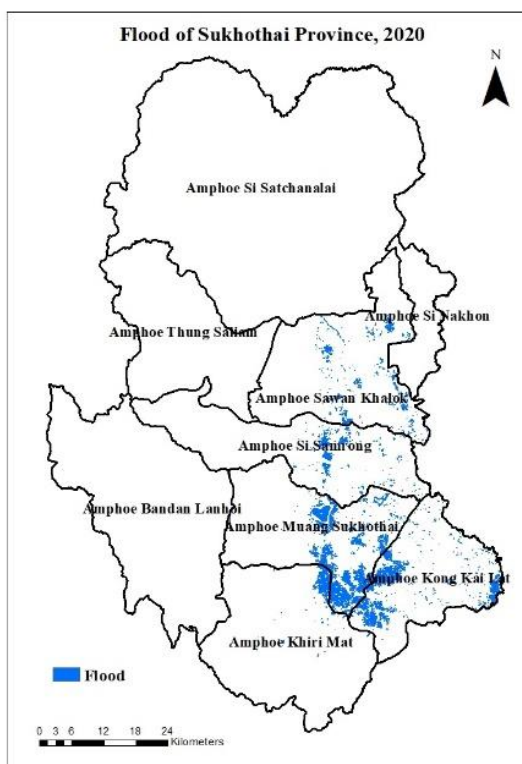


Figure 2. Area flooded by data analysis.



Figure 3. Area flooded by GISTDA.

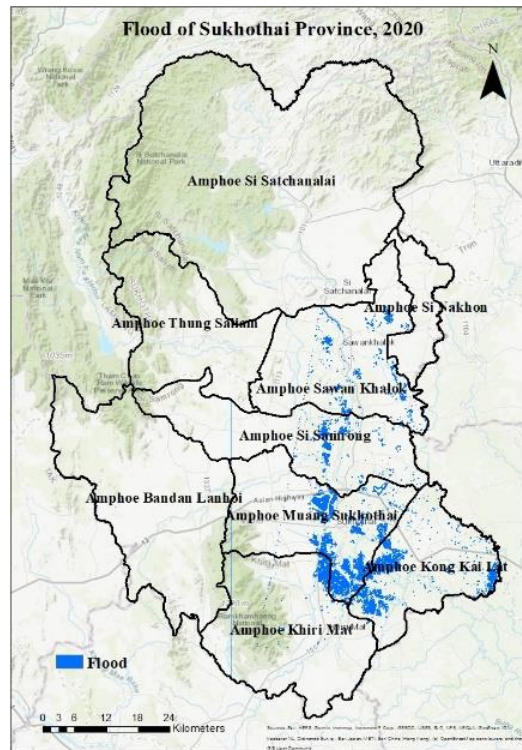


Figure 4. Area flooded by data analysis.



Figure 5. Area flooded by GISTDA.

When analyzing flood data from the Sentinel-1 satellite on August 25, 2020, the results showed a total flood area of 96.751 km^2 compared to flood area data obtained by GISTDA, which had a total flood area of approximately 106.632 km^2 . As shown in Figure 2, it is a map

of flood-affected areas obtained from ArcMap program, Figure 3 is a flood-affected area, which is obtained from the data file from GISTDA. It can be opened with the Sukhothai Map, Figure 4 is a map of areas affected by flooding that have been analyzed and then opened in ArcMap based on an online map of Sukhothai, and Figure 5 is a flood-affected area from GISTDA.

5. CONCLUSION

Analyzing and identifying flooded areas with data from the Sentinel-1 satellite, Sukhothai province, which performs data analysis with SNAP and ArcGIS programs. Each program has different pros and cons, but for effective results, it shares the program, allowing for effective results, being able to find space and create flood maps from open sources and open code software. According to the data from August 25, 2020, the flood area was 96.751 km². Compared to the flood area data obtained from GISTDA, which has a total flood area of approximately 106.632 km², it was found to be about 9.593% difference. The differences may be due to different actions in data management and creation. Sukhothai's geographical characteristics are found to have rivers flowing from north to south, passing about 170 km, which causes repeated flooding, especially in Si Satchanalai, Sawankhalok, Sri Samrong, Sukhothai, and Kong Krailat districts. This research provides a way to process data from open sources with open code software to find flood areas of Sukhothai. This research can be applied to determine the likelihood of flood areas preparing prevention, surveillance, or immediate evacuation of populations to reduce the impact of a wider range, but the use of data from open sources must be carried out carefully and the accuracy of the data must be checked before use.

6. ACKNOWLEDGEMENT

This Research was Financially Supported by Defence Technology Institute.

7. REFERENCES

- Asian Disaster Reduction Center. (2012). Natural Disaster Data Book. Available at: http://www.adrc.asia/publications/databook/DB2012_e.html.
- Gašparović, M., & Klobučar, D. (2021). Mapping Floods in Lowland Forest Using Sentinel-1 and Sentinel-2 Data and an Object-Based Approach. *Forests*, 12(5), 553.
- Jomsrekrayom, N. Meena, P., & Laosuwan, T. (2021). Spatiotemporal Analysis of Vegetation Drought Variability in the Middle of the Northeast Region of Thailand using Terra/Modis satellite data. *Geographia Technica*, 16, Special Issue, 70-81.
- Laosuwan, T., & Uttaruk, Y. (2016). Application of Geoinformatics and Vegetation Indices to Estimate Above-ground Carbon Sequestration. *Studia Universitatis Vasile Goldis Arad, Seria Stiintele Vietii*, 26(4), 449-454, 2016.
- Ministry of Agriculture and Cooperatives. (2017). Prevention and mitigation plans caused by water (rainy season). Available at: <http://water.rid.go.th/hwm/wmoc/planing/wet/protect2561.pdf>. (In Thai)
- Phrae News. (2007). Project to Develop Strategic Alternatives for Yom River Basin Management Policy. Available at: http://www.phrae.go.th/news/news0650_45.html. (In Thai)
- Prohmdirek, T., Chunpong, P., & Laosuwan, T. (2020). The Relationship between Normalized Difference Vegetation Index and Canopy Temperature that Affects the Urban Heat Island Phenomenon. *Geographia Technica*, 15 (2), 222-234.
- Rotjanakusol, T., & Laosuwan, T. (2018). Inundation area investigation approach using remote sensing technology on 2017 flooding in Sakon Nakhon province Thailand. *Studia Universitatis "Vasile Goldis" Arad.Seria Stiintele Vietii (Life Sciences Series)*, 28(4), 159-166.

- Rotjanakusol, T., Sangyotha, U., & Laoauwan, T. (2019). Identifying Flood Areas from Satellite Data and Physical Model: A Case Study of Tha Yang District, Phetchaburi Province, 2018. Defence Technology Academic Journal, 1 (2), 64-73.
- Rotjanakusol, T., & Laosuwan, T. (2020). Surface Water Body Extraction Using Landsat 8 Images and Different Forms of Physical Models. The Scientific Journal of King Faisal University, Basic and Applied Sciences, 21 (2), 218 - 223.
- Singh, K.K., & Singh, A. (2017). Identification of flooded area from satellite images using Hybrid Kohonen Fuzzy C-Means sigma classifier. The Egyptian Journal of Remote Sensing and Space Science. 21(1), 147-155, 2017.
- Uttaruk, Y., & Laosuwan, T. (2016). Remote sensing based vegetation indices for estimating above ground carbon sequestration in orchards Agriculture & Forestry. 62(4), 193-201.
- Uttaruk, Y., & Laosuwan, T. (2018). Community Forest for Global Warming Mitigation: The Technique for Estimation of Biomass and Above Ground Carbon Storage using Remote Sensing Method. Agriculture & Forestry. 64(3), 47-57, 2018.
- Zhang, M., Chen, F., Liang, D., Tian, B., & Yang, A. (2020). Use of Sentinel-1 GRD SAR Images to Delineate Flood Extent in Pakistan. Sustainability, 12(14), 5784.

GENERATION OF INDICATORS TO ASSESS THE FLOOD VULNERABILITY INDEX IN HOI AN CITY, VIETNAM

Thuy Linh Nguyen¹, Chisato Asahi¹, Thi An Tran², Ngoc Hanh Le³

¹Department of Urban Science and Policy, Graduate school of Urban Environmental Sciences, Tokyo Metropolitan University, 1-1 Minami-Osawa, Hachioji-shi, Tokyo, Japan 192-0397

Email: nguyen-linh-thuy@ed.tmu.ac.jp, asahi@tmu.ac.jp

²Faculty of Management Science, Thu Dau Mot University, Vietnam
06 Tran Van On Street, Phu Hoa Ward, Thu Dau Mot City, Binh Duong Province, Vietnam
Email: tranthian.gis@gmail.com

³University of Science and Education, The University of Danang, 459 Ton Duc Thang, Danang City, Vietnam
Email: hanhlespdn@gmail.com

ABSTRACT

Floods, which are among the most-frequent types of natural disaster, have caused massive impacts on human health, socio-economic activities and the quality of the natural environment throughout history. Undertaking research or assessment on flood risk was and has been extremely necessary in the context of more uncertainties and risk associated with the climate system. Identifying the vulnerability is one step moving forward the assessment of flood risk and is also a supporting tool for policymakers in proposing compatible response solutions. The identification of vulnerability is based on analyzing various indicators which form the scientific basis for mapping flood vulnerability. This research aims at establishing indicators for assessing the vulnerable level of 9 wards and 3 communes in Hoi An where has high exposure level to flood but has not yet had comprehensive assessment of vulnerability. A set of indicators including totally 9 indexes covering three main components which are exposure (E), sensitivity (S) and adaptive capacity (AC) were selected for flood vulnerability index (FVI) calculation and the creation of flood vulnerability map in Hoi An city.

1. INTRODUCTION

Among the most frequent and devastating natural hazards, floods are the one that has caused massive damages to human life and ecosystems (Wallemacq *et al.*, 2018). In Southeast Asia countries, flood management is more on the side of being reactive in responding to disaster situations, rather than being proactive in minimizing the possibility in advance. This way of management shows its limitations when floods still cause serious damage to human's life and property annually. There are several reasons for developing countries to follow such a management approach, including the lack of budget, facilities, human resources, and more importantly the limitation in the number of comprehensive research on flood risk and vulnerability assessment. During thousands of years of history, Vietnam has faced many

floods with severe consequences across the country. The frequency and intensity of floods have caused significant difficulties in planning and management in Vietnam. In recent years, flood control actions have been more effective by applying flood risk assessment. Although it is difficult to quantify the risk of flooding because risks are the consequences of natural phenomena, flood risk can be minimized by reducing the vulnerability of the object or region which is affected by floods. This study applied the definition which has been agreed among most researchers that the vulnerability of a system is determined by three components: exposure (E), susceptibility (S), and resilience (AC) (Balica and Wright, 2010; UNISDR, 2009). In Vietnam, though there is still a limit on the number of research on vulnerability and assessment of flooding risks, the so far achievements have significantly contributed to the tightening of flood management. Studies on flood vulnerability in Vietnam mainly conducted in major river basin regions while studies on urban level have not yet received the deserved attention. This study aims at building spatial distribution of flood vulnerability (FVI map) in Hoi An city to answer the following questions:

- (1) Which area of the city most vulnerable to flood? And what factors make them most vulnerable?
- (2) What solutions can be proposed to reduce the vulnerability?

2. METHODS AND DATA SELECTION

2.1 Methods

Multi-criteria decision analysis employing geographic information system technique (GIS) and analytical hierarchy process ranking method (AHP) was used in this flood vulnerability evaluation. AHP has been considered as a practical method to address a broad decision-making problem involving a wide range of criteria (Saaty, 1990). In this study, AHP was used in selecting most appropriate indicators for FVI's components; and in identifying the weights for selected indicators. Questionnaire surveys were sent to three experts and officers from the people's committee of Hoi An city to build the initial AHP hierarchy. To solve the problems caused by the difference in units of selected indicators, all data were normalized to a standard scale from 0 to 1 employing minimum-maximum normalization (Krajnc and Glavič, 2005) before the ranking process. Afterward, the FVI was calculated as:

$$FVI = f(E, S, AC)$$

Where: FVI is the flood vulnerability index; E is exposure; S is susceptibility; AC is adaptive capacity.

2.2 The selection of indicators

Different types of data set from varied sources were collected for constructing spatial criterion layers employing geospatial calculation actions. Socio-economic data was obtained from the 2020 statistical yearbook of Hoi An city published by the Government, 10m Digital Elevation Model (DEM), land use map, The Open Street Map (OSM).

2.2.1 Exposure

-*Average elevation of terrain (AET)*: AET is considered to have the most priority in AHP

flood hierarchy since the topography directly influence on the level damage and the ability to recover after flooding (Tran *et al.*, 2014); therefore, this indicator was discussed and given the highest weight (an equal priority to flood frequency). The 10m Digital Elevation Model (DEM) data source provided by Quang Nam Department of Natural Resource and Environment (DONRE) was used to calculate AET. The administrative map and DEM surface were imported to GRASS GIS open-source software (using *r.stats.zonal* command) for elevation calculation for each ward/commune.

- *Average distance to the mainstream of Thu Bon River (DIST_R)*: The excess water-flow of Thu Bon mainstream causes most floods in Hoi An. The DIST_R data was generated by calculating the euclidean distance to the river channel using the *r.grow.distance* tool in GRASS GIS. The river network was extracted from hydrology data by Quang Nam DONRE and then was used as input data source for calculation of DIST_R. The zonal statistical method (*r.stats.zonal*) has been applied for calculation of average distance to river channels by ward/commune.

- *Flood frequency (EF)*: Since the FF values represent flood occurrence history, this indicator was considered to have the very strong importance as AET. Because the local community in Hoi An has not really taken radical measures to reduce flood risks and has not really adapted to this natural disaster, FE in this research is considered as an indicator that can increase the vulnerability rather than an indicator that reflects people's past experiences. EF was calculated by summing the total number of floods that occurred from 2016-2020 in Hoi An according to local statistics.

2.2.2 Susceptibility

- *Population density (P_DENS)*: The population growth and distribution, especially increased population density can increase the vulnerability to disasters (Perrow, 2007). In this research, P_DENS was considered as a strong important indicator due to its direct impact to the level of loss of life in a disaster. P_DENS was taken from Hoi An statistical yearbook 2020.

- *Number of historical sites (HIS)*: Historical sites in Hoi An need particular attention in flood management due to their irreplaceable cultural value and their sensitive constructive typologies (Fabiana and Tiago, 2019). In consequence of that, considering historical sites as a vulnerable indicator is necessary. HIS was taken from the 2020 statistical yearbook. Hoi An has 23 sites that have been certified as national historical sites and 47 sites that have been certified as provincial historical sites by the Ministry of Culture, Sports and Tourism of Vietnam in 2020. The higher HIS value in the ward, the greater the risk of damage.

- *Number of households in vulnerable groups categorized by economic status (VUL_ECO)*: VUL_ECO covers the number of poor and near-poor households in the research area. According to article 2, decision No. 59/2015/QD-TTg of Vietnamese Government on the poverty line applied for the period 2016-2020, in terms of income, households with average income per month less than 700.000 Vietnamese Dong are considered poverty; meanwhile, near-poor households are those with monthly income of 700.000 to 1 million Vietnamese Dong.

2.2.3 Adaptive capacity

- *Number of working age adults (W_AGE)*: Children and the elderly are more vulnerable to flood hazard while people in working age are less vulnerable to flood due to the health status. Moreover, the working age group is the main source of labor force for economic development. Therefore, the ward or commune with the larger number of working age adults will be better able to cope with the consequences of floods. W_AGE was taken from Hoi An statistical yearbook 2020.

- *Road density (R_DENS)*: The OSM data was downloaded and then imported to GIS environment for updating the total road length and the road density by ward/commune. The zonal statistics method was applied in GIS to take the road length by commune with the base map as the administrative map and the cover map as the road map for Hoi An. These values of road length by commune then were divided into the area of each ward/commune to get the road density.

- *Annual average income per capita*: Income contributes to an individual's ability to prepare for a flood and rebuild (Rasch, 2015). Due to the uneven impact of covid-19 on different ward/commune, the data of average income per person per year in 2019 was used in this assessment to evaluate the degree of vulnerability.

3. RESULTS AND DISCUSSION

Before the normalization, each indicator was identified their relationship with FVI; in which EF, P_DENS, HIS and VUL_ECO have positive relation to FVI (an increase in the indicator value lead to an increase in FVI value); and AET, DIST_R, R_DENS, W_AGE and INC have an inverse relation to FVI (an increase in the indicator value lead to a decrease in FVI value). The normalized values and weights for 9 indicators of FVI's components are shown in Table 1.

Table 1. Normalization value and weights of vulnerability's indicators

Wards	AET	DIST_R	EF	P_DENS	HIS	VUL_ECO	W_AGE	R_DENS	INC
Minh An	0.49	0.04	1.00	0.96	0.95	0.00	0.84	0.16	0.00
Tan An	0.00	0.40	0.00	0.84	0.16	0.02	0.61	0.38	0.16
Cam Pho	0.45	0.14	1.00	1.00	1.00	0.00	0.41	0.39	1.00
Thanh Ha	0.36	0.25	1.00	0.18	0.53	0.04	0.00	0.95	0.55
Son Phong	0.52	0.14	0.93	0.73	0.37	0.07	1.00	0.00	0.03
Cam Chau	0.94	0.43	0.93	0.16	0.53	0.04	0.15	0.55	0.06
Cua Dai	0.97	0.36	0.33	0.21	0.00	0.74	0.67	0.69	0.09
Cam An	0.56	1.00	0.33	0.12	0.11	0.31	0.79	0.72	0.09
Cam Nam	0.91	0.00	1.00	0.11	0.11	0.24	0.62	1.00	0.42
Cam Ha	0.38	0.72	0.33	0.05	0.37	0.37	0.55	0.98	0.81

Cam Kim	0.82	0.03	1.00	0.01	0.21	1.00	1.00	0.94	0.67
Cam Thanh	1.00	0.18	0.93	0.00	0.58	0.63	0.43	0.98	0.64
Weight	0.40	0.20	0.40	0.31	0.46	0.23	0.40	0.40	0.20
<i>RI = 0.58, λmax = 3; CR = 0</i>									

The value of E, S, AC were calculated by multiply the normalized value of each indicator with its corresponding weight. In order to analyzing the impact of AC on the flood vulnerability result, the flood susceptibility map was calculated by integrating of flood exposure (E) and susceptibility (S) components (Equation 1). Subsequently, the flood vulnerability index was determined based on the investigation of flood susceptibility and the adaptive capacity (AC) as shown below (Equation 2).

$$FSI = \frac{1}{2}(E+S) \quad (1)$$

$$FVI = \frac{1}{3}(E+S+AC) \quad (2)$$

Where: FSI is Flood susceptibility index

FVI is Flood vulnerability index

Table 2. FVI value applying AHP weights

Wards	E	S	AC	FSI (without AC)	FVI (with AC)
Minh An	0.60	0.66	0.40	0.63	0.55
Tan An	0.08	0.27	0.43	0.18	0.26
Cam Pho	0.61	0.69	0.52	0.65	0.61
Thanh Ha	0.59	0.29	0.49	0.44	0.46
Son Phong	0.61	0.36	0.41	0.49	0.46
Cam Chau	0.84	0.29	0.29	0.56	0.47
Cua Dai	0.59	0.28	0.57	0.44	0.48
Cam An	0.56	0.17	0.62	0.37	0.45
Cam Nam	0.77	0.15	0.73	0.46	0.55
Cam Ha	0.43	0.30	0.77	0.36	0.50
Cam Kim	0.73	0.41	0.91	0.57	0.68
Cam Thanh	0.81	0.46	0.69	0.64	0.65

By applying the manual classification method (Samanta et al., 2016) with equal interval, the FVI values were categorized into 5 ranges. Without considering AC employing AHP: very low (0.18 - <0.27), low (0.27 - <0.37), medium (0.37 - <0.46), high (0.46 - <0.55), very high (>= 0.55); Considering AC employing AHP: very low (0.26 - <0.35), low (0.35 - <0.43), medium (0.43 - <0.51), high (0.51 - <0.59), very high (>=0.59).

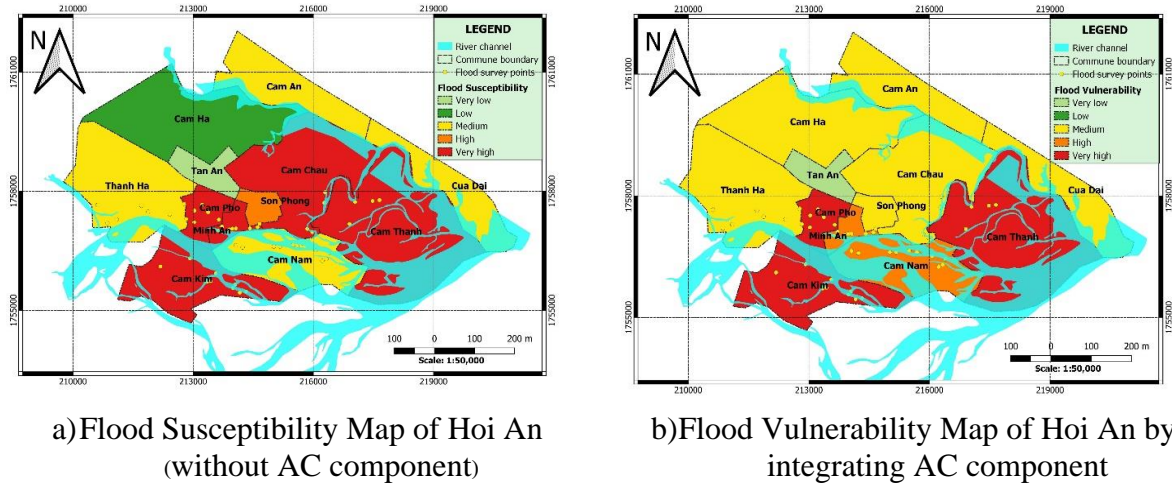


Figure 1. Integrated flood vulnerability map in Hoi An city

The flood susceptibility map of Hoi An generated by Equation (2) shows that there is a large area under very high level including the communes of Cam Kim, Minh An, Cam Pho, Cam Chau and Cam Thanh. These areas are located near the mainstream of Thu Bon River with relatively low elevation. The high level areas include Son Phong and Cam Nam wards which are also located along the mainstream of Thu Bon river. Thanh Ha, Cua Dai has medium level of vulnerability while Cam Ha, Cam An are communes under low level of flood susceptibility due to the location in the opposite side of main river and nearby the coastline which is usually well-drainage. Tan An is the ward with a very low susceptibility level due to its specific location and topography. Taking into account the AC, the flood vulnerability map has slightly changed in the categories compared to the flood susceptibility map. Minh An is the centered ward of the Hoi An City with relatively high economic condition as well as adaptive capacity, therefore these areas have fallen into the lower level compared to the flood susceptibility map. Son Phong, Cam Chau are the wards under the high speed of economic development and their AC are also increasing, therefore these areas have dropped to the medium level in the flood vulnerability map. Cam Pho, Cam Nam still retain their high level of vulnerability and Thanh Ha, Cua Dai have seen no changes in their medium rank. On the contrary, the Cam Ha, Cam An are the communes located in the suburb of Hoi An downtown with the considerably lower AC compared to other areas, hence they have become the medium flood vulnerability areas. These communities need to be enhanced both in awareness as well as the adaptive capacity to the flood and other disasters for sustainable development. Cam Kim and Cam Thanh are always under very high level both in flood susceptibility or vulnerability map. This indicates that there is an urgent need for promoting the local adaptive capacity as well as protecting these areas from the flood susceptibility. Tan An is the only ward which is always under very low level of flood susceptibility as well as vulnerability.

4. REFERENCES

- Balica, S., and Wright, N., 2010. Reducing the complexity of the flood vulnerability index. *Environmental Hazards* 9, 321-339.
- Fabiana, M.N., and Tiago, M.F., 2019. A simplified approach for flood vulnerability

- assessment of historic sites. *Natural Hazards* 96, 713-730.
- IPCC, 2014. Climate Change 2014: the Fifth Assessment Report (AR5) of the Intergovernmental Panel on Climate Change on Climate, Copenhagen
- Krajnc, D., and Glavič, P., 2005. How to compare companies on relevant dimensions of sustainability. *Ecological Economics* 55, 551-563.
- Perrow, C., 2007. *The next catastrophe: Reducing our vulnerabilities to natural, industrial, and terrorist disasters revised*. Princeton University Press, New Jersey.
- Rasch, R., 2015. Assessing urban vulnerability to flood hazard in Brazilian municipalities. *Environment and urbanization* 28, 145-168.
- Saaty, T.L., 1990. How to make a decision: The analytic hierarchy process. *European Journal of Operational Research* 48, 9-26.
- Tran, T. A., Raghavan, V., Masumoto, S., Vinayaraj P. and Yonezawa, G., 2014. A geomorphology-based approach for digital elevation model fusion - Case study in Danang City, Vietnam. *Earth Surface Dynamics* 2, 403-417
- UNISDR, 2009. *Global Assessment Report on Disaster Risk Reduction*. United Nations, Geneva, Switzerland
- Vietnamese Government, 2015. *Article 2, Decision No. 59/2015/QD-TTg Regulations on the poverty line applied for the period 2016-2020*. Hanoi.
- Wallemacq, P., Below, R., and McLean, D., 2018. *UNISDR and CRED report: Economic Losses, Poverty & Disasters (1998 - 2017)*. Centre for Research on the Epidemiology of Disasters. CRED

Machine Learning for Urban Types Detection Using Sentinel-1 And Sentinel-2

Niang Sian Lun¹ and Sarawut Ninsawat¹

¹ Remote Sensing & GIS

Department of Information and Communications Technologies (ICT)

School of Engineering and Technology (SET)

Asian Institute of Technology (AIT)

Email: sianlun10@gmail.com, sarawutn@ait.ac.th

ABSTRACT

The urban various categories characteristics have emphasized the great importance of understanding and creating suitable land evaluations in the future. The overall objective of this study is to classified the urban zone utilizing building height and various satellite-based indexes of Sentinel-2A. First, the building height was estimated from the Sentinel-1A SAR. A new indicator VVH, which can provide a better performance, is produced from the dual-polarization information, VV and VH. Then, the building height model was developed using indicator VVH and the reference building height from NOSTRA building block data. The root mean square error (RMSE) between estimated and reference height is 1.413m. Then the machine learning to classify three urban types which are composed of the residential area, commercial area, and other areas including vegetation, waterbody, car parking, and so on were developed. To classify the urban types, the three-machine learning classifier; support vector machine, random forest, and k-nearest neighbours were developed by using the estimated building height and other satellite-based indices such as NDVI, NDWI, and NDBI. The classification is randomly trained data from eight focus areas and each area is divided into a 100x100m grid. Different parameter components of machine learning models are examined, for example, classification using only building height, and the only spectral indices. There are a total of 16 variables that are the minimum, maximum, mean and standard deviation building height, and the satellite-based indices of NDIV, NDWI, NDBI were used to classify the urban types with the models. Eventually, the Principal Components Analysis (PCA) was used to reduces the variables and get better performance of the models. SVM showed better accuracy than the other two RF and KNN. The accuracy of SVM, RF, and KNN are 0.86, 0.75, and 0.76 respectively.

Keywords: SAR, building height, urban types classification, machine learning

1. INTRODUCTION

Urban types identification is carried out for urbanization to comprehend how urban forms evolve and to manage environmental sustainability, congestion, pollution, and natural disasters such as floods and earthquakes (Misra et al., 2018). The utilization of remotely sensed data is becoming more common in distinguishing urban types for their high resolution and availability of information. As optical RS and SAR data are combined, the overall precision of urban classification is higher than when optical remote sensing or Sentinel-1A product is used alone (Corbane et al., 2008), (Bencure et al., 2010).

The objective of the study is to develop a machine learning model to classify urban types. The urban types were classified as (i) residential areas, (ii) commercial areas, (iii) other areas based on the parameters of building height and satellite-based indices. The classification was generated using the 16 variables of minimum, maximum, mean and standard deviation of building heights and the satellite-based indices.

2. STUDY AREA

Nonthaburi province is situated directly northwest of Bangkok on the Chao Phraya River. The population is 259,375 persons in 2019 and the area of Nonthaburi province is 38.90 sq-km which is registered as the second most populous city municipality in Thailand. The Nonthaburi research area is very wide and the process is carried out in the eight study areas in the province. The eight target zones of 500 x 500 meters are selected and each zone is divided into a 100x100m grid as shown in Figure 1, with different forms of the city, which are compact residential, industrial and high-rise buildings.

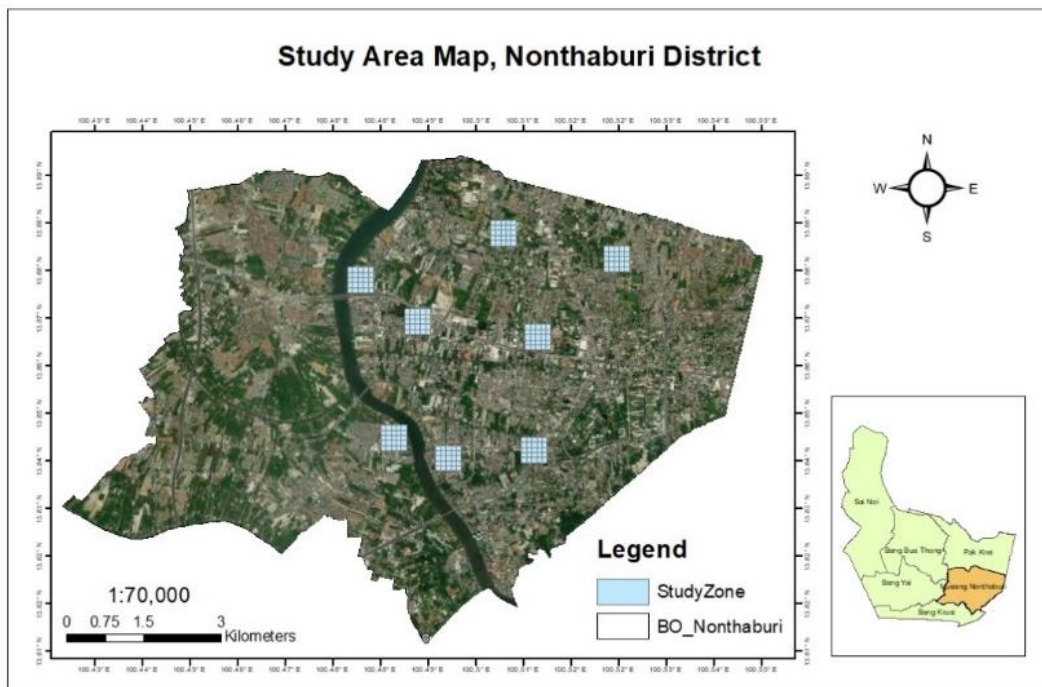


Figure 1 Study Area Map of Nonthaburi Province

3. METHODOLOGY

There are four main parts in the methodology as shown in Figure 2, including data preparation, building height estimation, urban types classification and accuracy assessment. The satellite data used for this research were from Sentinel-1A and Sentinel-2A in the year 2020 and the building block was a GIS shapefile which is developed by NOSTRA company. The data was published in 2012. In the data preparation section, SAR data was preprocessed with noise reduction, calibration, speckle filtering, and terrain correction using SNAP software. Moreover, the preprocessing of Sentinel-2A, multispectral data include atmospheric correction and surface reflectance computation, and the indices such as NDVI, NDWI, and NDBI were calculated. For the reference data, the raw building blocks from 2012 were checked and reorganized the data by adding or deleting the building blocks, calculating building heights from the number of floors.

After preprocessing, VV, and VH polarization were extracted from Sentinel-1A and the mean, minimum, maximum and standard deviation of VV and VH were used to estimate the height of each building. For the classification of urban types, both the estimated building height

from Sentinel-1A and satellite-based indices from Sentinel-2A were applied in the 100x100m grid-based zone. There are 100x100m grid zonal statistics of 12 parameters of the three satellite-based indices and 6 parameters from building height including mean, maximum, minimum, and standard deviation. The urban categorization was carried out as a grid-based classification using 194 sample grids in eight zones of the study area. All the minimum, maximum, mean and standard deviations were extracted using zonal statistic table in ArcMap. Three groups of urban types were identified using machine learning algorithms such as random forest, support vector machine, and k-nearest neighbours with the data standardization, principal component analysis, and tuning hyperparameter to reduce the processing time and increase the accuracy. To assesses the performance of urban types classification, the accuracy result was reported by precision, F1-score, recall, and accuracy values.

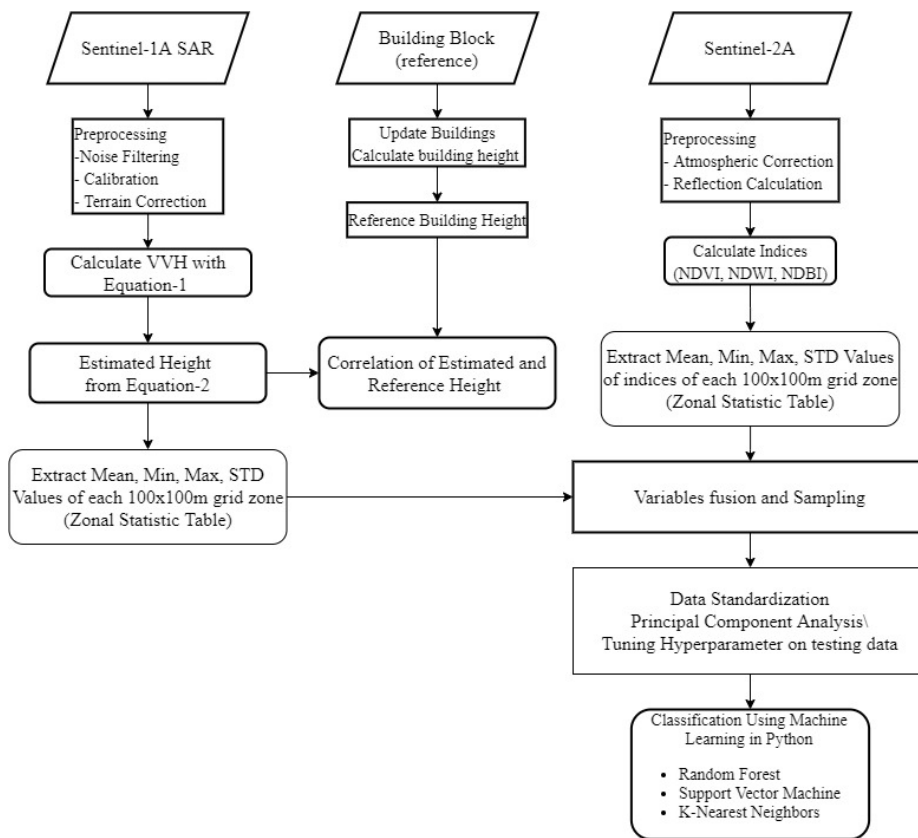


Figure 2 Overall Methodology of the Study

3.1 Building height model

A new indicator was processed for estimating building height in the first step after preprocessing Sentinel-1 GDR data. The mean value of the backscatter coefficient, VV, and VH, was extracted from the image to calculate the VVH indicator, equation 1 (Koppel et al., 2017). The equation for the new indicator of VVH shows better performance and a lower uncertainty range of estimated building heights (Li et al., 2020).

$$VVH = VV * \gamma^{VH} \quad (1)$$

To get the VVH value, the sigma 0 VV and VH value are calculated at different percentile levels that are ranging from 5% to 100% at a step of 5%. After that, VVH is enumerated with

Equation (1) using different γ values ranging from 1 to 10 and compared the results. The estimated height is extracted by using equation (2) from the 8 study zones and compare with the reference height.

$$\ln H = a * VVH^b + c \quad (2)$$

3.2 Machine learning classification of urban types

The machine learning model for urban types classification was developed by using building heights and satellite-based indices. The zonal statistic of mean, minimum, maximum and standard deviation of satellite-based indices include NDVI, NDWI, and NDBI of each grid were utilized to process the classification of the urban type. The 100m grid-level were generated in 500m eight zones.

In this study, three classifiers including support vector machine (SVM), random forest (RF), and K-nearest neighbours (KNN) were used. As shown in Table 1, a total of 194 sample grids were categorized for each urban type with a test size of 0.3. PCA and standardization which are for scaling and reducing the number of features were used. There are 5 experiments as shown in the Table 2 to distinguish urban types using a different composition of 16 parameters.

Table 1 Training Set Size for Training and Testing

Classes	Training	Testing
Residential Area	89	39
Commercial Area	26	12
Other Area	20	8

4. RESULT AND DISCUSSION

4.1 Building height estimation in the Nonthaburi

The VVH was calculated from VV and VH values which are percentile values, the output values change according to the γ value, gamma values are ranging from 1 to 10. Among them, $\gamma = 1$ produced the best R square value (0.8561). When γ values are higher, the R square of VVH dropped because γ is a parameter to characterize the relative impact of VH, which has negative values and is lower than VV values to the derived VVH. The VVH performs better and has a reduced uncertainty range of predicted building heights.

It should be emphasized that the term "building height" in this study refers to the average height inside the 100 m grid, which includes both buildings and non-building such as roadways and parking lots. To achieve a balance of model performance and spatial details of derived building heights, 100 m is the aggregation resolution with the equation (2) at $\gamma = 1$ of VVH value. The final parameters of a, b, and c are 0.2799, 1, and 5.727 respectively. The building height model using Sentinel-1A image and reference building height data performed well with root mean square error 1.413m and 0.8557 of R square value as shown in figure 3.

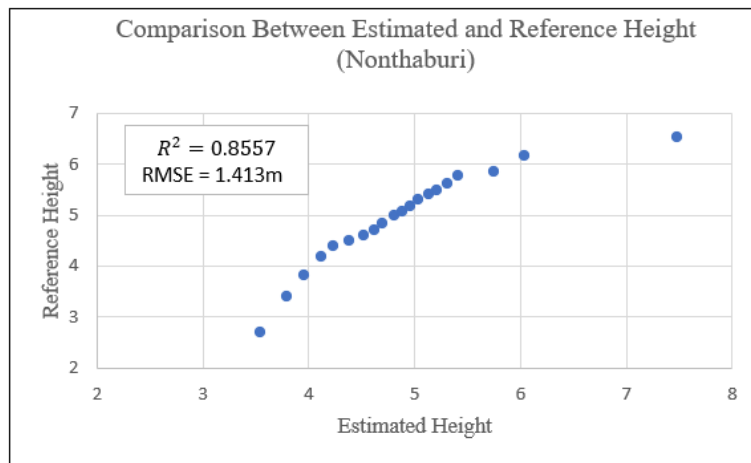


Figure 3 Chart Comparison of Estimated and References Height in Nonthaburi

4.2 Urban types classification

In this research, the classification results were produced and compared by combining different five cases as shown in table 2 to check which composition would provide good accuracy. Overall, the support vector machine worked very well as compared to other models. The results may change according to the variables which are used for classification.

The results of case 2, using the only average of all index and building height did not appropriate to classify the urban types and also all the classifiers performed poor accuracy ranging from 63 per cent to 71 per cent. Furthermore, cases 3 and 4 were analyzed, using separation of the height and indices show a better performance in some classifiers. RF has the highest result with 0.73 in the case of using only building height, classification with indices has the largest accuracy from the SVM classifier, 0.76.

Table 2 Parameters Used and Accuracy for Classification on Different Cases

Cases	Building Height	NDVI	NDWI	NDBI	RF	SVM	KNN
Case 1	mean, max, min, std	mean, max, min, std	mean, max, min, std	mean, max, min, std	0.75	0.86	0.76
Case 2	mean	mean	mean	mean	0.63	0.63	0.71
Case 3	mean, max, min, std				0.73	0.68	0.66
Case 4		mean, max, min, std	mean, max, min, std	mean, max, min, std	0.72	0.76	0.69
Case 5	mean, max, min, std	mean, max, min, std		mean, max, min, std	0.73	0.81	0.72

Case 5 (exclude NDWI index in this model) produced higher accuracy when compared with cases 2,3 and 4. Since there were numerous numbers of building and vegetated areas and less in the water body, the building height with NDVI, NDBI provided good accuracy for classification. However, the building heights and all satellite-based indices have the highest accuracy among all the combinations. All the variables are considered as mean, minimum, maximum, and standard deviation of each parameter (case1).

Additionally, the Principal Component Analysis (PCA) technique was adopted to minimizes the number of parameters and reduce the redundancy. The number of components in the PCA module was 0.95. After PCA, the new dimensionally reduced components were created. From table 3, the results were different because of high dimensionality with highly linked variables, PCA can increase the classification model's accuracy.

Table 3 The Accuracy Compared With PCA, Without PCA

PCA				Without PCA		
Cases	All parameter	Heights	Indices	All Parameter	Heights	Indices
RF	0.75	0.73	0.72	0.78	0.68	0.63
SVM	0.86	0.68	0.76	0.78	0.66	0.66
KNN	0.76	0.66	0.69	0.73	0.66	0.66

5. CONCLUSION AND DISCUSSION

Following the objectives, the building heights and classification were generated using Sentinel-1A and Sentinel-2A in the 100 x 100 m grid samples. The research information is beneficial for evaluating urban modelling, assessing changes in population density, energy usage, and so on. The method proposed for building height estimation in this work could be used to provide a global estimate of height. It would be better if more indices, urban layout and more detail classes were applied for the classification of urban types in the future. The number of algorithms will develop and be improved to be more suitable for usage in a variety of urban types.

6. REFERENCES

- Bencure, J., Tripathi, N. K., Gallardo, W., Boromthanarat, S., Ebbers, T., & Singhroy, V. (2010). Integration Of Sar, Optical Remote Sensing Data And Gis For Change Detection And Restoration Of Nipa Palm Plantation In Pak Phanang, Thailand. May 2010.
- Corbane, C., Faure, J. F., Baghdadi, N., Villeneuve, N., & Petit, M. (2008). Rapid urban mapping using SAR/optical imagery synergy. Sensors, 8(11), 7125–7143.
- Koppel, K., Zalite, K., Voormansik, K., & Jagdhuber, T. (2017). Sensitivity of Sentinel-1 backscatter to characteristics of buildings. International Journal of Remote Sensing, 38(22), 6298–6318.
- Li, X., Zhou, Y., Gong, P., Seto, K. C., & Clinton, N. (2020). Developing a method to estimate building height from Sentinel-1 data. Remote Sensing of Environment, 240(July 2019), 111705.
- Misra, P., Avtar, R., & Wataru Takeuchi. (2018). Comparison of Digital Building Height Models and SRTM Digital Surface Models over Yangon City.

ESTIMATING CHLOROPHYLL-A VARIATIONS WITH TEMPORAL MODIS DATA TIME SERIES

Phan Minh Thu^{1,2*}, Nguyen Thu Thao³ and Ho Dinh Duan⁴

¹Institute of Oceanography, Vietnam Academy of Science and Technology (VAST), Vietnam

²Graduate University of Science and Technology, VAST, Ha Noi, Vietnam

³HCMC University of Natural Resources and Environment, Ho Chi Minh City, Vietnam

⁴HCMC Space Technology Application Center, Vietnam National Space Center, VAST, Vietnam

Correspondence Email: phanminhthu@vnio.org.vn

ABSTRACT

Chlorophyll-a concentration (Chl-a) is an important factor in ecological property of the marine and coastal environment monitoring. It is a crucial index for water quality assessment in addition to others such as BOD, COD, TSS and etc. There exists an abundance of algorithms for estimating Chlorophyl-a concentration using Remote Sensing data, as well as its variation in time. In this study, we focus on analyzing the Chlorophyl-a concentration in surface water time series of Van Phong Bay area during the past 20 years based on the ocean MODIS data (NASA /OCEANDATA /MODIS-Aqua/L3SMI). Our approach used the Google Earth Engine (GEE) algorithms and processing capability of these tools. The study area, Van Phong Bay, is located in the vicinity north of Nha Trang City, a well-known tourism landmark of Vietnam, and also an important aquaculture site of the locality. Our study has revealed certain connection between the variation of Chlorophyl-a concentration in this area with the past incidents of algae bloom, as well as showing some trends and seasonal variation of the Chlorophyll-a index, which can be useful for prediction of water quality in the study area.

1. INTRODUCTION

Marine ecology has strong relationship with status and variation of Chlorophyll-a concentration (Chl-a). It is a key parameter in monitoring the marine and coastal environment, which has long been achieved by combining in-situ observations with remote sensing ocean color radiometry (OCR) (Shao *et al.*, 2011). The importance of understanding Chl-a in coastal waters has furthermore a particular interest, as it is an indicator for the health and nutrient status of the coastal habitats (Ferreira *et al.*, 2011; IOCCG, 2012). Chl-a has been well-known as an index of phytoplankton biomass, which is primarily responsible for the big process of carbon dioxide to organic carbon transformation (Falkowski & Kiefer, 1985; Sathyendranath *et al.*, 2019).

Estimation of Chl-a so far has been successfully achieved with satellite imageries and water sampling work, especially with the utilization of new remote sensing ocean color algorithms such as the OC2-6 for vast ocean regions as well as coastal areas (Gitelson *et al.*, 2011; O'Reilly & Werdell, 2019). Though these algorithms are by their nature either global or localized, which means there is a trade-off between using global models (lower accuracy) and regional models (higher accuracy, but for a specific area). In this aspect, a refined algorithm would be preferable for using the OCx algorithms to calculate Chl-a in coastal areas; but in the absence of an up-to-date formula of the algorithm, a multi-year thorough investigation with the presence of sufficient satellite data would be acceptable (Gitelson *et al.*, 2011; Hu *et al.*, 2012; O'Reilly & Werdell, 2019). One of the present-day tools that enables the harnessing of the huge inventory of satellite imageries for realizing the OCx algorithms, is the Google Earth Engine

(GEE) (Wang *et al.*, 2020). This tool provides a good time series of available cloud-based satellite data as well as a powerful computational capacity to support our study. In this study the temporal L3SMI MODIS dataset was used (NASA OB.DAAC, 2021), in combination with in-situ data of Chl-a.

The relatively rich variations of Chl-a in coastal waters partly reflects the unique features of the regional ecological system of a particular area, especially when it inherits a ubiquitous natural formation such as a half-closed bay with estuaries and a high tidal fluctuation. This is the case of our study. Van Phong bay is located north of Nha Trang city, a medium-size city with not only a unique landscape, but also under the process of rapid urbanization with plenty of tourism and aquaculture facilities. The human activities, together with the seasonal upwellings of the encompassing sea, are main factors that have long been contributing to the high variations of Chl-a in and near the bay (An, 2002). In the past, there have been several harmful algal blooms in these areas, which proved the extreme fluctuation of Chl-a concentration in the region. This kind of marine incidents have been recorded in 2007, 2011-2012, 2014, 2016- 2017, and 2018-2019, and to some extent has been studied and analyzed, which eventually showed a clue to Chl-a boom in the region (Doan-Nhu *et al.*, 2017; Luom *et al.*, 2021). With the data and computation engine provided by GEE, the present study aims at obtaining a picture of the variations through the years and an analysis of its trends and the seasonal behaviors. The mathematical tool used here is Fourier analysis. Through studying the extents of the multi-year Chl-a variations, a relationship with past algal blooms, though not very strong, could be revealed. The effects of upwelling, nutrient sources, and climatological factors, are with no doubt related to the Chl-a fluctuations, but they are beyond the scope of this paper, and should dedicate another discussion.

2. METHODOLOGY

2.1 Study area and materials

Van Phong Bay is located in the north of Khanh Hoa Province (Figure 1). The longitudinal coordinate of the bay has the easternmost position of Vietnam. It has a water surface area of 41,000 ha and a depth of 20-30 m, and is relatively free from wind. Thus, Van Phong Bay does not only contribute to fishing ground and aquaculture and but also targets to development of a region for international container transportation port and marine ecotourism. However, due to the impact of inland activities and marine aquaculture, the environment has been significantly degraded.

This study was conducted using MODIS data of Ocean Color SMI (Standard Mapped Image) MODIS Aqua Data, in which Chl-a (in mg m^{-3}) was collected in the period from 01 Jan 2003 to 31 Dec 2020 (NASA OB.DAAC, 2021). The daily data was used to calculate the monthly value for the inner and outside Van Phong Bay (Figure 1).

In addition, in-situ data from the surveys in 2018 - 2019 were used to compare with remote sensing derived values. The in-situ Chl-a data were analyzed from water samples collected at surface layers from stations allocated in the area (Figure 1). The water samples were filtered by Whatman GF/F 47 mm, then samples were extracted in acetone 90% in 4°C for 24 hours, after that the Chl-a concentration was measured in spectrophotometer U2900 following the method of Jeffrey *et al.* (Jeffrey *et al.*, 1997).



Figure 1. Study area with boundary of Van Phong Bay, Vietnam.

2.2 Data analysis

MODIS images were collected and processed on Google Earth Engine (GEE) platform (<https://code.earthengine.google.com/>). Daily Chl-a bands in the period of 2003-2020 were calculated for monthly averages for each region of inner and outside Van Phong Bay. The values of Chl-a were analyzed by classical decay method, which has been widely known in marine scientific literature (Mélin *et al.*, 2011; Vantrepotte & Mélin, 2010). According to this method, a time series of Chl-a concentration is described by the following equation (Mudelsee, 2014):

$$\{Y_t\}_{t=1}^N = S_t + T_t + R_t$$

Where Y_t is the monthly average time series of Chl-a, S_t is seasonal cycle component repeated with a frequency of 12 months, T_t is the trend component of changes over time; R_t is the seasonal stochastic component.

3. RESULTS AND DISCUSSION

3.1 In-situ vs MODIS Chlorophyll-a concentration

The survey results show the variation of Chl-a in Van Phong Bay between the rainy and dry seasons (Table 1). In-situ Chl-a in the rainy season (with a mean of $3.23 \pm 2.38 \text{ mg m}^{-3}$) was significantly higher than that in dry season (with a mean of $2.33 \pm 2.28 \text{ mg m}^{-3}$) ($p=0.05$). The

highest values in both seasons were found in the station VP03 in the upper bay; this station is shallow and influenced by nutrient suppling from wastewater of shrimp culture (An, 2002). A comparison between in-situ data with MODIS data in Figure 2 indicated that the average of Chl-a showed a decrease from in-situ value, to monthly MODIS and climatological monthly MODIS. In terms of spatial distribution, in-situ Chl-a reduced from the upper area to the southern opening of the bay (Minh-Thu *et al.*, 2014). In addition, in-situ, monthly and climatological MODIS Chl-a have the same trend and pattern in rainy and dry seasons. This fact suggests that monthly MODIS Chl-a could be used as a hint for the trend and variation of this index.

Table 1. Statistical values of in-situ Chlorophyll-a concentration in Van Phong Bay (Std: Standard Deviation)

Season	Min	Max	Average	Std
Rainy, 2018	0.67	8.37	3.23	2.38
Dry, 2019	0.57	8.33	2.33	2.28

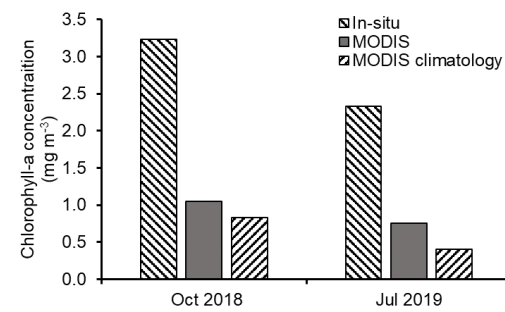


Figure 2. Comparison of Chlorophyll-a concentration in inner Van Phong Bay

Figure 3 shows the variation of monthly MODIS and climatological MODIS Chl-a in Van Phong Bay. In both the inner and outer regions, Chl-a has a reducing concentration from January to April, then a low pattern to August, after that Chl-a increased to the end of the year. The peak of Chl-a could be found in November and December.

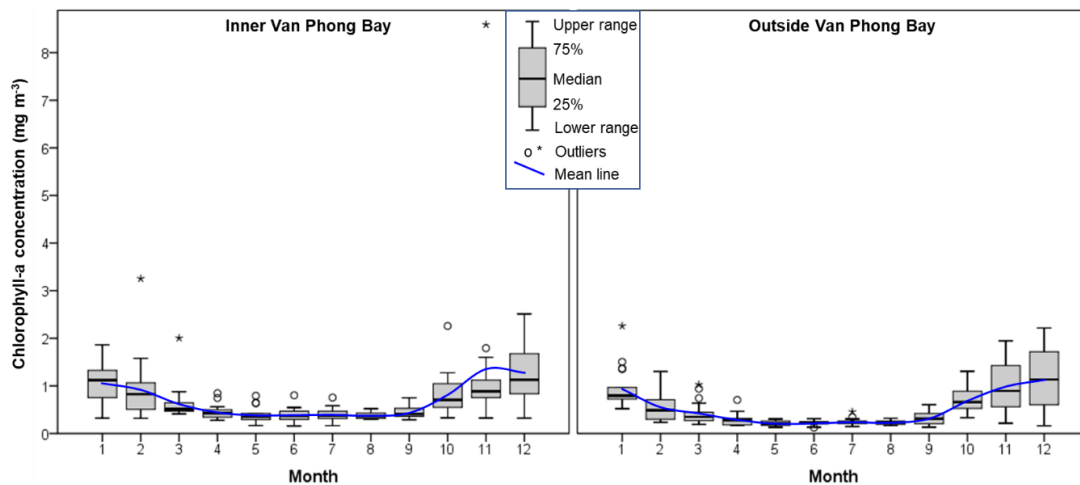


Figure 2. Box-whisker plot of MODIS Chlorophyll-a concentration in Van Phong Bay (p=0.05)

3.2. Trends and variations of MODIS Chlorophyll-a concentration

The seasonal pattern, trend and random components in the inner and outside Van Phong Bay was detected by decomposition of time series for monthly MODIS Chl-a. Figures 3 and 4 indicated the corrected magnitude of seasonal fluctuations as well as baseline of Chl-a. The seasonal fluctuations did not change overtime and the random value was variation around 0, whereas Chl-a trends have increases. However, in the inner bay (Figure 3), trend was significantly increased and slope with the graduated changes within the period of about 12 months. In contrast, the trend in outside bay (Figure 4) has more fluctuation.

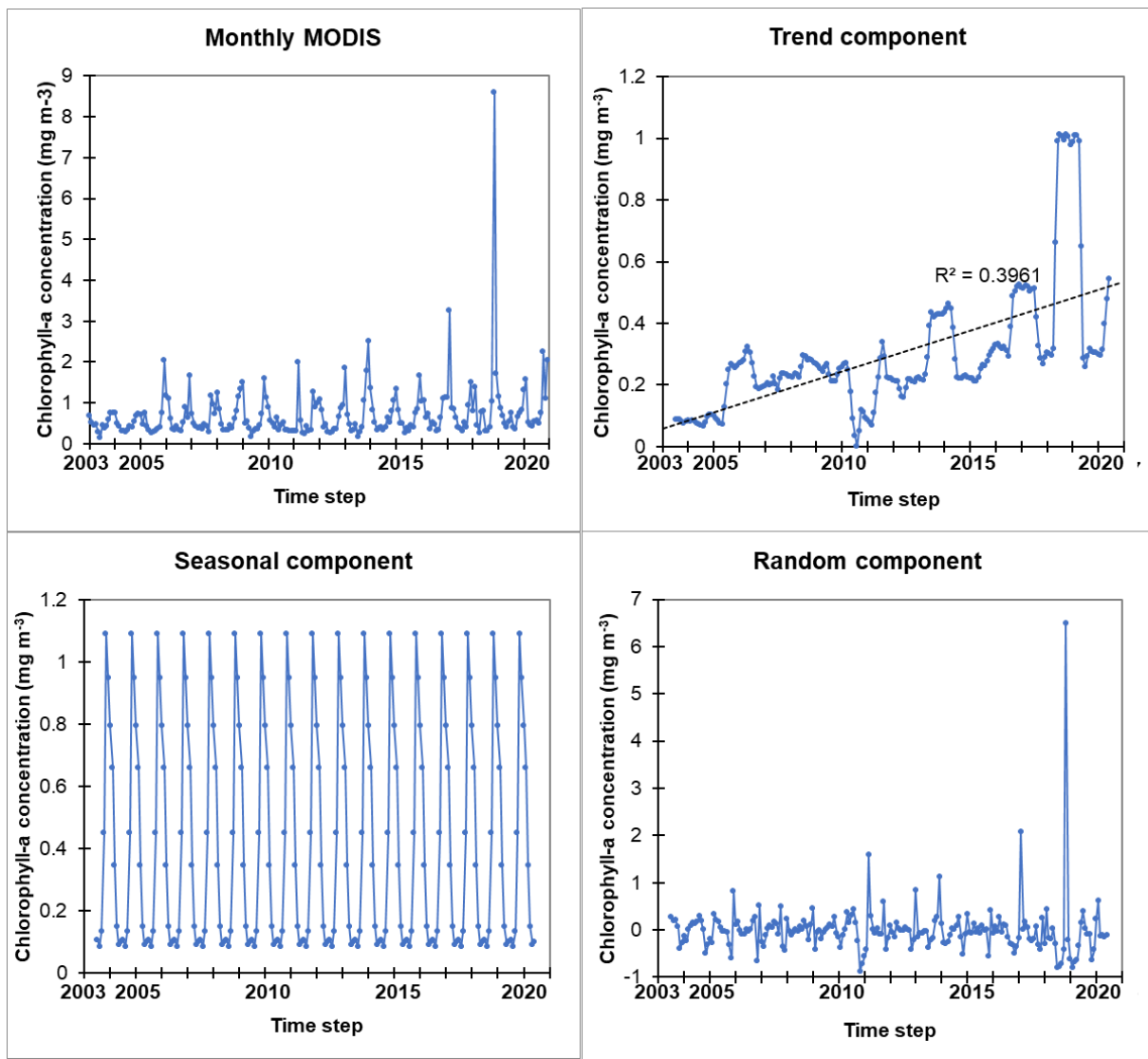


Figure 3. Trend components of monthly MODIS chlorophyll-a concentration in inner Van Phong Bay (from Jan 2002)

Based on the seasonal fluctuations, the baseline of Chl-a in the inner and outer bay are 0.084 mg m^{-3} and 0.049 mg m^{-3} , while the averages are $0.413 \pm 0.356 \text{ mg m}^{-3}$ and $0.357 \pm 0.314 \text{ mg m}^{-3}$, respectively. Figure 2 shows that the in-situ Chl-a has more than three times than that of MODIS Chl-a. It can be observed that the ratio of in-situ vs. monthly MODIS Chl-a does not change much, and the seasonal Chl-a mean in inner bay is $1.275 \pm 1.099 \text{ mg m}^{-3}$, with a range of $0.259 - 3.371 \text{ mg m}^{-3}$. Furthermore, based on trend and random components, Figure 3 could reveal the algal bloom events in early 2011, end of 2016 and 2019. The bloom in the end of 2016 was reported in (Doan-Nhu *et al.*, 2017; Luom *et al.*, 2021). As the same time, Chl-a was recorded an increase in the outer Van Phong Bay, without an occurrence of algal bloom.

4. CONCLUSIONS

An outlook on the variations and trends of Chl-a concentration in Van Phong Bay has been presented with in-situ and MODIS data. Seasonal, trending and random components were

detected by decomposition of the time series for monthly MODIS Chl-a. Chl-a time series showed a significantly increase in inner bay and a slightly increase in outer regions. Seasonal Chl-a has an average of $1.275 \pm 1.099 \text{ mg m}^{-3}$, with the range of $0.259 - 3.371 \text{ mg m}^{-3}$ in the inner bay and having a decreasing content from upper to the southern opening of the bay. Furthermore, the random component can help to determinate algal bloom events with sharply increases of Chl-a. This shows that the Fourier analysis is a powerful tool for studying such time series marine parameter like Chl-a concentration. The information is also helpful to support environmental management, marine culture development and zoning bivalve aquaculture.

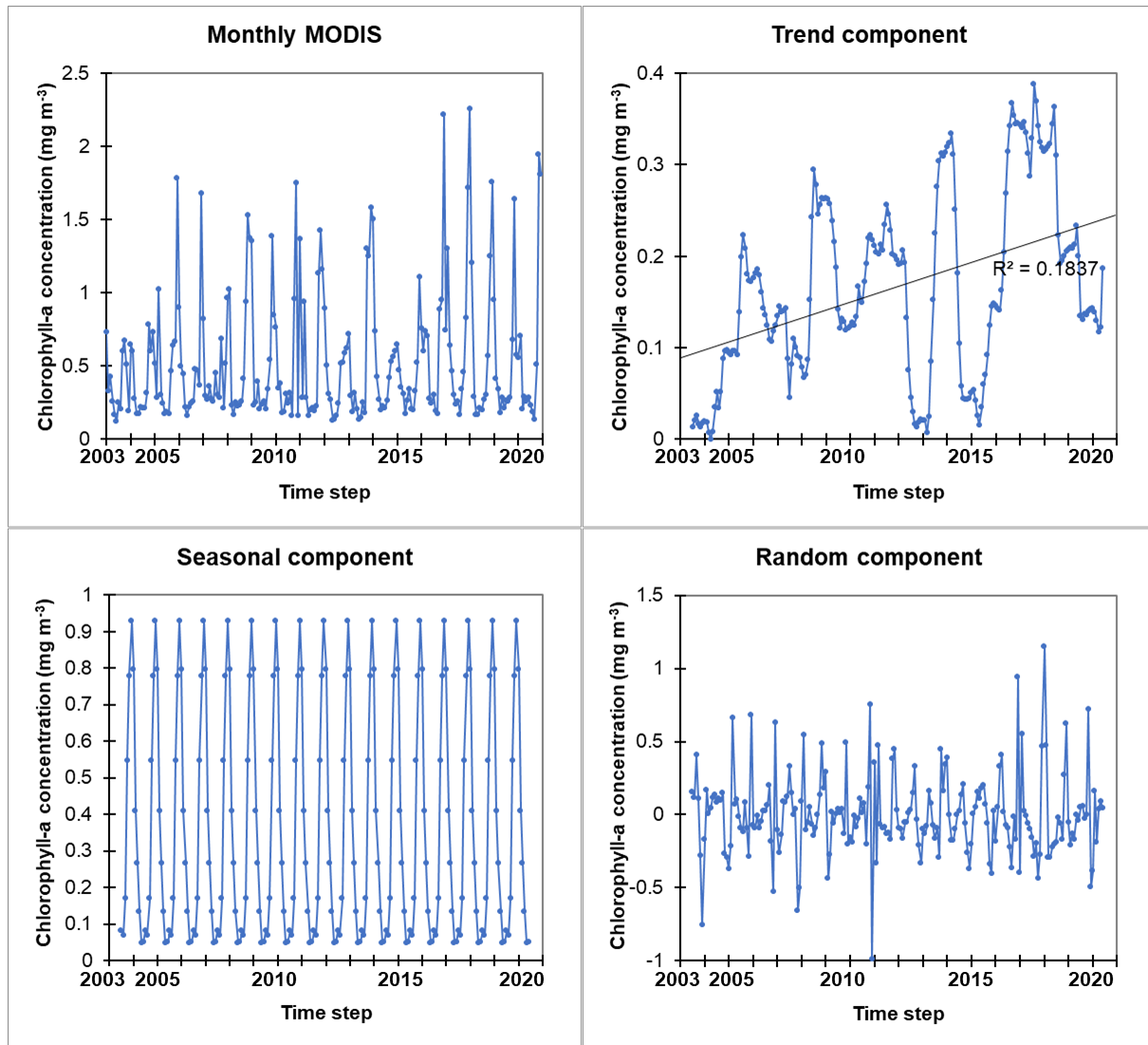


Figure 4. Trend components of monthly MODIS Chlorophyll-a concentration in outer Van Phong Bay

5. ACKNOWLEDGEMENT

The paper was funded by projects coded ĐT-2018-40502-ĐL2 and VT-UD.12/18-20. We also would like to thank the survey team from Institute of Oceanography, the HCMC Institute of Physics in collecting and analyzing water samples, the GEE and NASA for granting access to data and computing facilities.

6. REFERENCES

- An, N.T., 2002. Evaluation of the oceanographical conditions and environmental capacity for mariculture development in coastal waters of Khanh Hoa Province. *Collection of Marine Research Works* 12, 67-82.
- Doan-Nhu, H., Nguyen-Ngoc, L. & Bui-Minh, S., 2017. Unusual fish killing blooms of *Tripos furcain* Van Phong Bay, South Vietnam. *Harmful Algae News, An IOC Newsletter on Toxic Algae and Algal Blooms* 57, 1-3.
- Falkowski, P. & Kiefer, D.A., 1985. Chlorophyll a fluorescence in phytoplankton: relationship to photosynthesis and biomass. *Journal of Plankton Research* 7, 715-731.
- Ferreira, J.G., Andersen, J.H., Borja, A., Bricker, S.B., Camp, J., Cardoso da Silva, M., Garcés, E., Heiskanen, A.-S., Humborg, C., Ignatiades, L., Lancelot, C., Menesguen, A., Tett, P., Hoepffner, N. & Claussen, U., 2011. Overview of eutrophication indicators to assess environmental status within the European Marine Strategy Framework Directive. *Estuarine, Coastal and Shelf Science* 93, 117-131.
- Gitelson, A.A., Gurlin, D., Moses, W.J. & Yacobi, Y.Z., 2011. Remote Estimation of Chlorophyll-a Concentration in Inland, Estuarine, and Coastal Waters. In Weng, Q. (editor, *Advances in Environmental Remote Sensing: Sensors, Algorithms, and Applications*). CRC Press, Boca Raton. 439-468.
- Hu, C., Lee, Z. & Franz, B., 2012. Chlorophyll algorithms for oligotrophic oceans: A novel approach based on three-band reflectance difference. *Journal of Geophysical Research: Oceans* 117.
- IOCCG, 2012. Mission requirements for future ocean-colour sensors. In. The International Ocean-Colour Coordinating Group (IOCCG), Dartmouth, Canada
- Jeffrey, S.W., Mantoura, R.F.C. & Wright, S.W., 1997. *Phytoplankton pigments in oceanography : guidelines to modern methods*. UNESCO Publishing. Paris, France.
- Luom, P.T., Hai, D.N. & Lam, N.N., 2021. Dinoflagellate cysts in surface sediments at Van Phong Bay, Khanh Hoa Province, Vietnam: distribution, abundance and potentially harmful algal blooms. *Academia Journal of Biology* 43.
- Mélin, F., Vantrepotte, V., Clerici, M., D'Alimonte, D., Zibordi, G., Berthon, J.F. & Canuti, E., 2011. Multi-sensor satellite time series of optical properties and chlorophyll-a concentration in the Adriatic Sea. *Progress in Oceanography* 91, 229–244.
- Minh-Thu, P., Huan, N.H., Dung, L.T., Dung, L.T., Thi, V.H., Hue, T.T.M. & Du, H.T., 2014. Primary production in waters of Van Phong Bay. *Collection of Marine Research Works* 20, 60-69.
- Mudelsee, M., 2014. *Climate Time Series Analysis: Classical Statistical and Bootstrap Methods (2nd Ed)*. Springer. Cham, Switzerland.
- NASA OB.DAAC, 2021. Moderate-resolution Imaging Spectroradiometer (MODIS) Aqua Ocean Color Data. NASA Goddard Space Flight Center, Ocean Ecology Laboratory, Ocean Biology Processing Group. Greenbelt, MD, USA. Url: <https://doi.org/10.5067/AQUA/MODIS/L3M/CHL/2018>.
- O'Reilly, J.E. & Werdell, P.J., 2019. Chlorophyll Algorithms for Ocean Color Sensors - Oc4, Oc5 & Oc6. *Remote Sens Environ* 229, 32-47.
- Sathyendranath, S., Platt, T., Brewin, R.J.W. & Jackson, T., 2019. Primary Production Distribution. In, *Encyclopedia of Ocean Sciences* 10.1016/b978-0-12-409548-9.04304-9. 635-640.
- Shao, Y., Taff, G.N. & Lunetta, R.S., 2011. Review of Selected Moderate-Resolution Imaging Spectroradiometer Algorithms, Data Products, and Applications. In Weng, Q. (editor, *Advances in Environmental Remote Sensing: Sensors, Algorithms, and Applications*). CRC Press, Boca Raton. 31-56.
- Vantrepotte, V. & Mélin, F., 2010. Temporal variability in SeaWiFS derived apparent optical properties in European seas. *Continental Shelf Research* 30, 319–334.
- Wang, L., Xu, M., Liu, Y., Liu, H., Beck, R., Reif, M., Emery, E., Young, J. & Wu, Q., 2020. Mapping Freshwater Chlorophyll-a Concentrations at a Regional Scale Integrating Multi-Sensor Satellite Observations with Google Earth Engine. *Remote Sensing* 12, 3278.

ABOVE GROUND BIOMASS ESTIMATION USING MULTISPECTRAL SENTINEL-2 MSI DATA: A PRELIMINARY EXPERIMENT IN WANGCHAN FOREST LEARNING CENTER, THAILAND

**Sorasak Khoomboon^{1,a}, Tranid Prasertsri¹, Pudtraporn Napang¹, Natnicha Yooyen²,
Mattana Pongsopon², Suwit Navakam², Napak Karnasuta², and Sasawat Soontaros^{2,b}**

¹AI and Robotics Ventures Co., Ltd. Bhiraj Tower at Sathorn Building C 33, 31 31/1 S
Sathorn Road, Yannawa, Sathorn, Bangkok 10120, Thailand

²Reforestation and Ecosystem Institute, PTT Public Co., Ltd.
555 Vibhavadi Rangsit Road, Chatuchak Bangkok 10900 Thailand
Email: ^asorasakk@arv.co.th, ^bsasawat.s@pttplc.com

ABSTRACT

Dry Evergreen Forest above ground biomass (AGB) directly indicates conditions of the ecosystem, carbon cycle, and biodiversity conservation. Accurate AGB estimation is essential for the monitoring and supervision of the ecosystem and important parameters to calculate carbon sequestration, which is a method to determine carbon adsorption capacity of forest areas. This is an indicator to monitor the integrity of the forest within the area of interest that has been restored. The calculation of carbon sequestration is the most accurate and accepted method by Thailand Greenhouse Gas Management Organization (Public Organization) (TGO) through field survey to measure the parameters of several trees and calculation using allometric equations, which require more human resource, time, and expenses in large forest areas. However, using Sentinel-2, we can collect reflection data in various wavelengths within associated properties of plants and trees with large spatial measurements. It also has a high image resolution and can be downloaded for free to use in the interpretation and analysis of AGB estimation to handle resource problems. This study aims to carry out an experiment employing Sentinel-2 Multispectral Instrument (MSI) data to test the correlation between reflectance in the spectral channels and vegetation indices derived from imagery to model Dry Evergreen Forest AGB using Machine learning regressors (Random Forest, AdaBoost, Support vector machine, etc.) in the Dry Evergreen Forest at Wangchan Forest Learning Center in Rayong, Thailand, where the feasibility of model application was demonstrated.

1. INTRODUCTION

The above ground biomass (AGB) of forest accounts for 70-90% of total forest biomass, which directly indicates the abundance of ecosystems, carbon cycle, and biodiversity within the area (Prado-Junior et al., 2016). Moreover, forest AGB estimation is an important parameter to calculate Carbon Sequestration which leads to an assessment of the carbon absorption capacity in the area including forest resources management as well as monitoring and evaluating forest restoration, managing forest ecosystems to cope with climate change, and carbon credit trading (Muralikrishna, 2014).

The current method for forest AGB estimation in Thailand has been established by the Thailand Greenhouse Gas Management Organization (TGO), which involves field data collection by counting trees and plot sampling (*Thailand Voluntary Emission Reduction Program Reference Manual: Forestry and Agriculture Sector*, 2016). Tree counting is used for areas with plantation subplot sizes not exceeding 30 rai (4.80 hectare) and multiplied by a constant determined by the TGO. The sample plots for data survey should cover more than

1.0% of the total area to measure tree dimensions: diameter at breast height (DBH) and height. Biomass and capacity of carbon sequestration are determined by calculating from the allometric equations (Senpaseuth, 2009). The obtained result is multiplied with the Carbon Fraction according to TGO's guideline. Then, the carbon content in the plantation plot is determined and converted to the total amount of carbon dioxide. However, the area for sample plots will be larger according to the forest size, as well as a greater number of human resources, time, and expenses differently required in different areas of sample plots.

Although field data measurement is a method that has been recognized for its accuracy, it is not a practical approach for broad-scale assessments that require more resources and time. Therefore, to address these problems, remote sensing technology is introduced. This method has various advantages, especially in terms of resource reduction along with non-sampling whole plantation area assessment and accessibility in all areas. It has been reported the possibility of AGB estimation in sub-tropical buffer zone community forests from data collection on remote sensing technologies consisting of satellite data and optical remote sensing data using Sentinel-2 data (Pandit, Tsuyuki, & Dube, 2018).

This study aims to carry out an experiment by using Sentinel-2 Multispectral Instrument (MSI) data, which is a free optical imagery with 10 m resolution remote sensing data, to test the correlation between reflectance in the spectral channels and vegetation indices derived from imagery to estimate Dry Evergreen Forest AGB using Machine learning regressors at Wangchan Forest Learning Center in Rayong province, Thailand and to compare this data with the field measurement in order to find out the method and closest equation for this estimation, so that it can be applied to other forest areas.

2. MATERIALS AND METHODS

2.1 Study area

The study area is within the premises of Wangchan Forest Learning Center in Rayong province, Thailand (12.9948°N, 101.4421°E). The dry evergreen forest has been grown for about 6 years (since 2014) in the Forest Carbon Model Zone (FCMZ) covering a total area of 18.68 hectare.

2.2 Sampling strategy and field data collection

Field data collection and AGB calculation were performed following the TGO's guideline (*Thailand Voluntary Emission Reduction Program Reference Manual: Forestry and Agriculture Sector*, 2016). Three sample plots were selected from different locations of FCMZ, marked red in Figure 1. Each sample plot was further divided into 16 subplots, where 1 subplot has the size of 10 x 10 m to relate to the resolution of Sentinel-2. AGB of one data point is the summation of AGB of every tree within a single subplot. Hence, there are a total of 48 data plots in this study.

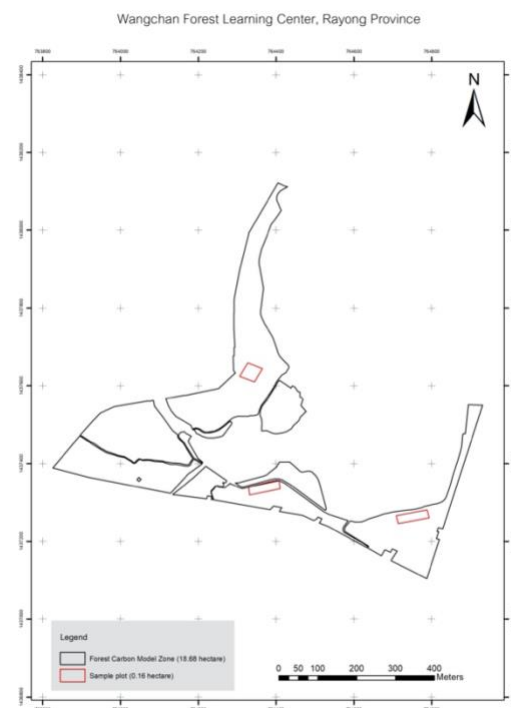


Figure 1. Study area for AGB estimation using sentinel-2 imagery.

2.3 Satellite image acquisition and variables for forest AGB estimation

Data of Single Tile Standard Sentinel-2 Level 2A on 26 July 2018 was downloaded from AWS earth ("Open Data on AWS," 2018), selected based on the cloudless condition in the area of interest and the time taken is similar to that of field data collection. The data we used in this study is acquired in 10 spectral bands or 'raw bands' which extend through (i) visible wavelength; B2, B3, and B4, (ii) near-infrared (NIR); B8, (iii) red-edge; B5, B6, B7, and B8A, and (iv) shortwave infra-red (SWIR); B11 and B12 wavelengths at 10 and 20 m spatial resolution. Subsequently, we re-sampled the resolution with B5, B6, B7, B8A, B11, and B12 to 10 m spatial resolution. To study the applicability of the Sentinel2 MSI sensor to estimate dry evergreen forest restoration AGB, raw bands and vegetation indices (VIs) were used. The selection of VIs was based on their performance in forest biophysical parameters introduced by Pandit and team as shown in Table 1 (Pandit et al., 2018).

Table 1. Vegetation indices calculated from Sentinel-2 previously introduced.

Vegetation Indices	Equations
NDVI	(B8-B4)/(B8+B4)
RGR	B4/B3
EVI	2.5*((B8-B4)/(1+B8+6*B4-7.5*B2))
SR	B8/B4
PSRI	((B4-B3)/B6)
NDII	(B8-B11)/(B8+B11)
SAVI	((B8-B4)/(B8+B11+1.5)) *1.5
IRECI	(B8-B4)/(B5/B6)
S2REP	705+(35*((0.5*(B7 +B4)/2)-B5)/(B6-B5))
RE1NDVI	(B8 -B5)/(B8+B5)
RE2NDVI	(B8 -B6)/(B8+B6)
RE3NDVI	(B8 -B7)/(B8+B7)
RE4NDVI	(B8 -B8A)/(B8+B8A)

2.4 Machine learning regression models

We used Sentinel-2 Multispectral Instrument (MSI) data to estimate AGB between reflectance in the spectral channels, vegetation indices derived from imagery, and field measurement data of 48 data points each data point represents a sample subplot. We divided these data points into 19 data points for training model and 13 data points for testing model using Machine learning regression models in Scikit-learn library (Pedregosa et al., 2011) which are random forest (RF) (Breiman, 2001), Adaptive Boosting/AdaBoost (ADA) (Freund & Schapire, 1997), Bagging (BAG) (Breiman, 1996), Gradient Boosting (GB) (Friedman, 2001), Support Vector Machine (SVM) (Platt, 1999), and least squares Linear Regression (LIN). Performance was tested to estimate AGB with the remaining unseen 16 data points. The overview method used in this study is presented in Figure 2.

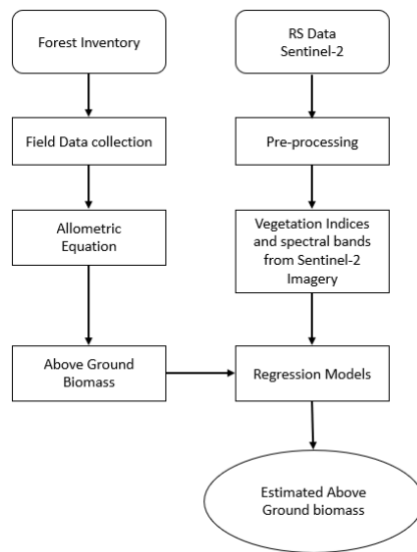


Figure 2. Method overview for AGB estimation using Sentinel-2 imagery.

3. RESULTS AND DISCUSSION

The experimental results of training with random RF, ADA, BAG, GB, SVM, and LIN from 19 data points of both data sets, data set A consisting of only raw bands (B2, B3, B4, B5, B6, B7, B8, B8A, B11 and B12) and data set B consisting of raw bands and VIs (B2, B3, B4, B5, B6, B7, B8, B8A, B11, B12, NDVI, RGR, EVI, SR, PSRI, NDII, SAVI, IRECI, S2REP, RE1NDVI, RE2NDVI, RE3NDVI, and RE4NDVI), revealed the feasibility in biomass estimation with the other 13 data points used in the testing model. Accuracy test of the experiment was obtained with R^2 showed greater than 0.80 as shown in Table 2. Using SVM with data set B, the most accurate value obtained was 0.88, which demonstrates the possibility of applying Machine learning regression models to estimate AGB in dry evergreen forest. However, when the resulting model is applied to 16 unseen data points, none of the models were able to estimate AGB as shown in Table 2. This could be caused by two reasons, one is the small sample size in which the amount of data points used for training is very low, since the number of sample subplots in this experiment is 48 in 3 sample plots, whereas the previously reported model study had a total of 113 plots (Pandit et al., 2018). The other reason is that the subplot location does not align with the direction of Sentinel-2 imagery (North-South direction), or the data measurement of the subplot location does not fit the pixel position of the satellite image.

Moreover, the study area is dry evergreen forest with a complex and multi-tiered canopy structure, hence it is necessary to take forest type and topography into account as well.

Table 2. R^2 with 13 test and 16 unseen data points.

Regression	13 Test data points		16 Unseen data points	
	A	B	A	B
RF	0.83	0.82	-6.82	-4.65
ADA	0.84	0.85	-3.86	-6.14
BAG	0.81	0.80	-5.09	-5.1
GB	0.83	0.83	-4.98	-4.76
SVM	0.83	0.88	-5.95	-5.97
LIN	0.81	0.81	-4.46	-5.4

4. CONCLUSION

We could carry out an experiment using Sentinel-2 Multispectral Instrument (MSI) data to demonstrate the feasibility of application of Machine learning regression models to estimate AGB in dry evergreen forest. However, this depends on the amount of data points used for training and strategic field data collection. Field data collection following the TGO's guideline resulted in misalignment to that of Sentinel-2 imagery which might have caused failure in AGB estimation using the unseen data. In future work, we plan to design a new strategy for field measurement to align with the direction of Sentinel-2 image sensing and divide contour level for location selection in the forest along with a higher number of sample size. Unfortunately, field experiments have been limited due to the situation of COVID-19 outbreak in Thailand which occurred during the study period. Hence, we have not been able to test the idea with larger samples yet. Nonetheless, once the situation is better to an extent that we can implement our field work, we are certain to develop and test the AGB assessment using Machine learning regression models to compute carbon storage estimations at the commercial level.

5. ACKNOWLEDGEMENTS

This research was co-supported by the Reforestation and Ecosystem Institute of PTT Public Co., Ltd. and the AI and Robotics Ventures Co., Ltd. We thank Thailand Greenhouse Gas Management Organization (TGO) and Faculty of Forestry, Kasetsart University for utilizing their expertise and providing us suggestions that greatly assisted the research.

6. REFERENCES

- Breiman, L. (1996). Bagging predictors. *Machine Learning*, 24(2), 123-140. doi:10.1007/BF00058655
- Breiman, L. (2001). Random Forests. *Machine Learning*, 45(1), 5-32. doi:10.1023/A:1010933404324
- Freund, Y., & Schapire, R. E. (1997). A Decision-Theoretic Generalization of On-Line Learning and an Application to Boosting. *Journal of Computer and System Sciences*, 55(1), 119-139. doi:<https://doi.org/10.1006/jcss.1997.1504>
- Friedman, J. H. (2001). Greedy function approximation: A gradient boosting machine. *The Annals of Statistics*, 29(5), 1189-1232, 1144. Retrieved from <https://doi.org/10.1214/aos/1013203451>
- Muralikrishna, I. (2014). Biomass Calculations for Carbon Sequestration in Forest Ecosystem. *Journal of Energy and Chemical Engineering*.
- Open Data on AWS. (2018). Retrieved from <https://aws.amazon.com/opendata/>
- Pandit, S., Tsuyuki, S., & Dube, T. (2018). Estimating Above-Ground Biomass in Sub-Tropical Buffer Zone Community Forests, Nepal, Using Sentinel 2 Data. *Remote Sensing*, 10(4), 601. Retrieved from <https://www.mdpi.com/2072-4292/10/4/601>
- Pedregosa, F., Varoquaux, G., Gramfort, A., Michel, V., Thirion, B., Grisel, O., . . . Duchesnay, É. (2011). Scikit-learn: Machine Learning in Python. *J. Mach. Learn. Res.*, 12(null), 2825–2830.
- Platt, J. (1999). *Probabilistic Outputs for Support Vector Machines and Comparisons to Regularized Likelihood Methods*: MIT Press.
- Prado-Junior, J. A., Schiavini, I., Vale, V. S., Arantes, C. S., van der Sande, M. T., Lohbeck, M., & Poorter, L. (2016). Conservative species drive biomass productivity in tropical dry forests. *Journal of Ecology*, 104(3), 817-827. doi:<https://doi.org/10.1111/1365-2745.12543>
- Senpaseuth, P., Navanugraha, C., & Pattanakiat, S. . (2009). The Estimation of Carbon Storage in Dry Evergreen and Dry Dipterocarp Forests in Sang Khom District, Nong Khai Province, Thailand. *Environment and Natural Resources Journal*, 7(2), 1-11. Retrieved from <https://ph02.tci-thaijo.org/index.php/ennrj/article/view/82564>
- Thailand Voluntary Emission Reduction Program Reference Manual: Forestry and Agriculture Sector.* (2016). (3rd ed.). Bangkok, Thailand: Thailand Greenhouse Gas Management Organization (Public Organization).

AIR POLLUTION NO₂ ASSESSMENT USING RS AND GIS IN HO CHI MINH CITY AND NEIGHBORHOOD PERIOD 2015-2019

Dinh Thi Kim Phuong¹ and Nguyen Duc Tri²

¹ Division of Environmental and Resources information System,
Faculty of Environment and Natural Resources,
(HCMUT), District 10, Ho Chi Minh City, Vietnam
Email: dtkphuong@hcmut.edu.vn

² Sub-National Institute of Agricultural Planning and Projection
District 3, Ho Chi Minh City, Vietnam
Email: ndtri88@gmail.com

ABSTRACT

The sources of air pollution are mainly from industrial activities, transportation and human activities. This research aims to assess the level of NO₂ pollution in the air from data collected by OMI (Ozone Monitoring Instrument) on AURA satellite of A-Train group. Pollution levels of NO₂ will be calculated, assessed. The results of the study showed that NO₂ concentration varies significantly with the seasons, relatively high in the dry season reaching 80 ($\mu\text{g}/\text{m}^3$) in Ho Chi Minh City, up to 70 ($\mu\text{g}/\text{m}^3$) in Binh Duong, Dong Nai, Long An province, and decreasing in the rainy season. Therefore, it is necessary to have quick and timely measures to monitor air pollution to minimize the consequences caused by air pollution in urban areas.

1. INTRODUCTION

At present, air pollution is not only in Ho Chi Minh City (HCMC) but also neighboring areas such as Long An, Binh Duong and Dong Nai which are increasing significantly in the dry season, especially on many main roads, there are often traffic jams everyday and city dwellers inhale a large amount of harmful emissions. In addition, the city's top priority; Ho Chi Minh City in solving air pollution include: reducing dust pollution in the building material manufacturing industry; SO₂ pollution from thermal power plants; as well as the amount of CO₂ and SO₂ generated from domestic activities by 2020 for urban and rural areas. Therefore, the control and reduction of air pollution in the urban area of Ho Chi Minh City must be based on a series of synchronous solutions, which must take into account climate and weather characteristics. Researches in Vietnam many research used to RS techniques to show air pollution for many years. In 2018, This paper presents the results of remote sensing application for mapping of air quality in mining area in Luong Son district, Hoa Binh province. Using Landsat 8 data with a resolution of 30m in three periods: 2013, 2015 and 2017 to calculate vegetation indices, air pollution index (API). The study also showed that the area with high forest cover would have better air quality than the area where mining activities were conducted (Tran Quang Bao et al, 2018). (Nguyen Hai Hoa, Nguyen Thi Huong, 2017) Using Landsat image to develop the distribution map of air pollution caused by mining activities in Hoanh Bo district, Quang Ninh province. Most of the dust concentration has increased from 2006 to 2010 because the mining industry has taken place extensively this period. The results also show that there is a relationship between vegetative cover and air quality, in which vegetation plays an important role in reducing air pollution and dust concentration from mining activities. In the world, there are related studies in the application of remote sensing techniques to evaluate NO₂ and SO₂ pollution, other air pollutants. In 2018, the study show impact of traffic-related air

pollution on morbidity and mortality in Copenhagen Municipality and the health gain of reduced exposure. The annual mean nitrogen oxide concentration is $19.6 \mu\text{g}/\text{m}^3$ in Copenhagen; One-year gain in life expectancy by lowering nitrogen oxide exposure to rural level (Henrik Brønnum-Hansen et al, 2018).

2. STUDY AREA

Ho Chi Minh City lives in the transitional zone between the Southeast and the Mekong River Delta. The general topography has a lower form from North to South and from East to West. Ho Chi Minh City is located in the subequatorial monsoon tropics, so it has a steadily high temperature throughout the year and has two distinct rainy and dry seasons affecting the air environment. The rainy season is from May to November, the dry season from December to April next year.

The HCMC region includes seven provinces and cities: Dong Nai, Binh Duong, Binh Phuoc, Tay Ninh, Long An, Tien Giang and HCMC. The task of adjusting construction planning has been approved by the Prime Minister, identifying this as a large urban area, the leading economic development engine of the country, also an international traffic hub, capable of adapting highly responsive, towards balanced and sustainable development, and at the same time a center of knowledge, modern services, and a unique cultural center. In particular, Ho Chi Minh City is a regional nuclear city, a multi-functional general economic center with synchronous and modern infrastructure on par with modern urban areas in the region. The development of industrial zones in the HCMC area is both an opportunity and a challenge in controlling and limiting air pollution.

3. METHOD AND DATA

3.1 Method

The research extracted air pollution information from data collected by OMI (Ozone Monitoring Instrument) on AURA satellite of the A -Train group, OMI data covers a period of more than 10 years for the analysis of pollution trends. It is important to correlate emissions with urban and industrial sources of emissions, to determine the location of emission sources from the VNREDSAT data. From the data set, ICST developed calculation techniques from the RT model (radiation propagation technique) to analyze remote sensing image data and extract NO_2 and SO_2 pollution data (Do The Hoang and ICST, 2018).

3.2. Data

- Collect monthly OMI data set from 2015 to 2019 in Ho Chi Minh City and surrounding areas to analyze the laws of change and the impact of air pollutants.

- Data NO_2 and SO_2 were extracted from the 2 km resolution image showing air pollutants for the HCMC area (90 km x 110 km).

- Interpolate extracted data for the study area, then display it on map and statistic data.

4. RESULT AND DISCUSSION

The concentration of NO_2 depends on time and according to the TCVN, in the area where the average NO_2 concentration does not exceed $100 \mu\text{g}/\text{m}^3$ according to the monitoring results, the air quality meets the allowable standards. Currently, the traditional method is to collect data from automatic air quality monitoring stations and show that NO_2 concentrations are increasing faster than the previous annual average. Especially, the evolution of NO_2 concentration in the air along the roads of the city. However, because the number of stations is not enough to

provide a city-wide pollution map, the solution to analyze OMI data to generate a map shows pollutants such as NO₂ collected on a monthly average for each month and surrounding areas are very helpful. Data's HCMC from 2015 to 2019 results show that the concentration of NO₂ clearly fluctuates with seasons which is relatively high in the dry months (Figure 1) and lower in the rainy season (Figure 2). Especially in 2018, the concentration exceeded 70 µg/m³ in January, February, November, December with the value of 74.2 µg/m³, 79.1 µg/m³, 82.7 µg/m³, 74.3 µg/m³, respectively.

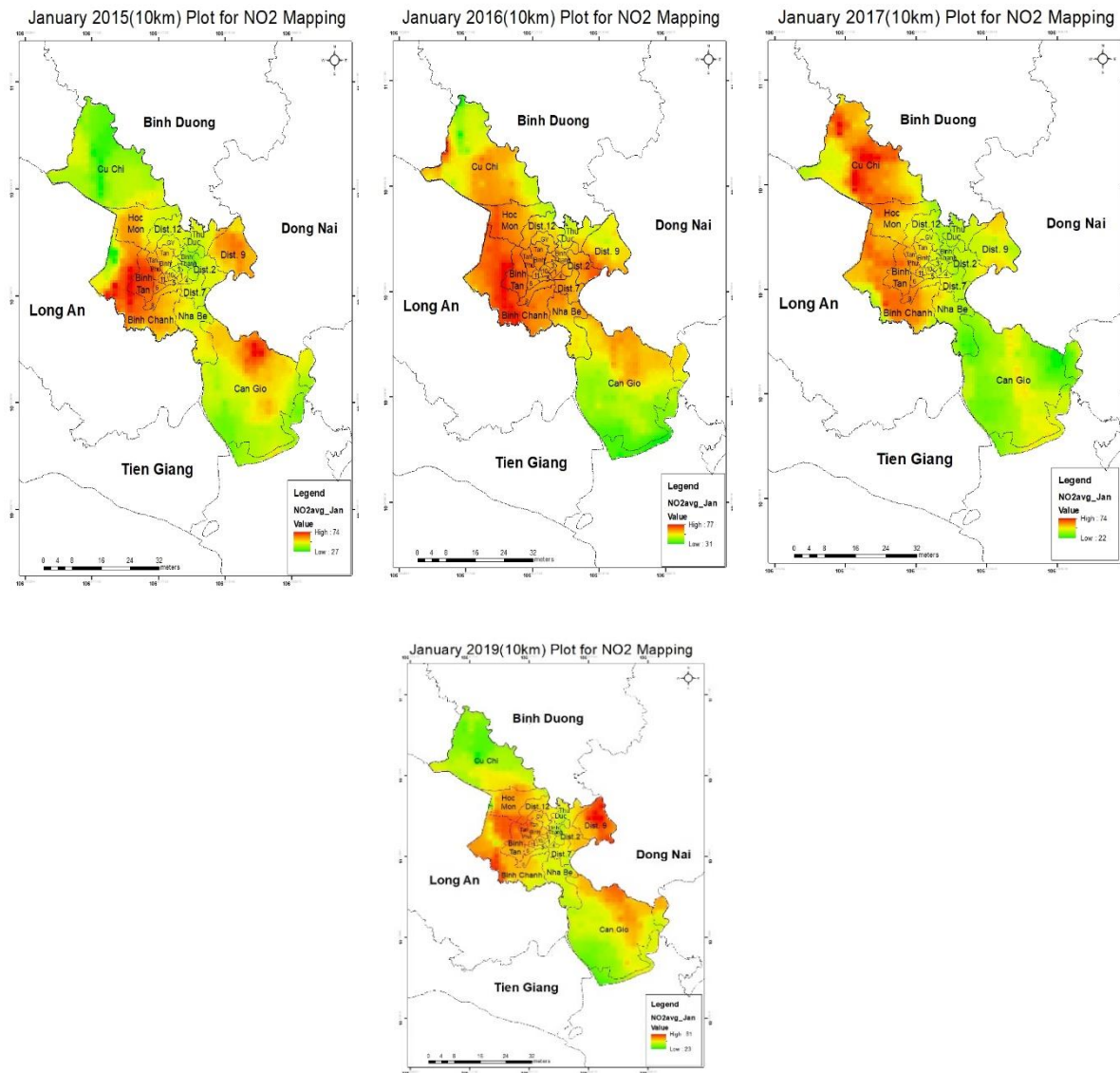


Figure 1. Trend of NO₂ concentration in dry season.

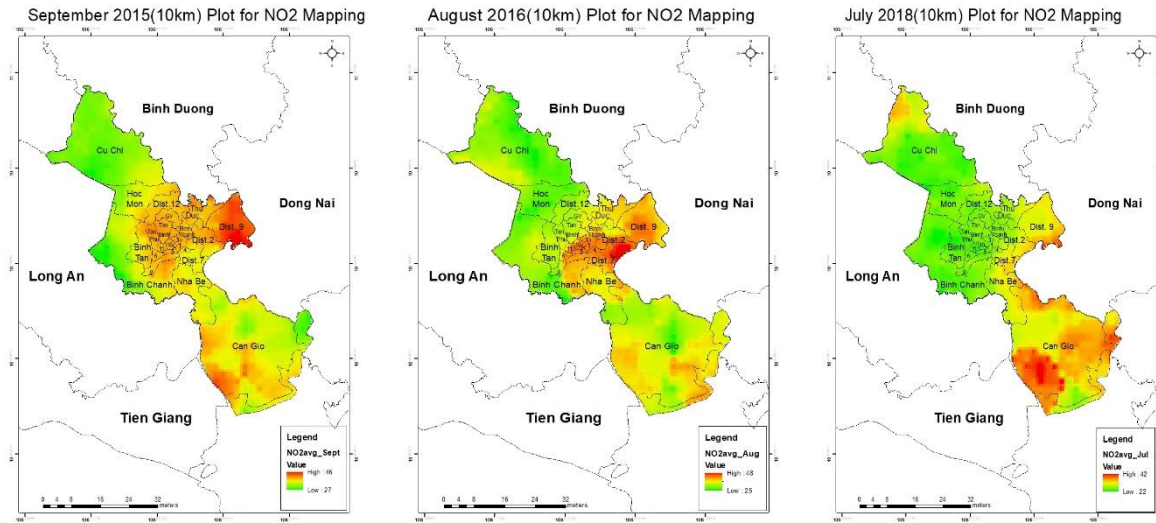


Figure 2. Trend of NO₂ concentration in rainy season.

As for the neighboring areas, in Long An provinces (Loc Hoa, Ben Luc, Can Giuoc districts) located in the humid tropical climate zone, due to the contiguity between the Southeast and Southwest regions, should bring both the characteristics specific to the Mekong Delta and the distinct masculinity of the Eastern region; In the dry season from November to April, there is a northeast wind with a frequency of 60-70%. The rainy season from May to October has southwest wind with a frequency of 70%. Binh Duong (Dau Tieng District, Ben Cat Town, Thu Dau Mot City, Thuan An City, Di An City) has tropical monsoon characteristics, rainy season from May to November; dry season from about December to April next year; the least rainy month is January; the wind regime is relatively stable, not directly affected by storms and tropical depressions; In the dry season, the prevailing wind is mainly in the East and North-East direction; the rainy season prevails mainly in the west, west-southwest; The highest observed wind speed is 12m/s, usually in the west, west-southwest direction. Dong Nai (Bien Hoa City, Long Thanh District, Nhon Trach District) has a sub-equatorial monsoon tropical climate; influenced by the Northeast and Southwest monsoons; in addition, it is also influenced by the tropical Pacific air from April to October; There are two distinct seasons: rainy and sunny. The dry season lasts for 5 to 6 months (from December to March or April of the following year), and the dry season for 6 or 7 months (from April or May to November). The end of the rainy season ranges from early October to December; Rainfall distribution gradually decreases from the North to the South and from the middle to the East and West of Dong Nai. It can be seen that the concentration of NO₂ pollution in neighboring areas also peaks in the dry season months, specifically in January and February, ranging from 70 to 80 ($\mu\text{g}/\text{m}^3$), especially in Dong Nai. reaching 81 $\mu\text{g}/\text{m}^3$ in 2019; Dong Nai currently has 35 industrial parks, including 31 industrial parks with active projects, but now the area of industrial parks has almost filled the area of the province based to many domestic and foreign investors. expanding production and Bien Hoa 1 industrial zone is considered a bomb of environmental pollution. Not only air pollution, but Dong Nai also faces with water pollution from Dong Nai river, dust pollution, noise pollution... HCMC reached 83 $\mu\text{g}/\text{m}^3$, Long An and Binh Duong respectively 77 $\mu\text{g}/\text{m}^3$, 74 $\mu\text{g}/\text{m}^3$ in 2019. Espeacially, in Long An province in 2018 this concentration exceeded the threshold of over 118 $\mu\text{g}/\text{m}^3$ due to the concentration of 16 industrial parks with the occupancy rate of more than 80% of the area of the industrial park.

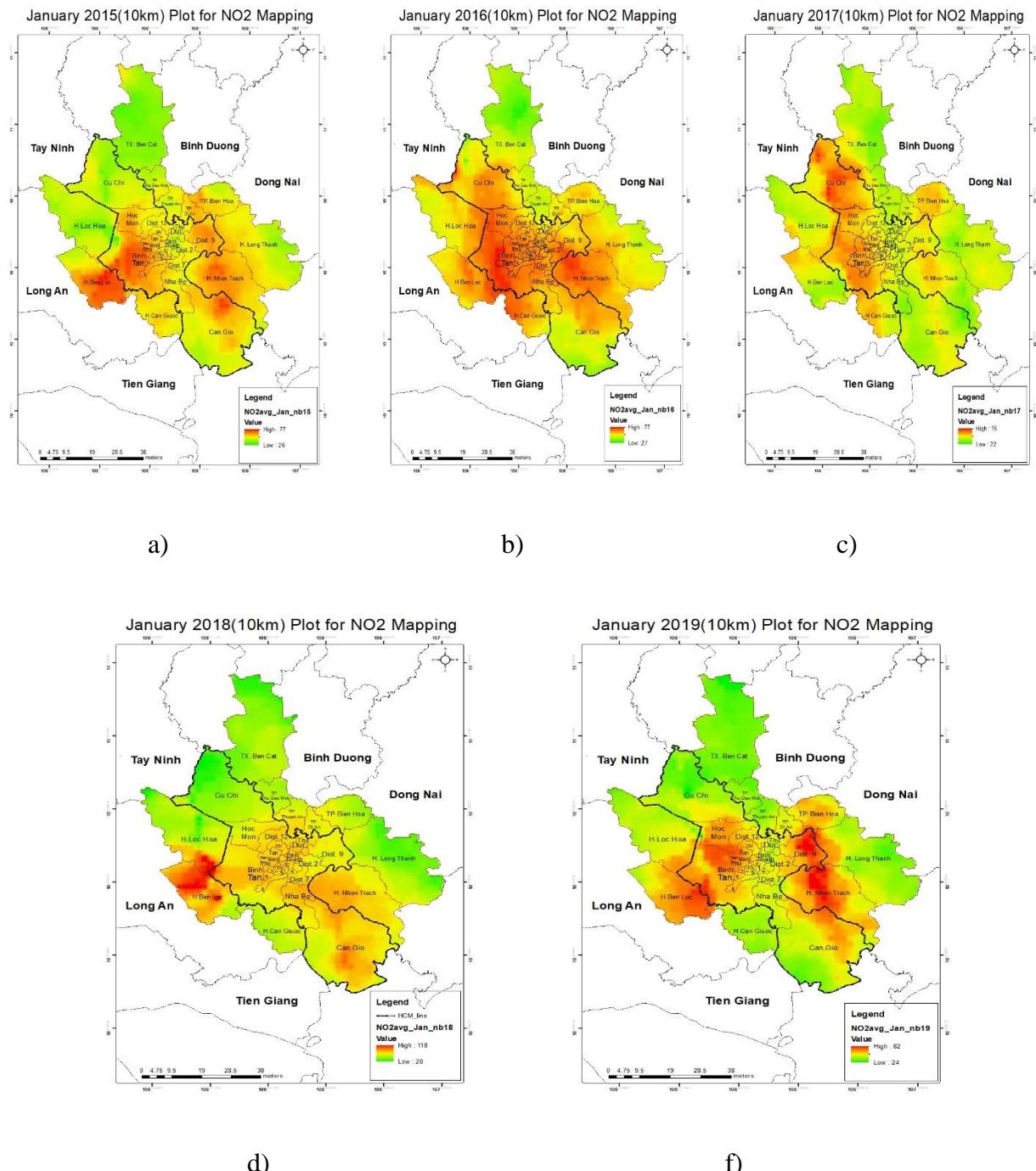


Figure 3. Trend of NO₂ concentration in January

a) 2015, b) 2016 and c) 2017, d) 2018 and f) 2019

Pollutant NO₂ concentrations decreased in the rainy season, and in August average concentrations ranged between 28-37 µg / m³ (table 1).

Table 1. Average NO₂ concentration in August, period 2015-2019 (µg/m³)

	2015	2016	2017	2018	2019
Dong Nai	37.5	34	39.9	31.9	34.8

Binh Duong	30.4	29	29.9	28.6	29.1
Long An	31.7	30.9	34.4	29.6	27.9
HCMC	34.8	32.9	34.9	32.3	32

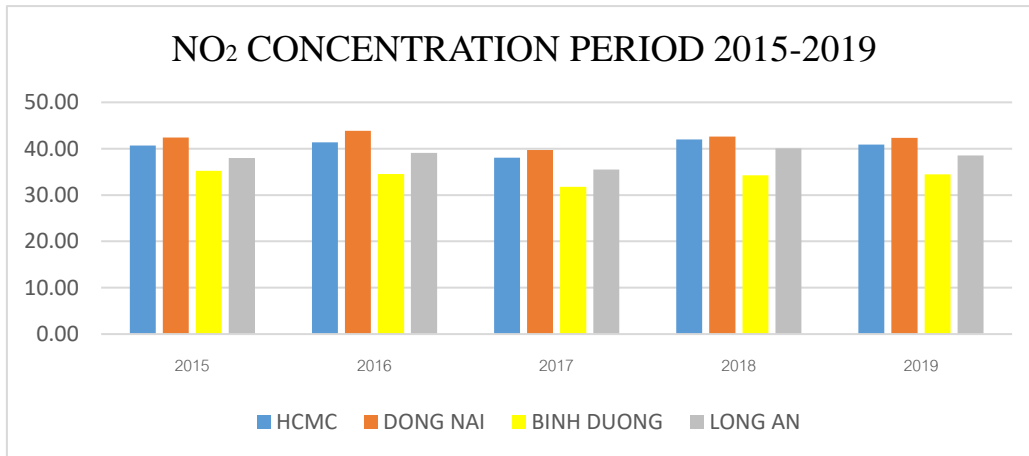


Figure 4. Chart of NO₂ concentration in neighboring areas of HCMC period 2015-2019.

5. CONCLUSION

This paper presents the results of extracting the pollution level of NO₂ from remote sensing images and develops a solution to map pollution trends over time. In addition, the data is analyzed and statistics to determine the location of emission sources in order to predict the exact change of pollutants to contribute very important to the development of an air quality management plan. The results show that the impact of air pollutants is usually concentrated in the dry season (from January to March) in Ho Chi Minh City and neighboring areas have higher pollution concentrations than other localities. Therefore, it is necessary to develop mainly clean industry with modern and advanced technology with high scientific content; great added value and above all does not pollute the environment.

6. REFERENCES

- Tran Quang Bao et al., 2018. *Application of GIS and RS for air quality assessing in mining area, Luong Son district, Hoa Binh province*. Journal of Sciences and forestry 6.
- Nguyen Hai Hoa, Nguyen Thi Huong., 2017. *Using landsat data to map spatial distribution of air pollution concentration due to mining activities in hoanh bo district, Quang Ninh province*. Journal of Sciences and forestry 4.
- Henrik Brønnum-Hansen et al., 2018. *Assessment of impact of traffic-related air pollution on morbidity and mortality in Copenhagen Municipality and the health gain of reduced exposure*. Environment International 121, 973-980.
- Do The Hoang and ICST., 2018. Reflectance spectra: *Dependence on Atmospheric Conditions*.

FLOOD RISK FIELD SURVEY USING MOBILE GIS IN PUA SUBDISTRICT, PUA DISTRICT, NAN PROVINCE, THAILAND

Phaisarn Jeefoo^{1,*} Watcharaporn Preedapirom² and Chamnan Kumsap³

¹Research Unit of Spatial Innovation Development (RUSID), Geographic Information Science, School of Information and Communication Technology (ICT), University of Phayao 19 Moo 2, Maeka, Muang, Phayao 56000 – Thailand

Email: p.jeefoo@gmail.com / phaisarn.je@up.ac.th

²Physiology, School of Medical Sciences, University of Phayao 19 Moo 2, Maeka, Muang, Phayao 56000 – Thailand

Email: watcharaporn.pree@gmail.com

³Defence Technology Institute, Office of the Permanent Secretary of Defence (Chaengwattana) 5th Floor, 47/433 Moo 3, Ban Mai, Pak Kret, Nonthaburi 11120 – Thailand

Email: chamnan.k@dti.or.th

ABSTRACT

This research paper presents the application of flood mobile field survey in Pua subdistrict, Pua district, Nan province by using free and open source software. Geographic Information Systems (GIS) technology is ideally suited as a tool for the presentation of data derived from continuous monitoring of locations and used to support and deliver information to environmental managers and the public. Combined with Google API AppSheet, it extended web capabilities to provide real-time data from notified activities. Both geographical data and remotely sensed and geo-referenced image data were provided, and the ground truth of Google map remote sensing was recognized and also further recommended for capability study. This application provided the opportunity to visualize and grasp the current situation of the flood and thereby managed to offer prompt decision making as an action plan immediately needed.

1. INTRODUCTION

Natural disaster compounded by climate change causes more than \$500 billion in losses every year (As Natural Disaster Rise, 2017). In particular, flooding is one of the most frequently occurring natural catastrophic events (Sanyal and Lu, 2004) impacting human lives, infrastructure and environment around the globe (Klema, 2014; Schumann and Moller, 2005; Anusha and Bharathi, 2019). Floods are among the most devastating natural hazards in the world and wildly distributed leading to significant economic and social damages than any other natural phenomenon (DMSG, 2001; Haq et al., 2012). Climate changes and human-induced land-use interventions are defined as important factors causing the flood hazard. There is a mutual trigger situation that the urban areas are the most influenced areas from flooding and also urbanization is the most important reason of the formation of flood (Ozkan & Tarhan, 2015). Remote Sensing has made substantial contribution in flood monitoring, mitigation and damage assessment that leads the disaster management authorities to contribute significantly. Geographic Information Systems (GIS) technology is ideally suited as a tool for the presentation of data derived from continuous monitoring of locations and used to support and deliver information to environmental managers and the public. GIS based spatial analysis and visual elements are used frequently in recent years for the detection of flood hazard areas and for the preparation of maps. GIS applications based on database and analysis tools have logical and mathematical relationships between the layers (Kourgiala & Karatzas, 2011).

Mobile GIS is a mature technology which takes geospatial technology beyond the walls of an office. Therefore, mobile applications have extended to field use which allows the user easy access, storage, updates, analysis and real time visualization of field data. Till recently, mobile GIS applications were mainly used as a navigation or location-aware system. Mobile GIS technology nowadays offers a potential alternative to fill the gaps of traditional GIS systems. With mobile GIS technology, officers and many other field workers have the potential to access the enterprise geospatial data from the server-side to accomplish their tasks with high level of accuracy. More importantly, it is also possible to update these geospatial enterprise data in real time (Choosumrong et al., 2016; Jeefoo, 2019).

The main objective of this research was to develop the mobile GIS field survey by using open source software for correcting flood risk hazards in Pua subdistrict, Pua district, Nan province, Thailand

2. MATERIAL AND METHOD

2.1 Study area: Pua subdistrict, Pua district, Nan Province

Pua subdistrict, Pua district, Nan province in the northern part of Thailand (Figure 1) was selected as the study area. Pua subdistrict comprises of 12 villages and covers an area of 23.9 sq.km. with geographical location between $19^{\circ}9'0''N$ to $19^{\circ}12'0''N$ and $100^{\circ}52'30''E$ to $100^{\circ}55'30''E$. It is mostly covered with forested mountain, with an approximate elevation of 310 meters about mean sea level.

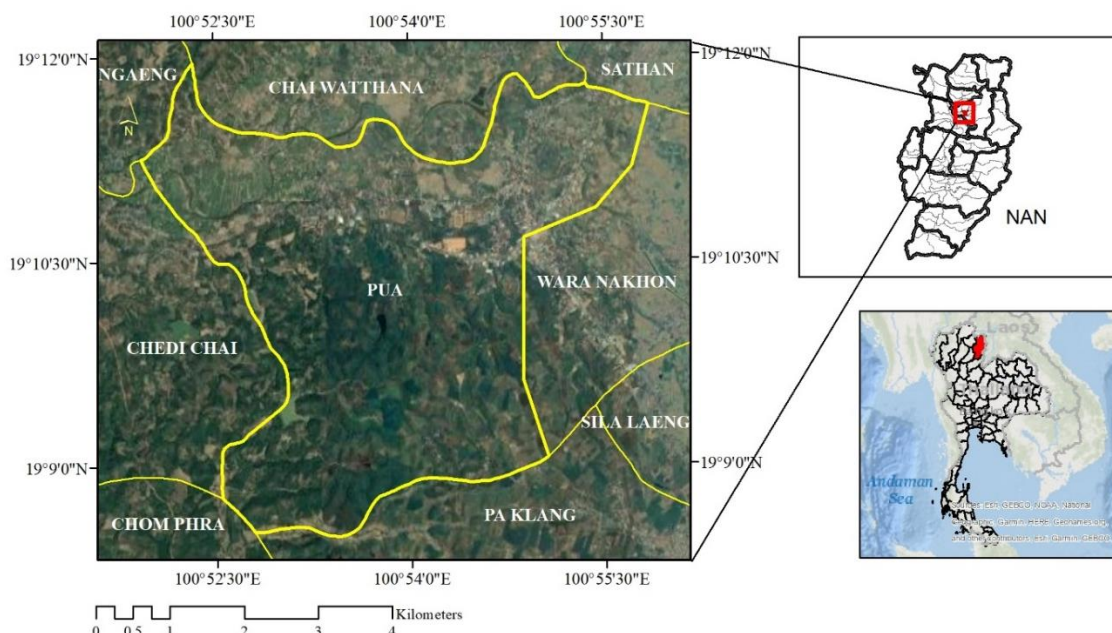


Figure 1. Geographic location of the study area.

2.2 Method

A smartphone running Android/iOS operating system was chosen to be a field device. The chosen smartphone was used for sending the flood risk field survey data in real-time to the base of operation to serve various purposes of field surveys. Real-time data availability provides many advantages.

Figure 2 shows the architecture of the flood risk field survey application. The application running on the device has two major modules: the map module and the survey module. The map module is used for retrieving the location data from the Google Maps. This location will

be sent along with other types of data to the cloud server, and it can be used to pinpoint the current location of the device when displaying a map. The second module is the survey module. This module takes care of getting the information from the flood data collector including type of the report, description, latitude-longitude and images.

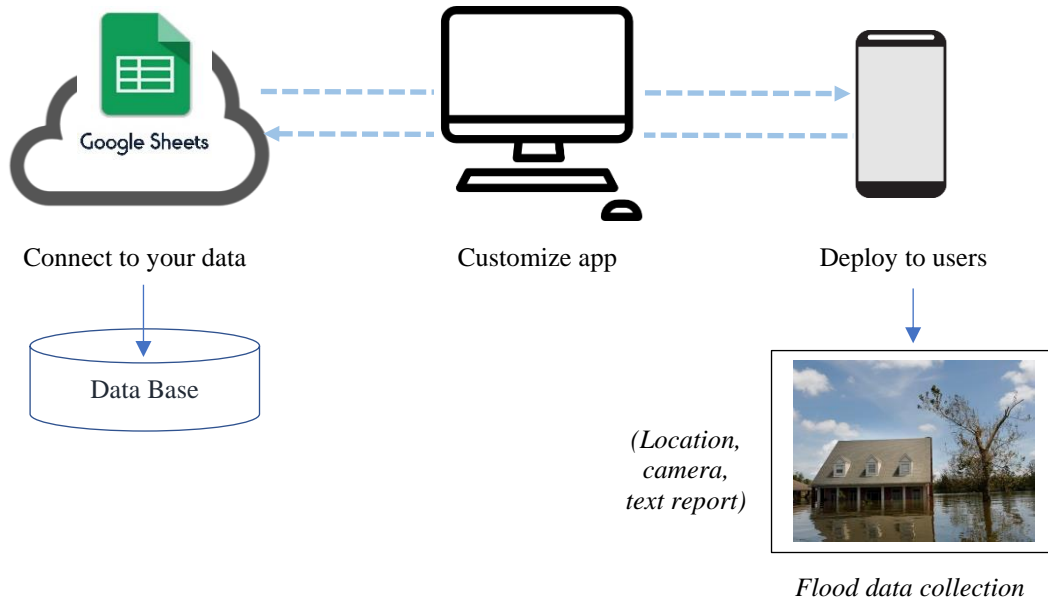


Figure 2. Architecture of the flood risk field survey application.

When the field data collector fills in details by clicking on the SURVEY button, the data will be sent to the cloud server via Wi-Fi network or mobile network (3G/4G/5G).

The system was being used in Pua subdistrict, Pua district, Nan province, Thailand. Field data collectors had the basic information of all the flood or flash flood in the area database such as elevation, slope, geography, climate, culture, etc. that was collected. However, they were unable to identify the location of the flood situation.

Google Sheet created the flood database and triggered the build app on AppSheet website (Figure 3 and Figure 4), <https://www.appsheet.com/>.

The screenshot shows the AppSheet interface for building a 'Mobile Flood Survey' application. The left sidebar lists various sections: **Views** (selected), Info, Data, UX (selected), Behavior, Automation, Security, Intelligence, Users, Manage, Learning Center, and a search bar. The main area displays the configuration for a 'MAP' view under the 'Views' tab. The 'MAP' view is set to display data from the 'SURVEY' table. The 'View type' is set to 'map'. The 'Position' is set to 'left'. The preview on the right shows a map with a survey point marked at coordinates 07140.012, 105.555. The preview also includes a 'Preview App as' section with the email address 'flood2nan@gmail.com'.

Figure 3. MAP page build app.

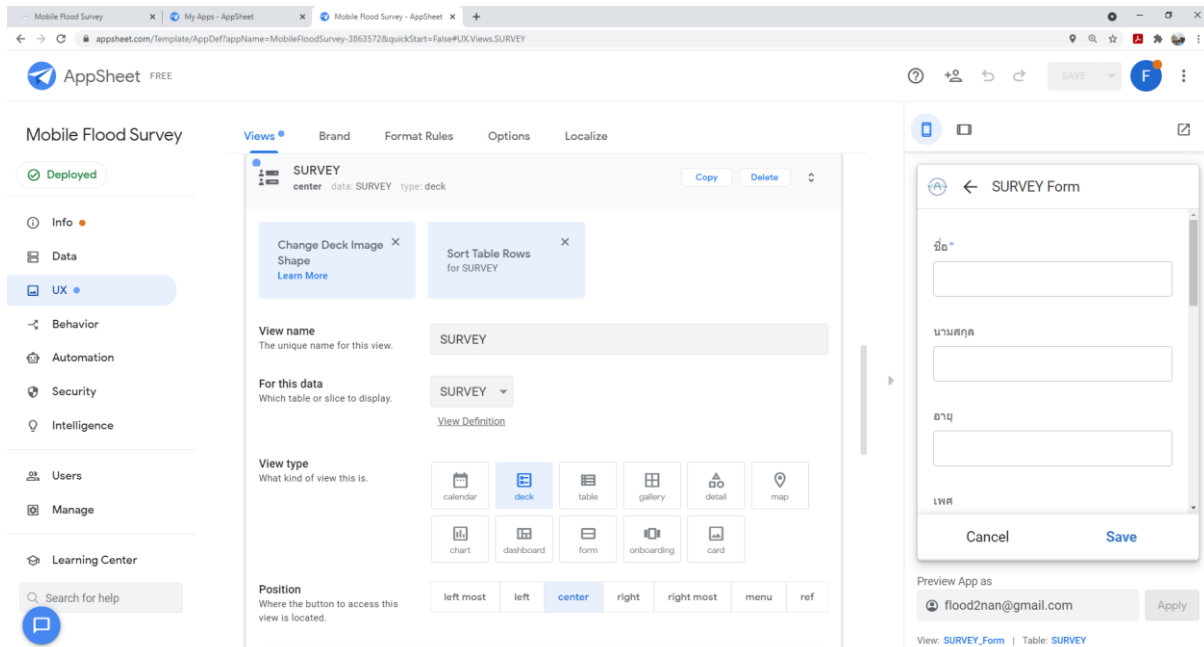


Figure 4. SURVEY page build app.

The server-side provided access to geospatial data and performed online spatial requests such as find, spatial query, measure, and closeness analysis based on requests made by from client-side. On the other hand, the user at the client-side could navigate and display through separate GIS layers of the geospatial data hosted by the server-side.

Application of the mobile side of the system was concentrated on the mobile GIS application. The previous application was used for field survey report from the geospatial field survey. The GPS location in the smartphone was adept of pinpointing the current lat/long location automatically. Once the existing location had been reached, the user would be able to start inserting the data using the input form.

3. RESULTS

The application of the mobile-side of the system was concentrated on the mobile GIS application. The previous application was used for flood situation report from the geospatial filed survey. The collectors got access to the app, then identified their existing location. The GPS location in the smartphone was adept of pinpointing the current location automatically. Once the existing location was found, the user started inserting the data using the SURVEY form.

Figure 4 below shows some screenshots of the application.

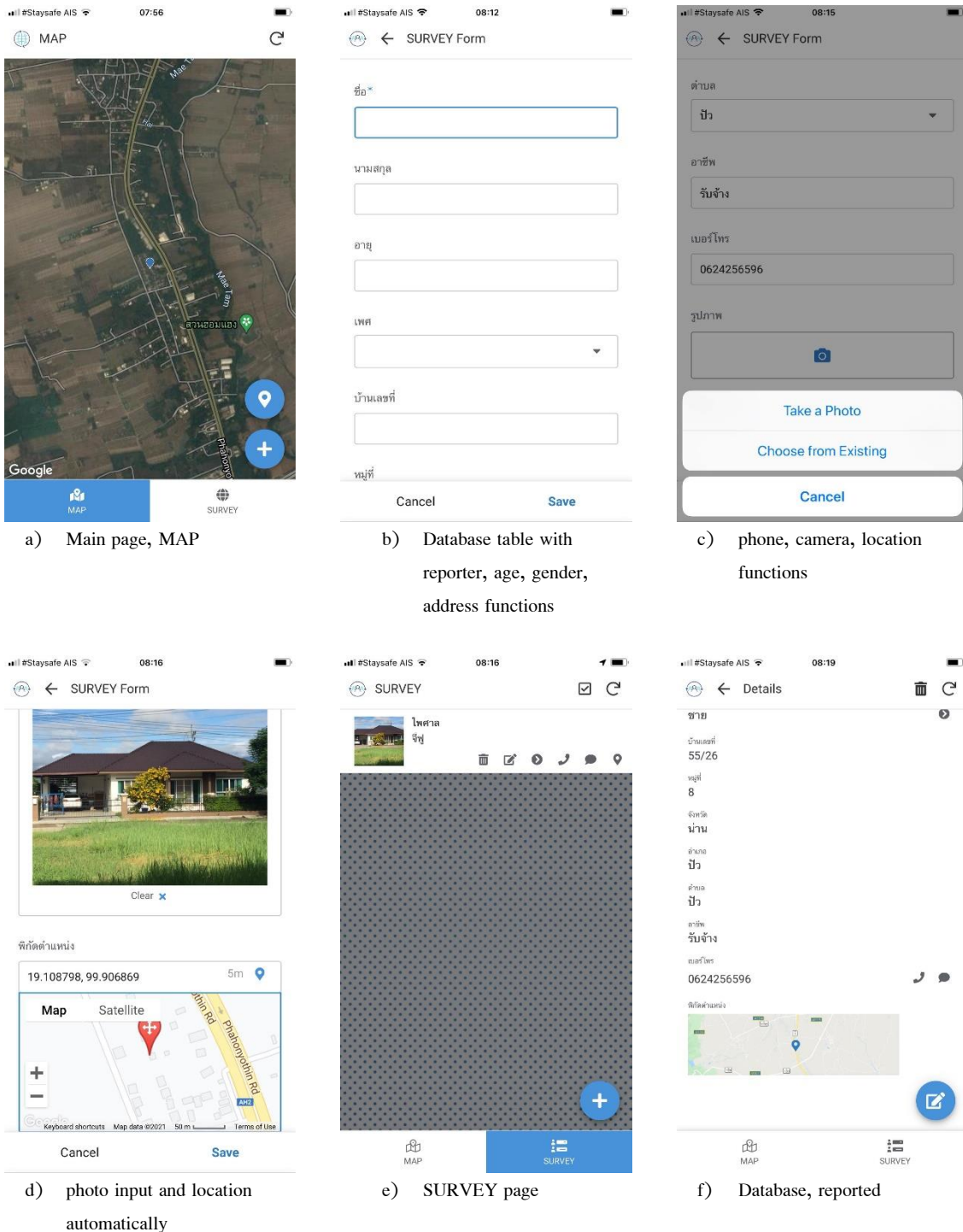


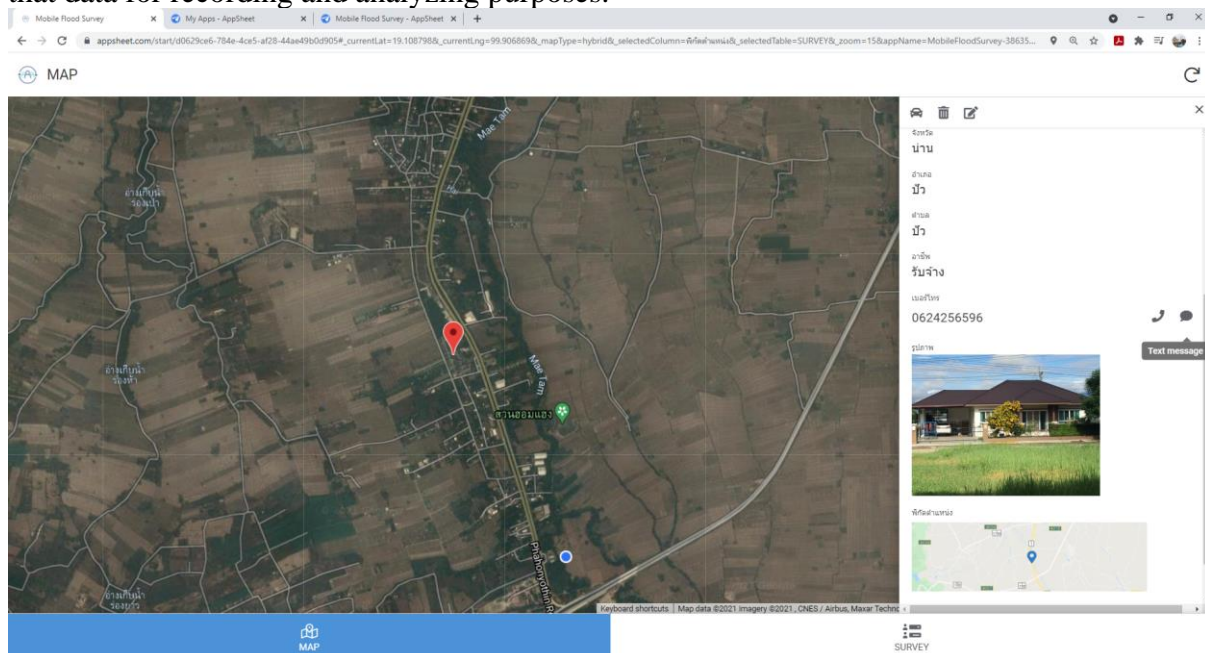
Figure 4. Screenshots of the flood risk field survey application.

The implementation of the flood data collection using mobile GIS field survey consisted of the software used and details of item software version. The flood risk field survey using Mobile GIS technology was designed and developed with a user-friendly main interface (Figure 4a). The main screen of the application provides access to the reporting tools. Reporting tool for field data includes data and image files of current location (Figure 4 (b, c, d, e, f)). The application development environment and tool are shown in table 1.

Table 1. Application development environment and tool.

No.	Flood Risk Field Survey using Mobile GIS <i>Software and Hardware</i>	Software
1.	Server	Cloud Server
2.	Operating System Server	Windows 10 Enterprise
3.	Web Server	AppSheet
4.	Application Server	AppSheet
5.	Database Server	Google Sheet
7.	User Interface	AppSheet
8.	Client Web Browser	Chrome, Firefox, Internet Explorer, Safari

The web interface for flood risk field survey is shown in Figure 5. The collectors can visualize the reporting points of real time field survey that send data, and they can make use of that data for recording and analyzing purposes.

**Figure 5. Web interface for flood risk field survey.**

By clicking on a pinpoint which was the location of the house that was flooded on the map, the information associated with the image such as latitude, longitude, flood status, reporter, and date was automatically linked with geographic data such as names of subdistrict, district, and province.

4. CONCLUSION

Google Maps provides its source of base map and user friendly applications. Freeware products can be easily and quickly downloaded and installed. The interface is well organized and easy to follow. Data recording tools are fairly user friendly, easy to figure out, and supportive to users with multiple data forms for output and sharing. This is a good free mobile tool, especially in the context of training others to use it, given its simple and easy to understand design. The implemented mobile GIS platform provides the basic GIS functionalities and

location. The new generation of mobile network technology advances rapidly, and the storage capacity of intelligent communication terminal increases substantially. So that the mobile GIS has become the new hot spot following Desktop GIS and Web GIS (Wu, 2012; Jeefoo, 2014). The client/server GIS framework that was developed was an independent application, which could be run in every modern mobile smartphone without requiring any other additional software. This application helped the field parties to gather data from flood risk field survey and provided inputs for monitoring and protection.

5. ACKNOWLEDGEMENT

This research was supported by Defence Technology Institute (DTI), Thailand. Spatial thanks go to the Mobile Development Unit 31 (MDU31) of Pua district, Nan province for supporting essential data and information.

6. REFERENCES

- Anusha, N., and Bharathi, B. 2019. Flood detection and flood mapping using multi-temporal synthetic aperture radar and optical data. *The Egyptian Journal of Remote Sensing and Space Sciences*, <https://doi.org/10.1016/j.ejrs.2019.01.001> (accessed 9 July 2021)
- As Natural Disaster Rise, Countries Call for Action on Resilient Crisis Recovery Planning, 2017. <https://www.worldbank.org/en/news/feature/2017/06/06/as-natural-disasters-rise-countries-call-for-action-on-resilient-crisis-recovery-planning> (accessed 10 July 2021).
- Choosumrong, S., Raghavan, V., Jeefoo, P., & Vaddadi, N. (2016). Development of Service Oriented Web-GIS Platform for Monitoring and Evaluation using FOSS4G. *International Journal of Geoinformatics*, 12(3), 67-77.
- DMSG, 2001. The Use of Earth Observing Satellites for Hazard Support: Assessments & Scenarios. Committee on Earth Observation Satellites Disaster Management Support Group, Final Report, NOAA, Dept. Commerce, USA.
- Haq, M., Akhtar, M., Muhammad, S., Paras, S., & Rahmatullah, J. (2012). Techniques of Remote Sensing and GIS for flood monitoring and damage assessment: A case study of Sindh province, Pakistan. *The Egyptian Journal of Remote Sensing and Space Sciences* 15, 135-141.
- Jeefoo, P. 2014. International Conference on Information Science & Application (ICISA), Real-time field survey using android-based interface of mobile GIS. <https://ieeexplore.ieee.org/document/6847455> (accessed 11 July 2021)
- Jeefoo, P. 2019. Wildfire field survey using mobile GIS technology in Nan province. The 4th International Conference on Digital Arts, Media and Technology and 2nd ECTI Northern Section Conference on Electrical, Electronics, Computer and Telecommunications Engineering, Nan, Thailand. <https://ieeexplore.ieee.org/document/8692291>
- Klemas, V., 2014. Remote sensing of floods and flood-prone areas: an overview. *J. Coast. Res.* 31 (4), 1005-1013.
- Kourgiala, N., & Karatzas, G. (2011). Flood management and a GIS modelling method to assess flood-hazard areas – a case study. *Hydrological Sciences Journal*, 56(2), 212-224.
- Ozkan, S. P., and Tarhan, C. 2015. Detection of Flood Hazard in Urban Areas Using GIS: Izmir Case. *Procedia Technology* 22, 373-381.
- Sanyal, J., and Lu, X.X., 2004. Application of remote sensing in flood management with special reference to monsoon Asia: a review. *Nat. Hazards* 33, 283-301.

Schumann, G.-J.P., and Moller, D.K., 2015. Microwave remote sensing of flood inundation. *Phys. Chem. Earth* 83-84, 84-95.

Wu, L. 2012. 2nd International Conference on Remote Sensing, Environment and Transportation Engineering, Research and development of mobile forestry GIS based on intelligent terminal, IEEE, 978-1-4673-0875-5/12. <https://ieeexplore.ieee.org/document/6260685> (accessed 11 July 2021).

Landslide susceptibility using Analytic Hierarchical Process in northern Thailand

**Sasithon Chatsudarat^{1*}, Nattapon Mahavik¹, Sarintip Tantanee²,
Charattdao Kongmuang¹, Polpreecha Chidburee²,
Kamonchat Seejata², Aphiththa Yodying²**

¹Department of Natural Resources and Environment, Faculty of Agriculture Natural Resources and Environment, Naresuan University, Phitsanulok, Thailand

²Department of Civil Engineering, Faculty of Engineering, Naresuan University, Phitsanulok, Thailand
Naresuan University, Phitsanulok, Thailand

Email: Sasithonc61@nu.ac.th

ABSTRACT

Landslides are one of the most common natural disasters. It causes a lot of damage to both people and property. This is triggered by a physical factor and the amount of rainfall is considered as the most important factor. The purpose of this research is to study susceptible zones to landslides in northern Thailand. This study used Analytic Hierarchy Process (AHP) integrated with Geographic Information Systems (GIS). Ten factors were considered namely, slope, slope aspect, slope angle, lithology, distance to lineament, distance to drainage, soil texture, rainfall, land use, and normalized difference vegetation index (NDVI). The study revealed areas that very high susceptible levels found in Lampang, Phrae, and Nan provinces. The Area Under Curve (AUC) method used to validate the map, showed the success rate accuracy of 59.67% and the prediction was correct 62.56%. Furthermore, these results will guide planning to deal with and prevent landslides in northern Thailand effectively.

Keywords : Landslides, Analytical Hierarchy Process(AHP), Geographic Information Systems (GIS), northern Thailand, Area Under Curve (AUC)

1. INTRODUCTION

Landslides are one of the most common natural disasters in the world. It causes a great deal of harm to both people and property. It also has an impact on the global and national economies. In the last 41 years, more than 150 landslides have occurred in Thailand, with the northern area bearing the brunt of the damage. According to data collected, the landslide caused total damage of 2,575.5 million baht and impacted the lives of approximately 286 people. (Soralump *et al.*, 2010). There have been numerous studies and assessments of landslide areas by considering many factors, including: geology, lithology, soil texture, land use, rainfall, and human activity (Guzzetti *et al.*, 2000; Intarawichian., 2008; Boroumandi *et al.*, 2015).

The analytical process is currently presented as a map qualitatively as well as quantitatively by integrating Geographic Information Technology (GIS) with Analytic Hierarchy Process (AHP). As extensively used in previous studies, GIS can be used to manage, process, and analyze landslide surveys due to its powerful tools. Therefore, this paper aims to; Landslide susceptibility zoning can substantially assist future risk mitigation and sustainability planning in areas. The Analytic Hierarchy Process (AHP) was a powerful tool for landslide susceptibility zoning. This technique is well-known applicability in multi-criteria decision making and the analytical capabilities of Geographic Information Systems (GIS).

2. DATA AND METHOD

2.1 Study area

In this study, we are focusing on Northern Thailand as the study area that covers an area

is approximately 93,691 km². The study area consists of nine provinces: Chiang Rai, Mae Hong Son, Chiang Mai, Lamphun, Lampang, Phayao, Nan, Phrae, and Uttaradit. Data collection on previous landslide events revealed that the majority of the events occurred in the north of Thailand and takes place between May and August. The data used in an analysis for this study ranging from 2002 to 2012. As shown in Figure 1, a total of 64 locations were discovered, which were divided into 45 locations for modeling success rate analysis accounted for 70 percent of success rate, while 19 locations used for model prediction rate accounted for 30 percent of success rate.

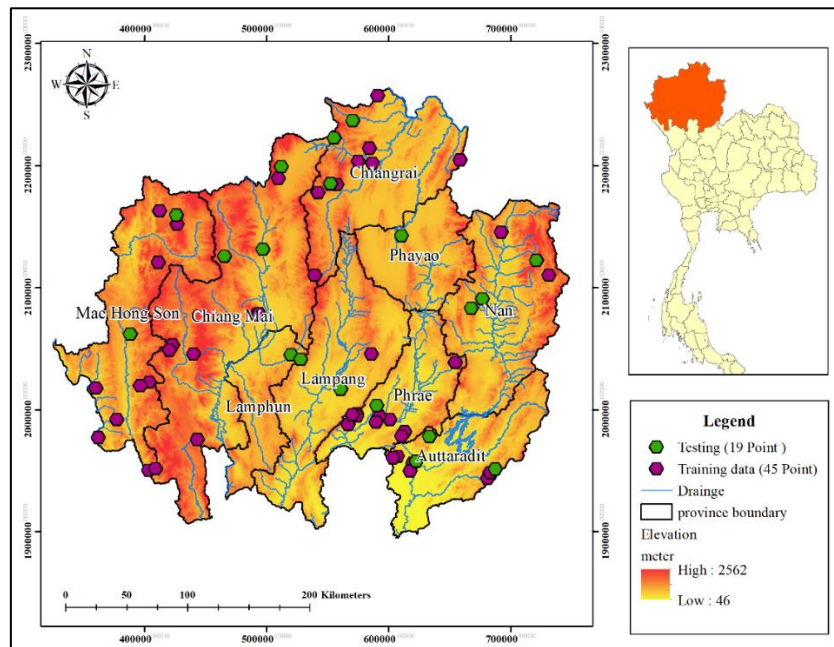


Figure 1. Study area with locations of landslides

2.2 Conditioning factors for landslide

Total ten causative factors were chosen for the susceptibility analysis of landslide based on the study by Intarawichian et al. (2008). A variety of data sources were used to collect landslide causative factors. These maps were prepared in GIS software by classifying and then reclassifying to create a landslide susceptibility map. In this study, the locations of landslide occurrences between 2002 to 2011 were derived from Geotechnical Engineering Research and Development Center (GERD). Rainfall: The annual rainfall average over the ten year was computed from daily rainfall extracted from TRMM 3B42 V.7 (<https://pmm.nasa.gov/data-access/downloads/trmm>). Elevation and slope angle were derived from Shuttle Radar Topography Mission Digital Elevation Model (SRTM DEM) and then generate slope aspect for the study area. Distance from drainage/Lineament was calculated from GIS data from the Department of Mineral Resources by creating a buffer at distance of 500 m for each interval. Soil texture was created by grouping soil types from the Land Development Department (LDD). NDVI was used as monthly vegetation indices L3 Global 0.05Deg CMG product (MYD13C2). Finally, Lithology was obtained from the Department of Mineral Resources as shown in Figure 2.

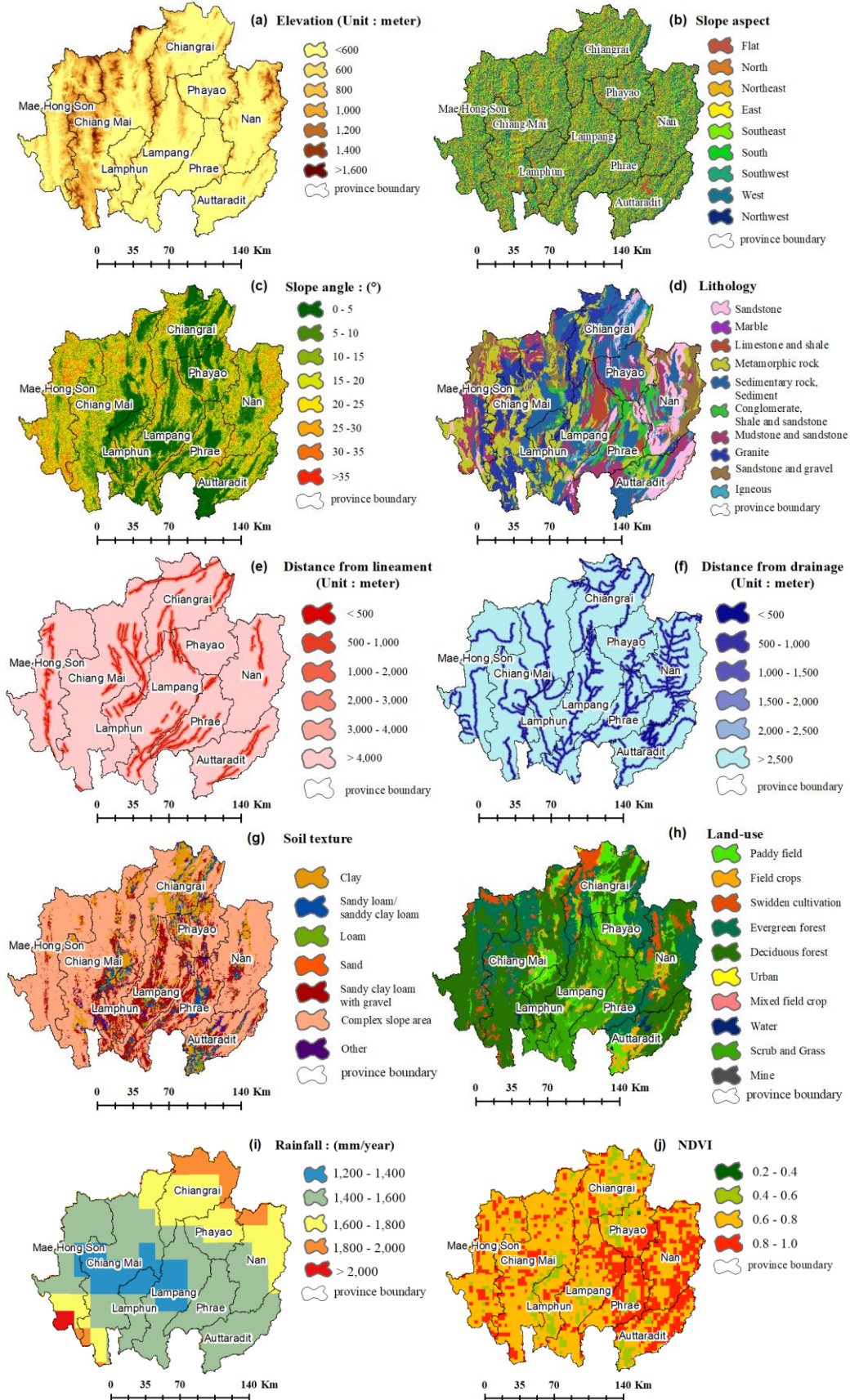


Figure 2. Map of physical parameters

2.3 METHODOLOGY

The present study is based on the AHP method for synthesizing weights of the factors/classes. AHP concept developed by Saaty (1980), we adopted to create the landslide susceptibility map. The computational steps to find criterion weights of a reciprocal matrix are as following operations (equation 1):

$$\text{Consistency Index (C.I.)} = \frac{\lambda_{\max} - n}{n-1} \quad (1)$$

Where λ_{\max} is the the most significant positive eigenvalue of the matrix and n is order of matrix. Finally, the Consistency ratio (C.R.) is calculated using the following (equation 2):

$$\text{Consistency Ratio (C.R.)} = \frac{CI}{RI} \quad (2)$$

Where R.I. is called Random Index and depends on the order of the matrix (n). The standard value of R.I. is represented (In this paper use R.I.= 1.49). If the threshold of Consistency ratio (C.R.) is achieved (C.R.<0.1), the weights of each row of the matrices are calculated.

Table 1. gives a comparison matrix for different classes of the thematic factors viz., elevation, slope aspect, slope angle, a distance from drainage, lithology, distance from lineament, soil texture, rainfall, land use and NDVI. Figure 3 presents the thematic maps generated for this study.

Table 1. Weight assignment of all factors based on AHP concept

Factor	[1]	[2]	[3]	[4]	[5]	[6]	[7]	[8]	[9]	[10]	Weight
[1] Elevation	1.00	1.00	0.20	0.50	0.20	0.33	0.50	0.20	0.25	0.33	0.03
[2] Slope aspect	1.00	1.00	0.25	2.00	0.20	0.20	0.33	0.17	0.25	0.33	0.03
[3] Slope angle	5.00	4.00	1.00	5.00	0.50	2.00	5.00	0.50	3.00	5.00	0.16
[4] Distance from drainage	2.00	0.50	0.20	1.00	0.33	0.25	0.33	0.20	0.33	0.50	0.03
[5] Lithology	5.00	5.00	2.00	3.00	1.00	2.00	2.00	0.33	4.00	5.00	0.17
[6] Distance from lineament	3.00	5.00	0.50	4.00	0.50	1.00	3.00	0.33	3.00	4.00	0.12
[7] Soil texture	2.00	3.00	0.20	3.00	0.50	0.33	1.00	0.20	0.33	0.50	0.06
[8] Rainfall	5.00	6.00	2.00	5.00	3.00	3.00	5.00	1.00	5.00	5.00	0.26
[9] Land-use	4.00	4.00	0.33	3.00	0.25	0.33	3.00	0.20	1.00	2.00	0.08
[10] NDVI	3.00	3.00	0.20	2.00	0.20	0.25	2.00	0.20	0.50	1.00	0.06
CR : 0.07											

The weights of classes of each of the 10 factors derived using AHP were assigned in the attribute Table to create weighted raster maps of the thematic layers. The weighted raster maps were loaded in the ArcGIS software. Then, the Landslide Susceptibility Index is applied in the raster calculator tool of Spatial Analyst Extension to produce the landslide susceptibility map of the study area, as (equation 3) :

$$\text{Landslide Susceptibility Index (LSI)} = \sum_{i=1}^n W_i \times R_i \quad (3)$$

Where W_i = Factor weight

R_i = Class weight/rating for factor i

Then, the resulting map is reclassified into five susceptibility classes. The final landslide susceptibility map is produced as shown in Figure 3.

3. RESULT AND DISCUSSION

3.1 Landslide susceptibility map

Landslide Susceptibility Map (LSM) was created using the AHP method. AHP was used to weight factors and their classes (Table 1) by overlaying the layers in the GIS environment and using relative weights. Accordingly, the LSI map is classified into the following five categories: Very low susceptibility, low susceptibility, moderate susceptibility, high susceptibility and very high susceptibility as shown in Figure 3. As shown in Table 2, we found that 11% of the entire area is accounts for very low susceptibility class, 13% in low susceptibility class, 30% in moderate susceptibility class, 33% in high susceptibility class and 13% in very high susceptibility. The results show that most of areas in Phrae, Lampang, and Nan provinces are in the very high susceptibility classes.

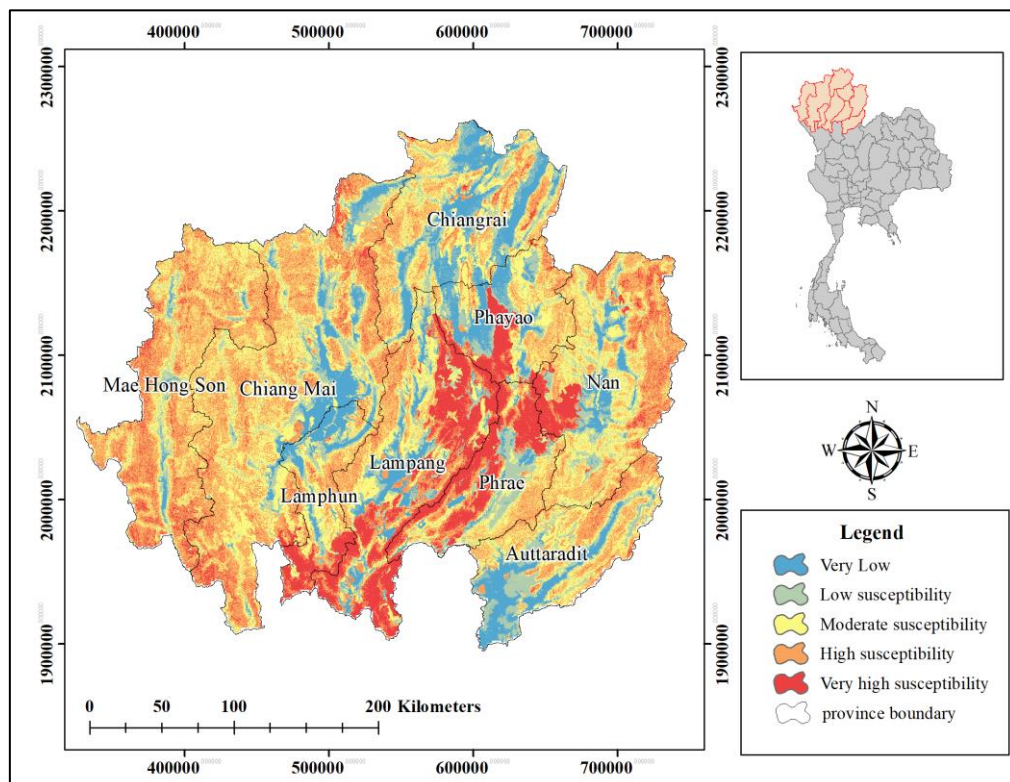


Figure 3. Landslide susceptibility map

Table 2. Landslide susceptibility classes, area and coverage percentage of the study area based on AHP

Landslide susceptibility classes	Number of landslide points (out of 64)	Area (km ²)	% of area
Very low susceptibility (VLS)	2	10,479.57	11.00
Low susceptibility (LS)	6	12,118.71	13.00
Moderate susceptibility (MS)	22	28,256.45	30.00
High susceptibility (HS)	21	31,620.76	33.00
Very high susceptibility (VHS)	12	12,185.14	13.00

3.2 AUC (Area Under the Curve) Validation

In this study, accuracy assessment results from Area Under the Curve. It was found that the hierarchical analysis process found that the accuracy of the success rate value was 59.67% and the prediction rate was 62.56%. A map that is susceptible to landslides can be prepared.

4. CONCLUSION

Demarcation of landslide zones in Northern Thailand, by using influencing analytical hierarchy process models in GIS. The goal of this paper was to use AHP to create a landslide susceptibility map. The results show that Phrae, Lampang, and Nan provinces are in the very high susceptibility classes. However, the most vulnerable areas to landslides were discovered. It was 31,620.76 Km² at the high susceptibility level, accounting for 33% of the total area. Finally, the susceptibility mapping method was found to be reliable with a success rate of 59.67 % and a prediction rate of 62.56%. In present days remote sensing and GIS tools are the most cost and time effective tools for landslide investigation.

5. ACKNOWLEDGEMENTS

This study was supported by “Advancing Co-design of Integrated Strategies with Adaptation to Climate Change in Thailand (ADAP-T)” (Grant Number: JPMJSA1502) supported by the Science and Technology Research Partnership for Sustainable Development (SATREPS), JST-JICA. We are also thankful to the Land Develop Department and Geotechnical Engineering Research and Development Center (GERD) for providing landslide inventory datasets.

6. REFERENCES

- Boroumandi, Mehdi, Khamehchiyan, Mashalah, & Nikoudel, Mohammad Reza. (2015). *Using of Analytic Hierarchy Process for Landslide Hazard Zonation in Zanjan Province, Iran*. Engineering Geology for Society and Territory, 2, 951-955. doi:10.1007/978-3-319-09057-3_165

Guzzetti, F., Cardinali, M., Reichenbach, P., & Carrara, A. (2000). *Comparing Landslide Maps: A Case Study in the Upper Tiber River Basin, Central Italy*. Environ Manage, 247-263.

Intarawichian, N. (2008). *A COMPARATIVE STUDY OF ANALYTICAL HIERARCHY PROCESS AND PROBABILITY ANALYSIS FOR LANDSLIDE SUSCEPTIBILITY ZONATION IN LOWER MAE CHAEM WATERSHED, NORTHERN THAILAND*. Doctor of philosophy in Geoinformatics Thesis, Suranaree University, Department of Technology.

Saaty, T. (1980). *Analytic Hierarchical Process*. Retrieved from Statistics Reference Online.

Soralump, S. (2010). *Rainfall-triggered landslide: from research to mitigation practice in Thailand*. Geotechnical Engineering, 41(1), 39.

FLOOD EXTENT DETECTION WITH DIFFERENCING WATER INDICES USING LANDSAT 8 DATA

Iyaratounrit¹, Somsarit Sinnung², Pattanapol Meena³, and Teerawong Laosuwan^{4*}

^{1,3,4} Department of Physics, Faculty of Science, Mahasarakham University, Maha Sarakham, Thailand

² Defence Technology Institute, Office of the Permanent Secretary of Defence, Nonthaburi, Thailand

*Corresponding author: teerawong@msu.ac.th

ABSTRACT

In the past, flood occurred in Thailand caused damage to people's lives and properties, environment and the ecosystem of a certain area. Flood occurs in Lainan sub-district, Wiang Sa district, Nan province every year. Major factors are from heavy rain influenced by monsoon wind and reinforcing factor like physical characteristics of the geography such as slope, stream density, land use including roads, etc. From the problem, the researcher focused on using data from Landsat 8 for conducting an analysis to detect flood affected areas in conjunction with 2 physical models; 1) Normalized Difference Water Index (NDWI) and 2) Modified Normalized Difference Water Index (MNDWI). The findings from the study showed that the water index from both methods; NDWI and MNDWI, could significantly detect flood affected areas. The NDWI method produced overall classification accuracy of 90.00% and Kappa statistics of 0.93 while the MNDWI produced overall classification accuracy of 95.00% and Kappa statistics of 0.95. In this regard, MNDWI was the method producing the most overall classification accuracy.

1. INTRODUCTION

Natural disasters or natural hazards have an impact on humans, making humans unable to live a normal life, causing huge damage to lives and properties and deteriorating societies (Blanc et al., 2012; Rotjanakusol et al., 2019). One of the most frequently occurring natural disasters is flood, accounted for 41.4%, followed by earthquakes and storms. Asia continental has the most impact (Milly et al., 2002). As for Thailand, it is found that damage from floods increased from 6,000 million baht in 1990 to 40,000 million bath in 2000 and 1.44 trillion baht in 2011 (Asian Disaster Reduction Center, 2012). The 2011 flood in Thailand was ranked as the world's fourth costliest disaster after the 2011 earthquake and tsunami in Japan, the 1995 earthquake in Japan and the 2005 Hurricane Katrina in the United States of America, respectively (Department of Disaster Prevention and Mitigation, 2013). Thailand occupies a total area of 513,115 km². It is a country at the center of Indochinese peninsula in Southeast Asia. In the past, Thailand experienced floods every year in every region of the country due to geographical factors. Thailand is located in a tropical climate zone, influenced by southwest monsoon and northeast monsoon as well as storms that pass throughout the year (Kim, 2014). An urgent necessity that cannot be missed for assessing levels of damage and severity of floods is information or maps showing areas affected by disasters (Rotjanakusol & Laosuwan, 2018). Conventional methods used in the past; for example, a flood map using ground surveying method, required a high cost and was time consuming. Furthermore, some areas are large and difficult to be accessible. In this regard, the application of remote sensing technology using data from a satellite that collects phenomena on the earth by means of the reflection of electromagnetic waves to sensors on the satellite (Uttaruk & Laosuwan, 2016; Laosuwan & Uttaruk, 2016; Uttaruk & Laosuwan, 2018) in conjunction with a physical model has been

carried out as a tool to assess the potential damage of a flood event. Satellite data can cover large areas or areas with difficult access with less costs compared to the ground surveying method (Singh & Singh, 2017; Rotjanakusol & Laosuwan, 2020).

Lainan sub-district, Wiang Sa district, Nan province is influenced by southwest monsoon that sweeps humidity to cover the whole region, bringing heavy rain during the rainy season from May to September. Consequently, Nan province is an area being at risk for flooding since it has a lot of mountains that lead to rapid flash flood, giving a direct effect on floods in lowlands. A study on areas of Nan province in 2016-2020 found that floods occur every year in lowlands, causing damage to properties, houses, agricultural areas including natural resources. As a consequence, this study focused on presenting a method to detect flood affected areas using Landsat 8 satellite data in conjunction with 2 physical models; 1) NDWI and 2) MNDWI in the area of Lainan sub-district, Wiang Sa district, Nan province in the years 2020.

2. AREA OF THE STUDY AND DATA

2.1 Area of the study

Lainan sub-district – is a sub-district in Wiang Sa district, Nan province (Figure.1). It is located in the east of the district on the left bank of Nan River. It occupies an area of 125.01 km².

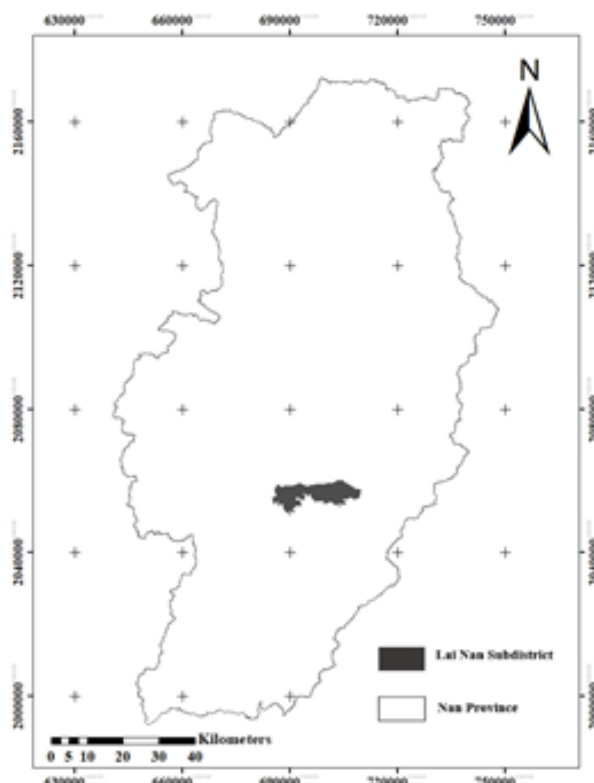


Figure 1. Lainan sub-district, Wiang Sa district, Nan province.

2.2 Satellite data

Landsat 8 is a satellite for surveying natural resources of United States of America. It was developed from the collaboration between NASA and USGS. On 11 February, 2013, it was launched into Earth orbit. It can collect repeated data of the same location every 16 days.

It has two main sensors; OIL and TIRS, with 11 wavelength ranges. For this study, Landsat 8 satellite data covering Lainan sub-district – is a sub-district in Wiang Sa district, Nan province in the years 2020 were employed.

3. METHODOLOGY

The details of the study can be described as follow:

1) NDWI analysis was proposed by McFeeters (1996), NDWI is calculated from the ratio between reflectance difference and sum of green band and NIR band of objects on the earth for separating Earth's water bodies. NDWI values range from -1 to +1 which help analyze and separate water bodies easier. NDWI ranging -1 to 0 represents vegetation fraction cover and NDWI close to +1 represents water bodies. NDWI calculation is shown in equation 1.

$$NDWI = \frac{GREEN - NIR}{GREEN + NIR} \quad (1)$$

Where;

GREEN = Green wavelength (Band 3)

NIR = Near Infrared wavelength (Band 5)

2) MNDWI was proposed by Xu (2006), MNDWI was developed to separate land areas and water areas with more precision. Emphasis is placed on spectral data of land cover being water on the surface of the earth and the reduction of wave disturbance from construction, vegetation and soil. MNDWI is calculated from the ratio between reflectance difference and sum of green band and MIR band. MNDWI values range from -1 to +1. Water has greater positive value than in NDWI as it absorbs more in MIR than in NIR and vegetation reflects more in MIR band than in green band. The calculation of MNDWI is shown in equation 2.

$$MNDWI = \frac{GREEN - MIR}{GREEN + MIR} \quad (2)$$

Where;

GREEN = Green wavelength (Band 3)

MIR = Middle Infrared wavelength or SWIR1 wavelength (Band 6)

The analysis results from both 2 models were used for field data survey. There were 30 surveying points around the area of the study. Kappa statistic was used to measure accuracy. Kappa statistic over 80% shows the data analysis result was high accurate, Kappa statistic ranging from 40-80% means the data analysis result is moderately accurate. Kappa statistic lower than 40% means the data analysis result is poorly accurate.

4. RESULT

4.1 Satellite data analysis result

Landsat 8 satellite data analysis results in conjunction with the 2 physical models: 1) NDWI and 2) MNDWI are shown below:

4.1.1 NDWI analysis result

NDWI is calculated from the ratio between reflectance difference and sum of green band and NIR band of objects on the earth for dividing Earth's water bodies. NDWI values range from -1 to +1 which help analyze and divide water bodies easier. NDWI ranging -1 to 0 represents vegetation fraction cover and NDWI close to +1 represents water bodies. In this study, the lowest value of NDWI was -0.549948, the highest value was 0.636856, the mean was -0.167055 and SD was 0.192698. As for spatial analysis, this study divided NDWI analysis result into 5 ranges (see in Figure 2), namely, the values of data range 1 were 1.000-to -0.700, representing high vegetation cover, the values of data range 2 were 0.700-to 0.400-, representing moderate vegetation cover, the values of data range 3 were 0.400 -to 0.100-, representing low vegetation cover, the values of data range 4 were 0.100 -to 0.200, representing areas with low to moderate water, and the values of data range 5 were 0.200 to 0.500, representing areas with a lot of water. According to NDWI spatial analysis, it was found that during flood occurrence, the data range 1 occupied the area of 0 km², the data range 2 occupied the area of 44.93 km², the data range 3 occupied the area of 66.94 km², the data range 4 occupied the area of 7.73 km² and the data range 5 occupied the area of 0.47 km².

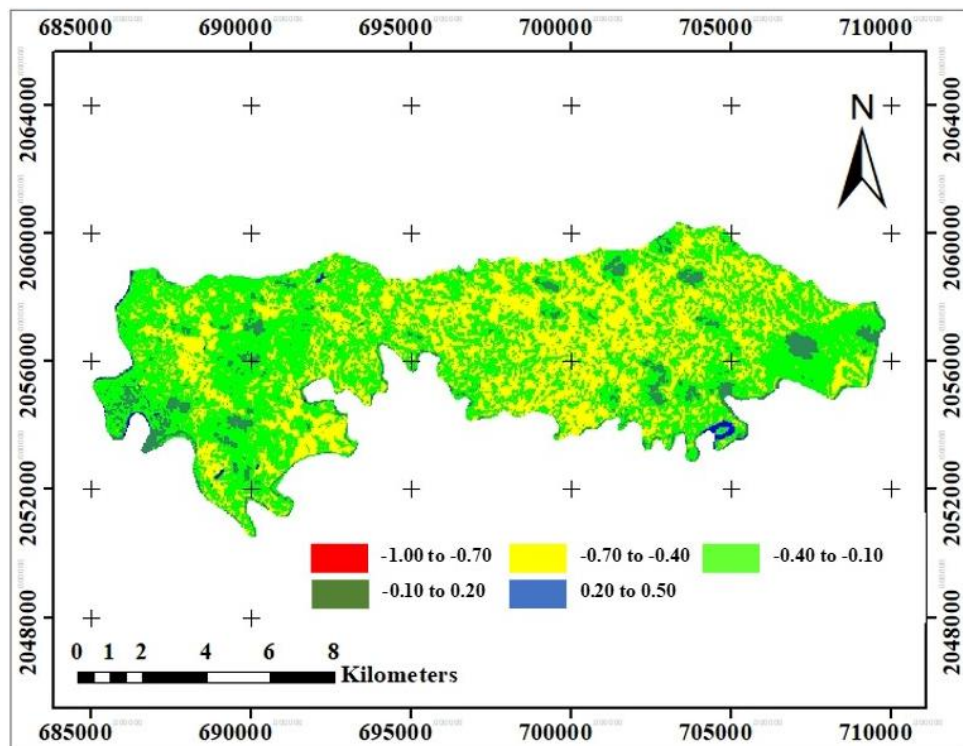


Figure 2. NDWI analysis result.

4.1.2 MNDWI analysis result

As mentioned above, MNDWI is a method used to separate water in soil or vegetation from the amount of solar radiation reflecting from soil or vegetation in green band and in MIR. The calculation of MNDWI produces 3 results: (1) water has greater positive value than in NDWI as it absorbs more in MIR than NIR and vegetation reflects more in MIR than green band. The values of MNDWI range from -1 to +1 similar to those of NDWI. According to the data analysis result in this study, the lowest MNDWI value was 0.405830, the highest value was 0.857356 , the mean was 0.582446 and SD was 0.040856. As for spatial analysis, this study divided MNDWI analysis result into 5 ranges (Figure 3), namely, the values of data range

1 were -1.000 to -0.600, representing high vegetation cover, the values of data range 2 were -0.600 to -0.200, representing moderate vegetation cover, the values of data range 3 were -0.200 to 0.200, representing low vegetation cover, the values of data range 4 were 0.200 to 0.600, representing areas with low to moderate water, and the values of data range 5 were 0.600 to 1.000, representing areas with a lot of water. According to MNDWI spatial analysis, it was found that during flood occurrence, the data range 1 occupied the area of 0 km², the data range 2 occupied the area of 0 km², the data range 3 occupied the area of 0 km², the data range 4 occupied the area of 67.11 km² and the data range 5 occupied the area of 52.96 km².

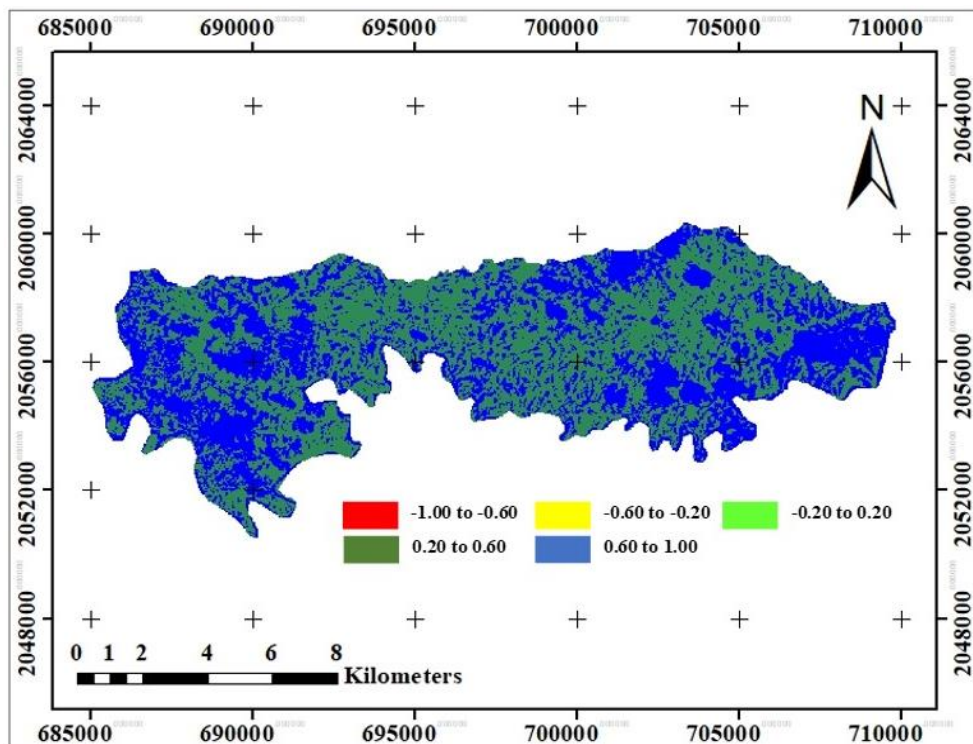


Figure 3. MNDWI analysis result.

4.2 Results from the field survey and accuracy assessment

In this study, accuracy assessment results from the separation of water bodies from lands were considered: 1) According to the NDWI model, overall classification accuracy was 90.00% and Kappa Statistics was 0.93 and 2) according to the MNDWI model, overall classification accuracy was 95.00% and Kappa Statistics was 0.95. The consideration of Overall Accuracy and Kappa Statistics of both physical models found the MNDWI model had the highest percentage of accuracy, based on the analysis.

5. CONCLUSION

Thailand is under the influence of 2 monsoons, namely southwest monsoon and northeast monsoon, making Thailand have 2 outstanding seasons, wet and dry seasons, alternately. As for drought season, consideration in detail stage finds it can be separated into 2 seasons as summer and winter. Therefore, there are 3 seasons in Thailand, namely, summer, rainy season, and winter. In this study, emphasis was placed on methods to detect flood affected areas using index by employing Landsat 8 satellite data in conjunction with the 2 physical models, NDWI

and MNDWI, in Lainan sub-district, Wiang Sa district, Nan province in the years 2020. The study result found the MNDWI model had the highest percentage of accuracy according to the analysis. This study result should be used as decision criteria for areas affected by flood rationally. It can be used to examine and warn areas that can be rapidly flooded. Relevant agencies can be used this method to analyze flood affected areas and prepare plans for flood prevention and mitigation in a sustainable manner.

6. ACKNOWLEDGEMENT

This Research was Financially Supported by Defence Technology Institute.

7. REFERENCES

- Asian Disaster Reduction Center. (2012). Natural Disaster Data Book. Available at http://www.adrc.asia/publications/databook/DB2012_e.html.
- Blanc, J., Hall, J., Roche, N., Dawson, R., Cesses, Y., Burton, A., & Kilsby, C. (2012). Enhanced efficiency of pluvial flood risk estimation in urban areas using spatial-temporal rainfall simulations. *Journal of Flood Risk Management*, 5, 143-152.
- Department of Disaster Prevention and Mitigation. (2013). Annual Report 2013. Available at <http://www.disaster.go.th/th/dwn-download-12-1/>.
- Kim, B., Sanders, B. F., Schubert, J. E., & Famiglietti, J. S. (2014). Mesh type tradeoffs in 2D hydrodynamic modeling of flooding with a Godunov-based flow solver. *Advances in Water Resources*, 68, 42-61.
- Laosuwan, T., & Uttaruk, Y. (2016). Application of Geoinformatics and Vegetation Indices to Estimate Above-ground Carbon Sequestration. *Studia Universitatis Vasile Goldis Arad, Seria Stiintele Vietii*, 26(4), 449-454, 2016.
- McFeeters, S.K. (1996). The use of normalized difference water index (NDWI) in the delineation of open water features. *International Journal of Remote Sensing*, 17, 1425-1432.
- Milly, P.C., Wetherald, R.T., Dunne, K.A., & Delworth, T.L. (2002). Increasing Risk of Great Floods in a Changing Climate. *Nature*. 415(6871), 514-517.
- Rotjanakusol, T., & Laosuwan, T. (2018). Inundation area investigation approach using remote sensing technology on 2017 flooding in Sakon Nakhon province Thailand. *Studia Universitatis "Vasile Goldis" Arad. Seria Stiintele Vietii (Life Sciences Series)*, 28(4), 159-166.
- Rotjanakusol, T., Sangyotha, U., & Laosuwan, T. (2019). Identifying Flood Areas from Satellite Data and Physical Model: A Case Study of Tha Yang District, Phetchaburi Province, 2018. *Defence Technology Academic Journal*, 1 (2), 64-73.
- Rotjanakusol, T., & Laosuwan, T. (2020). Surface Water Body Extraction Using Landsat 8 Images and Different Forms of Physical Models. *The Scientific Journal of King Faisal University, Basic and Applied Sciences*, 21 (2), 218 - 223.
- Singh, K.K., & Singh, A.(2017). Identification of flooded area from satellite images using Hybrid Kohonen Fuzzy C-Means sigma classifier. *The Egyptian Journal of Remote Sensing and Space Science*. 21(1), 147-155, 2017.
- Uttaruk, Y., & Laosuwan, T. (2016). Remote sensing based vegetation indices for estimating above ground carbon sequestration in orchards *Agriculture & Forestry*. 62(4), 193-201.
- Uttaruk, Y., & Laosuwan, T. (2018). Community Forest for Global Warming Mitigation: The Technique for Estimation of Biomass and Above Ground Carbon Storage using Remote Sensing Method. *Agriculture & Forestry*. 64(3), 47-57, 2018.
- Xu, H. (2006). Modification of Normalized Difference Water Index (NDWI) to Enhance Open Water Features in Remotely Sensed Imagery. *International Journal of Remote Sensing*, 27(14), 3025-3033.

Correlation of Drought Index Effected by El Nino Phenomenon Using Remote Sensing

Surat Khampangkaew¹ and Chanida Suwanprasit²

¹ Department of Geography, Faculty of Social Science, Chiang Mai University
Suthep Sup-district, Muang District, Chiang Mai 50200, Thailand
E-mail: surat.kpk@gmail.com

² Department of Geography, Faculty of Social Science, Chiang Mai University
Suthep Sup-district, Muang District, Chiang Mai 50200, Thailand
E-mail: chanida.suwanprasit@gmail.com

ABSTRACT

This study aims to analyze the correlation of the drought index in two periods: November - December 2015 and January - April 2016, where extremely severe El Nino occurred, and November - December 2017 and January - April 2018 and where it was at the normal condition. The results showed that in March 2016 and November 2017 there was a very severe drought level from VHI assessments of 9.574 and 7.625. The drought assessment from NDWI found that the level was at more or less risk of drought. There are no areas where there was no risk of drought. The highest value for the assessment of NDWI was 0.392. In December 2017, the drought level is at a slight drought risk. The lowest value in February 2018 was -0.680. The analysis of the correlation between VHI and NDWI was statistically significant in a positive same direction between two variables at a confidence level is 95 percent. The correlation coefficient values which were influenced by the El Nino phenomenon in November - December 2015 and January - April 2016 were 0.8668, 0.7842, 0.8107, 0.8108, 0.8407, and 0.8528 respectively. The correlation coefficients values which normal El Nino phenomenon in November – December were 0.6917, 0.8692, 0.7345, 0.7278, 0.6638, and 0.7200 respectively.

1. INTRODUCTION

El Nino phenomenon has the greatest impact on the global temperature rising than normal. The seasonal rain causing severe drought in many areas that are affecting the global environment and fertility of forests. Forest ecosystems changing may cause by drought. A very severe El Nino which in 2015-2016 cause rising to higher level drought in Thailand.

Nowadays, Remote Sensing Technology has an important role in various situations analysis that occurring in the world. According to the information services are accessible and comprehensive in various fields such as agriculture, environmental, and disasters, etc. Utilizing satellite images analysis can describe incidents that occurred in the study area in the past and can analyze the potential trend in the future. Remote Sensing Technology can be calculated the drought index for measuring the level of drought. It can be also applied for the correlations analysis between Vegetation Health Index (VHI) and Normalized Difference Water Index (NDWI) to explain the occurrence of droughts in El Nino Phenomena as information for monitoring droughts that may occur in the future.

2. MATERIALS AND METHODS

2.1 Study Area

The Nan River Basin is located in the northern of Thailand with a total area of 34,682.04 sq. km., covers 11 provinces. The position is along the North-South direction. The Nan River flows through the valley into the Sirikit Dam, both sides of the lower area are plain which is considered the most important large plain in Thailand. The Nan River flows along the Yom River until it joins at Chum Saeng District in Nakhonsawan province. Then flow through Bueng

Boraphet on the left before the confluence with the Ping River at Muang District, Nakhonsawan Province. When the Nan River joins together with the Ping River it becomes the Chao Phraya River.

2.2 Data Collection

This research used Landsat-8 OLI image, which covering Nan River basin area. The period was from November-December 2015 to January-April 2016 which extreme El Nino occurred, and November - December 2017 to January - April 2018 which normal event.

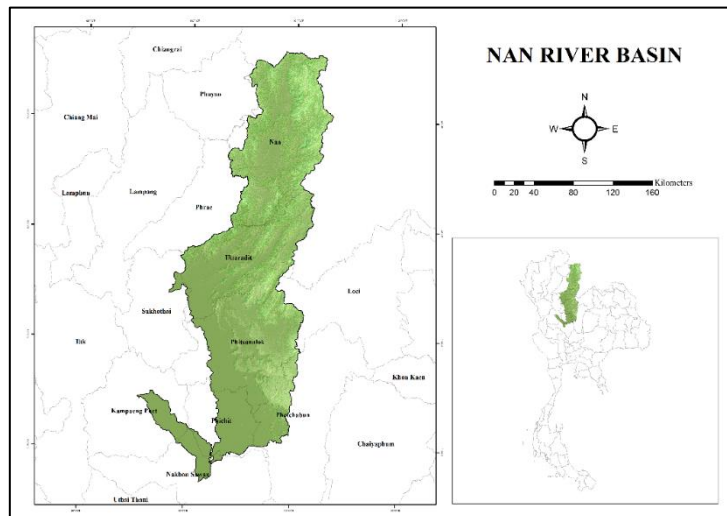


Figure 1. Nan River Basin

2.3 Data Analysis

2.3.1 Vegetation Health Index Analysis

VHI is an index developed to correct errors in the interpretation of drought conditions. It is a combination of the Vegetation Condition Index (VCI) and the Temperature Condition Index (TCI). VHI index is the representatives used to characterize the fertility of plants, by evaluating the mutual value between the humidity conditions and the thermal conditions of the area as shown in equation (1)

$$VHI = (0.7 \times VCI) + (0.3 \times TCI) \quad (1)$$

Where: VCI = Vegetation Condition Index
 TCI = Temperature Condition Index

VCI is a drought matrix calculated based on the Vegetation Index-Based Drought Metric which developed to monitor the Global Drought-Watch System. Vegetation Condition Index derived from NDVI data. It can be calculated from equation (2).

$$VCI = 100 \times \frac{NDVI - NDVI_{min}}{NDVI_{max} - NDVI_{min}} \quad (2)$$

Where: NDVI = Normalized Difference Vegetation Index in the study period
 $NDVI_{max}$ = The maximum value of Normalized Difference Vegetation Index in the study period
 $NDVI_{min}$ = The minimum value of Normalized Difference Vegetation Index in the study period

TCI is an index calculated from satellite data recorded in the Thermal Band of the Landsat-8 TIRS can capably detect surface thermal temperatures. TCI values can be useful for tracking drought conditions better than NDVI and VCI values, especially in the case of excessive soil moisture due to heavy rain or cloudy for a long time .It can be calculated from equation (3).

$$TCI = 100 \times \frac{T_{Max} - T_c}{T_{Max} - T_{Min}} \quad (3)$$

Where: T_c = Surface temperature of the study period (degree Celsius)
 T_{Max} = The maximum Surface temperature of the study period (degree Celsius)
 T_{Min} = The minimum Surface temperature of the study period (degree Celsius)

The land surface temperature from Landsat-8 TIRS, in the band 10 which is thermal infrared band which can be calculate as follows.

Step 1: Calculating the Top of Atmosphere (TOA) (Conversion to TOA Radiance) is a radiation correction by converting the reflectance value into light energy TOA which be calculated from the absorption data for each wavelength as shown in equation (4).

$$L_\lambda = M_L Q_{cal} + A_L \quad (4)$$

Where: L_λ = Reflected Value (Watts/(m² * srad * μm))
 M_L = Transformation of specific wavelengths
 A_L = Transformation of specific wavelengths
 Q_{cal} = Light intensity (Digital Number)

Step 2: Conversion of radiance to brightness temperature as shown in equation (5).

$$Tb = \frac{K_2}{\ln(\frac{K_1}{L_\lambda} + 1)} \quad (5)$$

Where: Tb = Brightness Temperature of satellite value (Degrees Kelvin)
 L_λ = Reflected Value (Watts/(m²*sradi*μm))
 K_1 = The conversion constant value of the thermal infrared wavelength.
 K_2 = The conversion constant value of the thermal infrared wavelength.

The conversion of temperature units from degrees Kelvin to degrees Celsius can be calculated from equation (6) as follows:

$$Tc = Tb - 273 \quad (6)$$

Where: Tc = The brightness temperature of the satellite Value (degrees Celsius)
 Tb = The brightness temperature of the satellite Value (degrees Kelvin)

2.3.2 Normalized Difference Water Index Analysis

Normalized Difference Water Index (NDWI) is used for drought, soil and vegetation monitoring based on the amount of solar radiation reflected in the Near-infrared band (NIR) and Shortwave Infrared (SWIR). NDWI index value ranges from -1 to 1 (with positive values representing water areas, negative values representing non-water features such as vegetation and open spaces) as shown in equation (7).

$$NDWI = \frac{NIR - SWIR}{NIR + SWIR} \quad (7)$$

Where: NIR = Near-infrared band
 SWIR = Shortwave Infrared band

2.3.2 Correlation Analysis

Data from Landsat-8 OLI with spatial resolution of 30 meters was randomly using stratified random sampling techniques and was classified into land use type categories using survey data based on binomial probability theory as follows:

$$N = \frac{Z^2(p)(q)}{E^2} \quad (8)$$

Where: N = Populations
 p = Percentage of expected accuracy
 q = Percentage of acceptable Error (1-p)
 Z = The area value from the standard normal curve table here defines the confidence level at 95 percent. (Confidence level at 95 percent is equal to 1.96)
 E = Percentage of acceptable survey errors

In this study, percentage of expected accuracy was set at 80%, and the error resulting from the survey points was allowed to be not more than 10%. These are 62 survey points classified by land use, including Forest land, Urban and built-up land, Agricultural land, Water body and Miscellaneous land. The drought index was calculated from Landsat-8 OLI which were VHI and NDWI to determine the correlation between the two indices during the dry season in the study area.

3. RESULTS

3.1 VHI value from Landsat-8 OLI

Based on the calculation of VHI from Landsat-8 OLI, the highest drought level was 9.57 in March 2016 and the non-drought level was 95.55 in December 2015 of the year influenced by the severe El Nino. The highest drought level was 7.62 in November 2017, and the non-drought level was 85.58, which was in November in a normal event (Figure 2).

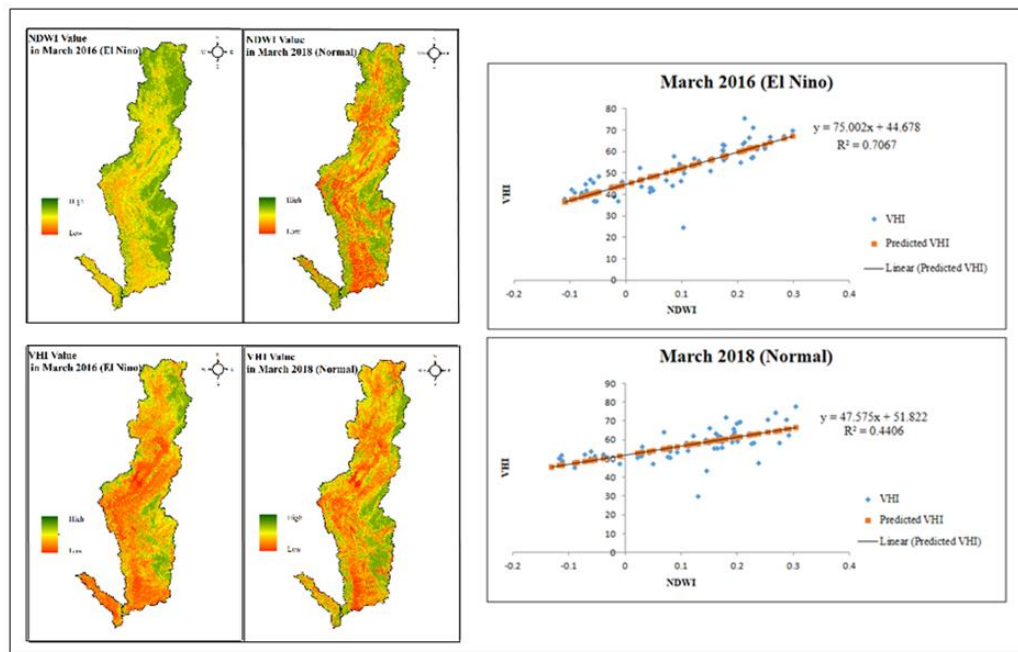


Figure 2. The correlation between VHI value and NDWI value.

3.2 NDWI Value from Landsat-8 OLI

NDWI was calculated from Landsat-8 OLI had a drought risk value was -0.653 in February 2016, and a no-risk value of 0.37885 in January 2016 of the year influenced by the severe El Nino. The drought risk value was -0.6795 in February 2018 and the drought no-risk value was 0.39218 in December 2017 of the normal event.

3.3 The correlation between VHI value and NDWI value

The correlation between the VHI value and the NDWI value was found that the VHI value and the NDWI value were statistically significant in a positive direction. The correlation was same direction for both variables, which was 95 percentage of confidence level. The correlation coefficient values which were influenced by the El Nino phenomenon were 0.8668, 0.7842, 0.8107, 0.8108, 0.8407 and 0.8528, respectively. The normal event values were 0.6917, 0.8692, 0.7345, 0.7278, 0.6638 and 0.7200, respectively.

Table 7. The correlation between VHI value and NDWI value.

Month	R	R Square	Month	R	R Square
November 2015	0.8668	0.7513	November 2017	0.6917	0.4784
December 2015	0.7842	0.6150	December 2017	0.8692	0.7556
January 2016	0.8107	0.6572	January 2018	0.7345	0.5394
February 2016	0.8108	0.6574	February 2018	0.7278	0.5296
March 2016	0.8407	0.7067	March 2018	0.6638	0.4406
April 2016	0.8528	0.7272	April 2018	0.7200	0.5184

4. CONCLUSION AND DISCUSSION

This research found out a correlation between the VHI and NDWI that analyzed drought levels from the Landsat-8 OLI. The drought levels from both indices were ranged from very severe drought to no drought occurrence in the whole of the study area. The results were consistent with the drought criteria derived from this study. In March 2016 and November 2017, there were severe drought levels with VHI value 9.574 and 7.625, respectively. In the NDWI drought assessment, the drought levels were slightly drought risk to highest drought risk level. There was no area that was not risk to drought. The highest value from the NDWI was 0.392 in December 2017, with a slightly drought risk level. The lowest value in February 2018 was -0.680.

The correlation between VHI and NDWI was positive or in the same direction. In other words, if the VHI value was higher, the NDWI value would also be higher. In this research discovered that the correlation coefficients had a positive value close to 1. The correlation coefficients in November-December 2015 and January-April 2016 during El Nino period were 0.8668, 0.7842, 0.8107, 0.8108, 0.8407 and 0.8528, respectively. In November-December 2017 and January – April 2018, the correlation coefficient in normal years were 0.6917, 0.8692, 0.7345, 0.7278, 0.6638 and 0.7200, respectively.

5. ACKNOWLEDGEMENTS

The author would like express the deepest appreciation to the advisor and the Department of Geography, Faculty of Social Sciences Chiang Mai University for supporting this research. Without their guidance and help this article would not have been successful and possible.

6. REFERENCES

- Chandrasekar K., Lingala S. and Ramana K.V., 2017. *Monitoring of Agricultural Drought using Satellite based Drought Severity Index over Andhra Pradesh State of India*, International Journal of Advanced Remote Sensing and GIS. Vol.6, No.1, 2017, pp. 2343-2359.
- Congalton R.G. and Green K., 1998. *Assessing the accuracy of remotely sensed data: principles and practices*. Lewis, New York.
- Kogan F.N., 1995. *Application of vegetation index and brightness temperature for drought detection*, Advances in Space Research. Vol.11, pp. 91-100.
- McKee, T.B., Doesken, N.J. and Kleist, J. 1993. *The relationship of drought frequency and duration to time scales*. Preprints, 8th Conference on Applied Climatology, 179184:17-22
- Pannual W., Chuchip K. and Jintana V., 2015. *Above-ground Carbon Stock Assessment of Khuan Khaeng Swamp Forest after severe Burning in 2012 using Satellite Imagery*., Thai Journal of Forestry Vol.34 (1), pp. 16-28.
- Peainlert S., Tongdeonok P., Kaewjampa N., 2018. *Drought Risk Area Assessment Using Remotely Sensed Data and Meteorological Data in Chern Sub-watershed*. KKU Research Journal (Graduate Studies), Vol. 18 no. 3, pp. 67-83.
- Pinthong A. and Kwanyuen B., 2016. *Drought Monitoring by Composite Drought Index*. Research Journal-Rajamangala University of Technology Thanyaburi, ISSN 1686-8420, Vol. 15(2)
- Pinthong A. and Kwanyuen B., 2018. *Testing the Use of Composite Drought Index to Monitoring Agricultural Drought in Thailand*, King Mongkut's Agricultural Journal, Vol. 36(3), pp.136-146.

COMPARISON OF GEOGRAPHIC IMAGES WITH SSIM AND MSE ALGORITHMS

Sukchatri Prasomsuk¹ Phuwitson Phumsaranakhom^{2*} Phaisarn Jeefoo³

¹Information Technology, School of Information and Communication Technology (ICT), University of Phayao
 19 Moo 2, Maeka, Muang, Phayao 56000 – Thailand
 Email: sukchatri.pr@up.ac.th / skchatri@hotmail.com

²*Computer Engineering, School of Information and Communication Technology (ICT), University of Phayao
 19 Moo 2, Maeka, Muang, Phayao 56000 – Thailand
 Email: narongchai.mo@up.ac.th / Corresponding

³Research Unit of Spatial Innovation Development (RUSID), Geographic Information Science, School of Information and Communication Technology (ICT), University of Phayao 19 Moo 2, Maeka, Muang, Phayao 56000 – Thailand
 Email: phaisarn.je@up.ac.th / p.jeefoo@gmail.com

ABSTRACT

This research, a system for comparing geographic images in the University of Phayao is proposed. The essential objective is developing an aerial photographic database system to support the future planning of the university's area development. Our application system development was separated into 2 modules: the first part is a database system for storing the selected university area map at different times, along with information regarding the photograph's area name, time, location and so on. The second part is a map image processing with two techniques: an algorithm of a perception-based model or structural similarity index measure (SSIM), and the mean squared error (MSE). QGIS, Python, PHP, MySQL was utilized all of most development as tools. The experimental results of the image processing and the similarity of a map comparison system are shown in term of mean (X-Bar) and standard deviation (SD), as well as the outcome of all sample area locations are excellent and to be satisfy.

Keywords: Geospatial database, GIS, Map comparison, SSIM, MSE

1. INTRODUCTION

In the private precincts of the university along with other environments and landscape in terms of their aesthetic appeal is indispensable to develop continuously. Most landscape developers or university administrators require a glance at both current and past data to plan the development of expansion construction to be appropriate for those area. In this research case, we desired to create a database system on web that could compare images and produce academic numerical results with some acceptable techniques for administrative support within the University of Phayao. This university is in Phayao Province at the north of Thailand, around 700 kilometers far from Bangkok as a capital. The campus area is approximately 9.12 square kilometers and is surrounded by agricultural fields, forests and mountains as backgrounds with a beautiful environment. This project is a system that consists of two parts: the first part is a database management system, which emphasized on map images preservation. Most of information would store in a form of image file at a different durations time. Thereafter, the second part is a different images calculation system at the same area maps with structural similarity index measure (SSIM) and the Mean Squared Error (MSE)

techniques to compare between two different image maps instead of visually looking by sight. The algorithms intended to compare images of geographic regions in terms of specific images from past to present. While nowadays, image map comparison can be done in a number of methods that available on internet including in group of GIS applications or other algorithms. Some methods are complicated, difficult to apply, but in this research focus on two techniques as mentioned above that can be attributed to our database system and issue numerical results of map differences as images to support easy-to-understand executive decision-making. For this reason, the SSIM, and the MSE were used as tools in this work.

The rest of this paper is organized as follows. After backgrounding introduction, follows by a brief review of previous related research, the methodology with SSIM and MSE to apply the comparing both map images and illustrates overall the system, the experimental results are demonstrated with the real area from the testbed, and finally is conclusion.

2. A BRIEF REVIEW

Comparison of aerial photographs or from satellite, it is one of the crucial works in the development of the area from the past until the present by using various techniques and methods in many ways since usage of various programs, both open source and commercial. All of programs can be used to assist with GIS work as well. In which those programs have different functions and techniques. We review from the previous research works as the following.

Anju Asokan and his colleges reviewed of the satellite image analysis with various processing techniques in terms of efficiency, quantitative and qualitative such as Peak-Signal-to-Noise Ratio (PSNR), MSE, Feature Similarity Index (FSIM), and SSIM and F-measurements (Anju, 2020).

In addition, there are other methods, which are common photographic comparison techniques, the SSIM method or a statistical method to determine the best image quality. The history and origins of SSIM are also discussed in detail for this research (Jim, 2020).

Another study is a program creation was called FLIP, it focused on image quality as well as the differences between rendered images and corresponding ground truths (Pontus, 2020).

Regarding the map comparison section to evaluate the image quality is a combination of methods, which divided into 4 groups: 1) Classical statistical methods : Fuzzy Kappa, Diagonal Proportion, and Geodetector, 2) Entropy-based methods : Symbolic Entropy, Average Mutual Information and V-measure, 3) Polygon-based methods : Mapcurves (V-measure), 4) Bivariate spatial association methods : Bi-Moran's I. and Lee's L. (Yue, 2020).

The K-Mean clustering algorithm is a technique to solve the segmentation problem of color images and to compare images for determine image quality also (Sadia, 2020).

A group of Umme Sara, they find out the different image quality metrics by to comparing two images between original images and the corresponding noisy and denoise with different noise levels. These experiments were not only considered on noise effects but also emphasizes

on pixel-by-pixel comparison two images values with various methods of the SSIM, MSE, PSNR and FSIM (Umme, 2019).

In 2017, Jake Snell and team have researched learning to visualize with perceptual similarity metrics. They examined the consequences of replacing pixel loss functions like MSE and MAE with grounded loss functions in SSIM and MS-SSIM recognition in neural networks that synthesize and transform images (Jake, 2017).

An interesting paper in 2014 of Anil Wadhokar, research on quality evaluation and comparison of the image capturing from different cameras by using SSIM values. They were focus on the different features values of images and comparison each image of Original (no distortion), Blurred image, Gaussian noise distortion, Salt & Pepper noise distortion, Poisson noise distortion and Speckle noise (Anil, 2014).

Some researches that involved concentrating on Full Reference (FR), Image Quality Assessment (IQA)-Both test and original images methods with SSIM and MSE (Swati, 2013).

As for the tools used in the development of Spatial Data Infrastructures (SDI) are separated in six categories; 1) Server software or web map and GIS servers: MapServer, QGIS, etc. 2) Spatial DBMS (Data Base Management Systems) and storages: PostGIS, SpatialLite, etc. 3) Registry/catalogue and metadata software: GeoNetwork, Deegree, MDWeb. 4) Client software: desktop GIS clients. 5) Web-GIS development toolkits: MapBender, MapFish, GeoMajas, SharpMap, etc. 6) Desktop GIS: Quantum GIS, GRASS, MapWindow, etc. (Erwan, 2012).

3. THE METHODOLOGY WITH SSIM AND MSE

3.1 Structural Similarity Index Matrices (SSIM):

In 2001, SSIM based on the name Universal Quality Index (UQI), which is published in April 2004 as a measure tool for image quality and is highly regarded in the field of image processing (Zhou, 2002). In addition, SSIM is still a popular technique and usage as a reference by considerable researchers for scholarly literature (Jim, 2020). The SSIM is a method for predicting of any picture quality from various sources for measuring the similarity between two images on an initial uncompressed or distortion-free image as reference. In the other word, SSIM is a model of perception-based that speculates, the structure change of information cause of image degradation, while also incorporating crucial perceptual phenomena, including veiling terms of both contrast and luminance. Hence, there are three parameters to effects as a consideration. The SSIM index method, a quality measurement metric is calculated based on the computation of three major parameters as mentioned. If we consider two non-negative images x and y where x is original discrete signal and y is distorted discrete signal, then SSIM index method can be expressed through these three terms as a formula equation (1) below (Umme, 2019).

$$\text{SSIM}(x, y) = [l(x,y)]^\alpha \cdot c[(x,y)]^\beta \cdot s[(x,y)]^\gamma \quad (1)$$

with : l = luminance, c = contrast, s = structure

α, β and γ are the positive constants.

where:

$$l(x, y) = \frac{2\mu_x\mu_y + c_1}{\mu_x^2 + \mu_y^2 + c_1} \quad (2)$$

$$c(x, y) = \frac{2\sigma_x\sigma_y + c_2}{\sigma_x^2 + \sigma_y^2 + c_2} \quad (3)$$

$$s(x, y) = \frac{\sigma_{xy} + c_3}{\sigma_x\sigma_y + c_3} \quad (4)$$

For above definitions: c_1 and c_2 are two variables to stabilize the division with weak denominator as $c_1 = (0.01*L)^2$, $c_2=(0.03*L)^2$, and $c_3= c_2/2$. Where: L is the dynamic range of the pixel-values and μ_x , μ_y are the local means, σ_x , σ_y are the standard deviations, and σ_{xy} is the cross-covariance for images x , y respectively. If $\alpha = \beta = \gamma = I$, then the index can be in a form of equation (5) as the following form by using Equations (2)-(4):

$$\text{SSIM}(x, y) = \frac{(2\mu_x\mu_y + C_1)(2\sigma_x\sigma_y + C_2)}{(\mu_x^2 + \mu_y^2 + C_1)(\sigma_x^2 + \sigma_y^2 + C_2)} \quad (5)$$

The values of SSIM is between ranges 0 to 1, which 1 is a perfect value of both the original image and the duplicate image.

3.2 Mean Squared Error (MSE)

Mean squared error (MSE) or Mean Squared Deviation (MSD) is derived from a comparing between an unknown quality estimation and random errors with a chance game by de Laplace Pierre Simon and Gauss Carl Friesrich in the early 19th century. MSE is the *Mathematical expectation* as the average of sum of squared difference between actual value and the predicted or estimated value (Yadolah, 2008). This method can be applied to many fields in estimating errors between two things, especially in many researches as mentioned in previous part. Particularly, popular works are used to compare identical images two pictures. Human would be able to inform a different two image in draft by them sense only. However, they cannot present in term of error values or different evaluation of image quality. Therefore, to find the error values for two images: I (the original image) and K (the second image) by using the equation formula (6) as below (Swati, 2013). The perfect value result of this method is reach to zero (Dominic, 2018).

$$MSE = \frac{1}{m n} \sum_{i=0}^{m-1} \sum_{j=0}^{n-1} [I(i, j) - K(i, j)]^2 \quad (6)$$

Where:

I : the matrix data of original image

K : the matrix data of copied or degraded image

m : the numbers of rows of pixels and i = the index of row

n : the number of columns of pixels and j = the index of column

4. EXPERIMENTAL RESULTS

This research presents a database system development on web technology for landscape map collection of University of Phayao. The main intent is to support executive and planning section. Most of sample image maps are from Google Earth at different time. The proposed system developed by using Visual Studio Code with Python, PHP, XAMPP and My SQL for database management system. The application consists of two main parts. The first part is a task of web and database system for administrator and users to view the image maps as information. The second part is a mechanism for comparison the same areas between two different time of image maps. The scope of research focuses on ten places in the university and the overview of the system operation displays in Figure 1. There are five stages of development the proposed system as the following.

- Stage 1: Requirement gathering; for this stage, collect all relevant information from executive and planning section, then take any area photo with ten map samples from Google Earth. Preparing information to develop the application, and make ensuring to meet user expectations. Typically, emphasizes on gather all related information with the software requirement specification (SRS) document for future reference.
- Stage 2: Design and data preparing into Server; at this point, the requirements from the SRS document references to create the software architecture and confirm outline a model. After that, all information are entered into the database system and high-angle photographs would resized in the determined dimension at 4800x2707 pixels to prepare for comparison process in next step.
- Stage 3: Coding and Implementation; this phase, the design is translated into source code. This is when software developers go in, implement the code, and revamp any algorithm code of SSIM and MSE with Python. Moreover, the database system part developed by various tools such as Visual Studio Code, PHP, HTML, QGIS and MySQL for managing our database. Finally, retest process is ran until to satisfy.
- Stage 4: Deployment; at this point, the software deployed into at planning section with executive of the university.
- Stage 5: Evaluation; this stage is a process of performance testing for overall programs, which the result shows in Table. 1.

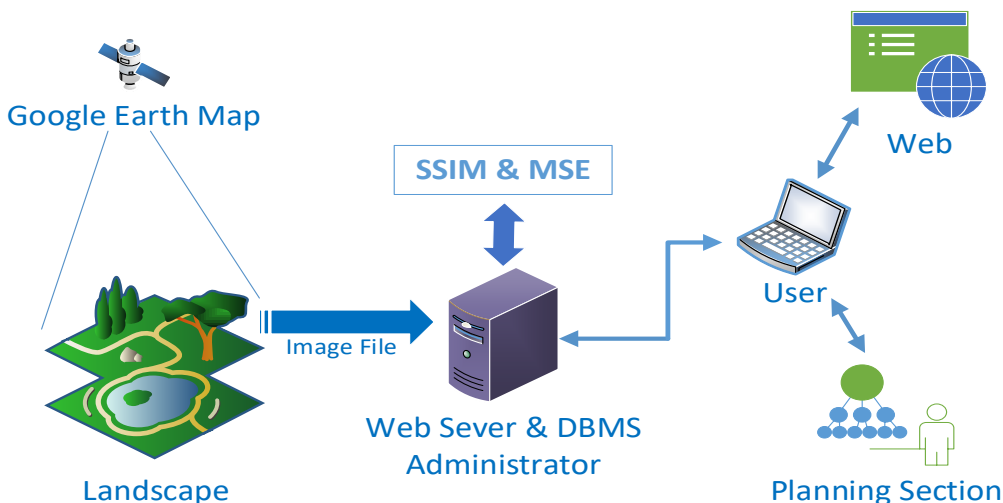


Figure 1. Overview of the system

A sample website screen of the university presents in Figure 2 as the user interface with the result of comparison on two different image maps at the right picture screen. The values of similarity (SSIM) and difference (MSE) display at the top of map as the both values multiply by 100 that to present in percentage.

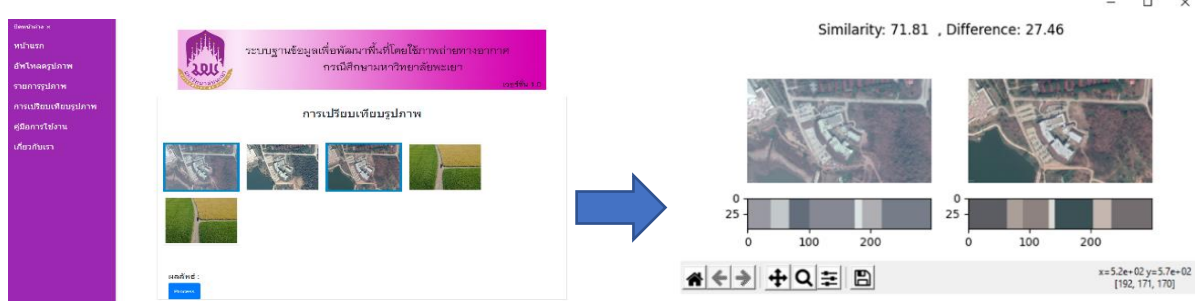


Figure 2. User interface

The operation of proposed comparison system can brief in process as Figure 3. According to area image A is the present map or original image, on the other hands, area image B is a map of previous time. Then, load two image files are into the system. Next step is convert the image colors into grayscale. Afterward, pass the grayscale values are into to the computational operation by SSIM and MSE modules. Finally, the result of similarity and difference reveal out.

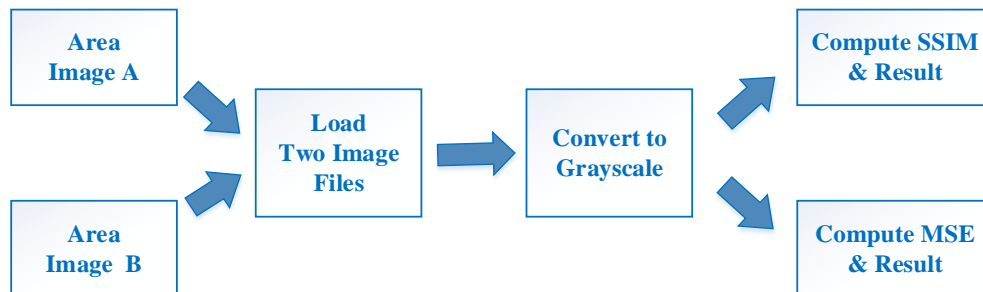


Figure 3. Image comparison process

For this research, we surveyed ten places of different time from Google Earth and comparison together, which shows in Figure 4 that composes of sample places *a-b*.

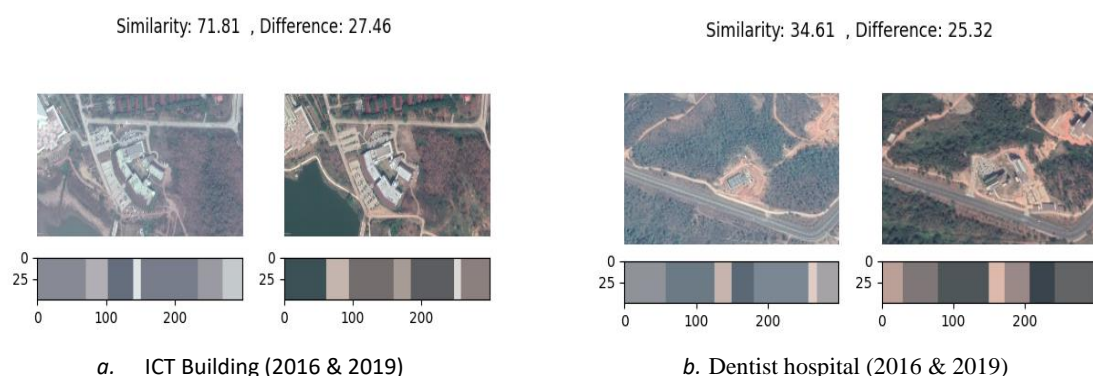


Figure 4. The image maps of each area comparison

5. CONCLUSION

In this article, we present a system development for comparing two images of ten places within the university. The proposed system focuses on the study of using the method of comparing map images by SSIM method to find a similarity value and the difference value between two image map from Google Earth to support the user in planning section in campus. The results of each place illustrates in Table 1.

Table 1. The results of the experiment to find SSIM and SME.

Map	Image Map Comparisons	(Similarity) SSIM	(Difference) SME
a.	ICT Building (2016 & 2019)	0.7181	27.46
b.	Dentist Hospital (2016 & 2019)	0.3461	25.32
c.	University of Phayao Hospital (2016 & 2019)	0.4309	19.15
d.	Pond of Agriculture Faculty (Feb. 2020 & Sep. 2020)	0.3484	16.06
e.	Agriculture Faculty (Feb. 2020)	1.00	0.00
f.	Ong Nakpok hill (2016 & 2017)	0.3675	25.74
g.	Ong Nakpok hill (2016 & 2019)	0.5527	26.70
h.	Arng Luang lake (2016 & 2019)	0.4812	33.53
i.	Arng Luang lake (2016 & 2019)	0.4879	9.42
j.	Sri Khorm Kam Gate (2 Feb. 2017 & 5 Mar. 2019)	0.5814	3.53

The experiment result as above demonstrates the SSIM or similarity values of mean (X -Bar) = 0.5314 with standard deviation (SD) = 0.2018 respectively. On the other hands, the MSE or different values of X -Bar = 18.68 with SD = 11.19.

6. ACKNOWLEDGEMENTS

We would like to give thanks to Sawarin Lerk U suke to assist any data of image maps and provide recommendations and special thanks to School of Information and Communication Technology (ICT), University of Phayao, Thailand for supporting some essential things.

7. REFERENCES

Anil Wadhokar , Krupanshu Sakharikar , Sunil Wadhokar , Geeta Salunke, 2014. SSIM Technique for Comparison of Images, *International Journal of Innovative Research in Science, Engineering and Technology* (An ISO 3297: 2007 Certified Organization) Vol. 3, Issue 9, ISSN: 2319-8753 Sep. 2014

Anju Asokan, J. Anitha, Monica Ciobanu, Andrei Gabor, Antoanelia Naaji and D. Jude Hemanth, 2020. Review Image Processing Techniques for Analysis of Satellite Images for Historical Maps Classification—An Overview. *Applied sciences* 10, 4207

Dominic Asamoah , Emmanuel Ofori , Stephen Opoku, Juliana Danso , 2018. Measuring the Performance of Image Contrast Enhancement Technique, *International Journal of Computer Applications*, Vol.181 – No. 22, Oct. 2018

Erwan Bocher, Markus Neteler, 2012. *Free and Open Source GIS Software for Building a Spatial Data Infrastructure*, Springer, p.247-261

Jake Snell, Karl Ridgeway, Renjie Liao, Brett D. Roads, Michael C. Mozer, Richard S. Zemel, 2017. Learning to Generate Images with Perceptual Similarity Metrics, *IEEE International Conference on Image Processing (ICIP)*, Sep. 2017

Jim Nilsson, Tomas Akenine-Möller, 2020. Understanding SSIM. *NVIDIA Research*, arXiv, <https://arxiv.org/abs/2006.13846>, 8 pages

Pontus Andersson, Jim Nilsson, Tomas Akenine-Moller, Magnus Oskarsson, Kalle Astrom, and Mark D.Fairchild, 2020. FLIP: A Difference Evaluator for Alternating Images. *Proc. ACM Comput. Graph. Interact. Tech.* 3, 2, Article 15, 23 pages.

Sadia Basar, Mushtaq Ali, Gilberto Ochoa-Ruiz, Mahdi Zareei, Abdul Waheed, Awais Adnan, 2020. Unsupervised color image segmentation: A case of RGB histogram based K-means clustering initialization, *PLoS ONE*, Oct. 2020, <https://doi.org/10.1371/journal.pone.0240015>

Swati A.Gandhi, C.V.kulkarni, 2013. MSE Vs SSIM, *International Journal of Scientific & Engineering Research*, Vol.4, Issue 7, July 2013, 930 ISSN 2229-5518

Sadia Basar , Mushtaq Ali, Gilberto Ochoa-Ruiz, Mahdi Zareei, Abdul Waheed, Awais Adnan, 2020. Unsupervised color image segmentation: A case of RGB histogram based K-means clustering initialization, *PLoS ONE*, Oct. 22, 2020, <https://doi.org/10.1371/journal.pone.0240015>

Umme Sara, Morium Akter, Mohammad Shorif Uddin, 2019. Image Quality Assessment through FSIM, SSIM, MSE and PSNR—A Comparative Study. *Journal of Computer and Communications*, 2019, 7, 8-18

Wang, Zhou, Bovik A.C., Sheikh, H.R., Simoncelli E.P., 2004. Image quality assessment: from error visibility to structural similarity, *IEEE Transactions on Image Processing*. 13 (4): 600–612

Wang, Z.; Simoncelli, E.P.; Bovik, A.C., 2003. Multiscale structural similarity for image quality assessment. *Record of the Thirty-Seventh Asilomar, Conference on Signals, Systems and Computers*, 2004. 2. pp. 1398–1402 Vol.2.

Yadolah Dodge, 2008. *The Concise Encyclopedia of Statistics*, by New York, Springer, p.337-338

Yue Lin, Jinfeng Wang, Chengdong Xu, 2020. Theoretical and empirical comparative evaluations on measures of map association. *Journal of Geographical Systems* 22, 361–390

Zhou Wang, Alan C. Bovik, 2002. A Universal Image Quelity Index, *IEEE Signal Processing Letters*, vol. 9, no. 3, pp. 81-84

LINKING BETWEEN METEOROLOGICAL DROUGHT AND LAND USE/LAND COVER IN THE BA RIVER BASIN

**Truong Nhat Kieu Thi¹, Pham Thi Mai Thy¹, Chau Nguyen Xuan Quang²,
Tham Thi Ngoc Han¹, Ho Van Hoa² and Lam Dao Nguyen¹**

¹HCMC Space Technology Application Center, Viet Nam National Space Center, Vietnam Academy of Science and Technology, 1 Mac Dinh Chi, Ben Nghe Ward, District 1, Ho Chi Minh City, Viet Nam

Email: tnkthi@vnsc.org.vn

²Institute for Environment and Resources – Vietnam National University Ho Chi Minh City, 142 To Hien Thanh, Ward 14, District 10, Ho Chi Minh City, Viet Nam

Email: cnxquang@gmail.com

ABSTRACT

Viet Nam is considered as one of the countries most affected by climate change, especially the Ba river basin. Objective of this study is linking between meteorological drought and land use/land cover in the Ba river basin. Penman - Monteith model and SWAT model are the main tools used in the calculation of climate change scenarios, especially climate extremes. The results of drought trend in the baseline scenario in 2019 and climate change scenarios RCP 4.5 and RCP 8.5 in the period 2046-2065 have changed drastically. In agriculture, the no drought level area has decreasing while the moderate drought and severe drought level area has increasing. In forest, the no drought level area has decreasing while the mild drought, moderate drought and severe drought level area has increasing.

1. INTRODUCTION

Viet Nam is considered as one of the countries most affected by climate change, especially the Ba river basin. In recent years, the frequency and intensity of extreme weather events has increased. Climate change also leads to changes in weather, directly affecting crops, production of agriculture, forestry, industry as well as aquaculture and fishing. Especially, the El Niño event in 2015-2016 caused the scorching temperatures and prolonged drought in the Central and Central Highlands in Vietnam, which affected agriculture activities [FAO, 2016].

Water shortages are getting worse with climate change. According to the statistics of the Departments of Agriculture and Rural Development in 2016, the total drought area was over 60,000 ha in the study area. In 2015-2016, the crop area had been damaged by drought of 60,588.6 ha. In 1998 and 2015-2016, the Ba River basin had the most forest area burned up to nearly 481.6 thousand ha (General Statistics Office of Viet Nam, 2018). The reason is El Nino Southern Oscillation (ENSO), which causes an increase in temperature and a decrease in precipitation leads to moisture to dry out.

The Ba river is the largest river in the central coastal region with a main stream length of 374 km. It flows through the four provinces of Kon Tum, Gia Lai, Dak Lak and Phu Yen into the East Sea. The Ba river basin has about 13,900 km² area and is located from 12°35' to 14°38'

North latitude and 108°00' to 109°55' East longitude [Directorate of Water Resources, 2010].

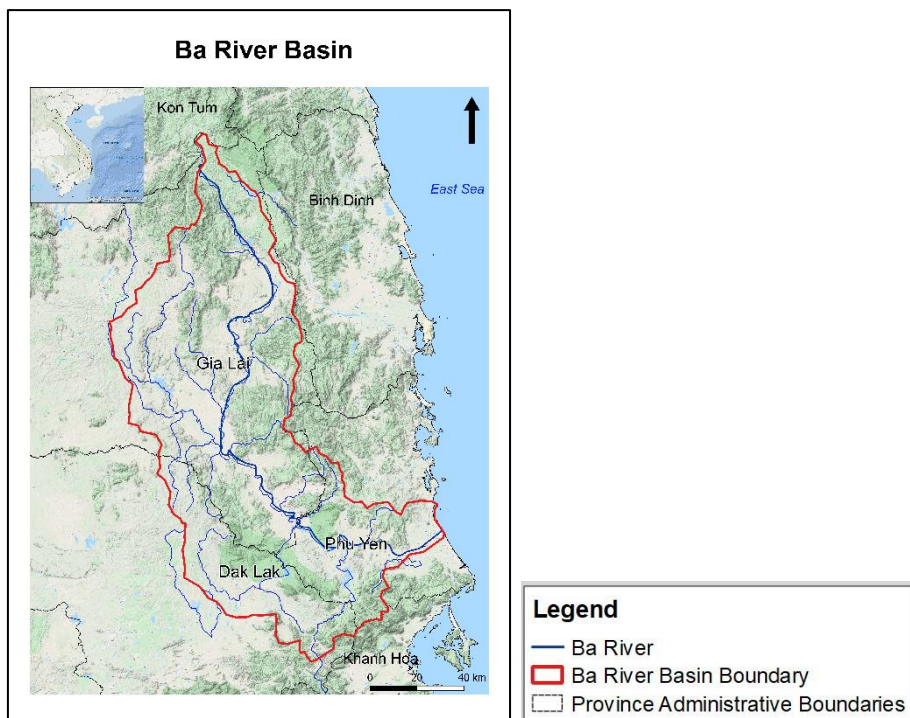


Figure 1. The Ba river basin location.

In recent decade, Remote Sensing (RS) and Geographic Information Systems (GIS) method have been widely applied to observe the surface of the earth such as environment, hydrometeorology, agriculture, land management, forecasting, etc. Therefore, objective of this study is linking between meteorological drought and land use/land cover in the Ba river basin, Viet Nam.

2. MATERIALS AND METHODOLOGY

2.1 Materials

Satellite images: Landsat 8 images were collected in dry season. They were collected from January to May in 2019.

Field data: Field survey samples were gathered in 2019 to assess the land use/ land cover (LULC) classification accuracy.

DEM, soil map, hydrometeorological data: current status, Representative Concentration Pathway (RCP) were also collected to aggregated into input data.

2.2 Methodology

Land use/land cover classification

Landsat image data was corrected atmospheric and removed cloud on the Google Earth Engine platform. Afterwards land use/land cover was processed and classified into forest, agriculture and others. Then the classification results were exported to the GIS formats to edit, evaluate the classification accuracy.

Develop maps of drought zoning

The study uses the results of “Investigating to develop maps of drought zoning in the Ba River basin in the context of climate change” (Thanh, 2019) based on the study method in the report based on the calculation of the drought coefficient (1) for sub-basins with potential evaporation calculated by Penman - Monteith model, average rainfall determined by Thiessen polygon method and average discharge of sub-basins:

$$K_{drought} = \sqrt{K_a K_b}; \text{ với } K_a = 1 - \frac{X}{ET_p} \text{ và } K_b = 1 - \frac{Q_{j,i}}{\sqrt{Q_i Q_o}} \quad (1)$$

K_a : dry coefficient of the level of meteorological drought

K_b : river depletion coefficient represents the abundance of water resources for a certain period of the year

X: monthly rainfall

ET_p : potential evaporation

$Q_{j,i}$: average river discharge in the jth period of the ith year

Q_i : average river discharge in the ith year

Q_o : average water flow for many years

Q: determined by SWAT model for Ba river basin to the outlet section of Song Hinh station

$K_{drought} = 0,5$: signs of drought

$0,5 < K_{drought} \leq 0,6$: mild drought

$0,6 < K_{drought} \leq 0,8$: moderate drought

$0,8 < K_{drought} \leq 0,9$: severe drought

$0,9 < K_{drought} \leq 1$: exceptional drought

Simulation scenario are set up for mapping the drought zoning of the Ba river basin in dry season:

- Scenario (BS): baseline scenario in 2019.
- Scenario 2 (RCP 4.5): the RCP 4.5 scenario in the period 2046-2065.
- Scenario 3 (RCP 8.5): the RCP 8.5 scenario in the period 2046-2065.

After the drought map (RCP 4.5 and RCP 8.5) is available, overlay drought map with LULC (agriculture and forest) in 2019 map by GIS tool.

3. RESULTS AND DISCUSSION

3.1 The change of agricultural and forest areas

The classification results for 2019 was demanding with kappa coefficient of 0.71 and overall accuracy of 89%.

Table 1. Land use/land cover in the Ba river basin in 2019.

LULC	Area (ha)	%
Agriculture	686,526	51.5
Forest	501,728	37.7

Others	144,356	10.8
--------	---------	------

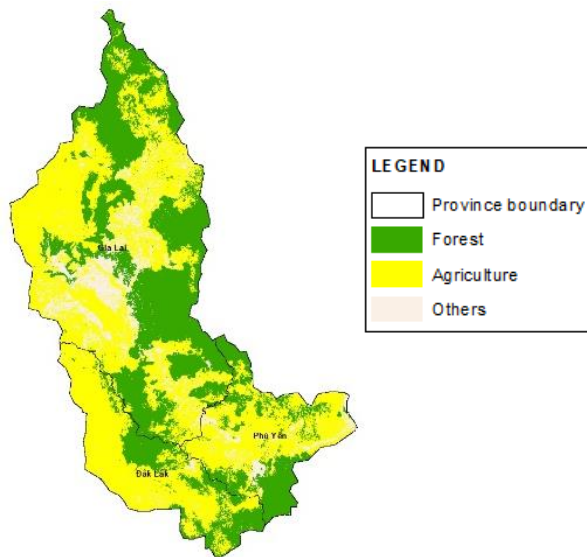
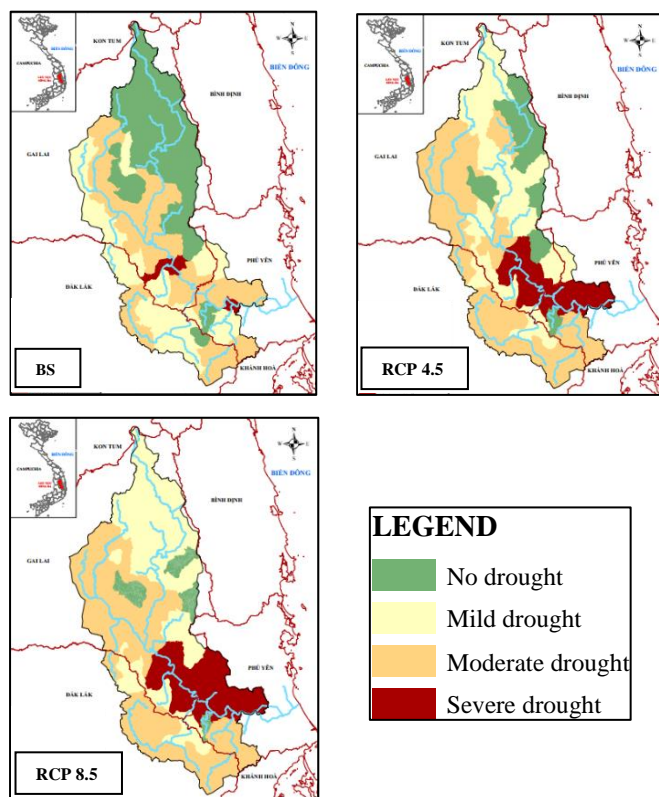


Figure 2. Land use/land cover change in the Ba river basin in 2019.

Table 1 and Figure 2 show that the forest cover was 37.7% (501,728 ha) while the agricultural areas accounted for 51.5% (686,526 ha) of the entire basin area in 2019.

3.2 Drought map of climate change scenarios



The data collected to forecast drought using the Penman - Monteith model is only limited to Cung Son station (Phu Yen province) because the water source is affected by salinity in the estuary, so the SWAT model and $K_{drought}$ Penman – Monteith coefficient can not be used. Thus, this study does not assess the drought in the entire Phu Yen province (excluding the estuary in Phu Yen province).

Simulation results of the climate change scenarios show that the no drought level area has decreasing while the severe drought level area has increasing according to the BS, RCP 4.5 and RCP 8.5. Besides, there is no exceptional drought in the Ba river basin (Figure 3).

Figure 3. Drought levels in the Ba river basin.

3.3 Linking between meteorological drought and land use/land cover

Agriculture drought and forest drought have changed drastically among climate change scenarios, especially no drought and severe drought levels. Mild and moderate drought are more dominant in 3 climate change scenarios (Figure 4 and Figure 5).

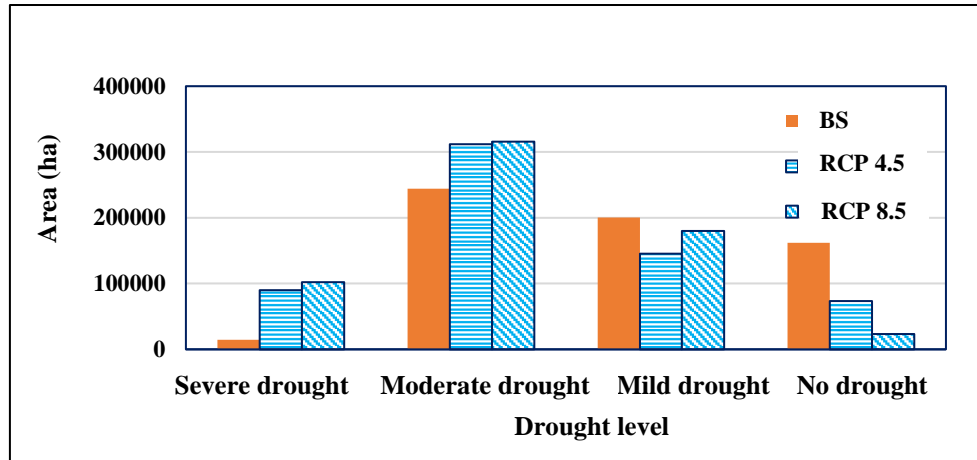


Figure 4. Agricultural drought area under climate change scenarios.

As described in Figure 4, the no drought level area in agriculture tends to decrease according to the BS, RCP 4.5 and RCP 8.5. The no drought level in agriculture in the BS scenario is the highest area, it is nearly 162,000 ha, in the RCP 4.5 scenario is 73,538 ha and the RCP 8.5 scenario is only 23,362 ha (decrease almost by 7 times). Therefore, it shows that future climate change will seriously affect the drought situation in the Ba river basin, the no drought level area in agriculture affected by drought is decreasing according to the simulation scenarios. In contrast, the moderate drought and severe drought level area in agriculture gradually increase according to the BS, RCP 4.5 and RCP 8.5. The area of moderate drought increases from 244,203 ha to 315,667 ha; especially severe drought has been much more serious, the area of severe drought in the RCP 4.5 and RCP 8.5 increases by 8 and 9 times compared to the area of severe drought in the baseline scenario. This will affect future agriculture, the trend of agricultural area can be reduced due to lack of water due to drought, especially in the upstream provinces of Ba River.

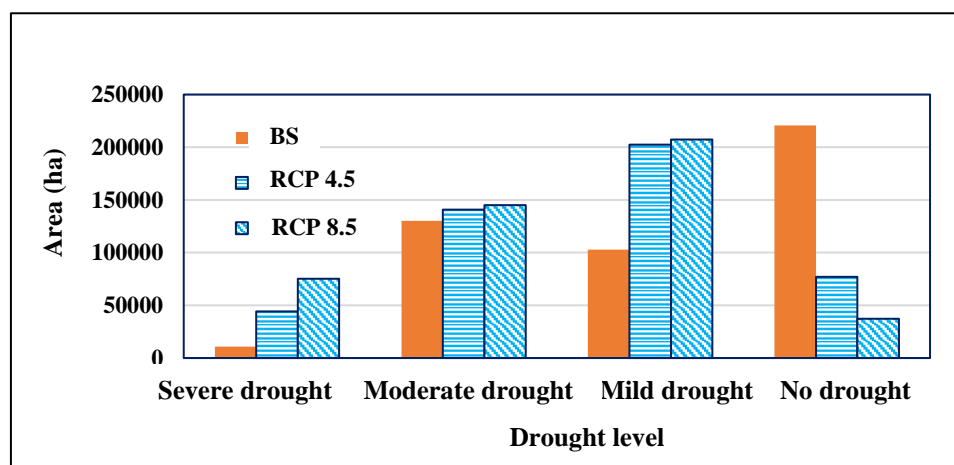


Figure 5. Forest drought area under climate change scenarios.

As agricultural drought, the no drought level area in forest also tends to decrease according to the BS, RCP 4.5 and RCP 8.5 (Figure 5). The no drought level in forest in the BS scenario is more than 220,000 ha, in the RCP 4.5 scenario is nearly 77,000 ha and the RCP 8.5 scenario is only 37,272 ha (decrease almost by 6 times). In addition, the mild drought, moderate drought and severe drought level area in forest also gradually increase according to the BS, RCP 4.5 and RCP 8.5. This shows that climate change seriously affects the level of drought in the Ba river basin. The mild drought area in the baseline scenario is just over 100,000 ha, then the area is more than doubled in the RCP 4.5 and over 207,000 ha in the RCP 8.5. The area of moderate drought in forest increases from 130,237 ha to 145,073 ha. Most notably, the area of severe drought in the RCP 4.5 and RCP 8.5 increases by 4 and 7 times compared to the area of severe drought in the baseline scenario.

4. CONCLUSIONS

Agriculture drought and forest drought have changed drastically among climate change scenarios (baseline, RCP 4.5 and RCP 8.5 scenarios). In agriculture, the no drought level area has decreasing while the moderate drought and severe drought level area has increasing. This will affect future agriculture, the trend of agricultural area can be reduced due to lack of water due to drought, especially in the upstream provinces of Ba River. In forest, the no drought level area has decreasing while the mild drought, moderate drought and severe drought level area has increasing. Severe drought seriously affects not only production but also seriously affects the supply of fresh water for daily life in the Ba river basin.

The results of this study analyzed the linking between meteorological drought and land use/land cover in the Ba river basin, which can serve as a basis for further development of other studies such as propose possible solutions to adapt to climate change, urgent actions to slow down the process of climate change, the effects of climate change on human and the environment...

5. REFERENCES

- Direcotorate of Water Resources, 2010. Integrated management of water resources in Ba river basin.
- FAO, 2016. El Niño event in Viet Nam: Agriculture, food security and livelihood need assessment in response to drought and saltwater intrusion.
- General Statistics Office of Vietnam, 2018. *Statistical yearbook of Viet Nam*.
- Nguyen Nam Thanh, Tran Hong Thai, Bach Quang Dung, 2019. Investigating to develop maps of drought zoning in the Ba River basin in the context of climate change. *Journal of Hydrometeorology*.

ECONOMIC CROPS PREDICTIVE SYSTEM USING ARTIFICIAL INTELLIGENCE AND GIS

Phanakron Kaewme^{1*} Phaisarn Jeefoo² Sukchatri Prasomsuk³ and Phuwitson Phumsaranakhom⁴

¹* Applied Geoinformatics, School of Information and Communication Technology (ICT), University of Phayao, 19 Moo 2, Maeka, Muang, Phayao 56000 – Thailand

Email: kaewmeeppy@gmail.com

²Research Unit of Spatial Innovation Development (RUSID), Geographic Information Science, School of Information and Communication Technology (ICT), University of Phayao, 19 Moo 2, Maeka, Muang, Phayao 56000 – Thailand

Email: phaisarn.je@up.ac.th / p.jeefoo@gmail.com

³Information Technology, School of Information and Communication Technology (ICT), University of Phayao, 19 Moo 2, Maeka, Muang, Phayao 56000 – Thailand

Email: sukchatri.pr@up.ac.th / skchatri@hotmail.com

⁴Computer Engineering, School of Information and Communication Technology (ICT), University of Phayao, 19 Moo 2, Maeka, Muang, Phayao 56000 – Thailand

Email: narongchai.mo@up.ac.th

ABSTRACT

This research presents a prototype development of geospatial database system for Pua distinct, Nan province, northern part of Thailand with the purpose to support an effective agricultural data management by integration of GIS technology and AI for agriculture area. The fourteen types of economic crops were studied, collected, and cleansed, including rice paddy, rainy season corn drought, tapioca, garlic, ginger, shallot, longan, lychee, rubber, palm oil, which there are different information in Pua district, Nan province area of each year. This system operates on any platform system whereat consists of three main functions are geographic map, statistical information with prediction, and information document format of all cropping areas in a form of annual report. The development tools were used by QGIS, Sumlime Text, intelXDK and cloud technology as database system including real-time Google map. The survey of satisfaction application usage showed that the confident users with the system very highly or ($\bar{X} = 4.00$, $S.D. = 0.78$).

1. INTRODUCTION

At present, with the area of Thailand being suitable for agriculture, it is undeniable that "plants" are what provide Thai people with food to feed their stomachs and also generate income for households, extending to generating income for the country until it becomes is "Economic crops" that many farmers take as a career. These cash crops are not just human consumption but also to be used to raise animals and other uses in order to get the most value. This is the good fortune of Thailand, with the right space and climate, it can grow a variety of different plants in a way that many countries can't. Help build the economy of Thailand better from "Economic Crops". Therefore, these plants are still referred to as cash crops today. as well as making money for farmers and the country continuously. Thailand is a country where most of the population is engaged in agriculture. Most of the areas are growing cash crops such as rice, cassava, corn, sugarcane, rubber, etc. From the past to the present, the government has always given importance and support in terms of knowledge and financial assistance to farmers. These economic crops grow in different regions.

Remote Sensing has made substantial contribution in flood monitoring, mitigation and damage assessment that leads the disaster management authorities to contribute significantly. Geographic Information Systems (GIS) technology is ideally suited as a tool for the presentation of data derived from continuous monitoring of locations and used to support and deliver information to environmental managers and the public. GIS based spatial analysis and visual elements are used frequently in recent years for detection of flood hazard areas and for preparation of maps. GIS applications area based on database and which analysis tools have logical and mathematical relationships between the layers (Kourgiala & Karatzas, 2011).

GIS technology has been developed in such a way that spatial information is stored and efficiently retrieved and modelling issues are appropriately embedded to support decision making and operational needs. The added value of GIS technology usage in managing crisis events is directly connected to the profits expected from the exploitation of such technologies designed for supporting decision making related to the geographical space, especially in the case of the operational field that intensely needs to make important decision of spatial nature (Buckeridge et al., 2002; Gavin, 2002; Vakalis et al., 2004).

Mobile GIS is a mature technology which takes geospatial technology beyond the walls of an office (Jeefoo, 2020). Therefore, mobile applications have extended to field use which allows the user easy access, storage, updates, analysis, and real-time visualization of field data. Till recently, mobile GIS application were mainly used as a navigation or location-aware system. Mobile GIS technology nowadays offers a potential alternative to fill the gaps of traditional GIS systems. With Mobile GIS technology, officers and many other field workers have the potential to access the enterprise geospatial data from the server-side to accomplish their tasks with high level of accuracy. More importantly, it is also possible to update these geospatial enterprise data in real time (Choosumrong et al., 2016).

The aim of this research is developed the Economic Crop System (ECS) by using free and open source software (FOSS) in Pua district, Nan province northern part of Thailand.

2. MATERIAL AND METHOD

2.1 Study area

Pua district, Nan province in the northern part of Thailand (Figure 1) was selected as the study area. Pua district comprises of 12 subdistrict and 107 villages and covers an area of 918 sq.km. with geographical location between 2100000 N to 2140000 N and 690000 E to 730000 E. It is mostly covered with forested mountain, with an approximate elevation of 430 meters about mean sea level.

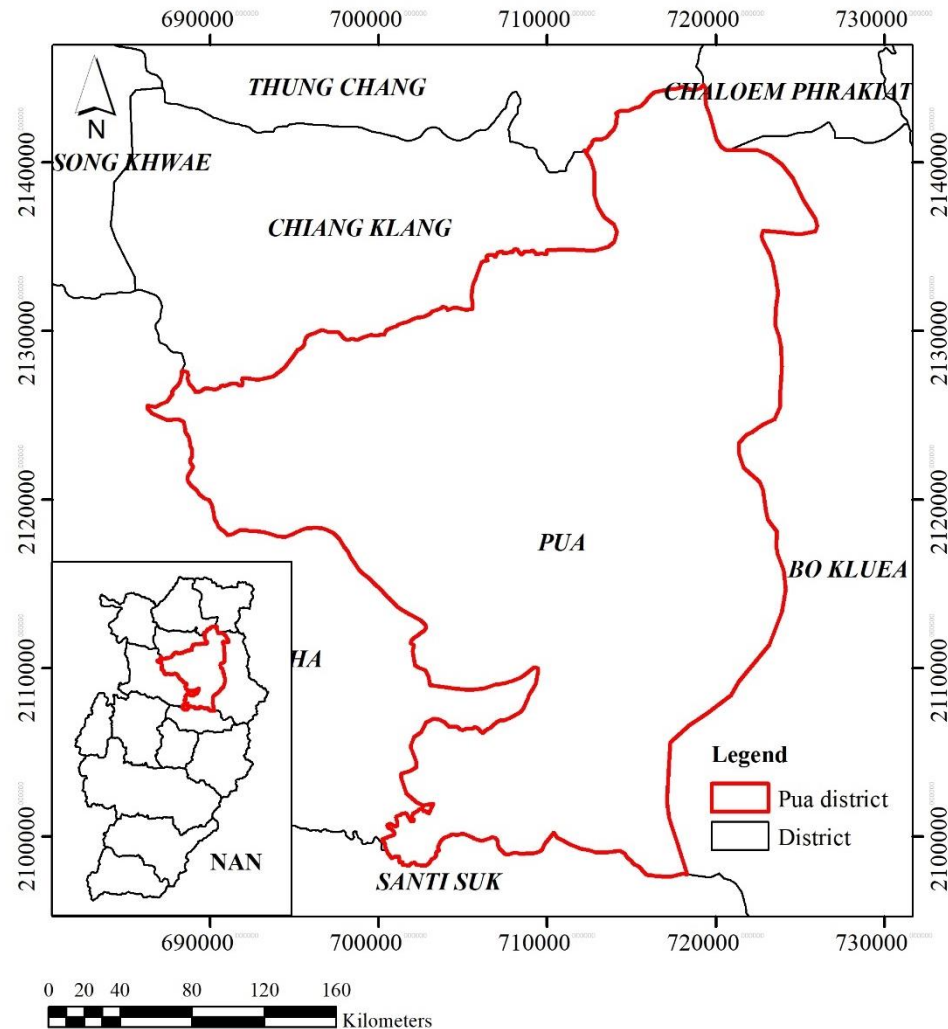


Figure 1. Study area, Pua district, Nan province.

2.2 Method

The ECS were developed by QGIS, Sumlime Text2, IntelXDK. The cloud server is data storage of the system. Administer office is checked data input – output and calculated results for each month of satellite image. Forecasting of the next month's yield calculations come out to be able to use a mobile phone to view the results of the geographic mapping of the cash crops of that area. You can also view the results of the next month's forecast.

2.2.1 Data collection

Collecting economic crop statistics each year information from Nan Provincial Agriculture and Cooperatives Office. They were randomly assigned to survey areas in each district to collect data from 9 types of farmers, namely, glutinous rice, longan, lychee, mango, sweet tamarind, coffee, tea, rambutan, and guava.

2.2.2 Data analysis

Firstly, admin section by managing information through web pages that can create, save, import or edit various data at any time. It works with databases that use cloud technology. Secondary, collect all data and the last display data in graphs or charts and documents (PDF

and MS Excel). Total year to date the relationship between the work of these 3 parts can be shown in figure 2.

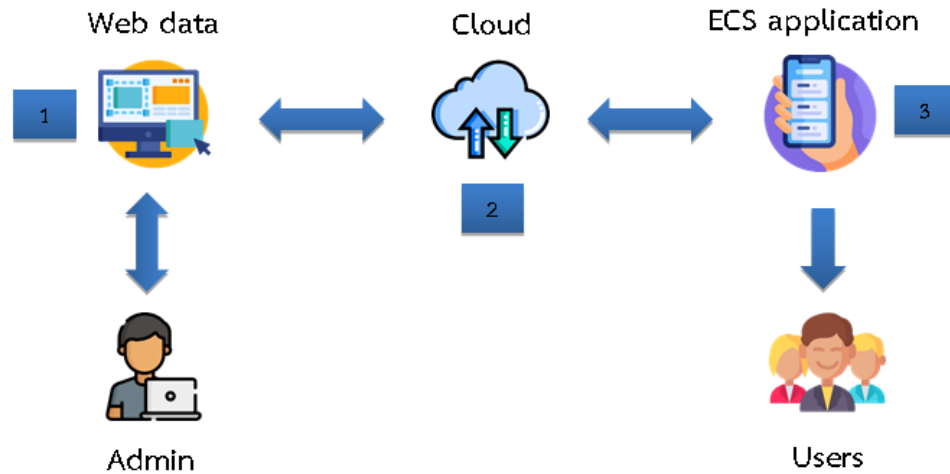


Figure 2. Overall ECS architecture.

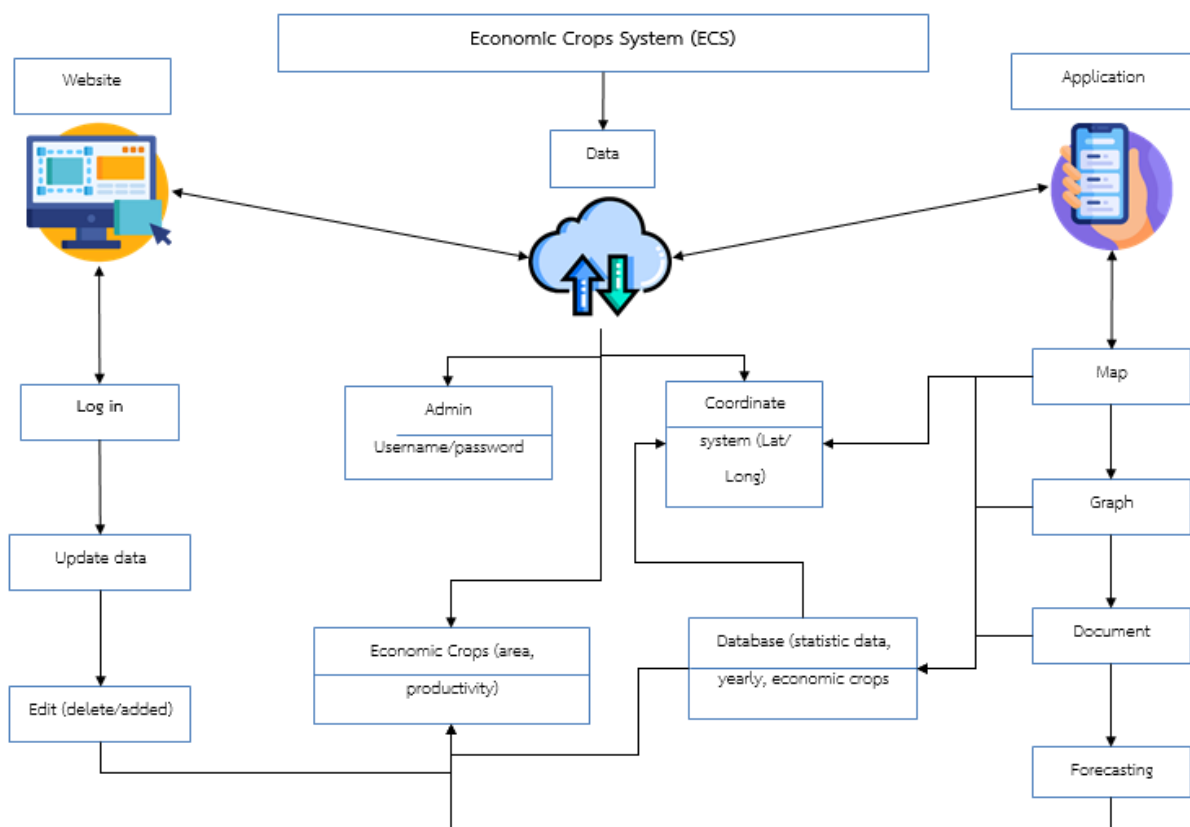


Figure 3. System design of ECS.

2.2.3 System development

This step was designed the system development including user interface (UI) and administrator.

- 1) User interface : 4 functions consist of (i) Map (ii) statistic data (iii) document data

- and (iv) forecasting
- 2) Administrator : updating, input data from MS Excel (coordinate system, crops data) and forecasting function.

3. RESULTS

3.1 Mobile Application : ECS application

Application of the mobile-side of the system was concentrated on the mobile GIS application. The function of predicting or predicting how much results will be achieved in the following year, where users have to select the crops they want to plant, then the application will display results individually. Year and calculate all the monthly cycles that the whole year will produce an estimation. Figure below shows some screenshots of the application.



Figure 4. Shown screenshots of the ECS application Pua district, Nan province.

The web interface for ECS is shown in Figure 5 to Figure 7. The agriculture office can visualize the reporting points of real time field survey that send data, and the can make use of that data for recording and analyzing purposes. For example, part of the economic crop prediction, fill in the numbers of the last year, such as 2016, etc. The system will calculate the results for the next year (Figure 5-7).

NameDis	Lat	Long	Update
จังหวัด	19.168	100.903	Update / Delete
จังหวัด	19.176	100.947	Update / Delete
จังหวัด	19.197	100.849	Update / Delete
จังหวัด	19.224	100.951	Update / Delete
จังหวัด	19.148	100.967	Update / Delete
จังหวัด	19.097	100.957	Update / Delete
จังหวัด	19.029	100.998	Update / Delete
จังหวัด	19.222	100.895	Update / Delete
จังหวัด	19.162	100.838	Update / Delete
จังหวัด	19.254	101.091	Update / Delete
จังหวัด	19.27	101.031	Update / Delete
จังหวัด	19.13	100.9	Update / Delete

Figure 5. Coordinate web page.

Figure 6. Date web page.

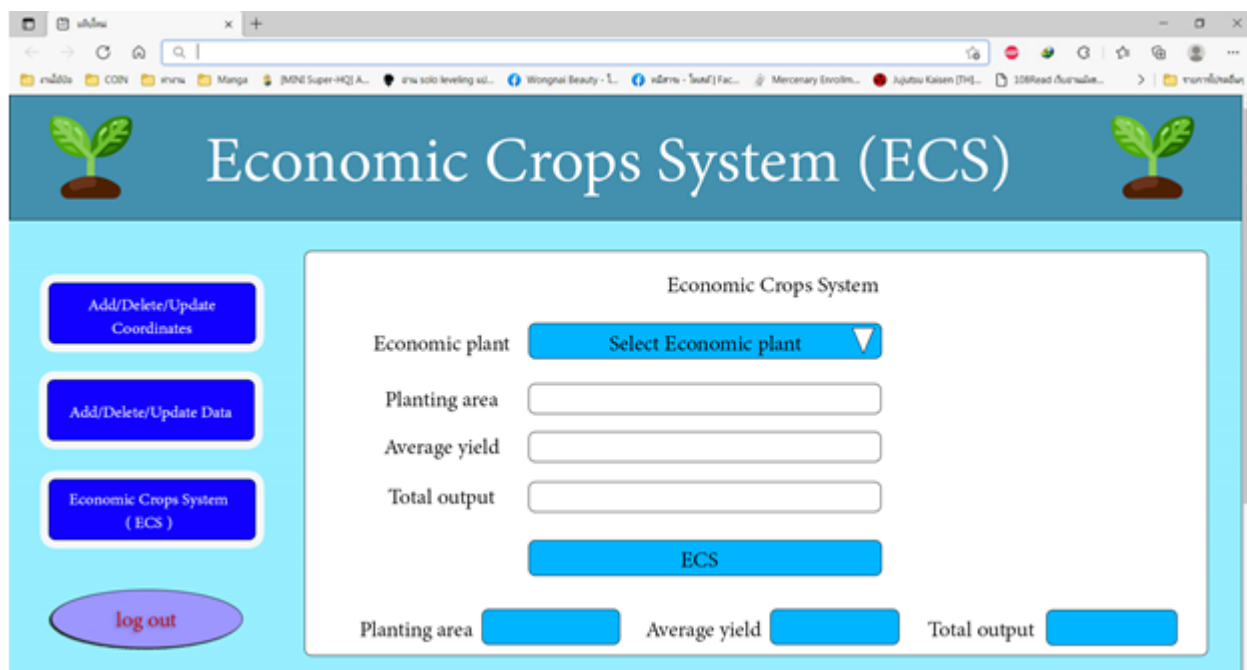


Figure 7. Forecasting web page.

4. CONCLUSION AND DISCUSSION

This research aims to develop a prototype of a system for predicting economic crops using artificial intelligence and GIS in Pua district. Nan province is a case study area for collecting data on economic crops. This system is designed to run primarily on applications, making it easy for users to browse and access information using information. In addition to updating the information through the web page administrator, the information will be stored on the cloud for ease of updating or editing. From the evaluation of the use of users from the system questionnaire in the form of averages in all 3 aspects of system design. The benefits of the system to use and the stability of the system is at a very good level, but if data can be collected in every area with more resolution, it should be expanded and surveyed to collect data at the village level in order to obtain complete information. more knowledge and further benefit to society. WebGIS is the integrated product of GIS and internet technologies; in WebGIS, the internet technologies are connected with GIS in order to take advantage of their special characteristics, such as easy usability, use of the GIS data such as input, adjustment, manipulation, analysis, and output of geographical information and to bring out related service on the internet (Miao & Yuan, 2013).

The system for predicting economic crops using artificial intelligence and GIS uses the area in Pua District. Nan Province is a case study area. There are research results from the assessment. It has been demonstrated to use for 2 groups of users who are personnel in the Phayao Provincial Agriculture Office. and interested individuals who were randomly selected from a total of 40 people assessed 3 aspects of competence from the user group at the satisfaction level. In terms of system design, it was at “very good” ($\bar{X} = 4.05$, $SD = 0.78$). The benefits of the system to use were at “very good” ($\bar{X} = 4.08$, $SD = 0.77$) and the system stability was at “Good” ($\bar{X} = 3.85$, $SD = 0.78$) the overall mean of overall system satisfaction was at “very good” ($\bar{X} = 4.00$, $SD = 0.78$).

The methodology is based on notions on general principles of Web GIS / Mobile GIS and has the potential for application for other economic crops of Thailand.

5. ACKNOWLEDGEMENT

This research is supported by School of Information and Communication Technology (ICT), University of Phayao, Thailand. Spatial thank would like to deliver to the Nan Provincial Agriculture and Cooperatives Office for supporting essential information.

6. REFERENCES

- Buckeridge, D.L., Mason, R., Robertson, A., Frank, J., R. Glazier, R., and Purdon, L., 2002. Making health data maps: a case study of a community/university research collaboration. *Soc. Sci Med.* 55(7): 1189-206
- Choosumrong, S., Raghavan, V., Jeefoo, P., and Vaddadi, N., 2016. Development of Service Oriented Web-GIS Platform for Monitoring and Evaluation using FOSS4G. *International Journal of Geoinformatics*, 12(3), 67-77.
- Gavin, E., 2002. Geo-Information Supports Decision Making in Africa – An EIS-AFRICA position paper. Pretoria, South Africa: EISAFRICA. Retrieved from <http://www.eis-africa.org/DOCS/A5-Engv7.pdf>.
- Jeefoo, P., 2020. A WebGIS Base Information System for Monitoring Wildfire Using Suomi-NPP (VIIRS) Satellite in Phare Province, Thailand. *Naresuan University Journal: Science and Technology (NUJST)*, 28 (2), 62-71.
- Kourgiala, N., and Karatzas, G., 2011. Flood management and a GIS modelling method to assess flood-hazard areas – a case study. *Hydrological Sciences Journal*, 56(2), 212-224.
- Miao, F., and Yuan, Q., 2013. A WebGIS-Based Information System for Monitoring and Warning of Geological Disasters for Lanzhou City, China. *Advances in Meteorology*, 2013, 9. [<http://dx.doi.org/10.1155/2013/769270>]
- Vakalis, D., Sarimveis, H., Kiranoudis, C. T., Alexandridis, A., and Bafas, G., 2004. A GIS based operational system for wildland fire crisis management II. System architecture and case studies. *Applied Mathematical Modelling*, 28(4), 411-425. [<https://doi.org/10.1016/j.apm.2003.10.006>]

GIS APPLICATION FOR UPDATING THE INFORMATION OF WASTE TRANSPORTATION IN LIEN CHIEU DISTRICT, DANANG CITY, VIETNAM

Tran Thi An¹, Le Ngoc Hanh² and Truong Van Canh²

¹Faculty of Management Science, Thu Dau Mot University, Vietnam
 06 Tran Van On Street, Phu Hoa Ward, Thu Dau Mot City, Binh Duong Province, Vietnam
 Email: tranthian.gis@gmail.com

²Faculty of Geography, University of Science and Education, The University of Danang, Vietnam
 459 Ton Duc Thang Street, Danang City, Vietnam
 Email: lhanh@ued.udn.vn, tvcanh@ued.udn.vn

ABSTRACT

Geographical Information System (GIS) has been widely used in many applications especially in geospatial data management. The main objective of this research is building a GIS database related to the municipal waste transportation in Lien Chieu District, Danang City, Vietnam. This GIS database includes the information about the traffic system and solid waste collection in Lien Chieu District was built based on the field surveys integrating with other referenced data sources such as OpenStreetMap (OSM) and data from local authority. These data were processed in a GIS environment to prepare for waste transported optimization through Network Analyst method in ArcGIS software. The optimal waste transportation route proposed from this study can save the travel time and distance compared to the current route. Especially for the forklift trucks, the waste transported time is reduced by nearly 40 minutes, traveling distance is reduced by about 14 kilometres and the number of transportation trips is also saver compared to the current route. This improvement will increase the efficiency of the waste collection process and reduce the environmental pollution in Lien Chieu District. Results from this study can be widely applied for solid waste management in other metropolitan areas where suffering high pressure of population as well as municipal waste growth.

Keywords: GIS database, network analyst, municipal waste, waste transportation, route optimization.

1. INTRODUCTION

Municipal solid waste (MSW) is one of the top concerns in many countries around the world. The problem of timely collecting and transporting solid waste from different sources to the collection centers in response to environmental pollution and urban beauty is an urgent need of many cities. A shortest waste collection and transportation strategy can effectively reduce waste collection and transportation cost (Swapan and Bidyut, 2015). This research aims to generate the GIS database related to the municipal waste transportation in Lien Chieu District which is currently a developing urbanized district in Danang City, Vietnam. It is observed that the amount of domestic waste is increasing along with the urban expansion and population growth (World Bank, 2018). Currently, Lien Chieu District is suffering about 160 tons of household waste per day and this amount of waste is forecasted about 280 tons per day by 2030 (Danang Urban Environment Company). In order to enhance the environmental situation as well as the urban beauty, the rapid movement of garbage from gathering points to the landfill sites while ensuring the efficiency of collection and transportation is a problem that needs to be studied and resolved. GIS combined with other analytical methods can be widely used in the waste management (Amirhossein *et al.*, 2013; Yadav Sk., 2013; Amjad *et al.*, 2016)

as well as optimization of waste transportation routes.

This study was conducted with the goal of building a GIS database for the purpose of optimization of the household waste transportation route in Lien Chieu District, Danang City, Vietnam. The traffic data including information about the route systems and their attributes were collected and standardized using the OpenStreetMap (OSM) application. Information about solid waste collection in Lien Chieu District was built based on the field surveys integrating with other referenced data sources. These data were processed in a GIS environment to prepare for waste transported optimization through Network Analyst method in ArcGIS software. The optimal waste transportation route proposed from this study can save the travel time and distance compared to the current route. Especially for the forklift trucks, the waste transported time is reduced by nearly 40 minutes, traveling distance is reduced by about 14 kilometers and the number of transportation trips is also saver compared to the current route. This improvement will increase the efficiency of the waste collection process and reduce environmental pollution.

2. METHODOLOGY

2.1 Study Area

The study area is Lien Chieu District which is a dynamic urban developing area of Danang City, Vietnam (Figure 1). This study area is also a hotspot of industrial as well as residential development. In accompany with the development process, the Lien Chieu District is also facing to a relatively large amount of solid waste. Regarding the waste transportation methods, there are two main methods in Lien Chieu District using forklift and compactor trucks in which transportation by forklift obtained 75 percent of the total collected waste volume of the study area. The authors had conducted tracking surveys of waste collection and transportation by using video camera recordings and GPS loggers, and collected the data on coordinates, transport locations (right of the road, left of the road or both sides of the road), transportation time, estimated waste volume, etc. These data are important sources for generating the solid waste GIS database and optimization of the waste transportation route for Lien Chieu District. This study focuses on building the optimal waste transportation route for forklift trucks which is the main vehicle using for waste collection in Lien Chieu District.

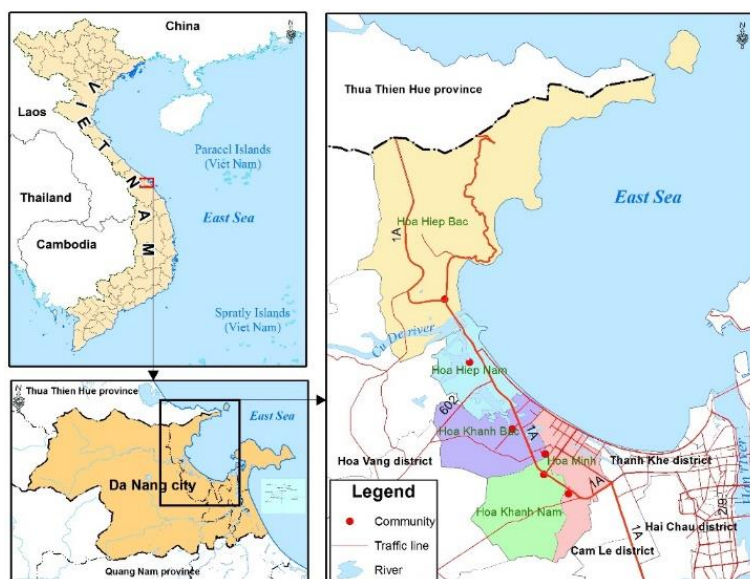


Figure 1. Overview of study Area.

2.2 Generation of GIS database

The OpenStreetMap data (Openstreetmap.org) which is a free and dynamic geospatial database was used to generate the traffic system map for Lien Chieu District, Da Nang City. Data collected on OSM is presented in vector which are in different formats (point, line, area) representing almost all spatial information about the real world. After collecting the road data from OSM, the study tried to extract the necessary traffic GIS data related to the construction of the waste transportation route such as roads, stops, obstacles, barriers, ... including both spatial and attribute information.

In addition, the traffic data collected from the local agencies was also utilized for validation of the road system. In this study, we extract data related to traffic of Danang City from the Department of Natural Resources and Environment, Department of Transport, etc. Subsequently, the filed survey data was also investigated as a supplement traffic data for OpenStreetMap (OSM). The road data on OSM sometimes lacks information such as road name, road type, traffic signs, etc. Therefore, updating the OSM data using field survey data is an effective solution to prepare the completed road system for the determination of the waste transportation route.

The data related to waste transportation includes the information on household waste, transportation vehicles and landfill sites. A field survey was conducted in the period from March 2020 to October 2020 in Lien Chieu area for the purpose of generation of GIS database related to solid waste transportation. In order to generate the data on waste gathering points, we have tracked the information on the location and volume of garbage as well as the collected time at each point in the Lien Chieu District with the help of video camera and GPS logger. The data on waste transportation means including the information on the type of vehicles, load capacity and operating time were also investigated in this field work.

2.3 Research workflow

The research workflow for generation of GIS database and optimization of waste transportation route for Lien Chieu District, Danang City is shown in Figure 2. The data on household waste and traffic system after being collected were standardized in both spatial and attribute information. In order to validate the spatial road data, the Topology tool in ArcGIS was used to identify the geometrical errors. Regarding the attribute data, the missing information on OSM data has been updated by using the supplemented data such as data collected from local authorities or field surveyed data. Subsequently, an application namely Network Analysis, was executed in GIS environment to generate the map of the optimal waste transportation routes in Lien Chieu District.

ESRI's ArcGIS Network Analyst extension allows users to perform complex calculations to solve the vehicle routing problems. The program performs analysis over a network of connected edges and decides fleet routing, travel directions, closest facility, service area, and location allocation (O'Connor, 2013). In addition, the Network Analyst allows the user to dynamically model genuine network situations, and hence facilitates finding the optimal route that is very important in solid waste transportation. Network Analysis is actually a tool to support fast and effective decision making for spatial analysis problems based on network systems such as: analyzing the shortest route, the optimal access, service delivery area, determining the nearest service facility, ... Network Analyst allows simulation of complex real-world network models with limited conditions such as one-way roads, forbidden roads, limits speed, time, vehicle limits, obstacles, ... In addition, the study also compares the proposed route with the current waste transportation one in the Lien Chieu area in order to evaluate the cost efficiency.

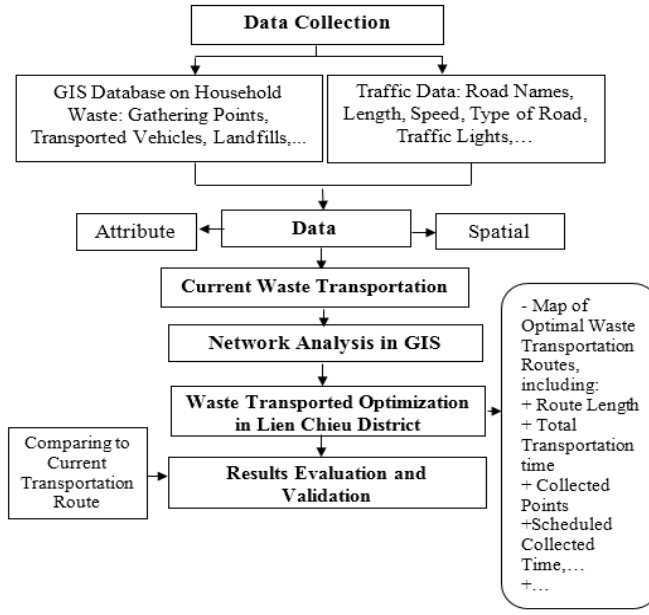


Figure 2. Study Workflow on Generation of GIS Database for Waste Transportation in Lien Chieu District

3. RESULTS AND DISCUSSIONS

3.1 GIS database for waste transportation in Lien Chieu

The traffic data is generated from OSM data combining with other supplemented data and transformed to the GIS format. The GIS database about traffic system in Lien Chieu District including both spatial and attribute dimensions has reflected adequately information for waste transportation in the study area. Based on the information about length and speed, the study calculated the travel time for each different road segment. In addition, traffic light data was also investigated in this study. The road system downloaded from OSM usually does not include all traffic light locations in the Lien Chieu area. In this case, the field survey data has been used to update information about these barriers of the waste trucks for the study area. In addition, the time for passing the traffic light was also modified in order to meet the requirement for Network Analysis.

Garbage data includes information about gathering points such as: the system of gathering locations, information of garbage trucks, landfill sites collected by field method. We have conducted a field survey to get information related to the waste collection such as order of points, type of bin, number of dustbins, estimated waste volume, collected time in the day, collected days of the week; transported location (on the right, left or both sides of the road), time to take garbage into the vehicle ... In addition, we also investigate the information of waste trucks in this area such as: vehicle, loading capacity, transported time of the day, ...Figure 3 shows the GIS database for determination of waste transportation route in Lien Chieu District that was generated from this study.

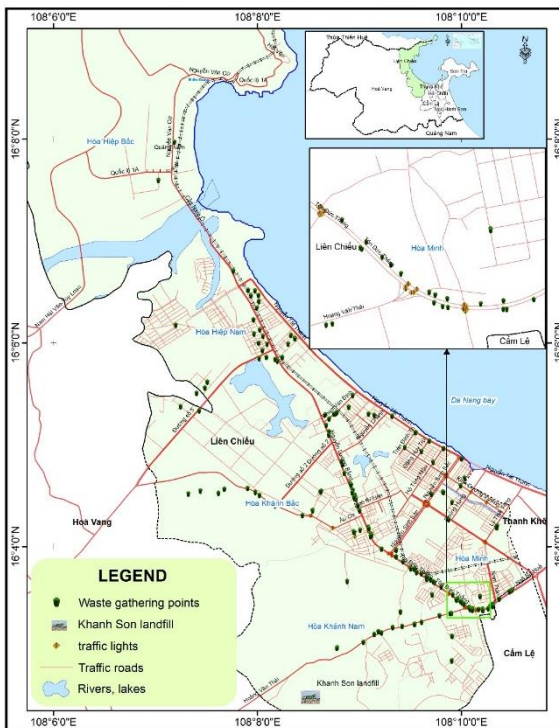


Figure 3. GIS database for building the waste transportation route in Lien Chieu District – Da Nang City

3.2 Generation of waste transportation map for forklift trucks in Lien Chieu District

3.2.1 Setting the parameter for Network Analysis

In this study, the waste transportation route was generated using the Network Analyst which is an extension in ArcGIS software that provides network-based spatial analysis including routing, travel directions, closest facility and service area analysis (Amirhossein *et al.*, 2013). There have been several studies on application of Network Analysis in waste transportation optimization (Amirhossein *et al.*, 2013; Apaydin and Gonullu, 2007; Phatsasi and Kampanart, 2018), however the results are still limited due to the parameter setting problem. This study experiences the method of using Network Analysis in generation of waste transportation route in Lien Chieu District, and proposed the optimal waste collection route.

The parameters for Network Analyst application in ArcGIS software includes the following key information: Orders (information about gathering points), Depots (information about the vehicle characteristics), Routes (information about transportation routes), Break (information about break time if any), Route Zones (information about the transporting area), Specialties (information about special points on the transportation route), Barriers (information about obstacles on the road including points, lines or polygons), etc.

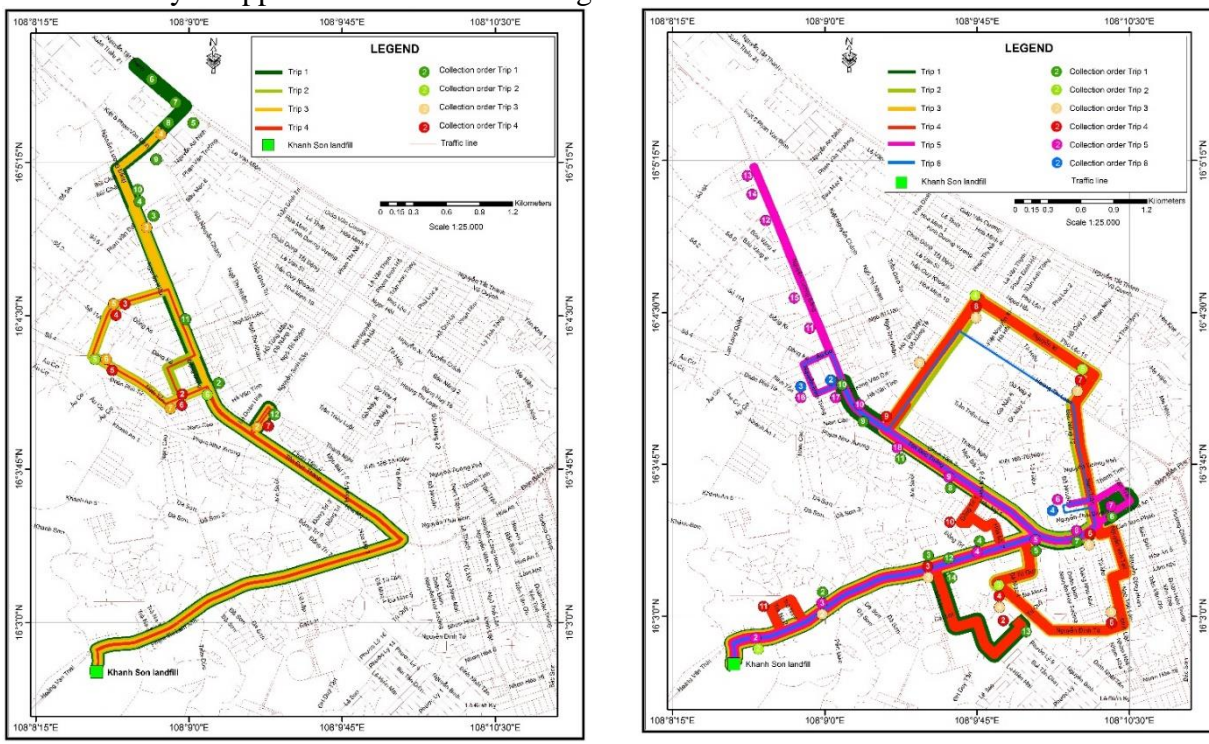
The data about garbage gathering points (Orders) has the following main information requirements: the consuming time when transporting garbage on the vehicle, the time of waste collection in the day, the waste volume at each point and garbage is taken from the right or left of the road, or both sides of the road, ...The data of the vehicle characteristics (Depots) includes the following main information: start and end locations of the waste trucks on the route; start time, end time; driving rules (left, right or can run on both sides), ...Subsequently, the Routes data includes the following information: route name; starting point, ending point; the earliest start time and the latest one; load capacity; maximum number of stops; transportation time, etc.

As a result, we have built a completed GIS database of garbage transportation. This is

the important input data source for establishing the network analysis in GIS to determine the optimal waste transportation route in Lien Chieu District - Da Nang city. This study has focused on optimization of the waste transportation route for the forklift trucks which are the major collection means in Lien Chieu District.

3.2.2 Current waste transportation map for forklift trucks in Lien Chieu District

In Lien Chieu District, there are currently two transportation routes of forklifts denoted Lien Chieu A (LCA) and Lien Chieu B (LCB). In this study, we use the network analysis in GIS to reconstruct the waste transportation route for the forklift trucks based on investigating the route-related information such as: gathering location, waste volume, transportation time, ... The waste transportation route includes the following major information: trip order, starting time, ending time, place, order of transportation, amount of garbage, distance, etc. Results of generation the current waste transportation map for forklifts in Lien Chieu District using the Network Analysis application are shown in Figure 4.



(a) Lien Chieu A forklift truck (LCA)

(b) Lien Chieu B forklift truck (LCB)

Figure 4. Current waste transport route map of Lien Chieu District, Danang City

3.2.3. Optimization of the waste transportation route for forklifts

The current waste transportation routes of Lien Chieu A and Lien Chieu B forklifts basically meet the needs of garbage transportation in the District. In this study, optimization of the current waste transportation route is the process of finding the optimal routes in case of the total waste collection volume of the forklift is not changed. In order to generate a better waste transportation route, we have adjusted the parameters on Network Analyst such as: transportation route, the amount of waste that can be collected at gathering points, Order of garbage transportation.

In this study, we tried to optimize the current waste transportation route based on the assumption that all the forklifts can load the maximum waste volume. In this case, we combined

the data of the LC A and LCB routes and break down the waste at gathering locations into smaller locations. The purpose is to increase the vehicle's loading capacity up to maximum volume. The results of optimal waste transportation for forklift trucks in response to the current waste volume of Lien Chieu District are represented in Figure 5 and Table 1.

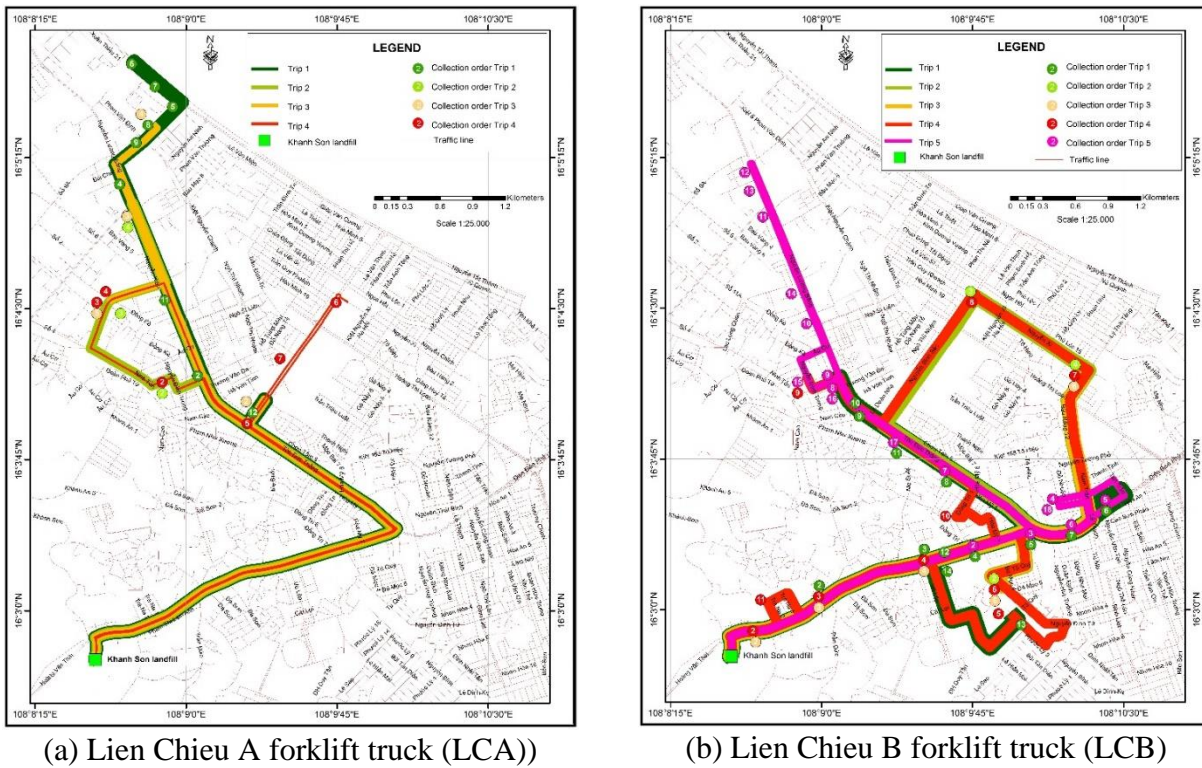


Figure 5. Optimal waste transportation route map of Lien Chieu District, Danang City

Table 1. Information on the optimal waste transportation of forklifts in Lien Chieu District, Danang City

Trip name	Total time (hours)	Starting time	End time	Distance (km)	The volume of garbage (tons)
LCA_1	1.65	6:00	7:39	18.3	11.0
LCA_2	1.28	9:00	10:16	15.6	11.0
LCA_3	1.28	11:00 am	12:16	17.4	11.0
LCA_4	1.42	13:30	14:54	17.2	10.1
Total LCA	5.62			68.5	43.1
LCB_1	2.05	6:00	8:03	16.5	11.0
LCB_2	1.23	9:00	10:14	14.3	10.6
LCB_3	1.28	11:00 am	12:17	11.9	9.7
LCB_4	1.57	13:30	15:03	18.8	11.0
LCB_5	2.32	18:00	20:19	20.4	11.0
Total LCB	8.45			81.8	53.4
Optimal route	14.07			150.4	96.5

It is obvious to see from Table 3 that the optimal waste transportation route can reduce the travel time and distance compared to the current route. Specifically, waste transportation time

is reduced by nearly 40 minutes, traveling distance is reduced by about 14 km and the number of trips is also saver with 1 trip smaller than the current route. This will increase the efficiency of the waste collection process and reduce the environmental pollution due to the saving of distance and travel transportation time.

4. CONCLUSIONS

MSW management is always a difficult problem of any urban area. This study has proposed an optimal waste transportation for forklift trucks in Lien Chieu District, Danang City that can bring the efficiency in time and travel distance. From the results of building and evaluating the efficiency of waste transportation routes using GIS in Lien Chieu District - Da Nang City, it can be concluded that integrating of GIS with the Network Analyst tool brings the high efficiency and quick results. Results from this study can help us to come up with the most reasonable waste transportation option according to the required conditions and the available database source.

5. REFERENCES

- Amirhossein M., Putri Md B., Munirah R. Md M., Noordiana K. (2013) Solid waste collection routes optimization via GIS techniques in Ipoh city, Malaysia. Fourth International Symposium on Infrastructure Engineering in Developing Countries; Malaysia.
- Amjad K., Mohamed M. S. and Moncef Z. (2016) Using GIS-Based Tools for the Optimization of Solid Waste Collection and Transport: Case Study of Sfax City, Tunisia. Journal of Engineering. Hindawi Publishing Corporation, Volume, Article ID 4596849, doi.org/10.1155/2016/4596849.
- Apaydin O. and Gonullu M. T. (2007) Route Optimization for Solid Waste Collection: Trabzon (Turkey) Case Study. Global NEST Journal, 9(1): 6-11.
- O'Connor, D. L. (2013) Solid Waste Collection Vehicle Route Optimization for the City of Redlands, California (Master's thesis, University of Redlands). Retrieved from https://inspire.redlands.edu/gis_gradproj/201.
- Phatsasi P. and Kampanart P. (2018) Application of GIS for analysis current waste collection routes and find potentiality routes of Thapho sub-District, Mueang Phitsanulok District, Phitsanulok Province. The International Conference on GeoInformatics for Spatial-Infrastructure Development in Earth & Allied Sciences (GIS-IDEAS); Can Tho, Vietnam.
- Yadav Sk. (2013) GIS Based approach for site selection in waste management. International Journal of Environmental Engineering and Management; 4: 507-514.
- Swapan Das, Bidyut Kr. Bhattacharyya (2015) Optimization of municipal solid waste collection and transportation routes, Waste Management, Volume 43, September 2015, Pages 9-18
- The World Bank (2018) Solid and Industrial hazardous waste management assessment: options and action areas, World Bank Publications, 156 pages.

Geo-Informatics evaluation of characteristics and amounts of microplastics contaminated in water surface level: Case of Songkhla Lake, THAILAND

**Supat Ponza*, Supattra Phaya, Pathipat Sanpapao, Pattareeya Ponza
and Chaiiwat Vansarochana**

Department of Agricultural science, Faculty of Agriculture Natural Resources and Environments, Naresuan University 65000, Thailand

*Corresponding author Email: supatp@nu.ac.th

ABSTRACT

Plastic waste causing significant problems to the aquatic ecosystems, especially plastic scraps smaller than 5 millimeters that are formed by breaking or decomposing of large plastic waste, which called microplastics, which affect more toxic to aquatic organisms. Microplastics might come from different waste sources such as agriculture, aquaculture, domestic wastewater etc. Songkhla Lake Basin has been diversely utilized, either land use types or diverse ecosystems, which stand for cause and effect of microplastics contaminated in Songkhla lake. This study aimed to identify the characteristics and amounts of microplastics at water surface level in Songkhla lake and use Geo-Informatics techniques to evaluation. Water samples were collected from 17 stations located around Songkhla lake at the surface level once in June 2020. The average amount of microplastics at the water surface level in Songkhla lake was 6.0 ± 3.6 pcs/L. Thale Noi area was higher contaminated level with 15.0 ± 11.5 pcs/L, and lower contaminated level at the middle lake of Thale Luang area with 0.6 ± 1.0 pcs/L. The major area of Songkhla lake ($506,029$ Km 2) was contaminated with microplastics about 4.7-6.8 pcs/L. Whereas the highest contamination level (12.9 - 15.0 pcs/L) was covered only about $5,591$ Km 2 in Thale Noi area. Fiber shape and black color particle were the most common characteristic of microplastic found in Songkhla lake.

Keywords: Microplastics, Songkhla lake, Water surface level, Geo-Informatics techniques.

1. INTRODUCTION

Plastic waste causing significant problems to the aquatic ecosystems, especially plastic scraps smaller than 5 millimeters that are formed by breaking or decomposing of large plastic waste (Browne *et al.*, 2007; Thompson *et al.*, 2004), which called microplastics, makes it easier for intake and toxic to aquatic organisms (Hall *et al.*, 2015; Teuten *et al.*, 2007). Microplastics may come from different waste sources such as agriculture, aquaculture, domestic wastewater etc. Songkhla Lake Basin is the only watershed in Thailand that has a lagoon system (Office of Natural Resources and Environmental Policy and Planning, 2014) which is diverse ecosystems consisting of freshwater lake (Thale Noi) at the upper north area, brackish water lake (Thale Luang) at the middle area and saltwater lake (Thale Sab Songkhla) at the lower south area. Therefore, majority land use in this area is diversified i.e., paddy field and moderate communities in the upper north area, paddy field and few communities in the middle area, paddy field and dense communities in the lower south area. This diversity of activities might cause microplastics contamination affecting the characteristics and amount of microplastics contaminated in Songkhla lake. To be able to effectively manage the problem of microplastic contamination in the Songkhla Lake, this study was therefore conducted to identify the characteristics and amounts of microplastics at water surface level in Songkhla lake.

2. METHODOLOGY

Water samples were collected from 17 stations located around Songkhla lake (Figure 1 and Table 1) at the surface level once in June 2020. Collected water samples were digested by Wet Peroxide Oxidation method (NOAA Marine Debris Program, 2015) then filled through GFC filter paper and oven dried at 30-60°C, after that microplastics remained were classified and counted under stereo microscope. The contamination level of microplastics were then evaluated through Inverse Distance Weighted (IDW) interpolation techniques (Burrough, 1986).

3. RESULTS

The average amount of microplastics at the water surface level in Songkhla lake was 6.0 ± 3.6 pcs/L. Data was indicated in Table 1 showing that Thale Noi was the most contaminated area (11.6 ± 4.7 pcs/L), which the highest contaminated level of 15.0 ± 11.5 pcs/L was found at Khlong Yuan Station (SK8). Thale Luang was lower contaminated area (4.7 ± 2.8 to 5.0 ± 2.7 pcs/L), where Khlong Ruea station (SK15) in the middle lake area was lowest contaminated level of 0.6 ± 1.0 pcs/L.

Table 1. Microplastics contaminated in water surface level of Songkhla Lake.

Lake Area	Sampling Station	Code	GPS Coordinates*	Amount of Microplastic (pcs/L)**
Thale Noi	Khlong Yuan	SK8	47N 0624920-858806	15.0 ± 11.5
	Khlong Kwai Klang	SK9	47N 0623800-861619	8.3 ± 5.6
			Average Amounts	11.6 ± 4.7
Thale Luang:				
Upper Lake	Khlong Hone	SK5	47N 0645062-839823	4.3 ± 0.5
	Khlong Rong	SK6	47N 0645451-850382	9.3 ± 7.0
	Khlong Chiang Phong	SK7	47N 0643968-857088	5.7 ± 1.9
	Klong Pak Pra	SK10	47N 0626445-854135	3.0 ± 3.0
	Khlong Lampam	SK11	47N 0627412-842570	2.7 ± 2.8
			Average Amounts	5.0 ± 2.7
Middle Lake	Khlong Sanamchai	SK4	47N 0654218-834772	3.3 ± 0.8
	Khlong Tha Maduea	SK12	47N 0632622-828961	6.3 ± 5.5
	Khlong Mha Khobdang	SK13	47N 0635203-825559	7.9 ± 0.8
	Pak Payoon	SK14	47N 0645922-814644	5.1 ± 4.6
	Khlong Ruea	SK15	47N 0648097-824737	0.6 ± 1.0
			Average Amounts	4.7 ± 2.8
Thale Sab Songkhla	Koh Yor	SK1	47N 0668935-790331	3.1 ± 2.0
	Khlong Sathing Mor	SK2	47N 0668222-798774	10.2 ± 6.4
	Khlong Pak Ror	SK3	47N 0658994-801858	9.8 ± 8.8
	Khlong Phumi	SK16	47N 0656522-794402	2.7 ± 1.0
	Khlong U-Tapao	SK17	47N 0661819-790412	5.0 ± 0.6
			Average Amounts	6.2 ± 3.6
Average Amounts of Songkhla Lake				6.0 ± 3.6

* UTM-a

** Mean \pm SD

The result from Inverse Distance Weighted (IDW) interpolation was showed in Figure 1. The major water surface area of Songkhla lake ($506,029 \text{ Km}^2$) was contaminated with microplastics about 4.7-6.8 pcs/L followed by contamination levels of 2.7-4.7, 6.8-8.8, 0.6-2.7, 8.8-10.9 and 10.9-12.9 pcs/L which covered about 264,183, 155,235, 41,152, 31,552 and 5,109 Km^2 respectively. The highest contamination level (12.9-15.0 pcs/L) covered only 5,591 Km^2 in Thale Noi area.

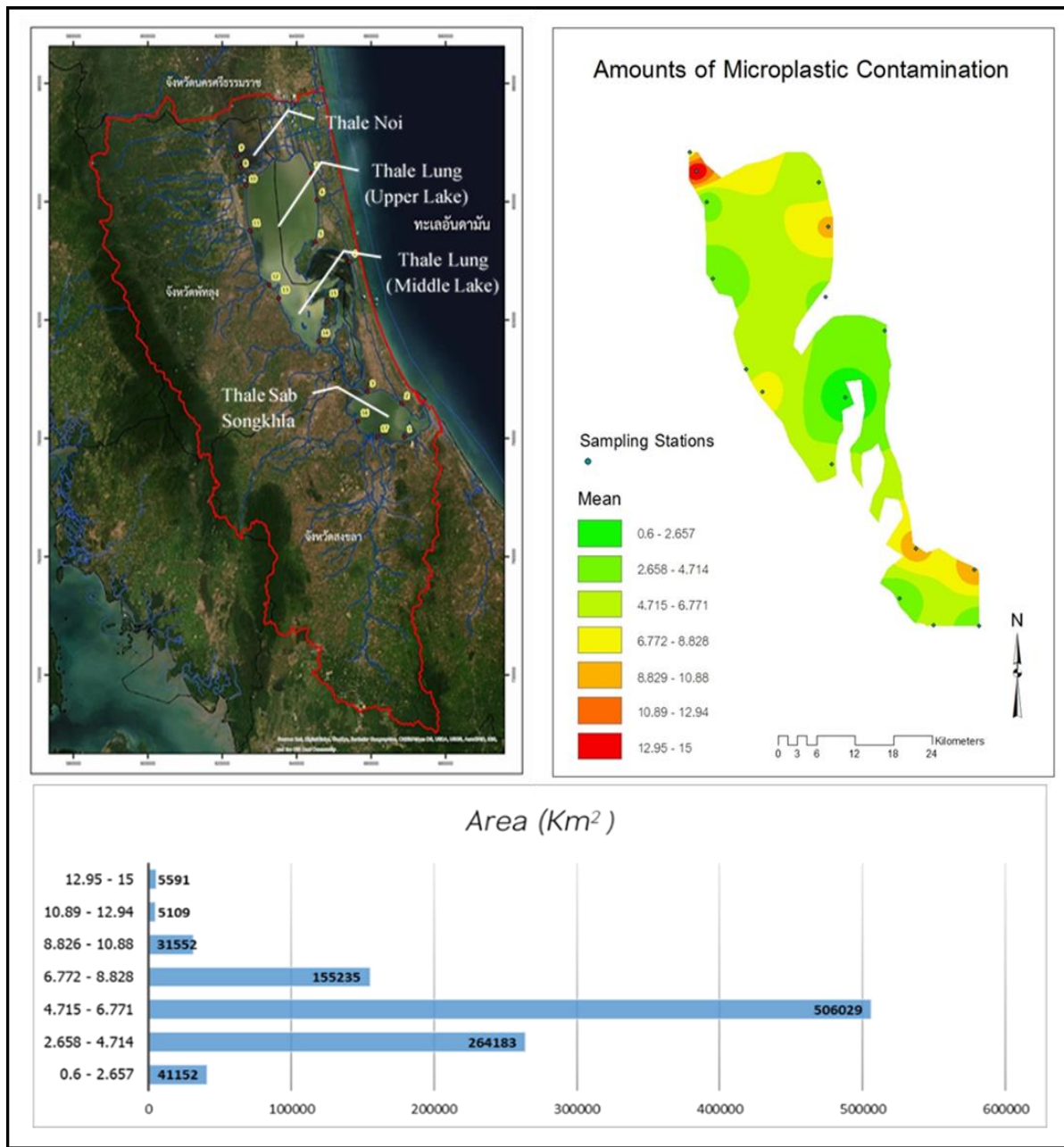
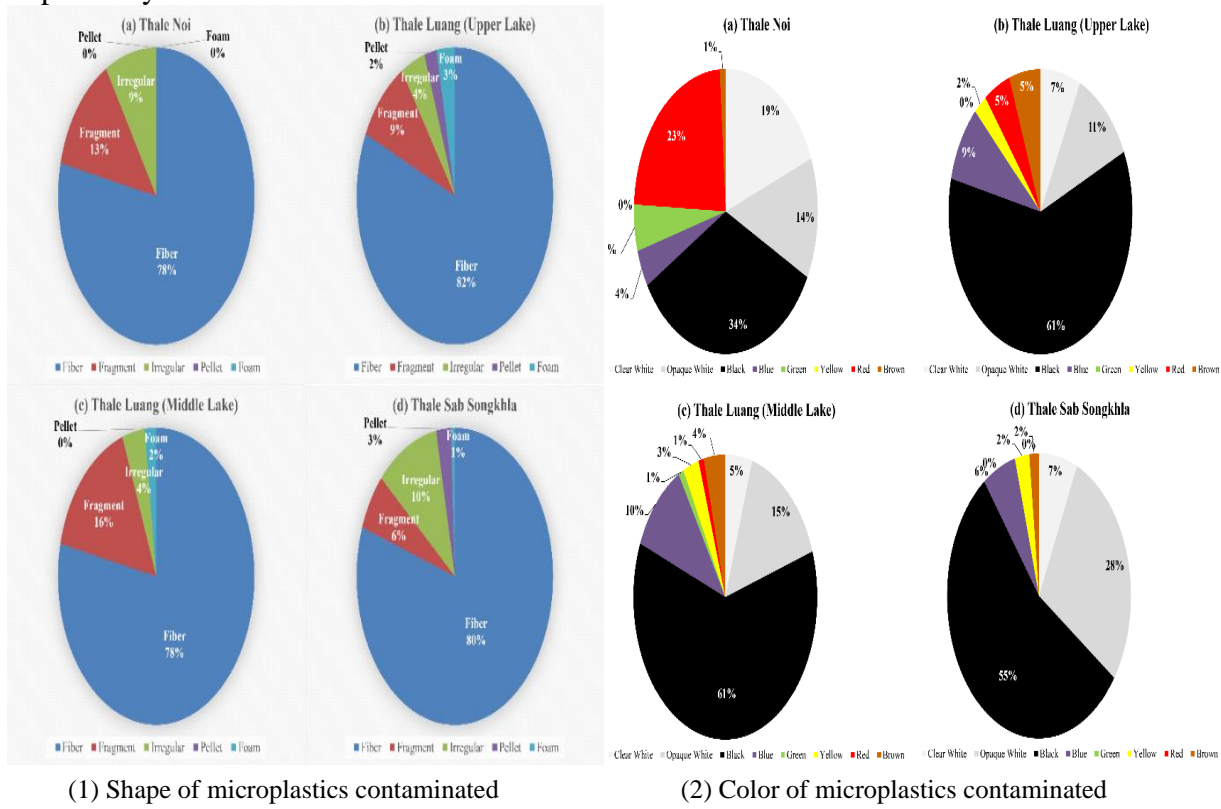


Figure 1. Contamination levels of microplastics in water surface level of Songkhla Lake.

As showed in Figure 2 (1), fiber shape was the most common characteristics of microplastic found in Songkhla lake (78%-82%). The highest amount of the fiber shape microplastic was found in upper lake of Thale Luang area, followed by fragment (6%-16%), irregular (4%-10%), foam (0%-3%) and pellet (0%-3%) respectively. Whereas the color of microplastics contaminated was showed in Figure 2 (2), Black color was the most common

characteristic of microplastic found in Songkhla lake (34%-61%), which highest in upper and middle lake of Thale Luang area, followed by opaque white (11%-28%), red (0%-23%), clear white (5%-19%), blue (4%-10%), brown (1%-5%), green (0%-5%) and yellow (0%-3%) respectively.



(1) Shape of microplastics contaminated

(2) Color of microplastics contaminated

Figure 2. Characteristics of microplastics contaminated in water surface level.

4. DISCUSSION AND CONCLUSION

The average amounts of microplastics found at the water surface level in Songkhla lake was similar to the other water reservoirs located in urban area. The major source of contamination along and surrounding lake area was human activities as indicated in Lake Geneva, Switzerland (Faure *et al.*, 2012) and Three Gorges Reservoir, China (Di and Wang, 2018). The microplastic materials found in this study consisted of polystyrene, polypropylene, and polyethylene. However, where the main contaminated sources in Thale Sab Songkhla were municipal wastewater, industrial plant, farming, and ranch indicating high contamination level since these point sources contained dense of both primary and secondary microplastics (Su *et al.*, 2016). In addition, various watershed development projects, especially the closure of the route linking the Gulf of Thailand to prevent saltwater invading to Songkhla Lake (Office of Natural Resources and Environmental Policy and Planning, 2014).

As compared to the other lake area, Thale Noi which the smallest water reservoir in Songkhla lake, was the highest contaminated area. These might cause by the morphology of the reservoir since Thale Noi had shallow water depth and dense of aquatic plants distributing along the shoreline. Moreover, most of domestic wastewater without any treatment processes was directly discharged into Thale Noi with only two small outlet canals connect to Thale Lung area would make this reservoir as the basin of microplastics. The contamination level would rapidly increase as occurred in the Dutch river delta and Amsterdam canals which contained more than 40 pcs/L (Leslie *et al.*, 2017), makes it more toxic to aquatic organisms (Hall *et al.*,

2015; Teuten *et al.*, 2007) in case of no actions to prevent and reduce growth of aquatic plant, and remove the organic rich sediment. The evidence from previous study in running and deep water showed lower microplastic contamination level (Lechner *et al.*, 2014). This indicated that water dept and flow could lower the contaminated load of microplastics.

In freshwater studies to date, microplastic particle counts ranged from around 0 to 1000 particles/L. Thus, contamination levels in water surface level of Songkha lake were in the average ranged. Most of Songkla lake water surface area of 998,151 Km² contained less than 10.0 pcs/L microplastic particle. The rest of 10,700 Km² water surface area contained more than 10.0 pcs/L microplastic particle. The contaminated level reported in this study could not directly compare to the other studies i.e., Laurentian Great Lakes, USA (Eriksen *et al.*, 2013), Hovsgol Lake, Mongolia (Free *et al.*, 2014), urban surface waters of Wuhan, China (Wang *et al.*, 2017), and Lake Winnipeg, Canada (Anderson *et al.*, 2017). However, this might be the prospective point of view for Local Administrative office which located along and surrounding Songkhla lake area to create microplastics management plans to avoid the same problems occurred in other water reservoir. In particular, the toxic of chemical adhesive on microplastics such as heavy metals such as iron (Fe), manganese (Mn), aluminium (Al), lead (Pb), copper (Cu), silver (Ag), zinc (Zn) and hydrophobic organic contaminants (HOCs) such as polyaromatic hydrocarbons (PAHs), organochlorine pesticides (OCPs) and polychlorinated biphenyls (PCBs) could be bioaccumulated through trophic levels (Verla *et al.*, 2019).

The shape of microplastics found tended to similar in each area of Songkhla lake, with fiber type being the most common microplastics shape. The types of fibers found might came from human activities included clothing scraps, fishing gears and aquaculture facilities mainly made up of fibers or ropes such as gill nets, cast nets, traps, cages, ropes, etc. Whereas the fragment and irregular shape might cause by large plastic dumping waste such as plastic bottles, plastic bags, bottle caps waste, etc. that breaks into a small plastic then floats along the canals finally sink into the lake (Mason *et al.*, 2016; Talvitie *et al.*, 2015). The most common colors of microplastics found in the Songkhla Lake area were black, blue, and opaque white respectively. These related to the colors of plastic waste from human activities i.e., clothing scraps, fishing gears, and aquaculture facilities. Particularly, the black-blue-colored waste from plastics commonly used to made ropes, such as nylon or fiber.

It could be concluded that Thale Noi area has the highest amount of microplastics contaminated in water surface level (11.6 ± 4.7 pcs/L) because it received wastewater from many sources, mainly domestic wastewater, farming, and ranch. The most common characteristics of microplastics found were fiber shape, especially in upper lake of Thale Luang area (82%). The found fibers were probably from pieces of clothing scraps, fishing gears, and aquaculture facilities, whereas black was the most common microplastic color found, particularly in Thale Luang area (61%).

5. REFERENCES

- Anderson, P.J., Warrack, S., Langen, V., Challis, J.K., Hanson, M.L., and Rennie, M.D., 2017. Microplastic contamination in Lake Winnipeg, Canada. *Environmental Pollution* 255, 223-231.
- Browne, M.A., Galloway, T., and Thompson, R., 2007. Microplastic—an emerging contaminant of potential concern. *Integrated Environmental Assessment and Management* 3(4), 559-561.
- Burrough, P.A., 1986. *Principles of Geographical Information Systems for Land Resources Assessment*, Oxford University Press, Oxford.
- Di, M., and Wang, J., 2018. Microplastics in surface waters and sediments of the Three Gorges Reservoir, China. *Science of the Total Environment* 616-617, 1620-1627.

- Eriksen, M., Mason, S., Wilson, S., Box, C., Zellers, A., Edwards, W., Farley, H., and Amato, S., 2013. Microplastic pollution in the surface waters of the Laurentian Great Lakes. *Marine Pollution Bulletin* 77, 177-182.
- Faure, F., Corbaz, M., Baecher, H., and de Alencastro, L.F., 2012. Pollution due to plastics and microplastics in Lake Geneva and in the Mediterranean Sea. *Archives Des Sciences* 65, 157-164.
- Free, C.M., Jensen, O.P., Mason, S.A., Eriksen, M., Williamson, N.J., and Boldgiv, B., 2014. High-levels of microplastic pollution in a large, remote, mountain lake. *Marine Pollution Bulletin* 85 (1), 156-163.
- Hall, N.M., Berry, K.L.E., and Rintoul, L., 2015. Microplastic ingestion by scleractinian corals. *Marine Biology* 162, 725-732.
- Lechner, A., Kechkeis, H., Lumesberger-Loisl, F., Zens, B., Krusch, R., Tritthart, M., and Schludermann, E., 2014. The Danuber so colourful: A potpourri of plastic litter outnumbers fish larvae in Europe's second largest river. *Environmental Pollution* 188, 177-181.
- Leslie, H.A., Brandsma, S.H., van Velzen, M.J.M., and Vethaak, A.D., 2017. Microplastics en route: Field measurements in the Dutch river delta and Amsterdam canals, wastewater treatment plants, North Sea sediments and biota. *Environment International* 101, 133-142.
- Mason, S. A., Garneau, D., Sutton, R., Chu, Y., Ehmann, K., Barnes, J., and Rogers, D. L., 2016. Micropalstic pollution is widely detected in US municipal wastewater treatment plant effluent. *Environment Pollution* 218, 1045-1054.
- NOAA Marine Debris Program, 2015. Laboratory Methods for the Analysis of Microplastics in the Marine Environment: Recommendations for quantifying synthetic particles in waters and sediments, *National Oceanic and Atmospheric Administration U.S. Department of Commerce Technical Memorandum NOS-OR&R-48*.
- Office of Natural Resources and Environmental Policy and Planning, 2014. *Sustainable Development of Songkhla Lake Basin Project*, Final Report, Bangkok.
- Su, L., Xue, Y., Li, L., Yang, D., Kolandhasamy, P., Li, D., and Shi, H., 2016. Microplastics in Taihu Lake, China. *Environmental Pollution* 216, 711–719.
- Talvitie, J., Heinonen, M., Pääkkönen, J. P., Vahtera, E., Mikola, A., Setälä, O., and Vahala, R., 2015. Do wastewater treatment plants act as a potential point source of microplastics? Preliminary study in the coastal Gulf of Finland, Baltic Sea. *Water Science and Technology* 72(9), 1495–1504.
- Teuten, E.L., Rowland, S.J., Galloway, T.S., and Thompson, R.C., 2007. Potential for plastics to transport hydrophobic contaminants. *Environmental Science and Technology* 41(22), 7759-7764.
- Thompson, R.C., Olsen, Y., Mitchell, R.P., Davis, A., Rowland, S.J., John, A.W.G., McGonigle, D., and Russell, A.E., 2004. Lost at sea: where is all the plastic. *Science* 304, 838.
- Verla, A.W., Enyoh, C.E., Verla, E.N., and Nwarnorh K.O., 2019. Microplastic-toxic chemical interaction: a review study on quantified levels, mechanism and implication. *SN Applied Sciences* 1, 1400.

- Wang, W., Ndungu, A.W., Li, Z., and Wang, J., 2017. Microplastics pollution in inland freshwaters of China: A case study in urban surface waters of Wuhan, China. *Science of the Total Environment* 575, 1369–1374.

Historical changes and variants of community level place names in the northeast of Thailand: A spatiotemporal-oriented study based on maps of early 20th century

Nagata Yoshikatsu¹

¹ Graduate School of Engineering, Osaka City University
3-3-138 Sugimoto, Sumiyoshi, Osaka 558-8585, Japan
Email: nagatay@osaka-cu.ac.jp

ABSTRACT

Place name is the important identification of a community. In many social studies, interviews to key informants are regular entrances to obtain general information of a community, and many old place names are to be mentioned. Such names in dialog can be hardly identified their corresponding locations because of historical changes in name. These missing locations are barriers to extend a study on social historical connections of a community.

From some old set maps covering Thailand issued in late 19th century and after, community level place names have been collected, and a spatiotemporal-oriented database of community level place names has been worked to be organized to record changes and variants of place names in the northeast of Thailand. Some place names can be linked to their corresponding present day communities, but still not a few notable names in old maps need more information on historical state of communities.

1. BACKGROUND

Place name is the important identification of a community, and it reflects many kinds of aspect such as natural environment, origin of early settlers, conceptual hope, and so on. In many social studies, interviews to key informants of a community are regular entrances to obtain its general information, and in such conversations many place names are to be mentioned. Place name is not always stable for long, so some old place names in dialog can be hardly identified their corresponding locations or place names which are currently in use. These missing locations are barriers to extend a study on social historical connections of a community.

2. OBJECTIVES

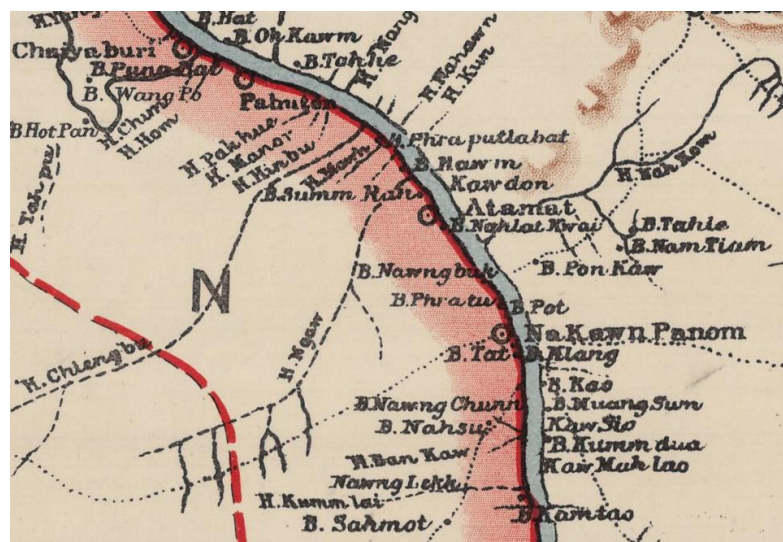
A spatiotemporal-oriented database of community level place names has been worked to be organized to record changes and variants of place names in the northeast of Thailand. In a previous article (Nagata 2019a), overview of similarity between old and present place name, and some typical cases of community level name were discussed. In another article (Nagata 2019b), regional tendency of locational difference of places shown on old maps was discussed. After these previous works, information of place names from other old maps has been added especially in Nakhon Phanom province and its adjacent areas. For enrichment of spatiotemporal-oriented database, some cases of changes and variants in place name are introduced. In this study, “community” means village or so-called “muban” in Thai.

3. MATERIALS

Information of place names has been collected from published materials, mainly maps and gazetteers. Modern topographic maps are used to collect place names of rural communities and their geographical locations. Some sets of old maps prepared in early 20th century or before can provide names of those days.

Some main sets of old maps described in below and topographic maps of L708 series scaled 1 to 50,000 are referred in this study.

(a) Maps comprised of 12 sheets with title “MAP OF SIAM” by the Survey of India Offices, Calcutta on a scale of 1 to 760,320 in 1896. These maps are noted as reproduction from an original supplied by the Royal Survey Department, Siam. (Figure 1)



Source) Sheet 4, MAP OF SIAM, published in 1896:
Collection of the Library of Congress

Figure 1. Around Nakhon Phanom on a part of “MAP OF SIAM”.

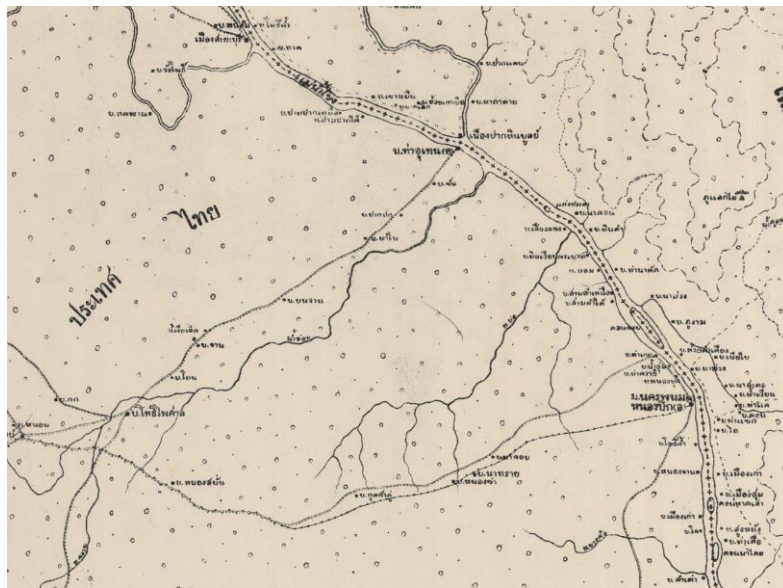
(b) Flight maps on a scale of 1 to 200,000 by Royal Survey Department. In the map titled Nakhon Phanom referred in this study for example, it is noted that this map was compiled from various scale maps in 1919, and printed in 1940 (Figure 2). Other sheets in this set maps were so far compiled around 1920 and printed from 1920s till 1940s. Some updated editions were continued to be printed in 1950s. Hereinafter these maps are referred as to the RSD maps.

(c) Maps by Japanese Army or so-called *Gaihozu*, the maps of areas outside the mainland Japan, on a scale of 1 to 200,000 in around 1940. *Gaihozu* covering Thailand are reproduction of the RSD maps described in above (Figure 3). Place names are transcript in Japanese from original in Thai. Some minor updates or additional information can be found in *Gaihozu*.

(d) Maps “Carte de l’Indochine” by the Service Géographique de l’Indochine on a scale of 1 to 500,000 in around 1930 (Figure 4). These maps include the north, the northeastern, and the eastern of Thailand as adjacent areas of French Indochina.

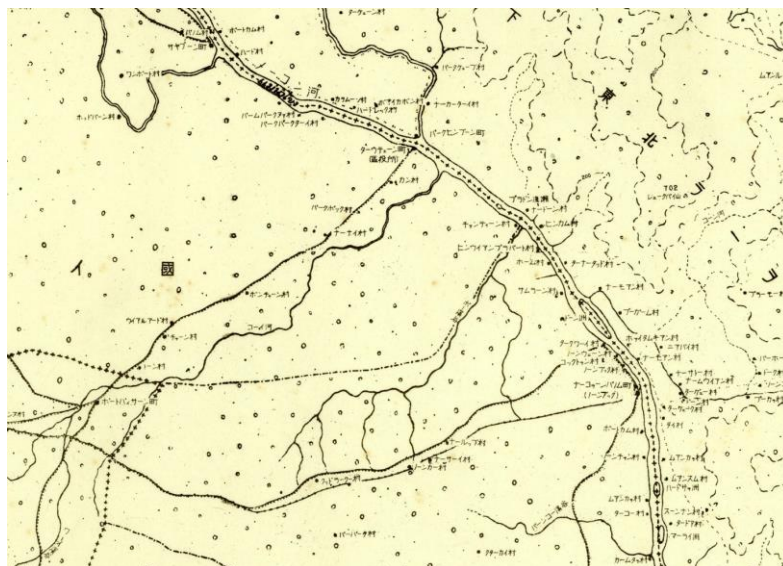
(e) Maps of Vietnam by Chinese Army on a scale of 1 to 500,000 in around 1940. Though no information of source nor surveying method is mentioned on maps, contents look reproduction from the Carte de l’Indochine above (Figure 5). Place names are described in

Chinese characters and their phonation is unknown because Chinese ideograph has many variation of phonation depending on regional dialects. As far as the author's experience, phonation of present day standard Chinese is far from Thai phonation of the corresponding place.



Source) นครพนม (๒๓) (Nakhon Phanom (23)), แผนที่การบิน
ฉบับเดิม (flight map), by the Royal Survey Department:
Collection of the Library of Congress

Figure 2. Around Nakhon Phanom on a part of flight map in Thai.

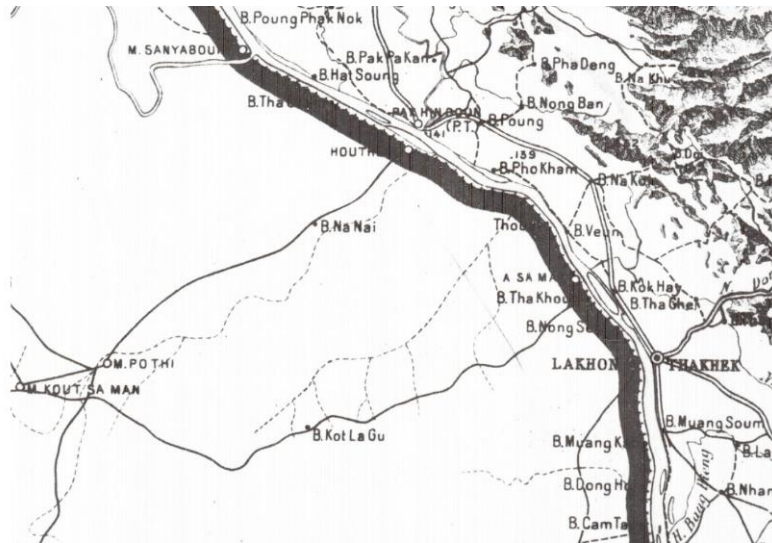


Source) Sheet 23, ナコーンパノム (Nakhon Phanom), タイ國二十万分一圖 (Thailand scaled 1 to 200,000), issued in 1941: Gaihozu Digital Archive, Tohoku University

Figure 3. Around Nakhon Phanom on a part of Gaihozu.

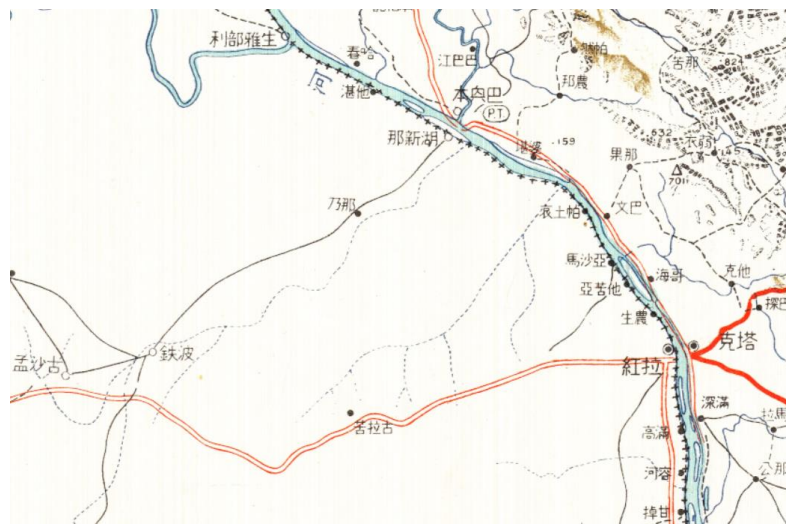
Beside old maps, some gazetteers provide both place names and their geographical

locations; however, geographical resolution varies from one minute to ten minutes, or from 2.5 km to 25 km in distance. It can be said that locations shown in such gazetteers can indicate only approximate locations, but they are not enough to distinguish a target community among nearby communities.



Source) Sheet 8, VINH, Carte de l'Indochine: Collection of the Library of Congress

Figure 4. Around Nakhon Phanom on a part of “Carte de l’Indochine”.



Source) Sheet 8, 義安 (Vinh), 越南圖 (Map of Vietnam), by the Chinese Army: Collection of the Library of Congress

Figure 5. Around Nakhon Phanom on a part of “Map of Vietnam”.

4. DISCUSSIONS

Place names described on a specific set of maps are so far snapshot names of those days, and form one layer of geographical 2D distribution. For the purpose of exploring local history of a community, linkage on temporal axis among such layers is indispensable.

Linkage of place names among different layers, or different ages, can be easy if these names are same or quite similar and their locations are so far same. But, it is not guaranteed that the place name of a community has kept same through generations. Slight change often happens by standardization so that a name in local language is adjusted to a name in national standard language. If the local language spoken in a community is far from national standard language, the name of a community is tend to be drastically changed to keep their original concept, or to be similarly pronounced in nationwide language. These changes bring difficulties in confirming linkages among different names. Cases that names on old maps are similar to those on present day maps are about 40 percent of communities shown on the RSD map for the area of Nakhon Phanom (Nagata, 2019a).

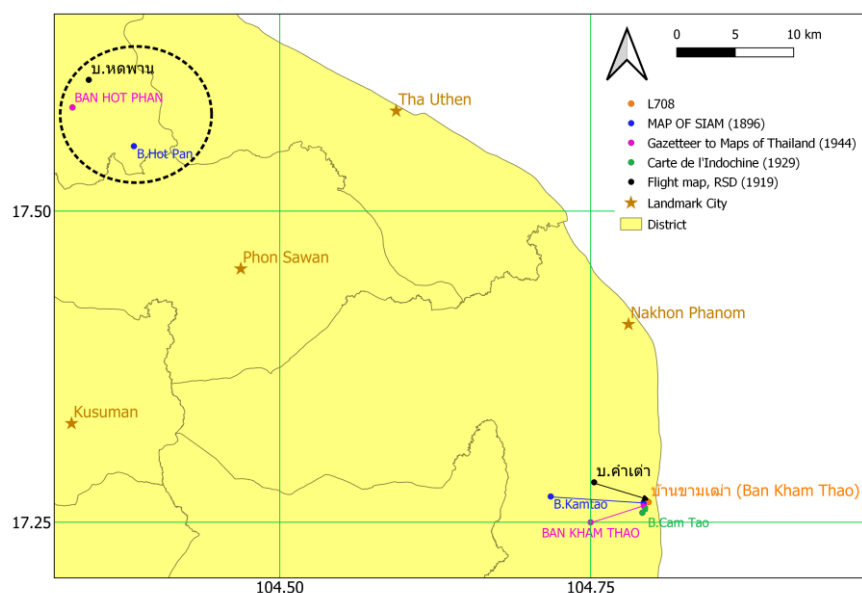


Figure 6. A linkable case and an unknown case.

At the right bottom of Figure 6, one example of linkable case, present day Ban Kham Thao, is shown. In this case, Ban Kham Thao was shown on all five old maps introduced in this study, and phonations look very similar (Table 1). “B.” is the abbreviation of “Ban” which is commonly used to represent “Village” in Thai. But at the same time, it should be keep in mind that described locations on such old maps are not always precisely corresponding to present day location. Relative position to landmarks, such as major rivers, big lakes, and notable cities, can give confirmable information to identify.

Another case in broken line circle at the left top of Figure 6 shows a missing community named Ban Hot Phan. This community is on the map “MAP OF SIAM” issued in 1896 and is listed in “Gazetteer to Maps of Thailand” published in 1944. The RSD map also describes this community (Table 2). But on the L708 series topographic maps, which are maps of 1960s, no community with similar name is shown in this area. In consideration that the MAP OF SIAM is a relatively small-scale map and was issued in late 19th century, communities shown on it must be notable in those days. Historical state of such communities may suggest an important aspect of history of the area.

Table 1. Place name descriptions of Ban Kham Thao.

Source	Description
(a) MAP OF SIAM	B. Kamtao
(b) Flight map by RSD	บ.คำเตา (B. Kham Thao)
(c) Gaihozu	カームタオ村 (Ban Kham Thao)
(d) Carte de l'Indochine	B. Cam Tao
(e) Map of Vietnam	甘掉 (* unknown pronunciation)
(f) L708 map	บ้านขามเตา (Ban Kham Thao)

Table 2. Ban Hot Phan, an example of unidentified current existence.

Source	Description
(a) MAP OF SIAM	B. Hot Pan
(b) Flight map by RSD	บ.หอดพาน (B. Hot Phan)
(c) Gaihozu	ホッドバーン村 (Ban Hot Phan)

For further information on such unidentified old communities, field interviews on site have been planned, but they cannot be conducted due to the still ongoing unsafe situation of the COVID-19.

5. ACKNOWLEDGEMENT

Many images of Gaihozu were referred in the Gaihozu Digital Archive web page by Tohoku University. Without map collections in the Library of Congress, this study could not be extended. This study was supported by JSPS KAKENHI Grant Number JP19K12700.

6. REFERENCES

- Nagata, Y., 2019a. Integrating Place Names of the Early 20th Century into a Spatio-Temporal Gazetteer of Northeast Thailand. *International Journal of Geoinformatics* 15(2), 69-78.
- Nagata, Y., 2019b. Community Level Old Place Names in the Northeast of Thailand for a Historical Digital Gazetteer. *Proceedings of the 2019 Pacific Neighborhood Consortium Annual Conference and Joint Meetings (PNC)*, 94-99.

A WEB-BASED SEASONAL GEOMORPHOLOGICAL AND COASTAL DYNAMICS MONITORING SYSTEM: CASE STUDIES IN MYANMAR

Dhyey Bhatpuria¹ and Thanapon Piman¹

¹ Stockholm Environment Institute, 10th Floor, Kasem Uttayanin Building, 254 Chulalongkorn University,
Henri Dunant Road, Pathumwan, Bangkok, 10330 Thailand
Email: dhyey.bhatpuria@sei.org; thanapon.piman@sei.org

ABSTRACT

Ayeyarwady River in Myanmar is one of the few free-flowing rivers in the South and Southeast Asian region. The river is also the most morphologically active in the region which is influenced by monsoon-induced high water levels and sediment loads. While such a morphologically active river in its natural state provides immense benefits for aquatic biodiversity and the ecosystem, it also poses a significant risk to riverine villages, urban infrastructure, agricultural lands, and ship navigation. In the coastal zone, the Sittaung River meets the Gulf of Mottama forming the Sittaung Estuary region which records powerful tidal surges resulting in erosion of its banks. The banks of this estuary experience a cycle of extreme erosion rates, of up to 1.6 km/y, which forces local communities to abandon their villages and farms, while elsewhere in the estuary accretion and growth of tidal flats allow for the development of new agricultural land.

A web-based monitoring system called “More Rivers” was developed for the Ayeyarwady River and Sittaung estuary region using long-term time-series Landsat (5,7,8) and Sentinel-1 imagery in Google Earth Engine (GEE). Pre-monsoon and Post-monsoon seasonal composites of satellite images are used to differentiate land-water pixels using Modified Normalized Difference Index (MNDWI) and Otsu thresholding for Landsat and Sentinel-1 respectively. Utilizing change detection method pre and post water surface, erosion, and deposition areas were identified for Ayeyarwady River as well as Sittaung estuary. For river morphology, River width change was quantified by estimating lateral changes in the demarcated stream centerlines and bank lines that were derived from the pre-and post-monsoon channel masks. Land Cover/Land Use data is integrated into the system to determine to affect land cover types and area loss and gain. It was observed that changes in river course in the upper estuarine region resulted in higher land loss whereas tidal impacts along with riverine water fluctuations resulted in changes of coastline in the lower part of the Sittaung estuary.

This information disseminated through stakeholder-centric User Interface (UI) will help government agencies to monitor changes and trends of the river and coastal dynamics as well as to conduct a rapid assessment of riverbank/coastline protection and investment needed. The major impact of this system stems from generating timely, user-required information for improved decision-making towards better river management.

1. INTRODUCTION

Rivers of South and Southeast Asia experience complex geomorphic changes like changes in flows, sediment, land use, and anthropogenic factors apart from Monsoon which exemplifies the complexities in the form of large variations in seasonal discharge and sediment loads (Abbas and Subramanian, 1984; Kummu and Varis, 2007). These induced geomorphic alternations in one season, in turn, influences local flood patterns in subsequent monsoon seasons. Over a long period, the local scale geomorphologic process may jointly function to alter the catchment scale process (Grabowski *et al.*, 2014).

Floodplains of morphologically active rivers in Asia like the Ayeyarwady and Ganges-

Brahmaputra-Meghna system hosts large populations and swathes of agricultural lands vital for the region's food security. Seasonal morphological change in these rivers erodes settlements and agricultural lands located in the floodplains thus directly affecting the riverine communities. Besides, these rivers also serve as key inland transport corridors, which are affected by seasonally changing river planforms. Monitoring river morphological change at high temporal and spatial resolutions is imperative to support sustainable river management. However, government agencies are constrained by the limited technology, human and financial outlays available to repeatedly cover the large spatial area while preferring to focus on field-based monitoring only in locations deemed critical (Newson and Large, 2006).

Freely accessible remote sensing data from multiple satellite platforms offer an efficient way to map river planform changes over large geographical domains at high temporal resolution which supports rapid assessment. Cloud-based remote sensing processing platforms like Google Earth Engine (GEE) (Gorelick *et al.*, 2017), enables planetary and regional scale computations using freely available satellite data like MODIS, Landsat, Sentinel series from their cloud repository without the need for downloading datasets. This facilitates focus on analysis and development of solutions with less dependence on remote sensing software techniques. This paper focuses on the development of a web-based, operational, large-scale seasonal river morphology monitoring system "More Rivers" for the Ayeyarwady river to map spatial and temporal erosion and accretion areas.

2. Materials and Methods

2.1 Study Area

Ayeyarwady River flows through Myanmar from North to South dividing the country into East and West half. Ayeyarwady River basin consists of Upper Ayeyarwady, Chindwin which merges downstream to Lower Ayeyarwady. The total length of the river is 2,170 km with a total basin covers 413,710 km². The river originates in Eastern Himalayas and receives high volumes of water during the monsoon months of May to October. The majority of cities within Myanmar like Yangon, Mandalay, Magway, etc. are along the Ayeyarwady River.

The Gulf of Mottama, located in the southwest of Myanmar and bordering the Andaman Sea, at its mouth is around 100 km wide and narrows into a funnel-shaped bay towards Sittaung River in the north. This region experiences a tidal bore phenomenon leading to high waves in the upper regions of the estuary which has resulted in a large mudflat area stretching a few 100 km. This forms the Sittaung river estuary.

2.2 Methodology

In this study, long-term time-series Landsat (5,7,8) from 1988-2019 and Sentinel-1 imagery from 2017-2019 available in Google Earth Engine (GEE) is used. Detailed methodology is shown in figure 2.

For riverbank erosion, Pre-monsoon and Post-monsoon seasonal composites of satellite images are used to differentiate land-water pixels using Modified Normalized Difference Index (Xu, 2006) and Otsu thresholding (Otsu, 1979) for both Landsat and Sentinel-1. The formula for Modified Normalized Difference Index (MNDWI) used is

$$\frac{Green-SWIR}{Green+SWIR}$$

(1)

Here, Green is the visible green band of Landsat series and SWIR is the Short Wave Infrared band of Landsat series.

Coastal erosion, tidal and intertidal dates were determined for each month, and images were aggregated to compare similar tidal conditions for pre and post-changes. Utilizing change detection method pre and post water surface, erosion, and deposition areas were identified for Ayeyarwady River as well as Sittaung estuary. Time-series changes in the area for each section were calculated. For river morphology, River width change was quantified by estimating lateral changes in the demarcated stream centerlines and bank lines that were derived from the pre- and post-monsoon channel masks. Land Cover/Land Use data is integrated into the system to determine to affect land cover types and area loss and gain. This was estimated at the village level using zonal statistics to estimate changes in each village administrative unit.

For ease of access to stakeholders, this methodology is transformed into an operational tool. A web-based tool “More rivers” is designed and developed which enables the user to select region/State, period of analysis to visualise and analyse changes in a particular area of interest. It also provides an estimation of land use changes in the form of spatial output apart from time-series changes in riverbank width. To support decision-making, the user can select 3 states to generate an automated 4-page report. “More rivers” is developed using a technology stack of GEE python api as backend with vue.js and html5.

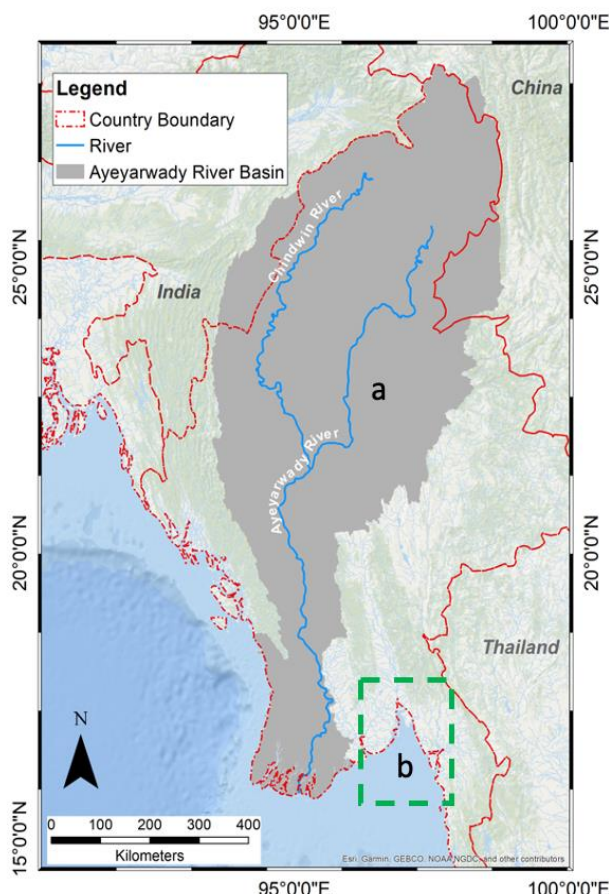


Figure 1: Study Area. Here a is the Ayeyarwady river basin and b is the Sittaung river

Estuary including the Gulf of Martaban.

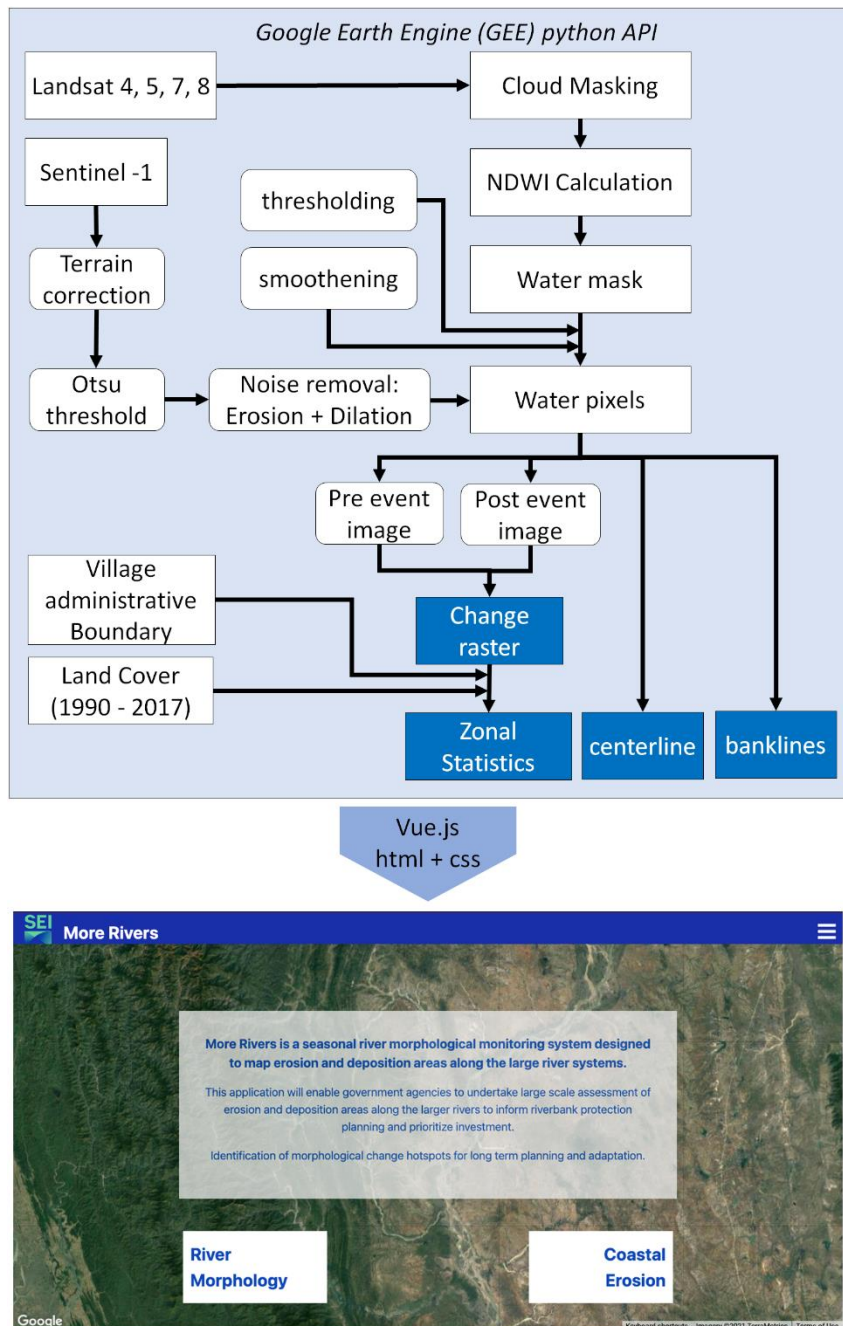


Figure 2: Methodology

3. Results

A comparison of the annual binary rasters river course of 2018 with 1988 is shown in figure 3. This area is downstream of the confluence of the Upper Ayeyarwady and Chindwin rivers and is observed to be highly dynamic. The red color represents the active river channel at the end of the study period (2019), the blue color represents the river channel during the start

of the study period (1989). The river is highly braided in this region and hence in the figure.3a island formations are ignored to get the final banks of the river. Figure 3b illustrates eroded and current river channel, and the green color is the accreted channel and depositions shows that a high degree of erosion and accretion occurred in multiple areas within this section of river along both banks. This is more prominent in the location of the confluence of upstream rivers and the following bend downstream. Ayeyarwady's river bank dynamics can be more clearly understood by observing at inter-annual intervals.

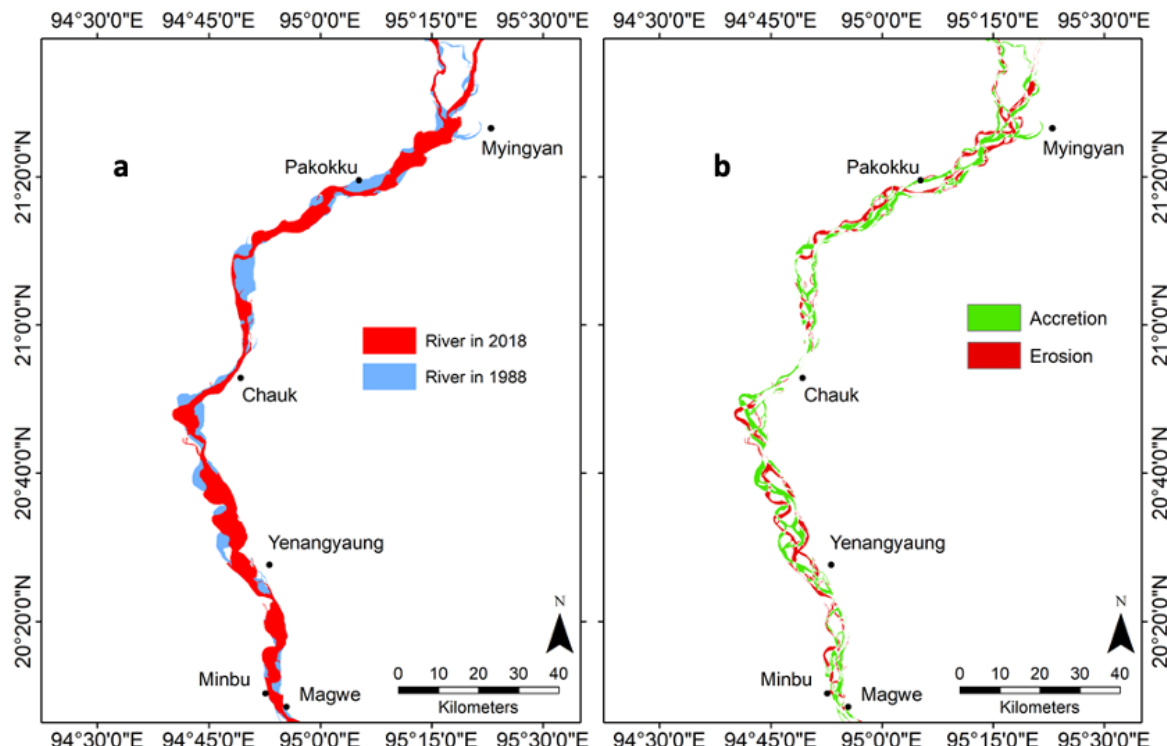


Figure 3: Changes in the river area during the study period. Figure a shows river area during 2018 (red) overlayed on river area during 1988. Figure b shows the difference of actual river area with all river braiding for the two years 1988 and 2018. Here Erosion (red) indicates the loss of land in 2018 while Accretion (green) depicts land gained in 2018 as compared to 1988.

Inter and Intra decadal changes in river course is shown in Figure 4 for 1988-1998 (a, d), 1999-2008 (b, e) and 2009-2018 (c, f). 4 a,b and c highlight Upper Ayeyarwady stretch from towns Tigyaing-Mya Taung to Takaung of Mandalay Region. 4 d,e and f shows s Lower Ayer stretch from Chauk town to Yenangyaung city of Magway Region. Here, binary annual river rasters are aggregated for each decade. Darker shades of blue represent low shifts in river course while lighter shades depict that river has been flowing through that location for a few years only during that decade. In Upper Ayeyarwady (figure 4 a-c), the river shows shifting in the course more prominently along the right bank before moving further downstream towards Mandalay city. Yellow circle highlights the location where the river shows high oscillation during each decade while by last decade it stabilizes with a net movement towards the right riverbank (figure 4a and c). Similarly in figure 4 d-f of the Lower Ayeyarwady also shows a significant shift in course gradually over three decades all along the stretch. Also, in the area highlighted by the red box, the river shows interdecadal oscillation in its course which causes

high braiding downstream to that area.

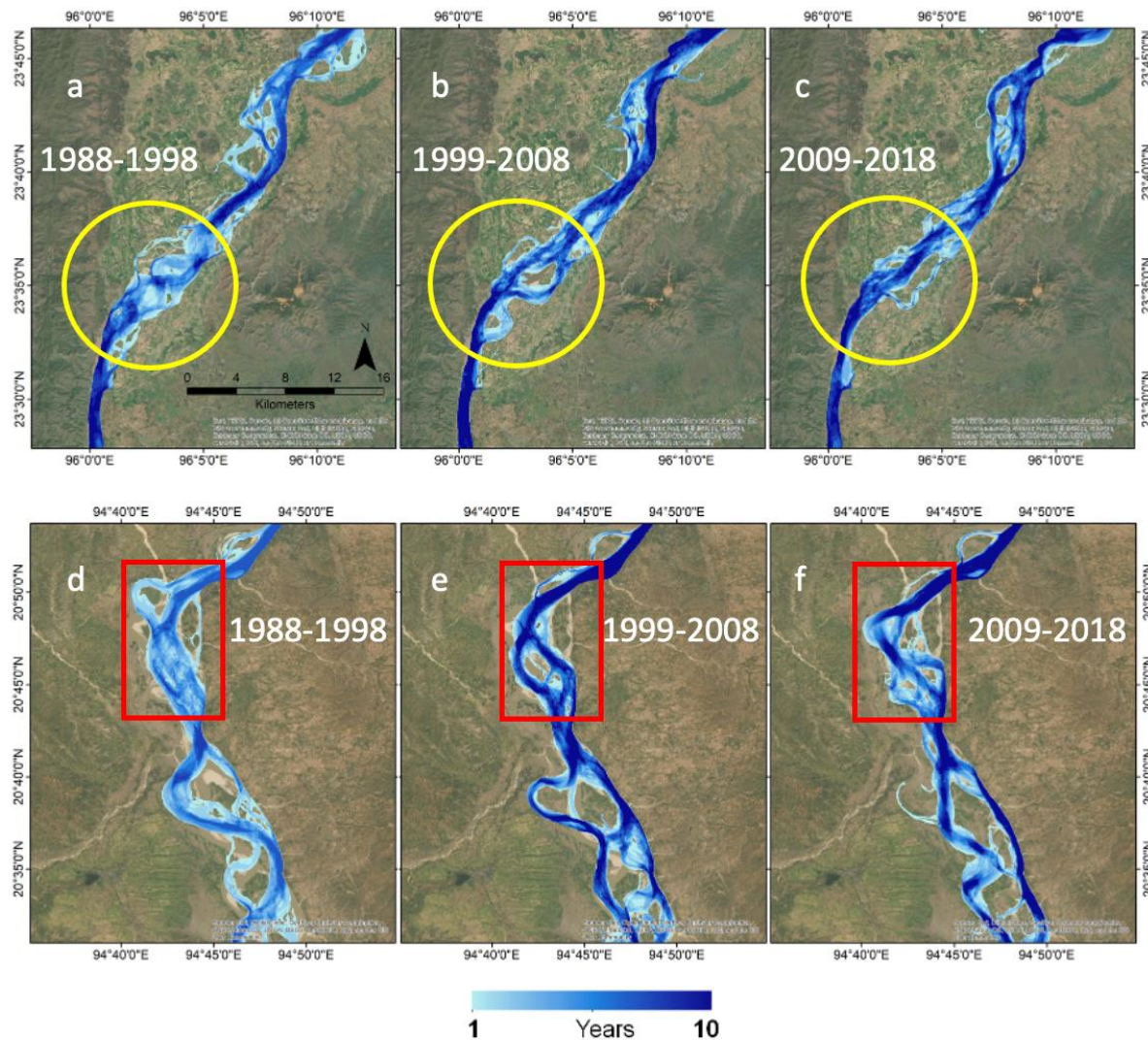


Figure 4: Decadal River course dynamics in Ayeyarwady from 1989-2019 for Upper Ayeyarwady(a,b,c) and Lower Ayeyarwady (d,e,f)

Figure 5 shows decadal changes in the river mouth region from 1989 to 2019 in false-color composite and land-sea map generated using Otsu thresholding of MNDWI. There have been conspicuous changes in the coastline along the geographic western side of the river mouth during the past 30 years. Also, during previous years, the river course was more convoluted as seen in 1989 which has been gradually changing to a more straight course, which would have led to change in streamflow and have an impact on the erosion of geographic western river mouth land. In 1999 we observed the formation of an intertidal island on the west coast which is downstream to areas with higher erosion while the lower part of the river mouth is comparatively unaffected by coastal erosion. Similarly, along the eastern side of the river mouth, we observe the development of a similar island in 2009 which gradually resulted in the gain of land.

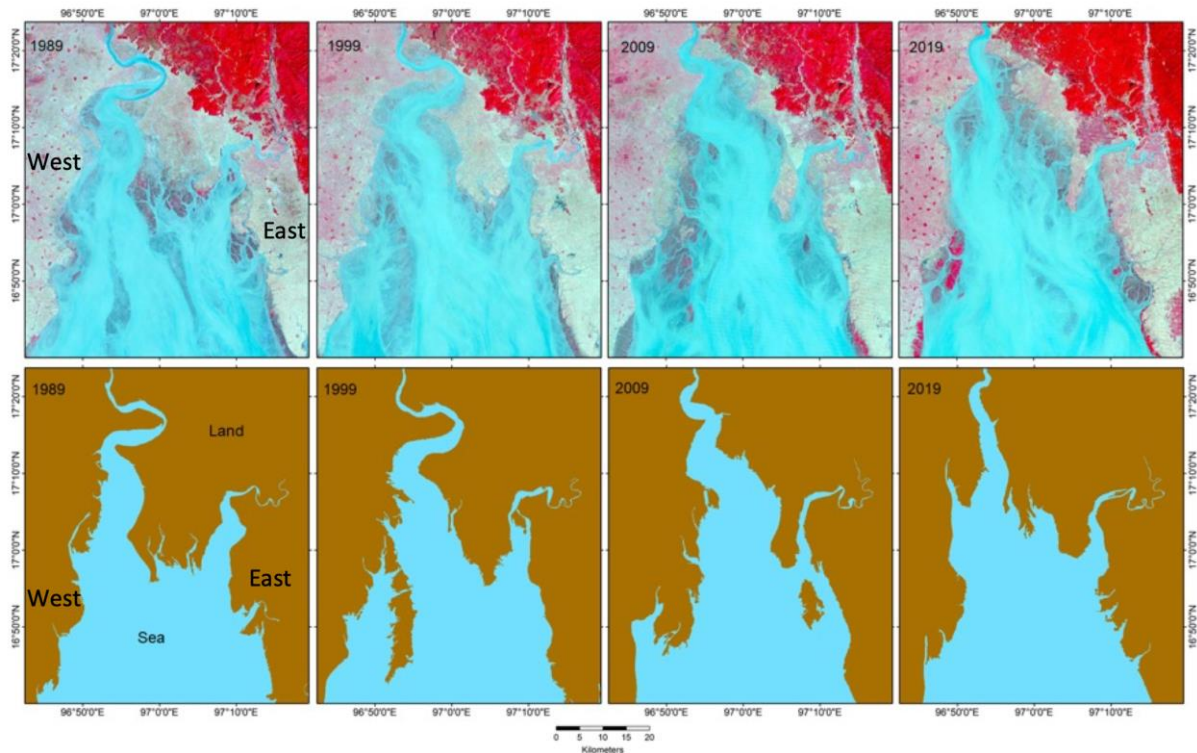


Figure 5. Decadal changes in the river estuary and coastal boundaries

4. Capacity Building and Stakeholder Engagement

Need assessment/stakeholder meetings were organized during the initial development phase of the tool to incorporate needs of the end users and decision makers. The Directorate of Water Resources and Improvement of River Systems (DWIR) of Myanmar which is a national governmental agency with a responsibility for managing river systems was identified as one of the primary stakeholder. DWIR conducts extensive task of monitoring river morphological change over several thousand kilometres of river in the country. During stakeholder meetings, challenges in conducting monitoring as well as expected outputs which would augment existing methods along with addressing knowledge gaps were discussed. Web tool is being used by the key stakeholders to build better plans for management of riverbank and coastal erosion.

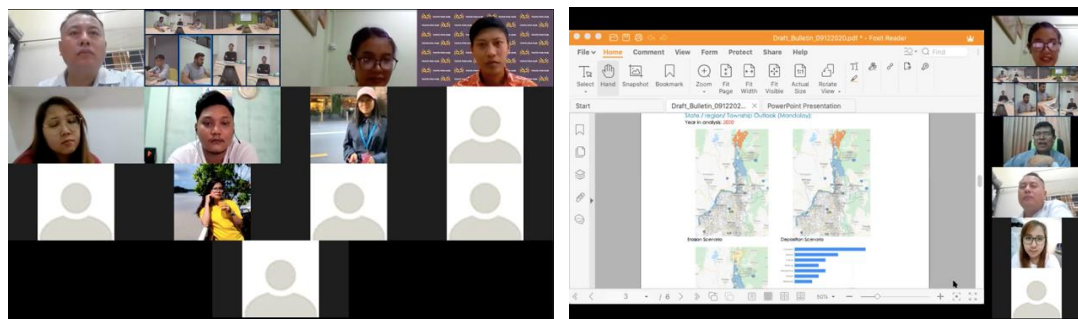


Figure 6. Online Stakeholder meeting on web tool with DWIR, Myanmar

5. Conclusion

Long-term seasonal analysis of Ayeyarwady reveals a significant change in the riverbank width. This change in river width is the consequence of erosion or deposition. Also in specific sections near Magway and above Mandalay cities, changes in the form of oscillation of the river course are observed. The Sittaung estuary region shows a high impact of tidal waves which causes a high degree of erosion. There is more land gain in the eastern bank of the estuary in recent years which was witnessing higher erosion in previous decades, while the opposite trend is observed for the western bank of the Sittaung estuary. The tool can support in monitoring riverbank and coastal erosion for a large scale area and identify the hotspots to manage the erosion better. Google Earth Engine's repository of freely available satellite data and powerful cloud computing capabilities facilitate rapid calculations and on-the-fly analysis. The development of a web application equipped with processed data and results creates a digital playground for the end-users and stakeholders to visualise and analyse information to actionable intelligence.

6. REFERENCES

- Abbas, N., Subramanian, V., 1984. Erosion and sediment transport in the Ganges river basin (India). *Journal of Hydrology* 69, 173–182. [https://doi.org/10.1016/0022-1694\(84\)90162-8](https://doi.org/10.1016/0022-1694(84)90162-8)
- Gorelick, N., Hancher, M., Dixon, M., Ilyushchenko, S., Thau, D., Moore, R., 2017. Google Earth Engine: Planetary-scale geospatial analysis for everyone. *Remote Sensing of Environment* 202, 18–27. <https://doi.org/10.1016/j.rse.2017.06.031>
- Grabowski, R.C., Surian, N., Gurnell, A.M., 2014. Characterizing geomorphological change to support sustainable river restoration and management: Characterizing geomorphological change in rivers. *WIREs Water* 1, 483–512. <https://doi.org/10.1002/wat2.1037>
- Kummu, M., Varis, O., 2007. Sediment-related impacts due to upstream reservoir trapping, the Lower Mekong River. *Geomorphology, Monsoon Rivers of Asia* 85, 275–293. <https://doi.org/10.1016/j.geomorph.2006.03.024>
- Newson, Malcolm.D., Large, A.R.G., 2006. ‘Natural’ rivers, ‘hydromorphological quality’ and river restoration: a challenging new agenda for applied fluvial geomorphology. *Earth Surf. Process. Landforms* 31, 1606–1624. <https://doi.org/10.1002/esp.1430>
- Otsu, N., 1979. A Threshold Selection Method from Gray-Level Histograms. *IEEE Trans. Syst., Man, Cybern.* 9, 62–66. <https://doi.org/10.1109/TSMC.1979.4310076>
- Syvitski, J.P.M., Vörösmarty, C.J., Kettner, A.J., Green, P., 2005. Impact of Humans on the Flux of Terrestrial Sediment to the Global Coastal Ocean. *Science* 308, 376–380. <https://doi.org/10.1126/science.1109454>
- Xu, H., 2006. Modification of normalised difference water index (NDWI) to enhance open water features in remotely sensed imagery. *International Journal of Remote Sensing* 27, 3025–3033. <https://doi.org/10.1080/01431160600589179>

POSSIBILITY IN IDENTIFYING SUITABLE AREAS FOR URBAN GREEN SPACE DEVELOPMENT USING GIS-BASED MULTI-CRITERIAL ANALYSIS AND AHP WEIGHT METHOD IN DONG HA CITY, VIETNAM

Do Thi Viet Huong, Doan Ngoc Nguyen Phong, Le Tan Tuyen

Department of Geography and Geology, University of Sciences, Hue University, Vietnam

77 Nguyen Hue Str., Hue city, Vietnam

E-mail: dtvhuong@hueuni.edu.vn; phong080595@gmail.com; letantuyenypu@gmail.com

ABSTRACT

Urban Green Spaces (UGS) is an essential component of the urban environment and provides the community's critical ecosystem services. The administrators face difficulties selecting the multi-level capabilities site for urban green space under the pressures of population growth dynamic, unplanned urban development, and environmental, socio-economic, cultural, and other sociopolitical risks. This study evaluates the possibility of expanding UGS in Dong Ha city using a GIS-based multi-criteria and analytical hierarchy process (AHP). Variables including slope, existing land use/land cover, proximity to the main road, waterbody, pollution sources, park, historic place; land price, population density, and land surface temperature took for suitable analysis. The dasymetric mapping technique utilized for retrieving population density factors demonstrated more accurately for proper evaluation modelling. The findings suggested the spatial distribution of 0.36%, 5.32%, and 23.18% of the area's highly suitable, relative suitable, suitable, respectively. While the most crucial site, 62.03%, is less suitable, and 9.10% is not suitable for UGS development. These research findings could assist the city planner, the government authority, examines the optimal urban green spaces for improving the environmental sustainability in urban areas.

Keywords: Urban Green Spaces, AHP, GIS, Dasymetric, suitable analysis

1. INTRODUCTION

By 2050, 68 per cent of the world's population is projected to be urban and approximates 50 per cent of the level of urbanization in Asia [5]. This unprecedented urban growth leads to post tremendous pressure on natural resources and the ecological environment.

Urban Green Space (UGS) is an essential component of the urban environment and provides the community's critical ecosystem services and the quality of human well-being [2], [4]. Municipal governments in developing countries face difficulties selecting the optimal locations for UGS under the pressures of dynamic population growth, unplanned urban development, and environmental, socio-economic, cultural, and other sociopolitical risks [6]. The suitable land analysis determines the fitness of a given tract of land for a defined use, which is considered vital in UGS planning. The multi-criteria analysis (MCA) with the Analytic Hierarchy Process (AHP) weighting method approach incorporated into GIS-based suitability procedures has been increasingly used in UGS proper evaluation by various parameters such as bio-physical, socio-economic, environmental, policy-related, accessibility factors in decision-making processes [4], [6], [8].

Dong Ha is a young city in Quang Tri province, central Vietnam, facing fast urbanization and the threat of climate change. As a result of the rise of impervious surfaces, green spaces are becoming increasingly limited. Therefore, this study aims to select potential UGS sites to assist in an effective planning process of green areas. A GIS-based multi-criteria and AHP framework was carried out to indicate different parameters for evaluating the possibility of expanding UGS in Dong Ha city. The findings may benefit city planners, real estate developers, and government officials in ensuring the proper land use planning and management of the urban areas.

2. MATERIAL AND METHOD

2.1 Study area

Dong Ha is the capital city of Quang Tri province, central Vietnam. Located between $16^{\circ}07'53''$ - $16^{\circ}52'22''$ north latitude and $107^{\circ}04'24''$ - $107^{\circ}07'24''$ east longitude. It has nine wards, with a total natural area of 7,308.53 hectares. As of April 1, 2019, Dong Ha city's population was 95,658 people; after ten years (April 1, 2009 - April 1, 2019), the city's population increased by 14,497 people, an average growth rate of 1.7% people. Some wards have a fast average population growth rate: Dong Luong ward 4.1%; Ward 2 2.2%; Dong Le ward 2.2%; Dong Thanh Ward 2.2%.

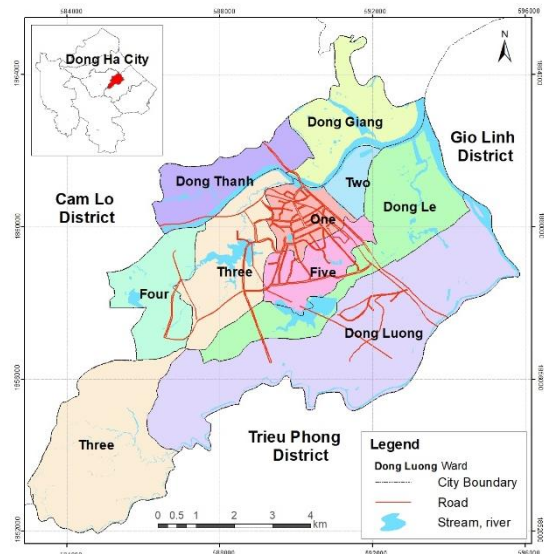


Figure 1: Map of the study area

2.2 Materials

The spatial and non-spatial data were gathered from various government departments and authorities such as the Department of Natural Resources & Environment (DONRE), Department of Statistic (DS), People's Committee of Quang Tri Province (PC). The collected data showed in table 1.

Table 1. Data collection for analysis

Data	Sources	Type	Year	Resolution /Scale	Purpose
Landuse map			2020	1:10.000	Proximity analysis
Topographic map	DONRE	Vector	2015	1:10.000	Slope
Master plan and land use planning			2030	1:10.000	Reference
Land price information	PC	Excel	2020 - 2024	Ward level	Landprice
Population census	DS	Excel	2020	Ward level	Population density analysis
Landsat 8 TIRS	UGSS	Raster	2020	30 x30 m	Land surface temperature analysis

3. METHODOLOGY

3.1 Determination of criteria

The criteria that affect selecting suitable UGS vary from researcher to researcher and are grouped into some dimensions, i.e., physical, socio-economic, environmental, accessibility [4], [9], [12]. Based on the synthesizing literature review, expert consultation, and study area condition, the optimized UGS suitability evaluation criteria were adopted, including ten measures in table 2. The level of suitability for urban green space development is defined by the Food and Agricultural Organization and classed in each sub-criteria as follows: Highly suitable (S1), relatively suitable (S2), suitable (S3), less suitable (S4), and Unsuitable (N) for urban green space corresponding to the score of 5, 4, 3, 2, 1, respectively [1] (Table 2).

3.2 GIS-based multi-criteria analysis and AHP framework for suitable analysis

GIS-based analysis was conducted to derive the selecting criteria map indicating in table 2. Population density mapping at a finer scale and higher resolution can play an essential role in understanding urban spatial features, especially in analysis for urban green space. Therefore, dasymetric mapping effectively helps allocate population data to more delicate spatial units with ancillary data [11]. Dasymetric mapping technique was utilized for extracting the population density through spatial analysis, population distribution over a given territory based on the weighting of each land-use/surface cover category to distribute population data shown on the map more accurately in geographical space [3],[10]. The slope criteria map was derived by interpolation from the elevation data of the topographic map. Land surface temperature criteria were obtained from an algorithm from Landsat 8 TIRS. The proximity analysis was established with the different distances for the pollution sources, road, waterbody, historic place, park criteria. The land price information is joined with the administrative unit for deriving the land price criteria.

Table 2. The criteria for site selection and suitable analysis of urban green space

Criteria	Description	Level of suitability				
		S1 (5)	S2 (4)	S3 (3)	S4 (2)	1 (N)
Slope (%) - SL	The areas with low slopes are highly suitable for developing UGS	0-5	5-10	10-15	15-30	>30
Proximity to waterbody (m) - PW	The closer to waterbody gets more preferences, contributing to maintaining the area's environmental health.	0-20	20-40	40-60	60-80	>80
Proximity to road (m) - PR	The UGS site is preferable when it is located at a suitable distance from roads to easily access transportation, enhance the possibility of monitoring, and maintain their security for citizens.	0-25	25-50	50-75	75-100	>100
Proximity to pollution source (km) - PPo	Noisy areas are not suitable for UGS like the factory area because of high sound pollution and smoke.	>20	15-20	10-15	5-10	0-5
Proximity to history place (km) - PH	The development of UGS must ensure that there is no encroachment on the relic.	0-0,5	0,5-1	1-1,5	1,5-2	>2 and the historic areas
Proximity to park (km) - PPa	The area farthest from the existing park requires green space due to the lack of green space or vegetation, balancing the number of green spaces and gardens between the regions.	>3	2-3	1-2	0,5-1	<0,5
Existing land use - LU	The capacity of land use type can be changeable into UGS	Bare land	Green Space	Forest	Agriculture	Construction land
Population density (people/ha) - PD	The areas closer to residential areas are highly suitable for developing green space.	>100	50-100	20-50	S4: 5-20;	<5
Land price (1.000 VND/m ²) - LP	The areas with the lower price will be priority than those areas with the higher price for UGS development	<3.000	3.000-6.000	6.000-9.000	9000-1.5000	> 1.5000
Land surface temperature (°C) - LST	UGS is considered an appropriate way to reduce urban heat; Areas with high temperatures will be prioritized to develop UGS	>34	32 - 34	30-32	28-30	<28

The MCA with the AHP method is an effective tool for dealing with the complex decision-making process. Based on pairwise comparisons to rank the selected criteria. The AHP weighted score for each criterion is determined based on its importance to the development of UGS. Questionnaires for each measure have been prepared. The requirements are weighted by consulting ten experts in land use or urban planning fields based on their desired priorities following Saaty's 9 point scale. The formula checked the consistency check

of the pairwise comparison matrix: $RC = IC/IR$ (1) to ensure the result meets the requirement ($RC < 0.1$). Where CR=Consistency ratio, CI=referred to as consistency index, RI=is the random inconsistency index whose value depends on the number (n) of factors being compared [7]. The MCA has incorporated ArcGIS 10.4 to select an appropriate location for the development of UGS.

In potential UGS suitable analysis, each criterion (vector layer) was normalized by turning it into a raster layer with a resolution of 30×30 m. The weighted linear combination technique was adopted to aggregate the standardized layers using the formulation to derive the potential land suitable map for urban green space development [2], [4]:

$$S = \sum_{i=1}^n W_i X_i \quad (2)$$

where S is the total value of the UGS suitability evaluation, n is the total criteria number; W_i is the combined weight result of criteria i, and X_i is the suitability value for standards i. Figure 2 depicts the framework of GIS-based multi-criteria analysis and the AHP weight method to select the suitable places for urban green space in Dong Ha city.

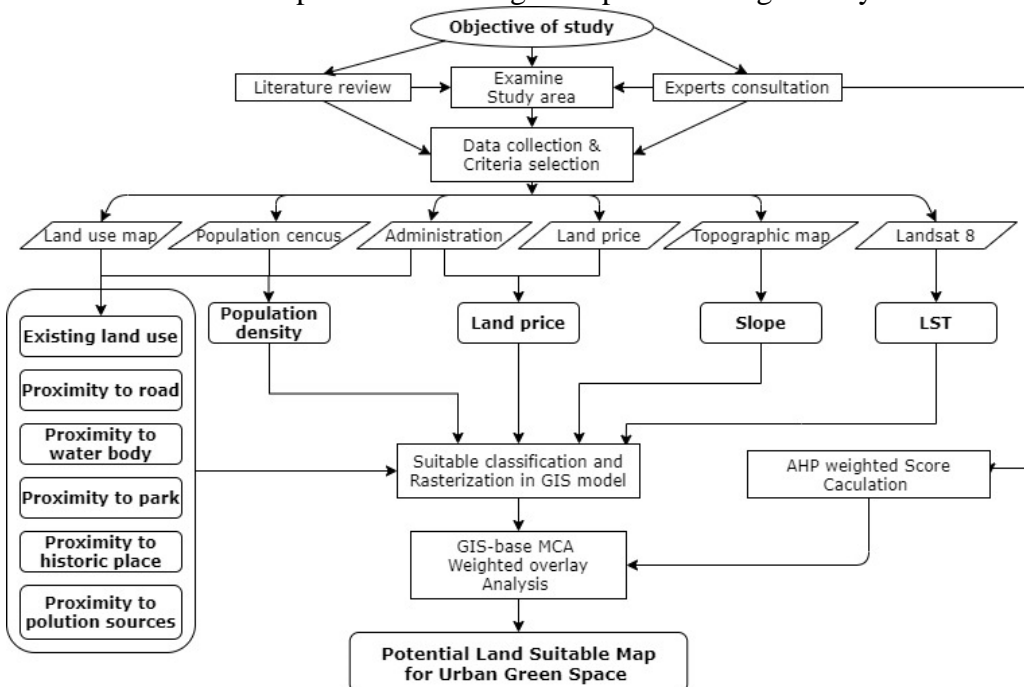


Figure 2. Flow chart of GIS-based multi-criteria analysis and AHP weight method to select the suitable places for urban green space

4. RESULT AND DISCUSSION

4.1 Mapping and weighting each criterion

The results of computing AHP weights for each criterion by comparing the pairs of evaluation criteria according to the importance scale, with the consistency coefficient $CR = 8.9\%$, satisfying the condition AHP analysis. The degree of influence on UGS varies depending on the criterion. The indicators that greatly influence UGS expansion are land surface temperature and population density with weights of 0.29 and 0.23, respectively. Meanwhile, the slope criteria and land price indicators have negligible influence on UGS expansion with the weight of 0.02 and 0.01, respectively, reflecting the reality with special conditions in the study area. The suitable thematic maps for ten criteria were done under the GIS platform in raster format for further appropriate analysis (Figure 4). Previous studies commonly derived the population density criteria under traditional density techniques of Choropleth [2], [3]. This method depicted the population distribution homogeneously throughout each administrative

boundary unit and significantly affected further spatial data analysis. In this paper, the Dasymetric mapping map technique was adopted for making population density maps because of its ability to distribute population data shown on the map more accurately in geographical space (Figure 4-PD).

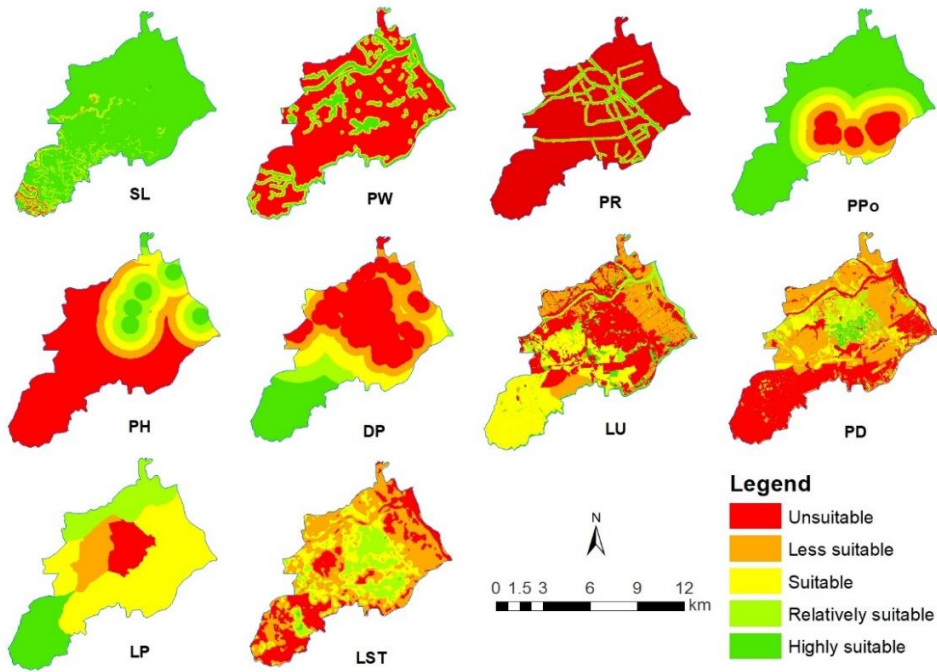


Figure 4. Suitability level of each criterion for urban green space development

4.2 The potential suitable land for expanding urban green space

A comprehensive overlay analysis was performed on each criterion following the AHP weighted score to derive the potentially suitable land for UGS development in Dong Ha city. The proper level was defined in 5 grades as highly suitable, relative suitable, suitable, less suitable, and unsuitable (Figure 5).

The results show that UGS suitability is concentrated in Ward 5, which covers a small area of 26.67 ha and accounts for 0.36% of the entire region. Most of the sites have high population density, building land with high temperatures, and high road density, which are ideal for UGS expansion. The analysis findings also show that the terrain slope is relatively flat adjacent to historical-cultural monuments. The relative suitability area is 388.62 ha, representing 5.32% of the total area, distributed mainly in wards 1 and 5. It belongs to the wards with high population density, high land price, and elevated green area coverage, such as wards 1 and 2. The suitability area encompasses 1,694.07 ha, or 23.18% of the total land area, and is primarily located in the city centre, encompassing wards 1, 2, 5, and Dong Luong and along the river. These areas contain many people and a lot of heat, but the rest of the conditions aren't ideal for UGS development. The location with the degree of unsuitability occupies the highest area of 4,533.72ha, accounting for 62.03% of the total

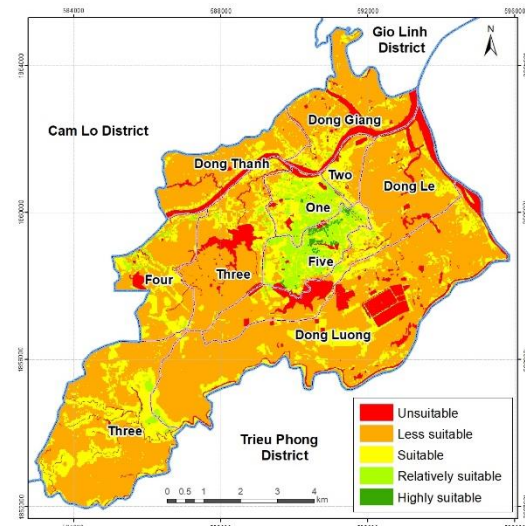


Figure 5. Final suitability map for urban green space development

area. These locations are primarily agricultural land, with relatively low density of main roads and low population density. In particular, the place to the southwest of the city is mainly suitable for low-density forest development. The location is not ideal, with 665.42 ha, accounting for 9.10% of the city area, particularly water surface land, parkland, and relic area.

5. CONCLUSION

In this study, the suitable region for urban green space development in Dong Ha city was determined using an integrated GIS-based multi-criteria with AHP weighted technique, which can aid in selecting suitable land for urban green space planning and development. The model of suitability assessment was established based on a weighted linear combination technique including ten criteria empowering various dimensions of physical, socio-economic, accessibility, environment for UGS development. The dasymetric mapping technique was utilized for retrieving population density factors demonstrated more accurately for suitable evaluation modelling. The suitability analysis results indicated the possibility of identifying the proper UGS development with suitable, relative appropriate and highly ideal for the areas located in the core city and the southwest of the town. These findings also meet Quang Tri Province's planning orientation on expanding the urban space and establishing new residential areas for economic development to the west and south. The open green space spread from the core city to the surrounding areas. Moreover, the findings provide a framework of GIS-based multi-criteria analysis and AHP weighted method in UGS development for Dong Ha city planning green spaces in the backdrop of climate change challenges in recent years.

6. REFERENCES

- [1]. FAO 2006. Guidelines for soil description. Fourth Edition, Rome, Italy, ISBN 92-5-105521-1.
- [2]. Eshetu Gelan 2021. GIS-based multi - criteria analysis for sustainable urban green spaces planning in emerging towns of Ethiopia: the case of Sululta town, *Environmental Systems Research*, 10;13, pp.1-14.
- [3]. M. H. Hamza, A. S. Al-Thubaiti, M. Dhibe, A. Bel Haj Ali, M. S. Garbouj, M. Ajmi 2016. Dasymetric Mapping as a Tool to Assess the Spatial Distribution of Population in Jeddah City (Kingdom of Saudi Arabia), *Current Urban Studies*, Vol. 4, pp.329-342.
- [4]. Zhiming Li, Zhengxi Fan, Shiguang Shen, 2018. Urban Green Space suitability evaluation based on the AHP-CV combined weight method: A case study of Fuping country, China, *Sustainability* 10, no 8:2656, <https://doi.org/10.3390/su10082656>.
- [5]. United Nations, Department of Economic and Social Affairs, Population Division 2019. World Urbanization Prospects 2018: Highlights (ST/ESA/SER.A/421).
- [6]. Shiva Pokhrel 2019. Green space suitability evaluation for urban resilience: an analysis of Kathmandu Metropolitan city, Nepal, *Environ. Res. Commun.*, Vol 1, 105003, pp 1-16.
- [7]. Saaty L T 1980. The analytical hierarchy process: planning, priority setting Resource Allocation (New York: McGraw Hill Company).
- [8]. Arjun Saha and Ranjan Roy 2021. An integrated approach to identify suitable areas for built-up development using GIS-based multi-criteria analysis and AHP in Siliguri planning area, India, *SN Applied Sciences*, Vol.3:395, doi.org/10.1007/s42452-021-04354-5.
- [9]. Tania Sharmin, Koen Steemers 2018. Effects of microclimate and human parameters on outdoor thermal sensation in the high-density tropical context of Dhaka, *International Journal of Biometeorology*, Vol. 64, pp 187-203.
- [10].Alena Vondraskova, Jan Kolarik, 2013. Dasymetric mapping as an analytical tool for the city development identification and its cartographic visualization, *GIS Ostrava 2013 - Geoinformatics for City Transformation*, pp. 1-11.
- [11]. Hao Wu , Lingbo Liu, Yang Yu and Zhenghong Peng, 2018. Evaluation and Planning of Urban Green Space Distribution Based on Mobile Phone Data and Two-Step Floating Catchment Area Method, *Sustainability*, Volume 10, Issue 1, doi: 10.3390/su10010214.
- [12].Elham Yousefi, Esmail Salehi, Seyed Hamid Zahiri, Ahmadreza Yavari 2016. Green Space Suitability Analysis Using Evolutionary Algorithm and Weighted Linear Combination (WLC) Method, *Space Ontology International Journal*, Vol. 5, No. 4, pp. 51-60.

BUILDING A GIS-BASED DECISION SUPPORT MODEL ON LAND USE PLANNING FOR RUBBER PLANTATION UNDER THE EFFECT OF TYPHOONS IN QUANG BINH PROVINCE, VIETNAM

Pham Huu Ty¹, Nguyen Van Binh¹, Nguyen Ngoc Thanh¹, Pham Thi Trieu Tien¹

¹University of Agriculture and Forestry, Hue University
102 Phung Hung, Hue city, Vietnam

Corresponding author's email: phamhuuty@huaf.edu.vn

ABSTRACT

Quang Binh province, Vietnam had a large rubber area, more than 17000ha before 2013. However, due to the impact of many typhoons after 2013, over 7000ha of rubber trees were damaged. For sustainable rubber tree development, a planning support model is needed. The application of GIS and remote sensing is capable of supporting scenarios for planning to adapt to the effects of typhoons. This study uses Landsat 8 OLI satellite images from 2013-2020 to assess the damage level of rubber trees caused by typhoons and uses a multi-criteria method to build a model to support the rubber-plantation use land planning. The Maximum likelihood algorithm and the object-based image classification were combined to classify rubber plantation land cover before and after typhoons. The opinions of local experts and officials have been collected to determine the criteria for building a model to support planning decisions. The result of image classification shows that the overall accuracy is quite high, 84.4% and the Kappa coefficient is 0.69. There are 04 criteria selected to evaluate the impact of storms on rubber plantations, including slope, elevation, slope direction and distance from the coastline. The results also show that rubber trees were severely damaged in the land 10-20km from the coast, the area with the elevation <50m, the slope <5°, and the aspect in the East and Northeast. Based on these criteria, two planning options have been proposed for local reference.

Key words: Typhoon, rubber tree, remote sensing, Quang Binh province

1. INTRODUCTION

Quang Binh province, Vietnam has a large area of rubber tree, about 18.220 ha. However, due to the impact of many typhoons in 2013, more than 12.174ha of rubber trees were damaged (Nguyen, 2014) and the Doksur typhoon damaged nearly 7,000 rubber trees in Quang Binh province (Nhat Linh, 2017) that changed the mindset of local leaders and people to re-think about the future of rubber tree development. In 2019, Quang Binh Provincial People's Committee approved a scheme on converting inefficient rubber trees to other crops for the period of 2019 – 2025 according to Decision No. 4909/QD-UBND dated on December 19, 2019. This scheme outlined general principles of planning that focused on maintaining the rubber tree plantation with a high productivity and less impacted by typhoons, while eliminated the rubber tree plantation areas damaged by typhoons to other crops (Quang Binh Provincial People' Committee, 2019). The decision of the scheme was made mainly based on statistics and data from localities, and opinions of local rubber plantation companies, but lacked specific criteria and spatial analysis to identify areas where are not suitable for rubber plantations because of the high risk of typhoons to prevent the damage of typhoons. Therefore, this study used the GIS and remote sensing approach in combination with a multi-criteria decision support model to identify areas at high risk of being affected by typhoons, thereby proposing the appropriate planning scenarios for an adaptive planning and meeting the planning objectives of local leaders.

2. MATERIALS AND METHODS

2.1 Secondary data

Data and documents on natural, economic, and social conditions of Quang Binh province

are collected to obtain general information on the provincial portal of the People's Committee of Quang Binh province (Quang Binh People's Committee, 2020). The reports in the Proceedings of the Workshop on Solutions to improve the efficiency and sustainable development of rubber trees in Quang Binh province in 2017 (Quang Binh Department of Science and Technology, 2017), including 25 presentations by departments, departments, localities, and scientific research units. The report on the project on restructuring crops on inefficient rubber plantations in Quang Binh province in the period of 2019-2025 is also collected with a lot of information related to planning, expert opinions on regulatory criteria plan.

2.2. Remotely sensed data

This study used 02 types of remote sensing data from satellite, Landsat 8 OLI and digital elevation model from SRTM satellite. Landsat 8 OLI satellite image data from 2013 to 2020 and the DEM SRTM model were downloaded from the US Geological Survey website <https://earthexplorer.usgs.gov/>. The image in May 2013 was collected before the typhoon No. 10 in 2013 (named Wutip) occurred, the photo in October 2013 was the time right after the typhoon Wutip occurred. The image of April 2017 was the one before the time of typhoon No. 10 in 2017 (named Doksur) and that of April 2018 was the time after the storm Doksur happened 6 months because there was no image right after the typhoon happened. This research used images from April 2018 to evaluate the change of rubber cover and to assess the impact of Doksur typhoon on the damaged rubber area in 2017. Image in July 2020 was used to assess the status of rubber tree cover, and at the same time was used as an input information for a model to support land use planning for rubber trees in Quang Binh province.

2.3. Data pre-processing: Landsat 8 OLI and SRTM DEM

Landsat 8 OLI satellite images were downloaded and geometrically corrected on the WGS-UTM 48N system (north direction) to ensure consistency with the vector data. The Resample function of ArcGIS software was used to convert the spatial resolution to 30m x 30m. The boundary of Quang Binh province was used to extract the Region of Interest (RoI) by using the Extract command in the Spatial Analyst/ArcGIS. The image channels were imported into the IDRISI TerrSet software to preprocess the image by using the Stretch, Filter, and Pan-sharpen tools. The Simple Linear method was used in the STRETCH tool to generate a new image with a new value that is determined by the upper and lower bounds of the values in the input image. The FILTER tool was used to create a new image, where the value of each pixel was based on its value and the values of neighboring pixels in the input image. The PANSHARPEN tool was applied to increase the high resolution of images to 15m (Padwick, 2014). BandBQA image channels were used to remove clouds and cloud shadows using the Raster Calculator tool in ArcMap 10.8. After the image channels were enhanced, the 6.5.2 channel was used to generate the 6.5.2 pseudo-color composite image. The SRTM DEM from 03 image scenes were merged into one image by using the Create Mosaic Dataset tool in Arc-tool box of ArcMap 10.8 software.

2.4. Image classification and rubber tree cover map

To classify rubber tree cover, 07 land cover types were identified, including: natural forest, planted forest, mixed vegetation, and other vegetation (agricultural and shrub cover), which were numerically coded from 1 to 7. The 6,5,2 channel pseudo-color composite image

was used to create the decoding pattern layer. The training samples were mainly selected based on Google Earth images with images corresponding to the month of Landsat 8 OLI satellites and field surveys. Three 6,5,2 channels were used to create segments using the Segment Mean Shift tool in ArcGIS to group pixels that are adjacent to each other and have similar spectral characteristics. After that, the Training Sample Manager tool and the Select Segments tool in the Image Classification of Spatial Analyst were exploited to create sample regions. Sample regions were selected according to the reference of sample points collected from Google Earth images. Then, the Create Signature File tool was utilized to create a reflectance layer file for the corresponding decoding key samples. The reflectance class file of these key samples was used to classify images according to the Maximum Likelihood Classification algorithm in the Image Classification module of Spatial Analyst.

2.5. Accuracy evaluation

To evaluate the accuracy after image classification, the representative classes of the land covers were selected based on the Google Earth image scenes corresponding to the time of Landsat 8 OLI image collection. The procedure was like creating the training samples. For the classified images of May 2013; October 2013; April 2018; and July 2020, the total number of points used to evaluate the accuracy was respectively 84, 65, 66, 82 points. Particularly for the image of April 2018, the total number of points used to evaluate 7 object classes was 556 points. Because the province-wide data is too large, the scope of the study only tests the overall accuracy, the actual user accuracy, the interpretation accuracy, and the Kappa coefficient in 2017 by the error matrix through the Compute Confusion Matrix function in the Segmentation and Classification module. In the error matrix, there are the following indicators to evaluate classification accuracy including (Tsutsumida& Comber, 2015). Other years, classified images are evaluated by accuracy frequency between classified images and sampling points on Google Earth images based on the Frequency tool in the Arctool box of Arcmap. From there, the percentage of accuracy was calculated.

2.6. Building a model to support land use planning for rubber plantations based on GIS and remote sensing in typhoon-affected conditions in Quang Binh province

This study combined AHP and GIS methods based on expertise of local leaders and staff to construct some rubber-tree-plantation land use planning scenarios adapting to the impact of typhoons (Malczewski, 2006; Saaty, 2008; Ahmed et al., 2016; Akinci et al., 2013). However, ranking of criteria was not done by local experts, it was conducted by the estimation of damaged rubber tree scale based on the criteria identified by experts. It was similar to the crop suitability evaluation, but it determined non-suitable areas to plant rubber trees because of high risk of typhoon damage.

Step 1: Determine criteria to evaluate by local experts and create thematic layers: To come up with a planning adjustment method for rubber plantation areas, the criteria were discussed and consulted with two scientists studying rubber trees at Hue University of Agriculture and Forestry, 05 leaders at the Department of Agriculture and Rural Development in Quang Binh province, 02 technical staff of the Center for Agro-Forestry Planning in Quang Binh Province. Some criteria were also collected from the documents of the technical Procedures for Rubber Plantation of Ministry of Agriculture and Forestry, Vietnam. Based on expert opinions, this study selected 04 criteria, including elevation, slope, aspect, and distance to the coast, to identify areas that were not suitable for rubber trees because of high-risk tolerance under the impact of typhoons. Criteria layers were converted to shapefiles for use in the next step.

Step 2. Ranking the damage scale of rubber tree according to the four criteria: This study used the second layer of rubber trees damaged by Typhoon Wutip in 2013 to assess the damage levels of rubber trees based on the information layers. The damaged rubber tree cover in 2013 and the assessment criteria layer were superimposed through the Intersect tool in ArcGIS. Then, the Dissolve tool was exploited to combine the criteria classes and calculate the damaged area for the subclasses in the criteria, thereby calculating the percentage and ranking the influence of the subclasses in the criteria layers.

Step 3. Developing scenarios for adjusting rubber tree planting planning: To adjust the rubber tree planting planning, this study overlayed the 2018 rubber tree layer with the evaluation criteria layers by Intersect tool in ArcGIS to create land units according to the criteria. Then, the Selection tool with logical overlapping commands (And, Or...) was used to select the unsuitable land units to remove out of the 2018 rubber tree areas because of the greatest typhoon-induced damage level. After obtaining the planning adjustment scenario, the results were sent to experts of Department of Agriculture and Rural Development, Department of Natural Resources and Environment, and Center for Agro-Forestry Planning in Quang Binh province for comments and synthesis for adjustment.

Step 4. Editing the map of the adjustment method of rubber tree planning: After removing the unsuitable land units, the remaining rubber tree area was edited to include in the adjustment map layer for rubber tree planning.

3. RESULTS

3.1. Training sample evaluation

Table 1 show that the segment training samples have different combinational color values and the distribution among the channels is suitable. This distinction helps to classify land cover types quite well. In addition, the training samples are tested to calculate the scores of the samples. The mean score for all samples is 0.77, for the following samples: rubber tree (0.75); shrubs (0.63); bare soil (0.75); water (0.97); natural forest (0.71); and mixed vegetation (0.93). Thus, the training samples are used to classify images ensure good quality.

Table 1. Pixel value of composite images for segment samples

Land cover code	Land cover types	Pixel value of composite images		
		Red	Green	Blue
1	Rubber tree	165	245	122
2	Bare soil	255	127	127
3	Mixture (vegetative and residential)	0	92	230
4	Water	0	255	197
5	Natural forest	38	115	0
6	Production forest	85	255	0
7	Other plants (shrubs, short-term agricultural crops)	0	92	220

3.3. Accuracy assessment after classification

The results of the accuracy evaluation are as follows: the accuracy rate of May 2013 is 88.3%, October 2013 is 82.6%, and April 2018 is 88.3%, and July 2020 is 82.9%. For image classification as of 4/2018, the accuracy assessment is done by the error matrix through the Compute Confusion Matrix function in the Segmentation and Classification module. The evaluation results shown in Table 2 show that the overall accuracy is high, 84.4% and the Kappa coefficient is 0.69. This result shows that the interpretation results have high reliability (Tsutsumida et al., 2015).

Table 2. Confusion matrix assessment for image classification in April 2017

Land cover types	Rubber	Bare soil	Mixed vegetation	Water	Natural forest	Plantation forest	Shrubs	Total	User's accuracy
Rubber	91	2	15	0	0	0	11	119	76,5
Bare soil	0	60	1	0	0	0	1	62	96,8
Mixed vegetation	0	0	81	0	8	0	10	99	81,8
Water	0	0	0	18	0	0	0	18	100,0
Natural forest	0	0	0	0	50	0	1	51	98,0
Plantation forest	0	0	0	0	20	80	3	103	77,7
Shrubs	0	0	1	0	14	0	89	104	85,6
Total	91	62	98	18	92	80	115	469	
Producer's accuracy	100,0	96,8	82,6	100,0	54,4	100,0	77,4		
Overall accuracy =84,40%									
Kappa coefficient = 0,69									

3.4. Maps of rubber tree land cover

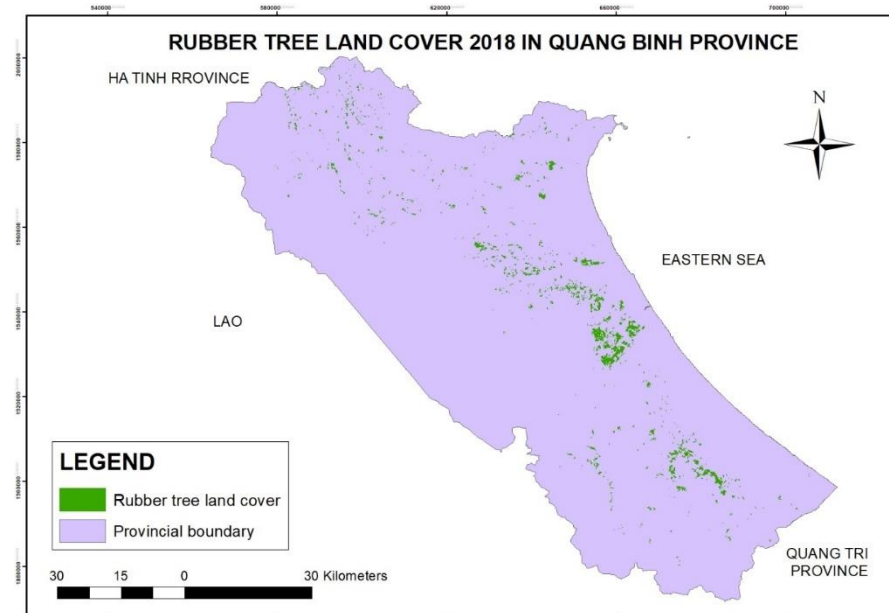


Figure 1. Rubber tree land cover in 2018, Quang Binh Province

Table 3. Changes of rubber tree land cover area in the period 2013-2020

Years	2013	2017	2018	2020	Change (+/-)		
					2013-2017	2017-2020	2013-2020
Rubber land cover area (ha)	17.654	13.084	13.407	9.776	-4570	-3308	-7878

Table 3 shows that the area of rubber trees decreases sharply in the period 2013-2020, by nearly 45%, an average of nearly 8% of the total area each year. In which, the period 2013-2017 and the period 2017-2020 reduces more than 25% of the total area.

3.5. Results of building a model to support land use planning for rubber trees based on GIS and remote sensing in the affected conditions of typhoons

3.5.1. Maps of criteria layers

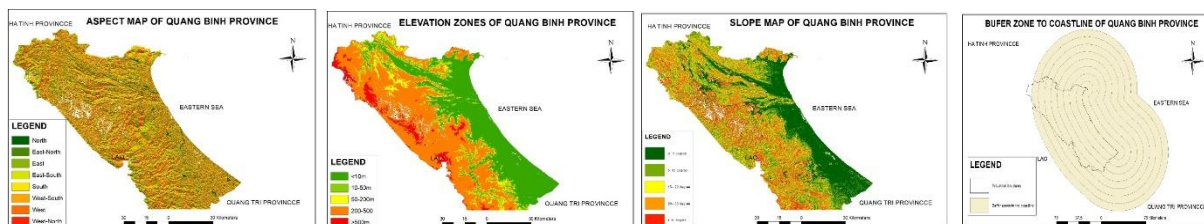


Figure 2. Maps of criteria layers: slope, aspect, elevation, and distance to coastline

3.5.2. Typhoon-induced rubber tree damage for each criterion

The land cover map layer for rubber plantations damaged by the 2013 Wutip typhoon and the attribute map layers including slope, elevation, slope direction and distance from the coastline were superimposed by the command Intersect to determine the area of damaged rubber trees according to the hierarchical information layers. The results are represented in Table 4,5,6 and 7 as follows:

Table 4. Damaged rubber areas according to elevation

Elevation zones (m)	Damaged area (ha)	Rate (%)	Ranking (1-4 from most severe damage to lowest)
<50	8296	86,3	1
50-200	262	2,7	3
200-500	1042	10,8	2
>500	10	0,1	4

Table 5. Damaged rubber areas according to slope

Slope (m)	Damaged area (ha)	Rate (%)	Ranking (1-6 from most severe damage to lowest)
<5	7407	77,1	1
5-15	1958	20,4	2
15-20	150	1,6	3
20-25	66	0,7	4
25-30	22	0,2	5
>30	6	0,1	6

Table 6. Damaged rubber areas according to the distance to the coastline

Distance to the coastline (m)	Damaged area (ha)	Rate (%)	Ranking (1-7 from most severe damage to lowest)
10	2472	25,7	2
20	5405	56,2	1
30	463	4,8	5
40	111	1,2	7
50	559	5,8	3
60	489	5,1	4
70	115	1,2	6

Table 7. Damaged rubber areas according to aspect

Aspect	Damaged area (ha)	Rate (%)	Ranking (1-8 from most severe damage to lowest)
Northeast	1371	14,3	1
East	1352	14,1	2
South	1294	13,5	3
Southeast	1285	13,4	4
North	1243	12,9	5
Northwest	1067	11,1	6
Southwest	1043	10,9	7
West	955	9,9	8

3.5.4. Rubber tree plantation planning: two scenarios

Scenario 1: Remove the land units with the largest and second affected rubber trees (levels 1 and 2): The total area removed from the rubber tree planting plan is 131ha. In the opinion of experts from the Department of Agriculture and Rural Development and the Department of Natural Resources and Environment of Quang Binh province, this option has the advantage of selecting the areas where are the most affected by storms to remove from the planning. However, the disadvantage is that the areas excluded from the planning have a small area, are not suitable for local needs and located in many scattered locations, so it is difficult to implement.

Scenario 2: Only remove land units in the area with a distance less than 10km from the coastline, the remaining areas will be remained in the planning scenario but add forest belts to block the wind: This option removes 1692ha of rubber plantations located within 10km of the coast. According to experts in planning of the Department of Agriculture and Rural Development and the Department of Natural Resources and Environment of Quang Binh province, this option has the advantage of being suitable for the reality of storm damage, the strongest wind and storm when entering the mainland. And the area to be removed from the planning is quite suitable to the needs of the locality. Therefore, option 2 is more feasible than option 1.

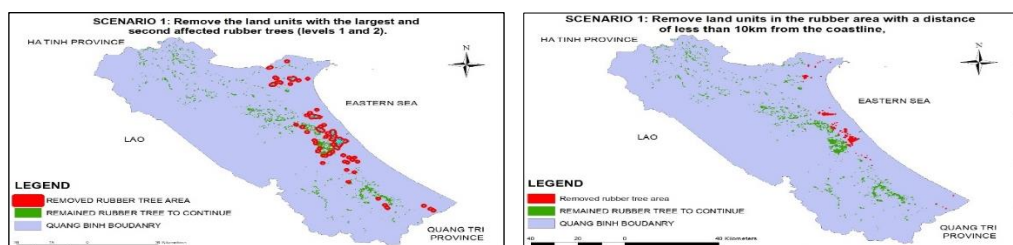


Figure 5. Two scenarios of rubber tree plantation planning

4. CONCLUSION

Landsat 8 OLI satellite images can be used to interpret, reclassify, and map rubber tree cover in Quang Binh province. The result of unsupervised and supervised classification combination in ArcGIS software based on Maximum Likelihood and Segmentation algorithms produced highly accurate results with an overall accuracy of 84,4% and the Kappa coefficient is 0,69. The area affected by the storm number 10 in 2013 was determined with a total damaged area of 9,612ha which is quite similar to the statistics of the Department of Agriculture and Rural Development of Quang Binh province, 9,091ha of damaged rubber area. There are 04 criteria selected to evaluate the impact of typhoon on rubber plantations, including slope, elevation, aspect, and distance from the coastline. Rubber trees were severely damaged in the land located in the distance 10-20km from the coast, the area with the elevation lower than 50m, the slope lower than 5°, and the aspect in the East and Northeast. Based on these criteria, two planning options are proposed for local reference.

5. REFERENCES

- Ahmed, G.B., Shariff, A.R.M., Balasundram, S.K. and bin Abdullah, A.F., 2016, June. Agriculture land suitability analysis evaluation based multi criteria and GIS approach. In *IOP Conference Series: Earth and Environmental Science* (Vol. 37, No. 1, p. 012044). IOP Publishing.
- Akıncı, H., Özalp, A.Y. and Turgut, B., 2013. Agricultural land use suitability analysis using GIS and AHP technique. *Computers and electronics in agriculture*, 97, pp.71-82.
- Department of Agriculture and Rural Development, 2019. Scheme on restructuring crops on inefficient rubber plantations in Quang Binh province in the period of 2019-2025.
- Department of Science and Technology of Quang Binh province. 2017. Proceedings of the Workshop on Solutions to improve the efficiency and sustainable development of rubber trees in Quang Binh province. Download at: <https://skhcn.quangbinh.gov.vn/3cms/ky-yeu-hoi-thao-giai-phap-nang-cao-hieu-qua-va-phat-trien-ben-vung-cay-cao-su-tren-dia-ban-tinh.htm>
- Malczewski, J., 2006. GIS-based multicriteria decision analysis: a survey of the literature. *International journal of geographical information science*, 20(7), pp.703-726.
- Nguyen Duc Ly, 2014. Solutions to improve efficiency and sustainable development of rubber trees in Quang Binh province, accessed on August 10, 2021 at <https://baoquangbinh.vn/khoa-hoc-cong-nghe/201403/cac-giai-phap-nang-cao-hieu-qua-va-phat-trien-ben-vung-cay-cao-su-tren-dia-ban-tinh-quang-binh-2113729/>
- Nhat Linh, 2017. Quang Binh: Damaged VND 7,800 billion after the storm, accessed on August 10, 2021 at <https://baotainguyenmoitruong.vn/quang-binh-thiet-hai-7-800-ty-dong-sau-bao-229668.html>
- Padwick, C. and Deskevich, M.P., 2014. Hyperspherical pan sharpening.
- Quang Binh Provincial People's Committee. (2019). Proposal of converting low-effective rubber plants in Quang Binh province for 2019-2025.
- Saaty, T.L., 2008. Decision making with the analytic hierarchy process. *International journal of services sciences*, 1(1), pp.83-98.
- Tsutsumida, N. and Comber, A.J., 2015. Measures of spatio-temporal accuracy for time series land cover data. *International Journal of Applied Earth Observation and Geoinformation*, 41, pp.46-55.

THE SURVEY OF VERTICAL TEMPERATURE DISTRIBUTION WITHIN SEA WATER COLUMN USING GEOINFORMATICS TECHNOLOGY, CASE STUDY: THE UPPER GULF OF THAILAND

Pongsakol Peatmak^{1,2}, Thaithaworn Lerdwithayaprasith³ and Suwisa Mahasandana^{1,2*}

¹ Department of Sanitary Engineering, Faculty of Public Health, Mahidol University, Thailand
Email: pongsakol_p@hotmail.com, suwisa.mah@mahidol.ac.th

² Center of Excellence on Environmental Health and Toxicology, Mahidol University, Thailand

³ Department of Marine Science, Faculty of Science, Chulalongkorn University, Thailand
Email: Thaithaworn.L@chula.ac.th
*corresponding author

ABSTRACT

Global warming and climate change are the current situation. This research focused on vertical temperature distribution within seawater column by using geoinformatics technology at the upper Gulf of Thailand. Sea temperature data were collected 2 seasons, wet season on 9-12 October 2019 and dry season on 8-11 March 2020. There were 20 sampling stations. The upper Gulf section maps of sea temperature distribution from both sampling presented similar heat distribution patterns which spread from the top to the bottom by the same highest temperature at around 12 A.M. – 4 P.M. The average of temperature difference, 9 A.M. – 5 P.M., between surface and bottom were 1.6°C in wet season and 1.2 °C in dry season while at low light time, 5 P.M.-9 A.M., were 0.01 °C and 0.4 °C respectively. From the linear correlation analysis, patterns of sea vertical temperature distribution from both samplings were correlated by the coefficient of determination (R^2) was 0.84. These sea temperature distribution patterns can be used for sea temperature prediction in the future for sea observation and monitoring.

Keywords: Vertical distribution, Sea temperature, The upper Gulf of Thailand (uGoT)

1. INTRODUCTION

At present, the warmer sea effected on every marine organisms' life including metabolic rate and population growth. Apart from marine organisms, the ecosystem also took damages from this situation such as coral bleaching. Moreover, the warmer sea affected the dissolved oxygen ability decreasing (Weis, 2015) that inversed with increase oxygen demand of marine organisms from their growth metabolic rates. For reducing damage and coping method preparation, the usual monitoring was routine necessary. Currently, geoinformatics technology was begun as an optional tool for better environmental monitor analysis. The tool could be used to presented better distributed pattern visualization and analysis.

Apart from marine environmental impact, the raised sea temperature also effects on marine agriculture. By the increased metabolic rate of marine organisms, marine parasites or pathogens gained this situation to outbreak (The UN Environment Programme World Conservation Monitoring Centre, 2009). In the same way, marine agriculture areas are affected by low oxygen conditions such as fishery, oyster farming etc. Higher sea temperature could reduce fish size 5% at each 1oC increasing (Forster, 2012). From above reasons, the economics of marine business was one of factors that was significantly affected.

The Upper Gulf of Thailand (uGoT) is the important area of Thais who takes several advantages including transportation, tourism, fishery, and marine agriculture. The uGoT had high diversity and resourcefulness because of various types of coastal zones, including beaches, marsh, rocky coasts, and coastal wetlands. Presently, the uGoT is affected by warmer sea especially coral reef where is marine larvae's habitat and important tourism site that influence economic directly. From above reason, this study focused on using geoinformatics technology to vertical investigation of temperature distribution within sea water column of the uGoT.

2. METHODOLOGY

The collections were assigned at the Upper Gulf of Thailand 2 times, wet season on October 9-12, 2019 (Oct) and dry season on March 8-11, 2020 (Mar). For covering all stations, the sampling spent 4 days per collection. The collection time was between 6 A.M – 6 P.M. The Buoy-data logger was floated approximately 40-45 minutes each station. The data logger, HOBO Pendant® Temp/Light,8K Part: UA-002-08, was set for temperature detecting every 5 minutes at all depth. The raw collected data was transferred to The Microsoft Excel files for correlation analysis between sea depth and temperature and was performed by line graph. The gathered data were analyzed by geographic information system (GIS) application using ArcGIS software and Ocean Data View (ODV), a free software, for mapping and vertical sea temperature distribution (Schlitzer and Reiner, 2021).

The Buoy-data logger preparation

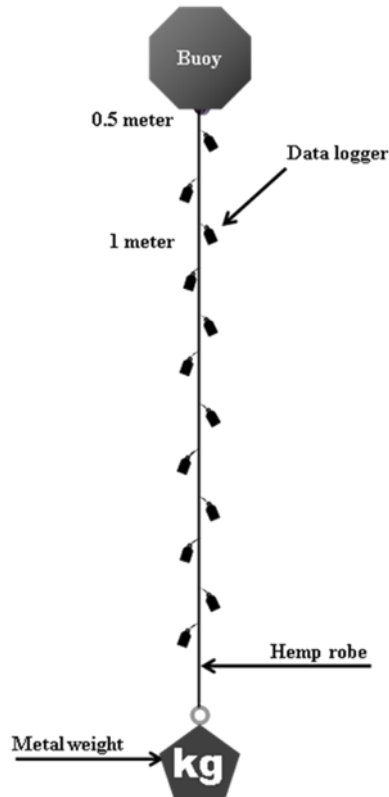


Figure 1. the model of the Buoy-data logger

- Prepared hemp rope 30 – 35 meters approximately.
- Fasten the data logger with the robe by cable tile or fishing line.
- Space between the data loggers was 1 meter each, except the first data logger at 0.5-meter, (Figure 1.)
- Adding metal weight at the end of robe for located the station to sea bottom.
- Binding the buoy at the top of the robe.

3. RESULTS AND DISCUSSION

3.1 Sea Temperature Profile

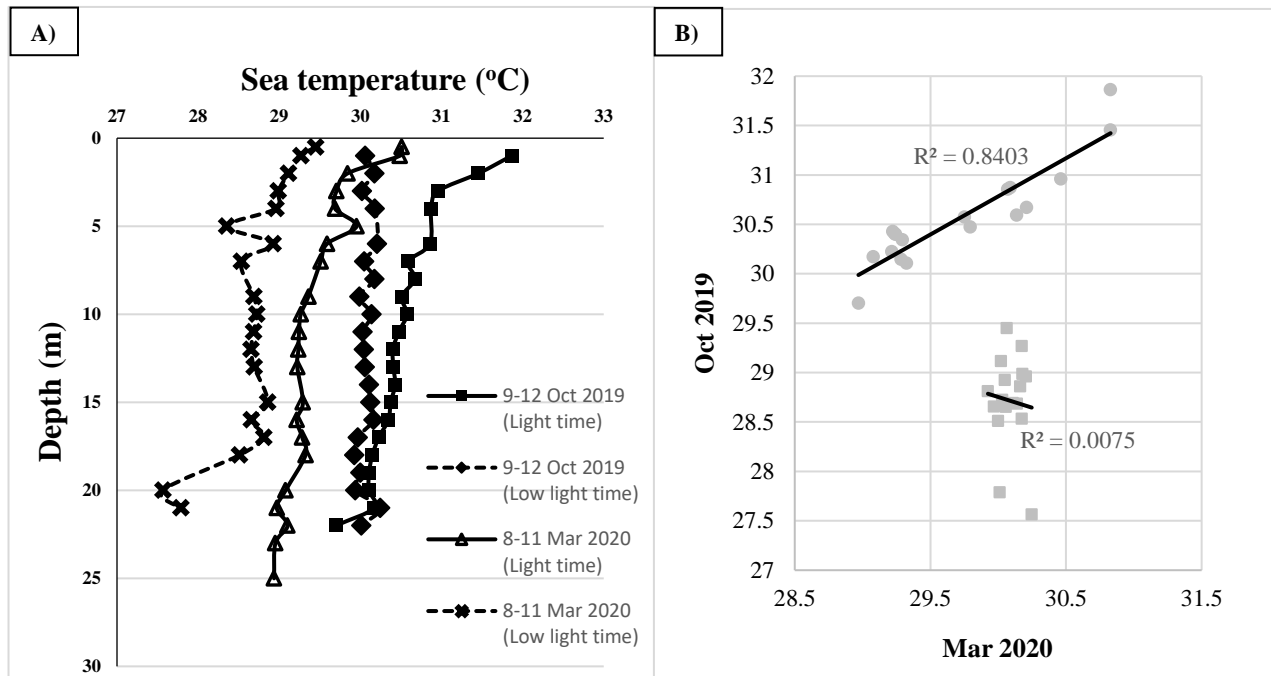


Figure 2. A shows the average of sea temperature profile of light time (around 9 A.M. – 5 P.M.) and low light time (around 5 P.M. – 9 A.M.) of the uGoT and B shows the linear correlation between the temperature of light time (●) and low light time (■)

The average sea surface temperature of 9-12 October 2019 and 8-11 March 2020 were 31.87°C and 30.51°C at light time while low light time were 30.06 and 29.45 respectively. The maximum of sea surface temperature of was 33.33 °C and 31.608 °C respectively at light time and 30.49 °C and 28.53 °C at low light time respectively. The minimum of sea surface temperature at light time was 30.26 and 28.12 while the low light time was 29.69 and 28.53 on 9-12 October 2019 and 8-11 March 2020 respectively. From surface to the bottom, the temperature will decrease apparently while both of seasons of temperature distribution at low light time were pretty stable because the sea surface was not affected by infrared rays from sun light directly as light time (Phongsathorn, 2019). Moreover, when comparing the average temperature of each depth follow by figure 2, the sea temperature profile of Oct 2019 and Mar 2020 are similar pattern because the linear correlation analysis (R^2) of light time between 2 profiles was 0.84 while the linear correlation of lightless time had no correlation, R^2 is 0.0075.

3.2 The section map of sea temperature distribution

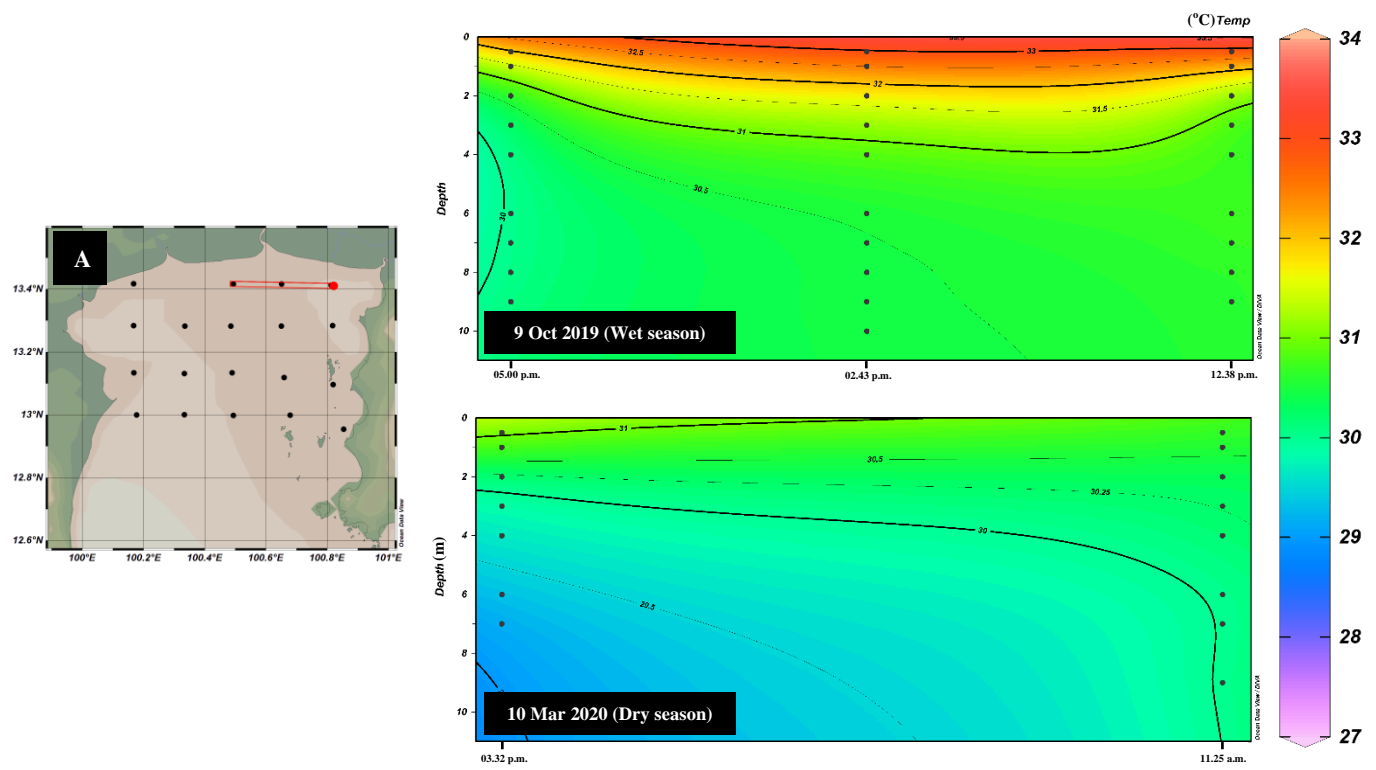


Figure 3. The selective section maps of wet and dry seasons and A is the selective stations

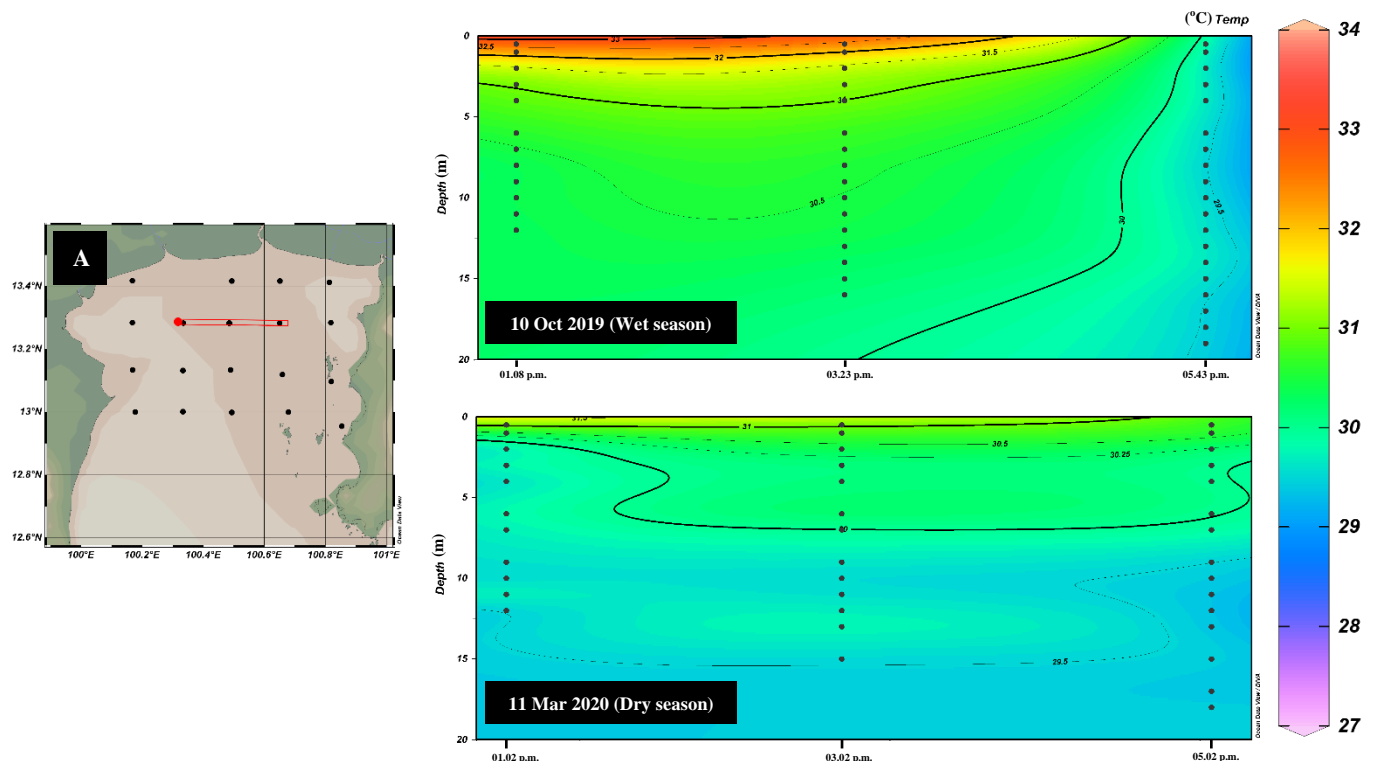


Figure 4. The selective section maps of wet and dry seasons and A is the selective stations

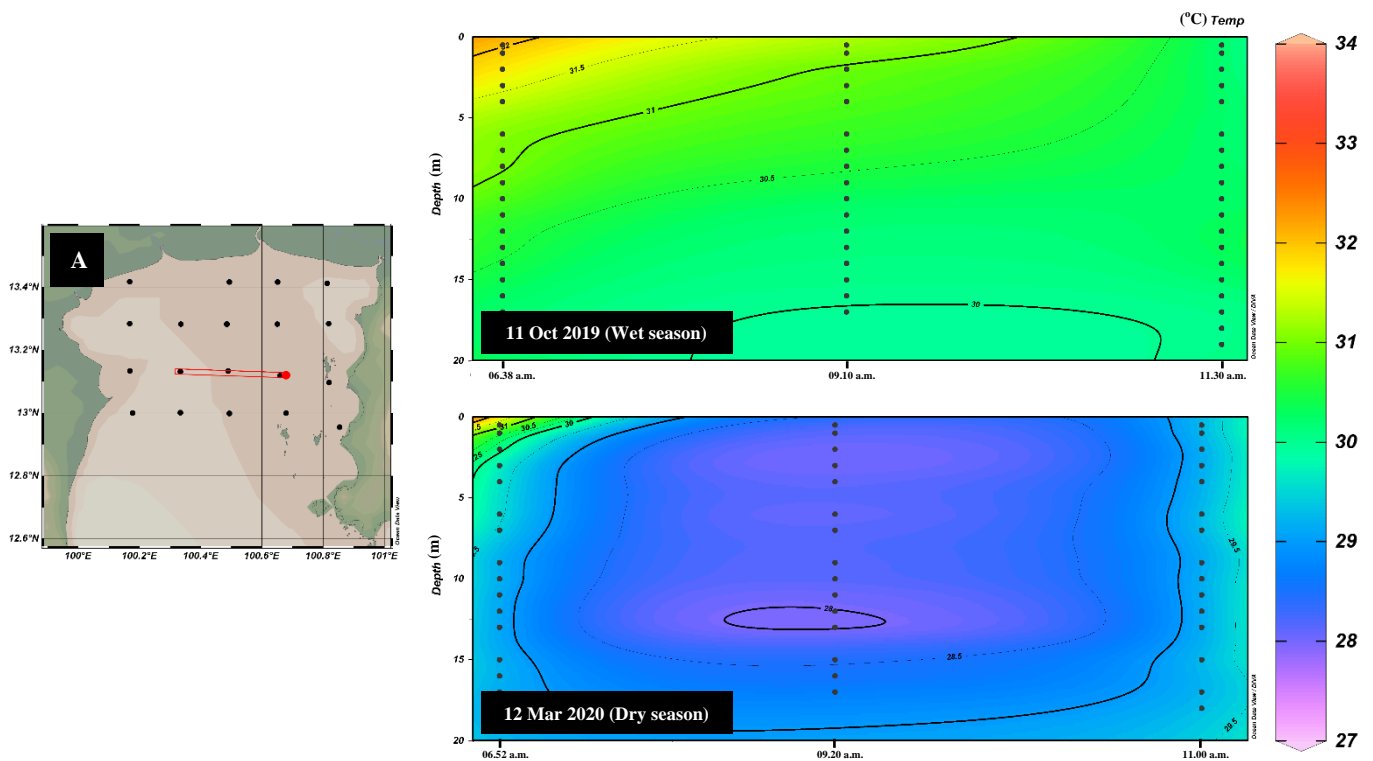


Figure 5. The selective section maps of wet and dry seasons and A is the selective stations

From the vertical temperature distribution maps which were developed from collected data within a day of both samplings (Oct 2019 and Mar 2020), the heat spread from the top to the bottom obviously. Light time collections between 9 A.M. – 5 P.M., sea water temperature raised at around 11 A.M. – 4 P.M. and cool down at low light time around 6 P.M. – 8 A.M. (Figure 3,4 and 5). Temperature difference between surface and bottom at the light time were 1.6°C (n=15) in wet season and 1.2°C (n=13) in dry season while the evening and the dawn, called low light time were 0.01°C (n=5) in wet season and 0.4°C (n=5) in dry season. The average of temperature difference of surface and bottom were 2.2°C in wet season and 1.6°C in dry season at light time. This temperature pattern results were correlated to the study of Thanyarat (2019) which gathered temperature data in 24 hours at Map Ta Phut coastal zone, Rayong Province, and found sea surface temperature had increased rapidly around 8 - 11 A.M. The highest sea surface temperature is approximately 11 A.M. – 1 P.M. and decreased slowly from the highest around 1 P.M. – 5 P.M. From Fig. 3-5, the temperature distribution was found higher temperature at the sea surface and decreased in the water column to bottom in every sampling station and both seasons. The average sea temperature of wet season was higher than dry season's both sea surface and within the water column.

4. CONCLUSION

1. The vertical distribution pattern of the light time (9 A.M.-5 P.M.) of Oct 2019 and Mar 2020 was similar by the linear correlation ($R^2 = 0.84$).
2. The sea surface temperature vertically distributed well at the time around 11 A.M. – 4 P.M. because the sea surface takes the heat directly from sunlight that affected the average of temperature difference of surface and bottom were 1.6°C in wet season and 1.2°C in dry season. After that, the sea temperature will cool down around 6 P.M. – 8 A.M.

3. The average sea temperature of wet season was higher than dry season's both sea surface and within the water column. The temperature was highest at sea surface at all sampling station and both seasons.

4. The sea temperature patterns might be furthermore studied to develop temperature forecasting models from the surface temperature that could be collaborated with remote survey technology such as satellite images for improvement sea temperature monitoring in the future.

5. ACKNOWLEDGEMENT

The authors were sincerely thankful to the department of marine science, Faculty of science, Chulalongkorn University, for vehicle support for temperature data collection at the Upper Gulf of Thailand. The Department of Sanitary Engineering, Faculty of Public Health, Mahidol University's advice and support is also appreciated.

6. REFERENCES

- Forster, J., Hirst, A., & Atkinson, D., 2012. Warming-induced reductions in body size are greater in aquatic than terrestrial species. *Proceedings of the National Academy of Sciences of the United States of America*, 109. doi:10.1073/pnas.1210460109
- Phongsatorn, E., 2019. *Temperature distribution model in the coastal water column: A case study of Map Ta Phut coastal zone, Rayong province*. Mahidol University, Bangkok, Thailand.
- Schlitzer, Reiner, 2021. Ocean Data View. Retrieved from: <https://odv.awi.de>.
- Thanyarat, A., 2019. *Sea surface temperature monitoring using satellite techniques: case study of Map Ta Phut coastal zone, Rayong province*. Mahidol University, Bangkok, Thailand.
- UNEP-WCMC. 2009. *Climate Change and Marine Diseases : The Socio - Economic Impact 2009* The United Nations Environment Programme World Conservation Monitoring Centre. Retrieved from: https://www.unep-wcmc.org/system/dataset_file_fields/files/000/000/125/original/Climate_Change_Marine_Diseases.pdf?1398683242.
- Weis, J. S., 2015. *Marine Pollution: What Everyone Needs to Know®*. New York: Oxford University Press.

APPLICATION OF KRIGING INTERPOLATION METHOD ON BUILDING THE DIGITAL ELEVATION MODELS FOR NINH KIEU AND CAI RANG DISTRICTS OF CAN THO CITY

Nguyen Thanh Ngan^{1,2}, Nguyen Hieu Trung³

¹Faculty of Environment, Ho Chi Minh City University of Natural Resources and Environment (HCMUNRE),
236B Le Van Sy Street, Ward 1, Tan Binh District, HCM City.

²College of Environment and Natural Resources, Can Tho University (CTU), Campus II, 3/2 Street, Xuan
Khanh Ward, Ninh Kieu District, Can Tho City.

Email: ntngan@hcmunre.edu.vn

³DRAGON Institute - Mekong, Can Tho University (CTU), Campus II, 3/2 Street, Xuan Khanh Ward, Ninh
Kieu District, Can Tho City.
Email: nhtrung@ctu.edu.vn

ABSTRACT

Ninh Kieu and Cai Rang are two urban districts established in 2004 of Can Tho City. These are thriving areas of the city and the Mekong Delta, with a long history of exploration and development. According to data from the Statistics Office of Can Tho City in 2019, Ninh Kieu District has an average population of 280,792 people and an area of 29.23 km², while Cai Rang District has an average population of 105,547 people and an area of 66.81 km². These two districts are currently facing major urban drainage challenges due to rapid urbanization. To address these challenges, it is necessary to develop a mathematical model for the urban drainage system in the study area, as a basis for providing appropriate solutions for drainage management. One of the important input data for the mathematical model building process is the digital elevation model. This paper initiates the preliminary results of building the digital elevation models based on Kriging interpolation method for Ninh Kieu and Cai Rang districts. This is also a useful data for drainage management and environmental management in the study area.

Keywords: digital elevation model, Kriging interpolation method, drainage management, Ninh Kieu District, Cai Rang District.

1. INTRODUCTION

Ninh Kieu and Cai Rang are two potential districts and also dynamic socio-economic centers of Can Tho City in the current period. These two districts were established in 2004 by the Government's Decree No. 05/2004/NĐ-CP (Vietnam Government, 2004). Due to the geographical position located in the right bank of the Hau River, these two districts have a system of rivers and canals that are greatly influenced by the tidal regime of this river (Can Tho City Department of Construction, 2016). Ninh Kieu and Cai Rang districts have a natural feature of low and flat terrain, so these two areas often experience heavy urban flooding (Can Tho City Department of Construction, 2016). Based on 2019 data, Ninh Kieu District has an average population of 280,792 people (133,911 men/146,881 women) and an area of 29.23 km², while Cai Rang District has an average population of 105,547 people (52,241 men/53,306 women) and an area of 66.81 km² (Can Tho City Statistics Office, 2020). The population densities of Ninh Kieu and Cai Rang districts in 2019 were 9,605 people/km² and 1,580 people/km² respectively (Can Tho City Statistics Office, 2020). Along with the socio-economic development, the urbanization process in these two urban districts has taken place at a fast pace and a complicated direction in recent years. This process has created major challenges for urban

management in these regions, among which is drainage management.

To address these challenges, managers in Ninh Kieu and Cai Rang districts need to apply new technologies to drainage management. One of the suitable solutions is to use urban stormwater modeling to solve the problems of urban drainage and flooding in these regions. This solution has been widely applied in many parts of the world and brought many practical and positive results in the field of drainage management (Montaseri *et al.*, 2015; Bisht *et al.*, 2016; Cipolla *et al.*, 2016; Chen *et al.*, 2017; Babaei *et al.*, 2018; Luan *et al.*, 2019; Macro *et al.*, 2019; Yazdi *et al.*, 2019.). To operate this mathematical model, one of the required input data types is the digital elevation model (DEM). This paper introduces the main results of building DEMs for Ninh Kieu and Cai Rang districts based on Kriging interpolation method (Goovaerts, 2019). Besides acting as an input data for the drainage mathematical model, DEMs are also a useful information for drainage management in particular and environmental management in general in the study area.

2. METHODS AND DATA

2.1 Research methods

Spatial interpolation method is used to generate DEMs for Ninh Kieu and Cai Rang districts. The interpolation algorithm used in this research is Kriging, also known as Gaussian process regression. Kriging is a type of spatial interpolation that estimates values at unsampled locations using a linear combination of measured values at nearby sampled locations (Goovaerts, 2019). The estimated result from the Kriging algorithm depends on three main factors: (1) the distance to the unsampled location, (2) the spatial arrangement of all sampled points, (3) the spatial correlation characteristics of the dataset (Goovaerts, 2019). The process of building DEMs for the study area is divided into five main stages: (1) collecting relevant data, (2) preprocessing digital map data, (3) interpolating point dataset to build DEMs, (4) correcting DEMs error with administrative boundary and hydrological network data, (5) evaluating results and drawing conclusions. The detailed implementation process of this research is shown in Figure 1.

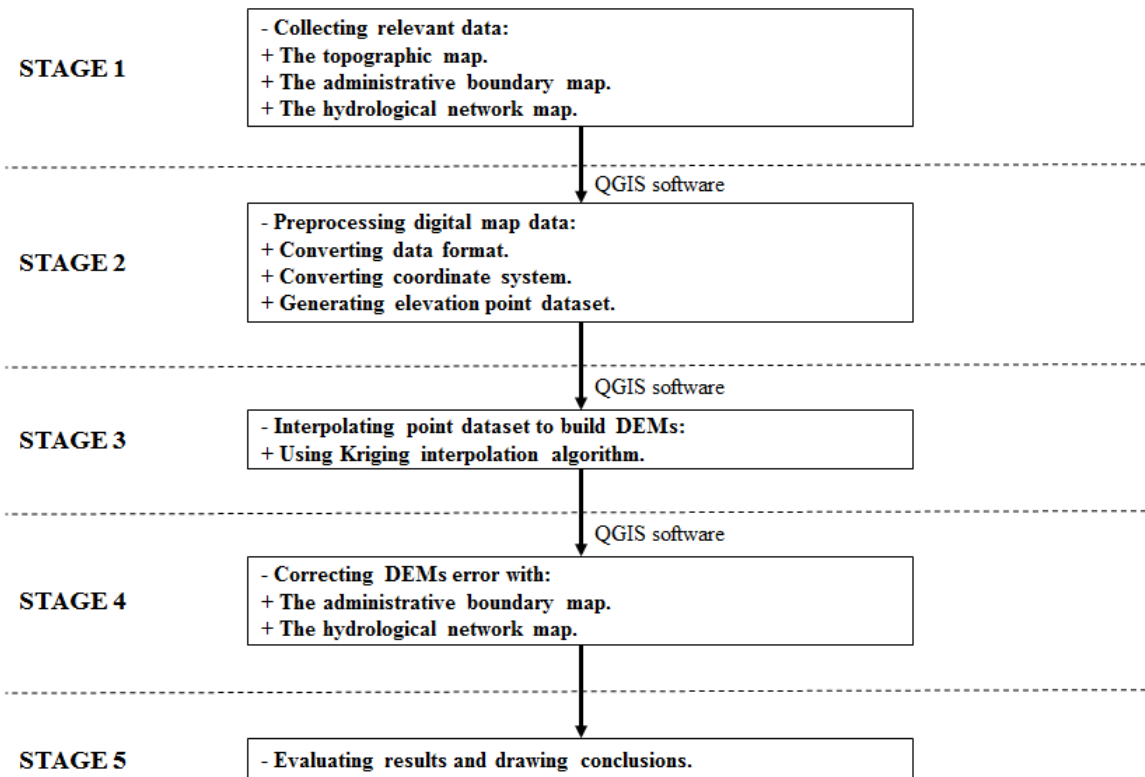


Figure 1. The detailed implementation process of the research.

2.2 Research data

The main data source used in this study is the digital maps of the two districts of Ninh Kieu and Cai Rang. The first type of digital map used is the topographic maps of the study area, which was collected from two main sources, the Mekong Delta Geographic Information Systems Project and the Can Tho City Department of Construction, in various formats. These topographic maps are reprocessed and converted into a uniform elevation point dataset in shapefile format. This elevation point dataset is the input data for spatial interpolation by Kriging algorithm to form DEMs using Quantum GIS (QGIS) software (Goovaerts, 2019). The second type of digital map used is the administrative boundary maps of the study area. These administrative boundary maps are used to define the spatial extent of the DEMs. The third type of digital map used is the hydrological network maps of the study area. These hydrological network maps are used to correct DEMs error by removing elevation values at water surface locations. Figure 2 depicts the administrative scope of the study area including Ninh Kieu and Cai Rang districts.

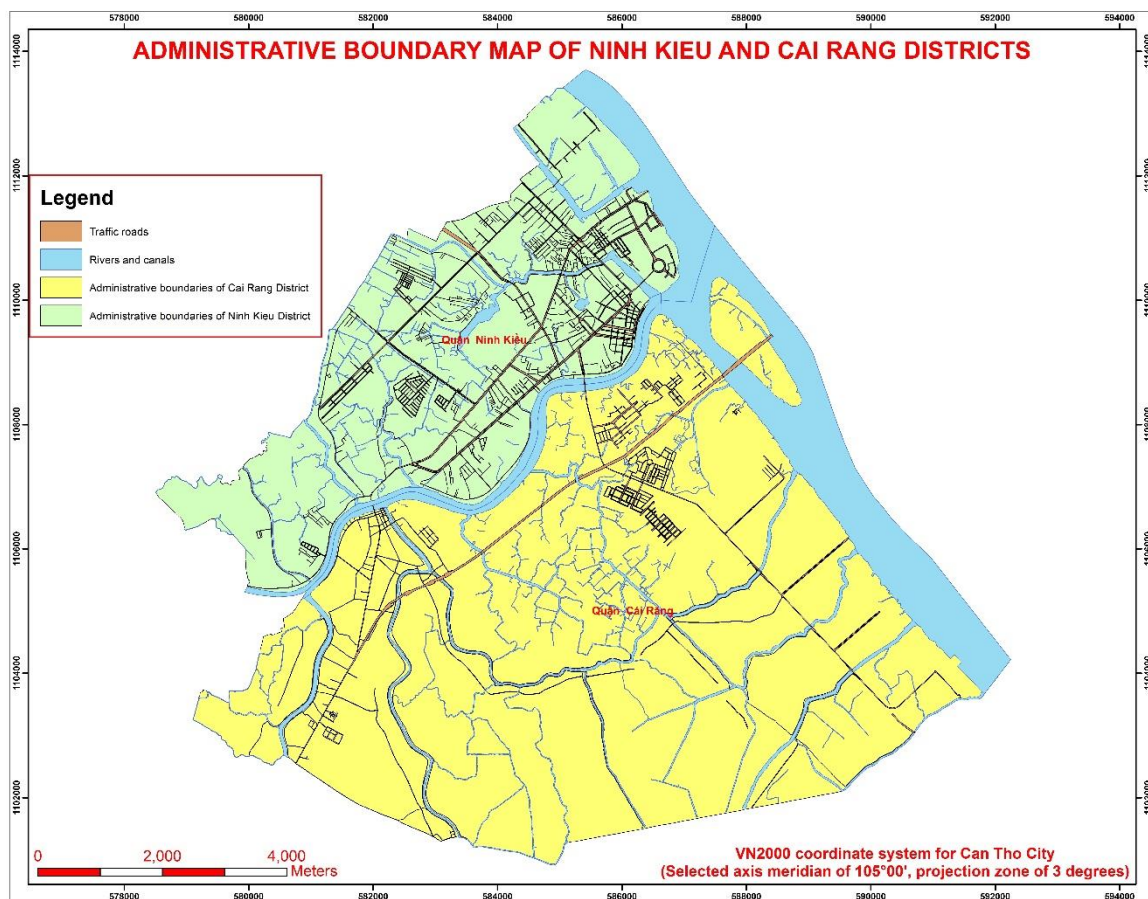


Figure 2. The administrative scope of the study area.

3. RESULTS AND DISCUSSION

In the first phase of the study, the topographic maps of Ninh Kieu and Cai Rang districts were collected from the Mekong Delta Geographic Information Systems Project and the Can Tho City Department of Construction in various formats. These topographic maps are reprocessed to the same format and geographic coordinate system, and then converted into an elevation point dataset. This elevation point dataset is the input data for the spatial interpolation process to create the DEMs on QGIS software. The SAGA toolkit operating on QGIS software is used to generate raster interpolated surfaces from the point dataset. The interpolation algorithm used in this process is Kriging. Location of elevation points in the study area is shown in Figure 3.

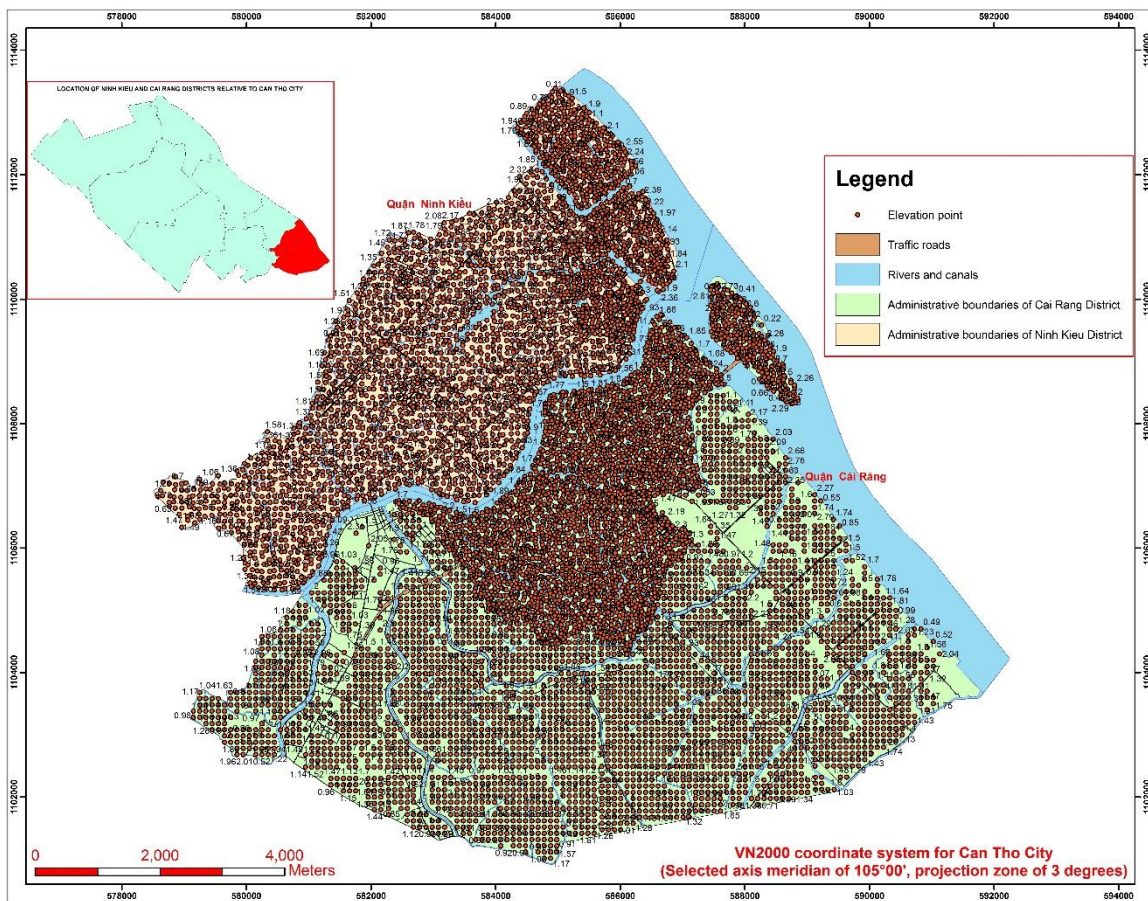


Figure 3. Elevation point locations in the study area.

After the spatial interpolation step, the generated DEMs are clipped based on administrative boundary vector data to remove the redundant parts that are outside the scope of the study area. The hydrological network data is converted from vector to raster using the Rasterize tool and then used to correct the clipped DEMs. This correction process removes the elevation values at the water surface grid cells on the clipped DEMs. The DEMs representing the topographical surface of the study area after correction are shown in Figure 4 and 5.

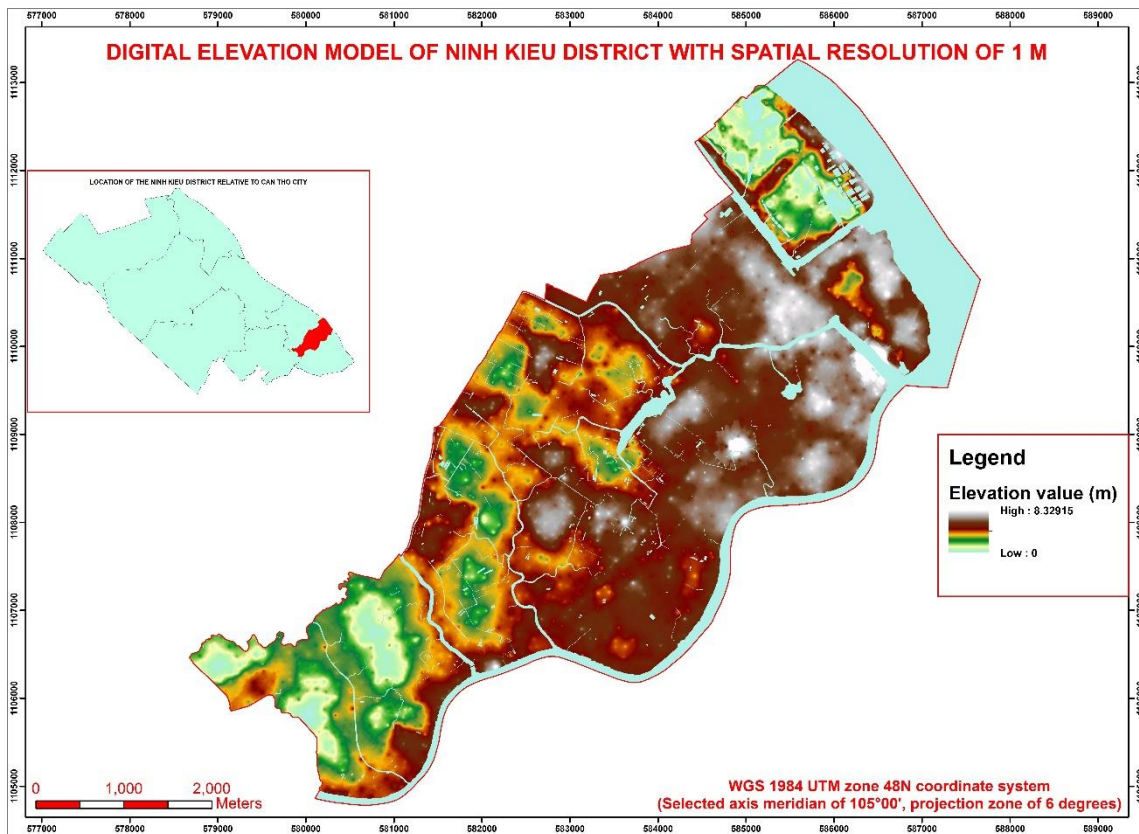


Figure 4. The digital elevation model of Ninh Kieu District.

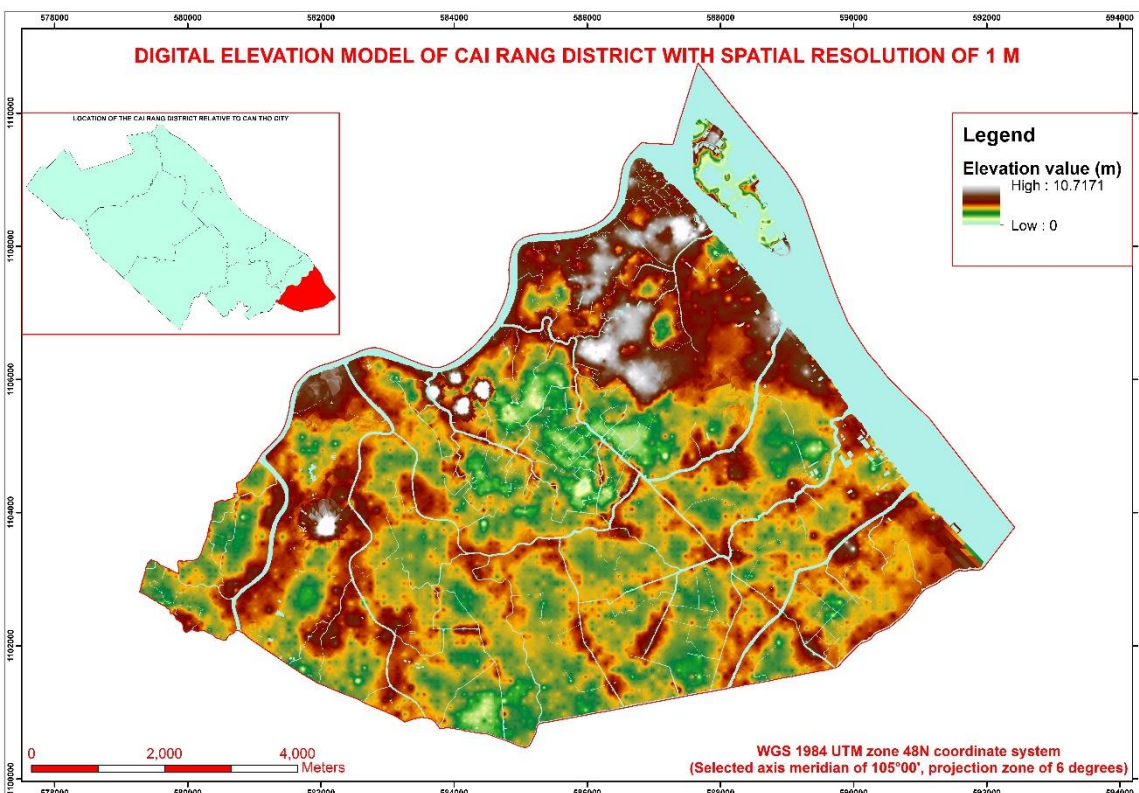


Figure 5. The digital elevation model of Cai Rang District.

The DEM created to represent the topographical surface of Ninh Kieu District has a total area of 29.06 km² with spatial resolution of 1.00 m, average elevation of 1.36 m, maximum elevation of 8.33 m and minimum elevation of 0.00 m. Meanwhile, the DEM created for Cai Rang District has a total area of 67.56 km² with spatial resolution of 1.00 m, average elevation of 1.15 m, maximum elevation of 10.72 m and minimum elevation of 0.00 m. Table 1 shows the basic statistics of the DEMs generated for the two districts of Ninh Kieu and Cai Rang.

Table 1. The basic statistics of the DEMs for Ninh Kieu and Cai Rang districts.

Statistics of the DEMs	Ninh Kieu District	Cai Rang District
Columns	8,986	13,147
Rows	8,476	10,285
Cells	29,063,042	67,557,805
Area Value	29.06 km²	67.56 km²
Spatial Resolution	1.00 m	1.00 m
Spatial Reference	WGS 1984 UTM zone 48N	WGS 1984 UTM zone 48N
Maximum Elevation Value	8.33 m	10.72 m
Minimum Elevation Value	0.00 m	0.00 m
Average Elevation Value	1.36 m	1.15 m
Standard Deviation	0.69 m	0.57 m

4. CONCLUSIONS AND RECOMMENDATIONS

The research has built DEMs for two districts of Ninh Kieu and Cai Rang from a dataset of elevation points in Shapefile format. These DEMs have a spatial resolution of 1.00 m, with a geographic coordinate system of WGS 1984 UTM zone 48N, built on the *.GIF raster format. The generated DEMs are input data for mathematical models used to simulate urban drainage systems in two districts of Ninh Kieu and Cai Rang. In addition, these DEMs are also a valuable reference source for environmental resource management in the study area. The future direction of the research is to use more elevation points to increase the accuracy of the DEMs.

5. ACKNOWLEDGMENTS

The authors would like to thank the ValBGI Project for sharing as well as supporting and introducing to collect data from the authorities of the Mekong Delta, the Mekong Delta Geographic Information Systems Project (MGIS) of Assoc. Prof. Dr. Le Van Trung for providing data support for this research.

6. REFERENCES

- Babaei, S., Ghazavi, R., Erfanian, M., 2018. Urban flood simulation and prioritization of critical urban sub-catchments using SWMM model and PROMETHEE II approach. *Physics and Chemistry of the Earth, Parts A/B/C*, 105, 3-11.
- Bisht, D. S., Chatterjee, C., Kalakoti, S., Upadhyay, P., Sahoo, M., Panda, A., 2016. Modeling urban floods and drainage using SWMM and MIKE URBAN: a case study. *Natural Hazards* 84(2), 749-776.
- Can Tho City Department of Construction, 2016. *Thuyết minh tổng hợp Quy hoạch thoát nước thành phố Cần Thơ đến năm 2030, tầm nhìn đến năm 2050: Chương 3 Hiện trạng thoát nước*. General explanation Can Tho City, III-2-III-53.
- Can Tho City Statistics Office, 2020. *Can Tho City Statistical Yearbook 2019*. Statistical Publishing House Publishing, Registration confirmation number: 2075-2020/CXBIPH/05-14/TK, 21-85.
- Chen, W., Huang, G., Zhang, H., 2017. Urban stormwater inundation simulation based on SWMM and diffusive overland-flow model. *Water science and technology*, 76(12), 3392-3403.
- Cipolla, S. S., Maglionico, M., Stojkov, I., 2016. A long-term hydrological modelling of an extensive green roof by means of SWMM. *Ecological Engineering* 95, 876-887.
- Goovaerts, P., 2019. *Kriging Interpolation*. The Geographic Information Science and Technology Body of Knowledge (4th Quarter 2019 Edition), John P. Wilson (ed.), DOI: 10.22224/gistbok/2019.4.4.
- Luan, B., Yin, R., Xu, P., Wang, X., Yang, X., Zhang, L., Tang, X., 2019. Evaluating Green Stormwater Infrastructure strategies efficiencies in a rapidly urbanizing catchment using SWMM-based TOPSIS. *Journal of Cleaner Production* 223, 680-691.
- Macro, K., Matott, L. S., Rabideau, A., Ghodsi, S. H., Zhu, Z., 2019. OSTRICH-SWMM: A new multi-objective optimization tool for green infrastructure planning with SWMM. *Environmental Modelling and Software* 113, 42-47.
- Montaseri, M., Afshar, M. H., Bozorg-Haddad, O., 2015. Development of simulation-optimization model (MUSIC-GA) for urban stormwater management. *Water resources management* 29(13), 4649-4665.
- Vietnam Government, 2004. *Decree on establishing Ninh Kieu, Binh Thuy, Cai Rang, O Mon, Phong Dien, Co Do, Vinh Thanh, Thot Not districts and communes, wards, towns of Can Tho City under the Central Government*. Number: 05/2004/NĐ-CP, 1-6.
- Yazdi, M. N., Ketabchi, M., Sample, D. J., Scott, D., Liao, H., 2019. An evaluation of HSPF and SWMM for simulating streamflow regimes in an urban watershed. *Environmental Modelling and Software* 118, 211-225.

IMPLEMENTATION OF WEB TECHNOLOGY FOR SMART FARMING MONITORING AND CONTROLLING USING IOT, BLYNK APP AND Nodemcu esp8622

Sittichai Choosumrong^{1*} and Natkamol Pinnok²

¹Department of Natural Resources and Environment, Faculty of Agriculture Nature Resources and Environment, Naresuan University, Phitsanulok Province, Thailand 65000

²Merakor Co., Ltd., Phitsanulok Province, Thailand 65000

* Corresponding author. E-mail: sittichaic@nu.ac.th.

ABSTRACT

At present, most of Thailand are engaged in agriculture. The major factor affecting plants is improper soil moisture content. Later innovations and technology were introduced to help in planning agriculture. The objective is to develop a real-time, low-cost sensor based data analysis system for measuring soil moisture spatially. To monitor the growth problems and increase plant yield through Internet of Things technology.

This paper presents about making farms smart and developed to help agriculture grow faster and safer. This paper expresses monitoring and controlling of parameters of the soil moisture. It contains controlling of solenoid valves using a blynk app with indication using NodeMCU ESP8266. The moisture sensors are strapped to the microcontroller. The Arduino software is used for getting the output of the sensors. These criterions are sensed by way of IoT to Blynk app. This Blynk app is used for controlling and monitoring the parameters of farms with different crops.

1. INTRODUCTION

Nowadays, most Thai people are farmers which is an important career for the economic system. According to the statistical data of Thai farmers from the Fiscal Policy Office, it reports that the area of Thailand is 320.6 million Rai, in 2018, 102.4 million Rai of forest, 149.2 million Rai of agriculture use, and 68.9 million Rai for other uses. It is obvious that most of the land of the country is used for agriculture. Later, there is a significant change of Thai traditional agriculture which depends on the weather. It became the era of Agriculture 4.0 in which changed from the traditional agriculture into agriculture integration with technologies and innovation to increase agricultural production. Technology and innovation are integrated into planting and management to control the process to achieve an accurate agriculture; for example, soil moisture sensor for planting environment data collection and to prepare for every condition. Since global climate change, farmers cannot predict any situations so the application of technology to increase production efficiency, reduce the long-term cost and errors from production by the farmers. It also increases the value and number of agricultural productions. Farmers can control everything through the internet which is the application of information technology for the most benefits of the users. There are also the uses of mobile tools such as smartphones or computer notebooks. They

become the major devices to access information through the internet. Therefore, IoT has a role to fill the gap between people of all ages and genders, for efficient and convenient work. It is easier to access the internet and use software.

This study aims to develop the data analysis from low-cost real time sensors to measure the areal soil moisture to monitoring the problems of growth and production by IoT. It can shorten the time and predict more accurately which can be monitored on a smartphone, so the information is quickly recognized, and the problems are in-time solved.

2. METHODOLOGY

2.1 Study Framework

The development of verifying and analyzing sensors from real-time sensors for integration of accurate agriculture consists of the following processes. The researcher studies and goes to the sample field to install the sensor of soil moisture with Wemos D1 R1 Bord. The sensor is installed in the sample field. The soil moisture values are transferred into the database phpPgAdmin. This sensor will transfer the moisture vale in the patterns of a website and an application.

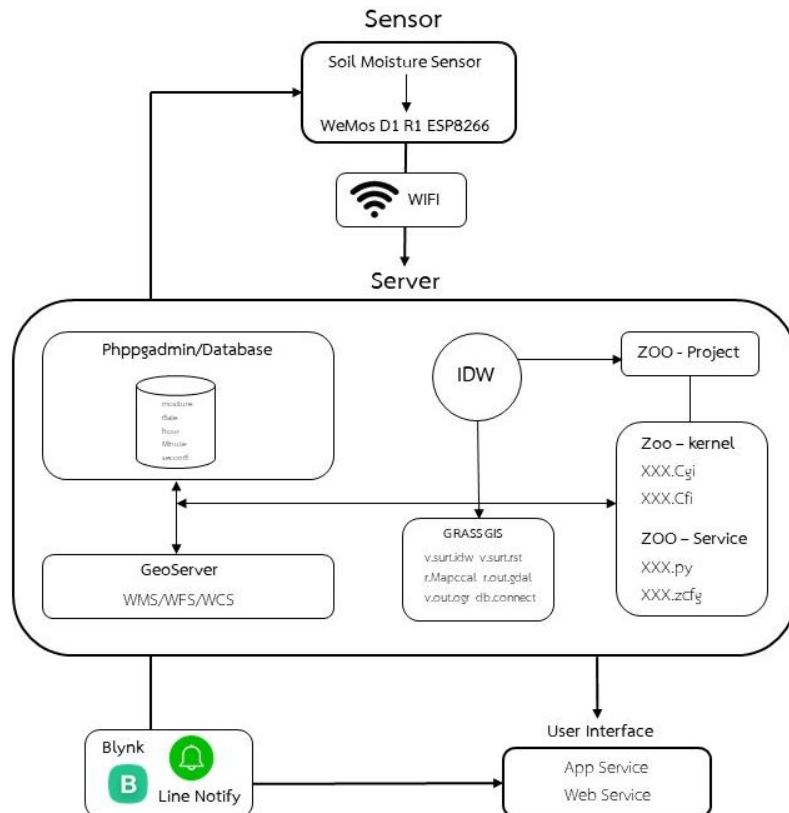


Figure 1. The designed framework.

2.2 System design and development

Figure 2 manifests the overall image of the moisture measuring sensor system by Wemos D1 R1 bord. This is the system that reports important physical factors of the plants. The result is in the pattern of relative humidity in which is transferred into the database. In addition, the sensor reports in the pattern of IDW in order to display on a website and an application real time, which displays images for the overall understanding.



Figure 2. The system overviews.

This development of the system employs Open-Source Software and Open Hardware. These programs are applied because Open Source is the effective and cheap program, as well as Open-Source software and Hard Software tools including Arduino IDE, PostgreSQL, LINE Notify, and Blynk App. he applied Open Hardware parts for developing the sensor are Wemos D1 R1 and Capacitive Soil Moisture Sensor Module.

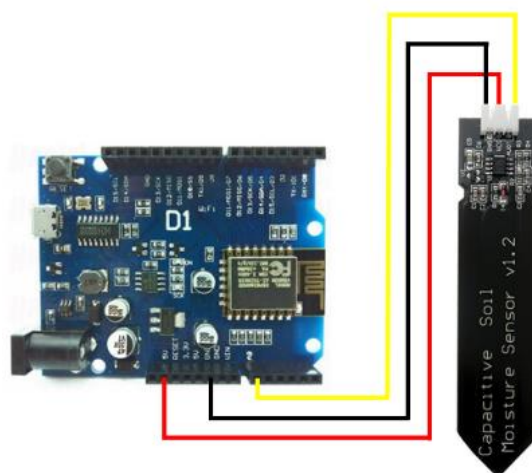


Figure 3. The soil moisture sensor with Wemos D1 board controller.

According to Figure 3 that shows the microcontroller connection WeMos D1 R1, the sensor displays relative humidity of the soil is adjoined with A0 leg, Ground, and 5V cable of the microcontroller WeMos D1 R1. The LED connection is also adjoined with Ground legs and thirteenth and fifth legs of the microcontroller. It is the serial communication.

3. RESULT

The set of sensor tools is a box with the boards inside. Its roles are to measure the properties or characteristics of any things around the target object, transfer the information from measurement into the process, and analyze the changes. This set of sensors can work with battery energy charged by solar energy.



Figure 4. The system experiment in the field.

For the monitoring and verifying systems via Web Service (Figure 5), it shows the values of the monitoring and verified soil moisture in the form of monitors and graphs. The system monitor the actual value of each sensor which displays real-time soil moisture.

The monitoring and verifying via Smartphone using Blynk Application are about monitoring and displaying the real-time sensor values like Web Service. The Blynk service includes a part of sensor monitoring and displaying in the forms of graph and monitor (Figure 6 a,b,c). For the test of LINE Notify, it is about to notify via LINE Notification in which the data are transferred as identified by the condition. The condition is set that if the soil moisture is lower than

10%, the sensor will notify the users. The information is from the sensor station and is notified of the soil moisture as condition indicated as shown in figure 6(d).



Figure 5. Real-time soil moisture monitoring dashboard based on Web Application



Figure 6. a-c is a Real-time soil moisture monitoring dashboard based on Blynk Application and (d) is LINE notify system

The real-time spatial data analysis for Smart Farming with IoT and Geographic Information System is about the measurement of soil relative moisture which continuously changes. According to the situation, there is an application of innovation. It is the process of WPS that is for data processing to develop the process on a website. ZOO-Project operation is employed for the Open-Source Software process. The results of the analysis manifest the density of the environment analyzed by GRASS GIS Software. The data of environment analysis by Inverse Distance Weight (IDW) presentation is shown in Figure 7.

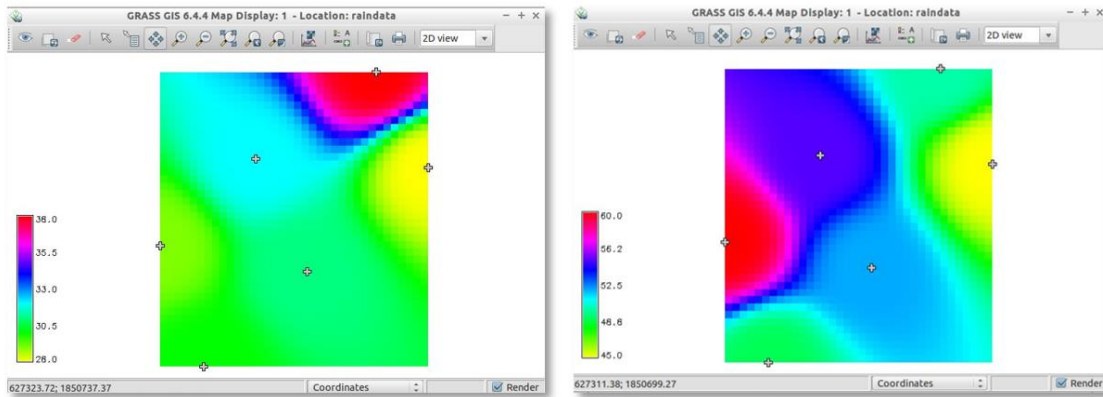


Figure 7. the real-time spatial data analysis using ZOO-WPS.

4. DISCUSSION AND CONCLUSION

This study is about the sensor system development by the application of IoT to measure the real-time soil moisture and to transfer the data to the host network. The objectives of this study are to develop the data analysis from a real-time sensor of soil moisture, to monitor the problems of growing, and to increase the production. In addition, the study improves notification and monitoring systems with Arduino IDE commands. When the sensor tool is connected to WIFI connection, the data of soil moisture are transferred to the database which are the real-time values on Web Service and Blynk App Service. The notification system will activate when the soil moisture is in LINE notify with the conditions. The operation of this soil property measurement tool records the data on the host network and calculates the Inverse Distance Weight (IDW) with ZOO - Platform, which is the Open-Source Software for spatial analysis. Moreover, the operation can manage and create WPS for cross-system processes. This set of sensor tools can actually monitor and check the soil properties real time as proposed, As a result, it is convenient, fast, and works better than general soil measurement machines so that it does not need to go to the area to collect data. This tool has higher accuracy than general measurement machines, therefore the farmers are less worried about the problems about the plants, and it increases the production efficiency.

5. REFERENCE

- Barbon, G., Margolis, M., Palumbo, F., Raimondi, F., & Weldon, N. (2016). Taking Arduino to the Internet of Things: the ASIP programming model. *Computer Communications*, 89, 128-140.
- Choosumrong, S., Raghavan, V. and Jeefoo, P. (2016) Development of the Real-Time Environment Monitoring System for Poultry Farm Based on IoT Technology, Proceedings of the International Conference on GeoInformatics for Spatial-Infrastructure Development in Earth & Allied Sciences (GIS-IDEAS), Hanoi, Vietnam, 12-15 November 2016.
- Choosumrong, S., Raghavan, V., Delucchi, L., Yoshida, D. and Vinayaraj, P. (2014) Implementation of Dynamic Routing as a Web Service for Emergency Routing Decision Planning, *International Journal of Geoinformatics*, Vol.10, No.2, pp.13-20 (ISSN 1686-6576)
- Shihong Wu, Kunlin Wu, Jian Liang, Zhengming Li and Ping Yang. (2011) Design of Remote Environment Control System of Intelligent Network Henhouse Based on ARM9. *Procedia Engineering*, Vol.15, pp.1056-1060.

ONLINE AND REAL-TIME ENVIRONMENT MONITORING SYSTEM USING ESP8266 AND WIRELESS SENSOR NETWORKS

Sittichai Choosumrong^{1*} and Krittapon Iamsaing²

¹Department of Natural Resources and Environment, Faculty of Agriculture Nature Resources and Environment,
Naresuan University, Phitsanulok Province, Thailand 65000

²Regional Center of Geo-Informatics and Space Technology, Lower Northern Region, Naresuan University,
Phitsanulok Province, Thailand 65000

* Corresponding author: E-mail: sittichaic@nu.ac.th.

ABSTRACT

According to the study, the major issue that effects on the field corn productivity in the planting period is found that most of the farmers do not measure the soil quality. In order to get the instant result, it is needed to have an experiment in a laboratory which takes at least 3-4 months to get the results. This is not a good option due to the fact that the soil quality. In the present day, there is an application of smart farm technology in agriculture to reduce that mentioned issue.

This research aims to develop a real-time soil quality measuring and notifying system. This study investigates users' problems and demands, analysis, and design of the model system software that is connected with temperature, humidity, and Potential of Hydrogen ion sensors, and the amount of nutrient in the soil. The measurement results will be transferred to the server and presented through a website in graphs and charts. The system also notifies the farmers through the LINE notification function within an appropriate environment. The developed system is based on a wireless sensor network (WSN), Internet of Things (IoT), and Free and Open Source Software for Geospatial (FOSS4G), which supports the increasing tools in the future. The result of the system performance is found at a good level. In addition, farmers can also access the model measurement tool at a reasonable price. It can reduce the cost of the model tool and adapt to other kinds of plants

1. INTRODUCTION

Nowadays, Internet of Things (IoT) has been applied to a lot of stuff all around the world, even to agriculture for the purpose of effective farm management and less human labor. This becomes the title Smart Farm in which employs RFID Sensors technology to connect agricultural tools so that they communicate with the main controller, for example weather station, soil sensor, plant disease sensor, yield monitoring sensor, etc. Those sensors can be set as wireless sensor network and set up in a field in order to collect data of soil humidity, temperature, light intensity, and chemical for the accurate problem solving.

Wireless Sensor Networks are the use of many small sensors to measure interested environment properties and to process the data for new knowledge about surroundings or automatic despondence to environmental surroundings. WSN is the integration between the embedded systems with wireless communication through node sensor in the platform of ad-hoc.

Mobile technology has been rapidly developed because of its benefits in several ways so that it has an important role for more convenient living. Therefore, consumers easily accept mobile technology as a part of daily life. In the present, the ability of smartphones is not only provide convenience, it also supports farmers to work more effectively by applying mobile technology with agricultural works; for example, agricultural planning system, agricultural farm problem management, and agricultural products follow-up. Geographic information technology is the integration of knowledge with Remote Sensing (RS), Geographic Information System (GIS), and Global Navigation Satellite System (GNSS), to apply with other tasks effectively. GIS is the important for many organizations to develop the country mission including agriculture, traffic and transportation, and natural disasters. The analysis results with information technology can be applied with decision-making planning accurately and fast.

Smart farming is the application of new technology with agricultural tasks to solve problems for farmers. It is in the concept of a modern farm called precision agriculture. The agricultural strategy is eco-friendly in which the farmers can adapt the resources to be mostly in accordance with area conditions, as well as to monitor effectively. This concept can be adapted with plant and animal farms. The smart farm differs from a general farm by its accurate resource usage for the needs of plants and animals. This decreases the resource loss and increases products based on the farmers' needs.

The purposes of this study are to develop the sensor system to verify the real-time soil properties in order to monitor and follow up the growth of corn in which is perhaps effected from the insufficient nutrient absorption, because the soil surface at the planting fields maybe too high or too low temperature and humidity.

2. METHEOLOGY

2.1 To investigate the problems and resolutions

The researcher investigates the problems of soil in the research field of Research Project of Growth and the Status of Nitrogen for applying fertilizers based on the potential of the corn production rate by Unmanned Aerial Vehicle (UAV), Tapho Sub-district, Muang District, Phitsanulok. This is to analyze the way and technical possibilities that solve the problems or demands as mentioned above. Then, the major question of the study is how to notify the farmers about the condition of soil in each spot in the cornfield conveniently and fast; and to identify the concepts and goals of the study framework, as well as necessary software and hardware tools for the model system development.

2.2 Microcontroller

The design of a measurement tool employs microcontroller model Wemos D1, which is an instant board including the connector between the board and other external tools. Even though there is a few connection ports, it can be used to connect with sensors sufficiently which is potential to evaluate data signal received from the sensor and to receive and send information through Esp8266 attached with the microcontroller. The Esp8266 is attached with Wi-Fi module so that is can connect with the network system to transfer information through protocol.

When the controller model Wemos D1 starts the work when the sensor system starts; this means that the system work begins. The sensor operates the serial port of each type of sensors that has been set up. When the sensor is active, it means that the sensor starts to read based on each sensor. The instruction is set that when the sensor reads the information, it will delay for 1 minute and then send to the database. On the other hand, if the sensor does not read the status of the soil, the process will be restarted. As a result, when it manifests that the temperature is higher than 25 degree Celsius, the system will notify through LINE Notify, and transfer the information to the database. This process is the acquisition of the 1-minute delayed information so that it will be transferred to the database.

2.3 The development of hardware system model

The model tool of system hard wear is designed to support the related sensors such as soil temperature measurement, soil humidity, soil's potential of Hydrogen ion (pH) sensor, and the amount of soil nutrients sensors. This depends on the budget of the farmers, for example farmers may needs to measure only the soil temperature so that it reduces the cost, as shown in Figure 1 showing the sensor model settings.

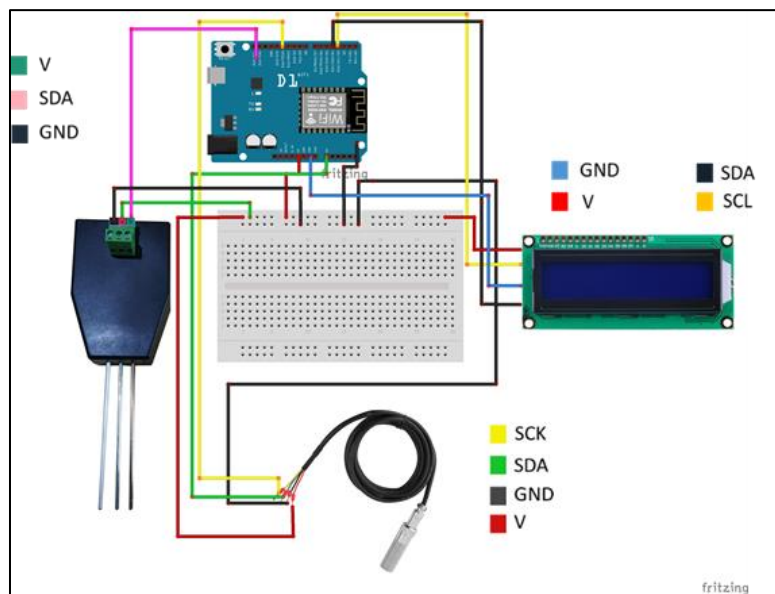


Figure 1. the sensor circuit connection

The energy resources used for the model tools can support solar energy. This study employs solar inverters to produce electric energy or solar cells. However, if the farms already have the electric providers, the tool can be applied with the house's electric energy through an electric transformer.

2.4 The development of Web Map Application

This study improves Web Map Application with Windows operation by applying Map Server for Windows (MS4W). MS4W is a free software designed to be applied with Map Server on Windows. In the past, users had to download and set up a lot of software, program by program, which resulted in difficulties. Therefore, there is the application of a software to work with Map Server together so that there will be no more difficulties, because the instant software helps the users work easier to create a web server even though they are not admins.

2.5 Mobile Application Development

The smartphone application with Android operation, version 8.0.0 with 17 level or above of API, has a major role to display and monitor sensor information from the soil measurement tool. That information include temperature, humidity, potential of Hydrogen ion (pH), and the amount of nutrient, in which are displayed in real time at the location of the tool.

2.6 LINE Notifications

This study set the notification to LINE application directly through Wemos D1 board because the board ship ESP8266 that can transfer information when connected to the internet. The soil temperature is already identified and when the temperature is higher than 25 degree Celsius, it will be notified via LINE application.

3. RESULE

3.1 Results of system experiment

The measurement of the soil sensor consists of temperature, humidity, potential of Hydrogen ion (pH), and the amount of soil nutrient sensors. The data can be continuously transferred. The settings must be deep at least 15 centimeter from the surface, which is the advice from the Agriculture Academician. For this study, the setting location should be

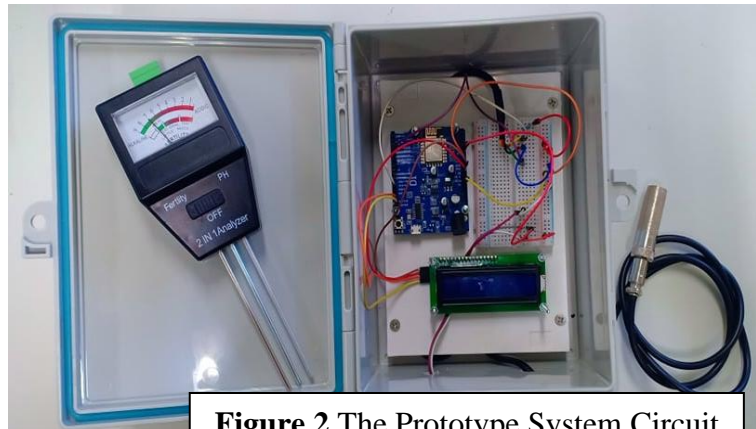


Figure 2 The Prototype System Circuit

around the corn tree but it does not have to be set on all the corn trees, where the sample location can be chosen. However, if it is in need of accuracy, more tools can be set up.

3.2 Results of application test

The pattern on Android operation can function with every section, including 1) user identification, 2) overall information from the measurement tool, 3) notification, and 4) graphs.

3.3 Results of Web Map Application test

When the data are transferred into the system, they are displayed on a parameter for sensor reading and graphs of measurement. The graphs include 2 characteristics, graphs for displaying each value of each sensor, graphs for displaying every sensor, and the 10-minute-back value.

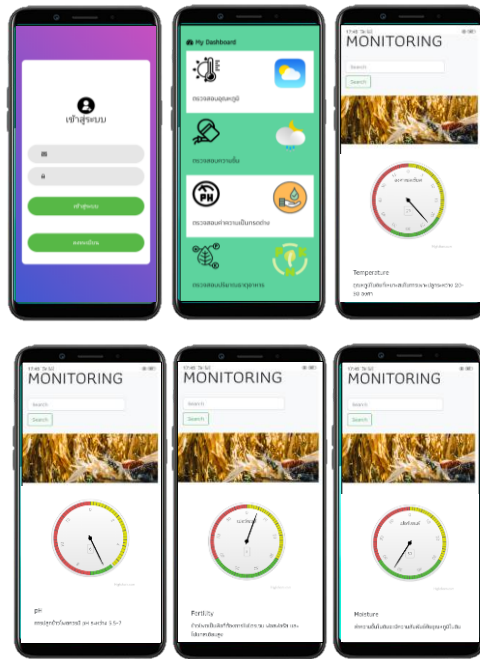


Figure 3. User interface for the mobile application.

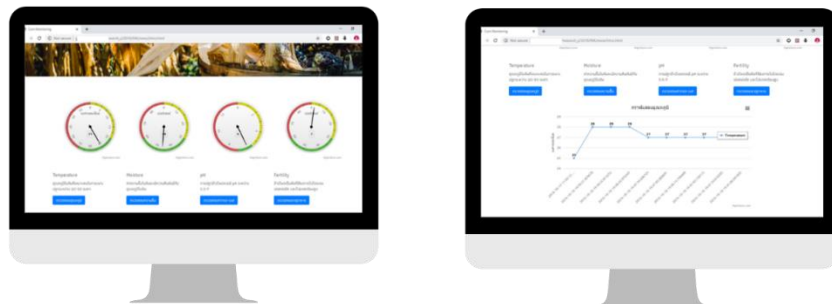


Figure 4 User interface for the Web Application.

3.4 Results of the expanses of the model measurement tools

Because the target of the researcher is a farmer, to apply the tools needs expenses as shown in Table. The basic system and sensor set are not more expensive than 1,600 baht. If the farmers already have their internet network transmitter and energy supplier, the price is acceptable. Moreover, only important sensors can be chosen, such as a temperature sensor, etc.

4. DISCUSSION AND CONCLUSION

From the purpose of the study to develop the real-time soil sensor system for monitoring the growth of corns, which may be affected from inappropriate nutrient, it reveals that the sensor actually works and can be tracked real time via both Web Application and Mobile Application. Furthermore, the system also notifies when the soil properties are not appropriate based on the conditions.

According to the development of soil properties measurement sensor tools, there is the usage of soil employing with Internet of Things to transfer information from the sensor and store as database through phpPgAdmin. Those mentioned development processes of soil properties tracking system are in accordance with the study of Pongpon N., et al (2021), which develops the soil monitoring and notification system in a durian farm and has a field study with minor group of farmers to solve the problems. The study investigates the problems and demands of the users, analyzes and designs the system, develops the model system in both integrated software with system database, and integrated hardware with potential of Hydrogen ion (pH), humidity, and soil and light intensity, as well as the system installation and technology transfer to the target groups. The study reveals that the model system installation that works well. Farmers can adjust the notifications of humidity and potential of Hydrogen ion (pH) as appropriate as the special equation directly through the application. The results of potential evaluation of the system and application users' satisfactions is scored 4.31 out of 5.00, which is ranked as Very Good. Furthermore, the minor group of farmers also access the model measurement tools with an acceptable price. In the future, the costs of the model tool will be reduced and can be integrated with the Smart Farming system with other kinds of plants.

5. REFERENCE

- Barbon, G., Margolis, M., Palumbo, F., Raimondi, F., & Weldin, N. (2016). Taking Arduino to the Internet of Things: the ASIP programming model. Computer Communications, 89, 128-140.
- Choosumrong, S., Raghavan, V., Jeefoo, P. and Vaddadi, N. (2016). Development of Service Oriented Web-GIS Platform for Monitoring and Evaluation using FOSS4G. International Journal of Geoinformatics, Vol. 12, No.3, 67-77.

DEVELOPMENT OF SMART LOCATION TRACKING SYSTEM BASED ON GPS GY-NEW-8M MODULE, RFID, AND ONLINE GIS TECHNOLOGY

Sittichai Choosumrong^{*} and Natima Udon

Department of Natural Resources and Environment, Faculty of Agriculture Nature Resources and Environment,
Naresuan University, Phitsanulok Province, Thailand 65000

* Corresponding author: E-mail: sittichaic@nu.ac.th.

ABSTRACT

The development of technology has increasingly sophisticated and has a positive influence on human life. The location tracking system that is currently overgrowing in the world of technology is required to be able to serve consumers until consumers can benefit from the technology. The case study of this research is to apply for a smart school bus tracking system. Not only has a location tracking system been developed but RFID technology also has developed.

This research has designed the school bus tracking system by creating work into 2 systems which are 1) GPS system and 2) RFID system. In which students will receive RFID tags via smart cards when students get on and off the shuttle bus, students must scan the card. Information on when and where the students board the car will be sent via the LINE application. On the guardians mobile phone via WiFi board to be used to verify that students have boarded the vehicle at the specified time and place safely. Then, designing a website for administrators (schools) and applications for general users (parents), while traveling to school, parents can track the location of the school bus where the location is installed. GPS through the application in real-time and the school will have a website to monitor the system, facilitate the management, and provide useful information about the students and the school bus. The mobile application prototype can increase the safety standards of students who are more likely to use school bus services in the future.

1. INTRODUCTION

Nowadays, the problem of traffic accidents is one of the problems that significantly cause lives and properties. Those accidents affect several groups of people; however the group that deeply affects the society every time it occurs is “the group of student”, especially “school-bus accidents”. School bus is one of the transportations of the students to schools. Some schools do not have many school buses while some other schools have almost a whole school that uses buses. The situation tends to be more school buses. There are several cases of school bus accidents; for example, a student falls from the bus along the way because there is no caretaker on the bus; or a kid is left in the car until dead. In all mentioned cases, the Department of Land Transport reiterates Provincial Transport Offices to verify safety and services of the school bus. It is identified that school buses must have complete control parts, registered rightly. This safety standard only relates to the vehicles and drivers, which only protect physically and does not cover the students' safety

or technical safety. Therefore, the researchers have an idea to improve the safety standard for students so that the parents can track their children's movement during the transportation with school buses via a mobile application.

It is currently obvious that sensor technology has been very popular for systems development, especially Smart City which will happen in the Thailand 4.0 era. Sensor technology has been continuously developed. One of the factors that significantly causes the progression includes the application of sensor technology. Furthermore, WiFi on smartphones is continuously improved with the ability to receive and transfer real-time data. The other important technology for the area is GIS or Geographic Information System, which is the currently used information technology for any tasks in a number of organizations in Thailand.

In conclusion, this study integrates sensor technology study, WiFi on smartphones technology study, and GIS study with IoT, Special Database Management, Web Map Application, and RFID. This study aims to improve the mobile application model of smart school-bus tracking systems in order to improve the safety standard to those students who go to school by school buses, and to parents' confidence to choose student-transportation service more than before.

The aim of this research is 1) to study and analyze the accident problems in case of school buses, and to analyze the standard of the vehicle's safety as indicated by the Department of Land Transport. 2) to develop the low-cost sensor for real-time tracking and notifying the vehicle's and children's status, e.g. going school and going back home, and to design an application model for tracking school buses via Internet GIS and Web Map Application. And 3) to develop the low-cost sensor for real-time tracking and notifying the vehicle's and children's status, e.g. going school and going back home, and to design an application model for tracking school buses via Internet GIS and Web Map Application.

2. METHODOLOGY

2.1 Study Area

The research chooses the area around Naresuan University, Phitsanulok Province, or surroundings to test the mobile application model for smart school-bus tracking. It is proposed to examine the performance of the mobile application model for smart school-bus tracking, in order to improve the safety for students with IoT, RFID, and Open Source Software.

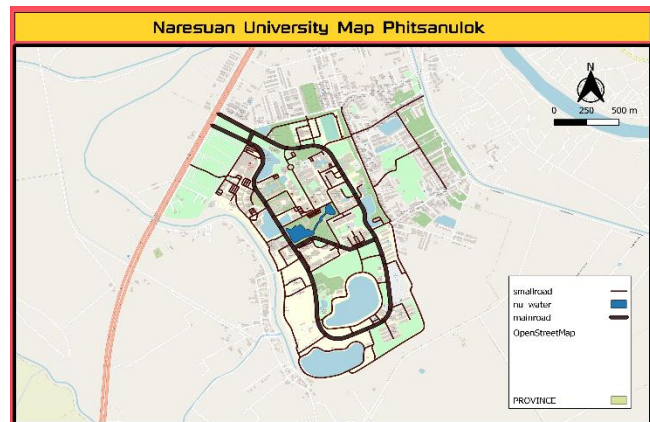


Figure 1. Naresuan University Map Phitsanulok Province.

2.2 Data

The data include cases of school bus accidents during 2015 - 2017, GPS data, and students' data.

2.2.1 School-bus accidents data management occurred during 2015 - 2017.

The data of accident cases are collected by each identified year, and then are analyzed to be statistical data. According to the data collection, there were 17 cases of accident, 212 cases of injury, and 7 cases of death in 2015. There was no case of accident in 2016 while cases of injury are 386 and cases of death are 7. In 2017, there were zero cases of accidents, 386 cases of injury, and seven cases of death. Comparing between 2015 and 2016, even though the cases of death reduces, the cases of injury increases. Types of the vehicle that cause accidents are pick-up trucks, followed by vans, buses, and trucks (AIP, 2018).

2.2.2 GPS data management

The GPS data are collected to create a database on phppgadmin, which the GPS data are from the sensor (Ublox Neo M8N). The sensor collects the data of latitude, longitude, and speed; and transfers these data to display on the real-time map and graph of the website speed and application on Leaflet map. The map displays an icon of a vehicle to represent the vehicle's location. When the icon color is blue, it means that the vehicle is moving. On the other hand, when the icon color is red, it means the vehicle is parked.



Figure 2. The map displays an icon of a vehicle and data from Sensor.

2.2.3 RFID data management

RFID is designed only as a model in which responses are just one set of data. These data are a lot related to the GPS information, they are only the designed system for message conveying when the students scan their cards. It starts with the examination of RFID cards for each card's code. After the examination, the result comes with UID values and completed code, then the conditions commands are input so that RFID can scan the cards. If the card is scanned one time, it will notify the parents that the students are online; while two times scanning means they are offline.

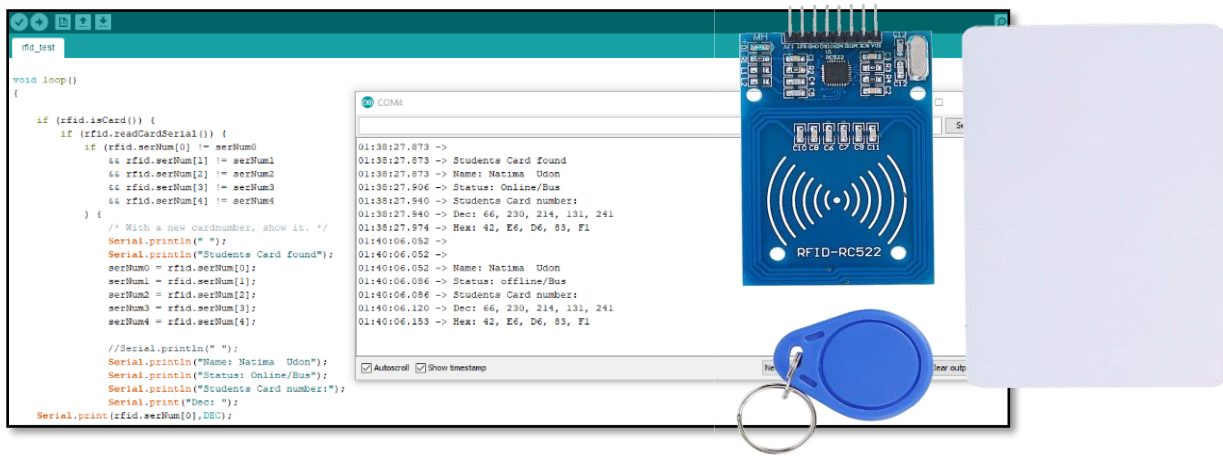


Figure 3. Code+Serial Moniter skewed from RFID terms.

2.3 Data management

The data of accident cases in Thailand during 2013 - 2018 are analyzed into statistical data in order to summarize the students' death rate from school bus accidents. The data are proposed to compare with the safety standard of school buses indicated by the Department of Land Transport, that whether the accident cases are less or not.

2.4 Research process and data analysis

First, the data about school-bus accident cases in Thailand during 2013 - 2018 are collected. Including i) the safety standard data for school buses are identified by the Department of Land Transport and ii) the school-bus accident cases during 2013 - 2018 are analyzed into statistical data. The safety standards for school buses as identified by the Department of Land Transport are analyzed whether there are errors or it reduces the accidents or not, comparing to the number of accident cases before indicating the safety standard. The tools information is collected for the development of both RFID and GPS Tracking sensors. Databases are designed and developed for creating an application and website for 3 groups of users: schools, school buses, and parents. Both RFID, GPS tracking and SMS Message systems tools are tested and installed in a school bus to check the sensor's working system. An application to display information through a smartphone

and computer are designed. The system is installed on the model vehicle and tested its working system with the mobile application, School-bus smart tracking system, within Naresuan University in order to investigate the errors. The infographic is created in order to present the mobile application about School-bus tracking system model information.

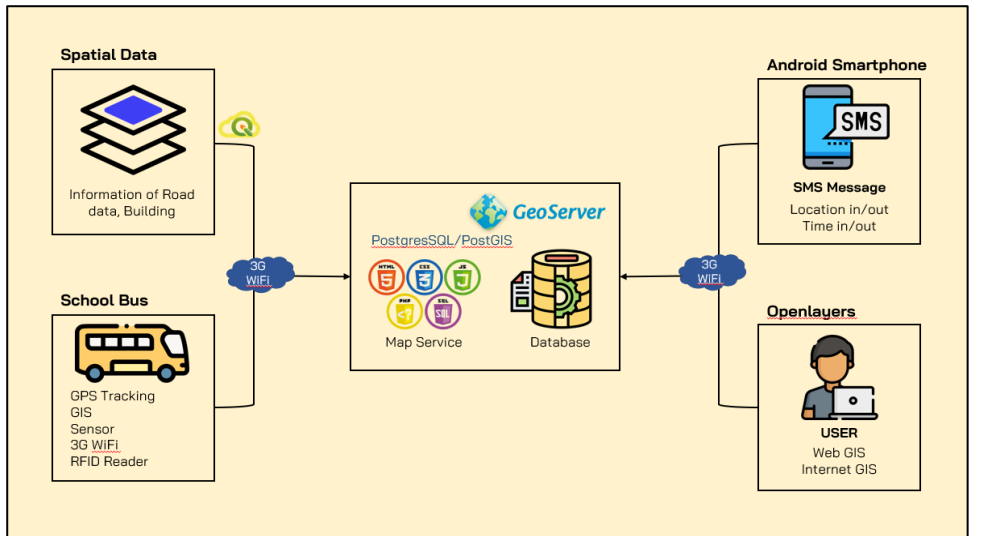


Figure 4. Conceptual Framework.

3. RESULT

According to the study, it becomes the “model of smart school-bus tracking system on a mobile application for the students’ safety, with the technologies of IoT, RFID, and Open Source Software”. The results from the development of GPS tracking in conveying the real-time current location and displaying the location information on a map to test for the location and GPS deviation are revealed as follows.



Figure 5. RFID Viewing Alert System.

The result of the RFID test reveals that it is the model system that is tested with only one user. When the system is activated (all systems are active when the vehicle is started), the system will send a message to the parents' LINE application immediately. If the students scan their cards the first time, the system will send the message that their children already get on the bus; whereas if the cards are scanned for the second time, the message sent is that the students already get out of the bus.

The students' data controlling website for the admins

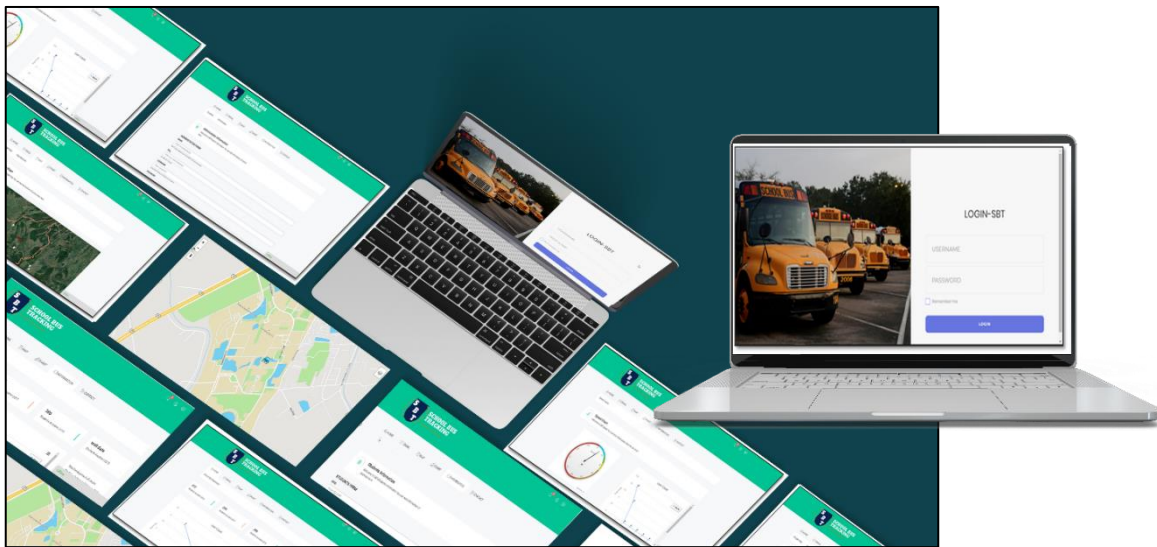


Figure 6. website for the admins.

The website is designed only for the admins, which they have to login and register through this website.

Web application for general users

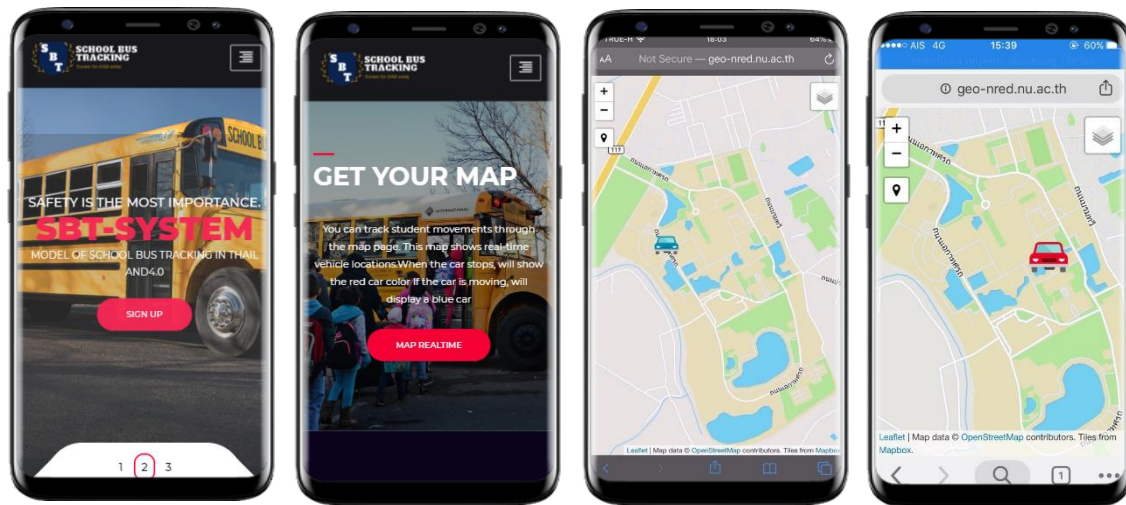


Figure 7. Interface Of Web Application for general users.

This web application is designed for the users to know the real-time location as well as the real-time speed. This application is just a model application.

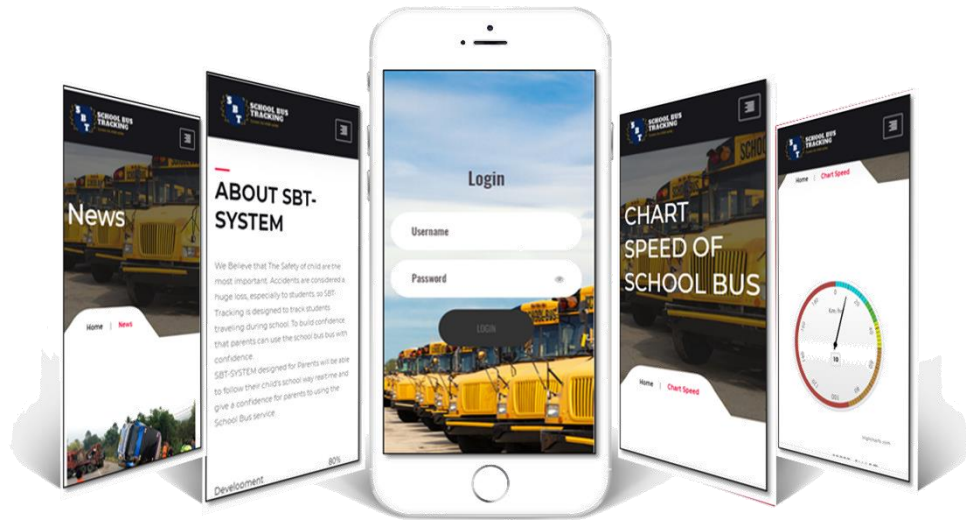


Figure 8. Web Application for general users.

4. DISCUSSION AND CONCLUSION

The development of a smart school-bus tracking system on application model for the safety of the students with the technologies of IoT, RFID, and Open Source Software is proposed to improve the system of GPS tracking to be able to convey the driver's real-time location data to the server. The notification system is developed by writing codes through Arduino IDE to be able to notify on the user LINE application. When the vehicle starts, all systems are working, and the RFID will send the message to the parents LINE application that the system is online. While the vehicles are moving, the GPS sensor will send the data into the database every five minutes and display the location on Leaflet Map real time. When the vehicle is moving, the icon color is blue; while the red icon means that it is stopped. The parents can check whether the vehicle is moving or stopped, where it is parked. In case the students get on the bus, they scan the RFID card before getting on, so the system will send a message to the parents' LINE application that the students are online. In the meantime, when the students are getting out of the bus, they will scan the card again and the system will send a message that the students are offline. For the website and application, this smart school-bus tracking system has been designed in the patterns of both website for the admins and application for the users. SBT-Website for the admins include real-time map, real-time speed standard, register page for admins, register page for students, and contact information. The users of this website must be those who already registered into the system. SBT-Application for general

users includes real-time map, real-time speed standard, and general information. The application works only with Android operation.

This system development applies the knowledge and understanding from document students and related studies. The researcher investigates and collects the data from school-bus accident cases to analyze the statistics and create the solutions by creating Smart school-bus tracking system model. This system design and development employs major languages including Javascript, php, and html; and retrieves the data from server to display on the leaflet map via PostgreSQL/PostGIS as the major program to manage databases to analyze data with SQL language. When the current location of the driver is developed by GPS Tracking system as well as the notification of the student's card scanning via Arduino IDE is improved, this system can be improved in the real server. According to the experiment of the system in the real route by driving around the university and activating a notification system, it reveals that the system can notify with sound when going into a risk area. The system stops notifying when going out of that risk area. In conclusion, this system can be developed and applied with other routes.

5. REFERENCE

- Bhor, M., Kadam, N., Shinde, D., & Mane, P. (2017). Children Safety and School Bus Tracking Solution. *International Journal of Electrical, Electronics and Computer Systems*, 5(1), 19-22.
- Klaus Finkenzeller, "RFID Handbook: Fundamentals and Applications in Contactless Smart Cards and Identification", John Wiley & Sons, 2003
- KUMAR, D. M., KONDURU, A. K., & GAIKWAD, N. (2016). School Children Transportation and Safety Enhancement System Based On RFID.
- Panchal, N. (2016). Track Anything and Using Analytics to Improve Performance (Doctoral dissertation, School of Engineering and Applied Science, Ahmedabad University).
- Quilatan, A. M., Sarin, J. I. D., & Sumagaysay, Z. T. (2015). Bus tracking and monitoring system for public transport terminals (Doctoral dissertation, De La Salle University-Dasmarinas).
- Shaaban, K., Bekkali, A., Hamida, E. B., & Kadri, A. (2013). Smart Tracking system for school buses using passive RFID technology to enhance child safety. *Journal of Traffic and Logistics Engineering*, 2(1), 196-191.

Isarithm Mapping of Pandemic Covid-19 Significant Area with Kriging Surface and Semi-Variance Analysis

Chaiwiwat Vansarochana¹ and Kankanit Pisamayarom¹

¹Faculty of Agriculture Natural Resources and Environment, Naresuan University
Naresuan University, Phitsanulok 65000, Thailand
Email: ChaiwiwatV@nu.ac.th; ChaiwiwatV@Gmail.com

ABSTRACT

Isarithm mapping shows statistical data aggregated over predefined regions. Pandemic Covid-19 situations can be represented as isarithm maps, depending on interpolation surface techniques. Kriging is the probabilistic interpolation surface that estimates semi-variance between pairs of data points over a range of distances. This study indicates a variance map of Thailand Covid-19 spreading, which gives any measure of uncertainty in the interpolated values and also being the example of estimation map for the pandemic significant area. Absolutely results are described.

Keywords: Isarithm mapping, Covid-19, Probabilistic interpolation, Semi-variance

1. INTRODUCTION

Currently, the world is in a situation of the covid-19 epidemic. Thailand, which is an important country in Southeast Asia was greatly affected by this epidemic disease. In the field of geospatial and cartography, we can present this epidemic in several ways. As an explorer and cartographer, therefore, I have applied the isarithm map method to be used with the geographic information program. To be intended as an epidemiological statistical surface mapping model. Those interested in the spatial analysis have brought this practice to further use.

In this study, the data of covid-19 infected people of the Department of Disease Control were used for analysis. This information is available online that the general public can download. However, because this isarithm thematic mapping involves a lot of fundamental statistical concepts, some interested students or researchers, which didn't have any good statistical background, should pay attention to study more from books or academic documents on statistics. To be integrated with the technique of using software GIS for mapping. It will be very useful.

2. MAIN CONCEPTS

2.1 Geostatistical Modelling

- Kriging

Kriging is a stochastic method for spatial interpolation. Based on the regionalized variable theory, kriging assumes that the spatial variation of an attribute such as changes in grade within an orebody or elevations of the land surface is neither totally random nor deterministic. Instead, the spatial variation may consist of three components: a spatially correlated component, representing the variation of the regionalized variable; a 'drift' or structure, representing a trend; and a random error term (Oliver and Webster, 1990).

- Semivariance and Semivariogram

Semivariance is the geostatistical method to express the degree of relationship between points on a surface. The semivariance is simply half the variance of the differences between all possible points spaced a constant distance apart. The semivariance at a distance $d = 0$ should be zero because there are no differences between points that are compared to themselves. However, as points are compared to increasingly distant points, the semivariance increases. If there is strong spatial dependence, points that are closer together will have a smaller semivariance (Hartmann. et al, 2018).

$$\text{Semivariance} = \frac{1}{n} \times \sum_{r_t < \text{Average}}^n (\text{Average} - r_t)^2$$

where:

n = The total number of observations below the mean

r_t = The observed value

Average = The mean or target value of the dataset

The semivariogram is a plot of semivariance as a function of the distance between the observations and is the source of information used in kriging to achieve optimal weighting functions for mapping. Kriging uses the semivariogram, or rather a mathematical model of the semivariogram, in calculating estimates of the surface at the grid nodes.

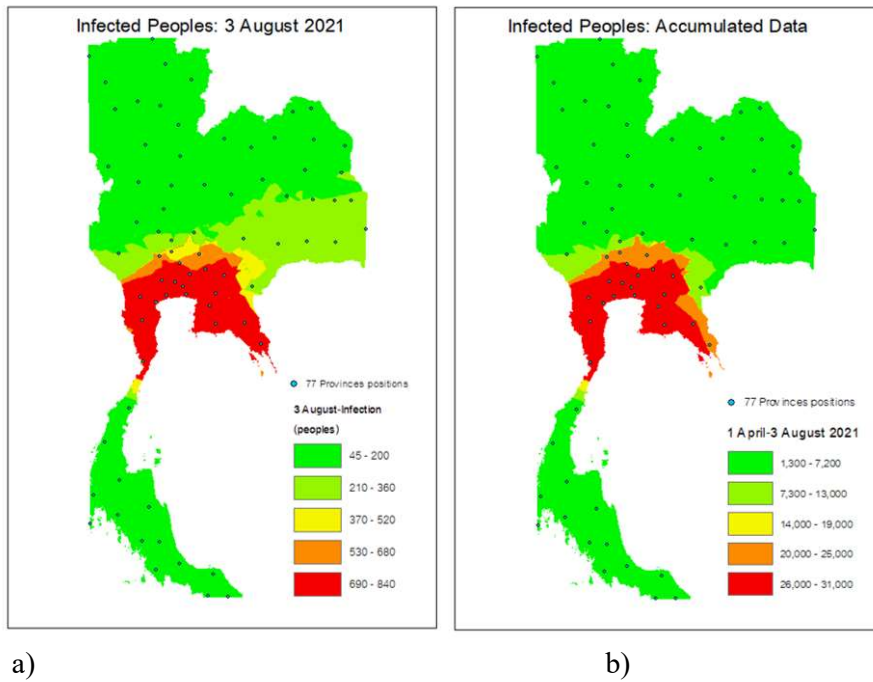
$$\text{Semivariogram}(distance h) = 0.5 * \text{average} [(\text{value at location i} - \text{value at location j})^2]$$

2.2 Isarithm map

Isarithm map uses isolines to depict continuous values like precipitation levels. These maps can also display three-dimensional values like elevation on topographic maps. Generally, data for isarithmic maps are gathered via measurable points. It must be feasible to consider the mapped phenomena continuous; discrete phenomena cannot be mapped isarithmically (Robinson et. al., 1995, and Dent, B. D., et, al, 2009).

Various advantages to the isarithmic technique must be weighed in the selection process:

1. Isarithmic mapping shows the total distribution of a spatially varying phenomenon.
2. It is flexible and can easily be adapted to a variety of levels of generalization or degrees of precision.
3. The technique is easily rendered by using computerized cartographic methods.



a)

b)

Figure 1. a and b., COVID-19 Infected peoples of THAILAND.

3. RELATED DATA AND METHODS

3.1 Thai Covid-19 Pandemic data

This study used data on people infected with the coronavirus pandemic from all 77 provinces of Thailand. Such information is from the Department of Disease Control. There are two types of data: 1) daily infection data on 3 August 2021 and 2) cumulative infected data (1 April – 3 August 2021). Some related information as being shown in Table 1.

Table 1. Some related Covid 19 information.

Provinces	3 August 2021 (peoples)	Accumulated 1 April – 3 August 2021 (peoples)
Bangkok	3566	161731
Samutprakarn	1361	41919
Chonburi	1359	29127
Samutsakorn	1282	34301
Nonthaburi	565	25989
Pathumthani	465	20840
Nakornratchasima	454	6201
Ubolratchatani	448	5868
Buriram	405	4507
Srakaew	382	3365
Srisaket	358	4943
Suphanburi	218	4838

3.2 Geostatistical method with GIS

I calculate covid-19 pandemic information base on geostatistical main concepts as to be represented in section 2.1 with ArcGIS software. I found any different views of data analysis results. As to be shown in fig. 1 a and b, represent the kriging surface of infected peoples of all 77 provinces of Thailand.

3.2.1 Semivariogram of Ordinary Co-Kriging Methods: 3 Aug 2021.

In statistic concept, “Group together data is bins”. The counts of detections have been binned logarithmically, within mass bins covering factors. For Semivariogram result, all bins are red color dots. Average points are shown as blue crosses and are generated by binning empirical semivariogram/covariance points that fall within angular sectors. Binned points show local variation in the semivariogram/covariance values, whereas average values show smooth semivariogram/covariance value variation (figure 2a).

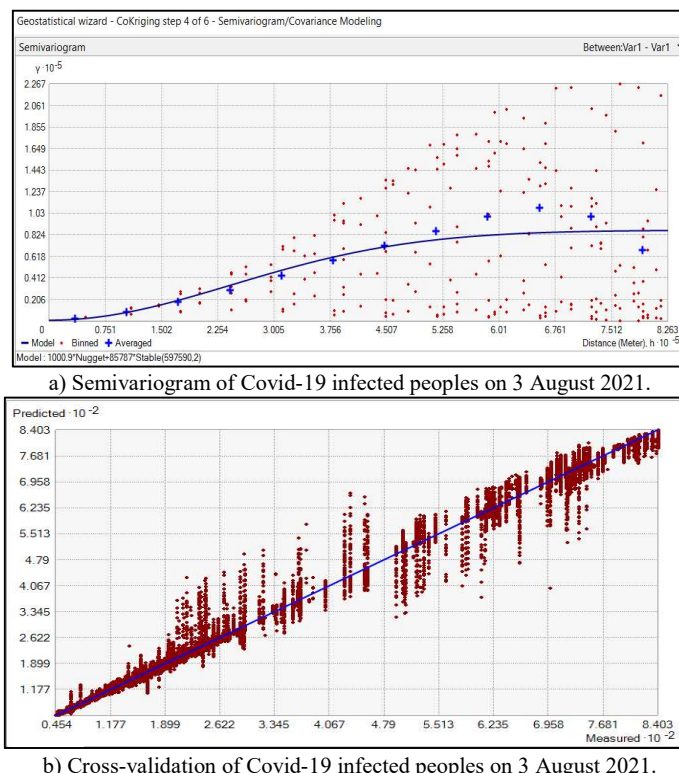


Figure 2. Semivariogram&Cross-validation of Covid-19 infected peoples on 3 August 2021.

This semivariogram comes from an ordinary kriging surface which interpolated from 77 province location points, also all points have their own infected covid-19 pandemic data. The range is the distance where the model first flattens out is nearly around $6.01(10^{-5})$, and the sill is mean the value on the y-axis that the semivariogram model attains at the range, is nearly around $0.824(10^{-5})$. The nugget is the semivariogram model intercepts the y-axis, as

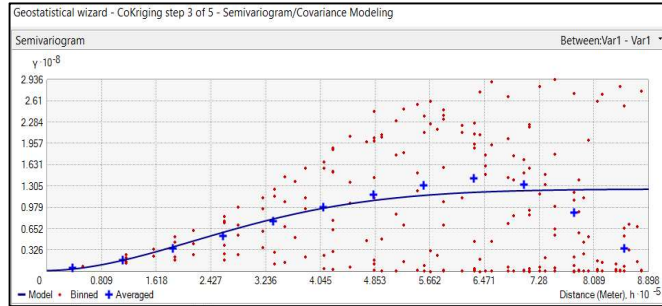
being around 0.001.

For cross-validation results, the root means the square error is 11.32, which means so much variate from stable, although, the calculation of Root Mean Square Standardized Error is 0.349, less than 1, this means we overestimate all variabilities of our prediction (figure 2b).

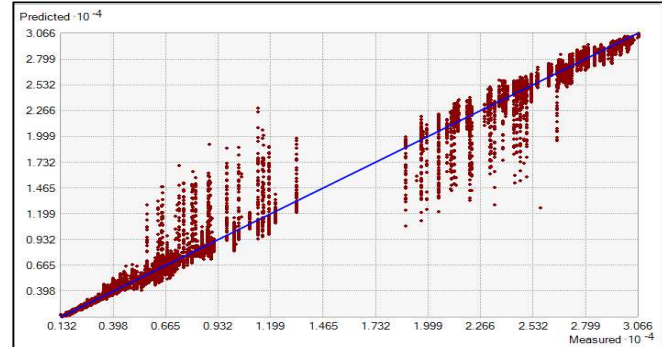
3.2.2 Semivariogram of Ordinary Co-Kriging Methods: Accumulated Data.

From section 3.2.1 we have considered semivariogram of covid 19 infected peoples with co-kriging method from daily infected data. For this topic, we will use cumulative infected data from April 2021 to August 3, 2021, to create a semivariogram. to consider the outcome.

From figure 3a, the range is around 7.28×10^{-5} . The sill was found as nearly 0.98×10^{-8} , and the nugget was very close to 0.01. For cross-validation results (figure 3b), the calculation of Root Mean Square Standardized Error is 0.395, less than 1, and this value is very close to the root mean square error of co-kriging method of daily infected peoples of section 3.2.1



a) Semivariogram of Covid-19 infected peoples: April - 3 August 2021.



b) Cross-validation of Covid-19 infected peoples: April - 3 August 2021.

Figure 3. Semivariogram & Cross-validation of Covid-19 infected peoples: Accumulated April to 3 August 2021.

4. The Results.

From the co-kriging method to consider the semivariogram. Those achievements can be used to create an isarithm map, as shown in Figures 4a and 4b, with map symbols and isarithm lines as a summary of the situation of covid-19 infection cases in Thailand, according to the range. all the time specified.

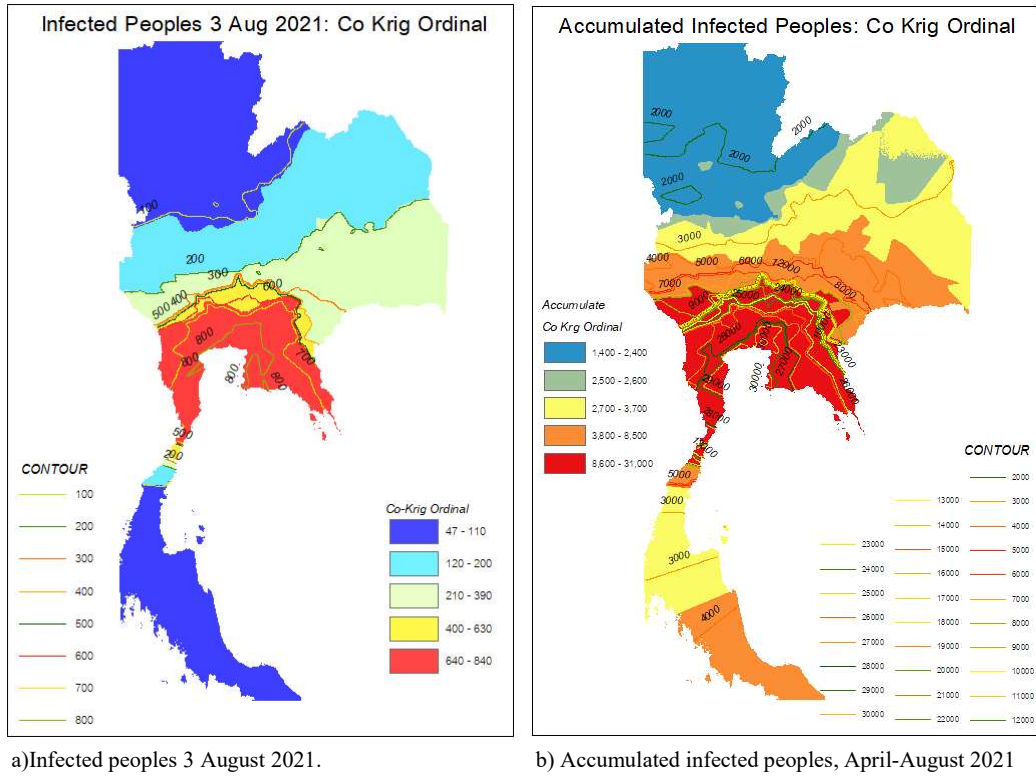


Figure 4. Isarithm Mapping of Pandemic Covid-19 Significant Area.

5. REFERENCES

- Dent, B. T., Torguson, J. S., and Holder, T. W., 2009. *Cartography: Thematic Map Design*. McGraw-Hill, New York.
- Hartmann, K., Krois, J., Waske, B. (2018): E-Learning Project SOGA: Statistics and Geospatial Data Analysis. Department of Earth Sciences, Freie Universität Berlin.
- Oliver, M. A., and R. Webster, (1990) Kriging: A method of interpolation for geographic information systems, International Journal of Geographic Information Systems, 4(3), 313-332.
- Robinson, A. H., Sale, R. D., Morrison, J. L., & Muehrcke, P. C., (1995) Elementary of Cartography. Wiley, New York.

A MACHINE LEARNING APPROACH TO BUILDING A DIGITAL MAP OF COVID-19

Thom Hue Huynh¹ and Son The Pham²

¹Faculty of Geography
 University of Social Sciences and Humanities, Ho Chi Minh City, Vietnam
 Vietnam National University, Ho Chi Minh City, Vietnam
 Email: 1856080099@hcmussh.edu.vn

²Department of Data Science
 Faculty of Information Science and Engineering
 University of Information Technology, Ho Chi Minh City, Vietnam
 Vietnam National University, Ho Chi Minh City, Vietnam
 Email: sonpt@uit.edu.vn

ABSTRACT

Coronavirus disease 2019 (COVID-19) has become more and more complicated from the end of 2019 until now. Information about the COVID-19 epidemic situation is a hot spot of interest. A problem is how to update the information about the COVID-19 epidemic quickly and accurately, simply and effectively. It can help managers and people capture information the most quickly. Therefore, we choose GIS applications as a powerful tool capable to solve the proposed problem.

The main objective of the project is to build a digital map application to support observing the COVID-19 epidemic situation in Vietnam. The map has the following features: (1) Automatically update new data about the epidemic situation; (2) Detailly present information about the developing epidemic situation by a digital map; (3) Allow users to search information about the epidemic; (4) Basically predict of the number of patients with days using a method of machine learning. Used dataset of this paper was collected until July 31, 2021.

1. INTRODUCTION

From the end of 2019 until now, the COVID-19 epidemic has spread all over the world, including Vietnam. Governments have promoted the development of many applications to limit the spread of the disease. Besides, there are also many types of research that have proposed GIS application solutions to monitor disease developments. Among them, we are especially interested in GIS applications to support building COVID-19 maps, statistical methods, and forecast models to predict the epidemic situation.

Specifically, GIS-based spatial modeling of COVID-19 (Mollalo, Vahedi, & Rivera, 2020) presented the rate in the United States, using maps to illustrate in the state area. Evaluation of map applications and analysis based on COVID-19 data sources in Europe's population (Pászto, Burian, & Macku, 2020). Reviews on spatial analysis and GIS in the research of COVID-19 highlighted important GIS applications to study COVID-19 (Franch-Pardo, Napoletano, Rosete-Verges, & Billa, 2020). Application of GIS map presented the status of COVID19 cases in Maharashtra state of India (Kodge, 2021). The Prophet package was used to predict covid-19 cases in India (Indhuja & Sindhuja, 2020). In general, the studies focused on forecasting and presenting maps showing the epidemic situation of countries.

In the scope of this research, we build a digital map application to support observing the COVID-19 epidemic situation in Vietnam. The map has the automatically update new data about the epidemic situation and detailly present information about the developing epidemic situation. And focus on analyzing epidemic data in the Ho Chi Minh City area to basically predict the number of patients with days using methods of machine learning. Because now the epidemic in the city is the most increasing. This issue is a concern to the whole society.

2. DATASET DESCRIPTION

2.1. Spatial data

Shapefile data of 63-province Vietnam was collected from the Open Development Mekong (ODM) at website (<https://opendevmentmekong.net/>). Shapefile is a type of vector data able to reference position, measurement unit, and spatial relationship. That means describe phenomenal shapes. The data is used to represent the scope of each administrative region on the map. The spatial reference system (SRS) on the project is UTM Zone 48-N to build the map.

2.2. Attribute data

Attribute data of COVID-19 cases is collected at the website of the Ministry of Health. The data daily updated as follows a total number of new cases of each region (province and city) in Table 1. Besides, we also collect detailed data of Ho Chi Minh City about the daily number of COVID-19 cases. The data is used to solve the forecasting problem that we introduced above. Data samples were collected until July 31, 2021. Nextly, we selected 5 data samples to present as follows:

Table 1. The five samples of cases of each region in Viet Nam

Region	Total
TP HCM	90243
Bình Dương	14679
Long An	5443
Đồng Nai	4126
Khánh Hòa	1710

Table 2. The five samples of cases in Ho Chi Minh City

Date	Total
2021-07-31	4180
2021-07-30	4282
2021-07-29	4592
2021-07-28	4449
2021-07-27	6318

3. PROPOSED METHOD

In this paper, we based on two main library packages: (1) The Arcpy package is used to support building a digital map representing the number of covid cases by areas. The digital map has the ability to automatically update the map state when the attribute data changes over real-time. In this section, the digital map will continuously automatically show the epidemic situation of provinces and cities so that managers can know the epidemic situation across the country. When the epidemic data changes, the map also updates. In addition, the map presents additional statistics on the epidemic situation. (2) The Prophet package supports building a machine learning model to predict the number of covid cases in the near future. In this forecast, we only focus on the Ho Chi Minh City area. Because this area has seriously been affected by the Covid-19 epidemic currently. The number of daily infections is increasing rapidly. Therefore, we are very interested and want to build a forecasting model

for that area. According to exploratory data analysis, we found the dataset to be very suitable for the Prophet forecast model we proposed.

3.1. ArcPy package

ArcPy is a package in Python programming that is able to perform geographic data analysis, map automation, data conversion, and data management (Zandbergen, 2020b, 2020a). ArcPy is a powerful and useful tool that is a product developed by ESRI. In this section, we apply ArcPy to build a digital map presenting an overview of the epidemic situation in Vietnam. The map can update itself when the attribute data changes. During the mapping process, we parallelly combine ArcPy and ArcGIS Pro to optimize the operation process. Some strengths of ArcGIS Pro as follow spatial analysis, image processing, and remote sensing, build maps and displays, real-time GIS data, data collection and management, and 3D GIS made us chosen it to develop the map (Allen, Znamirowski, & Chandler, 2021).

In the ArcPy package, there are many support modules for programmers to develop GIS applications, including the following: Charts module (`arcpy.charts`), Data Access module (`arcpy.da`), Geocoding module (`arcpy.geocoding`), Image Analysis module (`arcpy.ia`), Mapping module (`arcpy.mp`), Metadata module (`arcpy.metadata`), Network Analyst modules (`arcpy.nax` and `arcpy.na`), Sharing module (`arcpy.sharing`), Spatial Analyst module (`arcpy.sa`), Workflow Manager (Classic) module (`arcpy.wmx`). The modules covered other areas of ArcGIS. Besides, in the process of building the map, we have designed and built more tools embedded in ArcGIS Pro to automate operations with the following 5 processing tools: Add Data, Add Table, Join Table, Update Data, View Map.

3.2. Prophet package

The Prophet package in Python and R programming language is a machine learning model that is able to forecast many values in the future (Taylor & Letham, 2018). The forecast is based on time-series data collected and preprocessed in advance from the news website of the respiratory disease COVID-19 (Ministry of Health). The predictive model was installed with the 5 stages.

Firstly, preparing full data and follow/match the format of the model. They must be correct for the time series data type. The data of this step is the number of infections per day in Ho Chi Minh City. The city was a very serious Covid-19 epidemic now. Up to now (July 31, 2021), we have collected 96 statistical samples of the number of cases per day. Specifically, the five collected samples recently were presented in Table 2.

Secondly, based on the existing dataset to train the predictive model. As a result of this stage, we get a predictive model organized into an object in the programming language. Then set the number of predicting periods from the trained model. For the predicting periods of future cases, the periods are set up with 5 days. That is mean to predict the number of cases in the next five days. The 5-day period is just enough days to compare the actual values to calibrate and re-train the model. The results of the training model and the forecast results are visualized in Figure 1. In Figure 1, there are two visualization components: (1) visualization for the training data part and (2) visualization for the forecasting part. The forecasting section is marked with a red square in Figure 1. Figure 2 shows the forecast trend of the dataset calculated on a daily and weekly basis. In the weekly forecast trend, there is a negative value, because it is an overall value to represent the model. In the reality, the value will not happen.

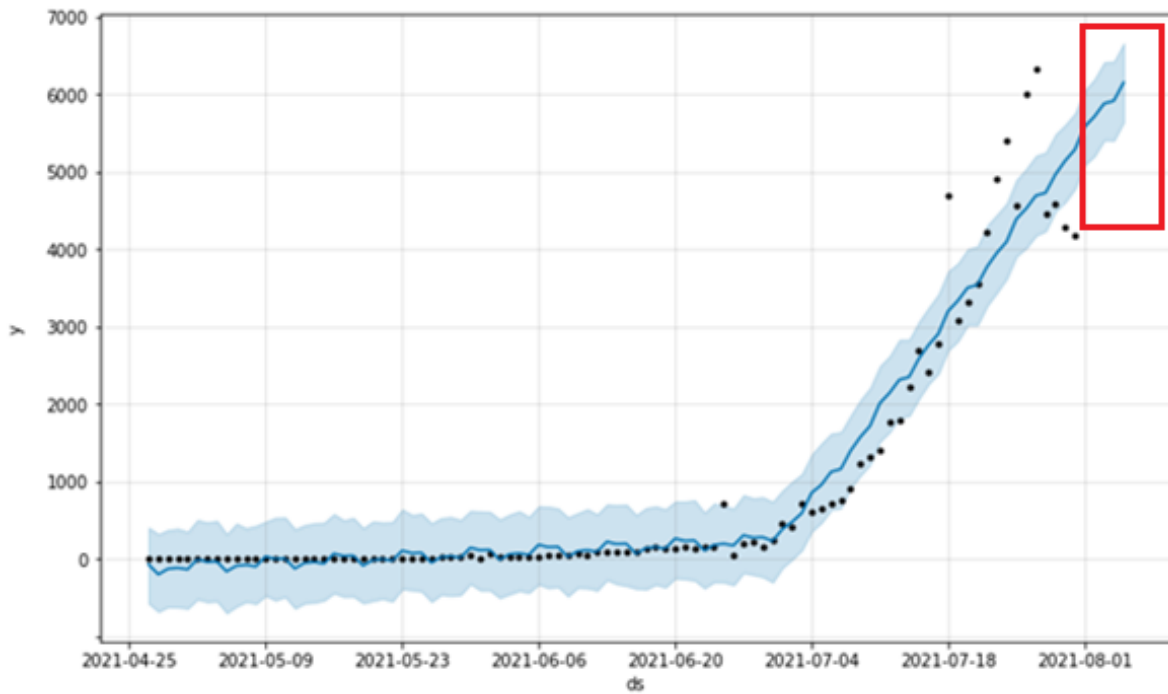


Figure 1. Result of build-in forecasting model.

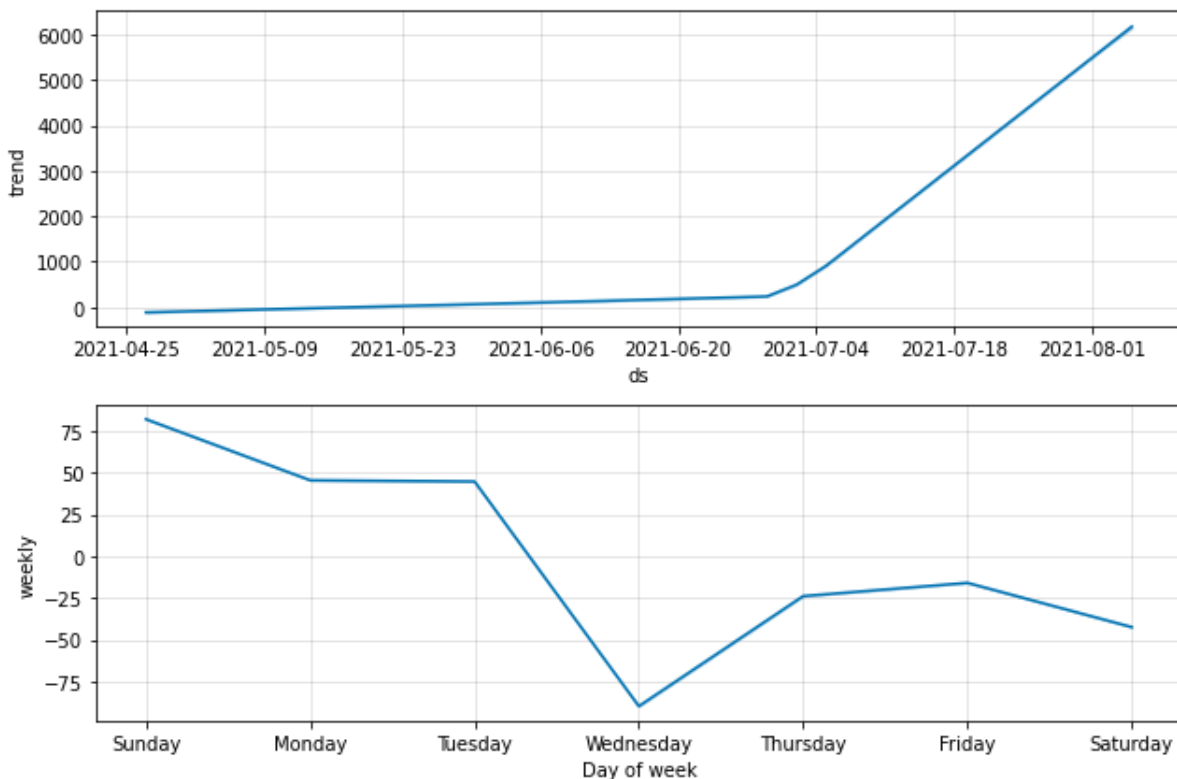


Figure 2. Trend of dataset using build-in forecasting model.

Thirdly, we will make future forecasts. From the obtained training model, we will proceed to get the prediction results. The forecast result will obtain the forecast value ($yhat$) and the upper and lower error range (called $yhat_lower$ and $yhat_upper$). The forecast result will be the real number. We will take the integer part to represent the number of COVID-19 cases in Table 3.

Table 3. Results of 5-day prediction in Ho Chi Minh City.

Day	yhat	yhat_lower	yhat_upper
2021-08-01	5575.304875 ~ 5575	5086.763709 ~ 5086	6047.794081 ~ 6047
2021-08-02	5708.581069 ~ 5708	5201.778696 ~ 5201	6195.450087 ~ 6195
2021-08-03	5877.611387 ~ 5877	5406.962430 ~ 5406	6413.376456 ~ 6413
2021-08-04	5913.098525 ~ 5913	5403.379973 ~ 5403	6423.361159 ~ 6423
2021-08-05	6148.652844 ~ 6148	5641.224548 ~ 5641	6658.201478 ~ 6658

Finally, based on actual data, then calibrate and retrain the model. The forecasting model will support predicting the next number of cases. But the model will not indicate when the peaking number of COVID-19 cases, or when the decreasing number of cases, or when there will be a complete decline. So, after the prediction is done and has more data of the new day. The model will be retrained one more so that the next prediction results are likely to be more accurate. Nextly, after retraining, there are 5 new forecasted results from the newly trained model.

4. RESULTS

Map of the situation of the COVID-19 epidemic in Vietnam by the method of representing the quality background. The map shows the epidemic situation distributed over 63 provinces in Vietnam with main information as follows: total number of cases and results of 5-day prediction in Ho Chi Minh City. The overview interface of the results is shown in Figure 3.

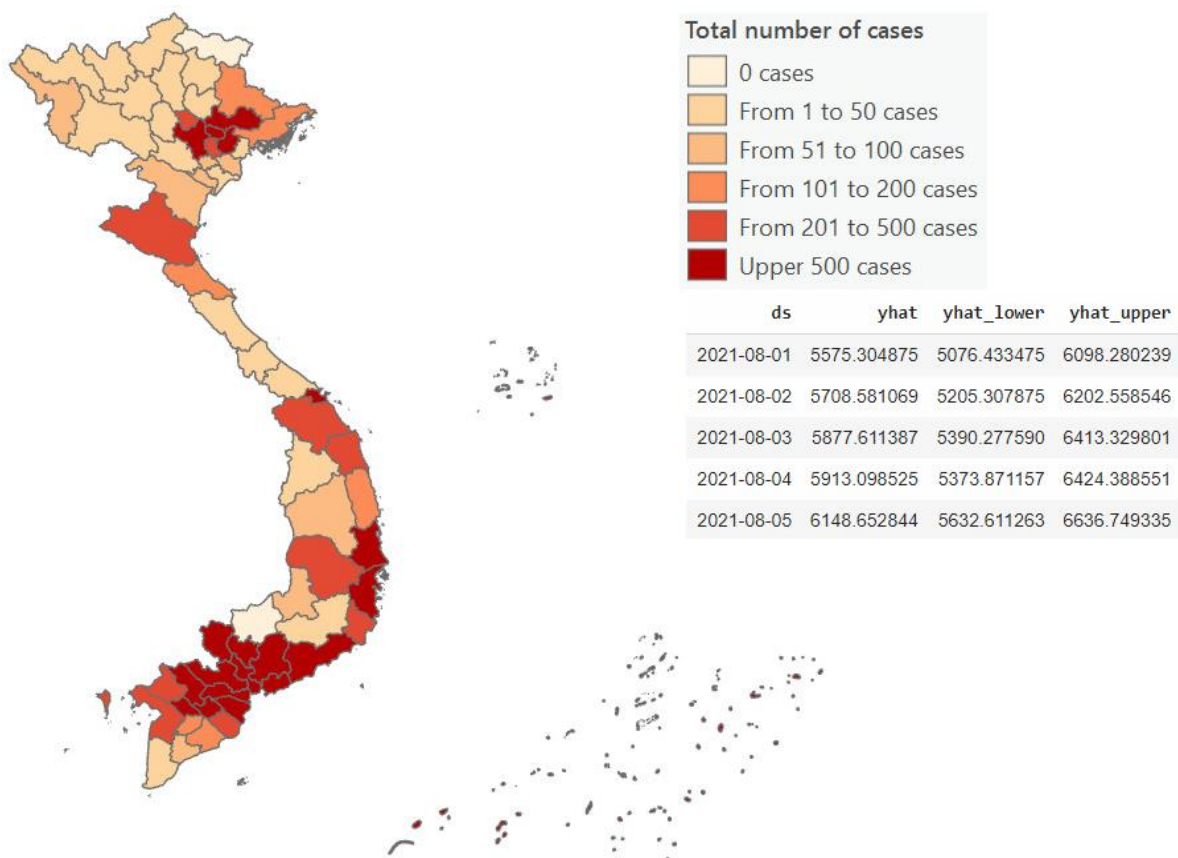
**Figure 3. Overall results.**

Figure 3 presents the results of the study. The left part is an automated map showing the COVID-19 epidemic situation of regions of Vietnam. The right part presents the scales showing the number of cases in the regions and the forecasted results of the total number of cases at Ho Chi Minh City in the next 5 days.

5. CONCLUSIONS

This paper presented a method for building an automatic digital map to visualize the COVID-19 epidemic situation of administrative regions in Vietnam and a forecast analysis of the number of cases in Ho Chi Minh City. The implementation method is based on two main approaches ArcPy package and Prophet package on Python programming. Firstly, after completing the application, the combination of both ArcGIS Pro and ArcPy for building an automatic digital map not only saves time and effort but also has high accuracy. That has helped us to complete an automated digital map of the covid-19 epidemic extremely smoothly. Secondly, the prediction results of the Prophet machine learning model are also acceptable. This forecast will help managers plan to respond to the growing number of patients. The downside of the Prophet model is that it only correctly predicts when the trend is up or down, does not predict when the number of cases will peak or when the epidemic is likely to end. The results are well applicable, taking advantage of the advances and new features of the software, contributing to improving the position of maps and geographic information systems in many fields.

In future work, we will conduct more automatic data collection from COVID-19 news websites of the Ministry of Health. That means we will build a website scraper and crawler that will automatically get the data when the source site changes. Then the map can perform real-time data updates.

6. REFERENCES

- Allen, D. W., Znamirovski, B., & Chandler, M. (2021). Focus on Geodatabases in ArcGIS Pro. *Photogrammetric Engineering & Remote Sensing*, 87(7), 468–469.
- Franch-Pardo, I., Napoletano, B. M., Rosete-Verges, F., & Billa, L. (2020). Spatial analysis and GIS in the study of COVID-19. A review. *Science of The Total Environment*, 739, 140033.
- Indhuja, M., & Sindhuja, P. P. (2020). Prediction of covid-19 cases in India using prophet. *International Journal of Statistics and Applied Mathematics*, 5(4), 103–106.
- Kodge, B. G. (2021). A review on current status of COVID19 cases in Maharashtra state of India using GIS: a case study. *Spatial Information Research*, 29(2), 223–229.
- Mollalo, A., Vahedi, B., & Rivera, K. M. (2020). GIS-based spatial modeling of COVID-19 incidence rate in the continental United States. *Science of the Total Environment*, 728, 138884.
- Pászto, V., Burian, J., & Macku, K. (2020). COVID-19 data sources: evaluation of map applications and analysis of behaviour changes in Europe's population. *Geografie (Utrecht)*, 125(2), 171–209.
- Taylor, S. J., & Letham, B. (2018). Forecasting at scale. *The American Statistician*, 72(1), 37–45.
- Zandbergen, P. A. (2020a). *Advanced Python Scripting for ArcGIS Pro*. Esri Press.
- Zandbergen, P. A. (2020b). *Python Scripting for ArcGIS Pro*. Esri Press.

The formal alleviation of people suffering and cost reduction during the COVID-19 epidemic in Thailand

**¹Pathana Rachavong, ¹Tanyaluck Chansombat, ²Jiranya Duangfoo,
and ³Wattananan Jaisa-ard**

¹Thailand Geographical Association, Email: pathanar@gmail.com, tanyalaks@nu.ac.th

²Geographic Information Sciences, Naresuan University, Email: jiranyad64@nu.ac.th

³Faculty of Social Sciences and Humanities, Nakhon Sawan Rajabhat University, Thailand,
Email: wattananun.j@nsru.ac.th

ABSTRACT

Remedial assistance and cost reduction for the people of the Thai government during the coronavirus disease 2019 epidemic is a review of the suffering of the people who have been healed by the Thai government. Remedies to reduce the burden of expenses on people in times of crisis. This research has therefore reviewed relevant research studies and used the Thai government's remedial information provided by the Fiscal Policy Office to show the spatial distribution of remedial assistance across different regions of the country. It was found that the government has directly provided assistance to people suffering from lack of income in 4 projects, namely the program to heal people during the first wave of the outbreak, paying 1,000 baht per month for 3 months from May to July 2020. There are participants in the project. 1.064 million.

The Roa Chana project has a weekly payout of up to 9,000 baht per person (February-May 2021). The project has 33.229 million people. The project to increase purchasing power for the welfare people has 3 phases. Phase one: October-December 2020, the government pays 500 baht per person per month, totaling 3 months, 13.808 million people are eligible. In the second phase, January-March 2021, the government pays 500 baht per person per month, for a total of 3 months, 13.718 million people are eligible. And in the third period of July-December 2021, the government pays 200 baht per person per month, for a total of 6 months, 13.581 million people are eligible. There is also a project to increase purchasing power for those who need special assistance up to 1,200 baht throughout the project period. There is a total of 2,285,429 people who are eligible, most of which are distributed in the Northeast. It shows the comprehensiveness of remedies and assistance that is beneficial to the further assistance of the relevant organizations.

1. INTRODUCTION

The pandemic caused a decline in economic growth and caused a sharp drop in employment in the second quarter (April-June) of 2020. However, consumer and business behavior has been supported by government-sponsored stimulus measures since March 2020, mainly social protection. It has a profound effect on poverty and employment. The impact of COVID-19 on social protection program recipients will depend on the level of investment in health and education as well as the macro-financial response in the medium to long term. Social protection programs provide access to social services such as health and education as well as act as a safety net to reduce negative income and health impacts for households.

Public health measures used to control disease are responsible for the direct impact on services, perhaps most notably in education. Public health measures have enormous economic impact, despite the changes made by macroeconomic stimulus and large payments to households. The cost of stimulus and the loss of GDP will have a lasting impact on public finances, reducing resources for future expansion projects. The Economist Intelligence Unit (EIU, 2020) estimates that the international recession and Thailand's public health measures will reduce the country's gross national productivity by 8.4 percent compared to the situation during the absence of the COVID-19 pandemic and will be reduced by 6.9 percent due to the impact of economic

stimulus measures. One of the main impacts of COVID-19 continues to be unemployment or job suspensions and continuing to lower incomes. UNICEF used data on sudden layoffs in Thailand to predict a modest increase in poverty in the second and third quarters to another level that hides more severe impacts in some groups. Because UNICEF only estimates the impact of COVID-19 on unemployment. It is therefore important to refer to other figures from the International Labor Organization. (International Labor Organization, 2020), with 6.6-7.5 million workers expected to be directly affected by the COVID-19 economic crisis.

In order to review the suffering of the people who were healed by the Thai government, especially the remedies to reduce the burden of expenses for people during the crisis. Therefore, this research study has reviewed various research studies. and use the Thai government's remedial information provided by the Fiscal Policy Office to show the spatial distribution of remedial assistance across different regions of the country. This study will reveal the breadth of remedies and assistance that will benefit further assistance to relevant organizations.

2. METHODOLOGY

This research was conducted in two parts: a review of relevant UNICEF research to study the relief of suffering in Thailand as a whole; and searching for information on Thai government assistance using the information collected by the Fiscal Policy Office. Descriptive statistical analysis is used to classification of the density of people in different regions of the country who receive the right to help and relieve suffering from the Covid-19 crisis.

3. RESULT AND DISCUSSION

This research has reviewed the measures taken to remedy the suffering of the Thai people from the United Nations in Thailand (2020) report, indicating that The pandemic will cause a deep reduction in economic growth and employment in quarter 2 (Q2) (April–June) of 2020, but consumption behavior and businesses are being supported by a series of stimulus measures put in place by the Royal Government of Thailand since March 2020 and summarized in the table below. These are in large part a social protection package and will have substantial impacts on poverty and employment. The impact of COVID-19 on recipients of social protection programs will depend on the level of investments in health and education, as well as the macro-fiscal response in the medium to long run. Social protection programs enable access to social services, such as health and education, as well as acting as a safety net to mitigate the negative impact on incomes and health shocks for households.

Healthcare spending is also expected to rise by 1.7%, supported by the direct allocation for the sector in the fiscal stimulus package in 2020. Currently, Thai formal workers are protected under the social security scheme and all workers (including informal workers) receive cash assistance to alleviate the poverty impact. Cash handouts may be insufficient to mitigate the impact of income lost overall, and they still exclude some vulnerable groups due to eligibility criteria.

It also surveyed the Thai government's assistance measures during the severe Covid-19 outbreak that prevented people from doing their jobs as usual. Government measures are considered as remedies, reduce cost burdens, support the spending of essential goods, and increase purchasing power for those who need special assistance. There are 4 government-assisted projects: 1) Aid/Remedy/Compensation Program to people affected by the coronavirus

disease 2019 outbreak to help those who have government welfare cards 2) Roa Chana project 3) the project to increase purchasing power for government welfare card holders and 4) the project to increase Purchasing power for those who need special assistance.

Table 2 Number of people eligible for state financial aid.

Project	Number of eligible persons
1. Financial assistance/remedial/compensation programs	1,064,166
2. Roa Chana Project	33,229,388
3. Increase purchasing power project	
3.1 Phase One (October-December 2020)	13,808,756
3.2 Phase Two (January-March 2021)	13,718,150
3.3 Third phase (July-December 2021)	13,581,033
4. Increase purchasing power for those who need special assistance Project	2,285,429

Source: Royal Thai Fiscal Policy Office, 2021

Table 3. Descriptive parameters

	welfare cards	Roa Chana	purchasing power	purchasing power	purchasing power	special assistance
AVG	13820.33766	431143.415	179334.4805	178157.6104	176377.039	29363.93506
MEDIAN	9789	341758	134459	133677	132230	25599
MODE	N/A	N/A	N/A	N/A	N/A	N/A
MAX	49735	1959234	615650	611248	605509	104748
MIN	1229	95154	23816	23720	23440	6985
STDEV	11904.23077	304717.8202	131651.0294	130706.9153	129315.5269	18704.45024
SKEWNESS	1.511823305	2.314602076	1.44640467	1.44562306	1.441379927	1.575018542

Source: Royal Thai Fiscal Policy Office, 2021

The program to help and compensate people affected by the coronavirus disease 2019 epidemic aims to provide relief to those who have a government welfare card who have not received medical assistance from any government program. with reduced income and unable to find other income to replace The government paid compensation of 1,000 baht per month for a period of 3 months between May-July 2020. A total of 1,064,166 people were eligible, mostly in the northeastern region.

But when considering the Roa Chana project, the objective is to help reduce the burden of living expenses for people due to the new wave of the Covid-19 epidemic. There is support for a budget of no more than 9,000 baht per person, paid weekly between February-May 2021. There are a total of 33,229,388 eligible people, mostly in the Northeast.

The project to increase purchasing power for people with government welfare cards is intended to help heal and reduce expenses for those who have government welfare cards during the epidemic situation of Covid-19. This measure is aimed at helping people with cardholders who are unable to do their jobs normally, have lower incomes, and are unable to find other incomes to replace them. Assistance is divided into 3 phases:

- Phase 1, implemented during October-December 2020, the government supported the budget for the purchase of essential consumer goods from low-cost Blue Flag stores to develop the local economy at 500 baht per person per month for 3 months, with a total of 13,808,756 eligible people. Most of them are distributed in the Northeast.
- Phase 2, conducted between January and March 2021, the government supported the budget for the purchase of essential consumer goods from Thong Fah stores at 500 baht per person per month for 3 months, with a total of 13,718,150 eligible people.
- Phase 3 will be implemented during July-December 2021. The government supports the limit for the purchase of goods from Thong Fah stores and supports the limit for the purchase of goods or service fees from shops or service providers participating in the 3rd phase of 200 baht per person per month for 6 months. There is a total of 13,581,033 eligible people, mostly scattered in the northeastern region.

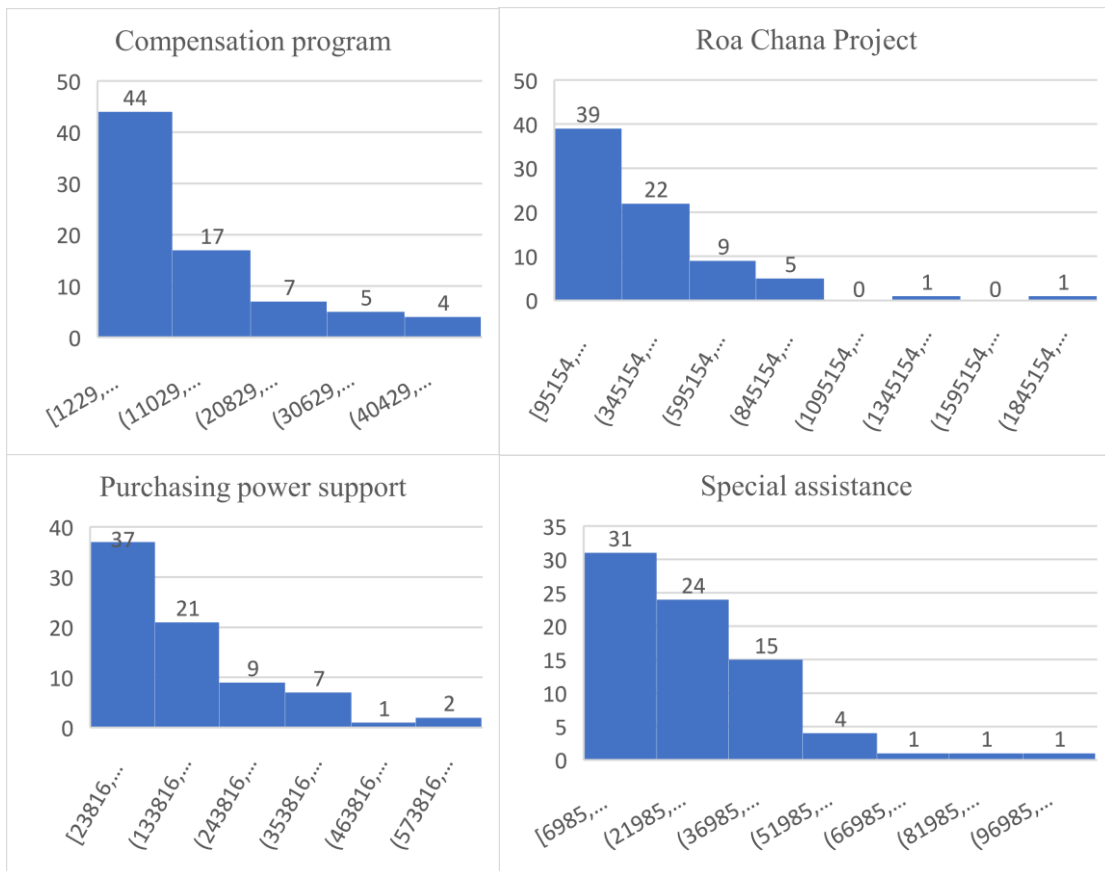


Figure 1. Distribution of government grantees in various projects during the COVID-19 crisis in Thailand

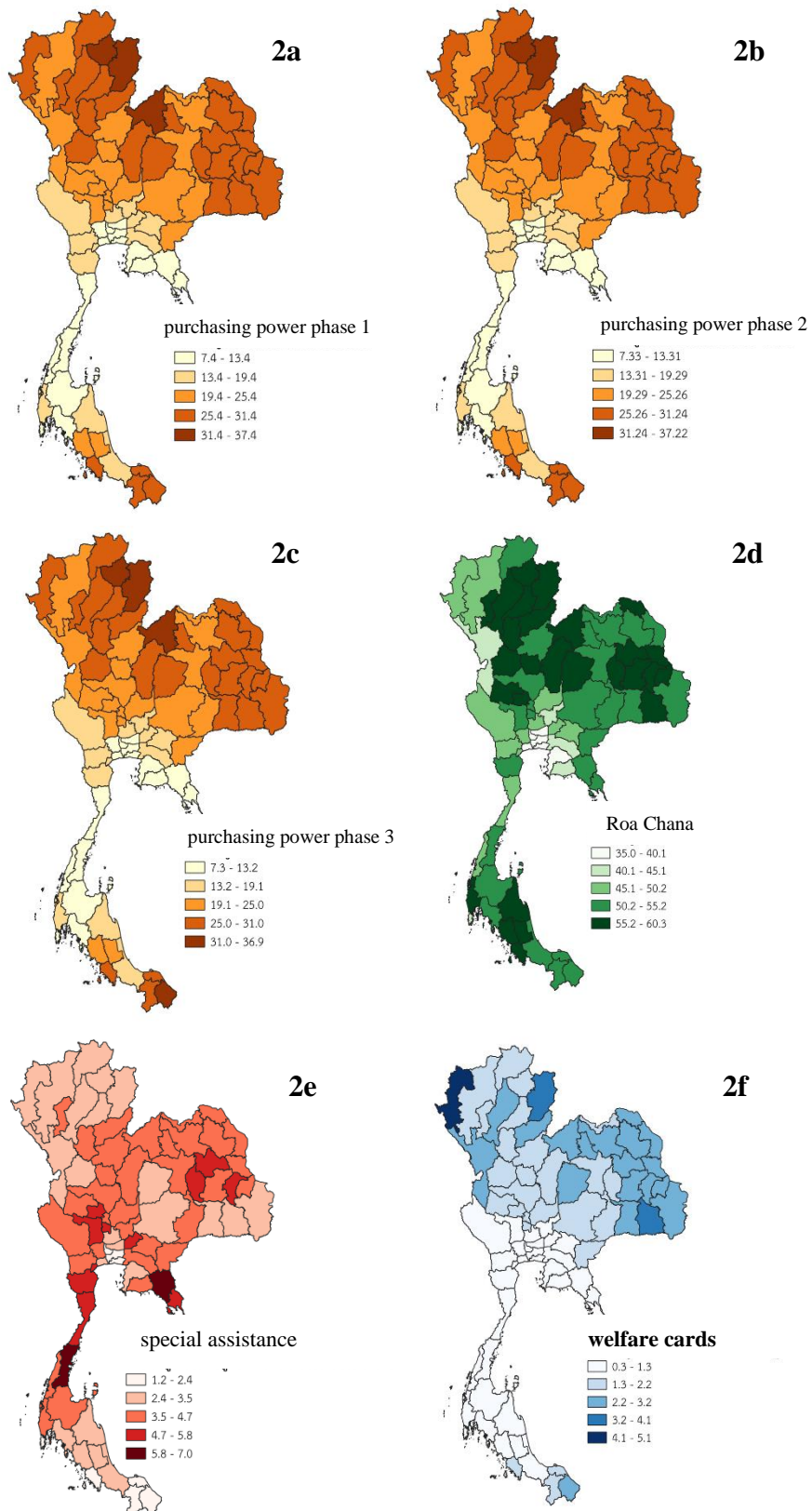


Figure 2. Distribution of government grantees in various projects during the COVID-19 crisis by regions in Thailand

The project to increase purchasing power for people with government welfare cards is intended to help heal and reduce expenses for those who have government welfare cards during the epidemic situation of Covid-19. This measure is aimed at helping people with cardholders who are unable to do their jobs normally, have lower incomes, and are unable to find other incomes to replace them. Assistance is divided into 3 phases:

- Phase 1, implemented during October-December 2020, the government supported the budget for the purchase of essential consumer goods from low-cost Blue Flag stores to develop the local economy at 500 baht per person per month for 3 months, with a total of 13,808,756 eligible people. Most of them are distributed in the Northeast.
- Phase 2, conducted between January and March 2021, the government supported the budget for the purchase of essential consumer goods from Thong Fah stores at 500 baht per person per month for 3 months, with a total of 13,718,150 eligible people.
- Phase 3 will be implemented during July-December 2021. The government supports the limit for the purchase of goods from Thong Fah stores and supports the limit for the purchase of goods or service fees from shops or service providers participating in the 3rd phase of 200 baht per person per month for 6 months. There is a total of 13,581,033 eligible people, mostly scattered in the northeastern region.

The project to increase purchasing power for disadvantaged groups aims to help and reduce the cost burden to those who need special assistance during the COVID-19 epidemic situation. The epidemic has left people in need unable to work as usual, their income is not enough to cover basic living expenses, and a dependency on their caregivers or family members. There is a credit limit for the purchase of goods from the Blue Flag Shop and support for the purchase of goods or service fees from participating stores or service providers, Phase 3, at 200 baht per person per month for 6 months between July and December 2021, the total amount is not more than 1,200 baht throughout the project period. There is a total of 2,285,429 eligible people, mostly scattered in the northeastern region.

4. CONCLUSION

This particular research has surveyed information on measures to help the Thai government during the severe outbreak of COVID-19, people are unable to do their jobs as usual as a remedy reduce the burden of expenses Support spending on essential goods and increase purchasing power for those who need special assistance. There are 4 government-assisted projects. Firstly, A project to help/heal/compensate for people affected by the coronavirus disease 2019 outbreak. This project aims to help those who have a government welfare card of 1,000 baht per month for a period of 3 months during May - July 2020, there are a total of 1,064,166 people receiving rights. Our winning project, secondly, is not more than 9,000 baht per person, paid weekly between February-May 2021, with a total of 33,229,388 eligible people. Thirdly, Project to increase purchasing power for people with welfare cards of the state. It has three phases to pay for the people: phase one, October-December 2020, pay 500 baht per person per month for 3 months, with a total of 13,808,756 eligible people; phase two, January - March 2021, pay 500 baht per person per month for 3 months, with a total of 13,718,150 eligible people; and phase three, July-December 2021 pay 200 baht per person per month for 6 months with a total of 13,581,033 eligible people. And the last project to increase purchasing power for those who need special assistance up to 1,200 baht throughout the project period.

There is a total of 2,285,429 eligible people. Most of them are distributed in the Northeast Thailand.

5. REFERENCES

- Asian Development Bank (2020). Proposed Countercyclical Support Facility Loans Kingdom of Thailand: COVID-19 Active Response and Expenditure Support Program: Report and Recommendation of the President to the Board of Directors. Project Number: 54177-001 June.
- Marome, Wijitbusaba and Shaw, Rajib. (2021). "COVID-19 Response in Thailand and Its Implications on Future Preparedness." *International Journal of Environment Research and Public Health*. 18, 1089. doi.org/10.3390/ijerph18031089
- Royal Thai Fiscal Policy Office, 2021
- Tantrakarnapa, Kraichat and Bhopdhornangkul, Bhophkrit. (2020). "Challenging the spread of COVID-19 in Thailand." *One Health*. Volume 11, 20 December, 100173. doi.org/10.1016/j.onehlt.2020.100173.
- UNICEF - Thailand (2020). *Socio-Economic Impact Assessment of COVID-19 in Thailand*. Bangkok: United Nations in Thailand.

Interests and Knowledge of the People on Non-Pharmaceutical Measures - DMHTT of Thailand During the Third Wave of the COVID-19 Pandemic

Pathana Rachavong¹, Tanyaluck Chansombat¹, and Jiranya Duangfu²

¹Thailand Geographical Association, Email: pathanar@gmail.com, tanyalaks@nu.ac.th

²Geographic Information Sciences, Naresuan University
Email: jiranyad63@nu.ac.th

ABSTRACT

Research on “Interests and Knowledge of the people on non-pharmaceutical measures - DMHTT of Thailand during the third wave of the COVID-19 pandemic.” The study aims to explore the knowledge, interests and practices of the people using data from Google Trend from searching with relevant keywords and then systematizing the data with words in a data mining program to find the spatial correlation of important measures with the Covid-19 epidemic situation in each region of Thailand. The results shows that Interest and behavior in response to non-pharmaceutical measures – DMHTT in Thailand was significantly correlated with the severity of the outbreak.

1. INTRODUCTION

Non-pharmaceutical or non-pharmaceutical intervention measures Interventions are the most effective public health measures for managing, preventing, and controlling the spread of SARS-CoV-2 in the communities that will cause the COVID-19 outbreak. Not only does it provide a moment for all countries to deal with epidemics without a vaccine to help control the outbreak, but also to prevent and control disease at a time when the health sciences have developed a vaccine. Such measures are still important to make effective control of this emerging disease more successful. The ECDC (ECDC, 2020) points out that non-pharmaceutical measures play an important role in reducing transmission rates and the impact of COVID-19 in the European Union, the European Economic Area and the United Kingdom. Until a safe and effective vaccine is available for everyone at risk of severe COVID-19, non-pharmaceutical measures will remain the primary public health tool against SARS-CoV-2.

Understanding of how the COVID-19 pandemic related to social distancing efforts to contain future outbreaks and to mitigate some of the lockdowns it is essential. Khataee et al. (2021) studied the quantitative relationship between key variables characterizing the epidemiological characteristics of COVID-19. and social distancing efforts of nine European countries. The study found that the epidemic was strongly correlated with the size of the reduction in people's movement. This made it possible to clearly decipher the relative impact of the timing and extent of social distancing on the total mortality burden of the pandemic. Meanwhile, Kim et al. (2021) demonstrated the effectiveness of social distancing in South Korea's spreading disease control, finding that the higher the level of social distancing, the higher the proportion of the effect. Negative respiratory viral PCR testing is also elevated, suggesting that national social distancing measures can help reduce the spread of common respiratory viral infections during the Covid-19 epidemic effectively.

Another personal measure that countries all over the world encourage people to take is hand washing. Li et al. (2021) reviewed six of the relevant research studies from four countries. In a total of 5,178 eligible databases and references, mask wearing was associated with a significantly reduced risk of SARS-CoV-2 infection ($OR=0.38$, 95% CI: 0.21-0.69, $I^2=54.1\%$)

for healthcare workers, it was found that masks reduce the risk of infection by almost 70 percent. For Thailand in early 2021, the Department of Disease Control, Ministry of Public Health has asked all citizens to cooperate to "Keep your guard up" even in the process of gradual vaccination against COVID-19. People still have a chance of getting infected. Therefore, the importance of self-protection measures should be strictly adhered to by wearing a mask 100%, washing hands frequently, keeping distance and avoiding entering community or crowded places, including risky places to prevent infecting and infecting family members and reduce the spread of disease in the community as well.

Department of Disease Control asks people to cooperate with the principle of "D-M-H-T-T" to protect themselves; D: Social Distancing Maintain a distance of 1-2 meters, avoid being in crowded places M: Mask Wearing Wear a cloth mask or hygienic mask at all times H: Hand Washing Wash your hands often with soap and water. or alcohol gel T: Testing, temperature measurement and T: Thai Cha Na, scan Thai Chana application before entering and leaving public places every time to make information easier to coordinate.

Based on the aforementioned policies, this research aims to explore the knowledge, interests and behavior of the people by using data from Google Trend from searching with relevant keywords and then organizing the data to find the spatial relationship of important measures to the epidemic situation of COVID-19 in each region of Thailand.

2. METHODOLOGY

2.1 Data Management

This research used data from keyword-driven google trend search results using keywords related to non-pharmaceutical interventions in accordance with guidelines recommended by the Ministry of Public Health for delaying progression. epidemic of covid-19

The Coronavirus Disease 2019 Epidemic Situation Administration has issued a notification to the provincial governor, provincial public health office doctors, and the provincial infectious disease committee asking all citizens to comply with DMHTT measures, including Distancing, Mask. wearing, hand washing, testing and inviting people to use the application "Thai wins" by adding 7 more words related to social distancing, mask wearing and hand washing that the World Health Organization has designated as an important measure. These are 3 words corresponding to Social distancing: Distancing, Isolation and Quarantine, 2 words corresponding to Mask wearing, Surgical mask and Mask, and 3 words corresponding to Hand washing: Hygiene, Alcohol and Bleach.

2.2 Method of Data Analysis

Spatial analysis of data to show distribution of popularity of COVID-19 epidemic prevention knowledge research using descriptive statistics. The spatial correlation model of knowledge obtained from public search related to the COVID-19 outbreak was analyzed using Geographically weighted regression Analysis by sorting Explanatory Variables and Dependent Variables by province for a total of 77 provinces as shown in Table 2 below.

Table 1. Systematization of data for GWR analysis.

	Variable I	Variable II	Variable III	Variable IV
Explanatory Variables	AVG Distancing	AVG Mask wear	AVG Hand wash	AVG Total
Dependent Variables	The number of cases in the first period	The number of cases in the second period	The number of cases in the third period	
Number of Cases	77 provinces			

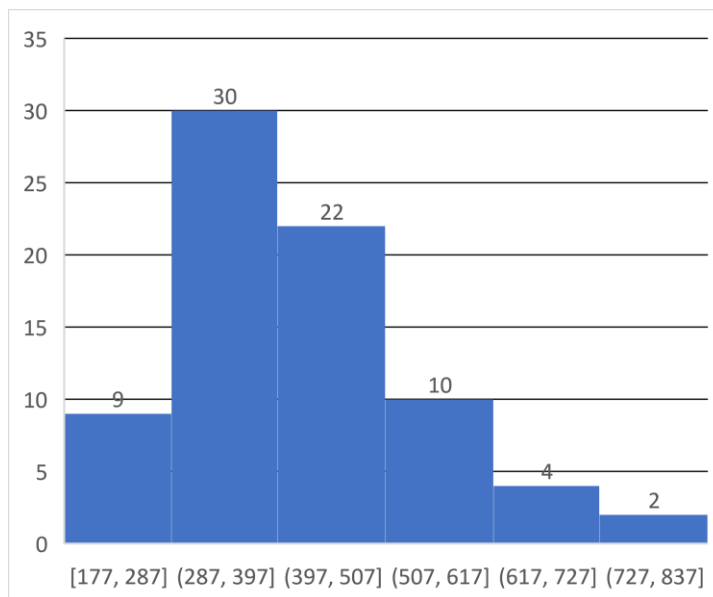
3. RESULT AND DISCUSSION

3.1 Properties of statistical distributions

On average, people in each province of Thailand had 418 searches for knowledge about self-protection against the COVID-19 outbreak, with a median of 396 and a baseline of 227 in the past 12 months. Phuket had the most searches at 809 times, followed by Bangkok at 770, and people in Yasothon province the least, only 177 times.

Table 2. Properties of statistical distributions.

MEAN	418	MAXIMUM	809
MODE	227	MINIMUM	177
MEDIAN	397	STD	127.3787075
		SKEWNESS	0.776320985

**Figure 1.** Distribution of the frequency of knowledge searching according to NPI of Thai people in each province.

3.2 Spatial relationship model parameters

Correlation analysis between the mean of keyword searches. These included four words of social distancing, three words of mask wearing, four words of hand washing, and the average of all keyword searches (AVG Total) and the number of confirmed cases during the first wave of outbreaks¹³, the second wave, and the third wave of the outbreak. The study found that the mean of the total number of search queries (AVG Total) correlated with the level of the COVID-19 outbreak, with values of R² = 0.383, 0.021 and 0.474, respectively.

Table 3. Properties of statistical distributions.

	The 1 st Pandemic	The 2 nd Pandemic	The 3 rd Pandemic
Bandwidth	2.879858	137.950868	2.813133
Residual Squares	2702209.332	186704849.9	14280243232
Effective Number	10.595343	2.006451	10.892975
Sigma	201.725233	1577.850477	14697.51778
AICs	1045.278114	1356.847422	1705.944049
R2	0.383345	0.021099	0.473759
R2Adjusted	0.29424	0.007962	0.395007

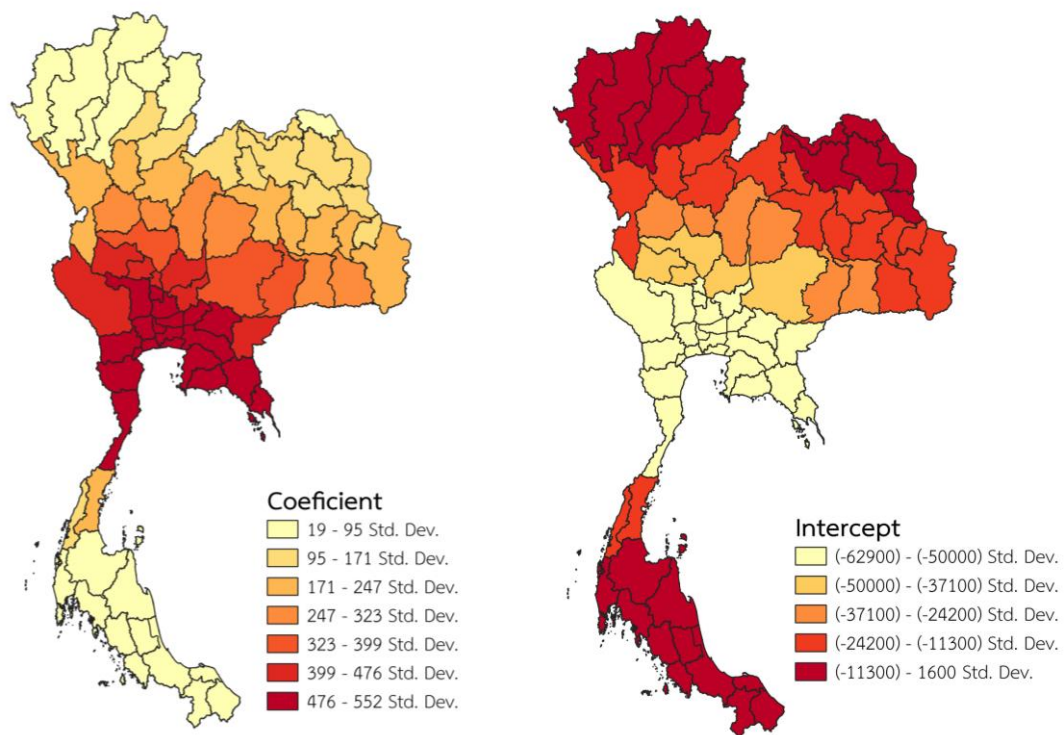


Figure 2. A map showing the spatial distribution of Explanatory variables' Influence towards Dependent variable through the two parameters: local coefficients and local intercepts.

The results of the GWR analysis were presented to show the importance of search in each province. It was found that there was a very high rational correlation in the central region, especially the provinces surrounding Bangkok, including the eastern region and the upper southern region as shown in the map in Figure 2.

4. Conclusion

A search of provincial residents' correlation with the level of infection within the province was evident during the third wave of outbreaks, with a correlation coefficient of 47.38 percent. The correlation between the first wave was 38.33 percent, while the second wave was only 2.11 percent correlation. People are more interested in searching for knowledge from the Internet for self-defense. The search data has a geographic relationship with distribution in the central, eastern and upper southern regions, which are areas with relatively high outbreaks of COVID-19.

5. REFERENCES

- Khataee, Hamid., Scheuring, Istvan., Czirok, Andras., and Neufeld, Zoltan. (2021). "Effects of social distancing on the spreading of COVID-19 inferred from mobile phone data." *Nature: Scientific Report*. 11(1661) (January) doi.org/10.1038/s41598-021-81308-2
- Liu, Yang., Morgenstern, Christian., Kelly, James., Lowe, Rachel., and Jit, Mark. (2021). "The impact of non-pharmaceutical interventions on SARS-CoV-2 transmission across 130 countries and territories." *BMC Medicine*. Vol 19, Number 40 (February). doi.org/10.1186/s12916-020-01872-8.
- Patiño-Lugo, Daniel F., Vélez, Marcela., Salazar, Pamela Velásquez., Vera-Giraldo, Claudia Yaneth., Vélez, Viviana., Marín, Isabel Cristin., Ramírez, Paola Andrea., Quintero, Sebastián Pemberthy., Martínez, Esteban Castrillón., Higuita, Daniel Andrés Pineda., and Henandez, Gilma. (2020). "Non-pharmaceutical interventions for containment, mitigation and suppression of COVID-19 infection." *Colombia Medica*. vol. 51, no. 2. (April). doi.org/10.25100/cm.v51i2.4266
- Rundle, Chandler W., Presley, Colby L., Militello, Michelle., Barber, Cara., Powell, Douglas L., Jacob, Sharon E., Atwater, Amber Reck., Watsky, Kalman L., Yu, Jiade., and Dunnick, Cory A. (2020). "Hand hygiene during COVID-19: Recommendations from the American Contact Dermatitis Society." *Journal of American Academic Dermatol*. 83(6) (December): pp.1730-1737. doi: 10.1016/j.jaad.2020.07.057.
- Li, Yanni., Liang, Mingming., Gao, Liang., Ahmed, Mubashir Ayaz., Uy, John Patrick., Cheng, Ce., Zhou, Qin., and Sun, Chenyu. (2021). "Face masks to prevent transmission of COVID-19: A systematic review and meta-analysis." *Am J Infect Control*. 49(7) (July): pp.900-906. doi: 10.1016/j.ajic.2020.12.007.

DEVELOPMENT OF WEB MAP APPLICATION FOR MAXIMIZING EMERGENCY VEHICLE SERVICE AREA FOR ELDERLY PEOPLE

Kampanart Piyathamrongchai, Wijitra Nakdang, Suwanan Sukjareon and Saowalak Thainsom

Naresuan University, Faculty of Agriculture, Natural Resources and Environment,
Department of Natural Resources and Environment.

99 Moo 9 Tambon Tha Pho, Amphoe Muang Phitsanulok, Thailand, 65000
Email: kampanart@nu.ac.th

ABSTRACT

The purposes of this study were 1) to study and analyze accessibility level of emergency medical service and 2) to develop a web application to locate EMS vehicle parking place in order to cover emergency medical service for elderly people. The web map application was developed using open-source spatial analysis Javascript library i.e. Leaflet and OpenRouteService. The aging population dataset of Thailand collected from Humanitarian Data Exchange was used to analyze 8-minutes-coverage of emergency medical service. The web application allows EMS planners to interactively locate desired standby points for emergency vehicles which can access to elderly people within 8-minutes service areas. The number of elderly population within service areas that correspond to any standby emergency vehicle parking spots would be calculated. The planners could daily use to allocate all available emergency vehicles to maximize the efficiency of services; or it would assist the planners to locate new emergency vehicles to new standby locations for serving the most effective areas without any duplication to other vehicles in the network. The application was tested in some major cities in Thailand and it showed admirable results. This study can be used as a guide for the EMS management to plan the covering of emergency service in order to improve the service efficiency; the relevant organizations will be able to reduce the possible losses in the future.

1. INTRODUCTION

United Nation defined that any countries which have number of over 60 years old population more than 10 percents of total population; these countries will become “aging society”, and more than 20 percents; those countries will call “aged society”. Nowadays, several countries in all over the world have been changed to aging and finally become aged society. Thailand is one of the countries that will turn fully to aged society soon in this decade. The National Statistical Office of Thailand (2018) reported that population aged 60 and above in year 2015 was approximately 13 millions or 19.2% of total population. The number would increase according to prediction model to be approximately 20 millions for population aged over 60 in year 2035, which is about 35% of total population. Thailand established the National Committee of Senior Citizens to provide current policies and programs in order to support older population in Thailand which focused on health, living and care, and social protection (Jitapunkul and Wivatvanit, 2009).

Emergency Medical Service (EMS) is one of a national service which the citizens lived in Thailand can publicly use. The number, 1669, is hotline number which can be used to call emergency vehicle (EV) to pick up people in case of accidents and any sicknesses. In Thailand, the emergency vehicle service is managed by a national organization called “National Institute for Emergency Medicine (NIEM)”. NIEM centrally organizes the EV service in all over country including both vehicles from public and private hospitals, and also vehicles from independent organizations in form of the voluntary foundation. Every major city of each

province in Thailand has at least one voluntary foundation that operates the service cooperated with hospitals within the city.

While every city in Thailand will soon turn to be aging and aged society, the EMS become more and more important. There are more aged people will need the EMS service in nearly future, especially in big cities with very complex transportation network and very traffic. Conventionally, the hospital's EVs stand by at the hospital. However, the EVs from voluntary foundation mostly stand by in any places distributed all over the city area according to the agreement with other foundations in the same city. It comes to state a problem that the standby locations of EV might not be able to cover the need of elderly people in the city.

In this study, a prototype of web map tool was developed in order to assist to better manage the standby locations for emergency vehicle in Thailand. The tool was created using open-source spatial analysis Javascript libraries and frameworks i.e. Leaflet, and OpenRouteService. Aged population dataset of Thailand collected from Humanitarian Data Exchange was used to analyze 8-minutes-coverage of emergency medical service. The web application can interactively be used as a guide for the EMS management to plan the covering of emergency service in order to improve the service efficiency; the relevant organizations will be able to reduce the possible losses in the future.

2. OBJECTIVES

- 2.1 to study and analyze accessibility level of emergency medical service.
 - 2.2 to develop a web application to locate EMS vehicle standby spot in order to cover emergency medical service for elderly people.

3. FRAMEWORK AND METHODOLOGY

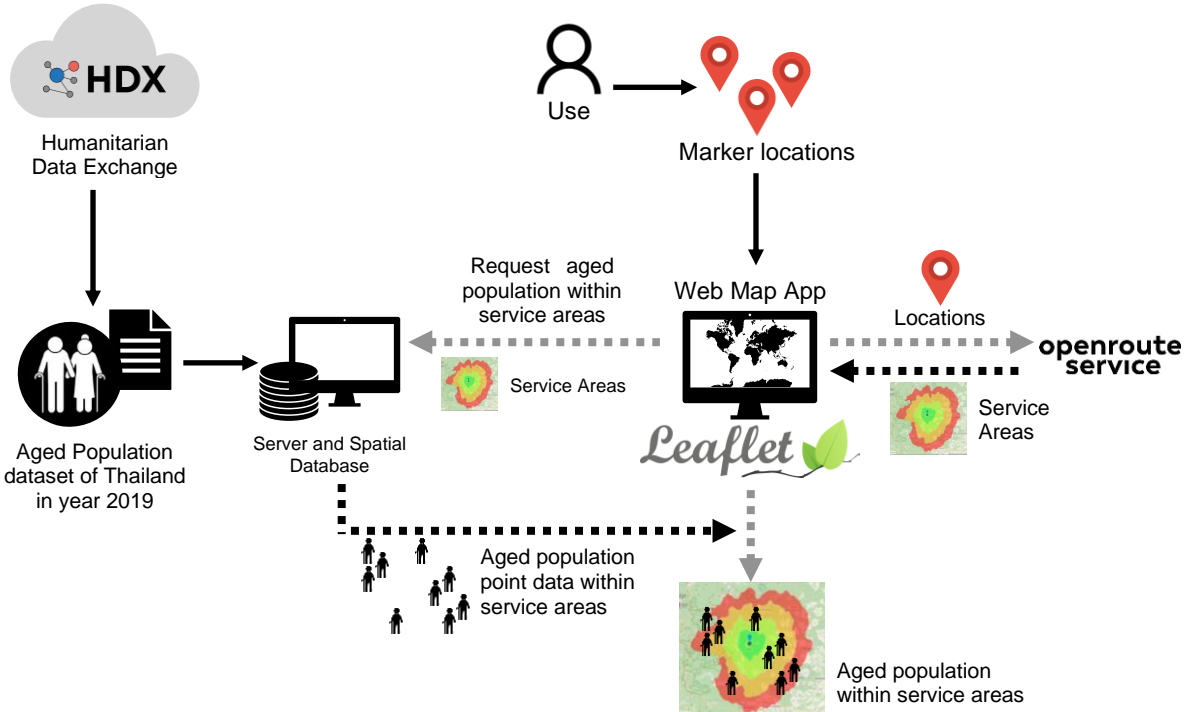


Figure 1. Conceptual Framework

Figure 1 represents the framework of this application. The aged population in year 2019 , which is in form of 30x30 meters resolution image, was collected from humanitarian data exchange (HDX). The dataset was converted into vector format and uploaded to PostgreSQL database server system. A web map application was simply developed based on Leaflet.js library. The

application was designed allowing users to define markers on the map in order to retrieve location information.

Once users determined desired location as standby positions for emergency vehicles, the web application would send a request to the database server according to the bounding box of markers defined to collect aged population within the bounding box. Whereas the web application also send location information to open route service to generate the 8-minutes service area based on submitted locations. Then the web application used spatial query in PostgreSQL to find the aged population which were within those service areas. Finally, the web application would calculate number of aged population within the service areas and report to the display.

4. IMPLEMENT THE APPLICATION

As described in the last topic, there are four major issues to be described: aged population information, web map interface, using OpenRouteService to generate the service area, and using spatial query to evaluate aged population within the service area. This section discusses each component in the way that were used in this study.

4.1 Aged population from HDX

Aged population data was downloaded from humanitarian data exchange website (<https://data.humdata.org/>). The data was in 30x30 meters Geotiff raster format— so it needed to be converted into vector data format as shown in Figure 2. Each point contains number of population data in the attribute table. The data was imported to PostgreSQL database system to provide as a service.

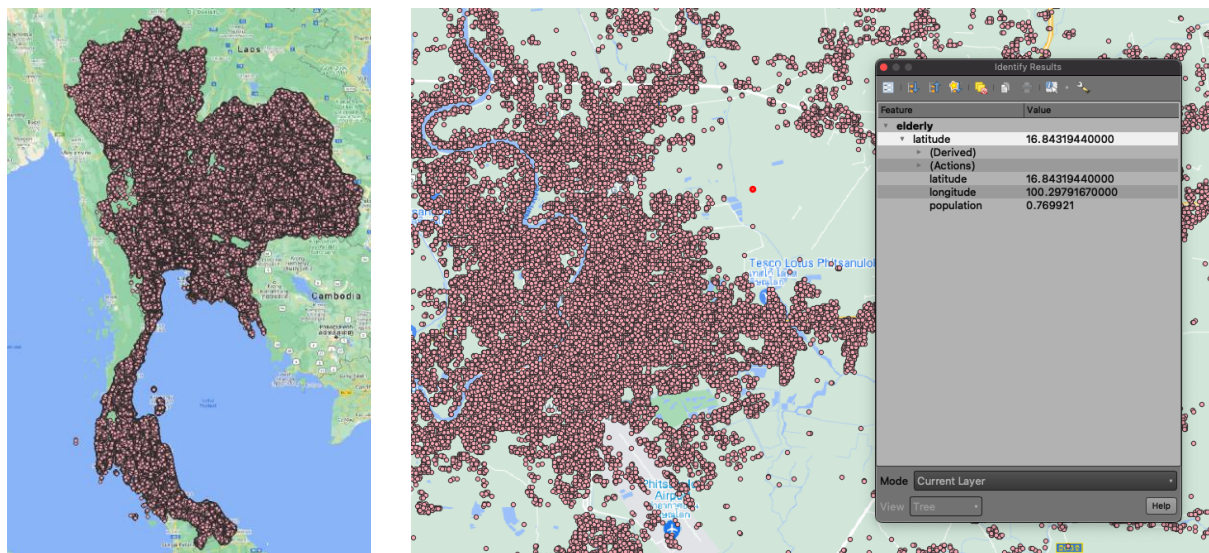


Figure 2. Aged Population from HDX

4.2 Web map interface development

The web map interface was simply developed using traditional web programming languages and using web map javascript library called Leaflet.js. In the application, users can choose the area and locate desired markers which is the standby spots for the EVs (in this



Figure 3. Web map interface and tool to locate standby spots for EV

prototype level, only 5 spots can be determined) as shown in Figure 3.

4.3 Generating service areas using OpenRouteService

When the user already located standby spots for the EV in an area, service areas can then be generated using OpenRouteService API. In this study, the service areas were created based on 8 minutes traveling time which is critical time to rescue patients in traumatic cases. Figure 4 represents examples of service area generation of Phitsanulok and Bangkok city. The service areas generated would measure from the standby spots covering 8 minutes traveling time along

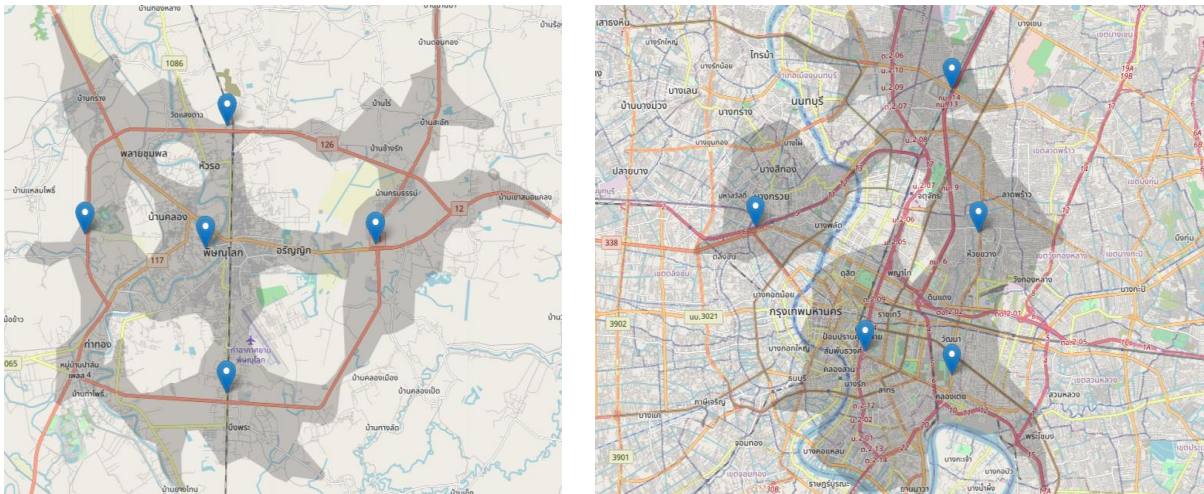


Figure 4. Example of service areas of Phitsanulok and Bangkok

the road network.

4.4 Evaluating aged population within the service areas

The service areas generated in the last section was sent as spatial logical request to the spatial database to compute the number of aged population within the service areas. The spatial SQL was used in order to filter the aged population point in the database which are within the service

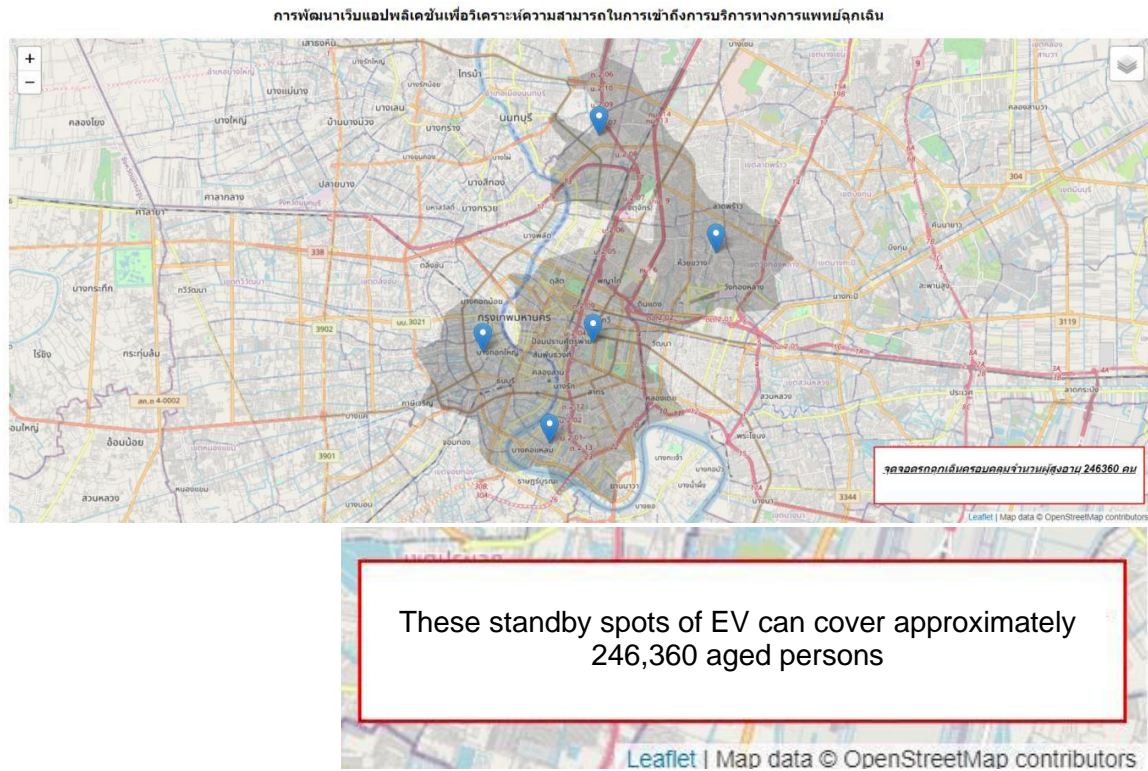


Figure 5. Example of 8-minutes service areas and number of aged population within the area in Bangkok city

areas. The number of aged population was reported in the web page as shown in Figure 5.

5. TESTING THE APPLICATION

As shown in Figure 2, the web application can be used in every city in Thailand. This section would represent some examples of city in Thailand which used this application to estimate the number of aged population within the service areas. Figure 6 represents six sample cities to create service area to calculate the number of aged people within the service areas. For example, if we planned to locate 5 standby spots for EV all over Chiang Mai city as shown in the figure, these 5 emergency vehicles could access to 36,500 aged people within 8 minutes. Therefore users can use the application to find the best standby spots that serve as many as aged people.

6. SUMMARY AND RECOMMENDATION

This prototype was developed by taking advantage of open source libraries and frameworks including Leaflet.js and OpenRouteService to create a simple application which can use to maximize the service of EV in the emergency medical service. Leaflet.js is ideal javascript library to create a web map with many splendid mapping tools and useful plugins. The OpenRouteService is perfect free API services for routing service and isochrone generation. The Humanitarian Data Exchange is a fine resource that provides demographic data in very detail up to 30x30 meters resolution covered the whole country. The application can be useful for planning suitable standby spots for emergency vehicles in order to maximize the coverage of service area.

Nonetheless, this is only a prototype stage that depict possibility to use big data in the

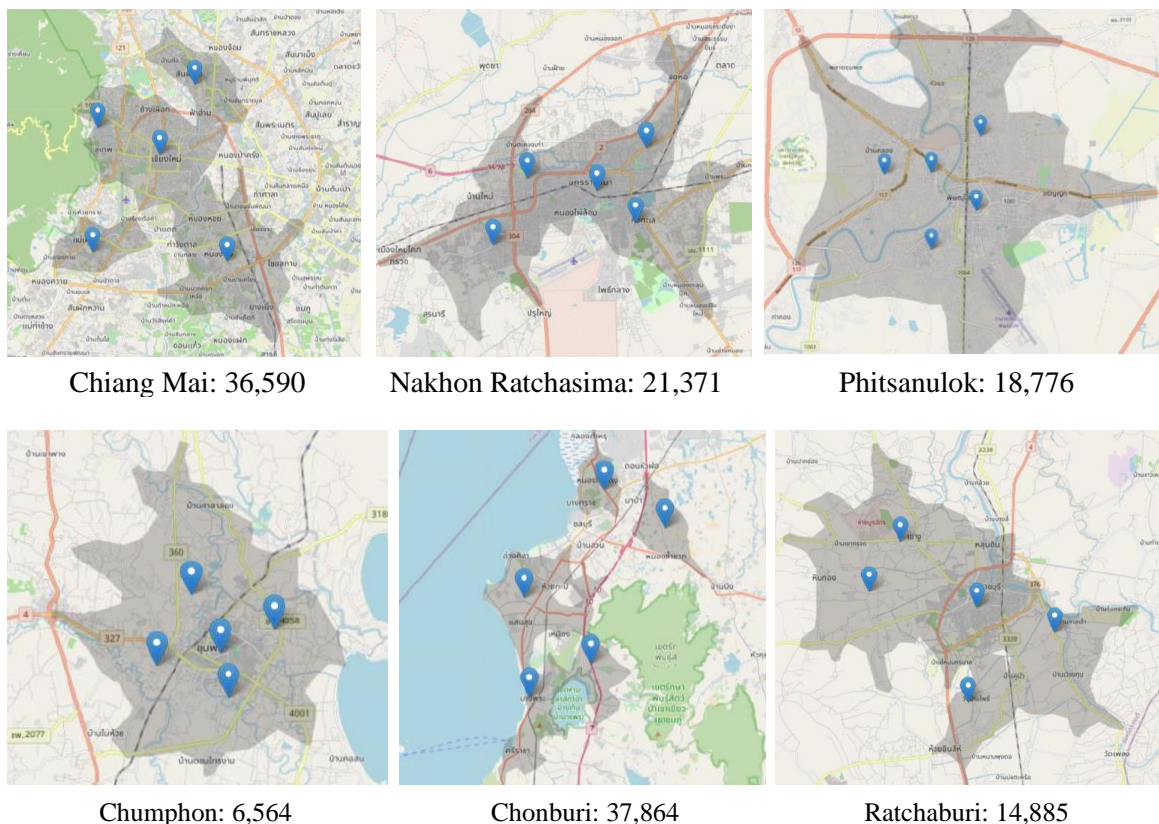


Figure 6. Applying the application to some examples of city in Thailand

open source web map application. It is feasible to make this application more efficient in several ways. For instance, we can extend the capability of the web application to find the best standby spots according to cluster of aged population without trial and error; we can also add up other map data layers to the application such as total population, other vulnerable demographic information or even accident incident points (Piyathamrongchai, 2018).

7. REFERENCES

- Humanitarian Data Exchange. Available Online at <https://data.humdata.org>.
- Jitapunkul, S and Wivatvanit, S. (2009). National Policies and Programs for the Aging Population in Thailand. *Aging International*, 33:62–74.
- National Institute for Emergency Medicine. (2020). Annual Report 2020, Available online at <https://www.niems.go.th/l/Ebook/Detail/12363?group=23>.
- National Statistical Office of Thailand (2018). Report on the 2017 survey of older persons in Thailand. Available online at http://www.nso.go.th/sites/2014en/Survey/social/domographic/OlderPersons/2017/Full%20Report_080618.pdf.
- Piyathamrongchai, K. (2018). Spatio-Temporal Pattern of Traffic Accident in Thailand in Year 2018. *Thai Geographical Journal*, 43, vol.2, Jul-Dec 2018.

Accuracy and effectiveness of 3D model reconstruction from UAV photogrammetry for physical road safety investigation

**Polpreecha Chidburee^{1*}, Boonphol Meechaiyo¹, Kumpon Subsomboon¹,
and Jittiwat Tonnamon²**

¹ Department of Civil Engineering, Faculty of Engineering, Naresuan University, Phitsanulok, Thailand

*Corresponding author: Email: polpreechac@nu.ac.th

Email: boonponm@nu.ac.th, kumpon@nu.ac.th

²Department of Natural Resources and Environment, Faculty of Agriculture Natural Resources and Environment, Naresuan University, Phitsanulok, Thailand.

Email: jittiwatt60@nu.ac.th

ABSTRACT

Traffic accidents are one of a serious cause that pose a threat to human life and economic loss. In particular, road safety is one of the keys to help prevent traffic accident. Hence, the risk assessment of physical factors for roads is very important for road safety audits. This research attempts to employ UAV photogrammetry for the three-dimensional model reconstruction of the physical road in order to help reduce the process of data collection for road inspector in risk assessment of road safety. The study area in the research is the intersection of road in the Naresuan University, Phitsanulok province, Thailand. Image acquisition of UAV photogrammetric approach was taken using DJI Phantom4 Pro V2.0 at 50 and 70 m of the flight height above the ground. Next, 3D reconstruction from the UAV imagery was performed using WebODM opensource software and ContextCapture commercial software to generate a 3D model for evaluating the physical conditions of the road by visualization. The results show that the use of opensource software has many benefits for UAV photogrammetric processing almost as potential as commercial software. Accuracy assessment of 3D models of the road obtained from between 50 and 70 meters at the UAV flight height was insignificantly different. Both models could provide accuracy in decimeter-level. However, the completeness and details of 3D model obtained from an UAV flight height at 50 meters above the ground were better than at 70 meters. For the risk assessment of physical roads from the 3D model, the optimal speed limits on the curve should be 40 km/hr following a guiding advice of road safety. Therefore, UAV photogrammetry can be utilized for the primary investigation of physical road safety and offering the guidelines for improving road safety to the relevant agencies.

1. INTRODUCTION

The physical road conditions are one of the factors in traffic accidents that can lead to damages to human life and properties. In order to reduce the impacts of traffic accidents, the risk assessment of physical factors on roads is essential for road safety. It should provide the guidelines for reducing traffic accidents to relevant agencies, especially improving road safety. For the improvement of road safety, there are four main stages, as follows: (i) survey the risk areas of traffic accidents in the community; (ii) analyze to find the points of high-risk areas for traffic accidents; (iii) draft the high-risky points of traffic accidents on a map; (iv) review and design the improvement of the high-risky points of traffic accidents. Therefore, the survey and improvement of high-risk points for traffic accidents are crucial to help decrease the negative impacts of accidents (Zahran et al., 2021).

Traditionally, the inspection of the physical roads for assessing road safety can use many methods such as field surveying and the use of tape measurement. If a road safety audit needs to inspect a large area, it will be time-consuming and labor-intensive to survey in the field.

Also, it might be very costly compared to conventional survey. In the present, the UAV photogrammetry has an important role in the applications of topographic survey because it can help for time-saving methods and reducing the cost of survey (Ismael & Henari, 2019). In particular, the UAV approach has been widely used that is concerned with the study of the physical factors for roads. For example, the use of an unmanned aerial vehicle (UAV) can apply to provide the topographic data for road design and traffic accident investigation (Outay et al., 2020; Pérez et al., 2019; Zulkipli & Tahar, 2018). Thus, the application of UAV photogrammetry has enormous potential for surveying the physical road conditions in order to assess the road safety. As a result, the information of the road safety will be utilized for effectively improving the physical factors of road.

In this paper, we present the potential of UAV photogrammetry to facilitate the assessment of the road safety from the physical factors for roads. The study area focused on places that had experienced traffic accidents. The image acquisition was taken using the UAV platform at different altitudes in order to offer the suitable photogrammetric results. For the 3D reconstruction of road obtained from the UAV imagery, the use of open source/free software were compared to commercial software in order to evaluate the photogrammetric results from different software packages for photogrammetric processing. The assessment of the physical factors for this road was preformed through 3D visualization method from 3D model. The outcomes of assessed physical conditions and guidelines for improvement will offer to relevant agencies in the university for improving the road safety.

2. MATERIALS AND METHODS

2.1 Study area

The study site focused in the road of the researcher's workplace that had used traffic accidents. The study area was located at the intersection of road, near the King Naresuan Monument, in Naresuan University, Phitsanulok province, Thailand, as shown in Figure 1. The type of this intersection is the three-leg or T-intersection. Each leg of intersection comprising two lanes of concrete roads. The main roads of intersection are cruve and many vehicles often use over speed limits at 40 km/hr. That is one reason why traffic accident at this intersection.

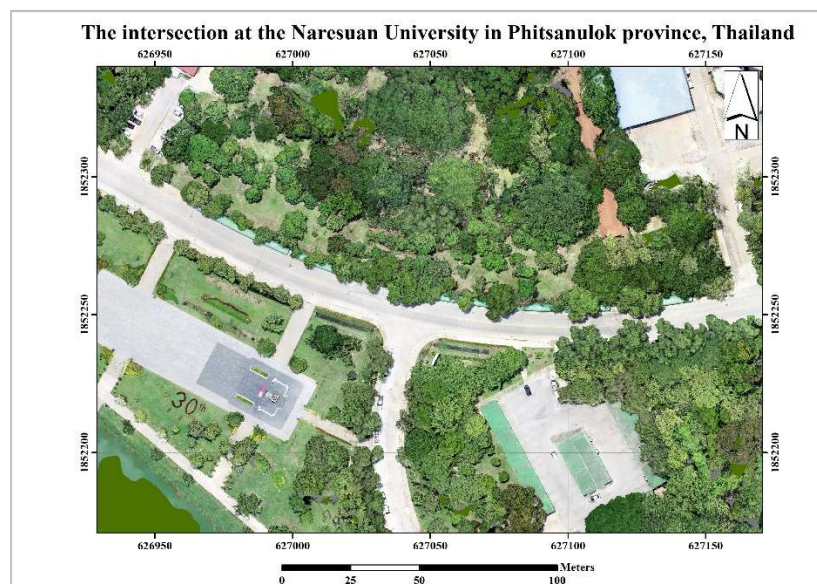


Figure 1. The intersection used in this study area.

2.2 Instruments and software packages

The UAV platform used for this study is the DJI Phantom 4 Pro V2.0 with 20MP of digital camera. The DJI GO 4 and the Pix4D capture mobile applications is used for setting up functions and flight plans for the DJI Phantom 4 UAV. For photogrammetric processing from the UAV imagery, the WebODM opensource/free software and the ContextCapture commercial software are utilized to generate a 3D model of the intersection and deliver photogrammetric results, such as orthophoto and Digital surface model (DSM). The visualization of 3D model for the intersection uses the CloudCompare opensource software. Finally, the QGIS opensource software help for assessing the quality and accuracy of photogrammetric results and calculating the design of speed limits on the road.

2.3 Methodology

The purpose of study is the application of UAV photogrammetry in order to inspect the physical factors of the intersection for evaluating the road safety. Figure 2 illustrates the methodology used for this study.

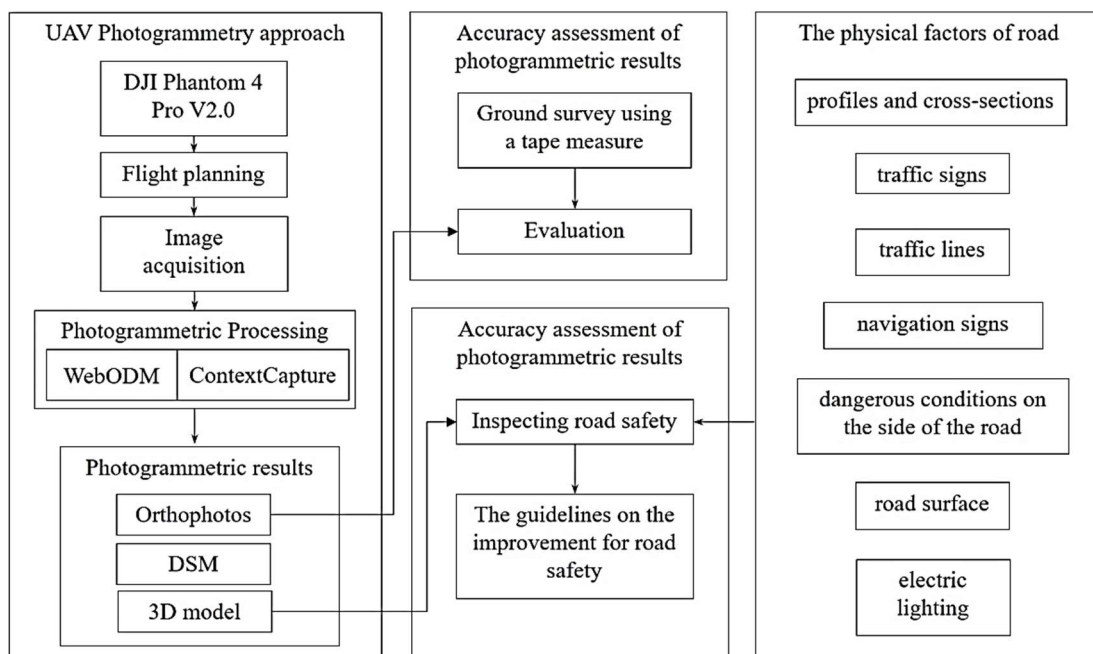


Figure 2. The methodology schema in this study.

2.3.1 Data acquisition

The flight planning for the UAV flying was designed using the Pix4D capture application on a mobile phone with the flying height at 50 meters and 70 meters above the ground, cross strips for flying direction and the 45 degrees of camera angle. As a result, there were two photosets, including: (i) 228 images for 50 meters of UAV flying height; (ii) 144 images for 70 meters of UAV flying height.

2.3.2 Photogrammetric processing and assessing photogrammetric results

After image acquisition, both photosets were processed using the WebODM software and the ContextCapture software for 3D reconstruction of the intersection. Georeferencing was based on the GNSS observation of UAV. The photogrammetric results obtained from the WebODM software were compared to the results of the ContextCapture software to evaluate

the potential of opensource/free software for photogrammetric processing. As the ContextCapture commercial software was able to provide high precision of photogrammetric measurement, that we assumed this software was used for a benchmark software in this study. To evaluate the accuracy of photogrammetric results, measuring the 30 widths of traffic lanes from the 3D models was compared to measuring the actual widths of roads in the field. The statistical errors such as Mean, Root Mean Squared Error (RMSE) from both photogrammetric software packages were calculated from the aforementioned comparison.

2.3.3 The investigation of road safety

Regarding the assessment of road safety for this intersection, the physical factors and characteristics of the road were analyzed following the principles for road safety of Department of Rural Roads (DRR), Thailand. To follow the recommendations for road safety, the roads should comprise physical factors or instruments on/alongside the road, such as profiles and cross-sections of the road, traffic signs, traffic lines, navigation signs, dangerous conditions on the side of the road, road surface, and electric lighting. The assessment of road safety was manually performed using 3D visualization on the CloudCompare software.

3. RESULTS AND DISCUSSION

Based on an UAV approach for the intersection of this study area, the results of 3D models obtained from the WebODM and ContextCapture photogrammetric software packages are presented in Figure 3.



Figure 3. The 3D models obtained from (a) WebODM, and (b) ContextCapture using the UAV flying height at (1) 50 meters, and (2) 70 meters above the ground.

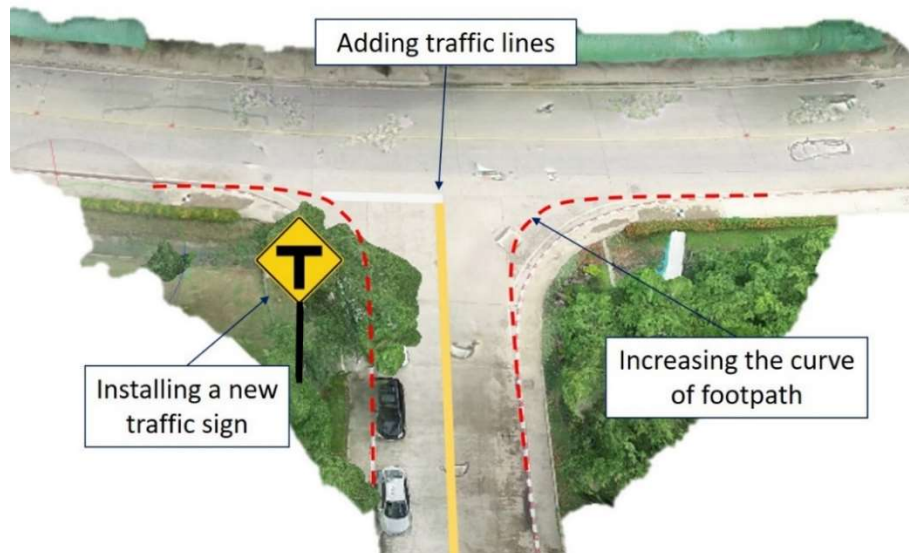
Regarding the comparison of 3D modeling results, as shown in Figure 3, the completeness of 3D model obtained from WebODM software had noticeably lesser clarity than from ContextCapture software. However, using different altitudes for UAV flying, the generated 3D models of each software were insignificantly different. For assessing the photogrammetric accuracy from different software packages and different altitudes of UAV, the values of statistical errors from both photogrammetric software packages are showed in Table 1.

Table 1. The statistical errors for the assessment of photogrammetric accuracy.

Software	UAV flying height (m)	Errors	
		Mean (m)	RMSE(m)
WebODM	50	0.073	0.088
	70	0.095	0.104
ContextCapture	50	0.042	0.071
	70	0.054	0.082

From Table 1, the accuracy of photogrammetric results obtained from ContextCapture software was higher than from WebODM software. Moreover, the accuracy assessment of 3D models at different altitudes of the UAV flying obtained from the same software was slightly different.

For the risk assessment from the physical factors of the road, the orthophoto from UAV photogrammetric results was used to calculate the radius of the curve using QGIS software. As a result, the radius of this curve was approximately 250 meters. Normally, the speed limits of this designed curve should not more than 60 – 70 kilometers per hour. However, the suitable speed limits of the curve for all vehicles should not more than 40 kilometers per hour following a guideline for road safety. That is the reason why traffic accidents might happen easily at the intersection. Road safety is not guaranteed by road design and construction regulations (Huvarinen et al., 2017). Hence, this intersection should have improved to increase road safety, as illustrated in Figure 4.

**Figure 4.** The guidelines on the improvement of the intersection for road safety.

4. CONCLUSIONS

The potential of the UAV photogrammetry has been utilized for inspecting preliminary road safety for this study. The application of UAV approach also helps decrease time-consuming and labor-intensive methods of road safety audits. Evaluating some physical factors of roads can identify on the 3D model reconstructed from the UAV imagery that facilitates extensively the assessment of the road safety. In this study, the photogrammetric accuracy from UAV approach depends on the photogrammetric software for processing. The WebODM opensource/free software can be potentially used for generating 3D models and photogrammetric results that provide accuracy at decimeter level. The outcomes of UAV photogrammetry (i.e. orthophotos) were used to analyze the causes of traffic accidents for decreasing human and economic loss. Moreover, a 3D model of the road was applied for offering guidelines on the improvement of road safety in the future.

5. REFERENCES

- Huvarinen, Y., Svatkova, E., Oleshchenko, E., & Pushchina, S. (2017). Road Safety Audit. *Transportation Research Procedia*, 20, 236-241. <https://doi.org/https://doi.org/10.1016/j.trpro.2017.01.061>
- Ismael, R. Q., & Henari, Q. Z. (2019, 23-25 June 2019). Accuracy Assessment of UAV photogrammetry for Large Scale Topographic Mapping. 2019 International Engineering Conference (IEC),
- Outay, F., Mengash, H. A., & Adnan, M. (2020). Applications of unmanned aerial vehicle (UAV) in road safety, traffic and highway infrastructure management: Recent advances and challenges. *Transportation Research Part A: Policy and Practice*, 141, 116-129. <https://doi.org/https://doi.org/10.1016/j.tra.2020.09.018>
- Pérez, J. A., Gonçalves, G. R., Rangel, J. M. G., & Ortega, P. F. (2019). Accuracy and effectiveness of orthophotos obtained from low cost UASs video imagery for traffic accident scenes documentation. *Advances in Engineering Software*, 132, 47-54. <https://doi.org/https://doi.org/10.1016/j.advengsoft.2019.03.010>
- Zahran, E.-S. M. M., Tan, S. J., Tan, E. H. A., Mohamad 'Asri Putra, N. A. A. B., Yap, Y. H., & Abdul Rahman, E. K. (2021). Spatial analysis of road traffic accident hotspots: evaluation and validation of recent approaches using road safety audit. *Journal of Transportation Safety & Security*, 13(6), 575-604. <https://doi.org/10.1080/19439962.2019.1658673>
- Zulkipli, M. A., & Tahar, K. N. (2018). Multirotor UAV-Based Photogrammetric Mapping for Road Design. *International Journal of Optics*, 2018, 1871058. <https://doi.org/10.1155/2018/1871058>

STUDY OF THE ACCURACY OF UAV SURVEY TECHNOLOGY FOR TOPOLOGY MAPPING ON DISCREPANCY TERRAIN CONDITIONS

Quang Khanh Nguyen¹, Anh The Hoang^{2,3*}, Thi Phuong Thao Ngo¹

¹HaNoi University of Mining and Geology
 18 Pho Vien, Duc Thang, Bac Tu Liem, Ha Noi, Vietnam
 Email: nguyenquangkhanh@humg.edu.vn; ngothiphuongthao@humg.edu.vn
²School of Agriculture and Natural Resource, Vinh University
 182 Le Duan, Vinh, Nghe An, Vietnam
 *Corresponding author Email: anhthe.dhv@gmail.com
³Department of Geophysics, School of Geodesy and Geomatics, Wuhan University
 Wuhan, HuBei, China

ABSTRACT

The create topographic map of hilly and mountainous area has long been a difficult problem for manufacturers in terms of both measurement methods and accuracy requirements. Traditional technologies such as total station method, aerial photography or RTK-GPS ... all have their own advantages and disadvantages. Currently, Unmanned Aerial Vehicles - UAV technology is being applied a lot in the field of mapping and is increasingly improving to have better results in production. But how much accuracy it has with comparing traditional survey methods in the discrepancy of terrain conditions? So, we have checked its in the 500ha hilly areas in Vietnam. Those areas have much different elevation (200m), hiking trails, build-up area, slope and flat area. The topographic map was conducted using UAV technology (with Phantom 4 RTK unmanned aircraft) had done the comparison with the checking points generated by RTK-GPS in term of accuracy. The result shows that the map produced by UAV technology matched with the topographic map do by RTK-GPS. Therefore, it can be concluded that the UAV technology can be considered as an alternative technique for production the topographic map.

Keywords: Unmanned Aerial Vehicles, UAV mapping, UAV, topographic map

1. INTRODUCTION

The topographic map play an important role in our daily life, it has been used in many fields such as urban planning, civil engineering, transportation, irrigation, ... The Independent Expert Advisory Group (2014) on a Data Revolution for Sustainable Development emphasized on the need for highquality and usable data, as “data are the lifeblood of decision-making”, and topographic maps is one of the accepted data. Therefore, the establishment of topographic maps is always interested in researchs by many organizations and individuals.

In creating the topographic map, the measurement in hilly and mountainous areas with many Discrepancy Terrain Conditions has been a difficult problem of both measurement methods and accuracy requirements for a long time. We can use the following technologies to create topographic map of hilly and mountainous areas: total station, RTK – GPS (Real Time Kinematic Global Position System), airborne LiDAR. In the above technologies, the total station technology and GNSS technology holds the highest accuracy level. With the total station technology, the measurement uncertainty is depends on the distance between points and other factors, but can get as low as in mm-level (Engberg 2015) and with the the RTK-GPS technology, precision can reach a level of some millimetres in post- processing, depending on the way the computation is done and the quality of the GNSS receiver (Royal Observatory of Belgium GNSS Research Group 2017). However, those technologies are very

laborious, time costing, and economically expensive. Airborne LiDAR technology allows to draw large areas with the accuracy required but the cost of implementing this technology is quite high, affecting the cost of the product. Therefore, finding solutions to create topology map of hilly and mountainous areas to ensure accuracy and economic savings is a problem that opens to scientists.

One of the emerging technologies being applied recently is Unmanned Aerial Vehicles (UAVs), which are being proved to be a good method to create topographic map. Unmanned aerial vehicles were initially used for military purposes, however, because of its advantages, nowadays UAV is applied in different fields, especially in civil and scientific research activities. For example, surveying and cadastral applications (Cramer et al. 2013; Barnes et al. 2014), coastal management (Delacourt et al. 2009), disaster response and monitoring (Molina et al. 2012; Boccardo et al. 2015), damage mapping (Vetrivel et al. 2015), forest and agriculture and geological investigations (Saari et al. 2011)... However, in UAV technology, with each flying device, each flight setting and different image processing software will give us different accuracy levels. And each discrepancy terrain (hills, plains, coastal, slope ...) will need to apply a different flight procedure, image processing method to produce consistent results. Each study will provide a new perspective on the application of flying equipment in topographic mapping. Therefore, we conduct to research the application of unmanned aerial vehicle (UAV) data to create topographic map of hilly area.

In this study, we propose the process of measuring mapping at mountainous areas using UAV technology and on the basis of applying Phantom 4 RTK unmanned aircraft data to create topographic map of the tea plantation hills of Phu Tho province of Vietnam.

2. RESEARCH APPROACH

2.1 Study Area

The study area is a tea growing area in Thanhson district, Phu Tho province, Vietnam (Figure 1a). The total study area is about 500 hectares. This is an area with high hill-mountain terrain, with alternating population (Figure 1b). The highest point in the study area has an altitude of 250 meters, the lowest point has an altitude of 70 meters. Because of the characteristics of the landform in this area including the large study area, high mountainous terrain, build-up, slope area and tea plantations, the researchers will take a long time and get a lot of difficulties in using the total station method to create topographic maps. Therefore, in this study, we will use the UAV method to create topographic maps and check the accuracy by RTK-GPS at some discrepancy terrain conditions.



Figure 1. a) The study area in Phu Tho, Vietnam. b) The terrain conditions in the study area

2.2 Methodology

In this study, the research methodology is done as showing in Figure 2. After choosing the Area for Topology mapping, we established the Ground Control Points (GCPs). The GCP is used for setting the Base Station for RTK UAV flying (translation the coordinates to the central images coordinates shooting on UAV) and for the Rover RTK GPS to measure the detail ground map. The topographic map was conducted by two methods (UAV Mapping and GPS Mapping). Finally, some tools will be used for analyzing the accuracy on the discrepancy terrain conditions. And the last phase is conclusion.

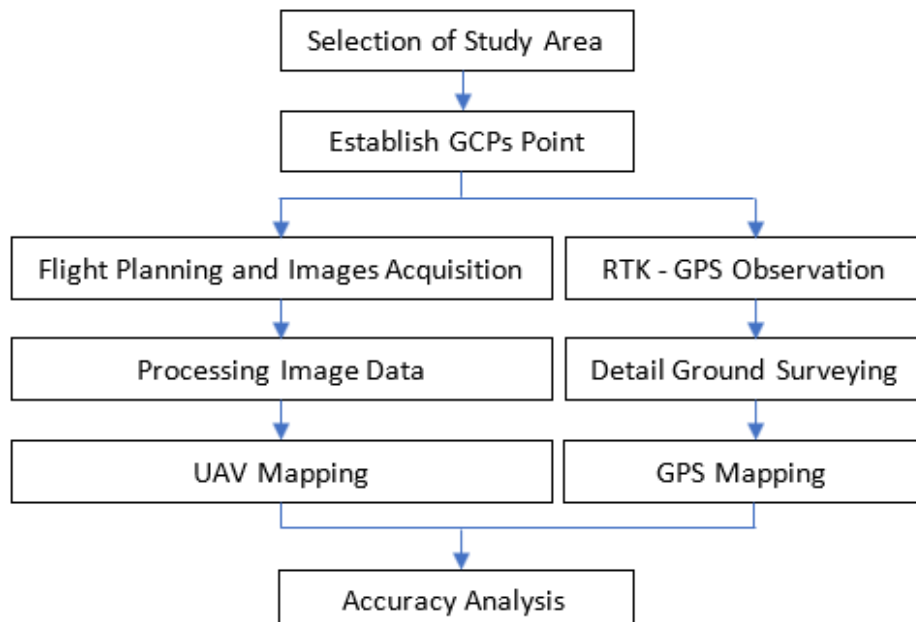


Figure 2. Research methodology framework

2.3 UAV mapping

2.3.1 Equipment

Unmanned aerial vehicles (UAV) has been known such as aircraft itself which is intended to be operated without a pilot-on-board, remotely or autonomously controlled by on-board computers.

Based on its structure and type of taking-off and landing operation, UAVs are divided into 2 main types: fixed-wing and rotary-wing. Each type has its own advantages and disadvantages, and when measuring in mountainous areas, they often use an airplane with rotary-wing. One of the most important details to consider on the specs of its camera, including its resolution and focal length. Different camera models will provide different resolution qualities, resulting in variety of the spatial resolution of the UAV (also called the ground sampling distance - GSD). Phantom 4 RTK type of rotary-wing aircraft with four powerful rotors is equipped with the positioning system GNSS and RTK receiver to achieve position accuracy of up to cm level. Phantom 4 RTK uses a camera with CMOS sensor of 1", resolution of 20 Mpx, focal length f2.8 - f11, lens field 84°, can recognize objects 2.74 cm at flight height 100m (<https://www.dji.com/phantom-4-rtk>).

The general structure of the UAV system includes four main parts: The aircraft; The digital camera; The ground control station; The image processing station. In this research, we used Phantom 4 RTK, the UAV mapping production of DJI, to do the UAV mapping (Figure 3).



Figure 3. Phantom 4 RTK unmanned aerial vehicles (UAV) system

2.3.2. *Ground Control Point (GCP)*

The use of Ground Control Points is an important element that could have a substantial impact on the accuracy of the DSM model. GCPs are elements which present in the field or artificial targets points (These points have known coordinates) and can be clearly recognized in the photo sequence acquired by UAV. The number of GCPs depend on the required final accuracy of the position of the DSM and the quality of the UAV positioning system. The coordinate of GCPs is acquired using GNSS or total stations.

In this study, we conducted field reconnaissance to select safe areas to place the GCPs. The number of GCPs is 03 point (namely GCP1, GCP2 and GCP3), evenly distributed over the study area. We use artificial marker, marked with highly reflective material, the geometry and the center is perfectly defined, and it can be correctly measured with high accuracy. We also set up 2 checking points (namely Check Pt1 and Check Pt2) to determine the accuracy of image model (Figure 4).



Figure 4. The position of GCPs and Checking point on the site

2.3.3 *Flight planning and Image acquisition*

One of the most crucial activities that should be considered for every aerial surveying project using UAVs, the first obligatory part is flight planning. When planning a flight, some important parameters need to be considered, such as: flying height, ground sample distance (GSD), camera information, UAV's batteries duration, maximum distance from the ground control station, availability and distribution of GCPs... Flight planning uses the software that comes with the aircraft.

To shoot the images of all the study areas cover 500 hectares, the flight planning has set up in three flight sections by the Control Station of the Phantom 4 RTK. The altitude for data acquisition of RGB images using UAV was 180 meter to get the image with size 5472x3648 pixels. Each flight, the Base Station was put at the GCP, the coordinate of GCP was input to the Base Station to transmit to the Aircraft (Figure 5). The result of the flight process, we had 641 images with means error of position center image coordinate was 0.018 meter.

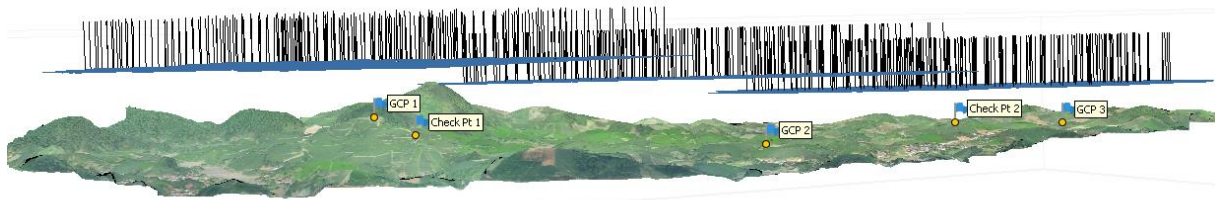


Figure 5. Image acquisition from three flights

2.3.4 Data Processing and Map Editorial

Image data processing is done by software. With an iterative procedure, this software is able to reconstruct firstly a sparse point clouds and then a dense one that is generally preferred in case of terrain/surface reconstruction. After, the dense point cloud could be interpolated, simplified, classified, and finally textured for photo-realistic visualization (Nex and Remondino 2015). All the data obtained from UAV observation were processed using Agisoft Metashape Professional 1.5.2.

Agisoft Metashape Professional software was used to mosaic the imagery and align it with georeferenced points using Structure from Motion (SfM) algorithms. For each set of images, Agisoft Metashape Professional software automatically aligns the images and builds point cloud models of the surface. Agisoft allows to generate and to visualize a dense point cloud model based on the estimated camera positions to combine into a single dense point cloud. The whole process flow of mosaicking RGB imagery is summarized as in Figure 6. The result of the mosaicking process is presented as in Figure 7a, Figure 7b.

Figure 7a shows the orthophoto image produced by the mosaicking process. The orthophoto is an aerial photograph or image geometrically corrected ("orthorectified") so that the scale of the map is uniform for the whole study area. The orthophoto image provides the information about the ground resolution of 7.8 cm per pixel for the study area.

Figure 7b shows the digital elevation model obtained from the mosaicking process. The digital elevation model provides information about the terrain surface of the study area with vertical resolution of 30 cm per pixel.

The topographic map was created by Civil 3D 2019 software, the Orthophoto Image was insetted to the drawing and using the drawing tools of Civil 3D to draw the hiking trails, vegetation area, build-up area of the topology map. The elevation of the topology map was created by Global Mapper V21.1.0 that is including the detail elevation points and the contour lines with 2m interval (Figure 7c).

2.4 GPS Mapping

The topographic map will be completed with the addition of measuring points at

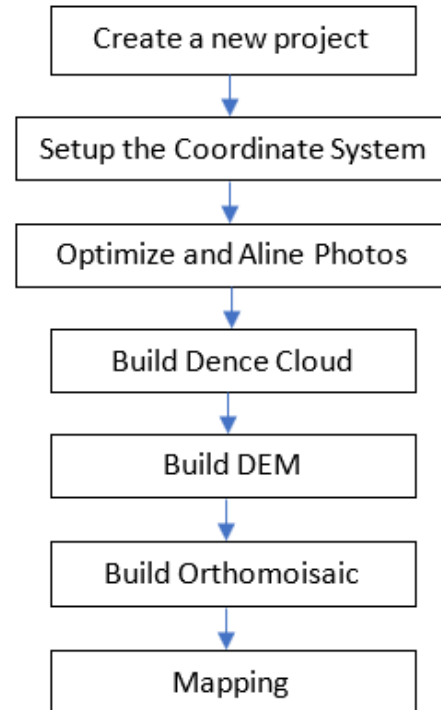


Figure 6. Flow chart for Mapping by Agisoft Metashape Professional software

difficult locations by using RTK-GPS surveying technology. The GPS equipment was used is Stonex 980A (integrated GNSS receiver tracks all satellite signals GPS, GLONASS, BEIDOU, GALILEO, QZSS and IRNSS). The data getting from RTK GPS surveying technique was imported to the AutoCAD 2019 to edit the topographic map.

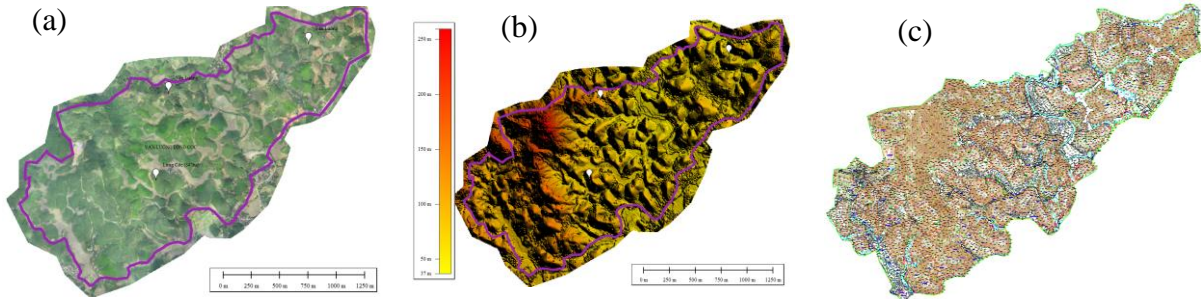


Figure 7. Data processing results
a. Orthophoto, b. Digital elevation model, c. Topographic map

3. ANALYSIS AND RESULTS

We selected areas with different topography to test (Figure 8). Quantitative analysis is about the numerical quantity that can be done by calculating or computation of the data. Quantitative assessment was carried out by calculating root mean square error (RMSE).



Figure 8. The areas of discrepancy terrain conditions for assessment the accuracy

The distance difference between UAV and RTK-GPS and RMSE are calculated by Eq. (1) and Eq. (2) as follows:

$$d = \sqrt{(X_{RTK_GPS} - X_{UAV})^2 + (Y_{RTK_GPS} - Y_{UAV})^2} \quad (1)$$

$$RMSE_{Coordinate} = \sqrt{\frac{\sum(d_i - \bar{d})^2}{n}} \quad (2)$$

The elevation difference between UAV and RTK-GPS are calculated by Eq. (3) and Eq. (4) as follows:

$$h = Z_{RTK_GPS} - Z_{UAV} \quad (3)$$

$$RMSE_{Elevation} = \sqrt{\frac{\sum(h_i - \bar{h})^2}{n}} \quad (4)$$

Where X , Y are horizontal coordinates and Z is elevation (obtained by UAV method and RTK-GPS method), \bar{d} and \bar{h} are the mean values, n is number of samples.

Table 1a: Comparison of coordinates (X-Y) obtained from UAV and RTK-GPS

POINT	UAV Coordinate (meter)		RTK-GPS Coordinate (meter)		Discrepancy Distance (meter)	Remark
	X (North)	Y (East)	X (North)	Y (East)		
1	2338441.558	533700.584	2338441.473	533700.522	0.105	House corner
2	2338472.092	533712.736	2338472.061	533712.643	0.098	-
3	2338468.009	533685.729	2338467.909	533685.671	0.115	-
4	2338500.807	533672.156	2338500.758	533672.122	0.060	-
5	2338507.844	533660.680	2338507.770	533660.654	0.078	-
6	2338408.781	533739.059	2338408.754	533739.006	0.059	-
7	2337599.136	532856.763	2337599.110	532856.696	0.072	-
8	2337617.996	532796.688	2337617.903	532796.649	0.101	-
9	2337599.152	532856.785	2337599.110	532856.696	0.098	-
10	2337506.914	532924.791	2337506.840	532924.722	0.101	-
11	2337487.165	532980.816	2337487.164	532980.807	0.009	-
12	2337387.179	532030.621	2337387.099	532030.547	0.109	-
13	2337279.669	531987.997	2337279.631	531987.961	0.052	-
14	2336926.255	532109.837	2336926.189	532109.759	0.102	-
15	2336898.437	532158.347	2336898.373	532158.301	0.079	-
16	2336828.387	532127.298	2336828.380	532127.221	0.077	-
17	2336761.658	532148.779	2336761.654	532148.715	0.064	-
18	2336696.192	532101.494	2336696.100	532101.412	0.124	-
19	2336675.493	532170.268	2336675.444	532170.242	0.055	Wall corner
20	2337167.304	533289.643	2337167.294	533289.621	0.024	-
21	2337250.685	533198.467	2337250.675	533198.443	0.026	-
22	2337543.886	533439.580	2337543.837	533439.510	0.086	-
23	2338315.287	533859.101	2338315.276	533859.056	0.046	-
24	2338474.912	533749.926	2338474.850	533749.916	0.063	-
25	2338822.250	534484.946	2338822.231	534484.846	0.102	-

Table 1b: Comparison of elevation (Z) obtained from UAV and RTK-GPS

POINT	X (North)	Y (East)	UAV	RTK-	Discrepancy	Remark
			Elevation (meter)	GPS Elevation (meter)		
1	2337304.910	532435.991	124.705	124.793	0.088	Slope area
2	2337459.278	532355.327	107.068	107.194	0.126	-
3	2337751.750	532232.373	148.675	148.551	-0.124	-
4	2337864.776	532313.287	166.951	166.905	-0.046	-
5	2337829.189	532357.063	152.044	152.037	-0.007	-
6	2337896.391	532457.572	114.040	114.229	0.189	-
7	2338062.956	532395.893	145.524	145.825	0.301	-
8	2338083.991	532247.060	239.935	240.363	0.428	-

9	2338216.721	532744.552	91.219	91.066	-0.153	-	
10	2338176.195	532463.735	106.080	106.206	0.126	Hiking Trails	
11	2338157.308	532590.399	86.080	85.821	-0.259	-	
12	2338342.568	532907.376	90.097	89.944	-0.153	-	
13	2337497.764	531851.680	126.638	126.539	-0.099	-	
14	2337917.371	532613.255	78.863	78.811	-0.052	Flat area	
15	2337841.585	532809.495	66.870	66.857	-0.013	-	
16	2337791.051	533105.523	61.583	61.619	0.036	-	
17	2337812.129	533155.164	60.447	60.482	0.035	-	
18	2337740.277	533207.286	61.716	61.691	-0.025	-	
19	2337863.410	533449.668	58.812	58.914	0.102	-	
20	2337853.591	533492.215	59.647	59.713	0.066	-	
21	2338679.953	534262.824	56.468	56.303	-0.165	-	
22	2338679.953	534223.839	56.809	56.818	0.009	-	
23	2338674.365	534189.398	56.763	56.694	-0.069	-	
24	2338721.826	534116.990	55.703	55.791	0.088	-	
25	2338747.239	534024.581	55.568	55.724	0.156	-	

Table 2: Comparison of coordinates (X-Y-Z) obtained from UAV and RTK-GPS.

Comparison obtained from UAV and RTK-GPS	Discrepancy of Coordination <i>Build-up</i>	Discrepancy of Elevation		
		<i>Slope area</i>	<i>Hiking trails</i>	<i>Flat area</i>
Average	0.076	0.089	-0.096	0.014
Max of Discrepancy	0.124	0.428	0.126	0.156
Min of Discrepancy	0.009	-0.153	-0.259	-0.165
Root Mean Square Error	0.030	0.020	0.169	0.064

The RMSE value determined the accuracy of coordinates and elevation of each point using different observation methods. The table 1a shows the comparison of coordinate for the checking points between UAV and RTK-GPS Survey, the checking points were chosen are build – up points like the corner house and wall corner. Here, we also show the exact location with elevation information for both UAV and RTK of elevation checking points in the same X-Y coordinates were taken within the open space area of the study area, showing in the table 1b. Equation (2) and equation (4) is used to determine the root means square error (Table 2).

4. CONCLUSION

This study presents an analysis of topographic map using UAV technology and RTK conducted in Phutho province of Vietnam. The accuracy of topographic map generated by Unmanned Aerial Vehicle (UAV) Imager compares to ground survey using Real Time Kinematic (RTK) which indicates the accuracy for X-Y coordinate is $0.076\text{m} \pm 0.030\text{m}$ and Z coordinate is $0.096\text{ m} \pm 0.169\text{m}$. This is good accuracy for a 1/2000 scale map. However with different type of UAV specifications, the accuracy value might get slightly different. Moreover, UAV technology allows to build maps in difficult terrain such as mountain area in this study in a very easy way, without spending too much time. In addition, the results of this study also show that using UAV technology to build topographic maps has a lower cost than

classical technologies. And the number of people participating in the survey work also needs less, just 2 to 3 people can carry out the task of controlling the aircraft to take survey photos. Therefore, it can be concluded that the UAV technology can be considered as an alternative technique to classical techniques in creating topographic map.

5. REFERENCES

- Barnes, G., Volkmann, W., Kelm, KM., 2014. Drones for peace : Part 1 of 2 design and testing of a UAV-based cadastral surveying and mapping methodology in Albania. In: *World bank conference on land and poverty*, Washington DC, USA, 24–27 March 2014.
- Boccardo, P., Chiabrandi, F., Dutto, F., Tonolo, F. G., Lingua, A. M., 2015. UAV deployment exercise for mapping purposes: evaluation of emergency response applications. *Sensors* 15(7):15717–15737
- Cramer, M., Bovet, S., Gütlinger, M., Honkavaara, E., McGill, A., Rijsdijk, M., Tabor, M., Tournadre, V., 2013. On the use of RPAS in national mapping —The EUROSAR point of view. *ISPRS – International archives of the photogrammetry, remote sensing and spatial information sciences*, XL-1/W2, 93–99.
- Delacourt, C., Allemand, P., Jaud, M., Grandjean, P., Deschamps, A., Ammann, J., Cuq, V., Suanez, S., 2009. DRELIO: an unmanned helicopter for imaging coastal areas. *Journal of Coastal Research*, 56 (SI), 1489–1493.
- Engberg, L.E., 2015. HMK-Geodesi: *Terrester detaljmätning*. Lantmäteriet.
<https://www.dji.com/phantom-4-rtk>
- Independent Expert Advisory Group on a Data Revolution for Sustainable Development, 2014. A world that counts: mobilizing the data revolution for sustainable development. [Accessed: 2021-07-20].
- Molina, P., Calaf, M. E. P., Colomina, I., et al., 2012. Drones to the rescue! unmanned aerial search missions based on thermal imaging and reliable navigation. *Inside GNSS*, 7, 36–47.
- Nex, F., Remondino, F., 2014. UAV for 3D mapping applications: a review, *Appl. Geomatics*, 6, 1–15
- Royal Observatory of Belgium GNSS Research Group. Who we are. <http://gnss.be/who.php>. [Accessed: 2021-07-20].
- Saari, H., Antila, T., Holmlund, C., Makynen, J., Ojala, K., Toivanen, H., Pellikka, I., Tuominen, S., Pesonen, L., Heikkila, J., 2011. Unmanned aerial vehicle (UAV) operated spectral camera system for forest and agriculture applications. In: *Proceedings of SPIE*, 8174.
- Vetrivel, A., Gerke, M., Kerle, M., Vosselman, G., 2015. Identification of damage in buildings based on gaps in 3D point clouds from very high resolution oblique airborne images. *ISPRS journal of photogrammetry and remote sensing*, 105, 61–78.

Shoreline change analysis using Sentinel-2A imagery data in Ben Tre, Vietnam

Le Huyen Tran, Nguyen Thi Phuong Doan and Huynh Yen Nhi

Faculty of Marine Resources and Management
 Ho Chi Minh City University of Natural Resources and Environment
 236B Le Van Sy street, Ward 1, Tan Binh District, Ho Chi Minh City, Vietnam
 Email: {lehuyentran.bt, doann9107}@gmail.com
 nhihy@hcmunre.edu.vn

ABSTRACT

In recent years, the process of erosion/accretion has become increasingly intense in coastal areas. With the advantage of low cost and large coverage, remote sensing and GIS have been widely applied in research and assessment of coastal erosion/ accretion in coastal estuaries. In this study, Sentinel-2A satellite images are used to extract the shoreline in Ben Tre province coast. Firstly, the obtained images are preprocessed and the SWIR band was enhanced in resolution. Subsequently, the boundary between land and water is determined by a two-step process: MNDWI ratio imaging and interactive thresholding. Finally, the DSAS statistics has also provided a detailed view of the change of shoreline at three periods (2016, 2018 and 2020). The study results show that from 2016 to 2021, The coast of Ben Tre province has the same phenomenon of erosion and accretion, but the trend of accretion is more dominant than erosion. The accretion phenomenon is concentrated in the area of Ba Lai estuary and coastal area of Thoi Thuan (Binh Dai). Erosion occurs strongly in the coastal areas of Bao Thuan, An Thuy (Ba Tri) and Thua Duc (Binh Dai).

1. INTRODUCTION

Nowadays, many sections of the coastline in Vietnam have been significantly changed due to the influence of climate change ([Trí et al., 2018](#)). In the coastal area of Ben Tre province, there are 20 places where strong erosion and accretion occurs with a total length of about 56 km ([Thanh, 2020](#)). Therefore, monitoring the coast morphology is practical, which contributes in limiting the damage to people and the economy.

The shoreline change is the basic geological change in the coastal area, which includes both the process of erosion and accretion ([Sheik, 2011](#)). Besides field survey data sources, multi-temporal remote sensing images are being widely applied in studying coastline morphology. Based on the spectral reflectance of land and water, the optical images provide a simple way to extract shorelines ([Ouma et al., 2006](#); [Sekovski et al., 2014](#))

There are many methods for coastline extraction, such as: edge detection algorithms ([Paravolidakis et al., 2016](#)), object-oriented multi-scale segmentation method ([Ge et al., 2014](#)), threshold segmentation method ([Zoran et al., 2007](#)), modified normalized water indexes ([Du et al., 2016](#); [McFeeters, 1996](#); [Xu, 2006](#))... In this study, The modified normalized difference water index (MNDWI) and threshold segmentation method are used to extract coastline information from sentinel-2A image. In addition, The Digital Shoreline Analysis System (DSAS) used to analyze the position change of the shoreline from 2016 to 2021.

2. STUDY AREA

The studied coastal area is located in Ba tri and Binh Dai district of Ben Tre province, which its length is approximately 40 kilometers. Located in the Mekong Delta area of Vietnam, its geographical coordinate has the range of the longitude ($106^{\circ}37'14''E$ – $106^{\circ}45'26''E$) and latitude ($9^{\circ}58'08''N$ – $10^{\circ}10'50''N$). Figure 1 depicts the research area.

The research area has a Tropical monsoon climate, with two primary wind directions: the Northeast Monsoon (December to April) and the Southwest Monsoon (May to November). The average annual temperature is between $26^{\circ}C$ and $27^{\circ}C$ and the annual average rainfall ranges from 1,250 to 1,500 millimeters. The tidal range oscillates with the highest value of 3.5 m during the day (Hung, 2019). This coastal area is invested to develop marine economic sectors, especially aquaculture. In recent years, the phenomenon of accretionary erosion has affected people's lives and economic activities.



Figure 1. Map of the study area

3. DATA AND METHODS

3.1 Data

Second order headings like the one above are in 12 pt bold face, one line (12 pt) below the preceding paragraph and one line (12 pt) above the succeeding text.

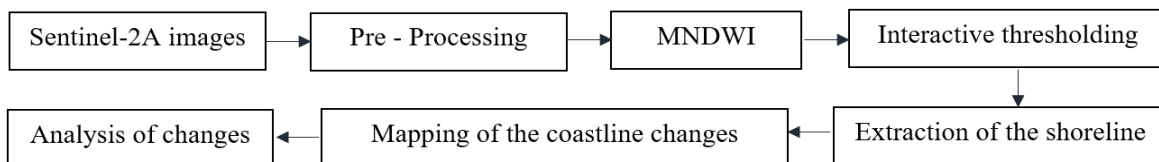
The image data is obtained free of charge from the United States Geological Survey (USGS) with UTM/WGS84 projection. Sentinel-2A carries an innovative wide swath high-resolution multispectral imager (MSI) with 13 spectral bands, of which four 10 m visible and near-infrared (NIR) bands, 20 m short wave infrared (SWIR). Wind direction should be considered during data collection in order to minimize tidal influence on multi-temporal shoreline change analysis. For that reason, the Sentinel-2A images are collected between March and April, when the Northeast Monsoon is active. Information about the collected image data is described in the Table 1.

Table 1. Characteristics of Sentinel-2A product used in this study.

Date	Acq. GMT (HHMM)
04 March 2016	10 :06
24 March 2018	10 :05
7 April 2021	10 :05

3.2. Methods

The implementation method includes the steps as shown in Figure 2.

**Figure 2. Processing workflow**

3.2.1. Pre-Processing

All collected Sentinel-2A Level-1C satellite images are atmospherically corrected through the Sen2cor tool in SNAP, which is intended to remove haze and thin cirrus clouds. The result of this process is a Level-2A Bottom-Of-Atmosphere (BOA) reflectance product. The geographic coordinate system is the World Geodetic System 84 (WGS 84) and the selected projection is UTM zone 48 North. For a resolution compatible with Green and NIR bands, the pan-sharpening is applied using Resample to increase the resolution of the SWIR band from 20 m to 10 m.

3.2.2. Extraction of the shoreline

In this study, the shoreline information is extracted from Multi-Temporal Sentinel-2 Data using the spectral water index MNDWI. The MDNWI is calculated from the Green and Shortwave-Infrared (SWIR) bands to clarify the boundary between land and water. The MNDWI is expressed as follows ([McFeeters, 1996](#)):

$$MNDWI = (Green - SWIR)/(Green + SWIR)$$

An optimal histogram thresholding is chosen as 0.2575 in this case, which is used to create binary images from MNDWI images. The coastline is extracted as the boundary line between land and water. In order to evaluate the accuracy of the extracted coastlines, the shoreline results are overlayed on the Google Earth image with the corresponding time intervals. In this study, the tidal correction is ignored for the following reasons: the image acquisition time in years was similar (March and April), the largest tidal range during the day is 3.5m ([Hung, 2019](#)) and the resolution of Sentinel-2 image is 10m.

3.2.3. Shoreline change assessment

The DSAS tool is used to calculate the shoreline change in the study area over the period 2016-2018 and 2018-2021. The following steps are used to calculate DSAS parameters: determine the baseline and shoreline, build perpendicular lines, and calculate the coastline rate. The net shoreline movement (NSM) and endpoint rate method (EPR) are used to analyze the erosion/accretion trend of the coastline.

4. RESULTS AND DISCUSSION

Period 2016-2018: The results of analysis of coastline changes show that the accretion trend clearly prevails in the study area (Figure 3). The average accretion rate in Ba Tri and Binh Dai districts is 12 m/year and 9 m/year, respectively. However, erosion still occurs in some locations in the study area. In Ba Tri district, erosion occurs in Bao Thuan and An Thuy areas with an average erosion rate of 1.5 m/year, of which the highest erosion rate is 39 m/year. This observation is consistent with statistics, which show that a high tide in February 2017 caused a 50m landslide in coastal Bao Thuan ([Hien, 2017](#)). In Binh Dai district, erosion occurs in the Dai estuary (Thua Duc) with an erosion rate of 4 m/year.



Figure 3. The shoreline extraction result for the period 2016-2018

Map of coastline changes in Ba Tri and Binh Dai districts in the period 2018-2021



Figure 4. The shoreline extraction result for the period 2018-2021

Period 2018-2021: The results of analysis of shoreline changes show that there are alternating between erosion and accretion trends in the study area, but in general, the accretion trend still prevails (Figure 4). In Ba Tri District, the coastline has a similar rate of erosion and accretion. DSAS analysis results show that the average accretion rate is 5 m/year and the average erosion rate is 4 m/year. The place where the most obvious erosion occurs is in the Ham Luong estuary (An Thuy) and Con Nhan (Bao Thuan) area with the maximum erosion length of 17 m/year. In Binh Dai district, the accretion trend prevails with an accretion rate of 7 m/year, which is concentrated in the Ba Lai estuary (Thoi Thuan) and a section of the Thua Duc coast. Besides, erosion continues to occur the Dai estuary (Thua Duc) with an erosion rate of 5 m/year, which is an increase compared to the period 2016-2018.

5. CONCLUSION

The results of the analysis of shoreline changes over two periods show that the accretion trend prevailed in the change of coastline morphology in Ben Tre province. Besides, the research results show that the trend of erosion is increasing in both districts, in which the strongest erosion is in Bao Thuan, An Thuy (Ba Tri district) and Thua Duc (Binh Dai). These analysis results are consistent with the survey results of the Ben Tre Provincial Irrigation Sub-Department, which indicated that these areas are the severe coastal erosion sites of Ben Tre Province (Minh đầm, 2019). The analysis of factors affecting the trend of erosion and accretion in the coastal area of Ben Tre province will be carried out in further research.

The research results indicate that the method of extracting coastline information by MNDWI ratio imaging and interactive thresholding can be suitable for rapid assessment of shoreline changes in a large area. Sentinel-2A satellite images are useful data in supporting the monitoring of coastline changes that contribute to making reasonable plans for erosion and accretion in coastal areas.

6. REFERENCES

- Du, Y., Zhang, Y., Ling, F., Wang, Q., Li, W., & Li, X. (2016). Water bodies' mapping from Sentinel-2 imagery with modified normalized difference water index at 10-m spatial resolution produced by sharpening the SWIR band. *Remote Sensing*, 8(4), 354.
- Ge, X., Sun, X., & Liu, Z. (2014). *Object-oriented coastline classification and extraction from remote sensing imagery*. Paper presented at the Remote Sensing of the Environment: 18th National Symposium on Remote Sensing of China.
- Hien, T. (2017). Triệu cường gây sạt lở bờ biển Bến Tre ngày càng nghiêm trọng. Retrieved from <https://baotintuc.vn/>
- Hung, B. V. (2019). *Xác định mực nước triều cao trung bình nhiều năm trên địa bàn tỉnh Bến Tre*. Retrieved from Department of Natural Resources and Environment, Bến Tre:
- McFeeters, S. K. (1996). The use of the Normalized Difference Water Index (NDWI) in the delineation of open water features. *International journal of remote sensing*, 17(7), 1425-1432.
- Ouma, Y. O., & Tateishi, R. (2006). A water index for rapid mapping of shoreline changes of five East African Rift Valley lakes: an empirical analysis using Landsat TM and ETM+ data. *International journal of remote sensing*, 27(15), 3153-3181.
- Paravolidakis, V., Moirogiorgou, K., Ragia, L., Zervakis, M., & Synolakis, C. (2016). Coastline extraction from aerial images based on edge detection. *ISPRS Annals of the Photogrammetry, Remote Sensing and Spatial Information Sciences*, 3, 153.
- Sekovski, I., Stecchi, F., Mancini, F., & Del Rio, L. (2014). Image classification methods applied to shoreline extraction on very high-resolution multispectral imagery. *International journal of remote sensing*, 35(10), 3556-3578.
- Sheik, M. (2011). A shoreline change analysis along the coast between Kanyakumari and Tuticorin, India, using digital shoreline analysis system. *Geo-spatial information Science*, 14(4), 282-293.
- Thanh, B. (2020). Bến Tre: Sắp hoàn thành dự án Thiết lập hành lang bảo vệ bờ biển. Retrieved from <https://baotainguyenmoitruong.vn/>
- Trí, Đ. Q., Thủy, N. B., & Thủy, N. T. (2018). Đánh giá ảnh hưởng của biến đổi khí hậu tới xói lở đường bờ biển Nghệ An.

- Xu, H. (2006). Modification of normalised difference water index (NDWI) to enhance open water features in remotely sensed imagery. *International journal of remote sensing*, 27(14), 3025-3033.
- Zoran, L., Golovanov, C. I., & Zoran, M. (2007). A threshold method for coastal line feature extraction from optical satellite imagery. Paper presented at the Remote Sensing for Environmental Monitoring, GIS Applications, and Geology VII.

THE USE OF NDVI AND NDBI TECHNIQUES FOR MONITORING THE GROWTH OF MAIZE; A CASE STUDY OF MAE PHRIK DISTRICT, LAMPANG PROVINCE

Prasit Mekarun, Sirintorn Tongkam and Sittichai Choosumrong*

Department of Natural Resources and Environment, Faculty of Agriculture Nature Resources and Environment,
Naresuan University, Phitsanulok Province, Thailand 65000

*Corresponding author: E-mail: sittichaic@nu.ac.th.

ABSTRACT

Maize are very important to the animal husbandry industry, the demand for domestic maize has increased considerably, the production of maize is insufficient to meet the demand and the volume is uncertain due to the production. With the soil, the weather causes heat to heat from the very quiet and risks having to compete with other economic crops that yield better returns than usual. Mae Prik District, Lampang Province, most farmers cultivate maize for animal husbandry. This study was conducted to study the classification of maize acreage areas using the Vegetation Index (NDVI) and the Building Index (NDBI) for classification and comparison. It was correct that both techniques were effective. Different or not according to the growing period, divided into 3 phases: start planting, growing, harvesting. To compare the statistical value

1. INTRODUCTION

Maize is considered a very important farm plants. The need of maize in the country tends to be increasing after the animal culture has been expanded since 1992. Nowadays, planting maize is not enough for internal usage. The quantity is inconstant because the production depends on the weather so that there is a risk of drought. The area for planting is in need to compete with other kinds of plants for more income in the following 4-5 years. The Government solves these problems by managing a Project of Maize Planting to be in accordance with academic principle, to reduce the area of planting maize at the inappropriate area and increase the planting area in drought season for maize planting, in order to have enough production for the market demands.

Since Mae Phrik District, Lampang Province, farmers from this District like to plant several maizes. The researcher emphasizes the production of maize so the study of NDVI and NDBI technique is conducted to find out which technique is more accurate and efficiency for planting maize, and whether they are different. The study employs satellite photos, Sentinel-2, as a tool to evaluate the planting area. Statistical methods are compared with the production of Mae Phrik District.

The purposes of this study are to 1) apply the techniques of NDVI and ADBI to track the maize planting in 2019, Mae Phrik District, Lampang Province; and 2) compare the efficiency values (NDVI, NDBI) of the maize planting.

2. STUDY AREA

The study area covers all the area of Mae Prik District, Lampang Province. It is in the southern west of the province, geographic location falls on 17 degrees, 26 minutes, 54 northern seconds; and 99 degrees, 6 minutes, 54 western seconds. The area covers 538.921 square kilometers (208.079 square miles). There are 16,021 populations. The density of population is 29.72 people/square kilometer (77.0 people/square miles). The location is 268.80-meters above sea level. This area is connected to Li District (Lamphun Province) and Thoen District in the north. It relates to Thoen District in the North, Ban Tak and Sam Ngao Districts (Tak Province). In the South, it is connected to Sam Ngao District (Tak Province) and Li District (Lamphun Province).

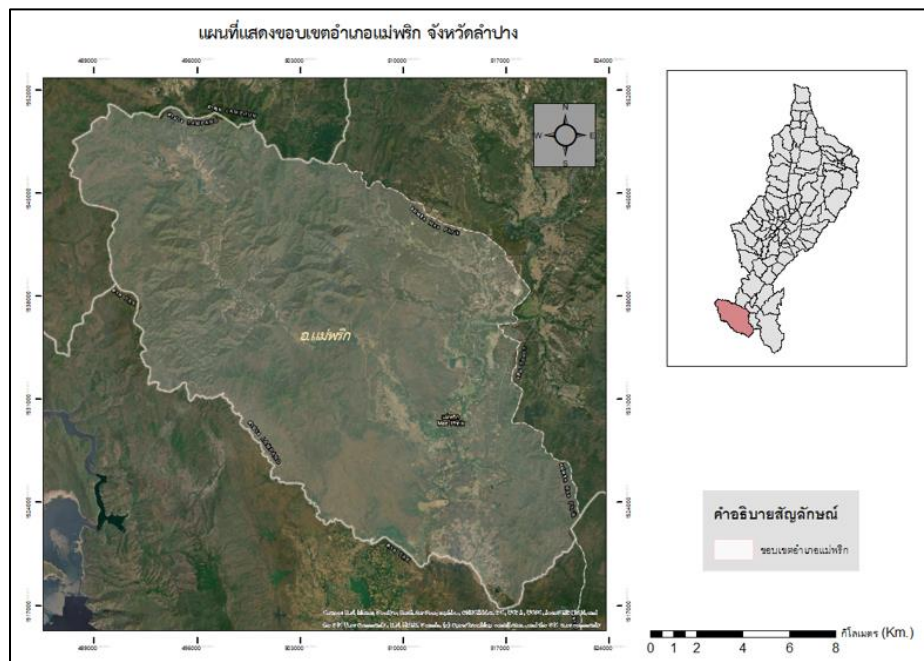


Figure 1. Study area.

3. TOOLS and METHODOLOGY

3.1 Normalized Difference Vegetation Index: NDVI

Vegetation Index is the portion of vegetation by calculating the vegetation waves related to vegetation. A famous method is Normalized Difference Vegetation Index (NDVI). The different reflection of the surface between the waves near infrared and the range of waves seen in red color by eyes are portioned with the adding values of the two ranges of waves to become the normal distribution as shown in Equation 1. Therefore, NDVI values are between -1 to 1, which is easier to be dynamic. This means that 0 is that there are no green plants in the observable area. Meanwhile 0.8 or 0.9 means that there are several green plants in the area. In case of area covered with vegetation, the reflection value near the infrared is higher than the waves seen in red color with

eyes. So, ADVI value is positive. In the meantime, the soil surface has reflection value between the two ranges of waves similarly so that NDVI value is nearly zero.

In case of water surface, the reflection value near the infrared is lower than the waves seen in red color by eyes. As a result, NDVI is negative. These values are normally between 0.1 - 0.7 only, as shown in the following Equation.

$$\text{NDVI} = \frac{(NIR - RED)}{(NIR + RED)} \quad (1)$$

When

NDVI is Normalized Difference Vegetation Index

NIR is the reflection waves near infrared

RED is red visible light of the wave's reflection

3.2 Normalized Difference Built - up Index: NDBI

The Normalized Difference Built - up Index (NDBI) is the analysis of relationship between the surface temperature and types of soil used, or soil covers. The analysis employs the data from the satellite which reflect the built-up objects in both nighttime and daytime, and the temperature of each period (Dousset and Gourmelon, 2003), as shown in the following Equation.

$$\text{NDBI} = \frac{(SWIR - NIR)}{(SWIR + NIR)} \quad (2)$$

When

NDBI means Normalized Difference Built - up Index

SWIR means Short-wavelength infrared

NIR means Near infrared spectroscopy

3.3 Research methodology

The researcher employs pictures from Sentinel-2 Satellite during May 2019 - January 2020. The study is classified into 3 phrases as described below.

1) Starting to plant phrase; 2) growing phrase; and 3) harvesting phrase, these phrases employ Normalized Difference Vegetation Index and Normalized Difference Built - up Index to classify the area for planting maize in each identified period. The results from the program are statistically analyzed to compare that which technique out of those two techniques is more accurate for planting maize.

Data and Data Resource

1. Pictures from Sentinel-2 satellite during May 2019 - January 2020.
2. Data of maize planting at Mae Prik District, Lampang Province during 2019 - 2020.

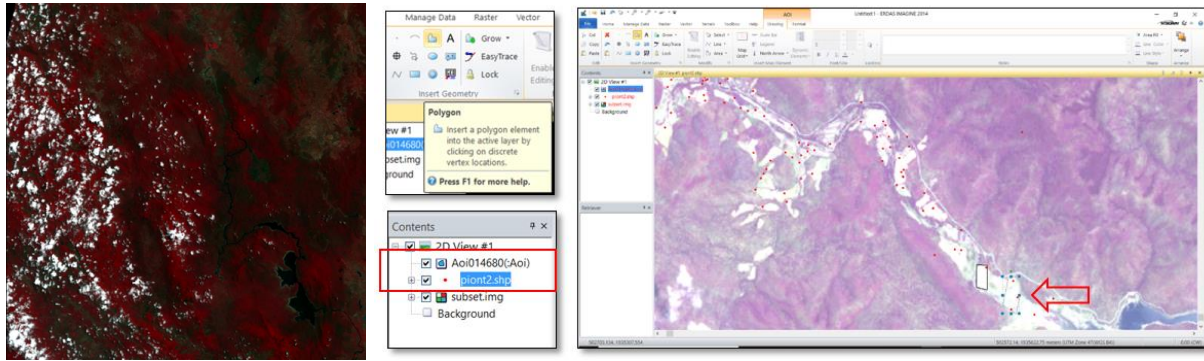


Figure 2. Sental-2 satellite image and maize planting in study area.

Data Analysis

1. Pictures from Sentinel-2 satellite during May 2019 - January 2020 are selectively downloaded.
2. All pictures from each period are collected into bands.
3. Study area are selected.
4. Areal data including maize planting are displayed as points of the field.
5. The pictures from satellite are mosaiced in order make the pictures affixed.
6. Pictures from the satellite are
7. The field area of maize planting is digitized.
8. NDVI and NDBI are analyzed.
9. NDVI and NDBI are compared whether they are related or not.

4. RESULT

4.1.1 Comparison of NDVI and NDBI via T-Test of the maize

The study is conducted to classify maize planting area, which the data are from the analysis of NDVI and NDBI of the satellite pictures for three phrases: planting, growing, and harvesting, during 2019 - 2020.

1. The hypothesis whether NDVI and NDBI of the maize planting area are different in utilizing other kinds of soil. The reliability is 95%.

Hypothesis

- Major hypothesis: the area of planting maize and other purposes of soil using are not different.
- Minor hypothesis: the area of maize planting and the other purposes of soil using are different.

ประเภท	NDVI	NDBI	t-Test: Paired Two Sample for Means	
			NDVI	NDBI
ข้าวโพดเลี้ยงสัตว์	0.053	0.177	Mean	0.15325
พื้นที่แปลงนา	0.029	0.022	Variance	0.01726425
พื้นที่ป่า	0.242	0.242	Observations	4
พื้นที่หมู่บ้าน	0.289	0.289	Pearson Correlation	0.87655392
			Hypothesized Mean Difference	0
			df	3
			t Stat	-0.924860248
			P(T<=t) one-tail	0.211626649
			t Critical one-tail	2.353363435
			P(T<=t) two-tail	0.423253298
			t Critical two-tail	3.182446305
			α	0.05
			Significanae	UnSig

Figure 3 display the results of the analysis Statistical value at the beginning of cultivation of maize compared to Other land use in hypothesis 2

4.2 Result of the test program

The analysis results reveal that the two-tail P($T \leq t$) value of NDVI and NDBI of maize comparing to the other purposes of planting is 0.42. It is higher than the significant value, 0.05. Therefore, it rejects H1 but accepts H0. This means that NDVI and NDBI of maize are not significantly different from other kinds of planting.

ประเภท	NDVI	NDBI	t-Test: Paired Two Sample for Means	
			NDVI	NDBI
ข้าวโพดเลี้ยงสัตว์	0.457	0.352	Mean	0.3995
พื้นที่แปลงนา	0.181	0.249	Variance	0.021859
พื้นที่ป่า	0.508	0.352	Observations	4
พื้นที่หมู่บ้าน	0.452	0.413	Pearson Correlation	0.851838039
			Hypothesized Mean Difference	0
			df	3
			t Stat	1.199643441
			P($T \leq t$) one-tail	0.1581909
			t Critical one-tail	2.353363435
			P($T \leq t$) two-tail	0.3163818
			t Critical two-tail	3.182446305
			α	0.05
			Significanae	UnSig

Figure 4 display the results of the analysis Statistical value during growth of maize compared to Other land use in hypothesis 2

5. DISCUSSION AND CONCLUSION

The adaptation of Sentinel-2 Satellite data to study the area of maize planting in 2020, at Mae Prik District, Lampang Province, with the techniques NDVI and NDBI. The Sentinel-2 Satellite includes the measurement tool called Multispectral Instrument (MSI), which consists of 12 bands and the analysis of NDVI and NDBI analysis from the Satellite.

$$\text{NDVI} = (\text{NIR}-\text{Red})/(\text{NIR}+\text{Red})$$

$$\text{Sentinel-2 :} (\text{Band8}-\text{Band4})/ (\text{Band8}+\text{Band4})$$

$$\text{NDBI} = (\text{R1650}-\text{R830})/(\text{R1650}+\text{R830})$$

$$\text{Sentinel-2 :} (\text{Band11}-\text{Band8})/ (\text{Band11}+\text{Band8})$$

According to the analysis of NDVI and NDBI classification when analyzed, it reveals that the applications of soil are different from other purposes of planting; for example, maize, water resource, forests, villages, etc., in different periods (planting, growing, and harvesting). As a result, all types of the Normalized Difference Vegetation Index, in 2019 - 2020, and Normalized Difference Built - up Index, in 2019 - 2020, slightly different in every period.

According to the analysis of classification of maize planting areas comparing with other purposes of planting; for example, maize, water resource, forests, villages, etc., with NDVI and NDBI, the results of the other purposes of planting by analyzing hypothesis via T-test manifest that NDVI and NDBI of planting area has two-tail $P(T \leq t)$ is significantly different from other purposes of planting, 0.5. Therefore, it accepts H_0 and rejects H_1 , which means that NDVI and NDBI of the maize planting area are not significantly different with 95% reliability.

In conclusion, the area of maize planting at Mae Phrik District, Lampang Province is obviously not different from other purposes of soil using in plantation.

6. REFERENCE

- D. W. Triscowati, B. Sartono, A. Kurnia, D. Dirgahayu and A. W. Wijayanto, "Classification of riceplant growth phase using supervised random forest method based on landsat-8 multitemporal data", International Journal of Remote Sensing and Earth Science, vol. 16, no. 2, pp. 81-90, 2020.
- Kshetri, T. B. NDVI, NDBI & NDWI Calculation Using Landsat 7, 8.
- Macarof, P., & Statescu, F. (2017). Comparasion of ndbi and ndvi as indicators of surface urban heat island effect in landsat 8 imagery: A case study of iasi. Present Environment and Sustainable Development, 11(2), 141-150.
- "United states department of agriculture (usda): world agricultural production july 2020", Circular Series WAP 7-20, vol. 2019, 2020.

APPLICATION OF UAV MULTI-SPECTRAL CAMERA FOR ESTIMATING BANANAS DISEASE INFESTATIONS IN COMPLEX FARMING IN PHITSANULOK PROVINCE

Sittichai Choosumrong*, Rhutairat Hataitara and Prasit Mekarun

Department of Natural Resources and Environment, Faculty of Agriculture Nature Resources and Environment,
Naresuan University, Phitsanulok Province, Thailand 65000

* Corresponding author. E-mail: sittichaic@nu.ac.th.

ABSTRACT

Phitsanulok Province located in the lower north, Thailand. The famous souvenir of Phitsanulok is dried bananas. The yield from bananas farm is essential as it is used as a raw material for production. The application of Remote Sensing methods to asses crop vigor and yields has had limited applications in Phitsanulok Province due largely to limitations associated with satellite images. The increasing use of Unmanned Aerial Vehicles (UAV) in recent times opens up new possibilities for remotely seeing crop status and yields even on complex smallholder farms.

This study demonstrates the applicability of a vegetation index derived from UAV multi-spectral cameras imagery to assess bananas crop vigor and yields at various stages of crop growth. The study employs a quadcopter flown at 80 m over farm and equipped with 6 bands cameras, RGB, Blue, Green, Red, Red Edge and Near Infrared. The Normalized Difference Vegetation Index (NDVI), Enhance normalized Difference Vegetation Index (ENDVI) and red-edge chlorophyll index (CI_{RE}) were compared. To Estimating bananas vigor and yields, we found that ENDVI and CI_{RE} is better indicator of crop vigor and a better estimator of yields than NDVI.

1. INTRODUCTION

Mali-Aong Banana is a widely grown cash crop in the Phitsanulok. In Bang Krathum District, Phitsanulok Province, there are products that are known as provincial products, famous abroad and have been registered as a type of intellectual property with Geographical Indication (GI) is Bang Krathum dried bananas. The most important raw material for making Bang Krathum dried bananas is bananas. The most suitable banana for making Bang Krathum dried bananas is Kluai Nam Wa Mali Ong (Mali-Aong bananas). Originally, Kluai Nam Wa Mali Ong planted a lot in the small fields at the end or border of the rice farm. After being used to make dried bananas, it has to know that this banana has possessions that are suitable for making dried bananas the most.

“Kluai Nam Wa Mali Ong” is considered an important alternative economic crop in the current situation. In the past few years, it has been affected by drought as well as the impact of deadly disease and banana borer. Make the banana price drop. Phitsanulok Province It is the largest source of dried banana products in Thailand. Farmers have a large demand for banana cultivars for planting. Instead, they pay more attention to the prevention of mortality before planting, and will

see the importance when the bananas show symptoms of disease, which is not timely and difficult to fix.



Figure 1. Kluai Nam Wa Mali Ong tree.

Banana borer of banana larvae are the larvae of weevils pierce banana stems. The scientific name is *Odoiporus longicollis* (Olivier, 1870). It is a beetle of the family Curculionidae. Characteristics of destruction and distribution generally, the adults of the banana larvae have a habit of laying eggs along the sheath of banana leaves in the trunk above the ground until about the middle of the trunk. When hatched from the eggs, the larvae from stage 1 will gradually penetrate and eat into the banana stems gradually to the center of the trunk. The external symptoms that are noticeable by the eye are around the banana plant is a common pore and dead banana.



Figure 2. Banana bore and the damage to banana plants.

If destroying in the near term until the chain falls will make the network break in the middle of the beginning or wither, perennial, die throughout the period of Ji Life will live in the area of the trunk and the leaf axils. The species can be found spreading in many areas around the world, including Bhutan, Cambodia, China, India, Indonesia, Laos, Malaysia, Myanmar, Nepal, Pakistan, Philippines, Singapore, Sri Lanka, Taiwan, Thailand and Vietnam.

Once a diseased plant has been found, ‘timely removal’ is the best way to avoid the formation of a disease center (Picq, 2020). Therefore, timely monitoring of banana disease is important for the disease treatment and crop planting adjustment. Traditional ground surveys to collect crop disease data are expensive and time-consuming (Shi Y Y *et al*, 2018). Remote sensing technology has become a feasible means for crop disease detection and assessment in the past few decades, including for detecting Fusarium head blight, dead bananas and rust infection in wheat (Jin X *et al* 2018, Mahlein A K *et al*, 2019, Huang W J *et al*, 2007) bacterial leaf blight in rice, and grey leaf spot in maize. When plants are infected with diseases, the leaf water, pigment content and internal structure undergo changes, which are reflected in the spectral signature of the plants. Many spectral features of vegetation were found in the red-edge, NIR, Red band that is related to changes in chlorophyll content and leaf area index, and significant changes were observed when bananas were infected with dead bananas. In recent years, various lightweight multispectral sensors that include the blud, green, red, red-edge nir and visible band (i.e., DJI Phantom 4 multi-spectral camera with RTK) were designed specifically for Unmanned Aerial Vehicle (UAV) platforms for vegetation monitoring. With the rapid development of UAV technology, UAVs have been increasingly used for acquiring imagery to extract phenotypic information of crops rapidly due to their advantages (i.e., high spatial resolution, ease of operation, high flexibility, and acquisition of data on demand). Moreover, scale effects and scaling have become one of the most important research topics in remote sensing. Different spatial resolution images show different landscape characteristics, and data with higher spatial resolution usually get more accurate estimates. However, seeking very high resolution data is unnecessary and unrealistic in the agriculture application at a regional scale as it is expensive and difficult to process. Therefore, it is very important to choose a suitable spatial resolution image for agricultural monitoring.

The objectives of this study were to (i) develop an identification method for the dead zone of banana using UAV-based multispectral imagery, (ii) determine the optimal VI for establishing an optimal identification model, and (iii) assess the effect of different image resolution on the identification accuracy of dead banana from disease to provide a reference for large-scale applications of satellite-based data.

2. METHEOLOGY

2.1 Study Area

The experiments were conducted at Bangkrathum district (Figure 3). Bang Krathum District is located in the upper central region and the lower northern region. The condition of the area is generally flat, no mountains and forests. The climate is divided into 3 seasons: summer, from late February to May. In summer the weather is very hot. Influenced by the southeast monsoon which is a hot wind. In the rainy season starting from May to October and in the next season from October to January which was influenced by northeast monsoon period of extreme cold from China.

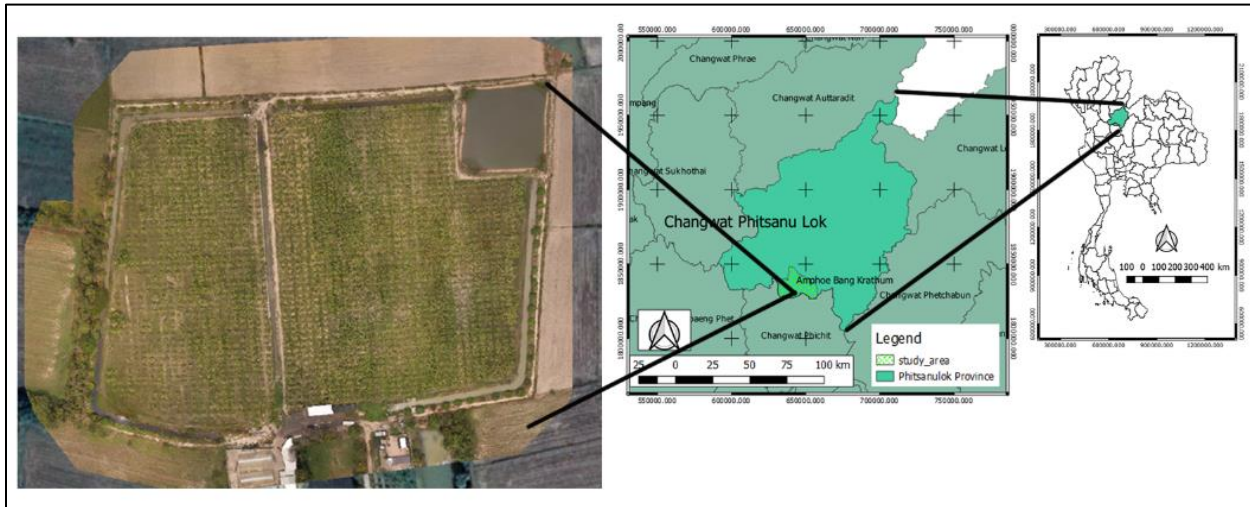


Figure 3. Location of the study area in Amphoe Bang Krathum.

2.2 UAV Multi-Spectral Camera and RTK Acquisition

The study area is located at the Banana Society Company. The surveys were done using a DJI Phantom 4 Multi-Spectral Camera with RTK (Figure 4).

This UAV was equipped with a five-band multispectral camera which has five narrow bands: Blue (465–485 nm), green (550–570 nm), red (653–673 nm), red edge (712–722 nm), near-infrared (800–880 nm) and one RGB (visible) band. The flight at the site was conducted between 14:00 p.m.–14:30 p.m. and covered an area of 21 ha. The flight at Hainan site was conducted between 11:00 a.m.–12:00 p.m. on 11 December 2018 and covered an area of 60,500 square meter. The flight plans were developed to ensure greater than 80% cross-track and along-track overlap rates. The multispectral imagery was acquired from a flying height of 100 m above the ground with a ground sample distance of 0.08 m. The multi-spectral imagery is 125 images



Figure 4. Phantom 4 Multi-Spectral Camera with RTK.

2.3 Data Analysis

In this study, different VIs were used to identify the infestation status of banana plants. These resolutions were selected because they were similar to those of several mainstream and easily accessible satellite imagery products (i.e., WorldView series with a resolution of 0.5 m, GF-2 with a resolution of 1 m, GF-1 and GF-6 with a resolution of 2 m, RapidEye with a resolution of 5 m, and Sentinel-2 with a resolution of 10 m) for agricultural applications.

2.3.1. Vegetation Indices

Considering the potential pathological characteristics of the Fusarium wilt disease infestations, eight VIs related to pigment absorption and plant growth were selected to characterize the biochemical and biophysical variations caused by individual infestations. The VIs included the Normalized Difference Vegetation Index (NDVI), Enhance normalized Difference Vegetation Index (ENDVI) and red-edge chlorophyll index (CI_{RE})

Table 1. List of vegetation indices developed for remote sensing applications.

Vegetation Index	Equation	Reference
Normalized Difference Vegetation Index (NDVI)	$NDVI = \frac{NIR - RED}{NIR + RED}$	Rouse et al., 1974
Enhance normalized Difference Vegetation Index (ENDVI)	$ENDVI = \frac{((NIR + Green) - (2 * Blue))}{((NIR + Green) + (2 * Blue))}$	Gitelson et al. 1996
red-edge chlorophyll index (CI_{RE})	$CI_{RE} = \frac{NIR}{(RE - 1)}$	Gitelson et al. 1996

3. RESULE

We analyzed the differences in the VI values between the healthy and diseased samples obtained from the experiment area, and conducted independent t-test analyses for each sample. The results showed that there were significant differences in the values of NDVI, GNDVI and CI_{RE} between the healthy and diseased samples.

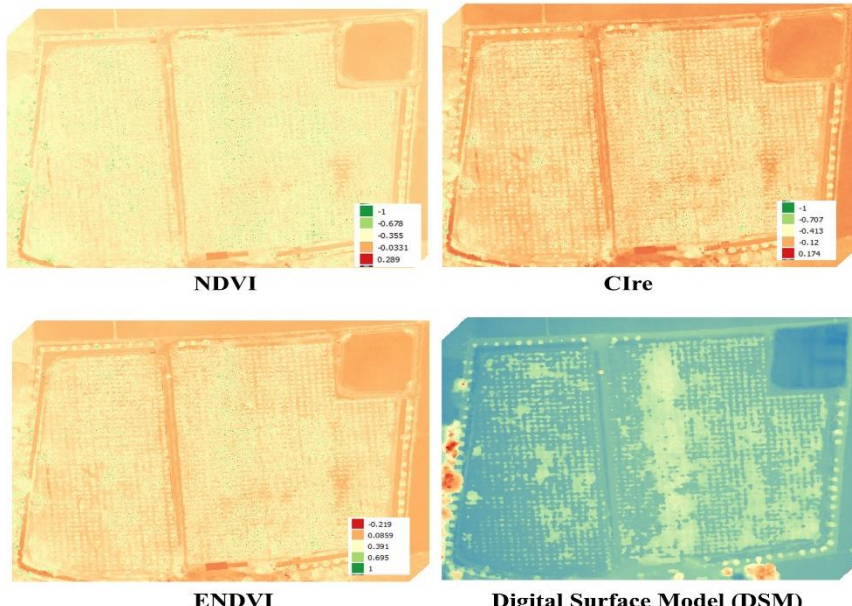


Figure 5. The result of all VI indexs.

4. DISCUSSION AND CONCLUSION

The results of this study indicate that the CI_{RE} was the optimal red-edge VI and the NDVI, ENDVI were the optimal non-red-edge VI for developing identification models for banana disease infestations. This is attributed to the fact that as the infection of disease progresses, the chlorophyll content decreases significantly, and the CI_{RE} values are sensitive to small variations in the chlorophyll content.

This study used VIs derived from UAV-based multispectral imagery and BLR to develop an identification method for detecting banana Fusarium wilt. The results showed that disease infestations of banana can be identified with this method.

5. REFERENCE

- Gitelson, A.; Merzlyak, M.N. Spectral reflectance changes associated with autumn senescence of *aesculus-hippocastanum* L and *acer-platanoides* L leaves—spectral features and relation to chlorophyll estimation. *J. Plant Physiol.* 1994, 143, 286–292. [Google Scholar] [CrossRef]
- Picq, C.; Fouré, E.; Frison, E.A. Bananas and Food Security; Bioversity International: Maccarese-Stazione, Italy, 1999. Available online: https://www.bioversityinternational.org/fileadmin/user_upload/online_library/publications/pdfs/709.pdf (accessed on November 2020)

- Rouse, J.W.; Haas, R.H.; Schell, J.A.; Deering, D.W. Monitoring vegetation systems in the great plains with ERTS. In Proceedings of the Third ERTS-1 Symposium NASA SP-351, Greenbelt, MD, USA, 10–14 December 1973. [Google Scholar]
- Shen, Z.; Xue, C.; Penton, C.R.; Thomashow, L.S.; Zhang, N.; Wang, B.; Ruan, Y.; Li, R.; Shen, Q. Suppression of banana Panama disease induced by soil microbiome reconstruction through an integrated agricultural strategy. *Soil. Biol. Biochem.* 2019, **128**, 164–174. [Google Scholar] [CrossRef]
- Shi Y Y, Huang W J, Ye H C, Ruan C, Xing N, Geng Y, et al. Partial least square discriminant analysis based on normalized two-stage vegetation indices for mapping damage from rice diseases using PlanetScope datasets. *Sensors*, 2018; **18**(6): 1901.
- Jin X, Jie L, Wang S, Qi H J, Li S W. Classifying wheat hyperspectral pixels of healthy heads and Fusarium head blight disease using a deep neural network in the wild field. *Remote Sens.* 2018; **10**(3): 395.
- Mahlein A K, Alisaac E, Al Masri A, Behmann J, Dehne H W, Oerke E C. Comparison and combination of thermal, fluorescence, and hyperspectral imaging for monitoring fusarium head blight of wheat on spikelet scale. *Sensors*, 2019; **19**(10): 2281.

Efficiency of MRC Flash Flood Guidance System (MRCFFGS) for Northeastern Thailand: Case Study of Tropical Strom Impact in 2019-2020

Fatah Masthawee^{1,2}, Chaiiwat Vansarochana¹, Pattara Sukthawee² and Banluesak Khorsuk²

¹Faculty of Agriculture Natural Resources and Environment, Naresuan University
Naresuan University, Phitsanulok 65000, Thailand

²Hydrometeorological Division, Thai Meteorological Department
4353 Shukhumvit Rd., Bangna, Bangkok 10260, Thailand
Email: fatah_m@yahoo.com

ABSTRACT

Flash flood is a globally drastic natural disaster. Hence, the World Meteorological Organization (WMO) arranges cooperation to develop a tool for flash flood forecasting in each WMO region which is Flash Flood Guidance System (FFGS). In Thailand, FFGS is implemented under a collaboration with the Mekong River Committee and it is called MRCFFGS. This system uses a hydrological model to calculate the capacity of water restoration inland before triggering flash floods in a small river basin. The study of MRCFFGS in Thailand shows that in the Northeast region affected by three tropical cyclones, KAJIKI, PODUL, and SINLAKU, it is found the statistic skill score callings as the following: The probability of detection (POD) is 0.14, and false alarm ratio (FAR) is 0.3. It is not a good score for prediction especially POD. After adjusting the FFG value by half, the result shows that POD is 0.50 and FAR is 0.36. While adapting the FFG value by one-third, the result reveals that POD is 0.50 and FAR is 0.42. In this study, it can be concluded that adjusting the FFG value by half shows the best result. It is suitable for flood simulation and prompt response to rainfall.

1. INTRODUCTION

Flash flood is one of the most dangerous natural disasters. In a year, at least 5000 people lost their lives and many people lost their properties, it is 85% of casualties of the flood came from the flash flood. Flash flood occurs in a short time and small particular area, unlike overbank flow which occurs in the large area in the basin. It is hard to predict this event precisely, flash flood warning is also uncertain and not in a time when it takes place, the main reason for damage to life and properties. The two main factors that trigger flash flood events are 1. rainfall and 2. the soil moisture properties, therefore, a flash flood is varying from place to place and depending on the micro-scale of weather in one another region (WMO, 2020)

The flash flood guidance system is supported by World Meteorological Organization, Hydrological Research Center, National Oceanic and Atmospheric Administration, and United States Agency for International Development. The mission of this system is to contribute to forecasting flash flood events for meteorologists and relate agents in each member country and regional area and enhancing flash flood warning for the overall area of the globe but separate responsibility by zone such as country. To launch flash flood warning issued, because of its flash in time and small of the region, some flash flood cases are miss and the information from FFGs show only heavy rainfall and soil moister saturation in area, meteorological and hydrological expertise is required to deal with flash flood warning issue inclusive with high-resolution weather station network and 24-7 monitoring (WMO, 2016)

FFGS use satellite-based rainfall with bias correction and put it into a physically-based hydrological model to explain flash flood event (WMO, 2007). Comparing observed rainfall with forecast rainfall and project to a characteristic of the basin in a specific time, the result of flash flood shows the difference value between soil capacity in basin and rainfall event. The flash flood guidance depends on basin drainage character which portrays by rainfall and evapotranspiration (Mutic et al., 2020)

FFGS that cover Thailand area is operated under MRCFFGS, system development in term of Mekong river basin view, the members country are Thailand Laos Cambodia and Vietnam. When it is applied to use in Thailand performance verification is necessary. The flood event in the past is used as ground truth for FFGs to improve efficiency.

FFGS case study in Thailand done Patsinghasanee et al. (2018), verified accuracy in the southern part of Thailand between 28 November 2007 and 4 December 2007- northeast monsoon period. The FFGS portrayed less rainfall significantly and recommended adding value by correcting soil moisture and rainfall.

This study aims to correct the product of FFGS by comparing it with ground truth. From flash flood operation finds that FFG rarely launch issue in flood warning which congenial with the study of Patsinghasanee et al. (2018) so bias correct as a result of the system are needed cause we cannot correct in process of the system.

2. METHODOLOGY

2.1 Study area

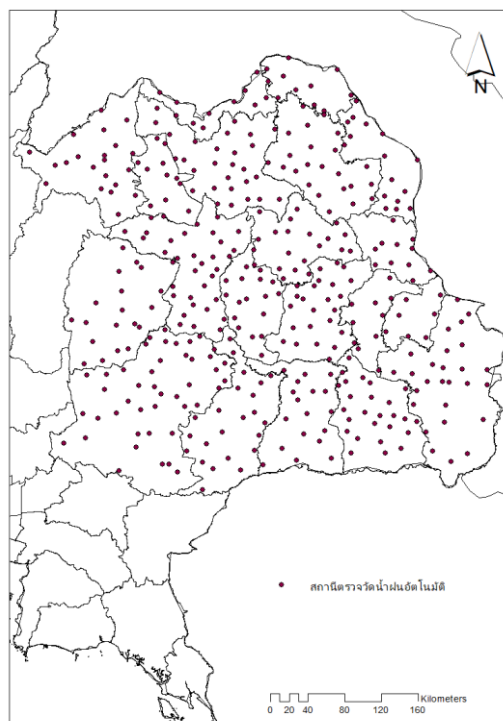


Figure 1. Rain Gauge Network in the study area

The Northeast part of Thailand was selected as a study. The picture1 shows automatic rain gauge network in this area (Figure 1)

2.2 Data collection

1. FFG data from MRCFFG center, located at Phnom Penh Cambodia, a two-period as following: 1. 28 August 2019 to 6 September 2019 and 2. 2 August 2020 to 5 August 2020. The data display the potential of a flash flood occurring by rainfall and soil capacity in the next six hours periodic calculation at 0000 0600 1200 1800 UTC.
2. TMD automatic rain network (403 stations) same period as 2.2.1 for comparing with FFGS record in ASCII file size is 1.4Mb per year
3. Report of flood in Thailand from Department of Disaster Prevention and Mitigation (DDMP) and Media news

2.2 Methods

1. Write Program computer script to download data from MRCFFGS and connect to TMD rainfall database for verification FFGs
2. Develop a script to transform format FFG from polygon of the small basin to grid cell of FFG and transform point rainfall to areal rainfall as grid cell of rainfall. The two grids are the exactly same size.
3. Comparing two types of data as mention earlier for two cases that have an influent of Tropical Cyclone (2019 and 2020).
4. Bias correction for FFGs

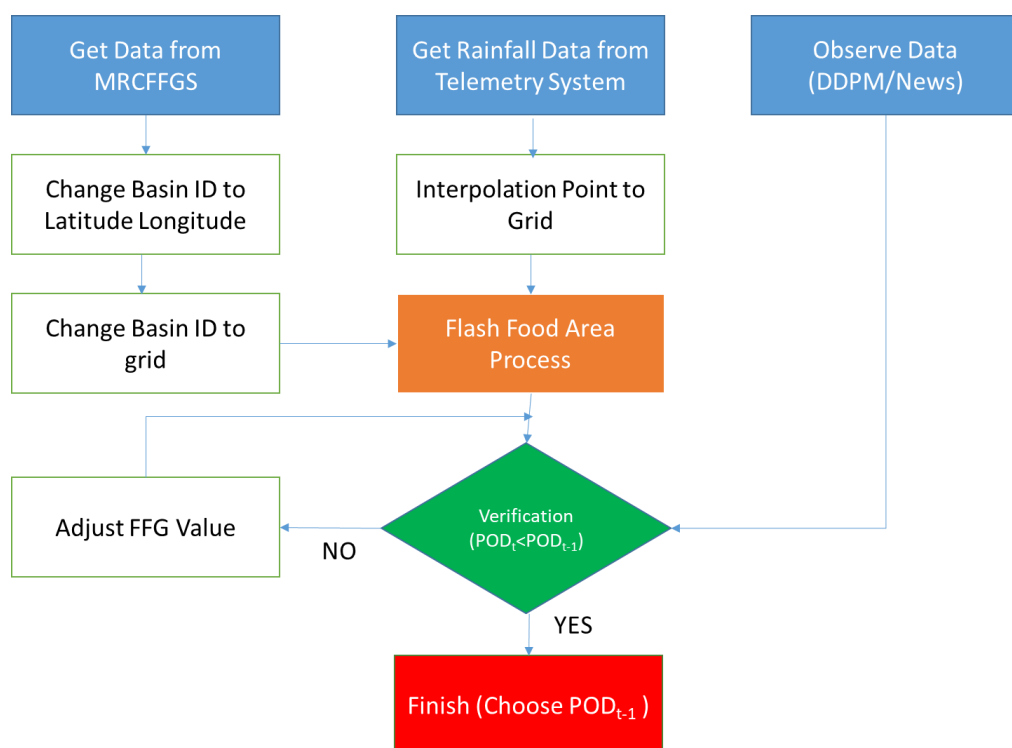


Figure 2. Flow chart of FFGs enhancing in Thailand (northeast part)

3. RESULT AND DISCUSSION

When comparing the value of FFG from the model with observation rainfall and flood event from the DDPM report. The result can show in Figure 3 that a separate category of adjustment technique and Tropical Cyclone case study. Unadjusted FFG has an area which smaller than decreased value of FFG. When more decrease FFG value, the flood area is wider. So, the verification technique is very necessary for the best adjustment value finding for flash flood forecasting.

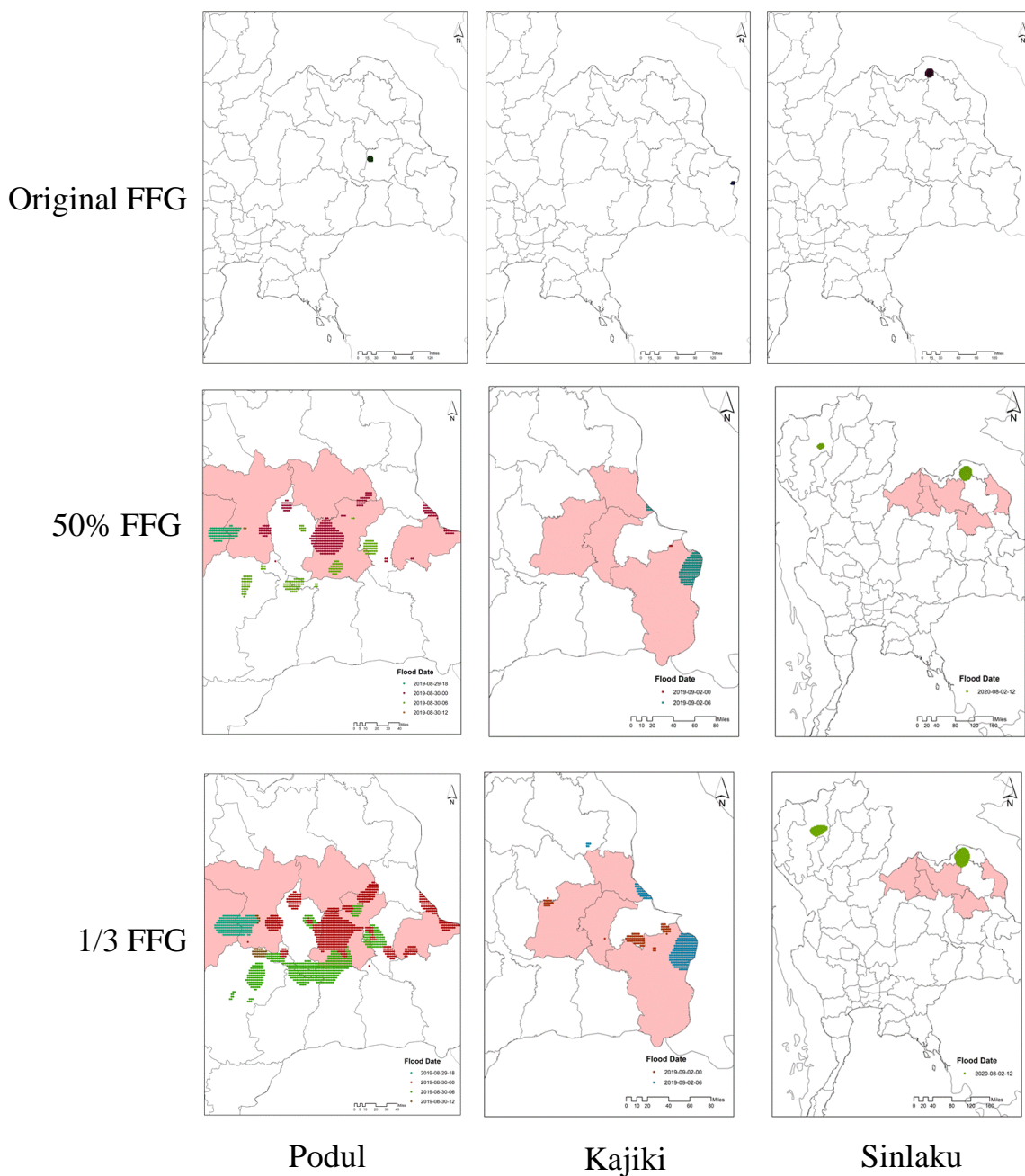


Figure 3. Comparison of FFG value and adjustment for three cases

Statistical verification showed that without a correction POD of FFG was 0.14 after being corrected by reduced FFG value by half and as one third, POD was up to 0.50, mean performance improved. In terms of FAR, FFG score as 0.33, after adjusted FFG by half, the value of FAR has more error score as 0.36 and adjusted as one third shown much more error (0.42) as the following table 1.

Table 1. Verification of FFG

FFG Value	POD	FAR
FFG (original)	0.14	0.33
50% FFG	0.50	0.36
1/3 FFG	0.50	0.42

FFGS, WMO supported system, in Thailand on the operation this system operating with numerical weather prediction by TMD (TMD-HPC) mostly miss flash flood event issue. This reason drives TMD to solve the missing issue and without authorizing to correct the system in the process, we tried to correcting and adjust the result as output by bias correction.

Tropical cyclone cases in this region were selected to fulfill the prediction. Because of the lack of efficiency to estimate rainfall from stratus clouds, vertical forming clouds are the best selection. The result is still poor as POD score 0.14, the event is correct only two provinces of 14 provinces congenial with the operation of FFG in Thailand

Two types of reducing rainfall are designed, 50% FFG and one-third FFG, to prove appropriate of the northeast of Thailand. POD scores are 0.5 in both cases but FAR scores are poorer in both cases especially in one-third score reduce to 0.42. 50%FFG is suitable for this area.

Too much soil capacity that FFG gives to this region is the main factor that FFG not triggering flash flood to launch warning issue. To solve this problem, the tropical cyclone case selected to play a vital to reduce the uncertainty of satellite-based rainfall which is the main trigger for MRCFFG, no adequate rainfall station, and radar-based rainfall.

Without bias corrections, POD score is less than 20 percent but the FAR score is high, the miss of situation has the disadvantage to warn flash flood issues which is the main purpose of the system. After adjusting FFG, scarify with more error but obtain POD is worth to be as the precaution principle and reduce the error with supervising by meteorological expertise who work in this field for a long time.

Bias corrections in this study are suitable only for the northeast of Thailand Area with ITCZ and monsoon, when applied in another region the forecaster must study in a particular area before launching warning issue from this FFGS

4. REFERENCES

- Mutic, P., Jurlina, T., Djordjevic, M. and Golob, A., 2020. *South East Europe Flash Flood Guidance System (SEEFFGS) Forecaster Guide*, Geneva.
- Patsinghasanee, S., Laonamsai, J., Suwanprasert, K. and Pracheepchai, J., 2018. Evaluation of MRC Flash Flood Guidance System for the Southern Thailand: Case study from 28 th November to 4 th December 2017. *The 23rd National Convention on Civil Engineering*. Nakhon Nayok, Thailand
- WMO, 2020. *Sustainability strategy for The Global Flash Flood Guidance System Initiative*, Geneva.
- WMO, 2016. *Flash Flood Guidance System (FFGS) with Global Coverage*. Geneva.
- WMO, 2007. *Prospectus, Implementation of a Flash Flood Guidance System with global coverage*. CBS-MG-VII/Doc. 5(7). Geneva.

WEB MAP OF VIETNAM PROTECTED AREAS

Van Ngoc Truc Phuong¹, Le Minh Vinh² and Le Duc Tuan³

¹ Faculty of Geodesy, Cartography and GIS

HCMC University of Natural resources and Environment, 236B LeVanSy, TanBinh, HCMC - Vietnam

Email: vntphuong@hcmunre.edu.vn

² Faculty of Geodesy, Cartography and GIS

HCMC University of Natural resources and Environment, 236B LeVanSy, TanBinh, HCMC - Vietnam

Email: leminhvinh@gmail.com

³ Faculty of Geography

University of Social sciences and Humanities - VNUHCM, 10 Dinh Tien Hoang, District 1, HCMC - Vietnam

Email: leductuan@hcmussh.edu.vn

ABSTRACT

Protected areas (PAs) are areas of particular importance for biodiversity and ecosystem services. Increasing awareness, sharing information and knowledge of PAs are key elements for their sustainability. Among sharing information media, web map has become a novel source that provides spatial information effectively and web maps of PAs have been paid attention. In Vietnam, using web maps for sharing information of PAs is less common. In the meantime, one of the cartography advancement results is multiscale map. Therefore, this study aims to develop a multiscale web map of Vietnam PAs. Its objectives are to create maps of PAs at different spatial extensions and publish them as a multi-level web map. This is an empirical research, beginning with literature review on multiscale and web map, to determining spatial extents intended to be viewed and rules for setting the scale range through those extents. Next step is to define symbol transformation across scale range to ensure visual continuity at all scales so that the map communicates effectively. Data was conducted with national parks (NPs) - the type of PAs with highest biodiversity importance. The web map was developed via Esri's ArcGIS Platform. Specifically, GIS data were manipulated, symbolized for desired scales, created as web applications and as web map with ArcGIS Desktop, ArcGIS Pro, ArcGIS online, ArcGIS Web AppBuilder and ArcGIS Experience Builder, respectively.

Research result is a web map of Vietnam PAs with the spatial extents spanning from national, regional, provincial to PA level. Spatial extents for experiment map at regional, provincial and PA level is North Centre Region, Quang Binh province and Phong Nha – Ke Bang NP, respectively. The web map configures basis interactive tools such as legend display, base-map gallery, layer management, measurement, radius search, and selection. Through web map services, spatial information of Vietnam PAs is accessible anytime and anywhere. The result shows that the rules for setting scale range for multiscale map of PA are reasonable and feasible. However, more experiments need to be done so that the rules can be applicable to elsewhere.

1. INTRODUCTION

Protected areas (PAs) are areas of particular importance for biodiversity and ecosystem services. PAs themselves become the Programme of Work in the Convention on Biological Diversity (CBD). They also form a central element of the other programmes of CDB Work. In the Programme of CBD Work on PAs and the World Parks Congresses of International Union for Conservation of Nature and Natural Resources (IUCN), increasing awareness, sharing information and knowledge of PAs are key elements for their sustainability. Among sharing information media, web map has become a novel source that provides spatial information effectively and web maps of protected areas have been paid attention.

With web map, one can access map from any device, anywhere and anytime. GIS technology advancements during last decades have led to multi-scale web map. Furthermore,

web map is currently not only the representation of map but also an interactive tool for spatial analysis (Neumann, 2016). In fact, such web maps of PAs have been developed, such as World Database on PAs, Protectedlands.net, Marine PAs Atlas, Atlas of Pálava protected landscape area, the Bay of Bangle Large Marine Ecosystem Atlas, Sequoia & Kings Canyon Parks Atlas, atlas of the Swiss NP, etc.

Being one of the Earth's most biodiverse countries, Vietnam have pushed efforts in elaboration of PAs management system. From which, the need for information sharing and awareness among stakeholders are vital (Chu, M. T., 2011). However, web maps for sharing information of PAs is less common. Therefore, this study aims to develop a multi-scale web map of Vietnam PAs. The objectives of the study are to create maps of PAs at different spatial scales and publish them as a web map.

2. THEORIES AND METHODS

2.1 Definition of PAs

The world first PA was established in 1872. However, until 1994, the first definition of PA was given by IUCN. The term was then revised in 2004. According to that, a PA is a "geographical space, recognized, dedicated and managed, through legal or other effective means, to achieve the long term conservation of nature with associated ecosystem services and cultural" (IUCN 2013) (p.7). By this, it is emphasized that conservation is needed to reach sustainability and that ecological services are major factors of sustainable conservation. The 2004 definition leads to six management categories of PAs, including Strict nature reserve, Wilderness area, national park (NP), Natural monument or feature, Habitat/species management area, Protected landscape or seascapes, PAs with sustainable use of natural resources. Due to historical circumstances, the classification of PAs varies all over the world.

Pursuant to the Vietnam Biodiversity Law 2018, the PAs system is categorized into four categories: NPs, nature reserves, species/habitat conservation areas and landscape conservation areas. A PA consists of functional zones such as no-take zone, ecological restoration zone, service-administrative zone. Meanwhile, pursuant to the Laws on Forestry 2017, PAs belong to special-use forests. Among PAs, NPs have highest biodiversity importance. This type of natural ecosystems is nationally and internationally important, specific to or representative of a natural ecoregion. They are the habitat of at least one endangered species; have special scientific and educational values; and have landscape and unique natural beauty of ecotourism value. Up to 2018, Vietnam has 170 PAs, 31 of which are NPs (Vietnam Administration of Forestry, 2019).

2.2 Multi-scale and web map

Differing from static maps which are designed to be viewed and output at a single scale, digital maps allowing one to change map zooms led to the birth of multiscale map – dynamic maps that display data in different ways across a range of scales. When map scale changes to certain levels (thresholds), map content and its visualization are required to change. Defining thresholds are a crux of multiscale mapping, which is driven by rules of map generalization and characteristics of the subject being mapped. Such maps are authored in ways that they have to ensure visual continuity throughout their scales so that the map can convey spatial information while striking the right balance between the map's purpose and the precise detail of map content. Generalization is not only the suitable cartographic symbolization across the scale range but also means that at a certain threshold, mapping method could change if necessary. Ideally, those changes are subtle by either privileging the feature density (for larger

scale; i.e. information is given per square kilometer) or spatial extension (for smaller scale), to avoid distraction from the map's content and overall message. Therefore, multi-scale mapping requires map-maker a skillful and delicate application of cartographic generalization rules and mapping methods (Van, N. T. P. and Le, M. V., 2016). Figure 1 illustrates a multiscale map of population.

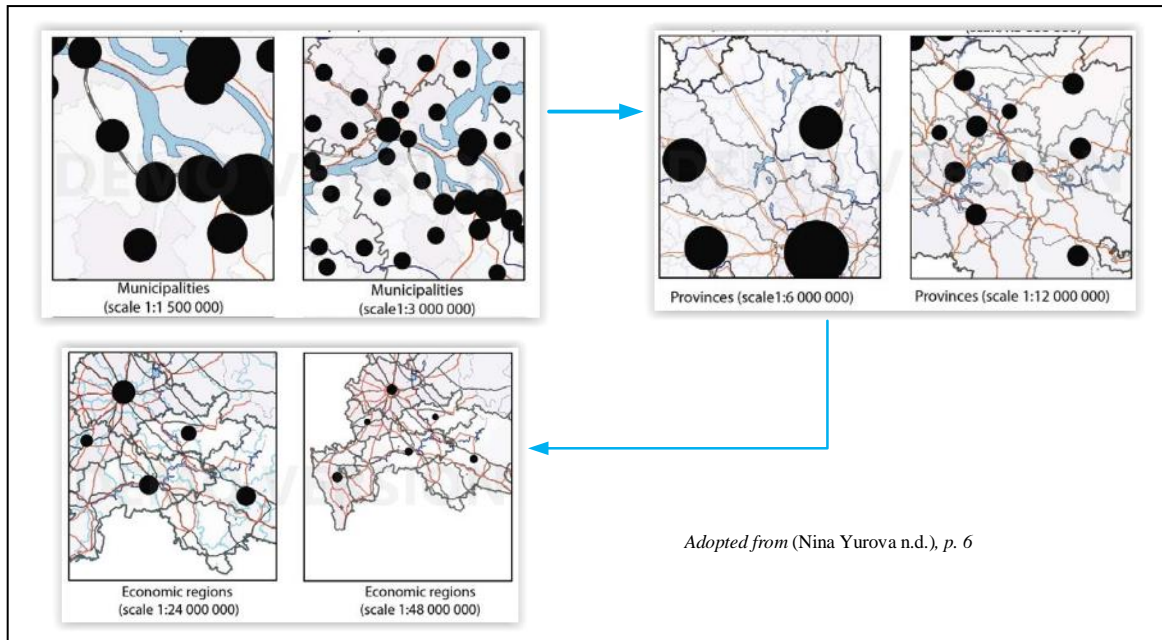


Figure 1. Multiscale map of population

For the last four decades, the multiscale mapping has become among the most prominent and problematic areas in modern cartography. Research work on multiscale mapping includes multi-resolution databases design (multiscale spatial database), real-time generalization, map layer structure, scale-dependent behavior and symbolization (multi-representation). Both multi-scale spatial database and multi-representation are driven by generalization when the map change from larger to smaller scale. The vision of map production is to develop the database that include a single database with the highest needed detail of subject to be mapped, called "master database". Through technical and technological solutions for automated map generalization, we can derive map on demand arbitrary scales from such a database. Some work on such geographical databases is still in progress. In fact, there is a substitute – the multiscale databases those that contain diverse data sets at different scales, called level of detail (Galanda, M., 2003). Large amount of work had been done on multi-scale database and map layer structure (Dumont, Touya, and Duchêne, 2015, 2020; Frye, 2006; Nyangweso, D. O., 2013). Meanwhile, multi-representation is the changes of symbol, geometry, content and label through scales (Brewer, Sparks, and Raposo, 2012). To a certain extent, the functionality of multi-representation may be supported in spatial databases by storing a collection of pre-designed maps (Zhou and Jones, 2013). Research on multiple representation for thematic maps was conducted with a few mapping methods such as graduated symbol, choropleth, dot density (Mai, T. H. and Lê, M. V., 2017; Yurova, N. snf Samsonov, T., n.d.; Van, N. T. P. and Le, M. V., 2016). Most of those studies are experimented with desktop software and the representation across scales is based on the density of field information.

In the meantime, the Internet has become a trendy medium for cartography. Maps in the internet are interactive and dynamic, which help to easy access and enable adaptation to user's need with respect to content and scale. According to Harder (2015), web map is online map that provides ways to work and interact with map layers. It contains a base map with thematic layers, and tools that enable users to interactive with these layers. The interactivities could be

basic, such as layer control, navigation (zoom in/out, pan, etc.), adaptive zooming, mouse over effects, click effects, interactive legend; or complex like spatial analysis, proximity... Web maps are shared on the web to work online and on any mobile devices. Therefore, they are accessible anywhere, anytime. In this paper, we present a multi-representation with a collection of pre-designed maps, based on the approach of spatial extension, and illustrate the implementation of multi-representation with web map demonstration.

2.3 Research methods

This study used the empirical research approach. The process of building experiment multiscale map of Vietnam PAs is shown as below (Figure 2):

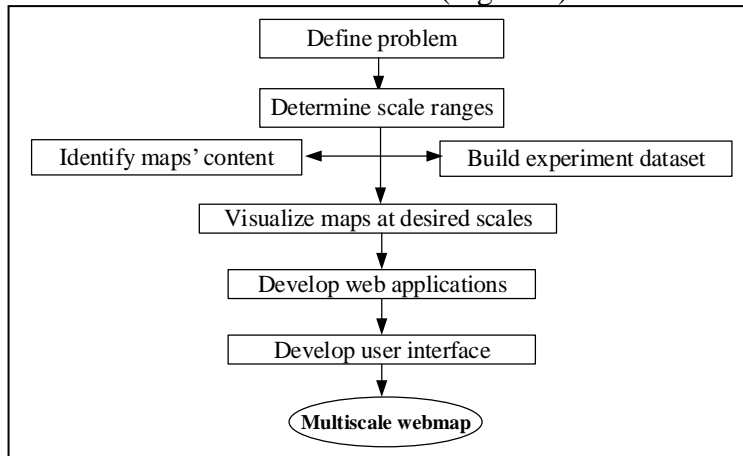


Figure 2. Research design process

According to that, to make multiscale map of Vietnam PAs, firstly, we determined spatial extents intended to be viewed. The spatial extents were set to fit administration levels which spanning from national, regional, provincial to PA level. The maximum and minimum visible scales for each administration level are the full map extent of that level and the full map extent of an adjacent higher level, respectively (Figure 3).

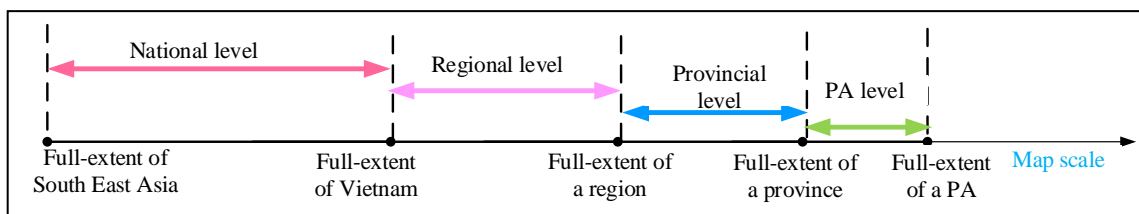


Figure 3. Rules for setting up scale range of multiscale map of Vietnam PAs

Then, we identified the contents for desired maps at spatial extensions, which include the distribution of PAs (national and regional level), of PA functional zones (provincial level) and of natural, socio-economic characteristics inside a PA (PA level). Meanwhile, input data (administration, PAs boundaries, PhongNha-KeBang NP or PN-KB NP map package) were also collected from online sources, including the World Database on PAs, Diva-GIS and ArcGIS online. They are manipulated as needed (i.e. update, re-projection, geometry conversion) and are authored pre-defined maps at desired scales. Each single map was designed for best view at the full-extent of an administration units to be viewed and we defined simultaneously symbol transformation across the range of scales to ensure visual continuity at all scales. All composed maps were then ready to make web map.

Technologically, the web mapping is implemented with ArcGIS platform. Specifically, ArcGIS Desktop was used to build dataset NPs for demonstration and then exported them to

ArcGIS Pro. In turn, ArcGIS Pro was used to compose and symbolize sets of pre-defined maps at desired scales. Next, those maps were shared as web layers to ArcGIS online to create and share web maps and ready-to-use web applications (called web apps) which allows to build user interface and interactive tools for exploit spatial information in the cloud. Finally, ArcGIS Experience Builder was used to transform the single-page web apps in a solely place.

3. RESULTS AND DISCUSSIONS

This study created a multi-scale web map of Vietnam PAs. The experiment was conducted at spatial extension of Vietnam, North Centre region, Quang Binh (QB) province and PN-KB NP, within the scale range (Figure 4). Pre-defined maps were conducted with computer screen and designed to be viewed at spatial extension of Vietnam (1:30,900,000 - 1:11,700,000), North Centre region (1:11,700,000 - 1:3,700,000), QB province (1:3,700,000 - 1:900,000) and PN-KB NP (1:900,000 - 1:300,000).

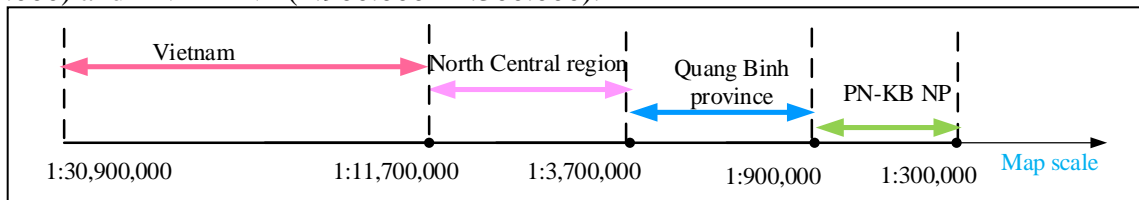


Figure 4. Scale range of experiment datasets

Within the experiment scale range, the content of map varies from the distribution of NPs (Vietnam and North Centre region), of functional and buffer zones of NP-KB NP (QB province), to that of natural and socio-economic characteristics. All contents are symbolized in ways that ensure visual continuity wherever applicable (Figure 5). The web map is held on Esri's GIS cloud and configured with basis interactive tools such as legend display, base-map gallery, layer management, measurement, radius search, selection.

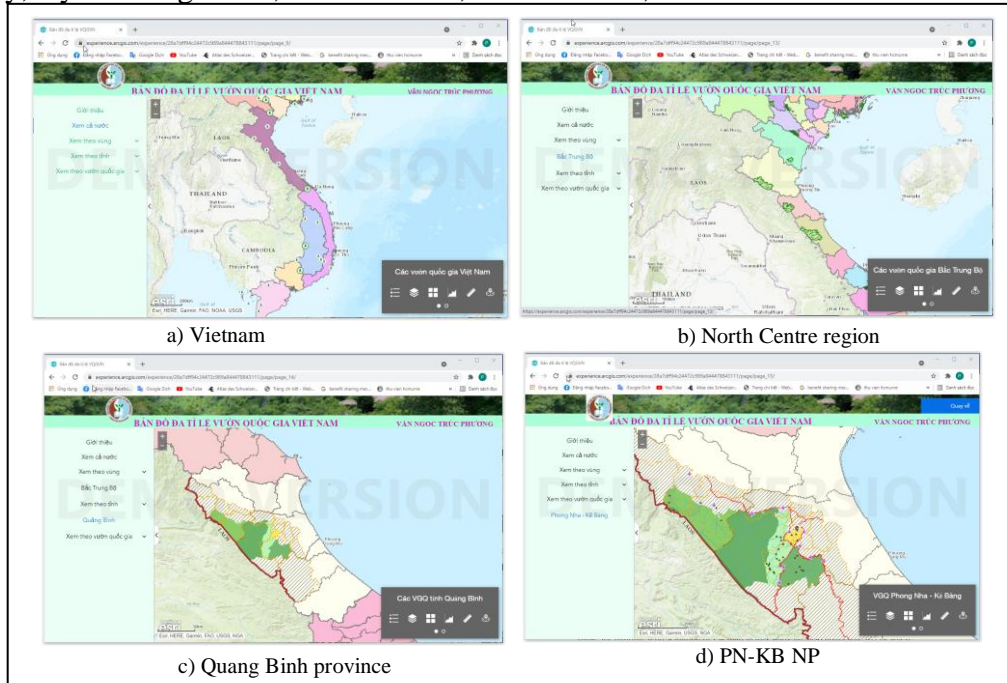


Figure 5. Experiment web map of Vietnam PAs

Through web map services, spatial information of Vietnam PAs is accessible from <https://experience.arcgis.com/experience/28a7dff94c24472c989a844478843111>. This study

proposed rules for setting scale range for multiple representation of PA map. They are reasonable and feasible, but require testing elsewhere in order to be applicable to other types of PAs.

4. CONCLUSIONS

Increasing awareness, sharing information and knowledge of PAs are key elements for their sustainability. Web map that provides spatial information of PAs has been paid attention. This study is aiming at develop a multiscale web map of Vietnam PAs and experiment with ArcGIS platform. Result is the web map with interactive tools, across spatial extensions, spanning from national, regional, provincial to PA level. The result shows that rules for determining scale range for multi-representation of PA map are reasonable and feasible. However, more experiments need to be done so that the rules can be applicable to elsewhere.

5. REFERENCES

- Brewer, C. A, Sparks, K., and Raposo, P.,. 2012. *Multiscale Design for The National Map 2011/12*
- Harder, C. 2015. *The ArcGIS Book: 10 Big ideas about applying geography to your world*. Esri Press
- Chu, M. T. 2011. *Xây dựng mô hình đồng quan lý tài nguyên môi trường tại KBT biển Cù Lao Chàm – tỉnh Quảng Nam*. Trường Đại học Khoa Học Xã Hội và Nhân Văn - ĐHQG TP. HCM.
- Dumont, Marion, Touya, and Duchêne. 2015. “Adding Intermediate Representations in a Multi-Scale Map to Enable a Smooth Zooming”. *CEUR Workshop Proceedings* 1598(c): 15–17.
- Dumont, Marion, Touya, and Duchêne. 2020. “Designing Multi-Scale Maps: Lessons Learned from Existing Practices”. *International Journal of Cartography* 6(1): 121–51.
- Frye, C. 2006. “A Product Driven Approach to Designing a Multi-Purpose Multi-Scale GIS Base Map Database That Supports High Quality Mapping.” *AutoCarto 2006*, 1–16.
- IUCN. 2013. “IUCN Protected Area Definition, Management Categories and Governance Types”. *The International Journal of Protected Areas and Conservation November* (19.2): 2.
- Mai, T. H., and Le, M. V. 2017. “Khái Quát Hóa Lớp Nội Dung Chuyên Đề Trong Bản Đồ Thông Kê Đa Tỷ Lệ”. *Kỷ yếu hội nghị khoa học và công nghệ 15*, Đại học Bách Khoa - TP.HCM, 145–54.
- Galanda, M., 2003. *Automated Polygon Generalization in a Multi Agent System*. University of Zurich.
- Neumann, A. 2016. “Chapter 379: Web Mapping and Web Cartography.” In Zhou X. Shekhar S., Xiong H. Cham (editors). *Encyclopedia of GIS*. Springer.
- Yurova, N., Samsonov, T., ?. *Automatic Selection of Symbols for Diagrams and Choropleths in Multiscale Thematic Mapping*.
- Nyangweso, D. O., 2013. *GIS Based Cartographic Generalization in Multi-Scale Environment: Lamu County*. University of Nairobi.
- Samsonov, Timofey. ?. *Multiscale Hypsometric Mapping*.
- Van, N. T. P. and Le, M. V., 2016. “Thiết Kế Hình Thức Bản Đồ Thông Kê Đa Tỷ Lệ Với Phương Pháp Đồ Giải.” *Tạp chí Phát triển khoa học và Công nghệ*, K4-2016 (tập 19): 51–58.
- Vietnam Administration of Forestry. 2019. *Báo cáo rừng đặc dụng và phòng hộ Việt Nam 2017-2018*. Hà Nội.
- Zhou, S., and Jones, C. B., 2013. “A Multi-Representation Spatial Data Model.” *Lecture Notes in Computer Science*.

WEB-BASED DATABASE AND SPATIAL DATABASE MANAGEMENT SYSTEM: APPLICATION OF DISABLED PERSON IN PHETCHABON PROVINCE

Gitsada Panumonwatee¹, Sudarat paluang², Jittrarat Chantana², Duangdao Sriyakun², Santi Lapbenjakul², and Sittichai Choosumrong^{1,*}

¹Faculty of Agriculture Natural Resources and Environment, Department of Natural Resources and Environment,
99 Moo 9 Tambon Tha Pho, Amphoe Muang, Phitsanulok, Thailand 65000,

²Reoriented Holistic Health Service Delivery Institution, National Health foundation, Ladyao, Chatuchak, Bangkok

* Corresponding author: E-mail: sittichaic@nu.ac.th.

ABSTRACT

Nowadays, widely used data warehousing technology is mostly due to its most efficient, easy-access, and analyzable. So, this work presents the approach to developing the service-oriented web-based application with spatial thinking of disabled persons quantitative. The Web-based database management system is one of the essential parts of Database Management System (DBMS) and is used to store web application data. A web-based database management system is used to handle those databases that are having data regarding E-commerce, E-business, blogs, e-mail, and other online applications. Not only has DBMS been implemented but spatial DBMS also has developed. Spatial DBMS can display, query and manage data in a Map format. This solution helps the care manager or disabled personal assistants (PA) manage the disabled person information as the database with the create, read, update, and delete the data (CRUD system) through Website. The application wasn't used only for data storage but also it was reflexed the disabled person needs e.g., job finding, PA-disable person matching, the disabled person mapping, and summarizing the information. The hypertext processor (PHP), JavaScript, CSS, PostgreSQL/PostGIS were used as the backend process of this application, through the hypertext markup language (HTML) with Bootstrap as the frontend development. The web mapping application using Leaflet and showing the summaries disabled person qualitative of each sub-districts, districts, or province. This solution could increase the disabled person database management and motivate the data analysis for better policy in the future.

1. INTRODUCTION

Web service technology is developing based on the concept of service-oriented computing. Service-oriented utilizes the rapid, easy distributed, and low cost that integrated web-based application through connecting and sharing the workflow (Papazoglou and Georgakopoulos, 2003). Web application technology refers to applications operated via multiplatform e.g., smartphone, tablet, and personal computer with the multi-operating system. This can be used on a web browser over the internet and developed using internet browser languages like HTML, PHP, JavaScript, etc. Sabah (2011) published the approach to developing a service-oriented web application for implement the business process as the customer-supplier interaction. Therefore, Data warehousing

can be developing under the Web-based database management system which is the key process of Database Management System (DBMS) and supported the decision support system (DSS).

Tongkaw and Tongkaw (2018) studied the geographic information system (GIS) with DSS for disabled person data management in Songkhla province, Thailand. They developed a prototype of a GIS-DSS web-based application for simulating the disabled person facilities tool to the better management plan and planning for Songkhla smart city in the future. GIS can be widely used and associated with decision supporting or spatial thinking. So, this could be appropriate for creating a new spatial database that interpreted especially disabled person information and personal assistants (PA) manage the disabled person information.

Create, read, update, and delete the data (CRUD system) is usually a function of database management which normally operates by Structured query language (SQL). This might be a barrier to data exploration and not suitable for everyone. So, web-application can solve this problem through CRUD through the Website. So, developing DNMS for disabled person management with CRUD through the web-based application is interested. This tool reflexes the disabled person's needs e.g., the suitable job finding, PA-disable person matching, the disabled person mapping, and summarizing the information.

So, we present the approach to developing the web-based database and spatial database management for the application of disabled person management in Phetchabun province. The disabled person information e.g., disabled type, location, care plan information, personal needs, and personal information was stored as an online database that can mange everywhere through the internet and smart devices. This solution could be solved the lack of data linking, connected the workflow, and integrated disabled person organization.

2. CONCEPTUAL FRAMEWORK AND MEHODOLOGY

Figure 1, This study developed 2 sectors including database design and web-based application. The database could be separated into 2 parts: disabled person databased and multi-level user databased. The database operated using PostgreSQL/PostGIS version 5.2 as the relational database management system (RDMS). The frontend was developed using hypertext markup language version 5 (HTML5) with Bootstrap5 as the cascading style sheets version 3 (CSS3). The hypertext preprocessor (PHP), JavaScript were used as the backend.

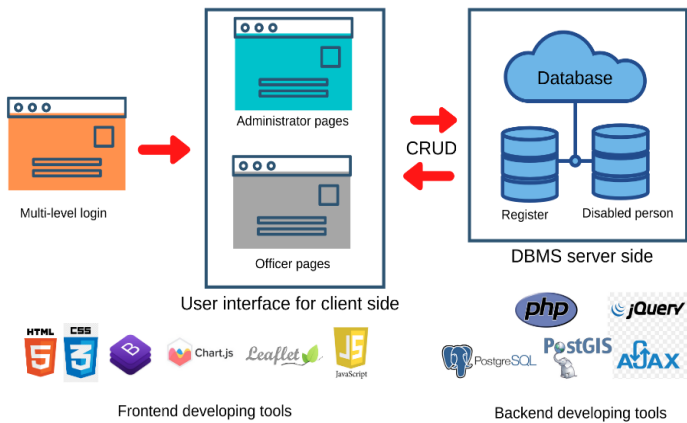


Figure 1. Conceptual framework

Disabled person databased obtained 4 schemes including disabled person data (DP), personal assistant data (PA), employment and job data (EM), and disabled person care center (Center). All of schemes related with the Center code, DP citizen ID, and PA citizen ID. Then, the data visualization was used the ChartJS through the Jquery. The database design was illustrated in Figure 2.

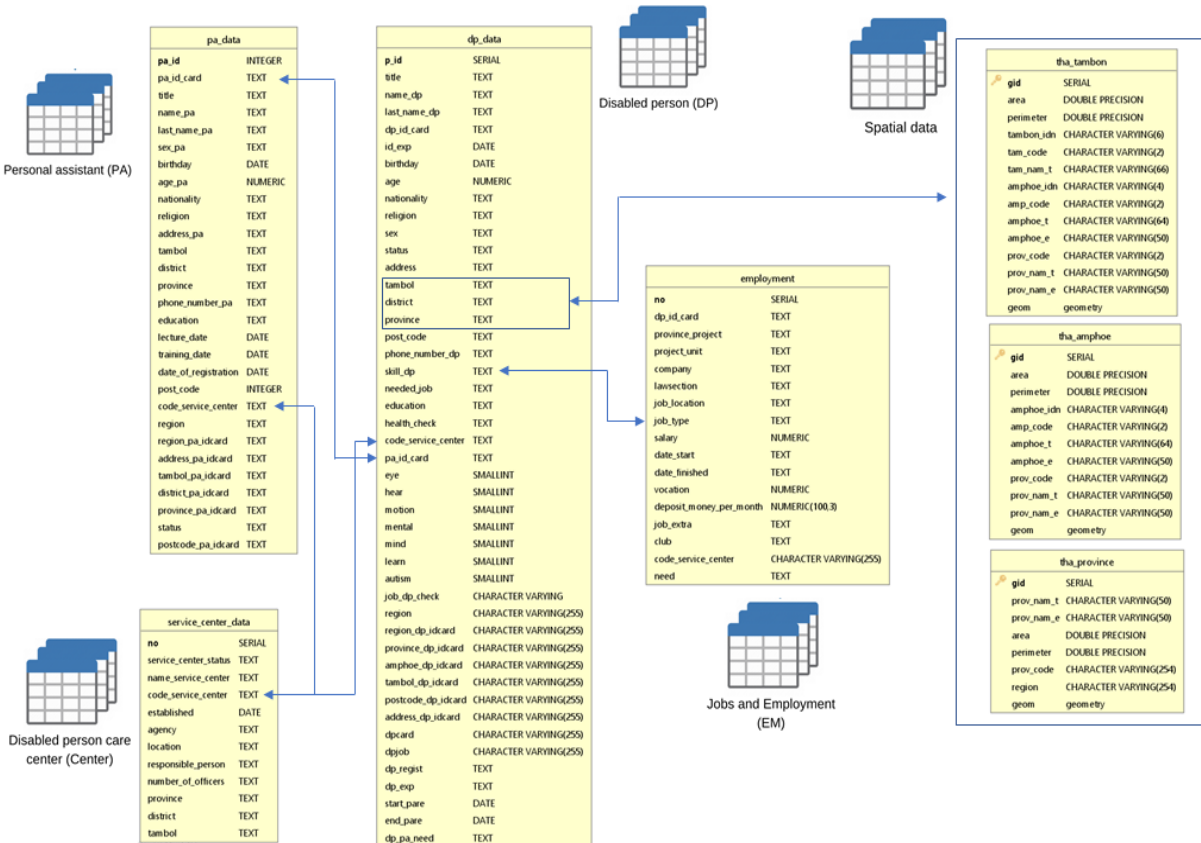


Figure 2. Disabled person database design.

Two-level user database designed to store the registered data e.g., username, e-mail, personal information, and password. The password is encoded as MD5 for the security data. The level is divided into 2 levels: administrator and officer. The officer rules can use CRUD the data of self-organization and disabled person under self-supervision. The administrator can access the data of every organization and can promote someone to the administrator level. The web application was design as the multi-view design relates to the user level. It contained 6 major pages: Dashboard page, DP page, PA page, Center page, EM page, and mapping page.

3. BACKEND AND FRONTEND DESIGN

3.1 Backend developing

Backend web development acts as the information source of the database that is required to operate the web application. Back-end was used for communication the client side to server side and server to client, likewise through the SQL. The SQL performs specific tasks like create, read, update, and delete; moreover, it can search, count, summation, or other analyses. It contains 3 majors parts: Server, Database, and Application. The server is a computer device that contains the computer program for processing the request through the network resources, normally, for storing the database, application, and web portal. The database collects all of the tables and these consisted of a variety of fields like a matrix of data. Figure 2. Showed the database design of disabled person web application (Browser-server (B/S) architectures) based on monolithic design.

From Figure 1., two types of login systems are allowed. The officer is responsible for add, edit, delete, and search, DP information e.g., Name, Last name, Citizen ID, address, disabled types, skill, and care plan. The permission was allowed only self-organization that was provided by the administrator. The center code was used for grouping the data and separation the permission of the officer. The address data of DP is linkage to the spatial data table. The geometry data was queried and showed on the mapping page. So, this could be applied to summary data such as disabled person per area, disabled person type per area, etc. Furthermore, the admin roles are showing more access to every center's data. The action of the officer/administrator was concluded and showed in Figure 3. In this section, many tools were applied to this work including AJAX-jQuery, PHP, and SQL for developed the CRUD system.

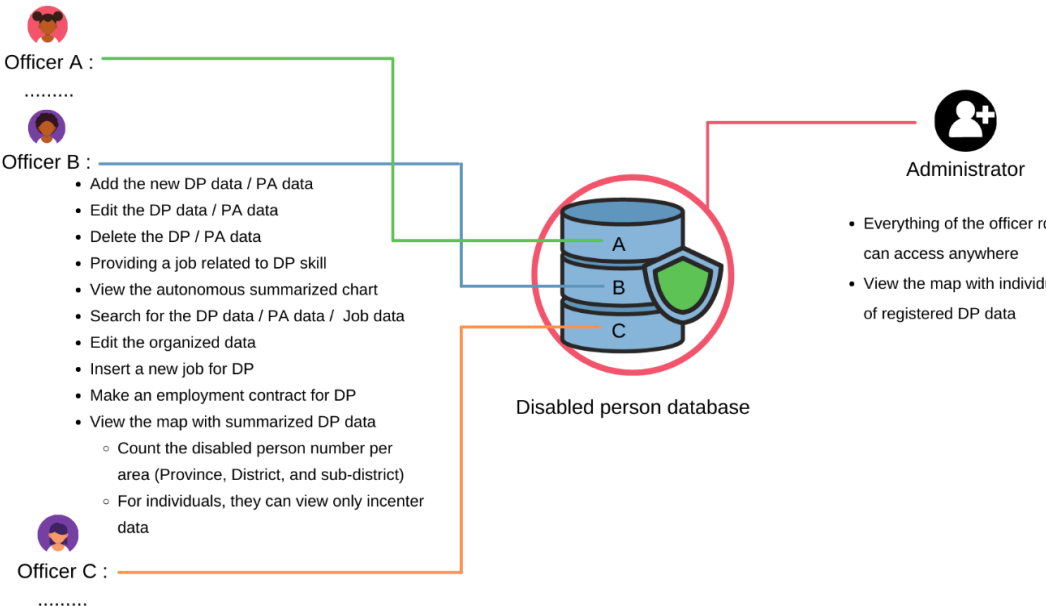


Figure 3. The backend design of web-application

PostgreSQL/PostGIS was used as the spatial mapping tool. The geography data of provinces, districts, and sub-districts were kept in the geometry type on the database. This function was designed to generate the location of a disabled person without a geographer technician. Moreover, the advantage of geometry data is analyzable. This function could help the officer or administrator (user) to manage the DP by spatial thinking. In addition, our solution motivates to help DP needs especially job-finding or job-matching. Spatial thinking enormously helps to match DP-job in the same area or in the range of agreement. Besides, the other functions like DP number per area (province, district, sub-district) nearest hospital or health promotion center, and disabled type per area were included in this work.

For the register database, we design to separate the database into another. The register database contained username, password, user information (name, last name, email, etc.), and user level. Start, we added the first administrator-level account for promotion to the other. The registration system was designed using object-oriented PHP with SQL.

3.2 Frontend developing

Frontend web development is programming which focuses on the visual elements of an application that a user will interact with the backend. They work together to create a dynamic website and allow the user to make the interactive activities: typing the data, submit the data, dynamic display, and everything as you see. For the better user experience, the frontend should break apart interesting with design engaging. Moreover, it should develop based on the user needs.

This work developed the responsive web application which supporting multi-platform access (mobile-friendly). The coding consists the HTML5, CSS, and JavaScript.

Bootstrap is one of the most popular open-source CSS framework for developing the responsive website. It contains the based components for design: forms, button, navigation, and grid. Bootstrap also comes with several JavaScript in the form of jQuery plugin. The HTML structure, CSS decorations, and accompanying JavaScript was included the Bootstrap framework. The basically layout component generating responsive design called “container”. Precompiled of Bootstrap is available in the form of one CSS file with three JavaScript. The frontend design was showed as Figure 4.

Leaflet is a free open-source JavaScript library for interactive map, one of the mapping Application programming interface (API). It designed with simplicity, usability, and multi-platform work-well. Leaflet has an ability to project the geographic data into online-mapping and work-well with the Google maps API. Figure 4 was showed the mapping web-application using leaflet, the geography data with related DP information was queried through the backend process.

ChartJS was used for visualizing the data to graph. It is a free open-source JavaScript library which supports many types of charts: bar, line, area, pie, etc.

4. THE IMPLEMENTATION SPATIAL THINKING FOR DISABLED PERSON MANAGEMENT

Our approach motivated us to develop the web application for DP information management. The data was stored in the database which has the ability to analyze. This application helps the officer and administrator can managing the data everywhere through various device types: smartphone, tablet, and personal computer. This work contained geospatial and non-geospatial information. The geospatial information is used for spatial thinking to planning the policy that might suitable for each area.

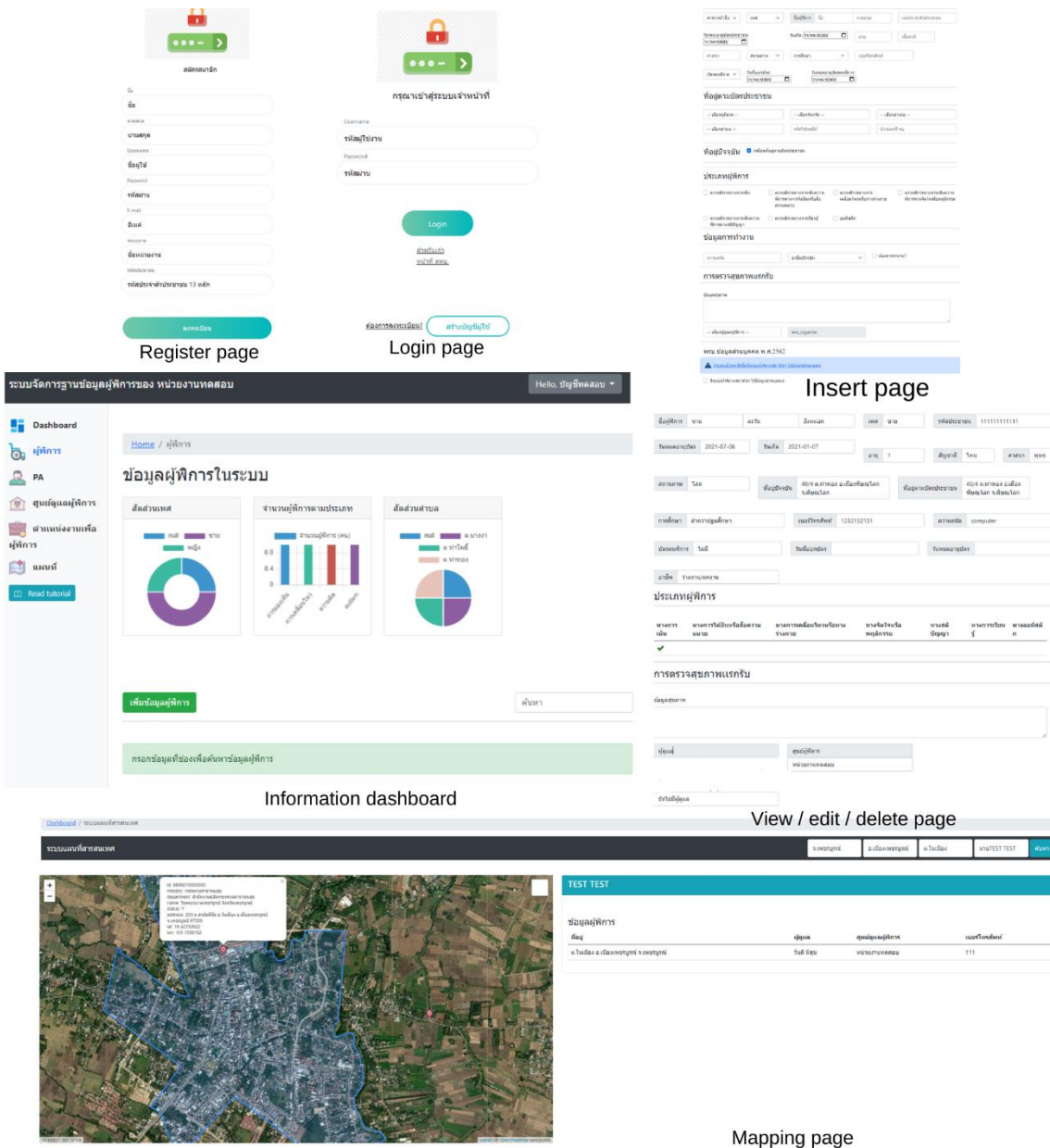


Figure 4. The frontend design of web-application using Bootstrap5, the mapping using Leaflet

For example, in an area that contains a high number of blind persons, there should be developing suitable facilities for the blind. The hospital geospatial data was projected. This could be used for finding the nearest. For non-geospatial information, PA could communicate with the Center, and access information of DP which care by himself e.g., health information, address, and work. The job-hiring for DP will be easier through our solution. The DP skill is the one of criteria for matching the job. The employment contract was stored on the database which is impartially both of employer and employee. Finally, this application facilitates the officer who working for

DP care. The data was analyzed into a real-time graph or table. This might motivate the data analysis for the better plan with support the policy makers.

5. CONCLUSION

A web-based database and spatial database management system for disabled persons in Phetchabun province was developed in this work. We designed a database to handle the disabled person information and the spatial database for the non-technician users. The backend and frontend were developed using the open-source library while showing effectiveness. This application presented the approach to spatial thinking for the decision support system. For the future, we suggested that gathering the coordinates data of each disabled person. This data might increase the function of applications like nearest hospital route, and the density of disabled persons per village.

6. ACKNOWLEDGEMENT

The authors would like to thank the Reoriented holistic health service delivery institution and the National health foundation for financial support.

7. REFERENCES

- Choosumrong, S., Raghavan, V., Delucchi, L., Yoshida, D. & Vinayaraj, P. (2014). Implementation of Dynamic Routing as a Web Service for Emergency Routing Decision Planning. *International Journal of Geoinformatics*, 10(2), 13-20.
- Choosumrong, S., Raghavan, V., Jeefoo, P. & Vadaddi, N. (2016). Development of Service Oriented Web-GIS Platform for monitoring and evaluation using FOSS4G. *International Journal of Geoinformatics*, 12(3), 67-76.
- Choosumrong, S., Rachavong, P. & Khamchiangngern, A. (2018). The study and explore the need for using public transportation services of the disabled to support the taxi service in Thailand era 4.0 using GIS tools. *Naresuan University Journal; Science and Technology*, Papazoglou, M. P., and Georgakopoulos, D., 2013 —Serviced-oriented computing, Communications of ACM, 46 (2003), 10, 25-28.
- Sabah A.F., 2011. Developing web applications. *International Journal of Software Engineering and Its Application* 5(2), 57-68.

USING GIS TO ANALYZE FACTORS AFFECTING THE APARTMENT PRICE. CASE STUDY: NEIGHBORHOOD OF HO CHI MINH METRO (LINE 1)

Nguyen Thi Cam Tien¹, Luu Dinh Hiep² and Le Thi Dung²

¹Center for Developing Information Technology And Geographic Information System, Ho Chi Minh City University of Technology, 268 Ly Thuong Kiet Street, District 10, Ho Chi Minh City, Viet Nam
Email: tienntc.hcmut@gmail.com

²Faculty of Environment and Natural Resources, Ho Chi Minh City University of Technology, 268 Ly Thuong Kiet Street, District 10, Ho Chi Minh City, Viet Nam
Email: hiepld_gis@hcmut.edu.vn

3Faculty of Environment and Natural Resources, Ho Chi Minh City University of Technology, 268 Ly Thuong Kiet Street, District 10, Ho Chi Minh City, Viet Nam
Email: dzungle1105@gmail.com

ABSTRACT

This study will explore the affecting price of the apartment where the research scope covers a 20km radius from Metro line 1. The data collected includes information about 300 units of apartments from Biggee.vn website and the local authority. The six variables are discovered to be affecting the apartment price after screening and standardizing the data with ArcGIS Pro. The price maps generated as a result of this study are used to visualize the unit price distribution of apartments in HCMC and the surrounding area. It will also assist property managers and home buyers in making informed decisions regarding apartment investments.

1. INTRODUCTION

Along with urbanization sprawl, Ho Chi Minh City (HCMC) land fund is becoming increasingly scarce. As a result of rising overpopulation, the HCMC Government forces have developed a population mechanism of control as well as new policies for expanding regional planning. That is why, in recent years, HCMC has increased its investment in infrastructure, particularly Metro line 1. It is expected to lower the pressure of overcrowding by resolving travel demand. This is because travel time can be shortened; for example, getting into the heart of HCMC takes only about 10-15 minutes. However, the real estate value surrounding this construction has become unpredictable. This results in exorbitant prices and an unstable investment trend. Besides that, the majority of new apartment projects evaluation is still subjective and imposing. It depends on appraise experience and knowledge or even the appraiser's priority. Because of that, the real value of the real estate is a public concern. Therefore, understanding the factors affecting the apartment price is critical. This helps the market to develop and be stable. This topic will focus in-depth on the impact of location, properties of apartments, and construction projects on the prices of surrounding apartments by using GIS.

2. METHODOLOGY

2.1 Research objectives and methods

The research objective is to study the determinants of the apartment price and apply it to the real estate market in the neighborhood of HCMC Metro line 1. In this topic, the linear

regression integrated GIS method is used. Specifically, determining the impact of factors like the population density of the region, distance to the CBD, and Metro line together with project scale (construction area and the highest floor). Considering entire model, which is the most dominant contribution to the price of an apartment. Finally, quantifies in detail how the modeled proxies affect the regional price market that contributes to consolidating knowledge about the real estate market in this market. In other words, the given findings could be used as preparation for investors, planners, or accommodation developers.

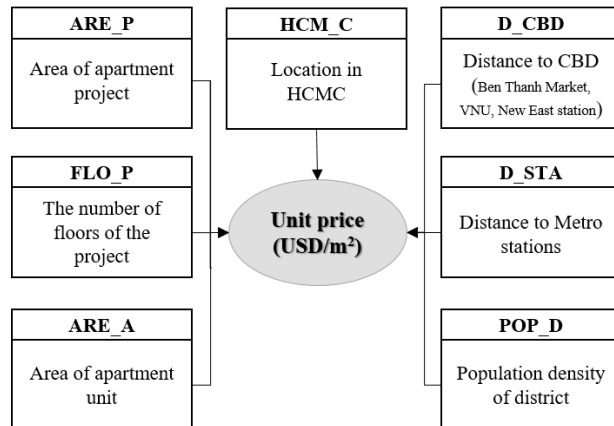


Figure 1. Research model

The dependent variable is the average sale price of the apartment in a project measured in USD/m². This price is the market price that has been collected and surveyed from many sources by the Biggee.vn website during August 2020. The data collection process takes about one month, so macro-factors will have very little impact on the research model because the real estate market has not fluctuated much. The topic uses the Logarithmic model and the logarithm form of apartment price variable (LnPRICE) as the dependent variable. When the PRICE variable is expressed as logarithms, the coefficients which be explained as the percentage shift in price resulting from an additional unit of the independent variable (Seo et al., 2018).

2.2 Data procedure

In this topic, 300 apartment projects in the vicinity of Ben Thanh – Suoi Tien Metro were surveyed and selected as a sampling population for the model. Data samples were collected in the research scope, commercial apartment projects located within 20 km of Metro lines

Table 1. Table of collected data description.

No.	Fields	Code	Unit	Description
A Variables				
01	Price of the apartment (Dependent)	PRICE	USD/ m ²	The average price per unit of an apartment
02	The number of the floor of the project	FLO_P	floor	The highest floor in the apartment project
03	Area of project	ARE_P	m ²	The total area of the apartment project
04	Apartment unit area	ARE_A	m ²	Average apartment unit area or size
05	Location in HCMC	HCMC	dummy	Apartment project in HCMC
06	Distance to CBD	D_CBD	km	Distance to the nearest CBD point (Ben Thanh Market, VNU, New East station)

No.	Fields	Code	Unit	Description
07	Distance to Metro stations	D_STA	km	Distance to the nearest station of Ben Thanh - Suoi Tien metro line
08	Population density	POP_D	Per/km ²	Population density of district where apartment located
B Other information				
09	Province		Text	Name of the province which apartment located
10	District		Text	Name of the district in which apartment located
11	Name of the project		Text	Name of the apartment project
12	X, Y		Double	The coordinate system of the apartment project

Following data collection, the project area was found that is the most heterogeneous variable. Therefore, the author group removes about 4% of the data sample in which four observations have the largest project area and eight ones have the smallest area, and 2.6% of apartment units having less than 45m² in size (8 observations). Elimination aims to optimize sample consistency and expect to limit bias in the regression process that could be caused by outliers. Finally, the size of the final sample is 280 observations.

3. FINDINGS AND DISCUSSION

As result from Table 2, it can be seen that the popular price ranges from 1,000–2,000 (USD/m²), in which the most traded price is ~1,300 (USD/m²). From the map, it can be seen that the prices of apartments in HCMC are very high (> 2,000 USD/m²). And the crowd density is high surrounding Ben Thanh Market. Meanwhile, projects with lower prices have scattered distribution and been located in the neighborhood areas (10km away from the metro).

Table 2. Descriptive statistical table of 280 observations.

Variables	Unit	Min	Max	Mean	Median	Mode	Std
PRICE	USD/ m ²	487.57	3,840.61	1,646.93	1,568.00	1,329.82	545.32
ARE_P	m ²	2,400.00	685,000.00	41,064.51	14,577.50	50,000.00	89,437.84
FLO_P	floor	5	50	22.70	22	18	7.41
ARE_A	m ²	45	167.85	76.38	70.50	60.00	21.61
HCMC	dummy	0	1	0.85	1	1	0.36
D_CBD	Km	0.81	17.56	6.11	5.81	-	2.85
D_STA	km	0.11	18.27	4.81	4.56	-	3.40
POP_D	Per/km ²	1,928.00	42,041.00	14,259.16	9,787.00	9,787.00	11,957.67

Out of 280 samples observed, the project has the smallest area of 0.24ha, and the largest area is 68.5ha. The average area of the project's sample is concentrated from 0.24 – 2.4ha.

These figures reveal a wide range gap of project area between the top and bottom points. Figure 2b shows that projects with size less than <2.4 ha account for most of the number of projects. Besides that, the project has the lowest floor of 5, the highest one is 50, the number of built popular floors is 20. The distribution of these apartments is broad across the research areas. For the project group with the number of floors above 32, it is found that clustered at the starting of the Metro line, district 2, and district 4 (HCMC). However, the Thuan An market (Binh Duong) is prominent with the appearance of many high-rise projects recently (Figure 2c).

Area of the apartment surveyed has ranged from 45 – 167.85m². Most of the area of the apartment is concentrated in the range of 55 - 75m². The popular area commonly chosen to buy an apartment is about 60m². There are 236 projects located in HCMC, accounting for 84.3% of the sample. The distance from 280 apartments to commercial and educational centers ranges from 0.81 - 17km, with an average distance of 6km. The shortest distance measured from the apartment to the nearest Metro station is 0.1km, and the furthest is 18km. It shows that within 1-5km around the metro line there is a high concentration of apartment projects (Figure 2d).

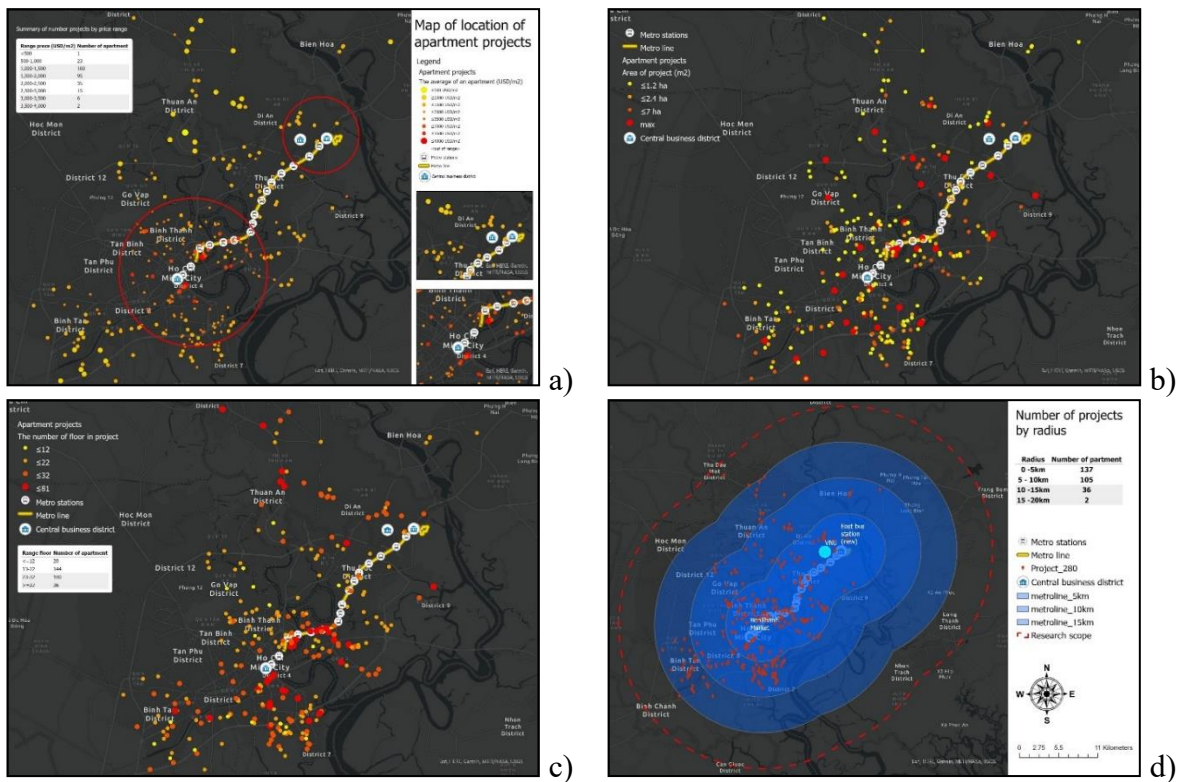


Figure 2. (a) Location of apartment projects by price, (b) Location of apartment projects by area of construction, (c) Location of apartment projects by the number of floors, (d) The apartment density by radius from Metro line 1

To explore possible combinations between the independent variables, the author will use the Exploratory Regression method. After analyzing, the variables HCMC, FLO_P, and ARE_A affect the price most, followed by POP_D, D_CBD, D_STA, and finally ARE_P. The group of project scale, the number floor of the project will have the biggest impact on the price of apartments. Meanwhile, the group explains the location factor, the project in HCMC will greatly affect the price. And finally, the area factor reflects the price. The remaining proxies of the location feature, also showing a huge effect on the price, > 80% as well. In contrast, a proxy represented the project size is the project area that exhibited a little effect (<20%). The model results show that with the seven variables, via the OLS regression, the proposed regression

models could be achieved a maximum of 61%. Data of 280 apartments were run OLS tool using ArcGIS Pro software, and gave the following results:

$$\begin{aligned} \text{Ln(PRICE)} = & 4.607 - 0.023 * \text{Ln(ARE_P)} + 0.396 * \text{Ln(FLO_P)} + \\ & 0.207 * \text{Ln(ARE_A)} + 0.285 * \text{HCM_C} - 0.032 * \text{D_STA} + 0.085 * \text{Ln(POP_D)} \end{aligned} \quad (1)$$

By IDW approach and mapping predicted metrics of each apartment resulted from OLS, the following maps are formed as Figure 3. The estimated zones having the highest price of the apartment are District 1,2 and Binh Thanh District, specifically the area surrounding Ba Son, Van Thanh, and Tan Cang stations of the Metro line. District 1, District 2, District 4, and Binh Thanh District (>2500 USD/m 2) are the zones with highly anticipated prices. Noticeably, house prices in District 9 and Thu Duc, part of Thu An Town and Di An city, Bien Hoa city also reached 1,500 USD/m 2 . The price of apartments along the Metro line is also estimated to be very high, ranging from 1,500 USD/m 2 to 3,000 USD/m 2 , gradually decreasing from Ben Thanh Market to Suoi Tien Terminal station. Besides, there is a clear difference between HCMC and neighboring provinces for the level of the apartment price or the market preference.

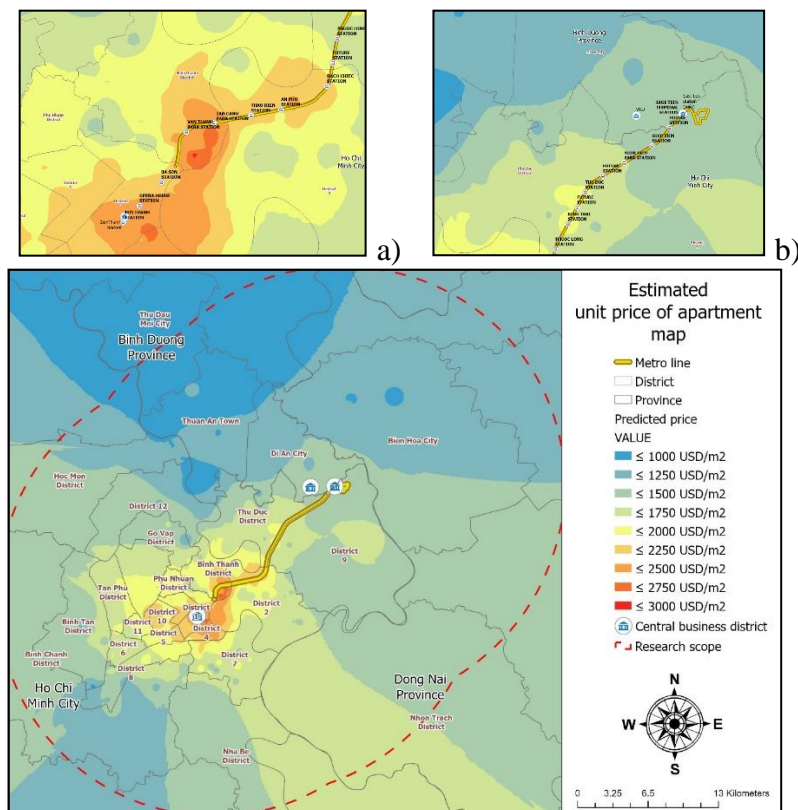


Figure 3. Estimated pricing map of apartments in HCMC and the neighborhood (a) Zone near the start point of Metro line 1, (b) Zone near the endpoint of Metro line 1

4. CONCLUSION AND RECOMMENDATION

4.1 Conclusion

From the inheritance of the results of previous studies, the author has built a price regression function. By this quantitative method, six factors have been identified that impact apartment prices in the scope within a 20km radius from Metro line 1. With only six

explanatory variables, the model can contribute 61% to the estimate of prices. Specifically, apartment prices will increase by 1 USD/m² when there is a 1-unit increase by one factor in the multi-factors such as high-rise buildings, apartment area, or population density. Meanwhile, with the apartment product title "location in HCMC", the price can increase up to 28.5%. Also, the distance to the Metro stations or the CBD will reduce the price of the apartment, when more than 1km away from Metro, the apartment can reduce 3.2% of the value.

The location in HCMC has the most impact on the price of an apartment in the study area. The real estate located in HCMC will be higher than the rest of the area. Because HCMC is the largest economic hub in the country, owning an apartment in this area gives buyers more opportunities to access the education system, well-paid jobs, public facilities, and social benefits that this area brings. Besides, the location of the apartment compared to the Metro line 1 will affect the apartment price here. This is because it will save travel time, especially with large-scale transportation systems such as Metro will greatly aid in accessing other transport networks, or inter-regional trade connections (Binh Duong - Dong Nai - HCMC). Currently, the number of projects around this metro line is growing more and more, which also explains the rapid increase in house prices in this area. The size of the project has a strong impact on apartment prices. In particular, the projects have more height, the apartment price is higher. The area of the apartment has the strongest impact on the price. This is also keeping in line with reality because the size is an important factor forming the value of the real estate, following the ancient idiom "golden square". Real estate prices will be high for real estate with large acreage due to meeting the diverse uses of owners or in other words maximizing usability by optimizing use purposes.

Through the application of the pricing model to determine the factors affecting apartment prices in the study area, partly understand the factors that affect apartment prices, which is the most important one. Thereby, this helping market participants will estimate transaction prices by relying on strong factors such as apartment area, the number of floors of the project, distance to the nearest Metro station, position, and population density of the area in which the apartment is located.

4.2 Recommendations

In the process of reviewing previous studies, the author found has only collected a small piece of factors, there are still many variables that also have an impact on apartment prices as such as building quality; the interior of the apartment, internal utilities of the project or information about the developers and owners as well as macroeconomic change (interest, government policies, ...) and so on. However, the datasets cannot meet this expectation because of difficulties in the process of collecting information and data about apartments. The other limitation is that the author does not re-examine the model and compare research results with previous studies in detail and reality data. These obstacles were recommended to solve in the next research.

5. REFERENCES

- Aladwan, Z., & Ahamad, M. S. S. (2019). Hedonic Pricing Model for Real Property Valuation via GIS - A Review. *Civil and Environmental Engineering Reports*, 29(3), 34-47. doi:10.2478/ceer-2019-0022
- Seo, D., Chung, Y., & Kwon, Y. (2018). Price Determinants of Affordable Apartments in Vietnam: Toward the Public–Private Partnerships for Sustainable Housing Development. *Sustainability*, 10(1). doi:10.3390/su10010197

INTEGRATION OF GEOGRAPHIC INFORMATION SYSTEMS AND UNIVERSAL SOIL LOSS EQUATION FOR SOIL EROSION ASSESSMENT IN DONG PHU DISTRICT, BINH PHUOC PROVINCE, VIETNAM

Nguyen Huy Anh¹, Gia Thanh Hoang¹ and Nguyen Thi Thao Nguyen¹

¹Ho Chi Minh University of Natural Resources and Environment
236B Le Van Sy street, Tan Binh district, Hochiminh city, Vietnam
Email: anhnhanh@hcmunre.edu.vn

ABSTRACT

The study evaluates soil erosion status in Dong Phu district, Binh Phuoc province, using the Universal Soil Loss Equation (USLE) and GIS methodologies. R (Rainfall erosivity factor), K (Soil erodibility factor), L x S (Slope length-gradient factor), C (Cropping management factor), and P (Pest management factor) were used in the calculation (Conservation practices factor). The generated maps depict soil erodibility and erosion condition, with potential erodibility estimated at 3,568.72 tons per hectare per year. Soil erosion is very low (≤ 50 tons/ha/year) with an area of 63,645.98 hectares (68.04 percent of the natural area), low (1-5 tons/ha/year) with an area of 20,878.57 (accounting for 22.32 percent of the natural area), moderate (5-10 tons/ha/year) with an area of 6,791.15 hectares (accounting for 7.26 percent of the natural area), soil erosion is low (1-5 tons/ha (accounting for 0.33 percent of the natural area).

Keywords: soil erosion, Dong Phu district, GIS, USLE

1. INTRODUCTION

In earth science, erosion is defined as incorporation and transportation of material by a mobile agent, such as water, wind, or ice (Lutgens, 2016). Thus, soil erosion is a natural process that occurs regularly and continuously, affecting the characteristics and properties of the soil. Erosion can occur in all different types of terrain. Agricultural scientists believe that soil erosion is the process in which topsoil is removed due to physical factors such as water and wind or factors related to farming activities. Thus, erosion is considered one of the causes of soil degradation, especially in sloping areas. Factors affecting soil erosion are mainly terrain slope, soil characteristics, rainfall, vegetation cover characteristics and farming techniques. In recent years, climate change is becoming more evident in Vietnam such as the increase in temperature, changes in rainfall and sea level rise. All of which can be potential causes for exacerbation of soil erosion.

Dong Phu is a district located in the southern major economic zone of Binh Phuoc province. It offers a lot of advantages in terms of territory, natural resources, people, and economic potential. Dong Phu district is an important location in Binh Phuoc province, with the National Highway 14 serving as an arterial artery connecting Dong Phu to the Central Highlands, Ho Chi Minh city and Cambodia. Soil deterioration is becoming more likely as a result of socioeconomic development, population growth, and changing farming circumstances. As a result, research to assess soil erosion is critical.

Researches on erosion and erosion protection measures to protect slopes in the world have been deployed by scientists from the 18th century. One of popular methods is universal soil loss equation (USLE) by Wischmeier and Smith (1978). USLE has been used in various case studies for tropical region (Ali and Hagos, 2016), (Lai, 2011), (Tung et al., 2018). Soil

erosion assessment and its verification using the Universal Soil Loss Equation and Geographic Information System: a case study at Boun, Korea (Saro L., 2004). Rapid Assessment of Soil Erosion in Central America's Rio Lempa Basin The estimated erosion rates were compared to sediment delivery ratios utilizing the Universal Soil Loss Equation and geographic information systems and remote sensing technology. (John B. K., 2005). This study analyzed soil erosion changes in the Kondoa degraded area and investigated reasons of change using the Universal Soil Loss Equation, Geographic Information Systems, and a socioeconomic survey. To forecast soil erosion, researchers employed soil data, digital elevation models, rainfall, and land use/cover visually assessed from multitemporal satellite imageries. (Ligonja P.J., 2015). The goal of this study was to quantity and map mean annual soil erosion and sediment deposition using a geographic information system in Thailand (GIS). The revised universal soil loss equation (RUSLE) model was used to examine soil loss in each grid cell. (Prem Rangsiwanichpong, So Kazama, (Luminda G., 2018).

In Vietnam, after 1990s studies on soil erosion gradually shifted to using GIS and remote sensing methods, notably the studies by Mai (2007), Ho (2000), My (2005), Huong (2015). Thus, it can be seen that the integration of GIS and RS technology for soil erosion assessment research is currently of interest. GIS can support modeling and assessment of the current situation and using mathematical models to find areas of high soil erosion proneness to propose measures to minimize and prevent soil erosion.

2. RESEARCH METHOD

2.1 An overview of the field of study

Topographic: The district of Dong Phu is situated at a height of roughly 100 to 120 meters above sea level. Red soil grows on basalt soil and gray soil develops on ancient alluvium in this low undulating terrain, which is generally found in the district. The landscape is low-lying, with undulating low-hill terrain intermingled; the common soil is mostly sloping ground.

Soil resources: With a total natural area of 93,542 ha, red-yellow shale soil accounts for 42.53 percent, red-brown basalt soil accounts for 23.90 percent, yellow-brown basalt soil accounts for 9.13 percent, and soil on basalt accounts for 9.13 percent. Gray on ancient alluvium makes up 14.47 percent of the total, with yellow-brown soil on ancient alluvium and sloping soil accounting for the remainder.

Climate: The climate is mild, with two distinct seasons each year; the average annual temperature is around 27.8° C; high air humidity, rarely influenced by storms; and ideal growing conditions for plants and animals. The temperature is typically cold at night in the latter months of the rainy season and the beginning of the dry season. The daytime temperature is generally the greatest in the country during the dry season, although the high temperature only lasts approximately a month before progressively decreasing.

2. Research method

In addition to traditional research methods such as collecting and analyzing secondary data from available documents and literature in combinatin with field survey, the research also uses modern methods such as the application of remote sensing technology to determine the characteristics of plant cover, geographic information system (GIS) to integrate various

elements into USLE model to assess soil erosion in Dong Phu district, Binh Phuoc province, Vietnam. The method used in this study is presented in Figure 1.

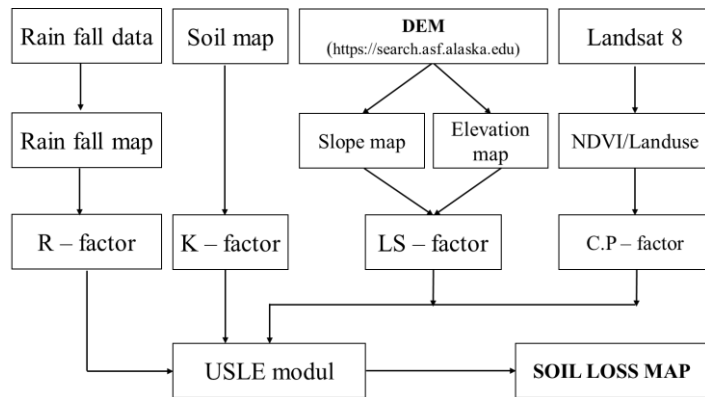


Figure 1. Flowchart of the methodology.

To prepare a soil erosion map, the study used USLE and GIS models. Factors affecting soil erosion are performed according to USLE developed by Wischmeier and Smith in 1978 (equation 1):

$$A = R \times K \times (L \times S) \times (C \times P) \quad (1)$$

In which:

- | | |
|--|---|
| A: Average annual soil loss (ton/ha/year); | R: Rainfall erosivity factor |
| K: Soil erodibility factor | L x S: Slope length-gradient factor (m) |
| C: Cropping management factor | P: Conservation practices factor |

3. RESULT AND DISCUSSION

3.1. Factors for erosion

3.1.1 Rainfall erosivity factor

Rain immediately impacts the soil surface, which, when coupled with topographic circumstances, creates surface runoff, which transports that soil layer to another location. The rainfall erosivity is calculated by multiplying the kinetic energy by the maximum rainfall intensity during a period of 30-minutes for each rainstorm. The R-factor averages the erosivity of individual rainy occurrences across several years (equation 2).

$$R = \frac{E * I_{30}}{1.000} \quad (2)$$

In which: E: total kinetic energy of precipitation (J/m^2); I_{30} : maximum rainfall intensity during a period of 30 minutes for each rainstorm (mm/h); R: rainfall erosivity factor ($MJ/ha.mm/h$).

Without 30-minute rainfall data, the authors employed annual average rainfall to calculate R using the method in Ha N.T. in 1996 (equation 3).

$$R = 0.548257 \times M_{TB} - 59.9 \quad (3)$$

In which: (R) rainfall erosivity (J/m^2); (P) annual average rainfall (mm/year); From equation (1), a map of R was developed for the district, showing value in range of 872.13 – 1091.43.

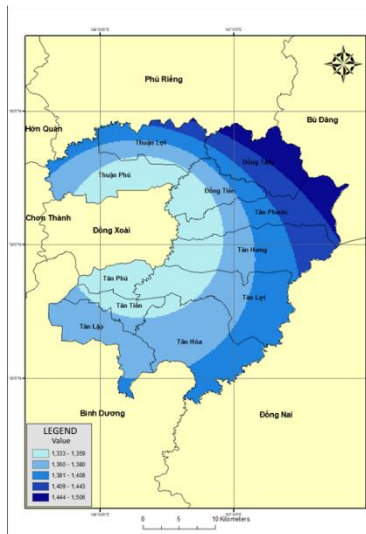


Figure 2. R factor.

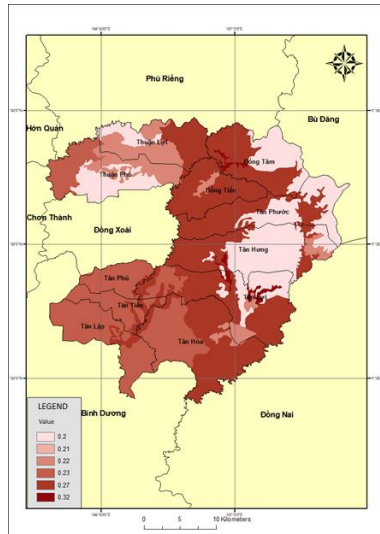


Figure 3. K factor.

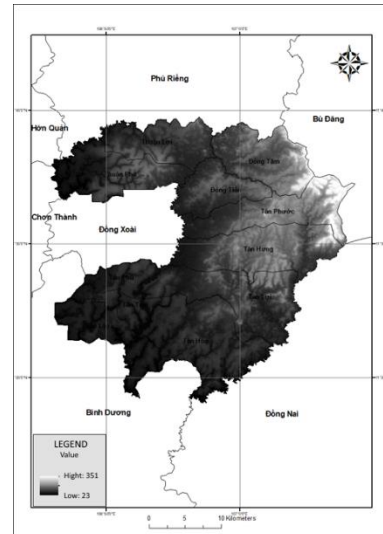


Figure 4. DEM.

R factor is highest in the east in the communes of Dong Tam, Tan Phuoc, Tan Hung, Thuan Loi. Communes of Dong Tien, Tan Hoa, Tan Lap have an average R factor and account for up to 30% of the district area. The lowest R factor is in the west area and a part of the central area of the district (Figure 2).

3.1.2 Soil erodibility (K)

K is depended on both soil physics and chemistry, namely soil structure, permeability and chemical composition.

According to Ha, N.T. in 1996, K factor for different soil type is as follow (Table 1).

Table 1. K factor of different soil types in Dong Phu District

No	Type	WRB (World Reference Base for Soil Resources)	K – factor	Area (ha)	Ratio (%)
1	D	Umbric Gleysols	0.32	1,000.90	1.07
2	Fk	Acric Ferralsols	0.20	22,356.54	23.9
3	Fp	Haplic Acrisols	0.23	8,315.88	8.89
4	Fs	Haplic Acrisols	0.27	39,783.41	42.53
5	Fu	Acric Ferralsols	0.21	8,549.74	9.14
6	X	Haplic Acrisols	0.22	13,535.53	14.47
<i>Total</i>				<i>93,542.00</i>	<i>100.00</i>

From map of soil type in Dong Phu District, Figure 3 was developed. The result shows that in Dong Phu District, K factor is from 0.2 to 0.32, in which K at 0.27 accounts for most of

the area (42.53%). K factor shows small difference, indicating that that the erosion resistance of the above soils is not much different (Figure 3).

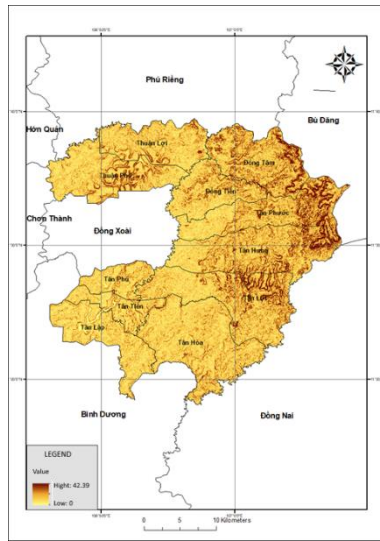


Figure 5. Slope

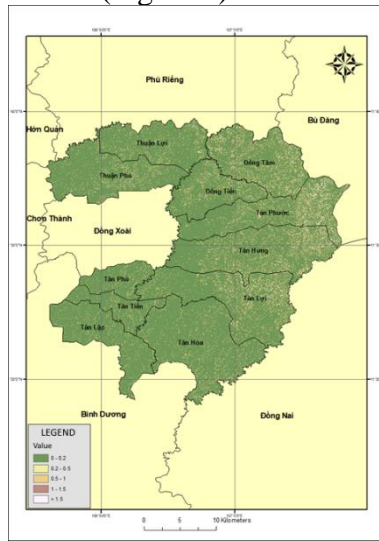


Figure 6. LS factor



Figure 7. NDVI

3.1.3 Slope-length and steepness

LS factor distribution map is developed from digital elevation model (DEM) and Wischmeier and Smith (1978) equation. DEM (Figure 4) is acquired from <https://search.asf.alaska.edu/> (equation 4).

$$LS = \left(\frac{X}{22.13} \right)^n * (0.065 + 0.045 * S + 0.0065 * S^2) \quad (4)$$

In which: (X) slope length in m, (S) steepness in %; (n) experiment coefficient, n = 0.5 if S > 5%; n = 0.4 if 3.5% < S < 4.5%; n = 0.3 if 1% < S < 3.5%; n = 0.2 if S < 1%.

Table 2. LS distribution

No	LS factor	Area (ha)	Ratio (%)
1	0 – 0.2	56,134.55	60.01
2	0.2 – 0.5	9,840.62	10.52
3	0.5 - 1	16,762.73	17.92
4	1 – 1.5	7,240.15	7.74
5	>1.5	3,563.95	3.81
<i>Total</i>		<i>93,542.00</i>	<i>100.00</i>

Table 2 shows the LS values of the region in the range 0 – 1.5 and divided into 5 levels. Out of the total area of 10,809.1 ha, 11.55% of area has LS value < 1.0 and 88.45% has LS value > 1.0 (Figure 6).

3.1.4 Crop management factor

Map of crop management factor (C) is developed from normalized difference vegetation index (NDVI – Figure 7) based on equation of Durigon (2014) as follow (equation 5):

$$C = \frac{-NDVI + 1}{2} \quad (5) \quad \text{in which} \quad NDVI = \frac{NIR - RED}{NIR + RED}$$

In which:

NIR and RED: reflection on near-infrared and red channels

In this study, data was collected from Landsat 8 image downloaded from: <https://earthexplorer.usgs.gov/>.

More than 85% of the area had a C ≤ 0.3 (Table 3). Specifically, C at 0 - 0.2 accounts for 22.16% of total area, at 0.2 accounts for 63.16%. The spatial distribution of current soil erodibility is a multiplication of all factors, which shows that soil erodibility of more than 90% of the area might have been halved thanks to existence of vegetation cover compared with non-existence of vegetation cover (Figure 8).

Table 3. Crop management factor (C)

No	C factor	Type	Area (ha)	Ratio (%)
1	0.0	Water (lake)	1,159.92	1.24
2	0.08	Forest, perennial plant	19,662.52	21.02
3	0.2	Rubber plant	59,081.13	63.16
4	0.3	Fruit plant	5,893.15	6.30
5	1.0	Other land	7,745.28	8.28
<i>Total</i>			93,542.00	100.00

3.1.5 Farming conservation practice (P)

P value is calculated according to Wischmeier and Smith (1978) from slope map using ArcGIS 10.3 software. As a result, P value map is developed (Table 4, Figure 9).

Table 4. P by steepness

No	P factor	Slope	Area (ha)	Ratio (%)
1	0.5	< 8	60,699.40	64.89
2	0.6	9-12	26,799.78	28.65
3	0.7	13-16	4,031.66	4.31
4	0.8	17-20	1,328.30	1.42
5	0.9	> 20	682.86	0.73
<i>Total</i>			93,542.00	100.00

3.2 Assessment of soil erosion status

Soil erosion status is developed from the integration of R, K, LS, C and P by using Raster Calculator in ArcGIS 10.3.

Table 5. Distribution of soil erosion status in Dong Phu District

STT	Level	Soil loss (ton/ha/year)	Area (ha)	Ratio (%)
1	No or negligible erosion	0 - 1	63,645.98	68.04
2	Mild erosion	1 – 5	20,878.57	22.32
3	Medium erosion	5 – 10	6,791.15	7.26
4	High erosion	10 - 50	1,917.61	2.05
5	Extreme erosion	> 50	308.86	0.33

<i>Total</i>	93,542.00	100.00
--------------	-----------	--------

Erosion level is divided into 5 level: Level I (no or negligible erosion); Level II (mild erosion); Level III (medium erosion); Level IV (high erosion); Level V (extreme erosion) (Table 5).



Figure 8: C factor

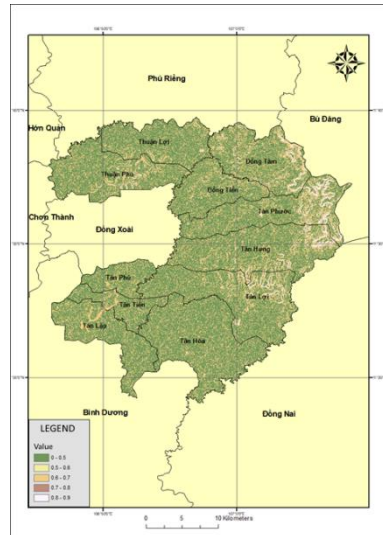


Figure 9. P factor



Figure 10. Soil erosion status map

It can be seen that the current erosion status in Dong Phu District is divided to the following levels (Table 5 and Figure 10):

- Level I (no or negligible erosion): accounting for 63,645.98 ha (68.04% of the entire area), distributed throughout the area, and with low terrain factors (LS).

- Level II (mild erosion): accounting for 20,878.57 ha (22.32%), sandwiched between Level I, Level III and Level IV land.

- Level III (medium erosion): most concentrated in the North, the central region and the South with an area of 6,791.15ha (7.26%).

- Level IV (high erosion): distributed in the entire district, accounting for 1,917.61ha (2.05%).

- Level V (extreme erosion): accounting for 308.86ha (0.33%).

4. CONCLUSION

The erosion map of Dong Phu district shows that in areas with high vegetation cover (high NDVI index), erosion value is low. Erosion in Dong Phu District is uneven among areas. In most of the district, area of negligible erodibility (from 0 to 5 ton/ha/year) is about 84,524.55 ha, accounting for 90.36% of the total land area. Extreme erodibility only accounts for 0.33% of the entire area. Therefore, it is necessary to take measures to prevent erosion especially on sloping land.

5. REFERENCES

- Ali, S. A., Hagos, H., 2016. *Estimation of soil erosion using USLE and GIS in Awassa Catchment, Rift valley, Central Ethiopia*. Journal of Geoderma Regional, Vol 7, 159-166.

Ha, N.T., 1996. *Factors on soil erosion and predicting soil erosion on slope land. University of Irrigation and Drainage*, Dissertation for Doctor of Philosophy, Hanoi (In Vietnamese).

- Ho, K., 2000. *Soil erosion and Accumulation evaluation on some popular farming systems on steep land in Huong river catchment, Thua Thien Hue province*. PhD Dissertation, University of Ha Noi Agriculture, Vietnam (In Vietnamese).
- John, B. K., Peter, S. and John, T. F., 2005. *Rapid Assessment of Soil Erosion in the Rio Lempa Basin, Central America, Using the Universal Soil Loss Equation and Geographic Information Systems*. Environmental Management, Vol 36, 872–885.
- Lai, V. C., 2011. *Soil erosion study by using RUSLE models - A case study in Quang Tri province, Central Vietnam*. VNU Journal of Science, Earth Sciences, Vol 27, 191-198 (In Vietnamese).
- Ligonja, P. J., Shrestha, R. P., 2015. *Soil Erosion Assessment in Kondoa Eroded Area in Tanzania using Universal Soil Loss Equation, Geographic Information Systems and Socioeconomic Approach*. Vol 26, 4, 367-379, <https://doi.org/10.1002/ldr.2215>.
- Lutgens, F. K., Tarbuck, E. J., & Tasa, D. 2017. *Foundations of Earth science*. Boston, Pearson.
- Mai, V. T. 2007. *Soil erosion and nitrogen leaching in northern Vietnam: Experimentation and modelling*. PhD Dissertation, University of Wageningen, Netherlands.
- My, N. Q., 1995. *Topographic factors on soil erosion in Vietnam*, VNU Journal of Science, Natural Sciences, Vol 11, 13-21 (In Vietnamese).
- Prem, R., So K., Luminda G, 2018. *Assessment of sediment yield in Thailand using revised universal soil loss equation and geographic information system techniques*. River Research and Applications, Vol 34, 9, 1113-1122, <https://doi.org/10.1002/rra.3351>.
- Saro, L., 2004. *Soil erosion assessment and its verification using the Universal Soil Loss Equation and Geographic Information System: a case study at Boun, Korea*. Environmental Geology, Vol 45, 457–465.
- Tung P. G., Degener, J. and Kappas, M., 2018. *Integrated universal soil loss equation (USLE) and Geographical Information System (GIS) for soil erosion estimation in A Sap basin: Central Vietnam. International*. Soil and Water Conservation Research Vol 6, 99-110.
- Wischmeier, W. H., and Smith, D. D. 1978. *Predicting rainfall erosion losses: A guide to conservation planning*. U.S. Department of Agriculture, Agriculture Handbook No. 537.
- Website: U.S. Geological Survey. <https://search.asf.alaska.edu/>.
- Website: Alaska Satellite Facility, Geophysical Institute University of Alaska Fairbanks. <https://earthexplorer.usgs.gov/>.

CAPACITY BUILDING ON WATER AND NATURAL RESOURCES IN SOUTH-EAST ASIA - BENEFITS FROM THE WANASEA PROJECT

Nguyen Vo Chau Ngan^{1*}, Truong Chi Quang², Lim Ngoc Han³, Tran Thi Minh Thao⁴, Tran The Nam⁵ and Phung Diep Anh⁶

¹Department of Water Resources, Can Tho University, 3-2 street, Xuan Khanh, Ninh Kieu, Can Tho, Vietnam
Email: nvcngan@ctu.edu.vn

²Department of Land Management, Can Tho University, 3-2 street, Xuan Khanh, Ninh Kieu, Can Tho, Vietnam
Email: tcquang@ctu.edu.vn

³International Relations Office, Can Tho University, 3-2 street, Xuan Khanh, Ninh Kieu, Can Tho, Vietnam
Email: Inhan@ctu.edu.vn

⁴International Relations Office, Can Tho University, 3-2 street, Xuan Khanh, Ninh Kieu, Can Tho, Vietnam
Email: minhthao@ctu.edu.vn

⁵International Relations Office, Vietnam Maritime University, 484 Lach Tray, Le Chan, Hai Phong, Vietnam
Email: thenam@vmaru.edu.vn

⁶Vietnam Graduate Academy of Social Sciences, 477 Nguyen Trai street, Thanh Xuan, Ha Noi, Vietnam
Email: fsp2s.bureau@yahoo.fr

ABSTRACT

Demand on water and natural resources are increasing among the people, communities, and governments of the Lower Mekong River and Delta. These demands are felt most acutely in Thailand, Cambodia and Viet Nam, where 80 percent of people depending on the river and its rich natural resources for their livelihoods. The issues of the region around the sustainable development of natural resources require more cross-sectorial coordination and policy integration. The WANASEA project is form up to improve the cooperation between these states on water and natural resource management. The project funded by the Erasmus+ program of the European Union and lead by University of Nantes. Three training courses related to GIS tool was implement focus on integrating water and socio-economic information with existing models. We will present the results of training courses which strengthen the multidisciplinary research and exchange of expertise and knowledge of project partners.

1. INTRODUCTION

Strengthen the production, management and outreach capacities of research in the field of WAtter and NATural resources in South-East Asia - WANASEA project has been granted in 2017 by Erasmus+ Programme of the European Union. The project includes 3 countries from Europe and Southeast Asia, respectively France, Denmark and Spain, and, Cambodia, Thailand, and Viet Nam. There are 15 partners namely University of Nantes (UN) - Leader, the French School of Asian Studies (EFEO), the French National Institute for Sustainable Development (IRD), the Center for Research and Expertise on Education and Development (CREED) in France; University of Southern Denmark (SDU) - Denmark; Universitat de Barcelona (UB) - Spain; Institut de Technologie du Cambodge (ITC), Royal University of Law and Economics (RULE), National University of Management (NUM) in Cambodia; Thammasat University (TU), Chiang Mai University (CMU) in Thailand; the Graduate Academy of Social Sciences (GASS), Can Tho University (CTU), Vietnam Maritime University (VMU), and RMIT University (RMIT-VN) in Viet Nam. In additional, the project has been supported by two associated partners: the Global Development Network (GDN) - India, and the Agence Universitaire de la Francophonie - France.



Figure 1. The WANASEA project consortium

(Source: WANASEA project, 2021)

The project aims to promote the multidisciplinary research, to foster an institutionally-supported research practice (in order to go beyond pure academic research and contribute to both creation of new knowledge, understanding and treatment of contemporary problem), and to help position universities as places for the production and transmission of knowledge open to both public and private actors to interact and involve in the process of changes. WANASEA also keeps on implementing its objective of enhancing the scientific cooperation between researchers, PhD students and non-academic stakeholders. Corresponding to these goals, the project developed five packages to strengthen not only scientific expertise but also the institutional capacities, create open spaces for exchange and develop channels of communication with other stakeholders, academic and non-academic, on an international scale, in order to improve the quality of high education institution curricula.

The third development package of the project aims to build the research capacity of students and young researchers related to Water and Natural Resources Management (WNRM). The main outcome of this package is launching the ASEAN Water Platform (AWP) in the year of 2018, 2019, and 2020. This platform is an annual research seminar and training which brought together young researchers from Asian and EU partners. Its main objective is to increase their research capacity by learning new innovative methodologies, multi-disciplinary approach to solve complex problems, and by creating durable links between each other.

For each AWP, around 80 people will be selected to participate to this annual 14-day event. The host country was changed every year among ASEAN countries partners. Furthermore, other countries such as Lao PDR and Myanmar will be contacted in order to expand the AWPs in other ASEAN states after the end of the project. This paper presents the results of AWP activities through the project lifespan, the contribution of the AWPs to the project, and also the lesson learnt from AWPs.

2. ACTIVITIES OF AWP EVENTS

2.1 Structures and presentations of the AWP

2.1.1 AWP program

In accordance to discussion from the Kick-off meeting, the title “Water and Its Many Issues - Methods and Cross-Cutting Analysis” was chosen and applied for annual AWP events. In the structure, each AWP was organized along two complementary axes: Plenary sessions (the first 2 days), followed by Thematic workshops (3 to 5 topics), and end by the Workshop restitution at the last day. Topics of plenary sessions and workshops would be drawn up at least 6 months, so that each partner could announce and pick-up participants on-time.

- For the plenary sessions, speakers from outside of project were invited to present their experiences, their point of view, or their project results which related to WNRM. The sessions were wound up with a round table that was open to organizations outside of the WANASEA consortium.
- For the thematic workshops: putting together of the team of trainers through the calls for candidates within the consortium so as to mix Asian and European teams. The training was wound up by a workshop summary session presented.

Table 1. Programs for annual AWP

AWP	Plenary sessions	Thematic workshops
Year 2018	<p>Session 1: Water resources changes - A great threat for sustainable development in the Mekong Basin</p> <p>Session 2: Global challenges for fisheries management and South-East Asian perspective</p> <p>Session 3: Holistic urban water resources management</p> <p>Session 4: An inquiry into the implementation of Phuoc Hoa Water project, Vietnam (video presentation)</p> <p>Session 5: Some examples about environmental and social challenges: Solid waste management and human impacts on deltas (video show)</p>	<p>Workshop 1: Risk management</p> <p>Workshop 2: Water management in an urban environment</p> <p>Workshop 3: Inputs of modeling for the analysis of saline intrusion in the Mekong Delta</p> <p>Workshop 4: Field research - Usage and management of the water resources in the context of change</p>
Year 2019	<p>Session 1: What role for a development bank in the improvement of the urban water supply and sanitation services? The case of AFD in ASEAN</p> <p>Session 2: Using simulations to design evacuation strategies in case of flooding</p> <p>Session 3: Knowing and governing water</p> <p>Session 4: Valuation of ecosystem services of mangrove forests in Cambodia</p> <p>Session 5: Equitable, reasonable and sustainable use of water resources in Cambodia</p> <p>Session 6: Inland commercial fishing lot and mobile gear fishing in Tonle Sap lake</p> <p>Session 7: Evaluating the success and sustainability of community fisheries in Tonle Sap lake after fisheries reforms</p>	<p>Workshop 1: Transboundary river management / water governance</p> <p>Workshop 2: Development of maritime policy in ASEAN and comparisons with the EU</p> <p>Workshop 3: Urban water risks: designing evacuation strategies in case of flooding with Agent-Based modeling and GAMA</p> <p>Workshop 4: Non-conventional water resources: Wastewater reclamation and reuse</p> <p>Workshop 5: Field research - Irrigation and agricultural management in Kandal Stueng system</p>

AWP Plenary sessions	Thematic workshops
<p>Year 2021</p> <p>Session 8: Knowledge and development - From principles to practice</p> <p>Session 1: Qualitative methodologies in social sciences</p> <p>Session 2: Sustainability of small-scale fisheries - Community based resource management approach in Cambodia, Vietnam and Bangladesh</p> <p>Session 3: Technology adoption in agriculture: Theory and application to irrigation technology</p> <p>Session 4: Water resources in the Mekong Delta</p> <p>Session 5: Bio-diversity versus climate change in the Mekong Delta</p> <p>Session 6: Restitution of inequalities and environmental changes Nexus project</p> <p>Session 7: Research on the Mekong River - Overview of the Mekong river ecology and its relationships with people livelihood</p> <p>Session 8: Research on the Mekong River - Role of Mekong River Commission and research on transboundary water governance</p>	<p>Workshops were implemented in specific program for each ASEAN country due to pandemic.</p>

(Source: Lagree, 2018, 2019, 2021)

For the AWP 2021, program was refined 14 days of training in Thailand namely AWP 2020, including two days of plenary sessions, four thematic workshops, among which a training workshop on field surveys in a district located 60 km from Chiang Mai, two days of parallel training (Doctoral student's days and a communication workshop), and a half day of restitution of the work of the two weeks in a plenary session. However, at the beginning of the year 2020, the emergence of Covid-19 has led the preliminary set-up of the AWP to be redefined due to the impossibility to carry out any mobility, both in the Asian region and from Europe to South East Asia. By that reason, the consortium to set the new dates of AWP on Feb - Mar 2021, but organized at each ASEAN country (Thailand, Cambodia, and Vietnam).

The realities of the field in each of the three Asian countries have led to specific organizations as detailed below:

- Plenary Sessions and Innovative Research Competition: face-to-face in Thailand and online for all other participants
- Face-to-face workshop in Thailand
- Face-to-face and online workshop in Phnom Penh: due to an increase in the number of Covid-19 cases in Phnom Penh just before the opening of the AWP, only the first day of the training could be held face to face, the other sessions were held online when possible
- Online workshop “Modeling and Simulation of Water Basin Integrated Management” in Vietnam
- Two different sites for the workshop “Qualitative methodologies in social science - Covid-19 as case study”, one in Hanoi city and the other one in Ho Chi Minh city, Face-to-face workshop for participants in these two cities and online workshop for participants from other provinces.

2.1.2 Support programs¹

Before the opening ceremony day, the AWP files were distributed to all participants. These files present: the program of the plenary sessions and the workshops accompanied by a synopsis of each presentation and a calendar of the week's work; reading texts - certain texts were transmitted by email; trainers' biographies; a list and contact addresses of the trainees in order to enable networking, etc.

The plenary sessions were all captured on film. The filmed presentations *in extenso* for viewing on the WANASEA web site; they are subtitled in English.

Filmed interviews were conducted with the speakers in the plenary sessions and those responsible for each workshop in order to present the goals and the methodological tools used in the course of the week. The video-clips available on the WANASEA website.

A common question grid was given to the trainees at the end of the training session in order to obtain feedback about the week's training.

Diffusion of economic, human and social science works at the heart of the WANASEA thematic that stem from the previous "Tam Dao Days" project (see: www.tamdaoconf.com). These textbooks are distributed free of charge during the WANASEA modules in the three Asian countries of the consortium (AWP and biannual training sessions to improve teaching and research)

- (2018) The challenges of energy transition in Vietnam and Southeast Asia, collection *Etudes de l'AFD*, n°16, AFD-ÉFEO - Tri Thúc, Hanoi, July.
- (2014) Perception and management of risks. Methodological approaches applied to development, collection *Conférences & Séminaires*, n°10, AFD-ÉFEO - Tri Thúc, Hanoi, July (reprint).
- (2013) Water and its many issues. Methods and multi-disciplinary analysis, collection *Conférences & Séminaires*, n°8, AFD-ÉFEO - Tri Thúc, Hanoi, July (reprint).

All the trainees and trainers participating were distributed by AWP labelled T-shirts (in the 2018 and 2019 edition) and water bottles (in the 2019 edition).

A master of ceremony (MC) and a moderator from the host institute facilitated the organization and hosted the two days of plenary sessions.

A certificate of participation and completion of training was awarded to each trainee during the AWP closing ceremony. This certificate had already been validated and signed by the representative of host institute and the University of Nantes.

For the AWP 2018, the IRD representation in Vietnam placed at the disposal of the AWP, with the agreement of CTU, a photographic exhibition about pollution by plastics in Vietnam in which the objects are followed from the places where they are produced, and then consumed in the privacy of everyday life, to the accumulation of plastic waste in the aquatic environment (trilingual exhibition in French, English and Vietnamese). Exhibition was particularly thorough about the sources and consequences of pollution by plastics; high-quality examples; opening out towards current issues.

¹ Some support programs not involved to the AWP 2021 as this event was organized online

2.3 AWP trainees' profiles and activities

At least 3 months prior each AWP, the call for attendance will announce at each partner institutes and also through project webpage. Enrolment in the AWP has been made easier by the placing online of a registration form via its Internet site. This form allows the examination and validation of the applications submitted, the identification of requests with regard to the four predefined workshops and the strengthening of the database for scientific networking.

Each application form had to meet the criteria that were explicitly stated on the selection sheet for candidates. From the registration forms of the selected trainees, the following profile emerges:

- A female majority: 62 percent (2018), 60 percent (2019), 53 percent (2021) of the trainees.
- A diversity of statuses and levels of education: master, master and teacher, master and development, doctoral student, doctor/doctoral student and teacher, researcher, researcher and teacher, teacher and development, development practitioner.
- High multi-disciplinarily and different fields of research: economics (macro, international, energy); environment (water management, risk management, climate change, maritime, law, biology); hydraulics and hydrology; remote sensing and geographic information systems; geography (human and physical); urban planning; development studies.
- Institutional opening out in Vietnam and Myanmar made possible through AUF, IRD, and UN co-financing methods.
- More participants attended in AWP 2021 due to the consortium would extend benefits both to people inside and outside of WANASEA partners as the event organized via online platform.

Table 2. Number of trainers and trainees to AWP events

	Trainer + trainee numbers		
	2018	2019	2020
<i>European partners</i>			
UN	4 + 1	3 + 0	2 + 0
IRD	4 + 1	5 + 0	6 + 0
EFEO	1 + 0	2 + 0	1 + 0
CREED	1 + 0	1 + 0	1 + 0
SDU	3 + 1	1 + 1	1 + 0
UB	2 + 1	3 + 0	-
<i>ASEAN partners</i>			
GASS	1 + 8	1 + 8	0 + 7
VMU	1 + 8	3 + 6	0 + 10
RMIT-VN	0 + 2	5 + 0	0 + 4
CTU	2 + 8	2 + 12	4 + 9
RULE	0 + 9	0 + 6	0 + 1
NUM	0 + 9	0 + 5	1 + 8
ITC	0 + 10	2 + 9	2 + 12
TU	0 + 9	1 + 8	2 + 5
CMU	0 + 6	4 + 8	6 + 16
Other institutions	-	-	10 + 38

(Source: Lagree, 2018, 2019, 2021)

2.4 Evaluation of the AWP

To evaluate for the success of the event, all trainees were required submitted their feedback on the AWP activities. Figures 2, 3, and 4 show that activities of AWP improve year-by-year as the trainees appreciate of good and excellent increasing at later events.

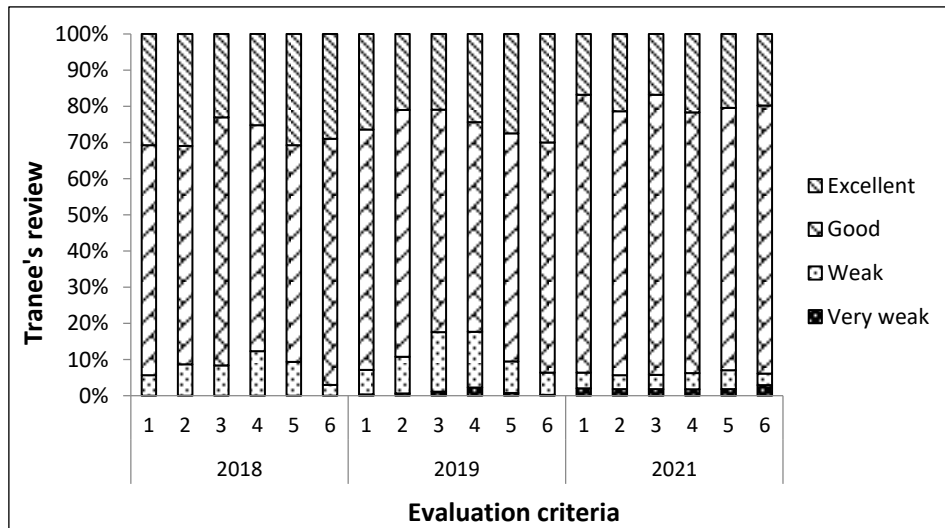


Figure 2. Feedback for plenary sessions (average recorded from all sessions)

Criteria: (1) Relevance of the subjects treated to the general thematic of AWP, (2) Overall quality of the presentation, (3) How enlightening was the presentation in terms of multidisciplinary approach, (4) New scientific or/and methodological perspectives, (5) Quality of the interactions with the speaker, (6) Quality of the organization of the plenary sessions

(Source: Derived from Lagree, 2018, 2019, 2021)

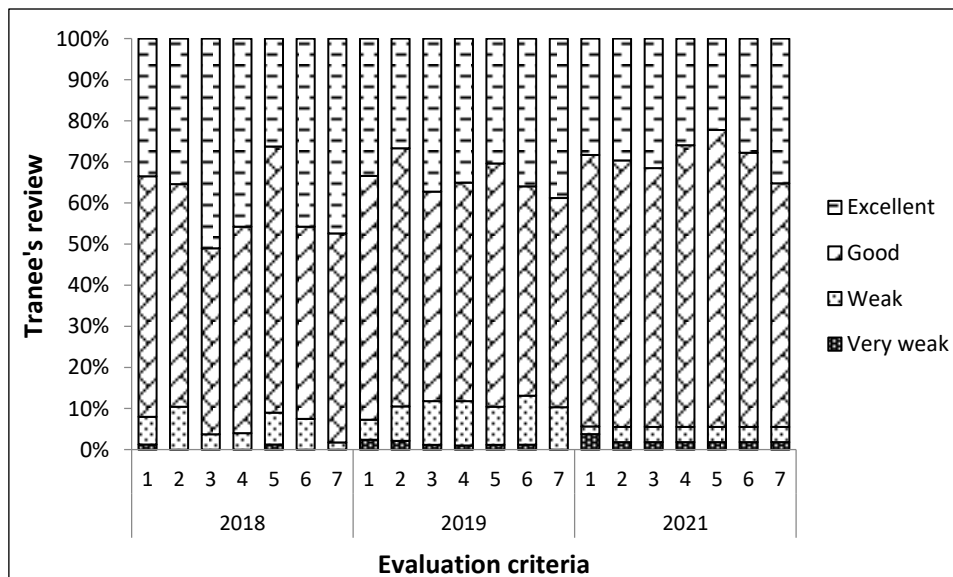


Figure 3. Feedback for thematic workshops (average recorded from all workshops)

Criteria: (1) Clarity of the program and objectives of your workshop, (2) Consistence between the program and its objectives, (3) Dedication and availability of trainers, (4) Collective and participatory approach of the teaching, (5) Amount of personal work required, (6) Improve your skills and abilities, (7) Relevant and useful knowledge

(Source: Derived from Lagree, 2018, 2019, 2021)

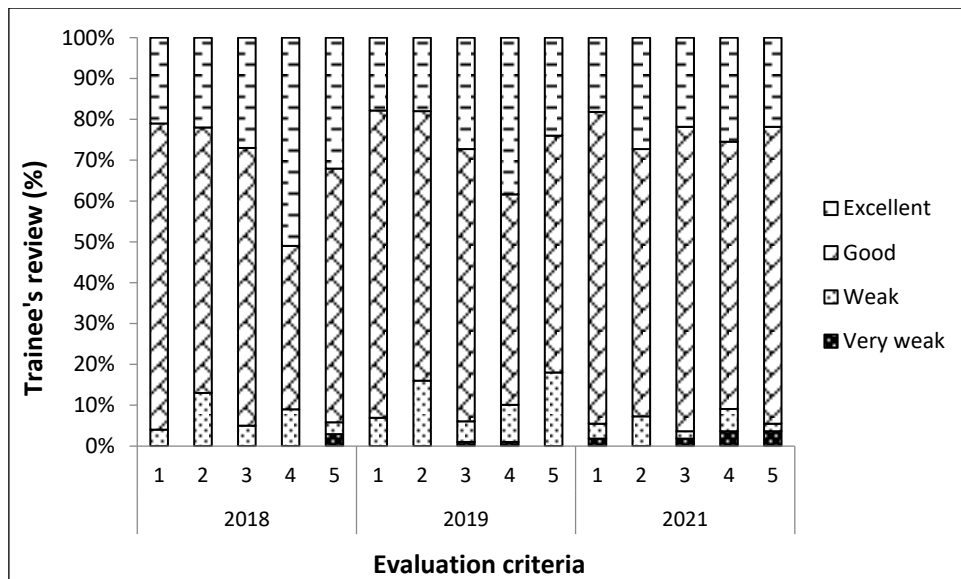


Figure 4. General appreciations for plenary sessions and workshops

Criteria: (1) Relevance of the thematic and program, (2) Balance between theory and practice, (3) Multidisciplinary approaches, (4) International networking and collaboration opportunities, (5) Quality of the organization (logistic and facilities, etc.)

(Source: Derived from Lagree, 2018, 2019, 2021)

The overall quality of AWP events combining plenary sessions and workshops is really satisfying according to both participant and trainer surveys. More than 90% of the trainees rated the event as good to excellent. Two points seem particularly satisfactory: the proposed thematic correspond to the audience's expectations, the organizational quality of the sessions. Although relatively marginal, there is some criticism of educational aspects in the course of the lectures and of the answers given during the exchanges with the audience; furthermore, the trainees remarked a certain weakness of methodological tools and the multi-disciplinary variations proposed.

Few trainees (less than 2%) stated that the AWP did not meet their expectations. The most recurrent criticisms concern a lack of equilibrium between theory and practice 12%, limited space for cooperation opportunities and certain organizational shortfalls 8%, and 2% regarding catering conditions. From a quality point of view, let us note the following requests: sending of PowerPoint presentations before the beginning of the training; slower delivery of plenary interventions, and more generally, a need to strengthen the level of English (both the trainees and speakers); greater integration of field visits, a stricter educational approach and greater open-mindedness from some of the trainers.

The mixed presentation of videos and lectures in the plenary session was greatly appreciated from trainees. The satisfaction rating "excellent" was noted for 40% of the trainees (Lagree, 2018). The format of these mix presentation should apply to further training events for both inside and outside WANSEA project.

For the AWP 2021, a characteristic of this workshop is the large number of trainers mobilized inside and outside the consortium; this dimension was particularly appreciated by the trainees. The most common criticisms basically refer to the lack of balance between theory and practice and a limited opportunity for networking and collaboration; the AWP 2021 online sessions can certainly explain a feeling of disappointment/frustration on both points.

Principal benefits of AWPs:

- Shared expertise;
- Disciplinary diversity; open-mindedness;
- Gain in self-confidence (possibility of speaking in group/public);
- Input of methodological tools (quantitative and qualitative);
- International, regional and personal networking;
- Linguistic enrichment.

However, there are some noticeable criticisms for improvement such as:

- Lack of balance between theory and practice, better to integrate field visits to each workshop;
- Limited space for opportunities to meet and network;
- Should have sent PowerPoint presentations before the beginning of the training;
- Speakers should deliver presentations slower for plenary sessions;
- Weak quality of the catering;
- Strengthening the selection by prioritizing the level of English for both trainees and trainers;
- A stricter educational approach and greater open-mindedness from some of the trainers;
- Too technical an approach;
- Strengthening group work for the restitution;
- Strengthening (trainers') knowledge about South-East Asia and develop case studies in Asia;
- A better qualitative/quantitative balance;
- Improving quality of Internet connection;
- Better collaboration between trainers during the training.

2.4 The AWP co-financing model

Each ASEAN partner of the WANASEA consortium has a budget that allows them to select nine candidates per AWP (one staff member, eight students), but the financing is not available for the partner that hosts the platform. Besides that, WANASEA AWPs 2018 - 2020 also benefit from distinct and complementary co-financing according to signed agreement between project consortium and AUF, IRD, UN and AFD partners. Total amounts of 68,528 euros co-financing to the annual AWPs.

- AUF financed actions: support the mobility and cost of stay to 4 and 12 trainees (from AUF member establishments outside of the consortium) in 2018 and 2019. Three professional internships. Consolidation for the identification of the needs and expectations of academic and non-academic players regarding the federating thematic of water and its associated resources.
- IRD financed actions: support the mobility and cost of stay to 5 trainees from Myanmar for each AWP. Construction of a new regional platform entitled "International JTDs" (output to AWP WANASEA) to widen networking in order to identify new financial and scientific partners, public and/or private, around the new model. Grant 6,000 euro for the AWP 2021's Innovative Research Competition module. This event attracted over 15 candidate's application, two laureates were nominated in Cambodia (ITC) and three in Vietnam (GASS, VMU and CTU).

- UN financed actions: selection of 3 trainees from Laos / Myanmar for the 2018 and 2019 AWPs; academic and non-academic networking (invitations to development practitioners and university teachers from outside the consortium).
- AFD financed action: since Jan 2019, WANASEA is eligible for new co-financing in order to consolidate the actions carried out within the framework of the project and its sustainability (non-earmarked financing).
- CTU financed action: sending 4 trainees from Vietnam, in which 2 trainees from government authority to the 2019 AWP in Cambodia. Funding to do research, sent 3 participants for oral presentation the two results at The first VietPhil Research Forum 2019 at Tra Vinh University, Vietnam.

3. CONCLUSION

Within the WANASEA framework, the training sessions and seminars AWPs gathered researchers, PhD candidates, professors and professionals from various fields around the topics of WNRM. This rise awareness about the current transboundary issues in the Greater Mekong Sub-region regarding WNRM. In parallel, WANASEA project generated and disseminated new knowledge which goes beyond methodological exchange. Participants on these events had chance to develop their research skills and learn how to work together on complex issues such as WNRM. AWP offered an excellent opportunity to connect Asian and European students with ASEAN and European professors.

4. ACKOWLEDGEMENT

The authors gratefully acknowledge the fund support from the Erasmus+ program of the European Commission on this study under the project “WANASEA - Strengthen the Production, Management and Outreach Capacities of Research in the field of WAtter and NAtural Resources in South-East Asia”.

5. REFERENCES

- Lagree, S., 2021. Report on AWP 2021. WANASEA project.
 Lagree, S., 2019. Report on AWP 2019. WANASEA project.
 Lagree, S., 2018. Report on AWP 2018. WANASEA project.
 WANASEA project, 2021. WANASEA’s partners. Link <https://wanasea.eu/about/partners/>

APPLICATION OF GEOGRAPHIC INFORMATION SYSTEM WITH FIELD EXPERIMENT TO ASSESS SUITABLE ZONATION MAPPING FOR RICE CULTIVARS UNDER PROJECTED GLOBAL WARMING IN LOWER NORTHERN THAILAND

Kanita Thanacharoenchanaphas¹, Fatah Masthawee² and Gitsada Panumonwatee^{1*}

¹Department of Natural Resources and Environment,
Faculty of Agriculture Natural Resources and Environment,
Naresuan University, Phitsanulok, Thailand

^{*}Corresponding author email: gitsadap@nu.ac.th
² Meteorological Department of Thailand

4353 Sukhumvit Road, Bangna, Bangkok, Thailand

ABSTRACT

The aims of this research were to assess the effects of increased temperature on total chlorophyll and grain yield of 5 commercial Thai rice cultivars (Chainat1, Pathumthani1, Phitsanulok2, KorKhor29, and Riceberry) in lower northern Thailand. Nine field-open top chambers (OTCs) with electric systems were applied from 2018 to 2020 in Phitsanulok to simulate projected 2 future temperature situations in 2100 which consistent with RCP4.5 and RCP8.5 scenarios (higher than ambient level by 2.6 °C and 4.5 °C, respectively). The results under field experiment revealed that the negative significant impacts on total chlorophyll were obvious appeared in KorKhor29 under RCP8.5 scenarios. In addition, results in grain yield indicated that decreases in yield were correlated with increased temperature under both of 2 situations. The high reduction in total grain yield (ton per ha) were also found in Riceberry and Phitsanulok 2 under RCP8.5 scenario by 88-95%. However, it seems that Chainat1 was heat-tolerant cultivars under both of 2 warming situations, by the way in which the property of increases in total chlorophyll and grain yield. Then all results were combined with the spatial temperature model and analyzed by the GIS to assess suitable zonation mapping for rice cultivars under projected global warming in lower northern area. As a result, we also found the positive effects of temperature rise on grain yields in Chainat1. These results are parallel to findings from the field experiment. The data indicated that under projected future temperature levels, it seemed that Tak province, Phitsanulok and Uttaradit provinces were suitable areas for rice cultivation. Chainat1 cultivar should be selected for cultivation in this area, especially in Tak province.

1. BACKGROUND

The Intergovernmental Panel on Climate Change (IPCC)'s Fifth Assessment Report (AR5) revealed that as global mean temperatures increase, there will be more frequent hot temperature extremes in the tropics regions. In the RCP8.5 scenario, which projects the most rapid global warming when emitting GHGs at their current level (with more than double emissions), projects 2.6-4.8°C temperature increase. In the RCP 4.5 scenario, where most GHG emissions are almost eliminated after the 21st century, the projected temperature range increase is 1.1-2.6°C (IPCC, 2013).

Rice is a staple food for approximately half of the world's population, however there is plenty of research evidence that rice yield will be influenced negatively by temperature increases in many parts of the world because physiological processes of crops are largely affected by high temperature stress (Thanacharoenchanaphas and Rugchati, 2018). IPCC has also reported that heat stress is projected to increasingly responsible for rice yield reduction in tropical regions without adaption (Shi et al., 2016). In Thailand, rice is the important economic crop. Meanwhile, the status of current mean temperature during the rice planting season has been changed at

meteorological observatories in the northern regions of Thailand (Limsakul et al., 2011). Hence, Thailand might affected on the food security under climate change.

Thus, it is necessary to analyze suitable zonation mapping for rice cultivars under projected global warming. The temperature dataset widely used for spatialization called interpolation techniques including Inverse Distance Weighting (IDW) Ordinary kriging (OK), temperature lapse rate (TLR), and Multiple linear regression (MLR). Chai et al. (2011) compared the technique for temperature interpolation from 38 meteorological stations for the period 1960- 2004 in Xinjiang Uygur, China. The result showed the performance of IDW technique while using the directly interpolating observed temperature. The IDW shows the strengths including rapid, accurate and easy to applied while using the non-complex method. Moreover, Jiang et al. (2021) also developed the adaptation modeling of maize under climate change situation. The temperature data set was interpolated using IDW technique with agrotechnology transfer (DSSAT) model. The result showed the slightly relative error (<5%) and high index of agreement (0.8).

Estimating the impact of climate change on yield of rice cultivars and the evaluation of appropriate adaptation and mitigation strategies are of extreme concern to development of new agricultural areas and use of heat resistant varieties to stabilize the rice yield in Thailand in future.

2. METHODS

2.1 Field Warming Experiment and Rice Planting Management

The experiment was conducted at Phitsanulok province ($16^{\circ}799790'$, $100^{\circ}225468'E$) in lower northern Thailand during 2018 to 2020. Nine field-open top chambers (OTCs) with electric systems were applied to simulate projected future temperature situations which consistent with RCP scenarios. Three controlled temperature levels with three replications were set up by black infrared bulbs and air conditioners that linked to the automatic controlling system to maintain at ambient level ($32.55 \pm 1.48^{\circ}\text{C}$; Control treatment) including two elevated air temperature by 2.6°C (HT4.5 treatment) and 4.5°C (HT8.5 treatment) under RCP4.5 and RCP8.5 scenarios, respectively. At seedling growth stage, all five cultivars of Thai rice (Chinat1, Pathumthani1, Phitsanulok2, KorKhor29, and Riceberry) were exposed to three different temperature situations for 10 hr. day⁻¹ exposure (7.00 am – 5.00 pm) in open top chambers until harvest.

2.3 Chlorophyll Analysis

At the flowering stage, rice fresh leaves were sampled and cut into pieces for determining total chlorophyll. They were extracted by 80 percent acetone. Then green pigment extract solutions of leaves samples were passed through a UV-VIS spectrophotometer at 2 wavelengths: 663 nm and 645 nm. Total Chlorophyll content for each sample was calculated according to Arnon (1949) as follows (equation 1):

$$\text{Total Chlorophyll (mg/g. fw)} = (20.2 \times \lambda_{645}) + (8.02 \times \lambda_{663}) \quad (1)$$

2.4 Yield Component Analysis

At the maturity stage, 12 plants per cultivar were harvested from each treatment. Total number of grains, filled grains (complete grains) and unfilled grains (incomplete grains) per panicle were counted manually from the panicles which were selected randomly. Total filled grains and unfilled grains per panicle was used to calculate percentage of filled grains panicle⁻¹.

The 1000 grain weight was determined by digital balance at about 14% moisture content. The thousand grains weight was expressed in gram (gm). The 1000 grains weight of grain from each cultivar was recorded. The data was converted and reported as grain yield as ton. ha⁻¹ by following equation 2 (Yoshida, 1981).

$$\text{Grain yield (t ha}^{-1}\text{)} = \text{no. of panicles per m}^2 \times \% \text{ filled grains per panicle} \times 1000 \text{ grain weight(g)} \times 10^{-5} \quad (2)$$

2.5 Modeling and Zonation Mapping

Daily temperature dataset was obtained from Meteorological Department of Thailand. The data was collected from weather station from 1950 to 2019. Pycharm 2021.1.1 (Python) was applied for the data screening and preparation. The prepared temperature data was interpolated using IDW by QGIS 3.14. The province boundary data was obtained from Royal Thai survey department. The rice paddy area data was obtained from Land development department.

2.6 Statistical Analysis

The total chlorophyll and yield component value data were analyzed statistically with analysis of variance (ANOVA). Significant difference of parameters were reported at $p<0.05$ by DMRT.

3. RESULTS

3.1 Total chlorophyll content

Results in total chlorophyll content showed the obvious positive by elevated temperature under HT4.5 situation. The significant increases ($p<0.05$) were shown in both Chinat1 and KorKhor29 cultivars. We found that, elevated air temperature by 2.6°C induced increase by 21.3% and 3.2% in Chinat1 and KorKhor29, respectively. However, the significant increase was not found under HT8.5 situation ($p>0.05$) (Table 1.).

3.2 Yield component

Grain yields under field experiment were harvested at maturing stage to assess grain quantity (Table1). The results showed the obvious negative significant impacts ($p<0.05$) on percentage of filled grains per panicle in Pathumthani1, Pitsanulok2 and Riceberry under both of 2 situations (HT4.5 and HT8.5). The percentage of filled grains panicle^{-1} of Pathumthani1, Phitsanulok2 and Riceberry fell 24 - 28% under the HT4.5 situation. The dramatic significant decrease higher than 50% under the HT8.5 situation appeared in Phitsanulok2 and Rice berry. However, the positive statistically significant results were shown in Chainat1 and KorKhor by 13.6% under RCP4.5 scenario.

Results in total grain yield (ton ha^{-1}) indicated that there were significant trends ($p<0.05$) of decreases in grain yield under increased temperature trend. The significant effects of the increase temperature at 2.6°C (under HT4.5) caused grain yield loss by 48% in riceberry. The results also showed that the cumulative effects of the elevated temperature at 4.5°C (HT8.5) obviously reduced grain yield by 94.9% and 88.1% in Phitsanulok2 and Riceberry, respectively. In contrast, the great significant increase of grain yield by 60.8% under increase temperature at 2.6°C was shown in Chainat1. Overall results in this part suggest that Phitsanulok2 and Riceberry are susceptible to heat stress during grain filling stage. In contrast, Chainat1 is highly tolerant to heat stress. Because, results under field experiment revealed that increasing temperature under RCP4.5 and RCP8.5 induced the positive responses in total chlorophyll content and grain yield.

It is possible that, a defense mechanisms might occurs in Chainat1 cultivar under increasing temperature. It is possible that they have the potential controlling heat tolerance genes during reproductive stage or grain filling stage (Ye et al., 2015; Wu et al., 2021).

3.3 Suitable Zonation Mapping for Rice Cultivars

Daily temperature dataset was collected form 118 weather stations but 16 stations were located in the lower northern part of Thailand. Then, the data was analyzed and calculated the

function of temperature increasing rate using linear regression. The differential of the linear function was determined as daily temperatures and calculated as the temperature over the next 100 years. The result was shown in Table 2.

The temperature dynamic data indicated that the highest increasing trend was found on the northern Tak, southern Nakhonsawan including southern and northern Phetchabun. The predicted temperature in these areas trended to increasing approximately 2.5-3.7°C which related with the RCP4.5. On the other hand, the surprised result which its temperature decreasing trend appeared in the south of Tak. The temperature level in this area trends to decrease by 3.65°C over the next 100 years. This might be the effect of western forest complex of Thailand. For the insanely results were the data from central of Sukhothai and central of Pichit, they were removed from our experiment due to its discrepancy.

Table 1. Mean values (\pm SD) of total chlorophyll, percentage of filled seed. ear $^{-1}$, and grain yield observed from samples of 3 treatments and exposed to elevated air temperature levels in 5 rice cultivars.

Rice Cultivars	Treatment	total chlorophyll (mg. g fw $^{-1}$)			filled seed. ear $^{-1}$ (%)			grain yield (t/ha)		
		\bar{x}	Change**	Sig.	\bar{x}	Change**	Sig.	\bar{x}	Change**	Sig.
Chainat1	CT	39.97 \pm 5.49 ^a			64.4 \pm 14.2 ^a			1.81 \pm 0.63 ^a		
	HT4.5	48.47 \pm 3.88 ^b	+21.27	p<0.05*	73.2 \pm 14.1 ^b	+13.62	p<0.05*	2.91 \pm 0.57 ^b	+60.77	p<0.05*
	HT8.5	47.73 \pm 0.98 ^{ab}	+19.41		55.7 \pm 10.5 ^a	-13.44		1.93 \pm 0.36 ^a	+6.62	
Pathum thani1	CT	35.51 \pm 5.25 ^a			63.7 \pm 16.4 ^b			1.55 \pm 0.73 ^a		
	HT4.5	36.35 \pm 6.99 ^a	+2.36	p>0.05	47.7 \pm 22.0 ^a	-25.08	p<0.05*	2.13 \pm 1.36 ^a	+37.42	p>0.05
	HT8.5	43.47 \pm 0.07 ^a	+22.43		49.1 \pm 15.2 ^a	-22.91		0.9 \pm 0.44 ^a	-41.94	
Phitsa-nulok2	CT	39.81 \pm 3.52 ^a			85.05 \pm 6.01 ^c			2.36 \pm 0.91 ^b		
	HT4.5	42.78 \pm 6.48 ^a	+17.31	p>0.05	64.43 \pm 4.56 ^b	-24.24%	p<0.05*	2.09 \pm 0.77 ^b	-11.44	p<0.05*
	HT8.5	41.44 \pm 4.88 ^a	+13.95		3.81 \pm 0.26 ^a	-95.52%		0.12 \pm 0.05 ^a	-94.92	
KorKhon 29	CT	44.06 \pm 0.76 ^{ab}			74.8 \pm 12.1 ^a			1.65 \pm 0.56 ^a		
	HT4.5	45.47 \pm 4.32 ^b	+3.19	p<0.05*	84.8 \pm 01.0 ^a	+13.36	p>0.05	1.94 \pm 0.35 ^a	+17.58	p>0.05
	HT8.5	39.10 \pm 0.57 ^a	-11.26		66.9 \pm 12.7 ^a	-10.55		1.18 \pm 0.25 ^a	-28.48	
Riceberry	CT	42.21 \pm 7.04 ^a			71.46 \pm 0.35 ^c			1.60 \pm 0.22 ^c		
	HT4.5	43.63 \pm 0.29 ^a	+3.36	p>0.05	51.77 \pm 10.59 ^b	-27.55	p<0.05*	0.83 \pm 0.21 ^b	-48	p<0.05*
	HT8.5	50.07 \pm 0.11 ^a	+18.63		12.06 \pm 2.48 ^a	-83.12		0.19 \pm 0.06 ^a	-88.13	

Note: The different letters for each treatment indicate a significant difference at $\rho<0.05$.

* A p-value less than 0.05 ($p\leq 0.05$) is statistically significant. ** Percentage change compared to control (CT)

Table 2. The dynamic temperature model of the lower northern part of Thailand

Station	Temperature change function	Differential	Temperature dynamic over the next 100 years (°C)
Tak (west)	6E-06x + 32.015	6.00E-06	0.22
Tak (south west)	-0.0001x + 32.446	-0.0001	-3.65
Tak (central)	3E-05x + 26.201	3.00E-05	1.10
Tak (north)	0.0001x + 31.97	0.0001	3.65
Tak (east)	3E-05x + 33.018	3.00E-05	1.10
Kamphaengphet (north)	7E-05x + 32.507	7.00E-05	2.56
Sukhothai (central)	-0.0004x + 39.868	-0.0004	-14.6*
Sukhothai (east)	4E-05x + 32.594	4.00E-05	1.46
Uttaradit (west)	-1E-05x + 33.994	-1.00E-05	-0.37
Nakhonsawan (central)	4E-05x + 33.583	4.00E-05	1.46
Pitsanulok (central)	9E-06x + 33.329	9.00E-06	0.33
Pichit (central)	-0.0004x + 38.638	-0.0004	-14.6*
Nakhonsawan (south)	0.0001x + 31.651	0.0001	3.65
Phetchabun (south)	8E-05x + 32.502	8.00E-05	2.92
Phetchabun (central)	2E-05x + 33.145	2.00E-05	0.73
Phetchabun (north)	7E-05x + 32.067	7.00E-05	2.56

*Outliner data was removed in next section.

Figure 1. shows the interpolation by using 350 m grid to assessed the predicted temperature increasing over the next 100 years using IDW. The areas of high increasing temperature trend in this figure were represented by four red areas: northern of Tak, central of Kamphaengphet, southern of Nakhonsawan, and northern of Phetchabun. In contrast, the decreasing trend was shown in the western of Tak which related to Table 2. The data presentation in Figure 1 was the overlayed with the paddy field data then the consequent result concerning the dynamic of rice yield (5 cultivars) over the next 100 years based on our temperature dynamic were estimated (Figure 2.). The results showed the increasing yield trend through the increasing temperature in Chainat 1 cultivar. The temperature levels in the areas like northern of Tak, central of Kamphaengphet, and Southern of Nakhonsawan might be appropriate to increased yield of Chainat cultivar higher than 50-60 % from the present (2020).

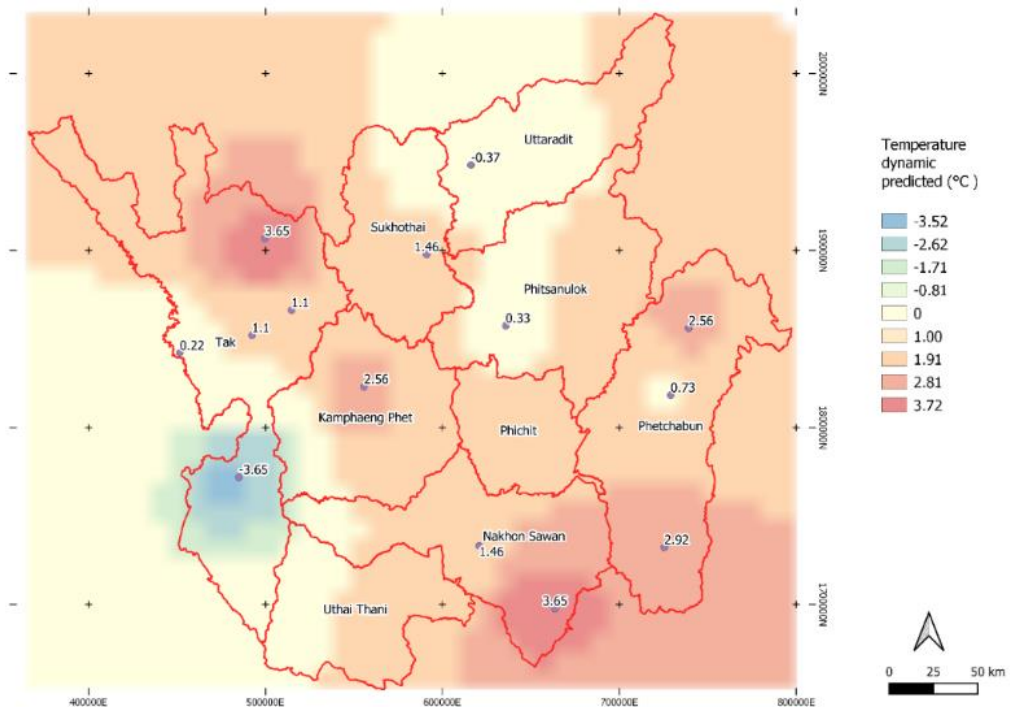


Figure 1. Temperature dynamic predicted over the next 100 years using linear regression and IDW.

However, other rice cultivars in ours experiment including Pathumthani 1, Phitsanulok 1, KorKhor 29, especially, Riceberry showed the decreasing yield trend. The result revealed that Riceberry was the most sensitive cultivar with the highest decreasing yield around 70% by the next 100 year from the present (2020).

Finally, the zonation mapping related with the temperature dynamic over the next 100 year showed the suitable rice cultivar that might be advantage on Chainat 1 yield. Temperature levels Northern of Tak and southern of Nakhonsawan areas showed its efficiency for yield increasing approximately 70% under global warming situation. The slightly effect under temperature levels in these areas appeared in Pathumthani 1 (up to 10%) except the temperature in the western of Tak might increase yield by 50%. This was found similarly result with the Korkhor 29. For the both of Phitsanulok 1 and Riceberry, the yield might be reduced approximately 50-70% yield under planting in Northern of Tak, southern of Nakhonsawan, northern and southern of Phetchabun, and

central of Kamphaengphet. We advised that they should be promoted to central of Phitsanulok, Uttaradit, and the western of Tak. Data revealed the evident increasing yield under the increasing temperature in Chainat1 cultivar. These results are parallel to results from the chamber experiment. Hence, Chainat1 cultivar should be selected for cultivation in this area.

4. CONCLUSIONS

The results from experiment with GIS showed that under projected future temperature levels based on RCP4.5 and RCP8.5 scenarios around the next 100 years, it seemed that Chainat1 is the tolerant cultivar, whereas Phitsanulok2 and Riceberry are susceptible cultivars. Finally, Tak province was the suitable areas for rice cultivation. Hence, Chainat1 cultivar should be selected for cultivation in this area, especially in Tak province.

5. ACKNOWLEDGEMENTS

The authors thank Biodiversity-based Economy Development Office (BEDO) for financial support. We also thank to Office of Agricultural Research and Development, Phitsanulok and Chainat for rice seed 5 cultivars.

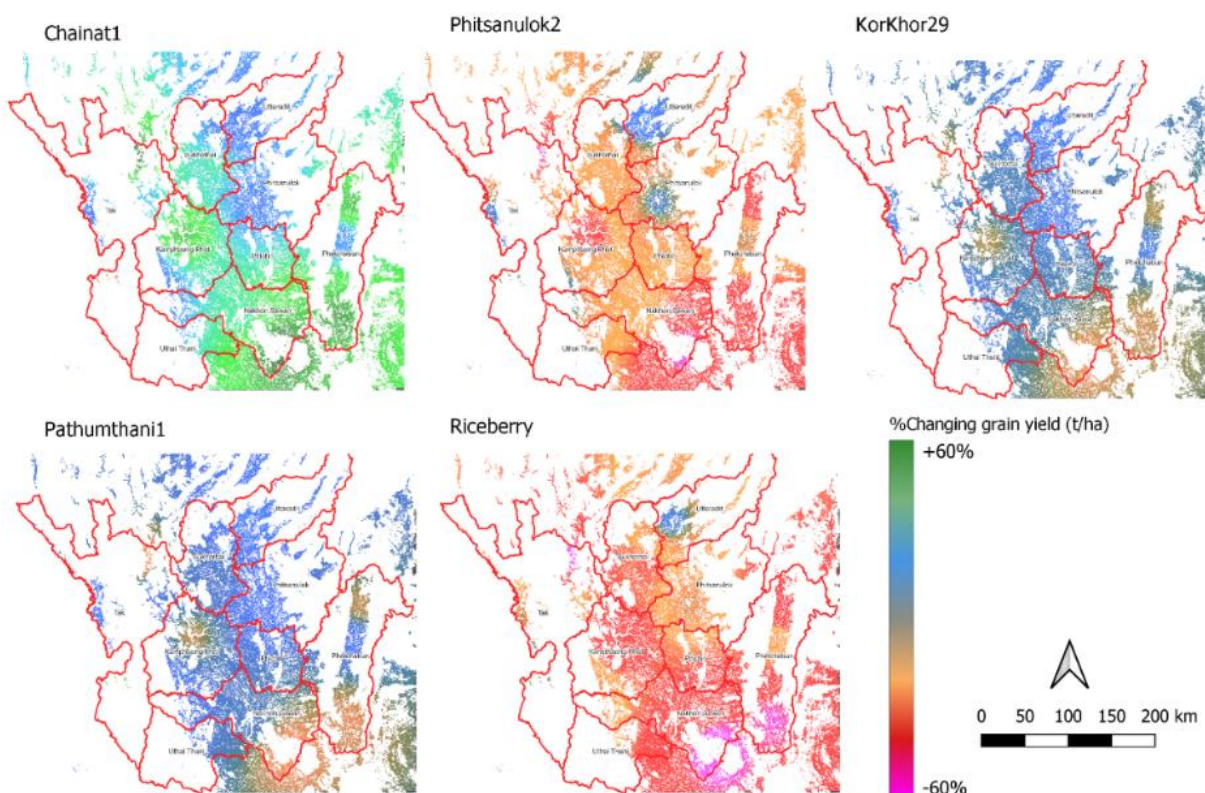


Figure 2. Rice cultivar zonation mapping under projected global warming

6. REFERENCES

- Arnon, DI., 1949. Copper enzymes in isolated chloroplasts polyphenol oxidase in Beta vulgaris. *Plant physiol* 24(1), 1-15.
IPCC., 2013. Summary for Policymakers. In: Climate Change 2013: *The Physical Science Basis*.

- Contribution of Working Group I to the Fifth Assessment Report of the Intergovernmental Panel on Climate Change*, Cambridge University Press, Cambridge, United Kingdom and New York, NY, USA.
- Limsakul, A., Limjirakan, S., Sriburi, T. & Suttamanuswong, B., 2011. Trends in Temperature and Its Extremes in Thailand. *Thai Environmental Engineering Journal (Thailand)* 25, 9-16.
- Thanacharoenchanaphas, K., and Rugchati, O., 2018. Changes in Yield and Essential Amino Acid Composition Associated with Air Temperature Stress in Thai Soybean Seeds, Sor Jor 5 Cultivar, *Journal of Fundamental and Applied Sciences* 10(3S), 703-714.
- Wu, C., Cui, K., Li, Q., Li, L., Wang, W., Hu, Q., Ding, Y., Li, G., Fahad, S., Huang, J., Nie, L., and Peng, S., 2021. Estimating the yield stability of heat-tolerant rice genotypes under various heat conditions across reproductive stages: a 5-year case study. *Scientific Reports* 11:13604, 1-11.
- Ye, C., Tenorio, F. A., Argayoso, M. A., Laza, M. A., Koh, H. J., Redoña, E. D., et al., (2015). Identifying and confirming quantitative trait loci associated with heat tolerance at flowering stage in different rice populations. *BMC Genetics* 16:41, 1-10.
- Davoren, A., and Mosley, M. P., 1986. Observations of bedload movement, bar development and sediment supply in the braided Ohau River. *Earth Surface Processes & Landforms* 11, 643-652.
- Mosley, M. P., 1979. Sediment sources in the Harper-Avoca Catchment. *Forest Research Technical Paper* 68, New Zealand Forest Service, Wellington.
- Mosley, M. P., 1997. Motu River. In Jayawardena, A. W., Takeuchi, K., and Machbub, B. (editors), *Catalogue of Rivers for Southeast Asia and the Pacific*, Vol 2, UNESCO-IHP Regional Steering Committee, Jakarta, 226-235.
- Schumm, S. A., Mosley, M. P., and Weaver, W. E., 1987. *Experimental geomorphology: the study of small landforms*. John Wiley, New York.
- Chai, H., Cheng, W., Zhou, C., Chen, X., Ma, X. and Zhao, S. 2011. Analysis and comparison of spatial interpolation methods for temperature data in Xinjiang Uygur Autonomous Region, China. *Natural Science* 3, 999-1010.
- Jiang, R., Wentian, He., Liang, He. Yang, J.Y., Qian, B., Zhou, W., Ping, He., 2021. Modelling adaptation strategies to reduce adverse impacts of climate change on maize cropping system in Northeast China. *Scientific Reports* 11, 810.

APPLICATION OF GIS ON BUILDING THE GEOGRAPHIC DATABASE FOR NINH KIEU AND CAI RANG DISTRICTS OF CAN THO CITY

Nguyen Thanh Ngan^{1,2}, Nguyen Hieu Trung³

¹Faculty of Environment, Ho Chi Minh City University of Natural Resources and Environment (HCMUNRE), 236B Le Van Sy Street, Ward 1, Tan Binh District, HCM City.

²College of Environment and Natural Resources, Can Tho University (CTU), Campus II, 3/2 Street, Xuan Khanh Ward, Ninh Kieu District, Can Tho City.

Email: ntngan@hcmunre.edu.vn

³DRAGON Institute - Mekong, Can Tho University (CTU), Campus II, 3/2 Street, Xuan Khanh Ward, Ninh Kieu District, Can Tho City.

Email: nhtrung@ctu.edu.vn

ABSTRACT

Ninh Kieu and Cai Rang are the two central districts of Can Tho City, established under the Government Decree No. 05/2004/NĐ-CP. These are two thriving and dynamic areas of the city, with a long history of formation and development. According to statistics in 2019, Ninh Kieu District has an area of 29.23 km² and an average population of 280,792 people. Also in 2019, Cai Rang District has an area of 66.81 km² and an average population of 105,547 people. In the current period, these areas are experiencing a rapid and strong urbanization. This has caused great pressure and challenges for drainage management in these two urban districts. To solve these major challenges, the managers in these areas must come up with reasonable solutions and policies for urban drainage. One of the input data needed for this process is the geographic database. This paper introduces the initial results of building a geographic database based on GIS for Ninh Kieu and Cai Rang districts. This is an important and useful data for drainage management in particular and urban management in general in the study area.

Keywords: GIS, geographic database, drainage management, Ninh Kieu District, Cai Rang District.

1. INTRODUCTION

Ninh Kieu and Cai Rang are two important urban districts of Can Tho City. These two districts are geographically located on the right bank of the Hau River, established in 2004 under the Government's Decree No. 05/2004/NĐ-CP (Vietnam Government, 2004). Ninh Kieu and Cai Rang districts have a natural feature of relatively low terrain following the general trend of the Mekong Delta (Can Tho City Department of Construction, 2016). Due to the characteristics of the districts located along the river, Ninh Kieu and Cai Rang districts are greatly influenced by the Hau river tidal regime (Can Tho City Department of Construction, 2016). According to statistics in 2019, Ninh Kieu District has an area of 29.23 km² and an average population of 280,792 people (133,911 men/146,881 women), while Cai Rang District has an area of 66.81 km² and an average population of 105,547 people (52,241 men/53,306 women) (Can Tho City Statistics Office, 2020). In recent years, the process of urbanization in these two areas has taken place at a rapid pace and in a complex direction. This process has created great pressures and challenges for drainage management in Ninh Kieu and Cai Rang because the drainage system is no longer able to meet the needs of communities in these two urban districts. To solve these difficulties and challenges, the managers in these areas need to have appropriate solutions and policies for urban drainage.

One of the appropriate technological solutions to solve the above problem is the application of GIS for drainage management in the two districts of Ninh Kieu and Cai Rang. This technology has been used to support drainage management in many parts of the world and has brought practical and positive results (Muthanna *et al.*, 2018; Wang *et al.*, 2018; Abbas *et al.*, 2019; Aguiar *et al.*, 2020; Martin *et al.*, 2020; Wang *et al.*, 2020; Guptha *et al.*, 2021). In recent years, the application of GIS to support drainage management in Vietnam has also been implemented by many domestic scientists (Trung *et al.*, 2014; Dang and Kumar, 2017; Nguyen and Dao, 2018; Dung *et al.*, 2021). To successfully apply this technology, one of the indispensable components is the geographic database. This work is carried out to build a geographic database for Ninh Kieu and Cai Rang districts, creating the initial basis for the gradual application of GIS to drainage management in these two areas.

2. METHODS AND DATA

2.1 Research methods

The geographic database supporting drainage management in Ninh Kieu and Cai Rang districts is built on the open source software Quantum GIS (QGIS). The general process of building this geographic database includes four main stages: (1) collecting relevant data, (2) processing data and maps, (3) building geographic database, (4) evaluating results. Stage (2) is the key stage because it directly affects the accuracy of the geographic database. The format for this database is SpatialLite with the four characteristics: (1) spatial data storage is in topological vector, (2) allows multiple objects to be used at the same time, (3) can be used on many software, (4) high data security features. The main stages of the research process are outlined briefly in Figure 1.

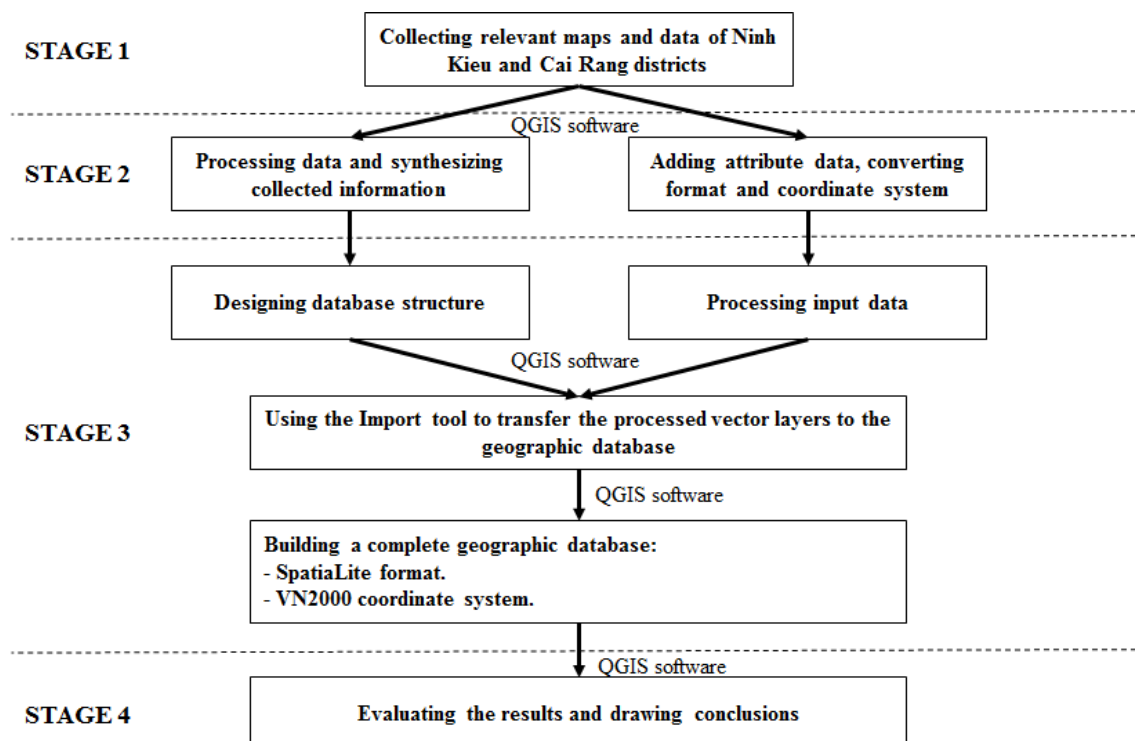


Figure 1. The detailed research flowchart to build geographic database.

2.2 Research data

The two main types of data were collected to build a geographic database for Ninh Kieu and Cai Rang districts including: (1) reports and statistics, (2) digital map data. The digital map data of the study area is assembled from many sources with following main formats: CAD file (*.dgn and *.dwg), Shapefile (*.shp), TAB file (*.tab). These digital maps include six main categories: (1) administrative map, (2) traffic map, (3) topographic map, (4) housing map, (5) land use map, (6) soil map. The boundaries of the study area cover the whole area of Ninh Kieu and Cai Rang districts. Figure 2 provides a general description of the administrative boundaries of the study area.

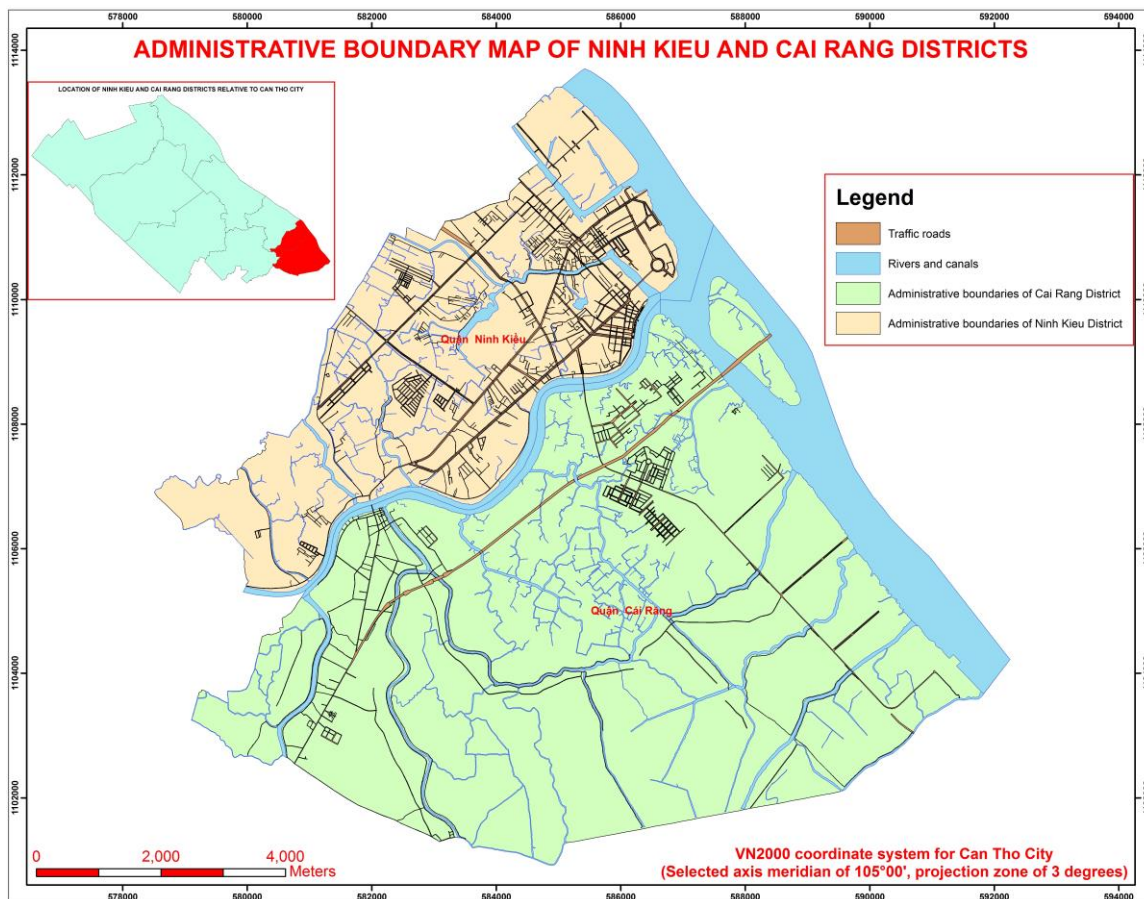


Figure 2. The location and scope of the study area - Ninh Kieu and Cai Rang districts.

3. RESULTS AND DISCUSSION

The process of building a geographic database for Ninh Kieu and Cai Rang districts is done on QGIS software with two main tools Create Layer and DB Manager. The main input data for this process are vector digital maps of the study area. These digital maps are processed and converted to the same format and geographic coordinate system (VN2000) before being imported into a SpatiaLite database. The structure of this SpatiaLite database is built on the basis of regulations issued by the Environmental Protection Agency in 2006. The SpatiaLite format is an extension of SQLite, a type of geodatabase that supports storing topological vector layers. This database is designed on the VN2000 coordinate system for

Can Tho city, with the projection zone of 3 degrees ($k = 0.9999$) and the selected axis meridian of $105^{\circ}00'$. The general structure diagram of this geographic database is shown in Figure 3.

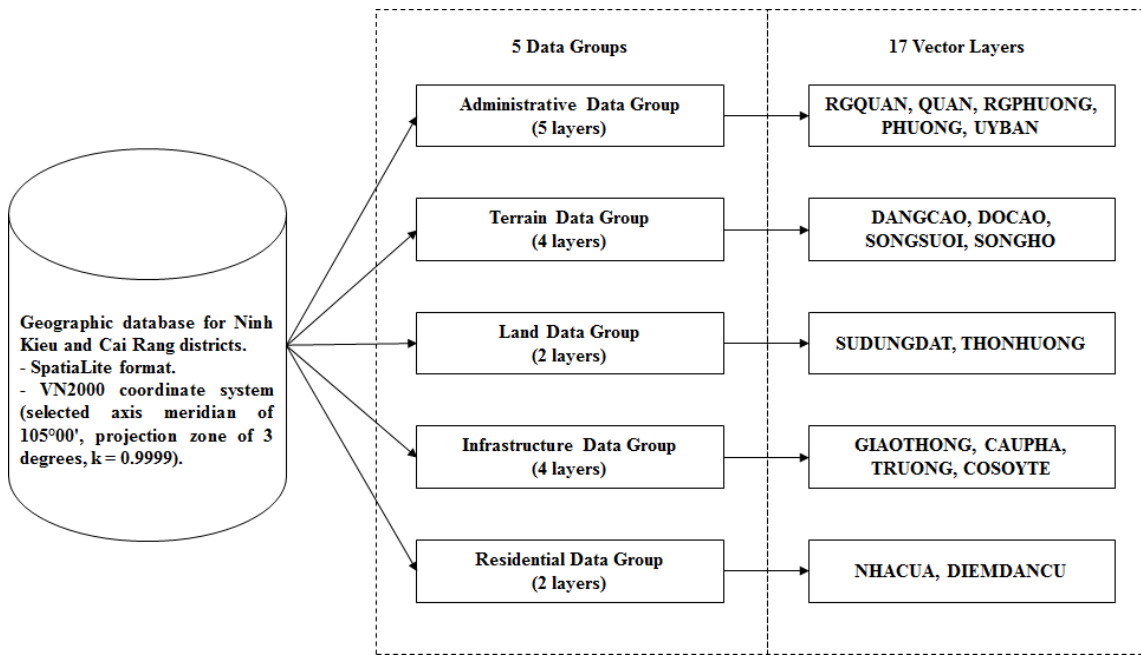


Figure 3. The general structure diagram of the geographic database for Ninh Kieu and Cai Rang districts.

The geographic database for Ninh Kieu and Cai Rang districts has five data groups, divided into 17 vector layers. The five main groups of this database include: (1) Administrative Data, (2) Terrain Data, (3) Land Data, (4) Infrastructure Data, (5) Residential Data. The main users of this geographic database are managers, policy makers, scientists and other stakeholders involved in drainage management. The vector layers stored in this geographic database are the basis for creating many different thematic maps for drainage management in particular and urban management in general in the study area. Figure 4 shows a map of houses in the study area, one of the products generated from the geographic coordinate for Ninh Kieu and Cai Rang districts.

In addition to building the SpatiaLite geographic database component, a system of processes to use data in this database is also designed to serve users. The main processes to use this geographic database include: adding new data, updating attributes, editing data, querying data, analyzing data, building thematic maps, extracting reports. This geographic database is designed to be used for many different fields, so it can be shared with other sectors in urban management of Ninh Kieu and Cai Rang districts.

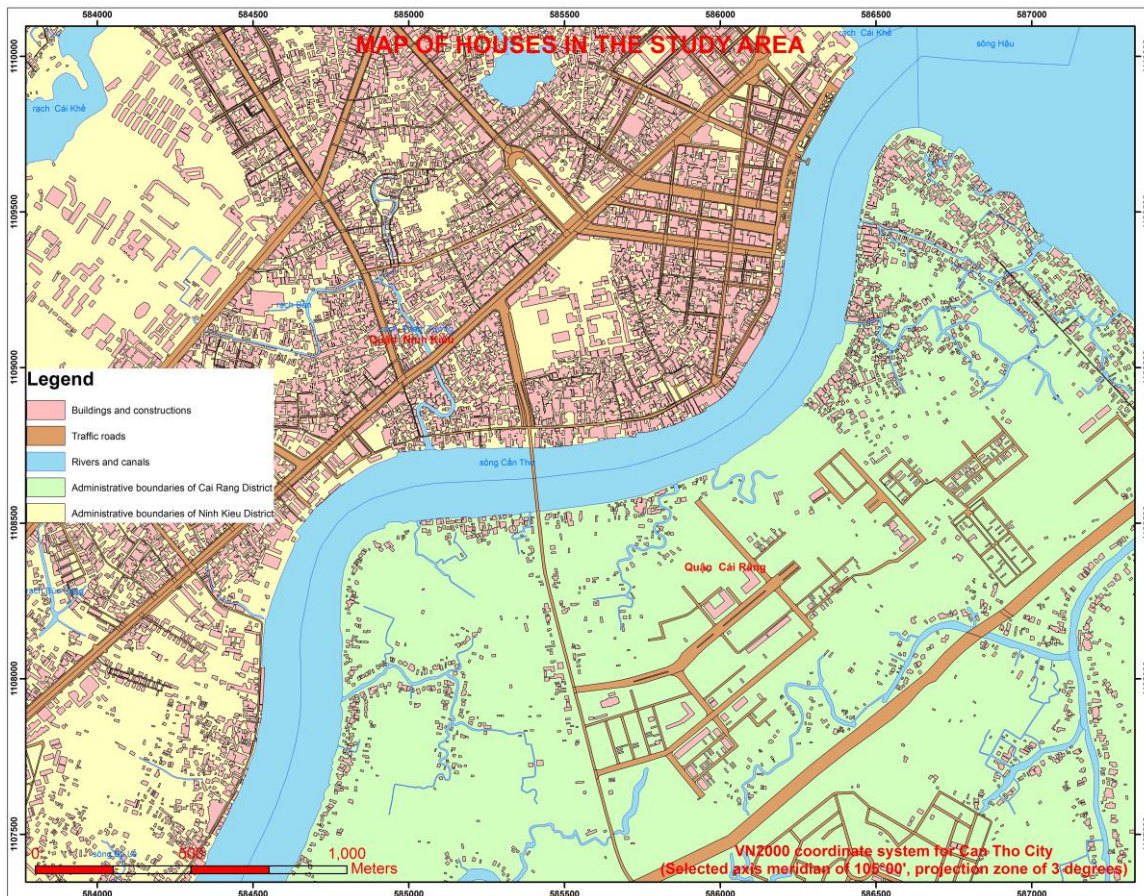


Figure 4. Map of houses in the study area - one of the objects of urban drainage management.

4. CONCLUSIONS AND RECOMMENDATIONS

The obtained results show that the research has achieved the set goal which is to build a geographic database for Ninh Kieu and Cai Rang districts with the structure in accordance with the regulations of the Ministry of Natural Resources and Environment. This geographic database is built on the VN2000 coordinate system, with five data groups, including 17 vector layers, meeting the requirements of the drainage management. With the SpatiaLite format, this geographic database can be used on many different types of GIS software. This geographic database is an important scientific basis for the application of GIS at different levels to drainage management in Ninh Kieu and Cai Rang districts. This database development process is a valuable reference for future research in the same field. The future development direction of the research is to add more layers and fields so that this database better reflects the current state of the study area, meeting the needs of managers in practice.

5. ACKNOWLEDGMENTS

The authors would like to thank the ValBGI Project for sharing as well as supporting and introducing to collect data from the authorities of the Mekong Delta, the Mekong Delta Geographic Information Systems Project (MGIS) of Assoc. Prof. Dr. Le Van Trung for providing data support for this research.

6. REFERENCES

- Abbas, A., Salloom, G., Ruddock, F., Alkhaddar, R., Hammoudi, S., Andoh, R., Carnacina, I., 2019. Modelling data of an urban drainage design using a Geographic Information System (GIS) database. *Journal of Hydrology* 574, 450-466.
- Aguiar, C. R. D., Nuernberg, J. K., Leonardi, T. C., 2020. Multicriteria GIS-Based Approach in Priority Areas Analysis for Sustainable Urban Drainage Practices: A Case Study of Pato Branco, Brazil. *Eng* 1(2), 96-111.
- Can Tho City Department of Construction, 2016. *Thuyết minh tổng hợp Quy hoạch thoát nước thành phố Cần Thơ đến năm 2030, tầm nhìn đến năm 2050: Chương 3 Hiện trạng thoát nước*. General explanation Can Tho City, III-2-III-53.
- Can Tho City Statistics Office, 2020. *Can Tho City Statistical Yearbook 2019*. Statistical Publishing House Publishing, Registration confirmation number: 2075-2020/CXBIPH/05-14/TK, 21-85.
- Dang, A. T. N., Kumar, L., 2017. Application of remote sensing and GIS-based hydrological modelling for flood risk analysis: a case study of District 8, Ho Chi Minh city, Vietnam. *Geomatics, Natural Hazards and Risk* 8(2), 1792-1811.
- Dung, L. T., Phu, V. L., Lan, N. H. M., Tien, N. T. C., Hiep, L. D., 2021. Sustainable Urban Drainage System Model for The Nhieu Loc - Thi Nghe Basin, Ho Chi Minh City. In *IOP Conference Series: Earth and Environmental Science*, IOP Publishing 652(1), 012012.
- Environmental Protection Agency, 2006. *Xây dựng bộ chuẩn cơ sở dữ liệu phục vụ việc xây dựng bản đồ môi trường Việt Nam, Phần “Nâng cấp cấu trúc cơ sở dữ liệu Hệ Thông tin Địa lý Môi trường”*. Ministry of Natural Resources and Environment, Report on performance of tasks, 45-204.
- Guptha, G. C., Swain, S., Al-Ansari, N., Taloor, A. K., Dayal, D., 2021. Evaluation of an urban drainage system and its resilience using remote sensing and GIS. *Remote Sensing Applications: Society and Environment* 23, 100601.
- Martin, C., Kamara, O., Berzosa, I., Badiola, J. L., 2020. Smart GIS platform that facilitates the digitalization of the integrated urban drainage system. *Environmental Modelling and Software* 123, 104568.
- Muthanna, T. M., Sivertsen, E., Kliewer, D., Jotta, L., 2018. Coupling field observations and Geographical Information System (GIS)-based analysis for improved Sustainable Urban Drainage Systems (SUDS) performance. *Sustainability* 10(12), 4683.
- Nguyen, A. T., Dao, H. S., 2018. GIS applications in urban management. In *MATEC Web of Conferences EDP Sciences* 193, 01004, 10.
- Trung, N. H., Tuu, N. T., Doan, T. C., Thinh, L. V., Tuan, D. D. A., Nguyen, M., 2014. Application of GIS to support urban water management in adapting to a changing climate: A case study in Can Tho city. *Vietnam Report number: UCCRN Case Study 14*.
- Vietnam Government, 2004. *Decree on establishing Ninh Kieu, Binh Thuy, Cai Rang, O Mon districts, Phong Dien, Co Do, Vinh Thanh, Thot Not districts and communes, wards, towns of Can Tho City under the Central Government*. Number: 05/2004/NĐ-CP, 1-6.
- Wang, J., Zhao, L., Zhu, C., Shi, B., 2018. Review and optimization of carrying capacity of urban drainage system based on ArcGIS and SWMM model. In book: *Advances in Hydroinformatics*, Springer, Singapore, 719-726.
- Wang, Z., Xu, J., He, X., Wang, Y., 2020. Analysis of spatiotemporal influence patterns of toxic gas monitoring concentrations in an urban drainage network based on IoT and GIS. *Pattern Recognition Letters* 138, 237-246.

MAPPING SURFACE WATER QUALITY ZONE BY GIS AND SPATIAL INTERPOLATION IDW - CASE STUDY IN CAN THO CITY, VIETNAM

Le Nhu Y, Nguyen Dinh Giang Nam and Nguyen Vo Chau Ngan

Department of Water Resources, College of Environment & Natural Resources, Can Tho University, 3-2 street, Xuan Khanh ward, Ninh Kieu district, Can Tho city, VietNam
Email: leny@ctu.edu.vn

ABSTRACT

Can Tho City - a biggest city in the Mekong Delta of Vietnam - has experienced rapid urbanization in recent years. It is also to deal with substantial water and climate change challenges ranging from urban to suburban areas, as well as surface water pollution. This paper calculated the Vietnamese Water Quality Index (WQI) values based on the database of water quality monitoring stations in Can Tho City in five years. Then the QGIS software and the Inverse Distance Weighted tool were applied to map out the surface water quality spatial distribution. The calculation results showed slightly temporal and spatial variation in water quality with WQI values range from 76 to 91 which indicate good condition. The lower WQI values recorded in the dry season and at the areas where concentrate more residential zones and industry factories. The spatial interpolate result showed the good condition of water quality through a thematic and visual map. The surface water quality map could use not only by scientists but also local authorities or decision makers.

Keywords: Can Tho City, Inverse Distance Weighted, QGIS, surface water quality, WQI

1. INTRODUCTION

Can Tho City is the largest city in the Mekong Delta of Vietnam - has experienced rapid urbanization in recent years. The river network plays an important role in supplying water for domestic use, agricultural production, industry, aquaculture and other activities. Under pressure from domestic and industrial discharge activities in the surface water area, there are signs of pollution. Recently, wastewater afore-mentioned activities which has been directly or indirectly affected to the source water quality; especially densely populated zones and intensive agricultural production (MRC, 2013). Monitoring results showed that almost all major water supply and drainage canals are contaminating at an alarming rate in Can Tho City (Center for Natural Resources and Environment Monitoring in Can Tho City, 2013). Many studies have evaluated water quality on the section of Hau River flowing through Can Tho in general and tributaries in the inner city in particular have indicated water quality according to each pollution parameter from direct sampling method. (Nguyen Thi Kim Lien *et al.*, 2016). The water quality in the Can Tho river has been polluted, most of the research indicators exceed the allowable limit, the average value of the water quality index (WQI) in the Can Tho river flowing through Ninh Kieu, Cai Rang and Phong Dien districts gradually increased over the years (Vo Thi Ngoc Giau *et al.*, 2019). The results of these studies have a certain contribution to the forecasting of water quality changes in the region. In order to improve efficiency in water resource management, besides assessing water quality fluctuations by WQI, the study also combines spatial interpolation method IDW (Inverse Distance Weighted) in the QGIS software (Quantum GIS) to distribute surface water quality on the river system. The results presented in a simple and understandable way is an appropriate source of information for the community and state management agencies in charge of the environment; organizations and individuals involved in the construction, announcing information on environmental quality to the community (General Department of Environment, 2019).

2. RESEARCH METHODS

2.1 Methods of data collection and analysis

Data are collected from the Center Environmental and Natural Resources Monitoring Can Tho City to calculate the WQI indicators. Data are collected continuously during the period 2014-2018. Monitored water quality parameters consisting pH, Arsenic (As), Chromium (Cr), dissolved oxygen (DO), chemical oxygen demand (COD), biological oxygen demand (BOD₅), Ammonium N-(NH₄⁺), Nitrate (NO₃⁻), Coliform. With sampling frequency 4 times/ year in March, June, September, December every year.

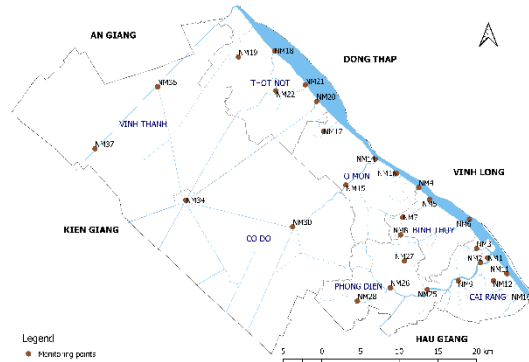


Figure 1. Monitoring location map

2.2 Calculating the water quality index WQI

Method for calculating the water quality index (WQI): the method adapted to Decision 1460/QĐ-TCMT of the General Department of Environmental is as follows:

$$WQI = \frac{WQI_I}{100} \times \frac{\left(\prod_{i=1}^n WQI_{II}\right)^{1/n}}{100} \times \frac{\left(\prod_{i=1}^m WQI_{III}\right)^{1/nm}}{100} \times \left[\left(\frac{1}{k} \sum_{i=1}^k (WQI_{IV})^2 \right) \times \frac{1}{l} \times \sum_{i=1}^l WQI_{V} \right]^{1/3}$$

In which:

WQI_I: calculation results for pH parameter (group I)

WQII: calculation results for the group of plant protection drug parameters (group II)

WQI_{III}: calculation results for heavy metal parameters (group III);

WQI_{IV}: calculation results for groups of organic and nutritional parameters (group IV)

WQI_V: calculation results for the group of microbiological parameters (group V)

The water quality index is calculated according to the scale (WQI value range) which corresponding to the symbol and the colors to assess the water quality (Table 1).

Table 1. Water quality rating scale

WQI value	Water quality	Suitable for the intended purposes	Colors
91 - 100		Good use for domestic water supply purposes	Blue
76 - 90	Good	Used for domestic water supply purposes, but needed appropriate treatment measures	Green
51 - 75	Medium	Used for irrigation and other equivalent purposes	Yellow
26 - 50	Poor	Used for navigation and other equivalent purposes	Orange
10 - 25	Very poor	Water is severely polluted, needs future treatment measures	Red
<10	Heavy pollution	Poisoned water, need to take measures to overcome and treat	Brown

(Source: General Department of Environment, 2019)

2.3 The IDW Spatial Interpolation Method by QGIS

From the results of WQI calculation, mapping water quality zone based on the WQI index was constructed by the IDW in QGIS software (version 3.18).

The IDW method determines the value of unknown points by averaging the distance-weighted values of the points with known values in the vicinity of each pixel. The IDW method has been evaluated optimally when there is no big difference between the interpolated value and the results of sample analysis at the laboratory in the study of constructing interpolated water quality maps (Asadzadeh *et al.*, 2013; Gong & O'Bryant, 2014).

3. RESULTS AND DISCUSSIONS

3.1 Calculation results of water quality index

Calculation results of WQI indicators for monitoring locations in Can Tho City during the dry season periods in March (1), the middle of the rainy season in June, September (2, 3) and the end of the rainy season in December (4).

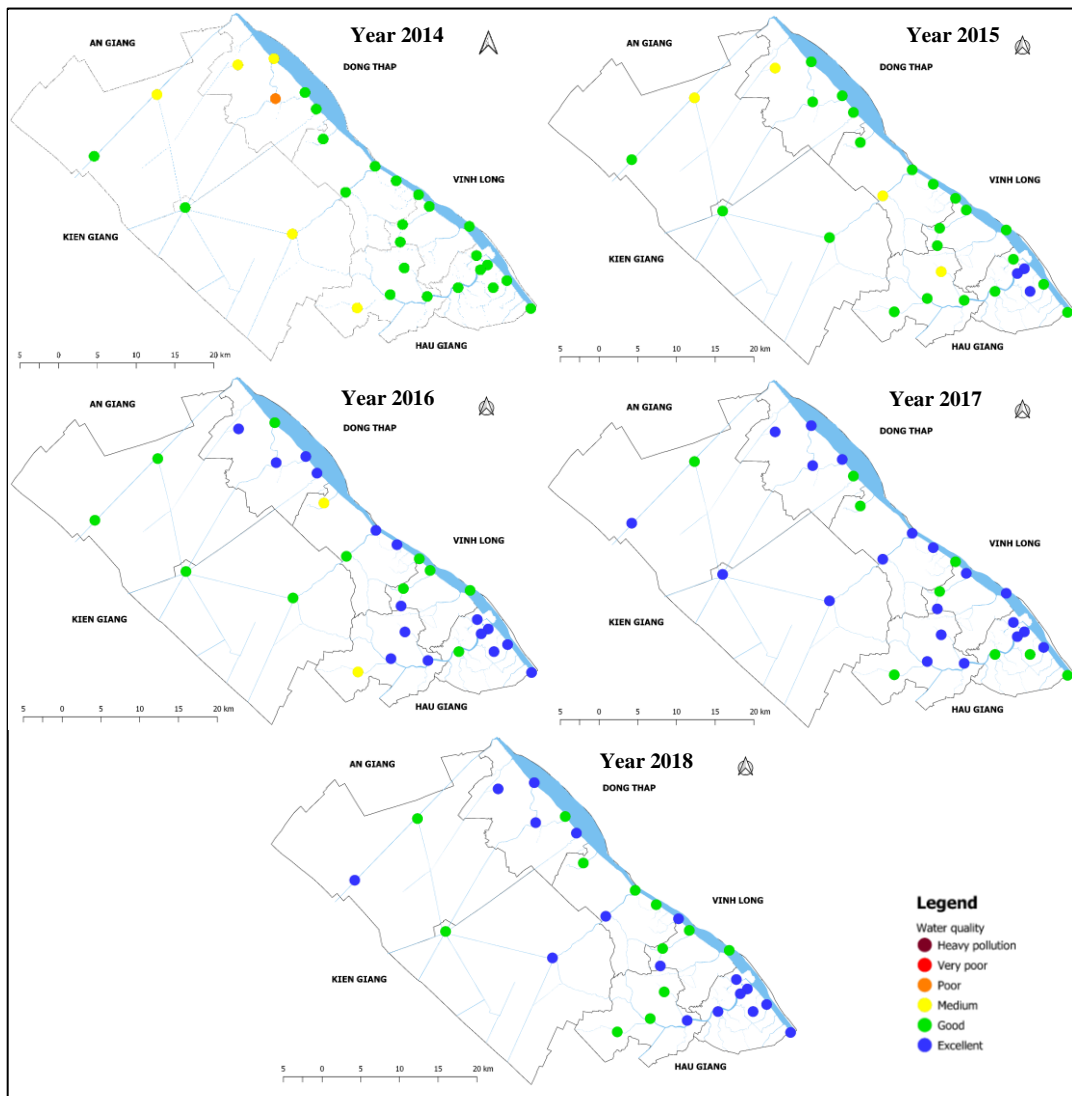


Figure 2. WQI map at the dry season from 2014 to 2018 in Can Tho

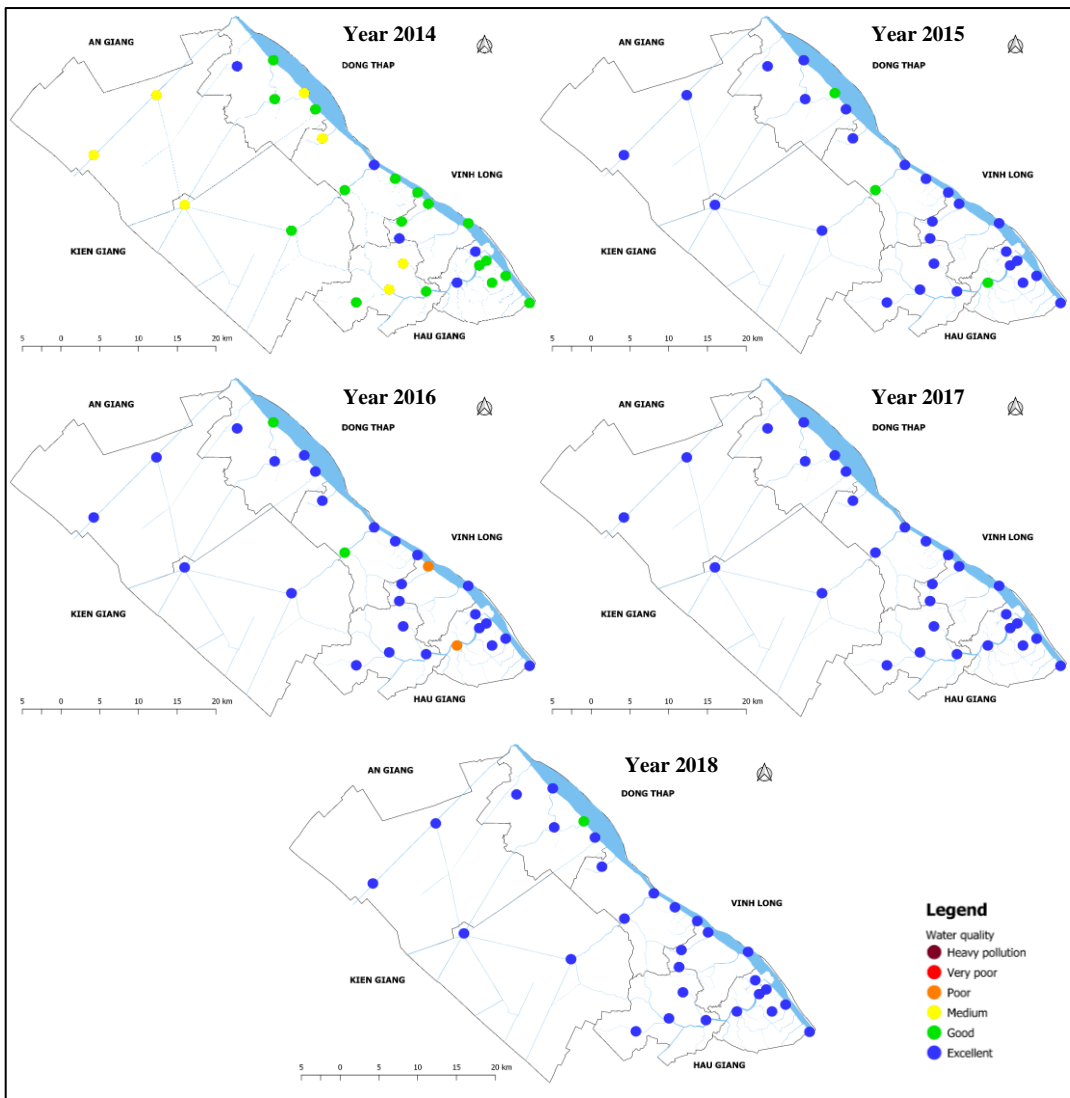


Figure 3. WQI map at the rainy season from 2014 to 2018 in Can Tho

The results of WQI calculation showed that in 2014 and 2015 water quality in the area is low, except for Ninh Kieu District (NM1, NM2, NM3), the remaining districts range from 26 to 75 corresponding to orange and yellow, and it could only be used for navigation purposes, some stations are still at level 25 (NM5). Until 2016, 2017, 2018 water quality will be improved, within range from 71 to 90 (corresponding to green) that can be used for irrigation and good water quality will reach the range from 91 to 100 (corresponding to blue) can be used for domestic water supply purposes.

The dry season and the beginning of the rainy season are the times when the water quality in the region is worse, the dry season period of all three years 2014, 2015, 2016 illustrated that the water quality in the region is mostly low and average. During the middle and the end of the rainy season, the water quality improves.

3.2 Mapping water quality zone

The evolution of water quality in the canal system in Can Tho City during the monitoring periods in 2018 showed that the water quality changes between the large river area and the inland area is quite large, the pollution level is non-partial at one site. In Ninh Kieu area,

water quality is relatively stable between seasons. The areas of continuous change in quality are mostly in market areas, typical industrial parks such as Tra Noc - Binh Thuy, Cai Rang and Phong Dien areas along the Can Tho river. The dry season (Figure 4) in the canals in this area has poorer water quality than the rest of the year. In addition, inland areas such as Vinh Thanh, water quality also decreases during the dry season.

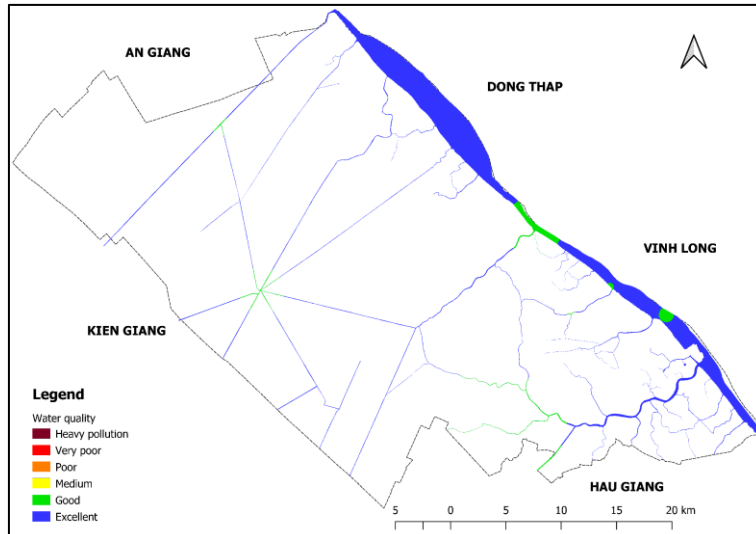


Figure 4. Mapping water quality zone at the dry season in 2018

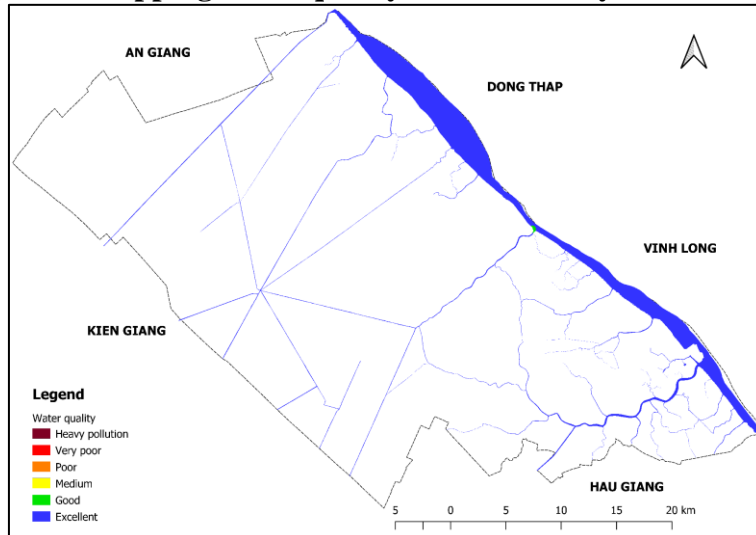


Figure 5. Mapping water quality zone at the rainy season in 2018

4. CONCLUSIONS

Research results indicated that water resources in the study area have uneven quality according to space and time. Water quality during the years 2014, 2015, and 2016 in several regions was only used for navigation. However, until 2017 to 2018 the water quality has improved from good to extremely wonderful and is capable of using water for domestic purposes. The water quality is better improved in the area adjacent to the Hau River, the more inland the water quality decreases. In the dry season and the beginning of the rainy season, the water quality is poor and gradually recovers in the middle and the end of the rainy season, which indicates that the self-healing capacity of the river system in the region is still very good. In some areas, there are signs of pollution, but it gradually improved over many years. Canals with low quality are often situated in the markets and next to large industrial zones. Hence,

the fundamental cause of water pollution afore-mentioned is mainly domestic and industrial wastewater.

The reliability of the IDW interpolation method has been proven and used by many authors to evaluate surface water quality in numerous previous publications. However, at points with limited density of monitoring such as Vinh Thanh and Co Do, the interpolation results are not very accurate. Therefore, at these points, the interpolation results from the IDW method are approximate and could be used for reference purposes.

Acknowledgements

This study is funded in part by the Can Tho University Improvement project VN14-P6 supported by a Japanese ODA loan.

5. REFERENCES

- Asadzadeh, F., Zareiyan-Jahromi, M., and Asadzadeh, F., 2013. Mapping the spatial variability of groundwater quality in Urmia (Iran): comparison of different interpolation methods. *Journal of International Environmental Application and Science*, 8(3), 359-368.
- Bui Thi Nga, and Bui Anh Thu, 2005. Surface water quality and household waste management at Rach Ban Canal, Can Tho City, Viet Nam. *Can Tho University Journal of Science*, 04, 26-35.
- Can Tho's Center for Natural Resources and Environment Monitoring, 2013. Report on the current state of the environment in Can Tho City 2012 - Internal circulation, Can Tho.
- Chau Hong Thang, Le Thi Thuy Van, Tran Sang, and Dong Thi Minh Hau, 2020. Application of geographical information system (GIS) to interpolate and manage water quality (WQI) of Dong Nai river from the Nam Cat Tien ferry terminal to Mui Den Do. *Ho Chi Minh City University of Education Journal of Science*, 17(6), 1088-1099.
- Chea R., Grenouillet G., and Lek S., 2016. Evidence of Water quality degradation in Lower Mekong Basin Revealed by Self Organizing Map.
- Gong, G., Mattevada, S., and O'Bryant, S.E., 2014). Comparison of the accuracy of kriging and IDW interpolations in estimating groundwater arsenic concentrations in Texas. *Environmental Research*, 130, 59-69.
- General Department of Environment, 2019. Decision No. 1460/QĐTCMT, dated December 11, 2019, on promulgating Technical Guidelines for calculation and publication of Vietnam Water Quality Index (VN_WQI).
- Mekong River Commission, 2013. Annual Water Quality Data Assessment Report. *MRC Technical Paper* No.40.
- Nguyen Thi Kim Lien, Lam Quang Huy, Duong Thi Hoang Oanh, Truong Quoc Phu and Vu Ngoc Ut, 2016. Water quality in mainstream and tributaries of Hau River. *Can Tho University Journal of Science*, 43, 68-79.
- Vo Thi Ngoc Giau, Phan Thi Bich Tuyen and Nguyen Hieu Trung, 2019. Assessing surface water quality of Can Tho river in the period of 2010-2014 using water quality indicator (WQI). *Can Tho University Journal of Science*, 55 (2), 105-113.

Monitoring The Multi-Temporal Pattern of A COVID-19 Situation in Thailand Through Geospatial Data

Chudech Losiri¹ Asamaporn Sithi²

Department of Geography, Faculty of Social Sciences,
Srinakharinwirot University 114 Sukhumvit 23, Bangkok 10110, Thailand

ABSTRACT

The current spread of COVID-19 is a severe situation that may affect all people regarding human health and social and economic well-being in Thailand. To continuously monitor the case at the national level, this research used the statistics of monthly patients in each province of Thailand from January 2020 to May 2021 to map and analyze the spread of the COVID-19 outbreak. This study used Morans I Index to identify a spatial pattern of the outbreak at the national level and utilized Getis-Ord Gi and Gi through a hot spot analysis to determine the intensity of the outbreak areas. Moreover, the correlation analysis was applied to identify the relationship between a number of patients and social and economic factors. The analysis results show that the spread of COVID-19 is concentrated in the major cities of various regions of the country, especially in Bangkok, which is the area where the epidemic concentration is the highest. In addition, the results from the analysis of the relationship between the number of cases and various factors revealed that COVID-19 cases show a low level of association compared with social and economic factors. It is because most of the epidemic is related to the travel activities of the local population. Finally, the results obtained from this study will lead to a greater understanding of the COVID-19 outbreak. They can also use the information for planning and organizing public health at the national level.*

MapMint: The service-oriented platform

Venkatesh Raghavan,¹Gérald Fenoy²

Graduate School of Engineering, Osaka City University, Japan,
GeoLabs SARL Futur Building 1 1280,
Avenue des Platanes 34970 LATTES FRANCE contact@geolabs.fr

ABSTRACT

MapMint is a comprehensive task manager for publishing web mapping applications. It is a robust open-source geospatial platform allowing the user to organize, edit, process and publish spatial data to the Internet. MapMint includes a complete administration tool for MapServer and simple user interfaces to create Mapfiles visually. MapMint is based on the extensive use of OGC standards and automates WMS, WFS, WMT-S, and WPS. All the MapMint functions run through WPS requests calling general or geospatial web services vector and raster operations, Mapfiles creation, spatial analysis and queries, and much more. MapMint server-side is build on top of ZOO-Project, MapServer, GDAL, and numerous WPS services written in C, Python, and JavaScript. MapMint client-side is based on OpenLayers and Jquery and provides user-friendly tools to create, publish and view maps. In this presentation, MapMint architecture and main features will be presented, and its modules: Dashboard, Distiller, Manager, and Publisher described with an emphasis on the OGC standards and OSGeo softwares they are using. Some case studies and examples will finally illustrate some of the MapMint functionalities.

Study on extending the supply water pipe network at Binh Thuy district, Can Tho city

Ngan Nguyen Vo Chau, Giang Nam Nguyen Dinh, Minh Khoa Tran

College of Environment and Natural Resources, Can Tho University,

College of Technology and Engineering, Can Tho University

ABSTRACT

The study aimed to determined the need of development and investment for water supply systems, then proposing a reasonable water supply pipe network for Binh Thuy district - Can Tho cities by 2030. Secondary data related to water is collected from local authorities, then EPANET model was applied to calculate flow, pressure in water supply system. The results show that water supply network of Binh Thuy has supplied water to 84.95% of households in the district, the pressure recorded at the end of pipelines is not up to standard. Thereby, the study also foresees the need to use clean water as a basis for the implementation of investment projects on new construction, renovation and upgrading of water supply network in the district. Based on that, the study has propose solutions to prevent water loss, preliminary calculate of the capacity of water supply, forecasting the flow rate and pressure in water pipe network.

**International Symposium on GeoInformatics for Spatial-Infrastructure
Development in Earth and Allied Sciences (GIS-IDEAS)
2-4 September 2021, Phitsanulok, Thailand**

CONFERENCE FOUNDERS

Dr. Nghiem Vu KHAI, Member of Parliament, S.R. Vietnam (VN)

Prof. Takashi FUJITA, Emeritus Professor, Osaka Institute of Technology (JP)

CONFERENCE CHAIRS

Prof. Vansarochana CHAIWIWAT (TH) and Prof. Venkatesh RAGHAVAN (JP)

ORGANIZING SECRETARY

Dr. Sittichai CHOOSUMRONG (TH) and Dr. Go YONEZAWA (JP)

STEERING COMMITTEE

Dr. Ho Dinh DUAN (VN)

Prof. Yasuyuki KONO (JP)

Assoc.Prof. Teerawong LAOSUWAN (TH)

Prof. Nguyen Kim LOI (VN)

Prof. Truong Xuan LUAN (VN)

Dr. Suwisa MAHASANDANA (TH)

Prof. Alaa A MASOUD (EG)

Prof. Shinji MASUMOTO (JP)

Prof. Muneki MITAMURA (JP)

Dr. Lam Dao NGUYEN (VN)

Dr. Thaworn ONPRAPHAI (TH)

Assoc. Prof. Chalermchai PAWATTANA (TH)

Dr. Kampanart PIYATHAMRONGCHAI (TH)

Assoc. Prof. Pathana RACHAVONG (TH)

Dr. Ornprapa Pummakarnchana ROBERT(TH)

Prof. Nitin TRIPATHI (TH)

Prof. Yasushi YAMAGUCHI (JP)

SCIENTIFIC COMMITTEE

Dr. Tran Thi AN (VN)

Dr. Tatsuya NEMOTO (JP)

Dr. Tran Van ANH (VN)

Dr. Sarawut NINSAWAT (TH)

Dr. Ho Dinh DUAN (VN)

Dr. Susumu NONOGAKI (JP)

Dr. Phaisarn JEEFOO (TH)

Dr. Thitirat PANBAMRUNGKIJ (TH)

Dr. Atsushi KAJIYAMA (JP)

Dr. Vinayaraj POLIYAPRAM (JP)

Dr. Rangsan KETORD (TH)

Dr. Pham Thi Mai THY (VNProf. Nitin TRIPATHI (TH))

Dr. Natapon MAHAVIK (TH)

Prof. Yasushi YAMAGUCHI (JP)

WORKSHOP COMMITTEE

Gérald FENOY (FR)

Jeff McKENNA (CA)

Prasong PATHEEPPOMEPMONG (TH)

Natraj VADADDI (IN)

CONFERENCE COORDINATORS

Ms. Tanyaluck CHANSOMBAT, Ms. Sanonoi FAKTHONGORN and Ms. Suthisa SANHAN

Author Index

Anh The Hoang	285	Nguyen Hieu Trung	219, 364
Bang Quoc Ho	1	Nguyen Huy Anh	339
Banluesak Khorsuk	313	Nguyen Ngoc Thanh	205
Boonphol Meechaiyo	279	Nguyen Thanh Ngan	219, 364
Bussaba Samdaengchai	83	Nguyen Thi Cam Tien	333
Chaiwiwat Vansarochana	26, 76, 178, 248, 313	Nguyen Thi Phuong Doan	294
Chamnan Kumsap	58, 121	Nguyen Thi Thao Nguyen	339
Chanida Suwanprasit	142	Nguyen Thu Thao	102
Charatdao Kongmuang	129	Nguyen Van Binh	205
Chau Nguyen Xuan Quang	156	Nguyen Vo Chau Ngan	347, 370
Chi Cong Nguyen	69	Niang Sian Lun	96
Chisato Asahi	89	Nuttapong Panthong	76
Dechen Wangmo	18	Pathana Rachavong	7, 38, 44, 64, 260, 267
Dhyey Bhatpuria	191	Pathipat Sanpapao	178
Dinh Thi Kim Phuong	115	Pattanapol Meena	83, 136
Do Thi Viet Huong	199	Pattara Sukthawee	76, 313
Doan Ngoc Nguyen Phong	199	Pattareeya Ponza	178
Duangdao Sriyakun	325	Phaisarn Jeefoo	121, 148, 162
Fatah Masthawee	76, 313, 357	Pham Huu Ty	205
Gia Thanh Hoang	339	Pham Thi Mai Thy	156
Gitsada Panumonwatee	325, 357	Pham Thi Trieu Tien	205
Ho Dinh Duan	102	Phan Minh Thu	102
Ho Van Hoa	156	Phanakron Kaewme	162
Hoang Ngoc Khue Vu	1	Phung Diep Anh	347
Huynh Yen Nhi	294	Phurba Tamang	18
Iyarat Ounrit	136	Phuwitson Phumsaranakhom	148, 162
Jigme Tenzin	18	Polpreecha Chidburee	129, 279
Jiranya Duangfoo	7, 44, 64, 260, 267	Pongsakol Peatmak	213
Jittiwat Tonnamon	279	Prasit Mekarun	300, 306
Jittrarat Chantana	325	Pudtraporn Napang	109
Kamonchat Seejata	129	Quan Le	1
Kampanart Piyathamrongchai	50, 272	Quang Khanh Nguyen	285
Kanita Thanacharoenchanaphas	357	Rajnish Rakholia	1
Kankanit Pisamayarom	248	Rattana Prakhammintara	76
Kazuma Kasahara	12	Rhutairat Hataitara	50, 306
Krittapon Iamsaing	234	Ricardo Simon Carbajo	1
Kumpon Subsomboon	279	Santi Lapbenjakul	325
Lam Dao Nguyen	156	Saowalak Thainsom	272
Le Duc Tuan	319	Sarawut Ninsawat	96
Le Huyen Tran	294	Sarintip Tantanee	129
Le Minh Vinh	319	Sasawat Soontaros	109
Le Ngoc Hanh	170	Sasithon Chatsudarat	129
Le Nhu Y	370	Sirintorn Tongkam	300
Le Tan Tuyen	199	Sittichai Choosumrong	50, 227, 234, 240, 300, 306, 325
Le Thi Dung	333	Somsarit Sinnung	83, 136
Lim Ngoc Han	347	Son The Pham.	254
Lobzang Dorji	18	Sorasak Khoomboon	109
Luu Dinh Hiep	333	Sudarat Paluang	325
Mattana Pongsopon	109	Sukchatri Prasomsuk	148, 162
Maythawee Jantha	7, 38	Supat Ponza	178
Muneki Mitamura	12	Supattra Phaya	178
Nagata Yoshikatsu	185	Surat Khampangkaew	142
Napak Karnasuta	109	Suriyawate Boonthalarath	58
Napatsawan Tubkrit	32	Suwanan Sukjareon	272
Natima Udon	240	Suwisa Mahasandana	213
Natkamol Pinnok	227	Suwit Navakam	109
Natnicha Yooyen	109	Tanyaluck Chansombat	7, 32, 38, 44, 260, 267
Nattapon Mahavik	76, 129	Teeranai Srithamarong	58
Ngoc Hanh Le	89	Teerawong Laosuwan	83, 136
Ngoc Hoan Nguyen	69	Thaithaworn Lerdwithayaprasith	213
Nguyen Dinh Giang Nam	370	Tham Thi Ngoc Han	156
Nguyen Duc Tri	115	Thanapon Piman	191

Thi An Tran	89	Tranid Prasertsr.	109
Thi Hai Yen Phi	69	Truong Chi Quang	347
Thi Phuong Thao Ngo	285	Truong Nhat Kieu Thi	156
Thi Thanh Thuy Pham	69	Truong Van Canh	170
Thi Thu Ha Le	69	Van Ngoc Truc Phuong	319
Thi Thuy Hang Nguyen	1	Vasker Sharma	18, 26
Thoai Tam Nguyen	1	Venkatesh Raghavan	50
Thom Hue Huynh	254	Watcharaporn Preedapirom	121
Thongley Thongley	18, 26	Wattananan Jaisa-ard	260
Thuy Linh Nguyen	89	Wijitra Nakdang	272
Tran The Nam	347	Xuan Luan Truong	69
Tran Thi An	170	Xuan Quang Truong	69
Tran Thi Minh Thao	347		



Organized by

Naresuan University, Osaka City University &
Japan-Vietnam Geoinformatics Consortium

Supported by

Hanoi University of Mining and Geology (VN)
Hanoi University of Natural Resources & Environment (VN) Japan
Geotechnical Consultant Association (JP)
Japan Society of Geoinformatics (JP)
i-bitz Company Ltd. (TH) and Geoinformatics International (TH)

ISBN 978-4-901668-37-8

9 781234 567897